C.-C. Jay Kuo
Shang-Ho Tsai
Layla Tadjpour
Yu-Hao Chang

Precoding Techniques for Digital Communication Systems

Springer

Precoding Techniques for Digital Communication Systems

C.-C. Jay Kuo · Shang-Ho Tsai · Layla Tadjpour · Yu-Hao Chang

Precoding Techniques for Digital Communication Systems

Springer

C.-C. Jay Kuo
Department of Electrical Engineering
EEB 440
Hughes Aircraft Electrical
Engineering Building
3740 McClintock Ave.
Los Angeles, CA 90089

Layla Tadjpour
908 N. Verdugo Rd.
Glendale, CA 91206

Shang-Ho Tsai
Department of Electrical
Engineering
R734 E5 Building
National Chiao Tung University
Taiwan, R.O.C.

Yu-Hao Chang
1 Dusing Rd.
Hsinchu Science Park
Hsin-Chu
Taiwan, 30078, R.O.C.

ISBN: 978-0-387-71768-5 e-ISBN: 978-0-387-71769-2
DOI: 10.1007/978-0-387-71769-2

Library of Congress Control Number: 2008926091

Printed on acid-free paper

springer.com

Preface

During the past two decades, many communication techniques have been developed to achieve various goals such as higher data rate, more robust link quality, and more user capacity in more rigorous channel conditions. The most well known are, for instance, CDMA, OFDM, MIMO, multiuser OFDM, and UWB systems. All these systems have their own unique superiority while they also induce other drawbacks that limit the system performance. Conventional way to overcome the drawback is to impose most of the computational effort in the receiver side and let the transmitter design much simpler than receiver. The fact is that, however, by leveraging reasonable computational effort to the transmitter, the receiver design can be greatly simplified. For instance, multiaccess interference (MAI) has long been considered to limit the performance of multiuser systems. Popular solutions to mitigate MAI issue include multiuser detection (MUD) or sophisticated signal processing for interference cancellation such as PIC or SIC. However, those solutions impose great burden in the receiver. In this case, precoding offer good solutions to achieve simple transceiver designs as we will mention later in this book.

This book is intended to provide a comprehensive review of precoding techniques for digital communications systems from a signal processing perspective. The variety of selected precoding techniques and their applications makes this book quite different from other texts about precoding techniques in digital communication engineering.

In the first part of the book, we overview the principles of precoding for channels with intersymbol interference (ISI) such as Tomlinson–Harashima precoding and Trellis precoding. We also introduce how the widely used OFDM systems can be treated as a special case of precoding techniques and introduce precoding schemes for OFDM systems. Furthermore, it is well known that the performance of code division multiple access (CDMA) systems is limited by the MAI. As the number of users increases, a light weight receiver may not be able to combat MAI efficiently. Thus, we introduce various existing precoding techniques that reduce the interference level while keeping the receiver design simple. Finally, we devote a whole chapter to the issue

of precoding for multiple input multiple output (MIMO) channels. In MIMO systems, the use of TH precoding at the transmitter will increase the capacity of a BLAST MIMO system. Precoding techniques can also use the channel stat information to optimally assign resources such as power and bits over multiple antennas or facilitates the design of space-time codes with maximum diversity/coding gain. We will review, joint linear/decoder design and linear precoding techniques for space-time codes systems, among other techniques. MIMO precoding with partial channel information is also included.

The second part of the book offers the recent state-of-the-art precoding techniques originated from several projects and research activities conducted by the authors in the field of multiuser OFDM transmissions and ultra-wideband (UWB) radio systems. For multiuser OFDM systems, we show that by properly designing transceiver and orthogonal code, the MAI induced from various sources such as multipath, time and frequency offsets, and Doppler effect can be completely eliminated or reduced greatly to a negligible amount for certain active users. Since some active users can enjoy a MAI-free or near zero MAI property, the computational complexity for MUD or sophisticated signal processing for interference cancellation can be significantly reduced. In the UWB channel, the signal power spread over a great number of multipath components leads to a challenging problem of received signal power collection at the receiver. We show that a channel phase precoding technique that concentrates on the signal power at the desired receiver output can greatly simplify the receiver complexity as compared to the conventional Rake receiver.

The book is written for graduate students, practicing engineers in telecommunications industry as well as researchers in academia who are already familiar with technical concepts such as probability, digital communication systems, and estimation theory. We hope that the book will contribute to a better understanding of the value of precoding techniques for digital communication system and may motivate further investigation in this exciting research area.

The authors would like to thank the anonymous reviewers for their constructive suggestions. C.-C. J. Kuo would like to thank his parents, his wife Terri and daughter Allison for their encouragement and support for years. Y.-H. Chang would like to thank his parents and wife Sophia for their support and encouragement during the preparation of this book. L. Tadjpour is grateful to her parents and sisters for their support and encouragement throughout this project. S.-H. Tsai would like to thank his parents and his wife Janet for their endless understanding and support during the time he devoted to writing this book, and his son Lawrence for his lovely smile.

National Chiao Tung University, *Shang-Ho Tsai*
University of Southern California, *Layla Tadjpour*
University of Southern California, *Yu-Hao Chang*
University of Southern California, *C.-C. Jay Kuo*
February 2008

Contents

List of Symbols

$\approx$	Approximately equal to
$*$	Time-domain convolution operator
$\otimes$	Kronecker product
$\mathbf{A}^{\dagger}$	Hermitian (Complex and conjugate) of $\mathbf{A}$
$\mathbf{A}^{t}$	Transpose of $\mathbf{A}$
$MAI_{i \leftarrow j}[k]$	The MAI from user j to user i at subcarrier k
$[x]_{\downarrow M}$	Signal x down-sampled by M
$[x]_{\uparrow M}$	Signal x up-sampled by M
$E\{x\}$	Expectation of x
$\mathcal{CN}(0,1)$	Complex circular symmetric Gaussian distribution
σ_x^2	Variance of x
J_n	Bessel function of the first kind of order n
$\mathrm{Re}\{x\}$	Real part of x
$\mathbf{F}$	Fourier matrix
$\mathbf{s}_k$	Spreading code of user k
$w(t)$	Unit power chip waveform defined as $\int_0^{T_c} \lvert w(t)\rvert^2 = 1$
$\delta_D(t)$	Dirac delta function
$\mathbf{I}_N$	An identity matrix of size $N \times N$
$\mathbf{e}_N^{(i)}$	the ith column of $\mathbf{I}_N$
$\mathbf{X}^{\ddagger}$	Pseudo inverse of matrix X
$\lvert\lvert\mathbf{x}\rvert\rvert$	Vector 2-norm
$\lvert\lvert\mathbf{F}\rvert\rvert_F$	Frobenius norm of matrix $\mathbf{X}$
$\lceil x \rceil$	A ceiling function of x
$\mathbb{F}\{\cdot\}$	Fourier transform operator
$\mathrm{diag}(x_1\ x_2\ \cdots x_N)$	$N \times N$ diagonal matrix with diagonal elements x_1,x_2,$\cdots$,x_N
T_c	Chip interval
$x(n)$	x in time domain
$X(k)$	x in frequency domain

L	Multipath length
$h(n)$	Channel impulse response
n and t	Time indices
T	Symbol period or number of users
k	Discrete frequency domain index
$\hat{x}$	Detected symbol, or estimated value of x
$\mathbf{R}$	Correlation matrix
F_c	Carrier frequency
F_s	Sampling frequency
V	Velocity
τ, D, or d	Delay
f_D	Doppler frequency
M_t	Number of transmit antennas
M_r	Number of receive antennas
$\mathbf{H}$	MIMO channel matrix
E_b	Bit energy
ϵ	Normalized carrier frequency offset (CFO)
τ	Time offset
ν	Length of cyclic prefix

Part I

Precoded Systems Overview

1

Introduction

Wireless communications have enjoyed exponential growth in the last few decades thanks to the development of reliable solid-state radio frequency hardware in the 1970s. Various paging, cordless, cellular, and personal communication standards have been developed for wireless systems throughout the world. The next generation of wireless systems will provide an end-to-end communication system where voice, data, and streamed multimedia can be served to users on an "anytime, anywhere" basis at hundreds of Mbits/s. For instance, current IEEE 802.11n standard (MIMO-OFDM) supports data rate up to 600 Mbps in physical (PHY) layer in quasi-static environment. The under constructing standard IEEE 802.16m (also MIMO-OFDM) aims to provide a gross data rate greater than 100 Mbps for mobile applications.

Data throughput is one of the most important performance indicators for communication systems. Before 1990s, multipath effect has long been considered as the main obstacle that prevents high throughput transmission [108]. This can be simply explained in the time domain. Due to the multipath effect, we may need to insert guard interval between transmitted symbols to prevent inter-symbol interference (ISI), where the guard interval should be larger than the channel delay spread. However, the insertion of guard interval limits the transmission data throughput. This limitation can also be explained in frequency domain. The multipath effect in time domain leads to frequency-selective fading in frequency domain. Hence, if the signal occupies the whole channel bandwidth, the signal will experience the frequency selective fading and the performance degrade significantly in this case. To avoid frequency-selective fading, we may transmit signal with narrow bandwidth (narrow band communications). In narrow band communication systems, such as the IS-95 (CDMA), the signal bandwidth is far less than channel coherent bandwidth. Hence, although the channel has frequency selective fading, the narrow band signal will not experience a dramatic frequency-selective fading since the signal occupies only a small portion of the channel bandwidth. However, transmit signal with narrow bandwidth implies that the data throughput cannot be high.

C.-C.J. Kuo et al., *Precoding Techniques for Digital Communication Systems*,
DOI: 10.1007/978-0-387-71769-2_1,

To overcome the multipath effect and achieve high throughput transmission, channel equalization or precoding techniques can be used. The original principle of precoding is that if transmit side knows channel information, we can design the transmit signal so that the ISI in the receiver side is greatly mitigated. For instance, the use of Tomlinson-Harashima precoding can be regarded as moving the feedback part of a DFE (Decision Feedback Equalizer) to the transmit side to avoid error propagation problem. Different from error correct coding that operates in Galois field, precoding deals with symbols in complex field and hence can help to rescue constellation-mapped symbols from impairments such as frequency selective fading [115].

An effective way to overcome multipath effect is using orthogonal frequency division multiplexing (OFDM) systems. OFDM has widely been used in both wireline and wireless communications. While the concept of OFDM has been known since 1966 [19], it was not employed in standard systems until 1990s when advances in digital signal processing (DSP) and VLSI technology made effective OFDM implementation possible with low-cost fast Fourier transform (FFT) chips. When used in wired environments, OFDM is also called discrete multitone (DMT) modulation, the technique used in xDSL (digital subscribe line). The primary advantage of the OFDM technique is its ability to effectively combat the inter-symbol interference (ISI) effect due to frequency-selective fading with a simple transceiver structure. OFDM system has proven its superior ability to combat ISI with simple implementation scheme in the past decade. In 1993, DSL adopted DMT and made it the first successful commercial product using OFDM instead of equalization-based technique. In 1995 and 1997, ETSI adopted OFDM in DAB (Digital Audio Broadcasting) and DVB-T (Digital Video Broadcasting-Terrestrial) systems, respectively. Later in 1999, IEEE 802.11a standard used OFDM and provided the Wi-Fi application a peak data rate up to 54 Mbps. Since 2002 till 2007, OFDM systems have been adopted for other standards such as IEEE 802.16x family (Wi-MAX) and IEEE 802.11n (MIMO Wi-Fi). In fact, OFDM system can also be regarded as a special case of precoding. In [5], the channel information of this multicarrier system was utilized to design the transmitting and receiving filter banks so that the ISI can be eliminated, which was called "vector coding." Vector coding may be regarded as a linear precoding technique and feedback from receiver to transmitter is needed since it assumes that the transmitter knows the channel information. The current OFDM system does not utilize the channel information to design the transmitting and receiving filter banks. Instead, it uses DFT and IDFT filter banks for transceiver design. As a result, transmitter does not need to know channel information. This kind of channel-independent OFDM scheme was generalized as precoding scheme in [76] and [115].

The increasing need for fast and reliable wireless communication links has lead to system with multiple antennas located at both the transmitter and the receiver. Multiple input multiple output (MIMO) systems are able to increase significantly the capacity and hence achieve higher transmission rates

than one-sided array links. The well-known Shannon theorem for capacity of bandlimited Gaussian channels shows that there is a fundamental limit (channel capacity) for transmission data rate over Gaussian bandlimited channels. With advances in communication theory and the growth of sophisticated signal processing and computation techniques, the possibility of achieving the fundamental information limit on channel capacity seems higher than ever before. In MIMO systems, if channel information is known to the transmitter, precoding can be used to further improve the system performance based on various design criteria such as maximum capacity or minimize the mean square error. In the current wireless standards, precoding (or beamforming) is adopted as an optional feature for IEEE 802.11n and IEEE 802.16 family, where full channel information or partial channel information are required to implement this feature. When channel varies rapidly, full channel information may not be available in the transmitter. In this case, some researches showed that "partial channel" information for MIMO precoding can still achieve satisfactory performance. This concept also motivated us to use partial channel information to perform precoding for UWB communication systems since the channel impulse response for such systems is long and full channel information may not be available in transmitter side (see Chapter 8).

As mentioned above, precoding schemes may be divided into three categories according to the accessibility of channel information. That is,

1. Transmit side has full channel information.
2. Transmit side only has partial channel information.
3. Transmit side does not have any channel information.

It is intuitive that the precoding scheme with full channel information can achieve better performance than other two schemes. However, sometimes full channel information may not be available in transmitter due to rapid channel variation (feedback is not in time) or long delay spread (too much feedback information). An example that full channel or even partial information may not be available is the uplink transmission in multiuser communication systems. In this case, the signal from different users will lead to multiaccess interference (MAI). To eliminate MAI using precoding technique with full channel information, the mobile station may need to know the channel information of all other mobile stations. However, this is somewhat impractical when the number of users is large. Although multiuser detection (MUD) can be used in the receiver to eliminate MAI, it demands high computational complexity, especially when the number of users is large. This motivates us to approach another research direction and we found that by properly designing transceiver and multiaccess orthogonal code schemes, we can achieve MAI-free or nearly MAI-free property without knowing channel information in the transmit side. Since this precoding scheme is channel independent, the transceiver design can be greatly simplified.

This book deals with precoding techniques in digital communication systems. Different precoding techniques can be employed in the transmitter

to improve the performance of wireline or wireless systems with affordable complexity. In the first part, we will provide an overview of several important existing precoding techniques. From this tutorial overview, readers can understand the evolution of precoding and the principles of various precoding schemes. In the second part, we will discuss the application of state-of-the-art precoding schemes to current and/or emerging communication systems to combat impairments such as ISI, MAI, and the Doppler effect. We will introduce the proposed MAI-free or near MAI-free multiuser systems, which combines CDMA and OFDM techniques. Unlike the multiuser systems without precoding that may lead to serious complexity burden in the receiver side to deal with MAI problem, the proposed MAI-free multiuser systems can achieve a good complexity leverage between transmitter and receiver. Consequently simple transceiver design is achievable. Different chapters are dedicated to different applications of precoding as outlined below.

1.1 Precoding for ISI Gaussian Channels

In Chapter 2, we discuss precoding techniques to eliminate ISI and achieve high throughput. To approach capacity, the transmission band must be expanded to the entire usable available bandwidth of the channel which leads to inter symbol interference (ISI). To mitigate the effect of ISI, equalization technique can be employed at the receiver side, or alternatively, when the channel state information is available at the transmitter, the interfering symbols can be subtracted from the transmitted bits with precoding techniques. Such precoders were independently proposed by Tomlinson [131] and by Harashima and Miyakawa [84] and is called Tomlinson–Harashima (TH) precoder. Tomlinson–Harashima precoding has been used in bandlimited telephone line modems to support data rates of 19.2 kb/s or above just short of the capacity 20 kbits/s. Theoretically, it has been shown that, with TH precoding and for high signal to noise ratio (SNR) channels, the capacity of any bandwidth limited Gaussian channel can be achieved as closely as the capacity of an ideal Gaussian channel. TH-precoding can be combined naturally with channel coding and also with trellis shaping which provide additional gain. In particular, trellis precoding, a combination of trellis shaping, trellis coded modulation (TCM), and TH precoding, yield very powerful scheme with remarkable performance.

OFDM is an effective technique to combat ISI. Representing OFDM systems using multirate filter banks structures will enable us to gain more insight on how to design precoder and postcoder to achieve different design criteria, since there have been many well-developed results for multirate systems. Also, with multirate representation, current widely adopted OFDM systems can be slightly modified to become other types of OFDM systems. For instance, the cyclic prefix (CP)-inserted OFDM can be modified to zero padding (ZP)-inserted OFDM to reduce transmitting power. It is also interesting to note

that precoding can also be added on current OFDM systems. One example is the channel independent Single Carrier with Cyclic Prefix (SC-CP) system [113], where a DFT precoder is added in the transmitter and hence the whole becomes a single carrier system. The SC-CP system enjoys a much lower peak-to-average power ratio (PAPR) than the widely adopted OFDM system. Furthermore, this system has been proven to achieve the minimum bit error rate (BER) with certain modulation schemes [78]. Since the transmitter of such precoding scheme does not need channel information in SC-CP systems, the transceiver design can be greatly simplified.

1.2 Precoding for CDMA Systems

In Chapter 3, we discuss different precoding techniques in the direct-sequence (DS) code division multiple access (CDMA) channel. As the number of co-channel users increases, the decoding performance suffers due to the increased level of multiple access interference (MAI). Even though several receiver-based MAI suppression schemes, such as multiuser detection [144], minimum mean square error (MMSE) receiver [83], and decorrelator [81], improve the receiver performance at the expense of high computational complexity and the knowledge of transmitted signals of all co-channel user, they are only suitable for the uplink, rather than the downlink channel. This is because the uplink receiver, namely the base station, is more likely to provide high computational power and to acquire the channel knowledge of all users than its downlink counterpart, namely the mobile unit. If the downlink channel information of each user is acquired by the base station based on the channel reciprocity assumption in the time division duplex (TDD) system, it is thus straight forward to consider different precoding techniques for the downlink channel. Here, three different precoding schemes, including transmit matched filter (Tx-MF), transmit zero-forcing filter (Tx-ZF), and the transmit Wiener filter (Tx-Wiener), for the CDMA downlink channel are derived and their performance and design trade-off are discussed.

1.3 Precoding for MIMO Channels

Multiple input multiple output (MIMO) and space-time processing techniques are by far the most promising existing wireless technologies. MIMO technology can provide channel capacity gain (multiplexing gain), if multiple independent data streams are sent simultaneously and in the same frequency band over multiple transmit antennas and recovered at the receiver via appropriate signal processing techniques, e.g. the V-BLAST scheme. This is usually called Spatial Division Multiplexing (SDM).

MIMO systems also offer potential spatial diversity that can be exploited by space-time codes, e.g. Alamouti code, among other techniques which essentially is a clever way to map data streams across time and space.

When the full channel state information is available at the transmitter, precoding can be used to improve the performance of MIMO system in variety of ways as follows:

- TH precoding can be used in a Spatial Division Multiplexing MIMO to subtract the interfering symbols from transmitted bits.
- Transmit and receive processing (linear precoding and decoding) can use the CSI to optimally allocate resources such as power and data rates.
- Precoding can also be combined with space-time codes to maximize the diversity and coding gain. In this particular form, the linear constellation precoding technique does not even require the knowledge of channel information state.

The MIMO precoding techniques are based on the assumption that the real-time channel knowledge at the transmitter is available. However, in a time varying channel environment where the channel information is updated often, the ideal channel information assumption is usually weakened by insufficient feedback channel capacity. Later in this chapter, two different precoding concepts are introduced to save the feedback overhead. The first precoder design explores the channel statistics, say, either channel mean or channel covariance, since they are relatively stable as compared to the current channel information and, therefore, less number of updates is required. Given either the channel mean or channel covariance matrix is available at the transmitter, the precoder is constructed by specifying a proper input covariance matrix at the precoder output so that the information rate is maximized. It is found that the maximum rate can be achieved by either the beamforming scheme or spatial multiplexing scheme, depending on the quality of feedback information. The other precoder design based on incomplete channel information is called unitary precoding. The idea of unitary precoding is as follows. A set of discrete codewords, i.e., codebook, is constructed off-line first and this codebook knowledge is shared at both sides of the link. Later, the receiver selects the best codeword from the codebook and sends the corresponding code index to the transmitter for precoding. Obviously, the size of codebook, which determines the quality of precoder, is limited by the number of feedback bits. The codebook design that minimizes the distortion due to discrete representation of the codeword is the key to this scheme and is detailed as well.

1.4 Precoding for Multiuser OFDM Systems

In Chapters 5–7, we introduce the precoding techniques for multiuser OFDM system to eliminate the MAI. Multiuser OFDM systems have been developed to meet the need of wireless multiaccess, including multicarrier code division multiple access (MC-CDMA) and orthogonal frequency division multiple

access (OFDMA). Multiuser OFDM systems generally suffer from multiaccess interference (MAI) which is caused by various environmental effects such as multipath, timing asynchronism, carrier frequency offset (CFO), or the Doppler spread. By using precoding techniques, the MAI caused by above environmental effects can be greatly mitigated or completely eliminated for a group of users.

In Chapter 5, we introduce a new family of multiuser OFDM transceivers, called the precoded multiuser (PMU)-OFDM to achieve approximately MAI-free with a low implementational cost. A code selection scheme based on Hadamard-Walsh code has been proposed for PMU-OFDM system so that the system is still approximately MAI-free in the environment with time asynchronism, CFO (carrier frequency offset), or the Doppler effects. That is, we use only the $M/2$ symmetric or the $M/2$ anti-symmetric codewords of the M Hadamard-Walsh codes. When the number of users is below $M/2$, all the $M/2$ users can enjoy the nearly zero MAI property. When the number of users exceeds $M/2$, MUD techniques can be used to further suppress the MAI. It is worthwhile to emphasize that even in the fully-loaded system, the complexity for MUD has been reduced since each user only needs to deal with $M/2$ interferers instead of M interferers.

Moreover, we proposed a code priority scheme based on the proposed code selection so that the PMU-OFDM can be more robust to CFO effect. That is, we rank the codewords according to their CFO robustness and form a code priority. This code priority can be used in three different ways. First, since not all the users are active simultaneously, the code priority suggests that we should assign the higher priority codewords to the first connected users. Second, when in a serious CFO environment, we can consider to support fewer users based on the code priority to maintain nearly MAI-free in this hostile environment. Third, in practical situations, individual users may have different CFOs. In this case, we should assign the codewords with higher priorities to the users who have larger CFOs and assign the codewords with lower priorities to the users who have smaller CFOs so that the overall performance will not degrade significantly. Furthermore, we evaluate the PMU-OFDM system in time-varying channel environments. We found that the PMU-OFDM system with the proposed code selection scheme can work robustly in such hostile channel environments.

It is known that MC-CDMA systems suffer from MAI when the channel is frequency-selective fading. In Chapter 6, we will introduce a Hadamard-Walsh code based MC-CDMA system that achieves zero MAI over frequency-selective fading channel. In particular, we will use appropriately chosen subsets of Hadamard-Walsh code as codewords. For a multipath channel of length L, we partition a Hadamard-Walsh code of size N into G groups, where G is a power of 2 with $G \geq L$. We will show that any of the G subsets yields an MAI-free system. It is also shown that the MAI-free property allows us to estimate the channel of each user separately and the system can perform chan-

nel estimation much more easily. Owing to the MAI-free property, every user can enjoy a channel diversity gain of order L to improve the bit error performance. Furthermore, the system has the additional advantage that it is robust to CFO in a multipath environment. That is, by partitioning those codewords into subsets, the number of supportable MAI-free users with Hadamard-Walsh codes is $1 + \log_2(N/G)$ in a CFO environment.

In Chapter 7, we show that the number of MAI-free users in CFO environment can be increased by partitioning the orthogonal carrier interferometry (CI) codewords [92]. Since some users can achieve the MAI-free property, in a fully-loaded MC-CDMA system, the complexity for MAI suppression can be greatly reduced. We will use existing interference suppression techniques to achieve fully-loaded user capacity in MC-CDMA with CFO and show that the receiver complexity is indeed simplified by adopting the proposed precoding scheme in the MC-CDMA system.

1.5 Precoding for UWB Systems

In Chapter 8, we study the precoding system design in UWB impulse radio (IR) systems. The UWB-IR system enjoys several advantages, such as an accurate ranging capability due to its fine multipath resolution, excellent fading immunity due to a great number of multipath components found in its channel response, etc. However, from a communication prospective, it is also important for the UWB receiver to acquire sufficient signal power spread among those many paths. The traditional Rake receiver used in the multipath CDMA channel is not applicable in UWB channels since it requires a huge number of Rake finger, and the associated cost is not cheap. The idea called time-reversal precoding (TRP) that shifts the complexity of multipath combining from the receiver to the transmitter is recently proposed to reduce the receiver hardware cost. By encoding the transmitted symbol with the time-reversed channel information, all the multipath components are automatically concentrated after certain delay and a simple MF filter can be applied to collect enough channel power. However, the deployment of TRP is limited by its high feedback overhead for those many multipath components. To reduce the feedback overhead while having the advantage of signal power focusing, the channel phase precoding UWB (CPP-UWB) is discussed in this chapter. The CPP transmitter that encodes the data symbol with the time-reversed phase information alone, demands only the phase information feedback, rather than the complete channel information feedback. Since each phase component in UWB channel is either $+1$ or -1 and it is represented by one signal bit, the feedback information quantity is greatly reduced. Owing to the concentrated signal power in the equivalent channel response after precoding, the ISI effect is somewhat mitigated for a fixed symbol interval. On the other words, the symbol interval of CPP-UWB system can be further shortened to speed up the data transmission rate for a given noise margin. For a given symbol

interval less than the channel response, we can adjust the phase codeword length so that the output signal-to-interference power ratio (SIR) is maximized. Although the optimal code length can be found via the exhaustive search, its computational complexity is high, especially when the number of channel taps is large. A fast search algorithm is also developed to determine the optimal codeword length with less computational power as compared with the exhaustive search algorithm.

2

Precoding Techniques in ISI Channel

One of the most critical issues in communication systems is the multipath effect. Multipath effect will cause inter-symbol interference (ISI) and hence it limits the transmission speed. In this chapter, we will review several techniques used to combat ISI. These include channel equalization, Tomlinson–Harashima precoding and Trellis precoding. Moreover, it is known that OFDM systems can compensate the ISI using simple transceiver scheme. Since multirate representation of OFDM systems can help us to gain more insight on the analysis, we will introduce the multirate representation of several OFDM systems. Further, channel independent precoding scheme for OFDM systems will also be developed based on the multirate representation.

2.1 Equalizers for ISI Cancellation

Communication channels are usually bandwidth limited. In order to approach capacity, the transmission band must be expanded to the entire usable available bandwidth of the channel. This will inevitably lead to the sever distortion of the signal spectrum at the band edges and inter-symbol interference (ISI). One way to reduce ISI is to use equalizers in the receiver. Three different equalizers, namely linear equalizers (LE), decision feedback equalizer (DFE), and maximum likelihood sequence estimation (MLSE) equalizers have been proposed.

Zero-forcing (ZF) DFE is depicted in Fig. 2.1 for a channel with impulse response $\mathbf{h}(D)$. It consists of one feedforward block $\mathbf{f}(D)$ whose task is to guarantee white noise at the decision devices and a casual minimum phase end-to-end impulse response. The causality ensures that each decision symbol x_i should only be disturbed by symbols with index $j < i$. Assuming all previous estimates are correct (ideal DFE assumption), i.e., $\hat{x}_i = x_i$, we can eliminate the tail $\sum_{j<i} h_j x_{i-j}$ or equivalently in D-transform $(\mathbf{h}(D)-1)\mathbf{x}(D)$ by subtraction as

C.-C.J. Kuo et al., *Precoding Techniques for Digital Communication Systems*,
DOI: 10.1007/978-0-387-71769-2_2,

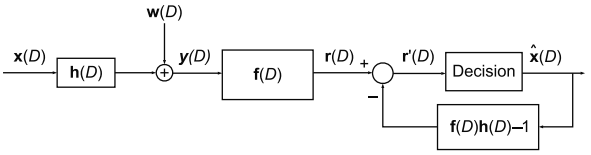

Fig. 2.1. Block diagram of ZF-DFE.

$$\mathbf{r}'(D) = \mathbf{r}(D) - (\mathbf{h}(D)\mathbf{f}(D) - 1)\hat{\mathbf{x}}(D). \tag{2.1}$$

Since

$$\mathbf{r}(D) = \mathbf{h}(D)\mathbf{f}(D)\mathbf{x}(D) + \mathbf{w}(D)\mathbf{f}(D), \tag{2.2}$$

we have

$$\mathbf{r}'(D) = \mathbf{x}(D) + \mathbf{w}(D). \tag{2.3}$$

We see that the ISI is completely cancelled and only white noise exists. The output signal to noise ratio is then given by

$$SNR_{ZF-DFE} = S_x/S_n, \tag{2.4}$$

where S_x and S_n are the average energy of input symbols x_i and noise, respectively. Note that for a ZF linear equalizer, the feedback section of Fig. 2.1 does not exist and $\mathbf{f}(D) = 1/\mathbf{h}(D)$. Then,

$$SNR_{ZF-LE} = S_x/S_n||1/h||^2$$

where

$$||1/h||^2 = \int_{-1/2}^{1/2} \frac{1}{|H(f)|^2} df$$

is the noise enhancement factor. Therefore, $SNR_{ZF-DFE} > SNR_{ZF-LE}$, i.e., ZF-DFE improves SNR_{ZF-LE} by the the noise enhancement factor. However, the ideal DFE assumption may not be practical. In fact, one of the main shortcomings of DFE is error propagation. Moreover, since the reliable detected decisions are only available after a delay, channel coding cannot be combined with DFE in a straightforward manner.

ISI cancellation can be performed by the optimum maximum likelihood sequence estimation (MLSE) equalizer. Suppose transmitting sequence $x(D)$ is drawn from an M-point constellation set. If channel impulse response has finite length L, it can be modeled as a shift register of length L with M-state memory. The Viterbi algorithm can be applied to optimally decode the received sequence $r(D)$ in the presence of noise. Although the output SNR for the MLSE equalizer can approach the effective SNR of the matched filter bound $SNR_{MFB} = S_x||h||^2/S_n$, the complexity of Viterbi algorithm grows exponentially with the channel length (M^L).

An alternative approach to equalizations in the receiver is to change the signal format at the transmitter by using channel state information so that the

effect of ISI is reduced or cancelled. This technique is called Precoding. In this chapter, we review the principles of the most famous precoding techniques, namely Tomlinson–Harashima (TH) precoding and trellis precoding.

2.2 Tomlinson–Harashima Precoding (THP)

Tomlinson–Harashima precoding (THP) technique was invented independently by Tomlinson in United Kingdom [131] and Hiroshima in Japan [84]. TH precoding is closely tied to the signal set. Figure 2.2 shows the block diagram of a transceiver in AWGN channel. We assume the discrete time channel impulse response is given by h_l. Let us assume without loss of generality, $h_0 = 1$. The channel sampled outputs are given by

$$r_i = \sum_{l=0}^{L-1} h_l x_{i-l} \tag{2.5}$$

We see that the symbols $x_i, x_{i-1}, \ldots x_{i-L+1}$ will interfere with each other. If the transmitter knows the channel impulse response, the inter-symbol interference (ISI) effect can be overcome by a precoder with a transfer function equal to the inverse of the transfer function of the channel as shown in Fig. 2.3(a).

However, when channel transfer function value is close to zero, the output of this precoder may increase or diverge to infinity.

To overcome this issue, a nonlinear block with transfer function $\mathbf{T}(D)$ is inserted before the $\mathbf{h}^{-1}(D)$ block, as shown in Fig. 2.3(b). The nonlinear function makes the sequence $\mathbf{z}(D)$ peak limited, i.e.,

$$z_{min} \leq \mathbf{z}(D) \leq z_{max}, \tag{2.6}$$

for some z_{min} and z_{max} and all D. Assume $z_{min} = -z_{max}$. Then, One possible construction of T can be constructed as follows [84]

$$\mathbf{y}(D) = \mathbf{x}(D) - 2Pz_{max}, \tag{2.7}$$

where P is an integer. Since $\mathbf{z}(D) = \mathbf{y}(D) - \mathbf{v}(D)$ and from Eq. (2.6), we can determine the condition for P to limit the peak value of sequence $\mathbf{z}(D)$ to be

$$(2P-1)z_{max} \leq \mathbf{x}(D) - \mathbf{v}(D) \leq (2P+1)z_{max}. \tag{2.8}$$

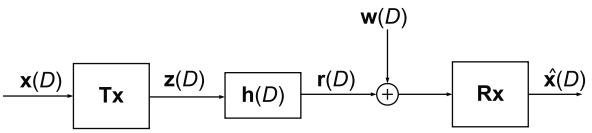

Fig. 2.2. Communication over AWGN channel.

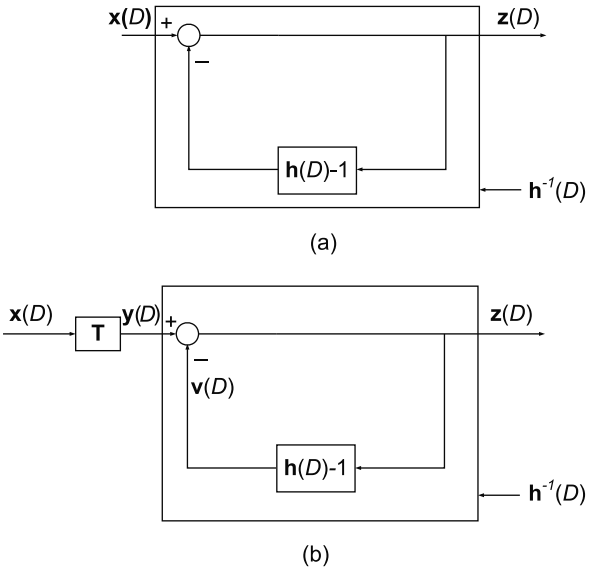

Fig. 2.3. (**a**) Block diagram of a precoder for ISI channel; (**b**) block diagram of Tomlinson–Harashima precoder [[84]©IEEE].

Therefore the value of $2Pz_{max}$ is actually the output of quantization operation on $\mathbf{x}(D) - \mathbf{v}(D)$ Q as show in Fig. 2.4. An implementation of T based on the above equations is shown in Fig. 2.5.

In the receiver, the estimation of $\mathbf{y}(D)$ is obtained by

$$\hat{\mathbf{y}}(D) = \mathbf{y}(D) + \mathbf{w}(D),$$

where $\mathbf{w}(D)$ is additive white Gaussian noise. After that, the inverse Transformation T^{-1} computes the estimated input sequence $\mathbf{x}(D)$ from

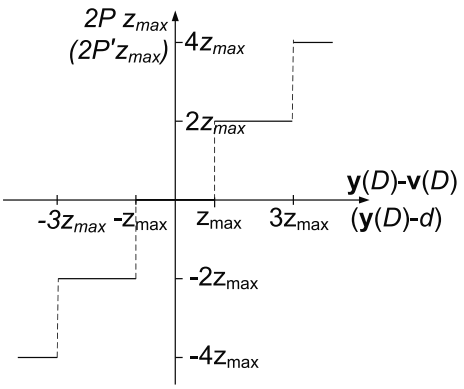

Fig. 2.4. Input–Output characteristic of quantizer Q[[84]©IEEE].

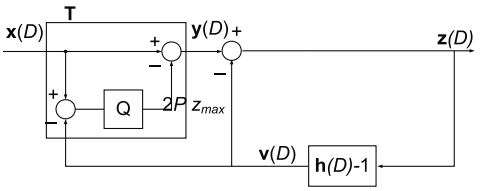

Fig. 2.5. Implementation of transmitter of TH precoding [[84]©IEEE].

$$\hat{\mathbf{x}}(D) = \hat{\mathbf{y}}(D) + 2Pz_{max}. \tag{2.9}$$

We assume the information sequence is also peak limited, i.e.,

$$x_{min} \leq \mathbf{x}(D) \leq x_{max},$$

for some x_{min} and x_{max}. Therefore,

$$x_{min} \leq \hat{\mathbf{y}}(D) + 2Pz_{max} \leq x_{max}, \tag{2.10}$$

or equivalently,

$$x_{min} - 2Pz_{max} \leq \hat{\mathbf{y}}(D) \leq x_{max} + 2Pz_{max}. \tag{2.11}$$

Assuming $x_{max} - x_{min} < 2\ z_{max}$, we have $x_{min} > x_{max} - 2\ z_{max}$ and $x_{maz} < x_{min} + 2\ z_{max}$. Therefore, we can rewrite Eq. (2.11) as

$$(2P'-1)z_{max} + x_{max} - z_{max} \leq \hat{\mathbf{y}}(D) \leq (2P'+1)z_{max} + x_{min} + z_{max}, \tag{2.12}$$

where $P' = -P$. Let

$$x_{max} - z_{max} \leq d \leq x_{min} + z_{max}. \tag{2.13}$$

Then, by comparing Eqs. (2.12) and (2.13), we conclude

$$(2P'-1)z_{max} \leq \hat{\mathbf{y}}(D) - d \leq (2P'+1)z_{max}. \tag{2.14}$$

We see that the term $2P'z_{max}$ can be obtained from $(\hat{\mathbf{y}}(D) - d)$ as the output from the quantizer Q shown in Fig. 2.4 which was inserted in the transmitter. From Eq. (2.9), $\hat{\mathbf{x}}(D))$ can be obtained from

$$\hat{\mathbf{x}}(D) = \hat{\mathbf{y}}(D) - 2P'z_{max}, \tag{2.15}$$

where $\mathbf{y}(D)$ varies according to

$$(2P'-1)z_{max} + d \leq \hat{\mathbf{y}}(D) \leq (2P'+1)z_{max} + d, \tag{2.16}$$

for all values of P'. Then, the input–output characteristics of T^{-1} is shown in Fig. 2.6. An implementation of T^{-1} function is shown in Fig. 2.7.

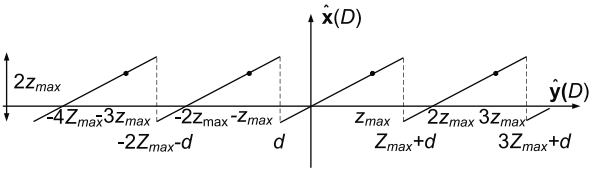

Fig. 2.6. Input–output characteristics of inverse transformation T^{-1} [[84]©IEEE].

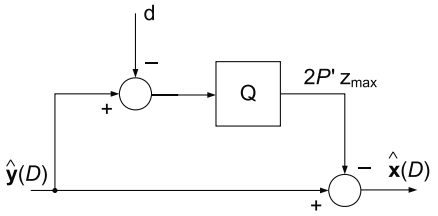

Fig. 2.7. An implementation of inverse transformation T^{-1} [[84]©IEEE].

For a special case where the information sequence is binary, i.e., $\mathbf{x}(D)$ can take either 0 or 1, we can set $z_{min} = -1$, $z_{max} = 1$, and $d = 1/2$. Then, from Fig. 2.7, it is clear that the original binary sequence can be restored by

$$\hat{\mathbf{x}}(D) = \begin{cases} 0, & \hat{\mathbf{y}}(D) = \text{even}, \\ 1, & \hat{\mathbf{y}}(D) = \text{odd}. \end{cases} \tag{2.17}$$

In other words, the T^{-1} is reduced to

$$\hat{\mathbf{x}}(D) = \hat{\mathbf{y}}(D) \mod 2. \tag{2.18}$$

Moreover, for a general case where the information sequence takes on values from M-level alphabet, $0, 1, \ldots, (M-1)$, T^{-1} function can be constructed by letting $z_{max} = -z_{min} = M/2$, and $d = (M-1)/2$, and

$$\hat{\mathbf{x}}(D) = \hat{\mathbf{y}}(D) \mod M. \tag{2.19}$$

Equivalently, if a signal set of $2M$-level PAM consists of points taking $\pm 0, \pm 1, \ldots, \pm(M-1)$ values, T^{-1} is equal to

$$\hat{\mathbf{x}}(D) = \hat{\mathbf{y}}(D) \mod 2M. \tag{2.20}$$

Note that the modulo-$2M$ block can be used in the transmitter as the nonlinear T transformation as demonstrated in [131] and shown in Fig. 2.8. In fact, the modulo-$2M$ operation reduces the transmit power by constraining the transmitted symbols to lie within $[-M,\ M]$.

2.2.1 Performance of TH Precoding

In 1972, Price [104] showed that for high signal to noise ratio, the gap (in dB) between the performance of an uncoded PAM with ideal (no feedback

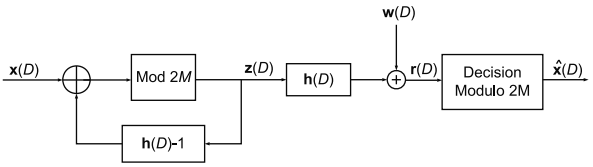

Fig. 2.8. Alternative representation of TH precoding [[84]©IEEE].

error) DFE or Tomlinson–Harashima precoding over any bandlimited AWGN channel and channel capacity at a given $P_r(E)$ approaches a constant value.

Consider a bandlimited Gaussian channel with bandwidth W. Assume the transmitted modulated signal is QAM with an $M \times M$ signal set. The transmitted power is constant for all frequencies within bandwidth W and zero elsewhere. Suppose either ideal zero forcing (ZF) DFE or TH precoding is used. Define normalized signal-to-noise ratio of an arbitrary transmission scheme with a data rate per two dimensions denoted by R as

$$SNR_{norm} = SNR_{DFE}/(2^R - 1), \tag{2.21}$$

where $SNR_{DFE} = S_x/S_n$ is the output signal power to noise power ratio of an ideal DFE. According to Price's results, at high SNR, the performance of all uncoded QAM signals over strictly bandlimited channels, regardless of channel characteristics (including the ideal AWGN channel), is the same with ZF-DFE or TH precoding. Thus, for high signal to noise ratio, the capacity of any bandlimited channel is approximated by [144]

$$C \simeq \log_2(1 + SNR_{DFE}). \tag{2.22}$$

Therefore,

$$SNR_{norm} \simeq (2^C - 1)/(2^R - 1). \tag{2.23}$$

Since $r < C$, $SNR_{norm} > 1$. Now, suppose the $M \times M$ square QAM scheme has minimum distance d_{min}. Since

$$S_x = (M^2 - 1)d_{min}^2/6, \tag{2.24}$$

and

$$R = \log_2(M^2), \tag{2.25}$$

and the noise is Gaussian, at high SNR, the symbol error probability can be approximated by [44]

$$\begin{aligned} P_r(E) &\simeq 4\, Q[(d_{min}^2/2S_n)^{1/2}] \\ &= 4\, Q[(3\ SNR_{norm})^{1/2}], \end{aligned} \tag{2.26}$$

where $Q(y) = \int_y^\infty f_X(x)dx$, and $f_X(x)$ is the Gaussian probability density function, with mean zero and variance one. The plot of $P_r(E)$ versus SNR_{norm}

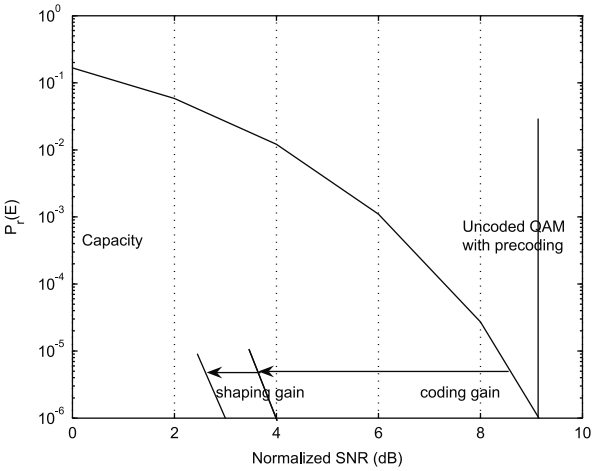

Fig. 2.9. Symbol error probability of uncoded QAM with precoding [[44]©IEEE].

is given in Fig. 2.9. It is seen that the gap difference between Shannon capacity limit and the performance of uncoded $M \times M$ QAM at $P_r(E) = 10^{-6}$ is about 9 dB. The key concept here is that the dB gap between uncoded QAM and capacity is approximately the same for over all strictly bandlimited high signal to noise ratio channels including the ideal AWGN channel.

The Tomlinson–Harashima precoding can be regarded an attractive alternative to the ZF-DFE when the channel state information is available in the transmitter, since as was shown by Price's result, it has the same performance for high SNR values over any ISI channel as ZF-DFE. It is nothworthy that TH precoding can be viewed as a DFE whose feedback section has moved to the transmitter. Therefore, it does not have the disadvantages of DFE mentioned before. That is, since the equalization is performed at the transmitter, the transmitting signals are perfectly known and the error propagation phenomena never occurs. Also, no immediate decision is required and hence channel coding can be combined easily with TH precoding.

2.2.2 Combined Precoding and Coding

The 9-dB SNR gap between performance of an uncoded QAM with Tomlinson–Harashima precoding over any bandlimited AWGN channel and the channel capacity at a given $P_r(E)$, observed from Fig. 2.9 can be reduced with coding and shaping gains achieved.

Precoding can be combined with coding to obtain additional coding gain. The combining can be preformed in a very natural way. Coded modulated symbols $\{x_i\}$ are sent into the TH precoder on which they perform the same precoding operation as before to produce $\{z_i\}$ symbols. For example, trellis coded modulated symbols can be used in conjunction with TH precoding.

The received symbols are the trellis coded symbols plus the additive Gaussian noise. The regular Viterbi algorithm can be used to find the closest sequence to the received sequence, which can then be reduced to modulo $2M$.

TH precoding combined with coded modulation schemes can achieve the same coding gain over partial response channel $(1-D)$ [43] or arbitrary channel response [15] and [35] as is achieved over the ideal channel, with about the same decoding complexity.

2.3 Trellis Precoding

It was shown in [29] that spherical lattice codes can achieve capacity at high SNR on ideal channels. Later, it was shown that the gain of a lattice code over uncoded QAM is due to both a coding gain and a shaping gain. The maximum shaping gain is shown to be about 1.53 dB. This means that a coding gain of 7.5 dB is required to fill the 9-dB gap with channel capacity. Since the complexity of spherical lattice codes is high due to prohibitive memory requirements, Forney and Eyuboglu [36] proposed trellis precoding, a combination of trellis shaping [42] and trellis coded modulation and precoding to leverage both coding and shaping gains. They argued that after the first 3–4 dB of coding gain, it is much easier to obtain the next 1 dB with shaping than with coding.

The concept of lattice and cosets is important in the discussion of trellis coded modulation (TCM) and trellis precoding. Here, we overview the basic concepts briefly. A lattice denoted by Λ consists of N dimensional vectors and is a subset of $\mathcal{R}^N$, where $\mathcal{R}$ denotes the set of real values. The simplest example of lattice is $\mathcal{Z}$, the set of integers. Z^2 and $\mathcal{Z}^N$ are two-dimensional and N-dimensional lattice, respectively. If we rotate each points of a lattice, e.g., $\mathcal{Z}^2$, we obtain a new lattice denoted by $R\mathcal{Z}^2$. Also, we can scale each point of $\mathcal{Z}^2$ by a factor of k, where k is any integer and obtain another lattice $k\mathcal{Z}^2$. A subset of lattice is called sublattice. Cosets are also subsets of lattice but they must be disjoint. Thus, a sublattice can have many cosets.

The two-dimensional lattice is the general form behind constellation sets used in digital communications such as M-PSK, M-QAM, etc. Higher dimension lattice have proven to be very useful in TCM. We assume that $\mathcal{A}$ is a conventional two-dimensional $M \times M$ square constellation. In lattice notation, $\mathcal{A}$ is the set of points from the two-dimensional half-integer lattice $\Lambda = \mathcal{Z}^2 + (0.5)^2$ that fall within the two-dimensional boundary square region $\mathcal{R} = \mathcal{R}_1 \times \mathcal{R}_2$, where $\mathcal{R}_1$ is the half-open interval $\mathcal{R}_1 = (-M/2, M/2)$. Figure 2.10 shows an 16×16 square two-dimensional constellation.

In the following sections, we first review the trellis shaping as described in [42] in Section 2.3.1. Then, in Section 2.3.2, we describe the principles of trellis precoding.

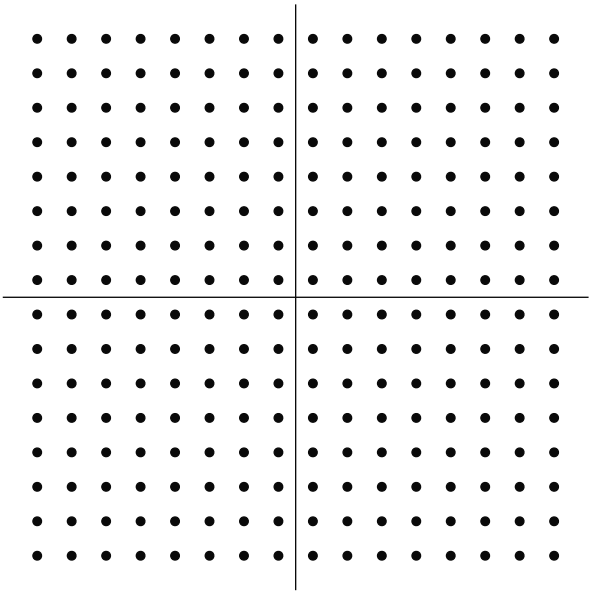

Fig. 2.10. Square 16×16 two-dimensional constellation.

2.3.1 Trellis Shaping

In TH precoding, the transmitted signals are uniformly distributed within a square region. Briefly, the goal of shaping is to reduce the average signal energy. This can be done by causing the probability distribution of signal set to be more like a Gaussian distribution than a uniform distribution.

Usually an $M \times M$ two-dimensional square constellation such as the 16×6 two-dimensional constellation shown in Fig. 2.10 is considered as the baseline constellation. For such a constellation with the minimum squared distance $d^2_{\min} = 1$, [42]

$$R = \log_2(M^2), \text{bits per two dimensions}, \tag{2.27}$$

$$S_x = (M^2 - 1)/6 = (2^R - 1)/6, \tag{2.28}$$

and

$$|\mathcal{A}| = M^2 = 2^R. \tag{2.29}$$

where $|\mathcal{A}|$ is the size of constellation. The base line average energy for a conventional $M \times M$ two-dimensional constellation or with $d^2_{\min} = 1$, data rate R and average energy S_X, is defined as

$$S_{x_0}(R) = 2^R/6. \tag{2.30}$$

The *shaping gain* γ_s is defined as

$$\gamma_s = S_{x_0}(R)/S_x. \tag{2.31}$$

The *shaping constellation expansion ratio* (CER) for a two-dimensional constellation is defined as

$$CER = |\mathcal{A}|/2^R. \tag{2.32}$$

Thus the shaping gain of a square two-dimensional is approximately 1 dB when R is large while CER is exactly 1 dB.

It was shown in [45] that $S_{x_0}(R)$ is a good approximation to average energy of any N dimensional square constellation with $d^2_{\min} = 1$. Thus, the shaping gain of any large constellation in the form of N-cube is 1 dB. It can be shown that an N-sphere constellation has a shaping gain of 0.2 dB in two dimensions, 0.98 dB in 16 dimensions, 1.10 dB is 24 dimensions and eventually reaches to the limit $\pi e/6$ (1.53) dB as N approaches infinity [45].

To have a shaping gain, the S_x must be reduced below S_{x_0}. One way to do it is through *sign bit shaping* . Consider 16×16 constellation shown in the Fig. 2.10 as the base line. Each coordinates can take values on from the 16-point PAM constellation $\{\pm 1/2 \pm 3/2, \ldots \pm 15/2\}$. In two's-complement notation, the most significant bit, t, is called *sign bit*. The remaining bits are called *the least significant bits*. For any of the 64 values of the least significant bits, we can form a square of side 8 whose vertices are the set of 4 constellation points corresponding to 4 possible sign bit combination. The set of such a four point set is called an equivalence class of points. An example of equivalence class is shown in Fig. 2.11(a).

The goal of sign bit shaping is to change the sign bit values such that the average energy is reduced, hence the shaping gain is obtained. Thus the

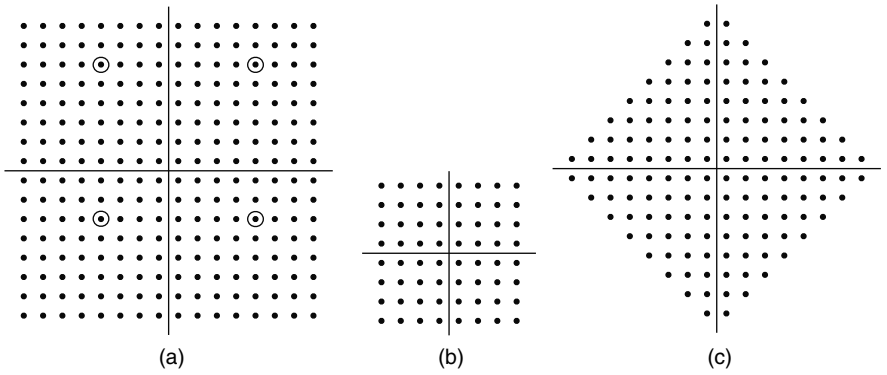

Fig. 2.11. (**a**) Equivalence class of 4 points with the same less significant bits for a square 16×16 two-dimensional constellation; (**b**) 64-point constellation consisting of least energy points in each equivalence class with no restriction on the sign bits; (**c**) 144-point constellation consisting of least energy points in each equivalence class if the parity of sign bits are preserved [[42]©IEEE].

shaping operation will choose the point with the least average energy in the class, which will be one of the 64-least energy points of Fig. 2.11(b).

Since sign bit carries no information, $R = 6$. Assuming all points are equiprobable, the average energy is reduced to $S_x = 63/6 = 10.5$ (10.21 dB). Therefore, the shaping gain γ_s is equal to 64/63 which is equal to that of a conventional 8×8 constellation.

If we demand the shaping operation change both sign bits together, then, we will have 144 point constellation as shown in Fig. 2.11(c). The reduced energy will be $S_x = 129/6 = 21.5$ (13.2 dB). Here, the sign bits carry one bit of information, hence R is 7 bits per second. However, we still do not have a shaping gain since the constellation shape is square ($\gamma_s = 128/129 \simeq 1$).

To obtain a shaping gain ($\gamma_s > 1$ dB), we can use a binary rate 1/2 convolutional code as shown in Fig. 2.12. The convolutional code is called shaping code $\mathcal{C}_s$ whose task is to modify the sign bit sequence $\mathbf{t}(D)$, which is a sequence of binary 2-tuples to $\mathbf{t}'(D) = \mathbf{t}(D) \oplus \mathbf{c_s}(D)$, where $\mathbf{c_s}(D)$ is any output sequence of the convolutional code and $\oplus$ denotes modulo sum operation [42].

Suppose any sequence of two-dimensional constellation point is denoted by $\mathbf{a} = \{a_i\} = (a_{i1}, a_{i2})$. Then, by modifying $\mathbf{t}(D)$ to $\mathbf{t}'(D)$, we will modify $\mathbf{a}(D)$ sequence to $\mathbf{x}(D)$ such that we minimize the average energy $S_x = E\{||\mathbf{x}||^2\}$. This is done via a Viterbi algorithm through a trellis search of the convolution code $\mathcal{C}_s$.

A trellis diagram is a way of visualizing all encoder's state transitions over time. Each state transition over time i to time $i + 1$ corresponds to a branch metric and is associated with encoder output sequence $c_{si} = (c_{s_{i1}}, c_{s_{i2}})$. Given constellation point $a_i = (a_{i1}, a_{i2})$, the modified output symbol x_i is constellation point a_i with sign bits modified with c_{si}, the binary 2-tuple at time i. If we assign to each branch labeled by c_{si}, a branch metric $||x_i||^2$ the Viterbi algorithm can search for a minimum weight path through the trellis diagram of $\mathcal{C}_s$. This search is equivalent to a search for the $\mathbf{c_s}(D) \in \mathcal{C}_s$ that results in modified output sequence $\mathbf{x}(D)$ with the least average energy. The complexity of the shaping is mainly determined by that of Viterbi decodes which grows exponentially with the number of states.

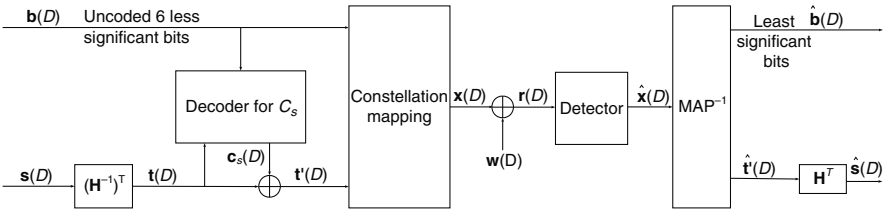

Fig. 2.12. Sign-bit shaping using the rate-1/2 convolutional code as the shaping code and square 16×16 constellation [[42]©IEEE].

At the receiver, if uncoded sequence $\mathbf{x}(D)$ is sent through a noisy channel, the received sequence $\hat{\mathbf{x}}(D)$ can be detected using conventional symbol by symbol detection techniques. From $\hat{\mathbf{x}}(D)$, the receiver can recover an estimate of $\hat{\mathbf{t}}'(D)$ of the modified sign bits. The modified sign bit sequence $\mathbf{t}' = \mathbf{t} \oplus \mathbf{c}_s$ is an element of the set $\mathcal{C}_s \oplus \mathbf{t}$ which is equal to a coset of the group code $\mathcal{C}_s$.

To limit the effect of propagation error associated with shaping code $\mathcal{C}_s$ on $\mathbf{t}'(D)$, the original two-tuple modified sign bit $\mathbf{t}(D)$ can be generated by a *syndrome sequence* $\mathbf{s}$ for the shaping code $\mathcal{C}_s$ at the transmitter.

For a rate k/n binary convolutional code with generation matrix $\mathbf{G}$, a *syndrome-former* is specified by an $n \times (n-k)$ transfer function $\mathbf{H}^T$ with rank $u - k$ such that

$$\mathbf{G}\mathbf{H}^T = \mathbf{0}. \tag{2.33}$$

For any code sequence $\mathbf{c_s}(D) = \mathbf{b}(D)\mathbf{G}$, we have

$$\mathbf{c_s}(D)\mathbf{H}^T = \mathbf{0}. \tag{2.34}$$

Also, for any n-tuple sequence $\mathbf{t}(D)$ which does not belong to C_s, $\mathbf{t}(D)\mathbf{H}^T = \mathbf{s}(D) \neq \mathbf{0}$. Since $\mathbf{t}'(D) = \mathbf{t}(D) \oplus \mathbf{c_s}(D)$, we have

$$\mathbf{t}'(D)\mathbf{H}^T = (\mathbf{t}(D) \oplus \mathbf{c_s}(D))\mathbf{H}^T = \mathbf{t}(D)\mathbf{H}^T = \mathbf{s}(D). \tag{2.35}$$

Therefore, regardless of the choice of $\mathbf{c}_s(D)$, the receiver can recover from $\hat{\mathbf{t}}'(D)$, the syndrome sequence $\mathbf{s}(D)$, provided $\hat{\mathbf{t}}'(D) = \mathbf{t}'(D)$. However, even if there is an error in the estimate of $\hat{\mathbf{t}}'(D)$, the resultant error propagation effect will be limited since it is known that for any linear, time invariant convolutional code, the syndrome-former can always be chosen to be feedbackfree.

As shown in Fig. 2.12, from the syndrome sequence $\mathbf{s}(D)$, the sign bit sequence can be generated as

$$\mathbf{t}(D) = \mathbf{s}(D)(\mathbf{H}^{-1})^T, \tag{2.36}$$

where $(\mathbf{H}^{-1})^T$ is an $(n-k) \times n$ left inverse matrix for $\mathbf{H}^T$ and is called *coset representative generator*.

The least significant bits, if sent uncoded over the channel, can be mapped directly into the estimates of the transmitted bits as shown in Fig. 2.12. The less significant bits of detected symbols $\hat{\mathbf{x}}(D)$ determines an estimate of the six corresponding input bits $\hat{\mathbf{b}}(D)$. The sign bits $\mathbf{t}'(D)$ are passed through a syndrome former $\mathbf{H}^T$ to produce an estimate of the syndrome sequence $\hat{\mathbf{s}}(D)$.

Figure 2.12 shows a sign bit shaping using a 256-point constellation and a rate 1/2 convolutional shaping code C_s, with data rate $R = 7$ bits per two dimension. It was shown in [42] that the shaping gain of such sign bit shaping depends on the window size of VA. As it approaches 20 symbols, the shaping gain increases to 0.9 dB. The shaping operation also changes the uniform distribution of input signal set to Gaussian distributions.

Sign bit shaping can be combined with any coding based on Ungerboeck's mapping by set partitioning [138]. According to Ungerboeck's set partitioning rule, the subsets are determined by the least significant bits. Since the sign

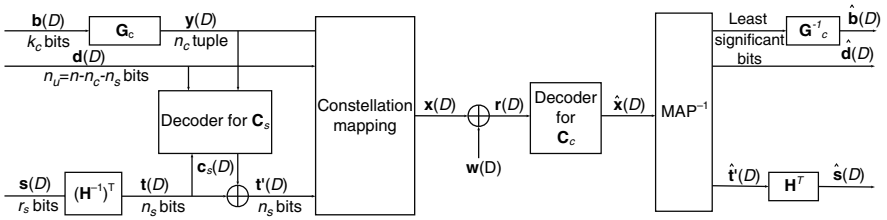

Fig. 2.13. Binary coded modulation shaping using the rate-k_s/n_s convolutional code as the shaping code and square 16×16 constellation [[36] ©IEEE].

bit does not change the partitioning of constellation points, the coding and shaping are completely compatible with each other.

In fact, sign bit shaping is only a special case of a more general trellis shaping depicted in Fig. 2.13. Here the constellation set $\mathcal{A}$ is N dimensional. Trellis shaping is used in conjunction with binary lattice-type channel trellis code $\mathbb{C}_c(\Lambda_c,\ \Lambda'_c,\ \mathcal{C}_c)$ which comprises the top section of Fig. 2.13. Trellis coded modulation [138] performs both coding and modulation without an increase in bandwidth. A trellis code is composed of a binary k_c/n_c convolutional code $\mathcal{C}_c$ and n_u uncoded bits. The encoder G_c generates an n-tuple code sequence $\mathbf{c}_s(D) = \mathbf{b}(D)\mathbf{G}_c$ from the k-tuple input sequence $\mathbf{b}(D)$. Each $\mathbf{c}_{si}$ partitions the constellation sets into 2^{n_c} cosets. In lattice notation, each $\mathbf{c}_{si}$ partitions a translate $\Lambda_c + a$ of an N-dimensional binary lattice Λ_c into $2^{n_c} = |\Lambda_c/\Lambda'_c|$ cosets of a sublattice Λ'_c [42]. The n_u uncoded bits $\mathbf{d}(D)$ determine the coordinates of points within each of these subsets. This set partitioning proposed by Ungerboeck guarantees that signal with the largest Euclidean distance have less bit differences.

The bottom section of Fig. 2.13 is trellis shaping which consists of a binary rate-k_s/n_s shaping convolutional code $\mathcal{C}_s$ and a partition of a region R of N-dimension into 2^{n_s} subregions $\mathcal{R}(z)$ and also a shaping decoder.

From what was said before, we know that $\mathbf{t}'(D)$ must fall in the same coset $\mathcal{C}_s \oplus \mathbf{t}$ as the initial sequence $\mathbf{t}$. The shaping decoder first selects the output code sequence $\mathbf{c}_s(D)$ to be any sequence that lies in the code $\mathcal{C}_s$. Then, using the Viterbi algorithm, the shaping decoder selects a label sequence $\mathbf{t}'(D) = \mathbf{t}(D) \oplus \mathbf{c}_s(D)$ that optimizes any desired characteristics, usually the average transmit energy, of the transmitted sequence $\mathbf{x}(D)$.

The sequence $\mathbf{x}(D)$ is then sent through the noisy channel. The receiver can use a conventional decoder for $\mathcal{C}_c$ to obtain the estimate of the sequence x_i, denoted by $\hat{x}_i$. The complexity and performance of this decoder is not affected by shaping operation. The coded information bits can be recovered with $\mathbf{G}_c^{-1}$ for the generating matrix $\mathbf{G}_c$ of the code $\mathcal{C}_c$. To obtain shaping bits, the received modified sign bits must be extracted from subregion $\mathcal{R}(z)$ and then sent through the syndrome-former $\mathbf{H}_s^T$ to obtain the syndrome sequence $\hat{\mathbf{s}}(D) = \hat{\mathbf{t}}'(D)\mathbf{H}_s^T$. If the estimate $\hat{\mathbf{x}}$ is correct, $\hat{\mathbf{x}}(D) = \mathbf{x}(D)$, then $\hat{\mathbf{s}}(D) = \mathbf{s}(D)$. Again, $\mathbf{H}_s^T$ can be chosen to be feedbackfree, and thus occasional error does not matter much.

2.3.2 Principles of Trellis Precoding

In short, trellis precoding is a combination of trellis shaping and precoding. Precoding is done to cancel the ISI effect when channel is not ideal, i.e., $\mathbf{h}(D) \neq 1$, where $\mathbf{h}(D)$ is any monic, causal, minimum phase channel transfer function, with a unique inverse $\mathbf{g}(D) = 1/\mathbf{h}(D)$.

For trellis precoding, we require the boundary region $\mathcal{R}$ of the $M \times M$ square constellation $\mathcal{A}$ be a fundamental region of a lattice Λ'_s, called precoding lattice. Let us denote the N-dimensional infinite array set by $\mathcal{S}$. Then, another property of the precoding lattice can be stated as follows: any element of precoding lattice added to any point in the coding subset of $\mathcal{S}$ results in another point in the same coding subset.

In trellis precoding, the information sequence is mapped into a sequence $\mathbf{x}(D)$. The sequence $\mathbf{x}(D)$ is then subtracted out from an N-dimensional symbols p_i from the precoding lattice $\Lambda'_s = M\mathcal{Z}^2$. In other words, a modulo device subtracts integer multiples of M (or $2M$) from each symbol. The resulting sequence $\mathbf{x}(D) - \mathbf{p}(D)$ is still a code sequence in $\mathcal{C}_c$. Finally the transmitted sequence $\mathbf{z}(D)$ is obtained by filtering $\mathbf{x}(D) - \mathbf{p}(D)$ through $\mathbf{g}(D) = 1/\mathbf{h}(D)$. Therefore, the received sequence $\mathbf{r}(D)$ is

$$\mathbf{r}(D) = [(\mathbf{x}(D) - \mathbf{p}(D))\,\mathbf{g}(D)]\,\mathbf{h}(D) + \mathbf{w}(D) = \mathbf{x}(D) - \mathbf{p}(D) + \mathbf{w}(D),$$

where $\mathbf{w}(D)$ is a while Gaussian noise sequence. The sequence $\{p_i\}$ can be chosen according to various criterion. In TH precoding, $\{p_i\}$ is determined by the simple memoryless modulo-M operation.

Figure 2.14 shows a trellis precoding composed of trellis shaping and TH precoding. The important block in trellis precoding is shaping decoder which selects not only the shaping code sequence $\mathbf{c}_s(D)$ from $\mathcal{C}_s$ but also the precoding lattice sequence $\mathbf{p}(D)$. The shaping decoder searches through all possible code sequence $\mathbf{c}_s(D)$ in $\mathcal{C}_s$ and precoding lattice sequence $\mathbf{p}(D)$ to optimize any desired property of transmitting sequence $\mathbf{z}(D)$ such as minimizing the average transmit energy S_z. In our case, the shaping decoder scans all possible sequence superstates $s'_i = (s_i, \mathbf{p}^{i-1})$, where s_i is a state of the convolutional code $\mathcal{C}_s$ and $\mathbf{p}^{i-1} = (p_{i-1}, p_{i-2}, \ldots,)$.

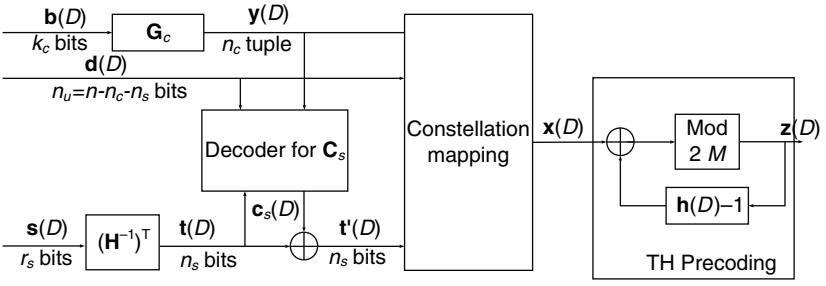

Fig. 2.14. Block diagram of trellis precoding transmitter [[36] ©IEEE].

The number of possible superstates is infinite, since $\mathbf{p}(D)$ can be any point from Λ'_s which is an infinite set. Since the optimum decoder resembles an MLSE of trellis-coded signals in the ISI channel, the VA-like reduced search estimation (RSSE) techqniques developed for combined decoding and equalization [38] has been suggested as the decoder for trellis precoding. The complexity of RSSE for trellis cods can range between that of the encoder trellis and that of the ML super-trellis. In the case in which the decoder trellis is equal to the encoder trellis, RSSE reduces to what is called parallel decision feedback decoding (PDFD).

In PDFD, the superstate is reduced to (s_i). The VA searches the trellis diagram of the shaping code $\mathcal{C}_s$ recursively to find a shaping sequence $\mathbf{c}_s(D)$ for which the transmit sequence $\mathbf{z}(D)$ has an energy

$$|\mathbf{z}(D)|^2 = |[\mathbf{x}(D) - \mathbf{p}(D)]\mathbf{g}(D|^2 . \tag{2.37}$$

For each state s of the trellis, the VA stores $\mathbf{z}^{i-1}(s) = [z_{i-1}(s), z_{i-2}(s), \ldots]$ and then computes the path metric as

$$\Gamma_i = \sum_{j<i} ||z_j|\,|^2, \tag{2.38}$$

where

$$|z_j|^2 = |x_j - (\sum_{k\geq 1} z_{j-k}(s)h_k) - p_j|^2, \tag{2.39}$$

where h_k are the coefficients of $\mathbf{h}(D)$.

The VA then selects the surviving paths for each branch, by selecting the nearest element $p_j \in M\mathcal{Z}^2$ that minimizes $|z_j|^2$. This can be done in two steps. First, the VA computes

$$f_j = x_j - \sum_{k\geq 1} z_{j-k}(s)h_k. \tag{2.40}$$

In other words, the VA subtracts the ISI from x_j using symbols $z_{j-k}(s)$. Then, the coordinates of f_j are reduced to the interval $(-M/2, M/2]$ with modulo M operations.

The VA will otherwise operates in a normal way, i.e., for each state, it selects the surviving path among the merging paths. The only constraint is that the final sequence $\mathbf{c}_s(D)$ must be a legitimate code sequence in the shaping code $\mathcal{C}_s$.

From the above discussion, we can see that the TH precoder is incorporated into the branch metric computations, and there is one precoder for each state of the trellis. Since PDFD does not make use of the component $\mathbf{p}^{i-1}$ of the superstate $s'_i = (s_i, \mathbf{p}^{i-1})$, it does not minimize the average transmit energy. In [37], it was shown that the shaping gain can be increased by expanded trellises that takes into account some part of the omitted component $\mathbf{p}^{i-1}$.

However, the above decoding technique offers the best performance/ complexity trade-off among the TH precoding the above precoder/decoder other decoders of RSSE family

2.3.3 Performance of Trellis Precoding

Recall that TH precoding (or ZF-DFE) have a 9-dB gap with channel capacity over any bandlimited or ideal channel as shown in Fig. 2.9. Suppose there is a coded modulation with coding gain γ_c and shaping gain γ_s. Then, the error probability is given by

$$P_r(E) \simeq BQ[(3\gamma_c\gamma_s SNR_{norm})^{1/2}], \tag{2.41}$$

where B is the error coefficient of the scheme and SNR_{norm} as defined in Eq. (2.23). Figure 2.9 shows the performance that would be obtained with a coding gain of 5 dB and a shaping gain of approximately 1 dB. In other words, the gap between channel capacity and performance of coded modulation is narrowed to 3 dB. The same improvement over the performance of uncoded can be obtained by a combination of coding, shaping, and precoding on any bandlimited, high SNR Gaussian channels.

We saw that trellis precoding is a combination of trellis coded modulation, trellis shaping, and precoding. Trellis coded modulation can achieve 5–6 dB coding gain. The shaping gain in trellis precoding is determined not only by the shaping code and the shaping decoder, but also by the channel response $\mathbf{h}(D)$.

Reference [36] showed a two-dimensional 4-state Ungerboeck code as the shaping trellis code and PDFD decoder can provide a modest shaping gain γ_s of 0.6−1 dB. These shaping gains were found to be independent of R at moderate to high data rates R. Also, it was found, while shaping gain is insensitive to the channel coefficients for small decoding delays, it starts to decrease as the decoding delay increases.

A maximum reduction of 0.3 dB in shaping gain was observed on severely distorted channels. It is possible to achieve a shaping gain as close to the ultimate shaping gain $\pi e/6$ (1.53 dB), with more complex trellis precoding. Therefore, with trellis precoding, the SNR gap of about 9 dB (at $P_r(E) \simeq 10^{-6}$) between capacity and uncoded modulation can be reduced by approximately 7 dB over any strictly bandlimited high SNR Gaussian channel. In other words, with the trellis precoding, the channel capacity of ISI channels at high SNRs can be approached as closely as channel capacity of ideal channels.

2.4 Multirate Representations for OFDM Systems

Multirate and filterbank design are very useful techniques for digital signal processing. By representing communication systems using multirate/filterbank forms, we can gain more insight into the systems since many important results can directly be derived from the existing multirate theories. This will greatly simplify the analysis. In this section, we introduce the basic multirate techniques [140] and represent the OFDM systems using multirate forms [76].

2.4.1 Multirate Fundamentals

Down-sample/Decimation. $x(n)$ is said to be down-sampled by M and results in output $y(n)$ if

$$y(n) = [x(n)]_{\downarrow M} = x(Mn). \tag{2.42}$$

That is, each sample of $y(n)$ is obtained by extracting every M sample of $x(n)$. The relationship between input and output for decimation in the z domain is given by

$$Y(z) = \frac{1}{M} \sum_{m=0}^{M-1} X(z^{1/M} e^{-j2\pi\ m/M}). \tag{2.43}$$

From Eq. (2.43), the decimated signal is the stretched and scaled version of the original signal in frequency domain. For convenience, we will use the block diagram as shown in Fig. 2.15 to denote sequence being decimated by M.

Up-sample/Interpolation. $x(n)$ is said to be up-sampled by M and results in output $y(n)$ if

$$y(n) = [x(n)]_{\uparrow M} = \begin{cases} x(n/M), & \text{if } n \text{ is multiple of } M, \\ 0, & \text{otherwise.} \end{cases} \tag{2.44}$$

That is, $y(n)$ is obtained by inserting $M-1$ zeros between every sample of $x(n)$. The relationship between input and output for interpolation in the z domain is given by

$$Y(z) = X(z^M). \tag{2.45}$$

The interpolated signal is the compressed version of the original signal in frequency domain. We will use the block diagram as shown in Fig. 2.16 to denote sequence being interpolated by M.

Noble Identities. In many cases, the decimator and interpolator are cascaded to other LTI systems. For instance, to relax the design effort of low pass filter in digital to analog converter (DAC), we usually interpolate the digital signal and then filter the interpolated signal before passing it to ADC. On the other hand, we will filter and decimate the digital signal after the analog to digital converter (ADC). In such cases, Noble Identities together with the polyphase decomposition (will be introduced later) provide good way to reduce the computational cost. Referring to Fig. 2.17, the Noble Identities provide rules so that we can interchange interpolation/decimation with system function. The interchanging rule for decimation can be expressed as

$$Y(z) = \left[X(z)H(z^M)\right]_{\downarrow M} = H(z)[X(z)]_{\downarrow M}. \tag{2.46}$$

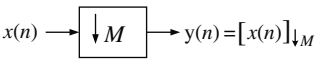

Fig. 2.15. Block diagram of decimation.

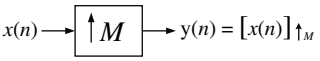

Fig. 2.16. Block diagram of interpolation.

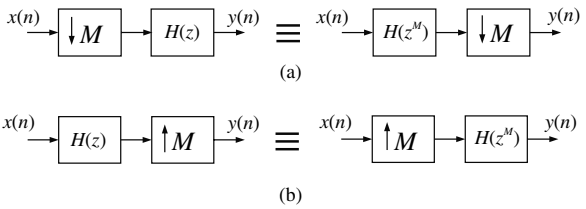

Fig. 2.17. Noble Identities: (**a**) interchanging decimator with system function, (**b**) interchanging interpolator with system function.

The interchanging rule for interpolation can be expressed as

$$Y(z) = H(z^M)[X(z)]_{\uparrow M} = [X(z)H(z)]_{\uparrow M}\,. \tag{2.47}$$

Polyphase Identity. If a system first interpolates its input by M, passing the interpolated signal through a system function and then further decimates the output by M, such system can use the Polyphase Identity as illustrated in Fig. 2.18. It can be expressed as

$$Y(z) = [H(z)[X(z)]_{\uparrow M}]_{\downarrow M} = [H(z)]_{\downarrow M} X(z). \tag{2.48}$$

Polyphase Decompositions. For a given system function, it can be decomposed into polyphase representations. Referring to Fig. 2.19, there are two types of polyphase decompositions. Type I decomposes the system function into polyphase with delay elements, i.e.,

$$F(z) = \sum_{k=0}^{N-1} z^{-k} G_k(z^N). \tag{2.49}$$

For instance, if $F(z) = a_0 + a_1 z^{-1} + a_2 z^{-2} + a_3 z^{-3} + a_4 z^{-4} + a_5 z^{-5} + a_6 z^{-6}$, let $N = 3$, we have $F(z) = (a_0 + a_3 z^{-3} + a_6 z^{-6}) + (a_1 + a_4 z^{-3}) z^{-1} + (a_2 + a_5 z^{-3}) z^{-2}$. In this case, $G_0(z^3) = (a_0 + a_3 z^{-3} + a_6 z^{-6})$, $G_1(z^3) = (a_1 + a_4 z^{-3} + a_1 + a_4 z^{-3})$, and $G_2(z^3) = (a_2 + a_5 z^{-3})$. Type II decomposes the system function into polyphase with advance elements, i.e.,

$$H(z) = \sum_{k=0}^{N-1} z^{k} S_k(z^N). \tag{2.50}$$

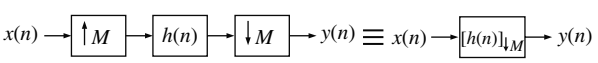

Fig. 2.18. Polyphase Identity.

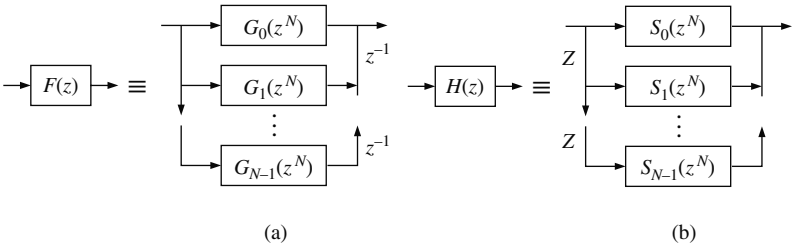

Fig. 2.19. Polyphase decomposition: (**a**) Type I (with delay elements), (**b**) Type II (with advance elements).

Continuing from above example and let $H(z) = F(z)$. Then, for $N = 3$, $H(z) = (a_0 + a_3z^{-3} + a_6z^{-6}) + (a_2z^{-3} + a_5z^{-6})z^1 + (a_1^{-3} + a_4z^{-6})z^2$. In this case, $H_0(z^3) = (a_0 + a_3z^{-3} + a_6z^{-6})$, $H_1(z^3) = (a_2z^{-3} + a_5z^{-6})$, and $H_2(z^3) = (a_1^{-3} + a_4z^{-6})$.

2.4.2 Multirate Representation for OFDM Systems

A multirate representation for communication systems with parallel symbol transmission is shown in Fig. 2.20 [76]. We will explain later that the OFDM systems can be represented using this model. In addition, several popular precoded OFDM systems can be extended based on this model as well. More detailed treatment and its extension for this subsection can be found in [100].

In communication systems, we usually choose $N > M$ to represent the insertion of redundancy to eliminate interference. More specifically, if the channel order is ν, we usually let $N \geq M + \nu$. In this chapter, we assume $N = M + \nu$.

To facilitate the analysis, we express the transmitter, channel, and the receiver using polyphase decomposition. Referring to Fig. 2.20, consider one of the filters in the transmitter (filter banks), i.e., the mth transmitter filter, $F_m(z)$. Using the Type I polyphase decomposition, $F_m(z)$ can be decomposed as

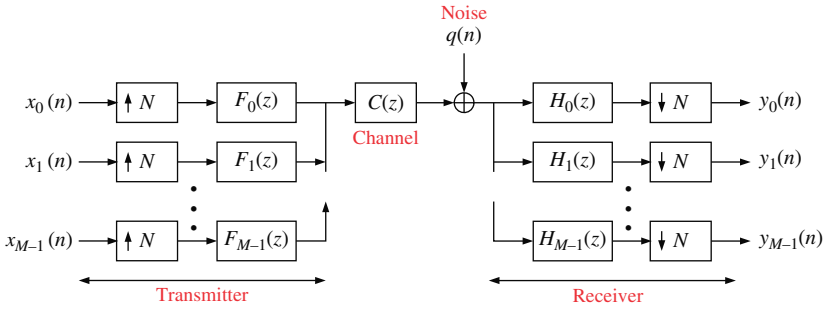

Fig. 2.20. A multirate representation for OFDM systems.

$$F_m(z) = \sum_{k=0}^{N-1} z^{-k} G_{km}(z^N), \quad m = 0,\ 1,\ \cdots,\ M-1, \tag{2.51}$$

where

$$G_{km}(z) = \sum_{k=-\infty}^{\infty} g_{km}(n) z^{-n} \quad \text{with} \quad g_{km}(n) \equiv f_m(k + nN). \tag{2.52}$$

The decomposition of Eq. (2.51) is shown in Fig. 2.21.

Similarly, let us consider the mth receiving filter in receiver (filter banks), $H_m(z)$. Using the Type II polyphase decomposition, $H_m(z)$ can be decomposed as

$$H_m(z) = \sum_{k=0}^{N-1} z^{k} S_{mk}(z^N), \quad m = 0,\ 1,\ \cdots,\ M-1, \tag{2.53}$$

where

$$S_{mk}(z) = \sum_{n=-\infty}^{\infty} s_{mk}(n) z^{-n} \quad \text{with} \quad s_{mk}(n) \equiv h_m(-k + nN). \tag{2.54}$$

The decomposition of Eq. (2.53) is shown in Fig. 2.22.

From Figs. 2.21 and 2.22, we can redraw the transmitting and receiving filter banks as in the left hand sides of Figs. 2.23 and 2.24. Since interpolation and symbol delay are linear operations, we can move the final summation for all filter banks to the front of the interpolation and symbol delay operations, and redraw the left hand side of Fig. 2.23 as the right hand side of the same figure. Similarly, we can redraw the left hand side of Fig. 2.24 as the right hand side of the same figure. Referring to the right hand side of Fig. 2.23, let

$$\mathbf{x}(n) = (x_0(n)\ x_1(n)\ \cdots x_{M-1}(n))^t$$

and

$$\mathbf{v}(n) = (v_0(n)\ v_1(n)\ \cdots v_{N-1}(n))^t .$$

We can represent the relationship of $\mathbf{x}(n)$ and $\mathbf{v}(n)$ using matrix form in z-domain, i.e.,

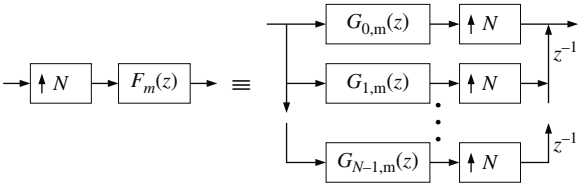

Fig. 2.21. Type I polyphase decomposition for $F_m(z)$.

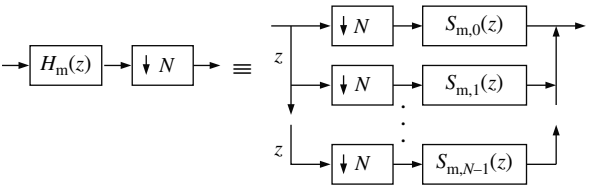

Fig. 2.22. Type II polyphase decomposition for $H_m(z)$.

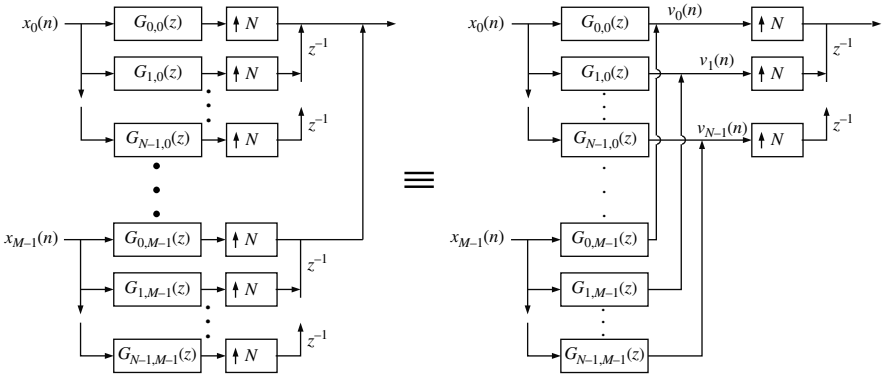

Fig. 2.23. Polyphase decomposition for transmitting filter banks $F_m(z),\ 0 \leq m \leq M-1$, and its simplified representation.

$$\mathbf{V}(z) = \mathbf{G}(z)\mathbf{X}(z), \tag{2.55}$$

where $\mathbf{G}(z)$ is of size $N \times M$ given by

$$\mathbf{G}(z) = \begin{pmatrix} G_{0,0}(z) & G_{0,1}(z) & \cdots & G_{0,M-1}(z) \\ G_{1,0}(z) & G_{1,1}(z) & \cdots & G_{1,M-1}(z) \\ \vdots & \vdots & \ddots & \vdots \\ G_{N-1,0}(z) & G_{N-1,1}(z) & \cdots & G_{N-1,M-1}(z) \end{pmatrix}. \tag{2.56}$$

Note that the ith column is corresponding to the ith transmitting filter. Also, the component $G_{j,i}(z)$ is the jth polyphase of the ith transmitting filter. Similarly, from the right hand side of Fig. 2.24, let

$$\mathbf{y}(n) = (y_0(n)\ y_1(n)\ \cdots y_{M-1}(n))^t$$

and

$$\mathbf{w}(n) = (w_0(n)\ w_1(n)\ \cdots w_{N-1}(n))^t.$$

We can represent the relationship of $\mathbf{y}(n)$ and $\mathbf{w}(n)$, i.e.,

$$\mathbf{Y}(z) = \mathbf{S}(z)\mathbf{w}(z), \tag{2.57}$$

where $\mathbf{S}(z)$ is of size $M \times N$ as follows:

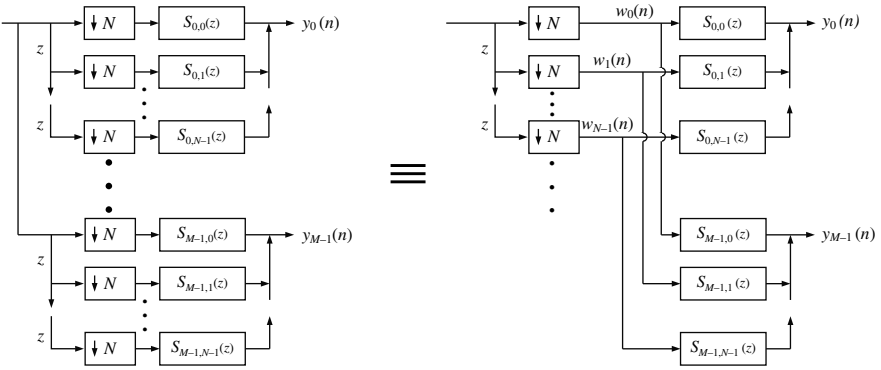

Fig. 2.24. Polyphase decomposition for receiving filter banks $H_m(z)$, $0 \leq m \leq M-1$, and its simplified representation.

$$\mathbf{S}(z) = \begin{pmatrix} S_{0,0}(z) & S_{0,1}(z) & \cdots & S_{0,N-1}(z) \\ S_{1,0}(z) & S_{1,1}(z) & \cdots & S_{1,N-1}(z) \\ \vdots & \vdots & \ddots & \vdots \\ S_{M-1,0}(z) & S_{M-1,1}(z) & \cdots & S_{M-1,N-1}(z) \end{pmatrix}. \tag{2.58}$$

Again, notice that the ith row is corresponding to the ith receiving filter. Also, the component $S_{i,j}(z)$ is the jth polyphase of the ith receiving filter.

From the discussion above, we can redraw Fig. 2.20 as in Fig. 2.25. Now we would like to discuss how to formulate the channel matrix $\mathbf{C}(z)$ in Fig. 2.25.

Polyphase Representation of the Channel. By using the Type 1 polyphase representation, we can decompose the channel as

$$C(z) = C_0(z^N) + C_1(z^N)z^{-1} + \cdots + C_{N-1}(z^N)z^{-(N-1)},$$

where $C_k(z)$ is the kth polyphase of $C(z)$. The shaded area in Fig. 2.25 is an $N \times N$ system. Each path can be described as a cascade of an interpolator, delays, $C(z)$, advances, and a decimator. The (m, n) path is shown in Fig. 2.26(a). Using Polyphase Identity, we can redraw Fig. 2.26(a) as in

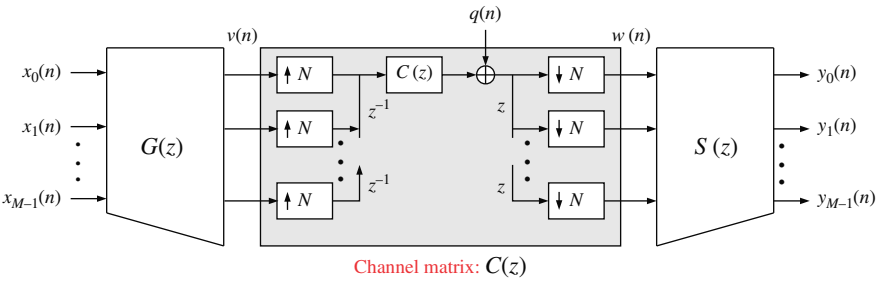

Fig. 2.25. Polyphase representation for the OFDM systems.

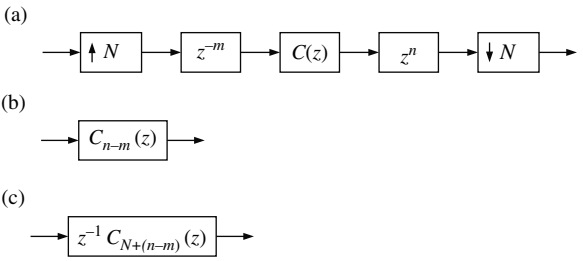

Fig. 2.26. (**a**) General block diagram for every path (from $v_n(n)$ to $w_m(n)$). When $n \geq m$, we can redraw (**a**) as in (**b**), when $n < m$, then (**a**) can redraw as in (**c**).

Fig. 2.26(b) when $n \geq m$, and redraw as in Fig. 2.26(c) when $n < m$. Although the decimator and interpolator are time-varing building blocks, the interconnection in Fig. 2.26(a) happens to be time-invariant and circuits (a) and (b) are equivalent, where $C_0(z)$ is the 0th polyphase component of the transfer function $C(z)$. Thus the transfer matrix $\mathbf{C}(z)$ is given by

$$\mathbf{C}(z) = \begin{pmatrix} C_0(z) & z^{-1}C_{N-1}(z) & \dots & z^{-1}C_1(z) \\ C_1(z) & C_0(z) & & \\ \vdots & & \ddots & \vdots \\ C_{N-1}(z) & C_{N-2}(z) & \dots & C_0(z) \end{pmatrix}. \tag{2.59}$$

This matrix falls into the category of the so-called pseudo circulant matrices [140]. Let the channel be finite impulse response (FIR) with order ν ($\nu < N$), and the kth channel tap be c_k, the polyphase terms of $C(z)$ is given by

$$C_k(z) = \begin{cases} c_k \text{ if } k < L+1, \\ 0 \quad \text{otherwise.} \end{cases}$$

We can partition $\mathbf{C}(z)$ as a constant matrix $\mathbf{C}_L$ and a matrix $\mathbf{C}_R(z)$, in particular

$$\mathbf{C}(z) = [\mathbf{C}_L | \mathbf{C}_R(z)], \tag{2.60}$$

where $\mathbf{C}_L$ is an $N \times M$ matrix and $\mathbf{C}_R(z)$ is an $N \times \nu$ matrix given, respectively, by

$$\mathbf{C}_L = \begin{pmatrix} c_0 & 0 & \dots & 0 & \dots & 0 \\ c_1 & c_0 & & & & 0 \\ \vdots & & \ddots & & & \vdots \\ c_\nu & c_{\nu-1} & & & & 0 \\ 0 & c_\nu & & & & 0 \\ \vdots & \vdots & \ddots & & \ddots & \vdots \\ 0 & 0 & & c_\nu & & c_0 \\ \vdots & \vdots & & & \ddots & \vdots \\ 0 & 0 & & 0 & \dots & c_\nu \end{pmatrix} \text{ and } \mathbf{C}_R = \begin{pmatrix} z^{-1}c_\nu & z^{-1}c_{L-1} & \dots & z^{-1}c_1 \\ 0 & z^{-1}c_\nu & & z^{-1}c_2 \\ 0 & 0 & & \\ \vdots & \vdots & \ddots & \vdots \\ c_0 & 0 & & z^{-1}c_\nu \\ c_1 & c_0 & & 0 \\ \vdots & & \ddots & \vdots \\ & & & 0 \\ c_{L-1} & c_{L-2} & \dots & c_0 \end{pmatrix}. \tag{2.61}$$

Based on the discussion above, the relationship between $\mathbf{Y}(z)$ and $\mathbf{X}(z)$ is given by

$$\mathbf{Y}(z) = \mathbf{S}(z)\mathbf{C}(z)\mathbf{G}(z)\mathbf{X}(z) + \mathbf{N}, \tag{2.62}$$

where $\mathbf{N}$ is the noise vector. Now we will represent OFDM systems using the above model. Since OFDM are systems with block transmission, the maximum length of the filters in transmitting filter bank $F_m(z)$ and receiving filter bank $H_m(z)$ cannot exceed N. Otherwise, the current transmission block $\mathbf{x}(n)$ will be affected by the blocks at other time instance k, where $k \neq n$, which is not block transmission. Given the maximum length N for all filters, from Eqs. (2.51) and (2.53), the matrices $\mathbf{G}(z)$ and $\mathbf{S}(z)$ become constant matrices. We can simplify the input and output relationship as

$$\mathbf{Y}(z) = \mathbf{S}\mathbf{C}(z)\mathbf{G}\mathbf{X}(z) + \mathbf{N}. \tag{2.63}$$

From (2.63), we still need to design $\mathbf{S}$ and $\mathbf{G}$ to avoid inter-block interference (IBI) due to $\mathbf{C}(z)$. The two popular methods are by inserting zeros or cyclic prefix. By the use of cyclic prefix or zero padding in matrix $\mathbf{G}$ and the redundancy removal in $\mathbf{S}$, although the channel matrix $\mathbf{C}(z)$ contains the z components, the current output block will only be affected by the current input block, and hence $\mathbf{X}(z)$ and $\mathbf{Y}(z)$ become constant vectors $\mathbf{X}$ and $\mathbf{Y}$ as we will see in the following subsections.

2.4.3 OFDM Systems with Cyclic Prefix

Now consider the OFDM system with cyclic prefix, which is widely adopted in current communications standards such as DVB-T, IEEE 802.11a/g/n, and IEEE 802.16x. At the transmitter side, due to the appended cyclic prefix with length L, the constant transmitting matrix $\mathbf{G}_{cp}$ is given by [77]

$$\mathbf{G}_{cp} = \begin{pmatrix} \mathbf{0}\ \mathbf{I}_{\nu} \\ \mathbf{I}_M \end{pmatrix} \mathbf{F}^{\dagger}, \tag{2.64}$$

where $\mathbf{F}$ is the $M \times M$ DFT matrix with the component at the nth row and mth column given by

$$[\mathbf{F}]_{n,m} = \frac{1}{\sqrt{M}} e^{-j\frac{2\pi}{M}nm}.$$

Consider zero forcing (ZF) equalization in the receiver side, due to the removal of CP, the constant receiving matrix $\mathbf{S}_{cp}$ is given by

$$\mathbf{S}_{cp} = \mathbf{\Lambda}^{-1}\mathbf{F}\left(\mathbf{0}\ \mathbf{I}_M\right), \tag{2.65}$$

where $\mathbf{\Lambda}$ is a diagonal matrix with its diagonal elements λ_k, $0 \leq k \leq M-1$. λ_k is the kth element of the M-point DFT of the channel coefficients, i.e.,

$$\lambda_k = \sum_{n=0}^{\nu} c_n e^{-j\frac{2\pi}{M}nk}. \tag{2.66}$$

From Eqs. (2.61) and (2.65), we find that $\mathbf{S}_{cp}\mathbf{C}(z)$ will lead to the removal of the upper ν rows of $\mathbf{C}(z)$ and is given by

$$\mathbf{S}_{cp}\mathbf{C}(z) = \mathbf{\Lambda}^{-1}\mathbf{F}\mathbf{C}_{cp}, \tag{2.67}$$

where $\mathbf{C}_{cp}$ is an $M \times N$ matrix given by

$$\mathbf{C}_{cp} = \begin{pmatrix} c_\nu & c_{\nu-1} & \cdots & c_0 & 0 & \cdots & 0 & \cdots & 0 \\ 0 & c_\nu & \ddots & & c_0 & \ddots & \vdots & & \vdots \\ \vdots & \ddots & \ddots & & & \ddots & 0 & \cdots & 0 \\ 0 & 0 & 0 & c_\nu & & & c_0 & \ddots & \vdots \\ \vdots & \vdots & & \ddots & \ddots & & & \ddots & 0 \\ 0 & 0 & \cdots & & 0 & c_\nu & \cdots & c_1 & c_0 \end{pmatrix}. \tag{2.68}$$

From Eq. (2.71) and (2.64), the overall system function $\mathbf{S}_{cp}\mathbf{C}(z)\mathbf{G}_{cp}$ can be manipulated as

$$\mathbf{S}_{cp}\mathbf{C}(z)\mathbf{G}_{cp} = \mathbf{\Lambda}^{-1}\mathbf{F}\mathbf{C}_{cir}\mathbf{F}^\dagger, \tag{2.69}$$

where $\mathbf{C}_{cir}$ is an $M \times M$ circulant matrix given by

$$\mathbf{C}_{cir} = \begin{pmatrix} c_0 & 0 & \cdots & \cdots & c_\nu & \cdots & c_1 \\ c_1 & c_0 & & & & \ddots & \vdots \\ \vdots & & \ddots & & & & c_\nu \\ c_\nu & & & \ddots & & & 0 \\ 0 & c_\nu & & & & & \vdots \\ \vdots & \ddots & \ddots & & & & 0 \\ 0 & \cdots & 0 & c_\nu & \cdots & c_1 & c_0 \end{pmatrix}. \tag{2.70}$$

The effect that the matrix $\begin{pmatrix} \mathbf{0}\ \mathbf{I}_\nu \\ \mathbf{I}_M \end{pmatrix}$ results in $\mathbf{C}_{cp}$ is to add the first ν columns to the last ν columns and then eliminate the first ν columns. Since $\mathbf{F}\mathbf{C}_{cir}\mathbf{F}^\dagger$ is a diagonal matrix with the diagonal elements being the M-point DFT of $(c_0,\ c_1,\ \cdots, c_\nu)$ [47], from Eqs. (2.63) and (2.69), current $\mathbf{Y}$(z) only depends on current $\mathbf{X}$(z). Hence there is no need to use z herein. The two vectors become constant vectors and their relationship of $\mathbf{x}$ and $\mathbf{y}$ can be expressed as

$$\mathbf{Y} = \mathbf{X} + \mathbf{\Lambda}^{-1}\mathbf{N}, \tag{2.71}$$

When the channel has zeros near the unit circle, the subchannels corresponding to these zeros have serious fading. In this case, λ_k are small in these subchannels. As a result, λ_k^{-1} are large and tend to enhance noise. Thus it leads to relatively high bit error probability (BEP) in these subchannels. To

avoid significant noise enhancement, we may use minimum mean square error (MMSE) technique. That is, define the averaged SNR

$$\gamma = E_s/\mathcal{N}_0, \tag{2.72}$$

where E_s is the averaged transmitted power and $\mathcal{N}_0$ is the noise variance. We can choose the receiving filter bank such that

$$\mathbf{S}_{cp}\mathbf{C}(z) = \mathbf{\Gamma}\mathbf{F}\mathbf{C}_{cp}, \tag{2.73}$$

where $\mathbf{\Gamma}$ is a diagonal matrix with its elements given by

$$[\mathbf{\Gamma}]_{k,k} = \frac{\gamma\lambda_k^*}{1+\gamma|\lambda_k|^2}. \tag{2.74}$$

When $\gamma \gg 1$, it is obvious that the MMSE equalization in Eq. (2.73) is reduced to ZF equalization in Eq. (2.67). Please note that both the ZF and MMSE equalizations described are called frequency domain equalization (FEQ) since they perform equalization in frequency domain.

2.4.4 OFDM Systems with Zero Padding

Zero padding is an alternative to avoid IBI. Instead of using cyclic prefix, it inserts ν zeros at the end of every transmitted block. If $\nu + 1 \geq L$, where L is the multipath length, the zero padded OFDM systems are free from IBI. The zero padded OFDM systems require less power consumption than that of cyclic-prefix OFDM systems. However, the zero padded OFDM systems need to perform extra manipulations in the receiver side. Fortunately, such manipulations only involve additions and have comparable computation complexity with cyclic-prefix OFDM systems as we will mention later.

Referring to Fig. 2.25, due to the insertion of zeros, the transmit matrix is given by

$$\mathbf{G}_{zp} = \begin{pmatrix} \mathbf{I}_M \\ \mathbf{0} \end{pmatrix} \mathbf{F}^\dagger. \tag{2.75}$$

The channel matrix remains the same as that in Eq. (2.59). Hence, from Eqs. (2.75) and (2.59), $\mathbf{C}(z)\mathbf{G}_{zp}$ is given by

$$\mathbf{C}(z)\mathbf{G}_{zp} = \mathbf{C}_L\mathbf{F}^\dagger, \tag{2.76}$$

where $\mathbf{C}_L$ is an $N \times M$ matrix as given in Eq. (2.61). From (2.76), the z term disappears and hence there is no IBI in this system. Let the receiving matrix be S_{zp}, the relationship between input and output blocks can be expressed as

$$\mathbf{Y} = \mathbf{S}_{zp}\mathbf{C}_L\mathbf{F}^\dagger\mathbf{X}. \tag{2.77}$$

From Eq. (2.77), for zero forcing reconstruction, we can choose $\mathbf{S}_{zp}$ as the pseudo inverse of $\mathbf{C}_L\mathbf{F}^\dagger$, i.e.,

$$\mathbf{S}_{zp} = \mathbf{F}(\mathbf{C}_L^{\dagger}\mathbf{C}_L)^{-1}\mathbf{C}_L^{\dagger}. \tag{2.78}$$

If we have the information of the averaged SNR as defined in Eq. (2.72), the performance can be further improved by choosing

$$\mathbf{S}_{zp} = \mathbf{F}(\mathbf{C}_L^{\dagger}\mathbf{C}_L + \gamma^{-1}\mathbf{I}_M)^{-1}\mathbf{C}_L^{\dagger}, \tag{2.79}$$

which is the MMSE receiver. However, the receivers implemented according to Eqs. (2.78) and (2.79) demand matrix multiplication and reversion and this leads to great computational complexity. To reduce the extra computational complexity, we can first perform manipulation of the received symbols and hence it makes the channel matrix $\mathbf{C}_L$ circulant as that shown in Eq. (2.61). After the manipulations, pass the signal into an DFT matrix $\mathbf{F}$. The input and output relationship can again be characterized by Eq. (2.71). To achieve this, let the receiving matrix be

$$\mathbf{S}_{zp} = \mathbf{F}\mathbf{\Phi}, \tag{2.80}$$

where $\mathbf{\Phi}$ is an $M \times N$ permutation matrix given by

$$\mathbf{\Phi} = \begin{pmatrix} \mathbf{I}_M & \begin{matrix} \mathbf{I}_\nu \\ \mathbf{0} \end{matrix} \end{pmatrix}. \tag{2.81}$$

Note that given an $N \times M$ matrix $\mathbf{A}$, the operation of $\mathbf{\Phi}\mathbf{A}$ is simply adding the last ν rows to the first ν rows and then eliminating the last ν rows. Hence, we have

$$\mathbf{S}_{zp}\mathbf{C}_L\mathbf{G}_{zp} = \mathbf{F}\mathbf{C}_{cir}\mathbf{F}^{\dagger}, \tag{2.82}$$

which again leads to the same input and output relationship as that in Eq. (2.71). Note that according to Eq. (2.80) although the OFDM systems with zero padding requires extra computations for $\mathbf{\Phi}$ in the receiver side, this matrix is a permutation matrix and can be implemented by additions. Hence, the complexity of OFDM with zero padding can use less transmitted power to achieve the same performance as that of OFDM with cyclic prefix while both systems can be implemented with comparable computational cost.

2.4.5 OFDM Systems with Transmitter Knows Channel Information

The transceiver filter banks as discussed above can actually be regarded as precoded communications systems. More specifically, we can regard the transmitting matrix $\mathbf{G}_{cp}$ and $\mathbf{G}_{zp}$ be the precoding/prefiltering to achieve ISI-free property. The DFT-based OFDM systems discussed above assume that only the receiver knows the channel information. If the transmitter knows the channel information, we can design non-DFT-based OFDM systems. For example, in [115], optimal transceiver design based on maximum output SNR and minimum mean square criteria were derived. In [76] and [77], transceiver that achieves optimal bit rate is considered. Based on the optimal bit rate, the transceiver that can achieve minimum transmit power is developed.

2.5 Precoding for OFDM Systems

Although the OFDM systems introduced in previous section can successfully overcome the ISI effect, the subchannels with serious fading will significantly degrade system performance. More specifically, the subchannels with the most serious fading will have the largest BEP. As a result, it dominates the overall system performance. In wireline communication systems, *e.g.* DMT-xDSL systems, such problems can be overcome by bit or power allocation. However, this demands feedback of channel information or SNR information for all subchannels and may somewhat infeasible in a rapid changing channel environment.

This problem may also be overcome by adding a proper precoder in the transmitter and the corresponding postcoder in the receiver. In wireless communication systems, however, channel may vary rapidly, and it is preferable that the precoder is independent of channel so that there is no need to use feedback. In this section, we will introduce a channel independent precoder to mitigate BEP. More detailed treatment and its extension for this subsection can be found in [75].

An OFDM system with precoder is shown in Fig. 2.27, where $\mathbf{P}$ is an $M \times M$ unitary matrix. At the receiver side, $\mathbf{P}^\dagger$ is placed after $\mathbf{S}$ so that the whole system can achieve perfect reconstruction property when there is no noise. In the following subsections, we will let the matrix $\mathbf{P}$ be the DFT matrix $\mathbf{F}$, and thus the OFDM systems become single carrier systems.

2.5.1 Single Carrier System with Cyclic Prefix (SC-CP)

Referring to Fig. 2.27, let the precoder $\mathbf{P}$ be an $M \times M$ DFT matrix and the transmitting matrix $\mathbf{G}_{cp}$ be that described in Eq. (2.64). In this case, the whole system becomes single carrier system with cyclic prefix. Figure 2.28 shows the block diagram of the single carrier system with cyclic prefix. The SC-CP

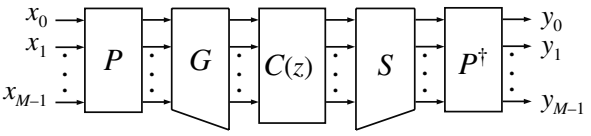

Fig. 2.27. Block diagram for a general OFDM system with precoder.

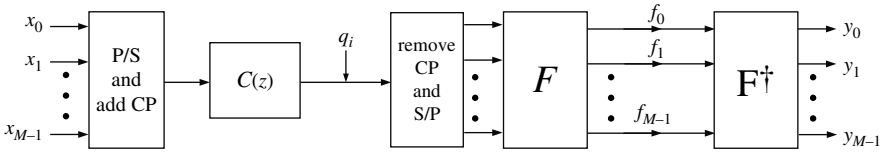

Fig. 2.28. Block diagram for a single carrier system with cyclic prefix.

system has the following advantages when compared with the conventional OFDM systems introduced in Sections 2.4.3 and 2.4.4.

1. **Mitigation for High PAPR.** It is well known that one of the critical issues of conventional OFDM systems is its high PAPR (peak-to-average power ratio) characteristic. Due to the use of IDFT in the transmitter, the dynamic range of IDFT output will increase, and hence the peak value increases. If we let the IDFT matrix be unitary, the average power of IDFT output remains the same as that in the IDFT input. As a result, the PAPR increases. It is intuitive that the PAPR increases as the number of subchannels increases. In the transceiver of DVB-T, the number of subchannels is up to 8192 and hence the system has large PAPR value. High PAPR will increase design effort for analog circuits such as power amplifier since the demand for linearity in systems with high PAPR is much higher than in systems with low PAPR. System performance will degrade significantly due to high PAPR. This drawback, however, can be overcome by using SC-CP systems. The reason is that there is no need to use IDFT in the transmitter side. Hence, the peak value of the transmit signal is completely dependent on the the modulation scheme. Take IEEE 802.11a/g/n for instance, the highest modulation scheme is 64-QAM. The corresponding PAPR for 64-QAM is around 1.63, which is much smaller than the PAPR in conventional OFDM systems whose PAPR is in general greater than 10 dB.
2. **Simplification of DAC.** Since there is no IDFT in the transmitter, it may be sufficient to put a low bit width for DAC design. For instance, for 64-QAM, the constellation level for both I and Q axes only have 8 different levels, i.e. $(-7\ -5\ -3\ -1\ +1\ +3\ +5\ +7)$. Under such situation, we may only require 3-bit DAC to represent such constellation level, which again greatly simplifies the design effort of analog circuits.
3. **Equalized BEP for All Subchannels.** Now let us discuss the most important characteristic of SC-CP system. That is, the SC-CP system has equal BEP for all subchannels. Referring to the receiving noise path of the SC-CP system in Fig. 2.29 and assuming that the receiving noise q_i is complex white Gaussian with zero mean and variance $\mathcal{N}_0$, due to the uncorrelated property of the noise, the correlation matrix of the noise vector is given by

$$\mathbf{R_q} = E\left\{\mathbf{q}\mathbf{q}^\dagger\right\} = \mathcal{N}_0\mathbf{I}_M. \tag{2.83}$$

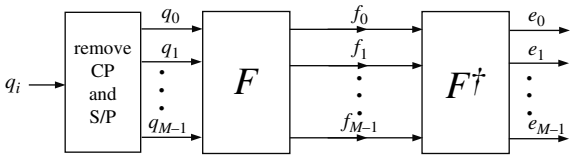

Fig. 2.29. Receiving noise path of a single carrier system with cyclic prefix.

Let the output noise vector be

$$\mathbf{e} = (e_0 \; e_1 \; \cdots e_{M-1}).$$

Now we would like to obtain the correlation matrix of $\mathbf{e}$. Assume that we are using the zero forcing equalization. In this case, the FEQ coefficients are

$$f_k = 1/\lambda_k, \quad 0 \le k \le M-1.$$

Hence, the output noise vector is given by

$$\mathbf{e} = \mathbf{F}^\dagger \mathbf{\Lambda}^{-1} \mathbf{F} \mathbf{q}. \tag{2.84}$$

Using Eqs. (2.83) and (2.84), we have the correlation matrix of the output noise vector given by

$$\mathbf{R_e} = E\left\{\mathbf{e}\mathbf{e}^\dagger\right\} = \mathbf{F}^\dagger \mathbf{\Lambda}^{-1} \mathbf{F} E\left\{\mathbf{q}\mathbf{q}^\dagger\right\} \mathbf{F}^\dagger (\mathbf{\Lambda}^{-1})^\dagger \mathbf{F} = \mathcal{N}_0 \mathbf{F}^\dagger (\mathbf{\Lambda}\mathbf{\Lambda}^\dagger)^{-1} \mathbf{F}. \tag{2.85}$$

To obtain the output noise variance, we only need to obtain the diagonal elements of $\mathbf{R_e}$ since the diagonal elements are the output noise variances. From Eq. (2.85), since $(\mathbf{\Lambda}\mathbf{\Lambda}^\dagger)^{-1}$ is diagonal with its diagonal element being $(1/|\lambda_0|^2 \; 1/|\lambda_1|^2 \; \cdots 1/|\lambda_{M-1}|^2)$, $\mathbf{R_e} = \mathbf{F}^\dagger (\mathbf{\Lambda}\mathbf{\Lambda}^\dagger)^{-1} \mathbf{F}$ is a circulant matrix and its diagonal elements are the 0th output component of the IDFT of $(1/|\lambda_0|^2 \; 1/|\lambda_1|^2 \; \cdots 1/|\lambda_{M-1}|^2)$, i.e.,

$$[\mathbf{R_e}]_{k,k} = \frac{\mathcal{N}_0}{M} \sum_{m=0}^{M-1} 1/|\lambda_m|^2, \quad \text{for all } k. \tag{2.86}$$

From Eqs. (2.85) and (2.86), the variance of output noise for every subchannel is the same, i.e.,

$$\sigma_{e_k}^2 = E\left\{|e_k|^2\right\} = [\mathbf{R_e}]_{k,k} = \frac{\mathcal{N}_0}{M} \sum_{m=0}^{M-1} 1/|\lambda_m|^2. \tag{2.87}$$

Assume the transmitter power is E_s. Due to the use of zero forcing equalization and from Eq. (2.87), the output SNR for all subchannel is the same and is given by

$$SNR_k = \frac{E_s}{\mathcal{N}_0} \frac{M}{\sum_{m=0}^{M-1} 1/|\lambda_m|^2}, \quad \text{for all } k. \tag{2.88}$$

Since the output SNR is the same (independent of k), all subchannels have the same BEP in this situation.

The BEP result for SC-CP is very different from that of the conventional OFDM systems. In conventional OFDM systems, the BEP of every individual subchannels is in general different. Thus, the performance corresponding

to the most serious fading will dominate the overall performance. Hence, we usually use channel coding to overcome the issue that subchannels have deep fading. On the contrary, SC-CP systems have the same BEP for all subchannels. In this case, if the unique SNR of SC-CP is good, there may be no need to use channel coding in this case. If the unique SNR of SC-CP is bad, however, using channel coding may not be able to rescue the system performance because the channel coding such as convolutional code is designed to correct burst error instead of block error. Observing from Eq. (2.88), if there is any value for λ_k is small (deep fading), the summation term $\sum_{m=0}^{M-1} 1/|\lambda_m|^2$ is large. Hence, the SNR value for all subchannels are the same bad. To overcome this problem, we can use the MMSE equalization instead of zero forcing equalization described as follows:

MMSE Equalization for SC-CP. Let the equalization coefficients be

$$f_k = \frac{\gamma \lambda_k^*}{1 + \gamma |\lambda_k|^2}, \quad 0 \le k \le M-1. \tag{2.89}$$

Let $\mathbf{\Gamma}$ be the diagonal matrix consists of f_k, i.e., $\mathbf{\Gamma} = \text{diag}(f_0,\ f_1\ \cdots f_{M-1})$. In this case, the input and output relationship is given by

$$\mathbf{Y} = \mathbf{F}^\dagger \mathbf{\Gamma} \mathbf{F} \mathbf{C}_{cir} \mathbf{X} + \mathbf{F}^\dagger \mathbf{\Gamma} \mathbf{F} \mathbf{q}, \tag{2.90}$$

where the first term is contributed from the transmitted symbols and the second term is contributed from noise. Since $\mathbf{C}_{cir} = \mathbf{F}^\dagger \mathbf{\Lambda} \mathbf{F}$, Eq. (2.90) can be rewritten as

$$\mathbf{Y} = \mathbf{F}^\dagger \mathbf{\Gamma} \mathbf{\Lambda} \mathbf{F} \mathbf{X} + \mathbf{F}^\dagger \mathbf{\Gamma} \mathbf{F} \mathbf{q} = \mathbf{X} + \underbrace{\mathbf{F}^\dagger (\mathbf{\Gamma}\mathbf{\Lambda} - \mathbf{I}_M)\mathbf{F}\mathbf{X} + \mathbf{F}^\dagger \mathbf{\Gamma} \mathbf{F} \mathbf{q}}_{\mathbf{e}}. \tag{2.91}$$

Note that the output noise vector in MMSE equalization contains the contribution from both noise and transmitted symbols. Let us obtain the output noise variance as follows. Assume the transmitted symbol vector $\mathbf{X}$ and the noise vector $\mathbf{q}$ are uncorrelated, using Eqs. (2.83) and (2.91), we have

$$\mathbf{R_e} = \mathbf{F}^\dagger \underbrace{\left(E_s (\mathbf{\Gamma}\mathbf{\Lambda} - \mathbf{I}_M)(\mathbf{\Gamma}\mathbf{\Lambda} - \mathbf{I}_M)^\dagger + \mathcal{N}_0 \mathbf{\Gamma}\mathbf{\Gamma}^\dagger \right)}_{\mathbf{D}} \mathbf{F}. \tag{2.92}$$

Since $\mathbf{D}$ in Eq. (2.92) is a diagonal matrix, $\mathbf{R_e}$ is again a circulant matrix. Next let us obtain the diagonal elements of $\mathbf{D}$, which is denoted by d_k, where $0 \le k \le M-1$. From Eqs. (2.89) and (2.92), we have

$$\begin{aligned} d_k &= E_s \left(|\lambda_k|^2 \left| \frac{\gamma \lambda_k^*}{1 + \gamma |\lambda_k|^2} \right|^2 - 2 \frac{\gamma |\lambda_k|^2}{1 + \gamma |\lambda_k|^2} + 1 \right) + \mathcal{N}_0 \left| \frac{\gamma \lambda_k^*}{1 + \gamma |\lambda_k|^2} \right|^2 . \\ &= \frac{E_s + \mathcal{N}_0 \gamma^2 |\lambda_k|^2}{(1 + \gamma |\lambda_k|^2)^2}. \end{aligned} \tag{2.93}$$

Since $\gamma = E_s / \mathcal{N}_0$, we can rewrite Eq. (2.93) as

$$d_k = E_s \frac{1+\gamma|\lambda_k|^2}{(1+\gamma|\lambda_k|^2)^2} = \frac{E_s}{(1+\gamma|\lambda_k|^2)}. \tag{2.94}$$

The diagonal elements of $\mathbf{R_e}$ is the 0th component of the IDFT of $(d_0\ d_1\ \cdots\ d_{M-1})$. Thus, we have

$$[\mathbf{R_e}]_{k,k} = \frac{E_s}{M} \sum_{k=0}^{M-1} \frac{1}{1+\gamma|\lambda_k|^2}. \tag{2.95}$$

From Eq. (2.95), the SNR is the same in individual subchannels and is given by

$$SNR_k = \frac{M}{\sum_{k=0}^{M-1} \frac{1}{1+\gamma|\lambda_k|^2}}. \tag{2.96}$$

Compared Eq. (2.96) with Eq. (2.88), even if some suchannels have deep fading, the MMSE equalization will not lead to bad SNR value for all suchannels.

2.5.2 Single Carrier System with Zero Padding (SC-ZP)

Another method for single carrier systems to avoid IBI is zero padding, which is similar to the OFDM systems with zero padding as discussed in Section 2.4.4 except that now we have a precoder. Referring to Fig. 2.28, SC-ZP is the same as that of SC-CP except that adding CP becomes zero padding. Hence, let $\mathbf{P} = \mathbf{F}$ and $\mathbf{G}_{zp}$ be the same as that in Eq. (2.75). For zero forcing and efficient implementation, $\mathbf{S}_{zp}$ can be chosen as that in Eq. (2.80). Hence, we have the input and output relationship given by

$$\mathbf{Y} = \mathbf{P}^\dagger \mathbf{S}_{zp} \mathbf{C}(z) \mathbf{G}_{zp} \mathbf{P} \mathbf{X} = \mathbf{X} + \mathbf{F}^\dagger \mathbf{\Lambda}^{-1} \mathbf{F} \mathbf{q},$$

which leads to the same results as that of SC-CP with zero forcing equalization in Eqs. (2.83–2.88).

If we keep all conditions unchanged except that $\mathbf{S}_{zp} = \mathbf{\Gamma F \Phi}$ as in Eq. (2.89), it becomes SC-ZP with MMSE equalization. In this case, the same results as in Eqs. (2.90–2.96) can be obtained. Similar to OFDM systems, SC-ZP can use lower transmitter power to achieve the same performance as SC-CP with little extra additions in the receiver.

We can also use the pseudo inverse solution with zero forcing to reconstruct the transmitted symbols. That can be done by keeping the transmitter unchanged as that in SC-ZP with MMSE equalization, and let $\mathbf{S}_{zp}$ be chosen as that in Eq. (2.80). In addition, let $\mathbf{P}^\dagger = \mathbf{F}^\dagger$. In this case, the input and output relationship is given by

$$\mathbf{Y} = \mathbf{X} + (\mathbf{C}_L^\dagger \mathbf{C}_L)^{-1} \mathbf{C}_L^\dagger \mathbf{q}.$$

For pseudo inverse solution with MMSE receiver, we can choose $\mathbf{S}_{zp}$ as that in Eq. (2.79) and $\mathbf{P}^\dagger = \mathbf{F}^\dagger$. The input and output relationship in this case can be expressed as

$$\mathbf{Y} = (\mathbf{C}_L^{\dagger}\mathbf{C}_L + \gamma^{-1}\mathbf{I}_M)^{-1}\mathbf{C}_L^{\dagger}\mathbf{C}_L\mathbf{X} + (\mathbf{C}_L^{\dagger}\mathbf{C}_L + \gamma^{-1}\mathbf{I}_M)^{-1}\mathbf{C}_L^{\dagger}\mathbf{q}.$$

For further reading, a channel independent OFDM precoder to combat subchannel nulls was proposed in [153]. Linear precoder for OFDM to achieve maximum diversity gain was considered in [149]. The SC-CP system was first proposed in [113] to investigate the possible application for digital terrestrial TV. In [78], the authors proved that SC-CP achieves the minimum BEP for a moderate SNR range over QPSK modulation. The results is further extended to higher constellation cases in [75].

3

Precoding Techniques in Multiple Access Channels

The direct-sequence code division multiple access (DS-CDMA) system accommodates more than one user in a single frequency band simultaneously by the use of spreading codes. For example, the data symbol of the kth user in the DS-CDMA system is first modulated onto an unique spreading code and then transmitted. If code information is available at the receiver, the kth receiver employs a matched filter (MF), which simply matches the received signal with the code sequence while rejecting the multiple access interference (MAI) for symbol decoding.

The MAI immunity of the MF receiver depends on both the spreading code design and the channel condition. In a synchronous frequency flat fading channel, the orthogonality between different code channels can be achieved by employing Hadamard-Walsh codes, which suggests that the MF receiver can completely remove MAI at its output. It is however that when the signal bandwidth is greater than the channel coherent bandwidth, the transmit signal undergoes a frequency selective fading channel, and multiple copies of the transmit signal coming from different propagation paths will be observed at different time delays at the receiver. This channel, known as a multipath channel, not only destroys the code orthogonality but also introduces overlapped transmit signals at the receiver. As a result, the system performance of the MF receiver degrades due to the presence of interference, namely, MAI, inter-chip interference (ICI), and possible inter-symbol interference (ISI) if a proper number of guard chips are not inserted between any two consecutive transmit symbols.

The DS-CDMA performance in the multipath channel can be saved by employing other receiver design schemes, such as the Rake receiver [105], the decorrelator [81], the minimum mean square error (MMSE) receiver [83] or the multiuser detector [144]. These schemes, which are complex in design and consume more power for symbol decoding than the MF receiver, are more likely to be implemented at the base station, rather than the mobile handset due to its size and battery constraints. Consequently, the performance of the downlink DS-CDMA system is worse than its uplink counterpart.

C.-C.J. Kuo et al., *Precoding Techniques for Digital Communication Systems*,
DOI: 10.1007/978-0-387-71769-2_3,

In order to improve the downlink performance while maintaining a simple receiver design, the idea of transmit precoding, which shifts the decoding complexity from the receiver to the transmitter, was proposed in different literature and gets more and more attention nowadays. Given the channel information of all users are known to the transmitter, the transmitter can pre-process the original transmit data according to the channel condition and the transmit signals of all co-channel users such that the resultant MF output contains either more signal power or less interference as compared to the system without precoding.

The precoder design necessitates the channel knowledge at the transmitter. If the channel varies slowly, the channel information can either be acquired via one feedback link from the receiver to the transmitter or be estimated at the transmitter by exploiting the channel reciprocity property, which is inherent in the time division duplex (TDD) system [12, 24, 25, 147]. It is however that the channel responses estimated at different ends may not be exactly the same due to imperfect RF circuits [96, 137]. Therefore, additional calibration is necessary. In this chapter, we do not consider the problem of channel information mismatch and simply assume that the channel knowledge at the transmitter is ideal. Next, three different linear precoding schemes, namely transmit matched filter (Tx-MF), transmit zero-forcing filter (Tx-ZF), and the transmit Wiener filter (Tx-Wiener), proposed in the previous literature, are reviewed in the following sections.

3.1 System Model

The block diagram of a generic downlink DS-CDMA system with precoding is given in Fig. 3.1, where the base station and each mobile user employ only one transmit and receive antennas, respectively. The binary symbol, $b_k(i) \in \{+1, -1\}$ equal-probable, which denotes the ith data symbol for the kth user, is modeled as an independent, identically distributed (i.i.d.) random variable for all i and k. The data symbol is first despread by the unit-power, N-chip spreading code, $\mathbf{s}_k$, given as

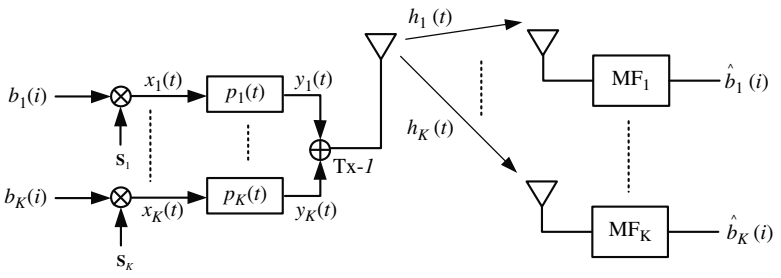

Fig. 3.1. The block diagram of the precoded SISO TDD DS-CDMA system.

$$\mathbf{s}_k = [s_{k,0}, \cdots, s_{k,N-1}]^t, \quad \mathbf{s}_k^\dagger \mathbf{s}_k = 1, \tag{3.1}$$

where $s_{k,i} \in \{+1/\sqrt{N}, -1/\sqrt{N}\}$, $\forall k, i$. The spread signal for the kth user, $x_k(t)$, is represented as

$$x_k(t) = \sum_{i=-\infty}^{\infty} \sum_{j=0}^{N-1} s_{k,j} b_k(j) w(t - jT_c - jT_s). \tag{3.2}$$

The precoder for the kth user $p_k(t)$, which is a L_p-tap finite impulse response (FIR) filter, is described as

$$p_k(t) = \sum_{i=0}^{L_p-1} p_{k,i} \delta_D(t - iT_c), \tag{3.3}$$

where $p_{k,i}$, which denotes the ith tap coefficient, is designed according to different criteria. The spread signal $x_k(t)$ is first passed through the corresponding precoder $p_k(t)$ before transmission and the output of the precoder $p_k(t)$ is

$$y_k(t) = x_k(t) * p_k(t). \tag{3.4}$$

The transmit signal $y(t)$, which is the sum of all K prefilter output signals $y_k(t)$, $\forall k = 1, \cdots, K$, is given as

$$y(t) = \sum_{k=1}^{K} y_k(t). \tag{3.5}$$

Please note that we omit the carrier frequency in $y(t)$ since we represent our transmit signal in the equivalent baseband.

Here we adopt the block fading channel model, i.e., the channel coefficients remain unchanged during a block of transmit symbols and then changes independently from block to block. Also, channels of different users are realized independently. Let $h_k(t)$ be the channel response for the kth user and is modeled as an L-tap FIR filter given as

$$h_k(t) = \sum_{i=0}^{L-1} h_{k,i} \delta_D(t - iT_c), \tag{3.6}$$

where the ith channel tap, $h_{k,i}$, is described as one complex Gaussian random variable whose mean is zero and has variance as σ^2, i.e.,

$$h_{k,i} \sim CN(0, \sigma^2). \tag{3.7}$$

After passing through the channel, the transmit signal is destroyed by the multipath channel and contaminated by the noise, and the received signal at the kth receiver is

$$r_k(t) = h_k(t) * y(t) + n_k(t), \tag{3.8}$$

where $n_k(t)$ is a zero mean, circularly complex Gaussian process with power spectrum density equal to σ_n^2. The kth mobile device performs the chip waveform match and then takes sample for every chip interval. As a result, the equivalent discrete representation for the received signal $r_k(t)$ becomes

$$\begin{aligned}\mathbf{r}_k(i) &= [r_{k,0}(i), \cdots, r_{k,L+L_p+N-3}(i)]^t, \\ &= \sum_{j=1}^{K} \mathbb{S}_j \bar{\mathbf{h}}_{j,k} b_j(i) + \boldsymbol{\mathcal{I}}_k(i) + \mathbf{n}_k(i), \\ &= \sum_{j=1}^{K} \mathbb{S}_j \mathbf{H}_k \mathbf{p}_j b_j(i) + \boldsymbol{\mathcal{I}}_k(i) + \mathbf{n}_k(i),\end{aligned} \tag{3.9}$$

where

$$\bar{\mathbf{h}}_{j,k} = [\bar{h}_{j,k,0}, \cdots, \bar{h}_{j,k,L+L_p-2}]^t = \mathbf{H}_k \mathbf{p}_j \tag{3.10}$$

denotes the effective channel response for the signal $b_j(t)$ to the kth receiver,

$$\boldsymbol{\mathcal{I}}_k(i) = [I_{k,0}(i), \cdots, I_{k,L+L_p+N-3}(i)]^t \tag{3.11}$$

and

$$\mathbf{n}_k(i) = [n_{k,0}(i), \cdots, n_{k,L+L_p+N-3}(i)]^t \tag{3.12}$$

denotes the corresponding interference and noise vectors for the kth user, respectively,

$$\mathbf{p}_j = [p_{j,0}, \cdots, p_{j,L_p-1}]^t \tag{3.13}$$

is a $L_p \times 1$ precoding vector for the jth user, and

$$\mathbb{S}_j = \begin{bmatrix} s_{j,0} & & \\ \vdots & s_{j,0} & \\ s_{j,N-1} & \vdots & \ddots \\ & s_{j,N-1} & \ddots \\ & & \ddots \end{bmatrix}_{(L+L_p+N-2)\times(L+L_p-1)} \tag{3.14}$$

and

$$\mathbf{H}_j = \begin{bmatrix} h_{j,0} & & \\ \vdots & h_{j,0} & \\ h_{j,L-1} & \vdots & \ddots \\ & h_{j,L-1} & \ddots \\ & & \ddots \end{bmatrix}_{(L+L_p-1)\times L_p} \tag{3.15}$$

are two Toeplitz matrices for the convolution operation. In addition, every element in $\mathbf{n}_k(i)$ is modeled as an i.i.d. circularly complex Gaussian random variable and is denoted as

$$n_{k,j}(i) \sim CN(0, \sigma_n^2). \tag{3.16}$$

To simplify the following analysis, we assume that the noise power is the same for all users. Here we restrict each receiver employing a simple MF receiver,[1] which first synchronizes to the L_pth effective channel tap in $\bar{h}_{k,k}$ and perform the despreading operation to get decision statistic $z_k(i)$, i.e.,

$$z_k(i) = \mathbf{f}_k^{\dagger} \mathbf{r}_k(i), \tag{3.17}$$

where

$$\mathbf{f}_k = [\underbrace{0, \cdots, 0}_{1\times(\mathrm{L_p}-1)}, s_{k,0}, \cdots, s_{k,N-1}, \underbrace{0, \cdots, 0}_{1\times(\mathrm{L}-1)}]^t. \tag{3.18}$$

By substituting (3.9) into (3.17), we can simplify $z_k(i)$ as

$$\begin{aligned} z_k(i) &= \mathbf{f}_k^{\dagger} \mathbf{r}_k(i) \\ &= \mathbf{f}_k^{\dagger} \left(\sum_{j=1}^{K} \mathbb{S}_j \mathbf{H}_k \mathbf{p}_j b_j(i) + \boldsymbol{\mathcal{I}}_k(i) + \mathbf{n}_k(i) \right) \\ &= \sum_{j=1}^{K} \mathbf{r}_{j,k}^{(0),\dagger} \mathbf{H}_k \mathbf{p}_j b_j(i) + \mathtt{I}_k(i) + \mathtt{n}_k(i), \end{aligned} \tag{3.19}$$

where $\mathtt{I}_k(i) = \mathbf{f}_k^{\dagger} \boldsymbol{\mathcal{I}}_k(i)$,

$$\mathtt{n}_k(i) = \mathbf{f}_k^{\dagger} \mathbf{n}_k(i) \sim CN(0, \sigma_n^2), \tag{3.20}$$

$$\mathbf{r}_{j,k}^{(0)} = [\mathbf{r}_{j,k}(L_p - 1), \cdots, \mathbf{r}_{j,k}(0), \cdots, \mathbf{r}_{j,k}(-L+1)]^t, \tag{3.21}$$

and

$$\mathbf{r}_{j,k}(d) = \sum_{i=0}^{N-1} s_{j,i+d} s_{k,i} \tag{3.22}$$

measures the cross-correlation between $\mathbf{s}_j$ and $\mathbf{s}_k$. Please note that the variables, vectors, and matrices shown in (3.19) are functions of the precoder length L_p and we simply omit it for notation simplicity. The kth receiver estimates the ith transmit symbol as

$$\bar{b}_k(i) = \mathrm{sign}\left\{ \Re\{ z_k(i) \} \right\}. \tag{3.23}$$

[1] It is worthwhile to point out that although a better system performance can be achieved by combining more than one channel tap in $\bar{h}_{k,k}(t)$. This idea, which necessitates a Rake receiver, is complicated for mobile devices and hence is not considered here.

3.2 Transmit Matched Filter

The frequency selective fading channel in nature leads to multiple propagation paths from the transmitter to the receiver, i.e., signal traveling along different path experiences independent path gain and arrives at the receiver at different time delay. The multipath channel provides additional frequency diversity, which prevents the received signal from deep fading since it is less likely that all the channel gains are in deep fading at the same time. Yet the conventional MF receiver, which synchronizes to some path only, fails to collect enough signal power scattered in the channel for symbol decoding. As a result, the performance of the MF receiver in the multipath channel is not good.

In order to enjoy this multipath diversity, the Rake receiver with several fingers, each of which is synchronized to an individual path, is usually adopted in the frequency selective fading channel [105]. Apparently, there is a trade-off between the system performance and the number of Rake fingers. The required number of fingers could be large, especially in some extremely frequency selective fading environment, such as the ultra-wideband (UWB) channel [151]. Since the receiver cost increases dramatically as the finger number grows, the Rake receiver is not attractive to the low cost mobile system design.

The idea of shifting complexity of multipath combining from the mobile receiver to the base station, called Pre-Rake, which utilizes the time-reversed channel impulse response as its precoder, is first proposed for the single-input single-output (SISO) TDD-DS-CDMA system by Esmailzadeh et al. in [34] and later generalized to the multi-input single-output (MISO) TDD-DS-CDMA system by Choi et al. in [24] to exploit additional transmit diversity at the base station. A similar idea, called time-reversal prefilter (TRP), was proposed first to the under water acoustic signal processing in [33, 40, 51] and later to the wireless communication scenarios in [68, 94, 123]. In fact, both TRP or Pre-Rake can be viewed as a special case of the transmit matched filter (Tx-MF), which will be derived next.

Usually, the precoder length is less or equal to that of the channel response, i.e., $L_p \leq L$. Let us now consider a special case when $L_p = L$. The idea of choosing $L_p = L$ will become clear later in this section. Given $L_p = L$, the decision statistic for the ith transmit symbol from the kth user $z_k(i)$ in (3.19) can be represented as

$$\begin{aligned} z_k(i) &= \sum_{j=0}^{K} \mathbf{r}_{j,k}^{(0),\dagger} \mathbf{H}_k \mathbf{p}_j b_j(i) + \mathtt{I}_k(i) + \mathtt{n}_k(i) \\ &= \mathbf{r}_{k,k}^{(0),\dagger} \mathbf{H}_k \mathbf{p}_k b_k(i) + \sum_{j=1; j\neq k}^{K} \mathbf{r}_{j,k}^{(0),\dagger} \mathbf{H}_k \mathbf{p}_j b_j(i) + \mathtt{I}_k(i) + \mathtt{n}_k(i). \end{aligned} \tag{3.24}$$

The first term at the right-hand side of (3.24) denotes the desired signal for the kth user. The goal of Tx-MF is to maximize the desired signal power in

$z_k(i)$ subject to the limited transmit power E_k. Hence, the precoder design problem can be reformulated as

$$\mathbf{p}_k^{(Tx-MF)} = \arg\max_{\mathbf{p}_k} E\left\{\left|\mathbf{r}_{k,k}^{(0),\dagger}\mathbf{H}_k\mathbf{p}_k b_k(i)\right|^2\right\} \quad \text{s.t.} \quad E\left\{|\mathbf{S}_k\mathbf{p}_k b_k(i)|^2\right\} = E_k. \tag{3.25}$$

Please note that $\mathbf{S}_k$ above is a $(L_p+N-1)\times L_p$ Toeplitz matrix, whose first column is

$$[s_{k,0},\cdots,s_{k,N-1},\underbrace{0,\cdots,0}_{1\times(L_p-1)}]^t. \tag{3.26}$$

The above constrained optimization problem is solved in Section 3.5.1, and we have the Tx-MF for the kth user as

$$\mathbf{p}_k^{(Tx-MF)} = \sqrt{\frac{E_k}{\mathbf{r}_{kk}^{(0),\dagger}\mathbf{H}_k\mathbf{R}_{\mathbf{S}_k}^{-1}\mathbf{H}_k^{\dagger}\mathbf{r}_{kk}^{(0)}}}\mathbf{R}_{\mathbf{S}_k}^{-1}\mathbf{H}_k^{\dagger}\mathbf{r}_{k,k}^{(0)}, \tag{3.27}$$

where $\mathbf{R}_{\mathbf{S}_k}$ is defined in (3.50). It is worthwhile to comment that different optimization criterion for Tx-MF, for example,

$$\mathbf{p}_k^{(Tx-MF)} = \arg\max_{\mathbf{p}_k} E\left\{\Re\left\{\mathbf{r}_{k,k}^{(0),\dagger}\mathbf{H}_k\mathbf{p}_k b_k(i)\right\}^2\right\} \quad \text{s.t.} \quad E\left\{|\mathbf{S}_k\mathbf{p}_k b_k(i)|^2\right\} = E_k \tag{3.28}$$

is also considered in [24] since the decoding performance is only related to the real part of the desired signal. However, it is easy to show that both (3.25) and (3.28) lead to the same solution.

Let us consider a special case when the autocorrelation property of $\mathbf{s}_k$ is ideal, i.e.,

$$\mathbf{r}_{k,k}(i) = \begin{cases} 1, i=0, \\ 0, \text{elsewhere.} \end{cases} \tag{3.29}$$

Therefore, $\mathbf{R}_{\mathbf{S}_k}$ and $\mathbf{r}_{k,k}^{(0)}$ become

$$\mathbf{R}_{\mathbf{S}_k} = \mathbf{I}_{2L-1} \tag{3.30}$$

and

$$\mathbf{r}_{k,k}^{(0)} = [\underbrace{0,\cdots,0}_{L-1},1,\underbrace{0,\cdots,0}_{L-1}]^t. \tag{3.31}$$

By substituting (3.31) and (3.30) into (3.27), the Tx-MF becomes

$$\mathbf{p}_k^{(Tx-MF)} = \frac{\sqrt{E_k}}{||\bar{\mathbf{h}}_k||}\bar{\mathbf{h}}_k, \tag{3.32}$$

where

$$\bar{\mathbf{h}}_k = [h_{k,L-1},\cdots,h_{k,0}]^t \tag{3.33}$$

is the reversed-order channel tap vector, and $||\mathbf{x}||$ denotes the 2-norm of vector $\mathbf{x}$. Equation (3.32) is the well-known Pre-Rake (or TRP), which is a special case of Tx-MF when the autocorrelation property of the spreading code $\mathbf{s}_k$ is perfect. In other words, the Pre-Rake or TRP, which utilizes the time-order reversed channel impulse response as its precoder, does not consider the spreading code structure into its precoder design. In addition, the MF receiver synchronizes to the channel tap $\bar{h}_{k,k,L-1}$, whose power is

$$\left(\bar{h}_{k,k,L-1}\right)^2 = \left(\mathbf{r}_{k,k}^{(0),\dagger}\mathbf{H}_k\mathbf{p}_k^{(Tx-MF)}\right)^2 = \sum_{l=0}^{L-1}|h_{k,l}|^2, \tag{3.34}$$

which suggests that the full multipath diversity is achieved at the MF receiver output. This is because all the channel taps are combined coherently after some delay and we denote $\bar{h}_{k,k,L-1}$ as the peak channel tap in $\bar{\mathbf{h}}_{k,k}$. On the contrary, the signal power of those off-peak signals $\bar{h}_{k,k,j}, \forall j \neq L-1$ are much weaker than that of $\bar{\mathbf{h}}_{k,k,L-1}$ since the original channel taps in $\mathbf{h}_k$ are combined excursively. Obviously, the precoder length L_p also affects the concentrated peak signal power in $\bar{\mathbf{h}}_{k,k}$. In order to achieve the full diversity, we let $L_p = L$.

Example 3.1: Rather than considering an autocorrelation function of a specific spreading code, a SISO Pre-Rake transmit filter example is given in Fig. 3.2. We assume that all the channel taps are real so that they can

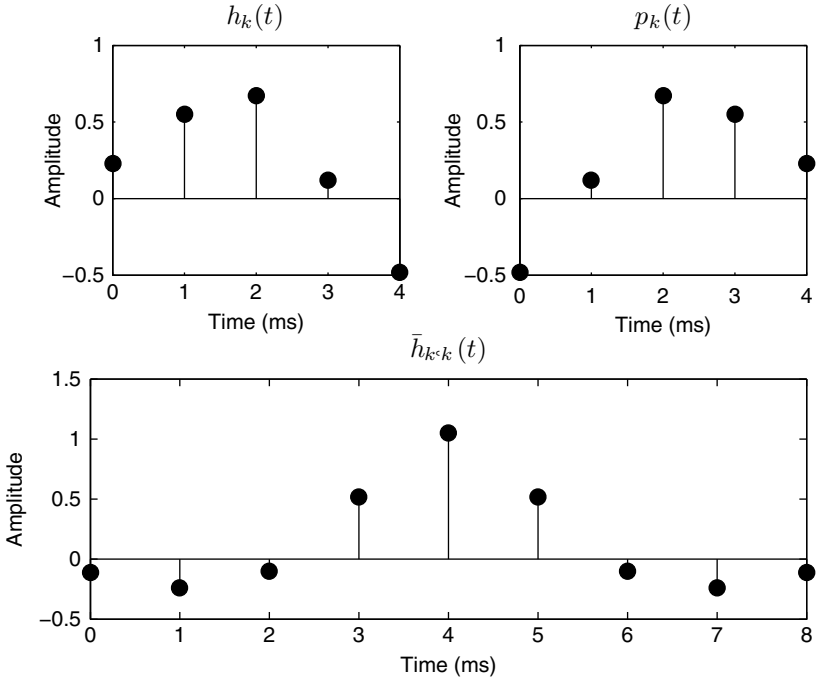

Fig. 3.2. The example of Pre-Rake transmit prefilter for the kth user.

be plotted in a two dimensional coordinate. $h_k(t)$, $p_k(t)$, and $\bar{h}_{k,k}(t)$ are the responses of the original channel, precoder, and the resultant channel for the kth user, respectively. In addition, the total power in $h_k(t)$ is normalized to one and the inter-arrival time between two consecutive taps is set as 1 ms. An obvious peak signal is presented in $\bar{h}_{k,k}(t)$ at 4 ms, which is the maximum tap delay of $h_k(t)$.

Example 3.2: In the following example, we demonstrate the performance improvement via additional Tx-MF precoding in this example. The downlink CDMA channel contains 10 users, each of which utilizes an unique Gold sequence of 31-chip in length. The channel response of every user consists of 5 multipath components, which are realized independently between different paths and different users. Furthermore, the length of the Tx-MF precoder is fixed as that of the channel response. The BEP curve corresponding to the Tx-MF is plotted in Fig. 3.3 at different SNR values. The performance curve from the conventional MF, which synchronizes to the strongest channel tap for decoding, is also provided as the performance benchmark. It is observed that the gap coming from additional Tx-MF precoding is at least 4 dB and it becomes more obvious while the signal power goes up.

The prefilter response depends on the current channel realization between the transmitter and the designated receiver. Therefore, the transmitted signal power will be concentrated at the desired receiver only rather than other

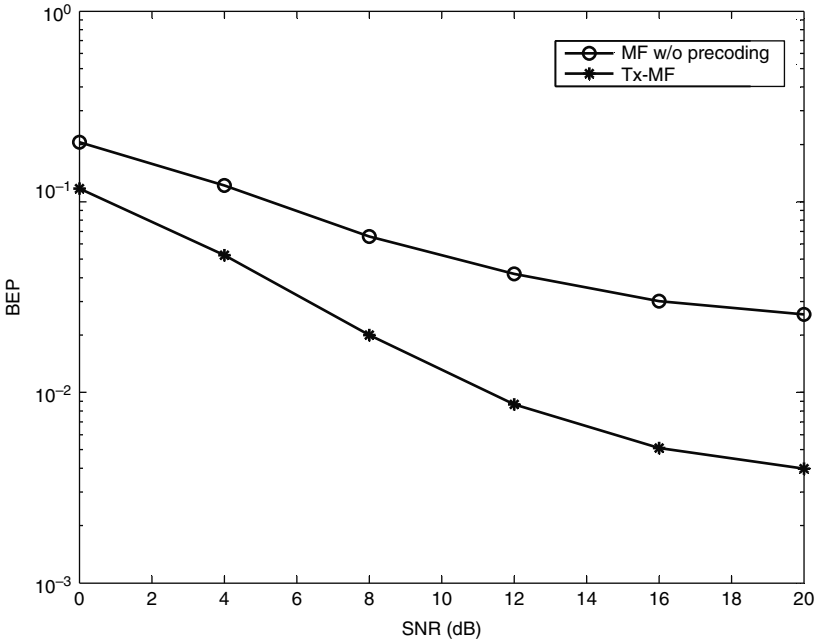

Fig. 3.3. Performance gap between the conventional MF without precoding and Tx-MF.

receivers in the system since the channel responses from different users are independent. Consequently, the MAI in the pre-Rake system is somewhat reduced as compared with that of the system without Tx-MF. It is however that the Tx-MF scheme, which does not consider the transmit signals and the downlink channel responses of other users in the system, may not suppress MAI efficiently at the receiver output. Two different precoder design schemes, namely Tx-ZF and Tx-Wiener, which remove or suppresse the possible interference, are reviewed next.

3.3 Transmit Zero-Forcing Filter

Although Tx-MF provided in the previous section achieves the maximal peak signal power at the desired receiver output, it may cause a strong interference to other co-channel users in the system since only the channel knowledge of the desired user is considered for the precoder design. In fact, a better system performance can be achieved by jointly designing all K precoders such that not only the peak signal power is maximized but also the interference is erased or minimized.

The transmit zero-forcing filter (Tx-ZF) is designed to decorrelate all the transmit signals such that the signal at every receiver output is free of interference and is derived as follows. Let us assume that every precoder is a L_p-tap FIR filter and both L_p and L are much smaller than N so that the inter-symbol interference (ISI) is dominated by previous one and next one transmit symbols only. Please note that the scheme discussed here can be generalized to different values of N, L_p, and L as well. If the kth MF receiver synchronizes to the L_pth effective channel tap $\bar{h}_{k,k,L_p-1}$ and performs signal despreading, the decision statistic for the ith transmit symbol in (3.24) can be represented as

$$z_k(i) = \sum_{l=-1}^{1} \sum_{j=1}^{K} \mathbf{r}_{j,k}^{(l),\dagger} \mathbf{H}_k \mathbf{p}_j b_j(i+l) + \mathtt{n}_k(i), \tag{3.35}$$

where $\mathbf{r}_{j,k}^{(0)}$ is given in (3.21) and

$$\mathbf{r}_{j,k}^{(-1)} = [0, \cdots, 0, r_{j,k}(N-1), \cdots, r_{j,k}(N-L+1)]^t, \tag{3.36}$$

and

$$\mathbf{r}_{j,k}^{(+1)} = [r_{j,k}(L_p-1-N), \cdots, r_{j,k}(1-N), 0, \cdots, 0]^t \tag{3.37}$$

denote different weight vectors for signals coming from the previous and followed symbols, respectively. By substituting (3.21), (3.36), and (3.37) into (3.35), $z_k(i)$ becomes

$$
\begin{aligned}
z_k(i) &= \sum_{j=1}^{K} \sum_{l=-1}^{1} \mathbf{r}_{j,k}^{(l),\dagger} \mathbf{H}_k \mathbf{p}_j b_j(i+l) + \mathtt{n}_k(i) \\
&= \mathbf{r}_{k,k}^{(0),\dagger} \mathbf{H}_k \mathbf{p}_k b_k(i) \\
&\quad + \mathbf{r}_{k,k}^{(-1),\dagger} \mathbf{H}_k \mathbf{p}_k b_k(i-1) + \mathbf{r}_{k,k}^{(+1),\dagger} \mathbf{H}_k \mathbf{p}_k b_k(i+1) \\
&\quad + \sum_{j=1, j\neq k}^{K} \sum_{l=-1}^{1} \mathbf{r}_{j,k}^{(l),\dagger} \mathbf{H}_k \mathbf{p}_j b_j(i+l) + \mathtt{n}_k(i),
\end{aligned} \tag{3.38}
$$

where the second and the third terms at the right-hand side of (3.38) are the pre-cursor and post-cursor ISI, respectively, and the fourth term is the MAI caused by all the other precoders $\mathbf{p}_j$, $\forall j \neq k$. In other words, the precoder $\mathbf{p}_k$ not only contributes ISI to the its receiver, but also causes MAI described as

$$
\sum_{l=-1}^{1} \mathbf{r}_{k,j}^{(l),\dagger} \mathbf{H}_j \mathbf{p}_k b_k(i+l)
$$

to the ith decision statistic of user j, $z_j(i)$.

Based on the similar scheme proposed in [12], we construct the Tx-ZF for the kth user $\mathbf{p}_k^{(Tx-ZF)}$, which is a symbol-wise FIR filter to remove the total interference caused by the transmit signal of user k while being subject to the total transmit power constraint, as follows.

$$
\mathbf{p}_k^{(Tx-ZF)} = \arg\max_{\mathbf{p}_k} \mathbf{r}_{k,k}^{(0),\dagger} \mathbf{H}_k \mathbf{p}_k \tag{3.39}
$$

subject to

$$
\begin{cases}
\mathbf{r}_{k,j}^{(l),\dagger} \mathbf{H}_j \mathbf{p}_k = 0, \ \forall 1 \leq j \leq K \text{ and } l = -1, 0, 1, \text{ except } (j,l) = (k,0), \\
E\left\{ |\mathbf{S}_k \mathbf{p}_k b_k(i)|^2 \right\} = \mathbf{p}_k^{\dagger} \mathbf{S}_k^{\dagger} \mathbf{S}_k \mathbf{p}_k = E_k,
\end{cases}
$$

where $\mathbf{S}_k$ is the same as the one given in (3.25). The Tx-ZF design problem in (3.39) can be solved in two steps, i.e., we design the precoder to satisfy the zero-forcing constraint first while maintaining the unit channel gain for the desired signal and then adjust the transmit power to confine the second constraint. Consider the following linear system equation,

$$
\boldsymbol{\mathcal{H}}_k \bar{\mathbf{p}}_k = \mathbf{e}_{3K}^{(3(k-1)+2)}, \tag{3.40}
$$

where

$$\boldsymbol{\mathcal{H}}_k = \begin{bmatrix} \boldsymbol{\mathcal{H}}_{k,1} \\ \vdots \\ \boldsymbol{\mathcal{H}}_{k,k} \\ \vdots \\ \boldsymbol{\mathcal{H}}_{k,K} \end{bmatrix}_{3K \times L_p}, \tag{3.41}$$

$$\boldsymbol{\mathcal{H}}_{k,j} = \begin{bmatrix} \mathbf{r}_{k,j}^{(-1),\dagger} \mathbf{H}_j \\ \mathbf{r}_{k,j}^{(0),\dagger} \mathbf{H}_j \\ \mathbf{r}_{k,j}^{(+1),\dagger} \mathbf{H}_j \end{bmatrix}_{3 \times L_p}. \tag{3.42}$$

The solution $\bar{\mathbf{p}}_k$ in (3.40) is found as

$$\bar{\mathbf{p}}_k = \boldsymbol{\mathcal{H}}_k^{\ddagger} \mathbf{e}_{3K}^{(3(k-1)+2)}. \tag{3.43}$$

Note that since the dimension of $\boldsymbol{\mathcal{H}}_k$ is $3K \times L_p$, $\bar{\mathbf{p}}_k$ is guaranteed if L_p is greater or equal to $3K$. In other words, the interference can be completely removed in this case. Otherwise, we need to resort to the least-square solution instead. However, the output of MF receiver is not free of interference. Next, we enforce the transmit power constraint into Tx-ZF design so that we have

$$\mathbf{p}_k^{(Tx-ZF)} = \frac{\sqrt{E_k}}{||\mathbf{S}_k^{\dagger} \bar{\mathbf{p}}_k||} \bar{\mathbf{p}}_k. \tag{3.44}$$

Another Tx-ZF design criteria is to maintain the channel gain for the desired signal while suppressing all the interference at K receiver outputs with the minimum transmit power. Mathematically, we can have

$$\mathbf{p}_k^{(Tx-ZF)} = \arg \min_{\mathbf{p}_k} \mathbf{p}_k^{\dagger} \mathbf{S}_k^{\dagger} \mathbf{S}_k \mathbf{p}_k \text{ s.t. } \boldsymbol{\mathcal{H}}_k \mathbf{p}_k = \mathbf{e}_{3K}^{(3(k-1)+2)}, \tag{3.45}$$

where we consider the equal gain for all K desired signals without the loss of generality. The solution to this alternative Tx-ZF design is provided in Section 3.5.2. In fact, the solution provided in Section 3.5.2 also minimizes the meas-square-error (MSE) between $b_k(i)$ and $z_k(i)$, $\forall 1 \leq k \leq K$. This is because the noise term at the MF filter output is independent of the precoder design and we can always design a proper Tx-ZF precoder to cancel all the interference before hand. The Tx-ZF design using MMSE criterion was also proposed in [147].

It is however noted that the zero-forcing precoder removes all the ISI and MAI at the expense of reduced desired signal power since part of the transmit power is used to cancel interference. On the contrary, more power is required to maintain the same power level of the desired signal as compared to the system without Tx-ZF. Therefore, when the transmit power limitation is imposed, the MMSE design criterion cannot lead to Tx-ZF precoder anymore.

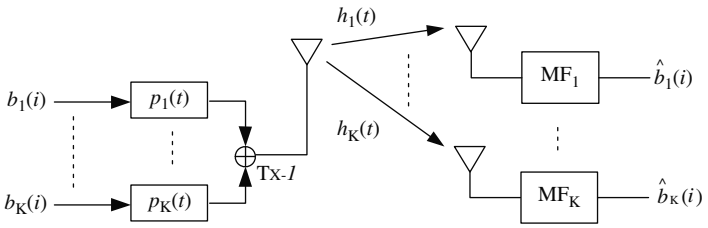

Fig. 3.4. The block diagram of the generalized SISO Tx-ZF DS-CDMA system in [12] [©IEEE].

The conventional Tx-ZF processes the transmit signal after despreading. It is however that the enforced spreading code structure limits the flexibility of its precoder design. In fact, a more generalized precoder scheme is to prefilter the original transmit symbol $b_k(i)$, $\forall k$, directly without the use of spreading code [12] while the kth receiver employs a known code $\mathbf{s}_k$ for signal despreading [12]. The corresponding system block diagram is given in Fig. 3.4. It was shown in [12] that this generalized precoder is more flexible and achieves even better performance than the conventional precoder with additional signal spreading operation at the transmitter [12].

3.4 Transmit Wiener Filter

In the previous sections, we introduced two precoder design ideas, namely Tx-MF and Tx-ZF. On the one hand, Tx-ZF, which focuses on the interference suppression alone, fails to provide better system performance than Tx-MF when the noise power is strong. On the other hand, when the noise power is weak, Tx-MF, which focuses the desired signal power without considering the interference structure into its precoder design, does not outperform Tx-ZF. In this section, we introduce another linear precoder design concept, called transmit Wiener filter (Tx-Wiener), which balances the noise suppression and interference cancelation.

We adopt the same system model and notations introduced in the previous Sections 3.2 and 3.3. Now we somewhat modify the receiver structure by placing one amplifier immediately before the signal despreading operator as shown in Fig. 3.5 where the gain of the receiver amplifier is α and is assumed to be

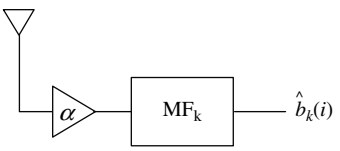

Fig. 3.5. The block diagram of the modified Rx structure for SISO Tx-Wiener SISO DS-CDMA system.

the same for all K receivers. Again, consider the case when Tx-Wiener precoder is a L_p-tap FIR filter and the kth MF receiver synchronizes to $\bar{h}_{k,k,L_p-1}$ for the received signal despreading. Thus, the output of the kth MF receiver for the ith transmit symbol, $z_k(i)$ is described as

$$z_k(i) = \sum_{l=-1}^{1} \sum_{j=1}^{K} \alpha \mathbf{r}_{j,k}^{(l),\dagger} \mathbf{H}_k \mathbf{p}_j b_j(i+l) + \alpha \mathtt{n}_k(i). \tag{3.46}$$

The Tx-Wiener $\mathbf{p}_k^{(Tx-Wiener)}, \forall 1 \le k \le K$, and the receiver gain $\alpha^{(Tx-Wiener)}$ are jointly adjusted to minimize the sum of K output MSE subject to the total precoder power constraint E_p, i.e.,

$$\begin{aligned} &\left\{ \mathbf{p}_1^{(Tx-Wiener)}, \cdots, \mathbf{p}_K^{(Tx-Wiener)}, \alpha^{(Tx-Wiener)} \right\} \\ &= \arg \min_{\mathbf{p}_1,\cdots,\mathbf{p}_K,\alpha} \sum_{k=1}^{K} E\left\{ \left| b_k(i) - z_k(i) \right|^2 \right\} \text{ s.t. } \sum_{k=1}^{K} \mathbf{p}_k^{\dagger} \mathbf{S}_k^{\dagger} \mathbf{S}_k \mathbf{p}_k = E_p. \end{aligned} \tag{3.47}$$

The Tx-Wiener filter and the optimal gain are derived in Section 3.5.3.

Recall that the receiver-based Wiener filter converges to the receiver-based ZF and MF when the noise power approach to zero or infinity, respectively. In fact, a similar property can be found in Tx-Wiener as well. Consider the case when the noise power approaches infinity, the Tx-Wiener for the kth user in (3.76) converges to

$$\lim_{\sigma_n^2 \to \infty} \mathbf{p}_k^{(Tx-Wiener)} = \sqrt{\frac{E_p}{\sum_{k=1}^{K} \mathbf{r}_{k,k}^{(0),\dagger} \mathbf{H}_k^{\dagger} \mathbf{R}_{\mathbf{S}_k}^{-1} \mathbf{H}_k \mathbf{r}_{k,k}^{(0)}}} \mathbf{R}_{\mathbf{S}_k}^{-1} \mathbf{H}_k^H \mathbf{r}_{k,k}^{(0)}, \tag{3.48}$$

which is the same as the Tx-MF filter shown in (3.27) with different scaling factors. This is because both systems are derived under different constraints, say, the individual transmit power limit for Tx-MF and the total transmit power limit for Tx-Wiener. On the contrary, when the noise power becomes infinitesimal, the Tx-Wiener is similar to Tx-ZF shown in (3.59) with different scaling factor. This interesting behavior of Tx-Wiener filter was first reported by Joham et al. in [61].

Example 3.3: The performance of different precoding schemes used to combat interference, such as Tx-ZF and Tx-MMSE, are provided in this example. The system parameters are the same as those in the previous example and the result we have is shown in Fig. 3.6. Please note that the curves for both Tx-MF and the conventional MF without precoding are plotted and served as the references. It is obvious that suppressing interfering signals improves the system performance. However, Tx-ZF with the fixed transmit power fails to provide a better decoding performance than Tx-MF when SNR is less than 10 dB. This is because it reduces the interference power at the cost of its output signal power.

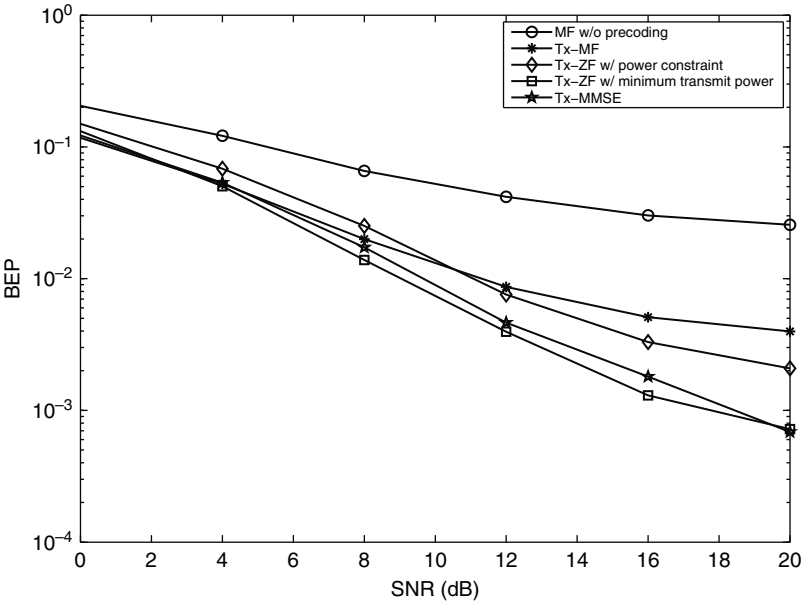

Fig. 3.6. Performance of different precoding schemes.

3.5 Appendix

3.5.1 Derivation of Tx-MF

The solution to (3.25) is given here. Let us first simplify the constrained optimization problem as

$$\mathbf{p}_k^{(Tx-MF)} = \arg\max_{\mathbf{p}_k} \left\{ \mathbf{p}_k^{\dagger} \mathbf{H}_k^{\dagger} \mathbf{r}_{k,k}^{(0)} \mathbf{r}_{k,k}^{(0),\dagger} \mathbf{H}_k \mathbf{p}_k \right\} \quad \text{s.t.} \quad \left\{ \mathbf{p}_k^{\dagger} \mathbf{R}_{\mathbf{S}_k} \mathbf{p}_k \right\} = E_k, \tag{3.49}$$

where

$$\mathbf{R}_{\mathbf{S}_k} = \mathbf{S}_k^{\dagger} \mathbf{S}_k = \mathbf{R}_{\mathbf{S}_k}^{1/2,\dagger} \mathbf{R}_{\mathbf{S}_k}^{1/2}, \tag{3.50}$$

is a $L_p \times L_p$ full-rank matrix. Since $\mathbf{R}_{\mathbf{S}_k}^{-1/2}$ is also a full-rank matrix, we can have the following transformation between $\mathbf{p}_k$ and $\mathbf{w}_k$ as

$$\mathbf{p}_k = \mathbf{R}_{\mathbf{S}_k}^{-1/2} \mathbf{w}_k. \tag{3.51}$$

By substituting (3.51) into (3.49) and performing some manipulation, (3.49) becomes

$$\mathbf{w}_k^{(opt)} = \arg\max_{\mathbf{w}_k} \left\{ \mathbf{w}_k^{\dagger} \mathbf{R}_{\mathbf{S}_k}^{-1/2,\dagger} \mathbf{H}_k^{\dagger} \mathbf{r}_{k,k}^{(0)} \mathbf{r}_{k,k}^{(0),\dagger} \mathbf{H}_k \mathbf{R}_{\mathbf{S}_k}^{-1/2} \mathbf{w}_k \right\}$$
$$\text{s.t.} \quad \left\{ \mathbf{w}_k^{\dagger} \mathbf{w}_k \right\} = E_k, \tag{3.52}$$

where the problem is transformed to find the optimal $\mathbf{w}_k$ with additional energy constraint on $\mathbf{w}_k$. It is easy to show that the best $\mathbf{w}_k$ satisfying (3.52) is

$$\mathbf{w}_k^{(opt)} = \sqrt{\frac{E_k}{\mathbf{r}_{kk}^{(0),\dagger}\mathbf{H}_k\mathbf{R}_{\mathbf{S}_k}^{-1}\mathbf{H}_k^{\dagger}\mathbf{r}_{kk}^{(0)}}}\mathbf{R}_{\mathbf{S}_k}^{-1/2,\dagger}\mathbf{H}_k^{\dagger}\mathbf{r}_{k,k}^{(0)}. \tag{3.53}$$

Therefore, the solution of $\mathbf{p}_k^{(Tx-MF)}$ is acquired by

$$\begin{aligned}\mathbf{p}_k^{(Tx-MF)} &= \mathbf{R}_{\mathbf{S}_k}^{-1/2}\mathbf{w}_k^{(opt)} \\ &= \sqrt{\frac{E_k}{\mathbf{r}_{kk}^{(0),\dagger}\mathbf{H}_k\mathbf{R}_{\mathbf{S}_k}^{-1}\mathbf{H}_k^{\dagger}\mathbf{r}_{kk}^{(0)}}}\mathbf{R}_{\mathbf{S}_k}^{-1}\mathbf{H}_k^{\dagger}\mathbf{r}_{k,k}^{(0)}.\end{aligned} \tag{3.54}$$

3.5.2 Derivation of Tx-ZF with Minimum Output Power Constraint

The Tx-ZF design problem in (3.45) can be rewritten as

$$\mathbf{p}_k^{(Tx-ZF)} = \arg\min_{\mathbf{w}_k}\mathbf{w}_k^{\dagger}\mathbf{w}_k \text{ s.t. } \boldsymbol{\mathcal{H}}_k\mathbf{R}_{\mathbf{S}_k}^{-1/2}\mathbf{w}_k = \mathbf{e}_{3K}^{(3(k-1)+2)}, \tag{3.55}$$

where $\mathbf{p}_k$ in (3.45) is replaced by $\mathbf{R}_{\mathbf{S}_k}^{-1/2}\mathbf{w}_k$ and $\mathbf{R}_{\mathbf{S}_k}$ is given in (3.50). Generally speaking, we can first figure out the optimal $\mathbf{w}_k^{(opt)}$ by using the pseudo-inverse of $\boldsymbol{\mathcal{H}}_k\mathbf{R}_{\mathbf{S}_k}^{-1/2}$, i.e.,

$$\mathbf{w}_k^{(opt)} = \left(\boldsymbol{\mathcal{H}}_k\mathbf{R}_{\mathbf{S}_k}^{-1/2}\right)^{\dagger}\mathbf{e}_{3K}^{(3(k-1)+2)}, \tag{3.56}$$

and then acquire $\mathbf{p}_k^{(Tx-ZF)}$ as

$$\mathbf{p}_k^{(Tx-ZF)} = \mathbf{R}_{\mathbf{S}_k}^{-1/2}\mathbf{w}_k^{(opt)} = \mathbf{R}_{\mathbf{S}_k}^{-1/2}\left(\boldsymbol{\mathcal{H}}_k\mathbf{R}_{\mathbf{S}_k}^{-1/2}\right)^{\dagger}\mathbf{e}_{3K}^{(3(k-1)+2)}. \tag{3.57}$$

Consider a special case when $\text{rank}\{\boldsymbol{\mathcal{H}}_k\mathbf{R}_{\mathbf{S}_k}^{-1/2}\} = L_p$, and

$$\left(\boldsymbol{\mathcal{H}}_k\mathbf{R}_{\mathbf{S}_k}^{-1/2}\right)^{\dagger} = \left(\mathbf{R}_{\mathbf{S}_k}^{-1/2,\dagger}\boldsymbol{\mathcal{H}}_k^{\dagger}\boldsymbol{\mathcal{H}}_k\mathbf{R}_{\mathbf{S}_k}^{-1/2}\right)^{-1}\mathbf{R}_{\mathbf{S}_k}^{-1/2,\dagger}\boldsymbol{\mathcal{H}}_k^{\dagger}. \tag{3.58}$$

Therefore, it can be shown that

$$\begin{aligned}\mathbf{p}_k^{(Tx-ZF)} &= \mathbf{R}_{\mathbf{S}_k}^{-1/2} \\ &\quad * \left(\sum_{j=1}^{K}\sum_{l=-1}^{1}\mathbf{R}_{\mathbf{S}_k}^{-1/2,\dagger}\mathbf{H}_j^{\dagger}\mathbf{r}_{k,j}^{(l)}\mathbf{r}_{k,j}^{(l),\dagger}\mathbf{H}_j\mathbf{R}_{\mathbf{S}_k}^{-1/2}\right)^{-1}\mathbf{R}_{\mathbf{S}_k}^{-1/2,\dagger}\mathbf{H}_k^{\dagger}\mathbf{r}_{k,k}^{(0)}.\end{aligned} \tag{3.59}$$

3.5.3 Derivation of Tx-Wiener

Let us first rewrite $z_k(i)$ in (3.46) as

$$\begin{aligned} z_k(i) &= \sum_{l=-1}^{1}\sum_{j=1}^{K} \alpha \mathtt{r}_{j,k}^{(l),\dagger}\mathbf{H}_k\mathbf{p}_j b_j(i+l) + \alpha \mathtt{n}_k(i) \\ &= \alpha\left(\sum_{l=-1}^{1}\mathbf{b}(i+l)^\dagger \mathbf{R}_k^{(l),\dagger}\mathbb{H}_k\mathbf{p}\right) + \alpha\mathtt{n}_k(i), \end{aligned} \tag{3.60}$$

where

$$\mathbf{b}(i) = [b_1(i),\cdots,b_K(i)]^t, \tag{3.61}$$

$$\mathbf{R}_k^{(l)} = \mathrm{diag}\left[\mathtt{r}_{1,k}^{(l)},\cdots,\mathtt{r}_{K,k}^{(l)}\right], \tag{3.62}$$

$$\mathbb{H}_k = \mathrm{diag}\left[\mathbf{H}_k,\cdots,\mathbf{H}_k\right], \tag{3.63}$$

$$\mathbf{p} = [\mathbf{p}_1^t,\cdots,\mathbf{p}_K^t]^t. \tag{3.64}$$

By substituting (3.60) into (3.47) and performing some manipulations, the summation of K MSE becomes

$$\begin{aligned} &\sum_{k=1}^{K} E\left\{\left|b_k(i)-z_k(i)\right|^2\right\} \\ &= K + \alpha^2\mathbf{p}^\dagger\left(\sum_{k=1}^{K}\sum_{l=-1}^{1}\mathbb{H}_k^H\mathbf{R}_k^{(l)}\mathbf{R}_k^{(l),\dagger}\mathbb{H}_k\right)\mathbf{p} \\ &- \alpha\left(\sum_{k=1}^{K}\mathbf{e}_K^{(k),\dagger}\mathbf{R}_k^{(0),\dagger}\mathbb{H}_k\mathbf{p} + \mathbf{p}^\dagger\mathbb{H}_k^\dagger\mathbf{R}_k^{(0)}\mathbf{e}_K^{(k)}\right) + \alpha^2 K\sigma_n^2. \end{aligned} \tag{3.65}$$

Next, we let

$$\mathbf{p} = \frac{1}{\alpha}\mathbf{R}_{\mathbf{S}}^{-1/2}\mathbf{w}, \tag{3.66}$$

where

$$\mathbf{w} = [\mathbf{w}_1^t,\cdots,\mathbf{w}_K^t]^t, \tag{3.67}$$

$$\mathbf{R}_{\mathbf{S}} = \mathrm{diag}\left[\mathbf{R}_{\mathbf{S}_1},\cdots,\mathbf{R}_{\mathbf{S}_K}\right] \tag{3.68}$$

and $\mathbf{R}_{\mathbf{S}_k}$ is defined in (3.50). By substituting (3.65) and (3.66) into (3.47), the constraint optimization is reformulated as

$$\begin{aligned} &\left\{\mathbf{w}^{(opt)}, \alpha^{(Tx-Wiener)}\right\} \\ &= \arg\min_{\mathbf{w},a}\left\{K + \mathbf{w}^\dagger\left(\sum_{k=1}^{K}\sum_{l=-1}^{1}\mathbf{R}_{\mathbf{S}}^{-1/2,\dagger}\mathbb{H}_k^H\mathbf{R}_k^{(l)}\mathbf{R}_k^{(l),\dagger}\mathbb{H}_k\mathbf{R}_{\mathbf{S}}^{-1/2}\right)\mathbf{w}\right. \\ &\quad \left. - \left(\sum_{k=1}^{K}\mathbf{e}_K^{(k),\dagger}\mathbf{R}_k^{(0),\dagger}\mathbb{H}_k\mathbf{R}_{\mathbf{S}}^{-1/2}\mathbf{w} + \mathbf{w}^\dagger\mathbf{R}_{\mathbf{S}}^{-1/2,\dagger}\mathbb{H}_k^\dagger\mathbf{R}_k^{(0)}\mathbf{e}_K^{(k)}\right) + \alpha^2 K\sigma_n^2\right\} \end{aligned} \tag{3.69}$$

subject to

$$\frac{\mathbf{w}^{\dagger}\mathbf{w}}{\alpha^2} = E_p. \tag{3.70}$$

Equation (3.70) implies that

$$\alpha^2 = \frac{\mathbf{w}^{\dagger}\mathbf{w}}{E_p}. \tag{3.71}$$

In order to simplify the constrained optimization problem, we substitute (3.71) into (3.69) to get rid of the power constraint, i.e.,

$$\begin{aligned}
&\mathbf{w}^{(opt)} \\
&= \arg\min_{\mathbf{w}} \left\{ K + \mathbf{w}^{\dagger} \left(\sum_{k=1}^{K} \sum_{l=-1}^{1} \mathbf{R}_{\mathbf{S}}^{-1/2,\dagger} \mathbb{H}_k^H \mathbf{R}_k^{(l)} \mathbf{R}_k^{(l),\dagger} \mathbb{H}_k \mathbf{R}_{\mathbf{S}}^{-1/2} \right) \mathbf{w} \right. \\
&\quad - \left(\sum_{k=1}^{K} \mathbf{e}_K^{(k),\dagger} \mathbf{R}_k^{(0),\dagger} \mathbb{H}_k \mathbf{R}_{\mathbf{S}}^{-1/2} \mathbf{w} + \mathbf{w}^{\dagger} \mathbf{R}_{\mathbf{S}}^{-1/2,\dagger} \mathbb{H}_k^{\dagger} \mathbf{R}_k^{(0)} \mathbf{e}_K^{(k)} \right) \\
&\quad \left. + \frac{K\sigma_n^2}{E_p} \mathbf{w}^{\dagger}\mathbf{w} \right\}.
\end{aligned} \tag{3.72}$$

The solution to the above unconstrained optimization problem can be easily shown as

$$\begin{aligned}
\mathbf{w}^{(opt)} &= [\mathbf{w}_1^{(opt),T}, \cdots, \mathbf{w}_K^{(opt),T}]^t \\
&= \left(\sum_{k=1}^{K} \sum_{l=-1}^{1} \mathbf{R}_{\mathbf{S}}^{-1/2,\dagger} \mathbb{H}_k^H \mathbf{R}_k^{(l)} \mathbf{R}_k^{(l),\dagger} \mathbb{H}_k \mathbf{R}_{\mathbf{S}}^{-1/2} + \frac{K\sigma_n^2}{E_p} \mathbf{I}_{KL_p} \right)^{-1} * \\
&\quad \sum_{k=1}^{K} \mathbf{R}_{\mathbf{S}}^{-1/2,\dagger} \mathbb{H}_k^{\dagger} \mathbf{R}_k^{(0)} \mathbf{e}_K^{(k)}.
\end{aligned} \tag{3.73}$$

Due to the block-wise matrix operation in nature in (3.73), $\mathbf{w}_k^{(opt)}$ can be individually represented as

$$\begin{aligned}
\mathbf{w}_k^{(opt)} &= \left(\sum_{j=1}^{K} \sum_{l=-1}^{1} \mathbf{R}_{\mathbf{S}_k}^{-1/2,\dagger} \mathbf{H}_k^H \mathbf{r}_{j,k}^{(l)} \mathbf{r}_{j,k}^{(l),\dagger} \mathbf{H}_k \mathbf{R}_{\mathbf{S}_k}^{-1/2} + \frac{K\sigma_n^2}{E_p} \mathbf{I}_{L_p} \right)^{-1} * \\
&\quad \mathbf{R}_{\mathbf{S}_k}^{-1/2,\dagger} \mathbf{H}_k^H \mathbf{r}_{k,k}^{(0)}.
\end{aligned} \tag{3.74}$$

Hence, we can have

$$\alpha^{(Tx-Wiener)} = \sqrt{\frac{\mathbf{w}^{(opt),\dagger}\mathbf{w}^{(opt)}}{E_p}} = \sqrt{\frac{\sum_{k=1}^{K} \mathbf{w}_k^{(opt),\dagger}\mathbf{w}_k^{(opt)}}{E_p}} \tag{3.75}$$

and

$$\begin{aligned}\mathbf{p}^{(Tx-Wiener)} &= \left[\mathbf{p}_1^{(Tx-Wiener),t}, \cdots, \mathbf{p}_K^{(Tx-Wiener),t}\right]^t \\ &= \sqrt{\frac{E_p}{\sum_{k=1}^K \mathbf{w}_k^{(opt),\dagger}\mathbf{w}_k^{(opt)}}}\mathbf{R}_{\mathbf{S}}^{-1/2}\mathbf{w}^{(opt)}, \end{aligned} \tag{3.76}$$

where

$$\mathbf{p}_k^{(Tx-Wiener)} = \sqrt{\frac{E_p}{\sum_{k=1}^K \mathbf{w}_k^{(opt),\dagger}\mathbf{w}_k^{(opt)}}}\mathbf{R}_{\mathbf{S}_k}^{-1/2}\mathbf{w}_k^{(opt)} \quad \forall k = 1, \cdots, K. \tag{3.77}$$

4

Precoding Techniques for MIMO Channels

4.1 Review of MIMO Systems

Multiple input multiple output (MIMO) systems have been the most desirable candidates for next generation of high data rate wireless communications. MIMO systems can offer spatial multiplexing gain and greatly increases the capacity of channels by independently sending streams of data across multiple antennas. The Bell Laboratory Layered Space-Time (BLAST) system is the most prominent example of this capacity achieving scheme. MIMO systems can also provide diversity and coding gain by using space time codes that map input symbols across time and space.

A block diagram of a MIMO system with either space-time code or multiplexing is shown in Fig. 4.1. Suppose there are M_t transmit antennas and M_r receive antennas. The MIMO system can be described by

$$\mathbf{y} = \sqrt{\rho}\mathbf{H}\mathbf{x} + \mathbf{w}. \tag{4.1}$$

where $\mathbf{x} \in \mathbb{C}^{M_t}$ is the transmit symbol, $\mathbf{y} \in \mathbb{C}^{M_r}$ is the received symbol, $\mathbf{w} \in \mathbb{C}^{M_r}$ is a circularly symmetric complex Gaussian noise vector and $\mathbf{H} \in \mathbb{C}^{M_r \times M_t}$ is channel matrix whose entries $h_{i,j}$ are the the complex gain of the transmission path from ith transmit antenna to jth receive antenna. Unless otherwise stated, the entries of $\mathbf{H}$ are considered statistically independent across space. ρ is the signal-to-noise ratio. When $\mathbf{H}$ is random matrix and

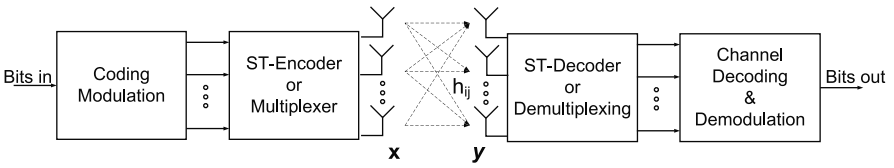

Fig. 4.1. Block diagram of a MIMO system

C.-C.J. Kuo et al., *Precoding Techniques for Digital Communication Systems*,
DOI: 10.1007/978-0-387-71769-2_4,

ergodic, we assume its entries are $i.i.d$ complex circularly symmetric Gaussian with zero mean and unit variance. That means, each entry of $\mathbf{H}$ has uniform phase and Rayleigh magnitude.

The capacity of an ergodic channel the capacity is achieved by maximizing the mutual information $I(\mathbf{x};\mathbf{y},\mathbf{H})$ with respect to the distribution of $\mathbf{x}$. It is shown that the capacity is achieved by transmitted signal $\mathbf{x} \sim \mathbb{C}N(0, \mathbf{\Sigma_x})$ and is given by [129]

$$C = E[\log_2 \det(\mathbf{I} + \rho \mathbf{H} \mathbf{\Sigma_x} \mathbf{H}^H)] \tag{4.2}$$

where $\mathbf{\Sigma_x} = E(\mathbf{x}\mathbf{x}^H)$ is the input covariance matrix.

If the channel state information (CSI) is known at both transmitter, $\mathbf{H}$ can be considered deterministic. In this case the channel capacity is given by

$$C = \max_{\mathbf{\Sigma_x},\, \mathrm{tr}(\mathbf{\Sigma_x}) \leq 1} \log_2 \det(\mathbf{I} + \rho \mathbf{H} \mathbf{\Sigma_x} \mathbf{H}^H) \tag{4.3}$$

Singular value decomposition (SVD) of $\mathbf{H}$ yields

$$\mathbf{H} = \mathbf{U} \mathbf{\Lambda} \mathbf{V}^H \tag{4.4}$$

where $\mathbf{U} \in \mathbb{C}^{M_r \times M_r}$ and $\mathbf{V} \in \mathbb{C}^{M_t \times M_t}$ are unitary and $\mathbf{\Lambda} \in \mathbb{C}^{M_r \times M_t}$ and its diagonal elements (singular values) are square roots of eigenvalues of $\mathbf{H}\mathbf{H}^H$.

If we multiply both sides of (4.1) with $\mathbf{U}^H$, we will obtain

$$\tilde{\mathbf{y}} = \sqrt{\rho} \mathbf{\Lambda} \tilde{\mathbf{x}} + \tilde{\mathbf{w}} \tag{4.5}$$

where $\tilde{\mathbf{y}} = \mathbf{U}^H \mathbf{y}$, $\tilde{\mathbf{x}} = \mathbf{V}^H \mathbf{x}$ and $\tilde{\mathbf{w}} = \mathbf{U}^H \mathbf{z}$. Since the rank of $\mathbf{H}$ is at most $m = \min(M_t, M_r)$, there are at most m non zero singular values denoted by $\sqrt{\lambda_i}$, $i = 1, 2, ...m$. Then, we can rewrite (4.5) as

$$\tilde{\mathbf{y}} = \begin{cases} \sqrt{\rho \lambda_i} \tilde{x}_i + \tilde{w}_i, & i = 1, ..., m \\ 0 & i = m+1, ..., M_r \end{cases} \tag{4.6}$$

where we assumed $M_r < M_t$. We see that SVD decouples the channel into a set of m parallel independent subchannels, known as eigen subchannels with eigenmodes λ_i.

The constrained optimization problem of (4.3) is simplified by using SVD of $\mathbf{H}$. The capacity is given by

$$C = \sum_{i=1}^{m} (\log_2(\rho \mu \lambda_i))_+ \tag{4.7}$$

where $(.)_+ = \max(0, .)$ and μ is chosen to meet the power constraint

$$\sum_{i=1}^{m} (\mu - \frac{1}{\rho \lambda_i})_+ = 1 \tag{4.8}$$

we see that the input power is given by

$$E\{\|x_i\|^2\} = (\mu - \frac{1}{\rho\lambda_i})_+ \tag{4.9}$$

Based on the above formulas, more power must be allocated to eigen subchannels with stronger eigenmodes. This type of power allocation policy is known as *water-pouring policy*.

Although spatial multiplexing and space time codes schemes do not need channel state information (CSI) at the transmitter, in a number of application, CSI is available at the transmitter. In such scenarios, precoding can optimally assign resources such as power and bits over multiple antennas using the channel state information. Precoding also can help us design better space-time codes. In this chapter, we explore various precoding techniques for MIMO systems. First, in section 4.2, we consider the use of TH-precoder for a MIMO system. Then In section 4.3 we show how to jointly design optimum linear precoder and decoder under certain criteria. We review the linear precoders with space-time codes in section 4.4. Finally, in section 4.5, we explain precoding techniques in the presence of incomplete channel information response.

4.2 Tomlinson-Harashima precoding (THP) for MIMO systems

In Chapter 2 we reviewed TH precoding for ISI channels. In this section, we show that TH precoding can easily be applied to a BLAST MIMO system [152]. In diagonal (D-BLAST), each codeword is transmitted using different antennas at different times. The Vertical (V-BLAST) architecture, however, places separate codewords in different antennas. Each of the M_r antennas receives a combination of M_t independent symbol streams. Recovering the independent data streams sent over multiple transmit antennas are essential to obtain the multiplexing (capacity) gain. Decoder then attempts to separate each independent symbol from others by canceling the interfering signals successively, similar to successive cancellation technique used in multiuser detection.

There exists a duality between canceling ISI in single input single output (SISO) systems, and canceling interference in Blast-based MIMO systems. Therefore, similar to SISO ISI channels, one can use linear equalization or non linear equalization e.g. DFE to separate the data streams spatially in MIMO systems.

Fig. 4.2 shows matrix DFE for a MIMO system. The MIMO system model is represented by (4.1). For simplicity, we assume that the number of transmit and receive antennas are the same and denoted by M. The feedforward $M \times M$ matrix $\mathbf{F}$ whitens noise and guarantees causality as in the case for the scalar DFE for ISI channel. Therefore $\mathbf{B} = \mathbf{FH}$ has to be lower triangular, where $\mathbf{B}$ and $\mathbf{H}$ are also $M \times M$ matrices.

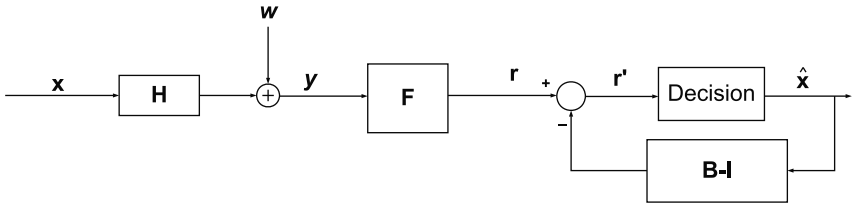

Fig. 4.2. Block diagram of Matrix ZF-DFE [[152]©IEEE].

F can also be chosen such that the main diagonal elements of **B** are one. The feedback matrix, $\mathbf{B}-\mathbf{I}$ cancels the interference caused by already detected symbol. However, matrix DFE suffers from the same shortcomings as scalar DFE for ISI channel. That is error propagation and the difficulty to combine with coding schemes. When the channel state information is available, the feedback section of the DFE can be moved to the transmitter so that linear pre-equalization of the cascade $\mathbf{B} = \mathbf{FH}$ can separate the signals from different transmit antennas.

However, the above pre-equalization technique can increase the transmit energy significantly. Therefore, a non linear function must be used to cripple the transmit energy. As shown in Fig. 4.3, this can be done by a modulo device as explained for TH-precoding for ISI channels in Chapter 2.

Ignoring the modulo device, the cascade of $\mathbf{B} = \mathbf{FH}$ is a lower-triangular and hence the output symbols y_i, $i = 1, 2, ...M$ are successively generated from the data symbols $x_i \in \mathcal{A}$ as

$$z_i = x_i - \sum_{j=1}^{i-1} b_{ij} z_j \tag{4.10}$$

Suppose, each symbol belongs to a square $M_c \times M_c$ constellation $\mathcal{A}$. each point in the constellation can take values from $\{\pm 1, \pm 3, \pm(M_c - 1)\}$. The constellation is bounded by by the square region of width $2M_c$. The function of the modulo $2M_c$ device of THP is to force the transmit symbols x_i, $i = 1, 2, ..., M_t$, into the boundary region of A. In other words as

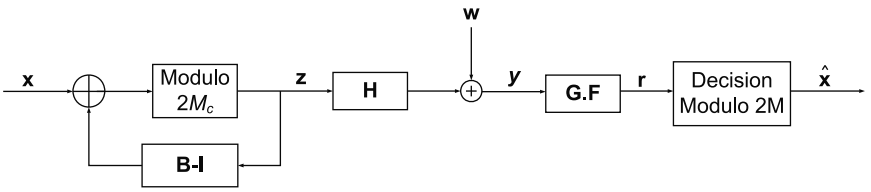

Fig. 4.3. Block diagram of TH precoding for MIMO channel [[152]©IEEE].

$$z_i = x_i + p_i - \sum_{j=1}^{i-1} b_{ij} z_j \tag{4.11}$$

where $p_i \in \{2\sqrt{M_c}.(p_I + jp_Q); p_i, p_Q \in \mathbb{Z}\}$. The channel matrix $\mathbf{H}$ can be factorized by *QL factorization* technique as

$$\mathbf{H} = \mathbf{F}^H \mathbf{S} \tag{4.12}$$

where $\mathbf{S}$ is a lower triangular matrix and $\mathbf{F}$ is the unitary feedforward matrix as defined before (preserving whiteness of the noise). By multiplying feedforward matrix with a scaling matrix $\mathbf{G} = \text{diag}(s_{11}^{-1}, ..., s_{NN}^{-1})$, we can keep the main diagonal elements of $\mathbf{B}$ equal to 1. Hence, $\mathbf{B} = \mathbf{GFH} = \mathbf{GS}$.

The received symbols $r_i, i = 1, 2..., M_r$ at the slicer are only corrupted by the noise thanks to the preequalization cascade $\mathbf{B} = \mathbf{FH}$ and can be written as

$$r_i = v_i + w_i' \tag{4.13}$$

where $v_i = z_i + w_i' = \tilde{w}/s_{ii}$ and $\tilde{\mathbf{w}} = \mathbf{Fw}$. We see that the MIMO channel is decomposed into M parallel AWGN channels with noise variance $\sigma_n^2/\|s_{ii}\|^2$, $i = 1, ...M$, where σ_n^2 is the variance of w_i.

The received symbols $r_i, i = 1, 2, ...M$ are first modulo reduced into the boundary region of signal constellation $\mathcal{A}$. Then, the estimates of the symbols $\hat{x}_i$ for each of M_t transmit antennas is recovered by a conventional slicer as shown in Fig. 4.3.

Eqs. (4.4) and (4.5) show that by singular value decomposition of channel and applying $\mathbf{V}$ at the transmitter and $\mathbf{U}$ at the receiver, MIMO channel can be transformed to M independent parallel eigen subchannels. Assumin high SNRs ($\rho \gg 1$), the capacity achieving power distribution approaches to a uniform one, *i.e.* $\mathbf{\Sigma_x} = E(\mathbf{xx}^H) = \mathbf{I}$. Hence by (4.3), the capacity of MIMO channel is given by

$$\begin{aligned} C_{SVD} &= \log\det(\mathbf{I} + \rho\mathbf{H}\mathbf{\Sigma_x}\mathbf{H}^H) \\ &\approx \log\det(\rho\mathbf{H}\mathbf{H}^H) = \log\det(\rho\mathbf{\Lambda}^H) = \log(\prod_{i=1}^{M} \rho\lambda_i) \end{aligned} \tag{4.14}$$

where λ_i and ρ were as defined before and we have assume that rank of $\mathbf{H} = M$.

As we showed above, MIMO system with THP (or with the error-free decision feedback equalization) result in parallel and independent AWGN channel with variance $\sigma_n^2/|s_{ii}|^2$, $i = 1, ...M$. Hence the capacity of THP MIMO for high SNR values is

$$C_{THP} = \sum_{i=1}^{M} \log(1 + \rho\|s_{ii}\|^2) \approx \sum_{i=1}^{M} \log(\rho\|s_{ii}\|^2) \tag{4.15}$$

But from (4.12),

$$\mathbf{H}^H\mathbf{H} = \mathbf{S}^H\mathbf{F}\mathbf{F}^H\mathbf{S} = \mathbf{S}^H\mathbf{S} \tag{4.16}$$

Since $\mathbf{S}$ is triangular, $\prod_{i=1}^{M} \|\lambda_{ii}\|^2 = \det(\mathbf{H}^H\mathbf{H}) = \det(\mathbf{S}^H\mathbf{S}) = \prod_{i=1}^{M} \|s_{ii}\|^2$. Thus, for $\rho \gg 1$,

$$C_{THP} = \log(\prod_{i=1}^{M} \rho\lambda_i) = C_{SVD} \tag{4.17}$$

In other words, precoding is asymptotically an optimal way for channel equalization. Fig. 4.4 [152] shows the capacity (in bits per M-transmit vector) versus SNR in dB for a MIMO system with $M = 4$. The entries of channel matrix were considered *i.i.d* complex Gaussian and the results were averaged over large number of channel realization. The capacity achieved by MIMO THP precoding and SVD were plotted for a flat (uniform) power distribution and also water pouring power allocation policy. We see that for high SNR, the water pouring power allocation merges to a flat one and the capacity achieved by TH precoding approaches to capacity of MIMO channel.

Symbol error rate for this MIMO system are also depicted in Fig. 4.5. The performance of SVD and preequalization schemes both sffer from small singular value which dominates the error rate. The THP system shows advantage over linear pre-equalization, SVD scheme and also the V-BLAST with non ideal DFE. However, with respect to gVBLAST with genie-aided (feedback error-free) DFE, THP suffers a small loss of performance.

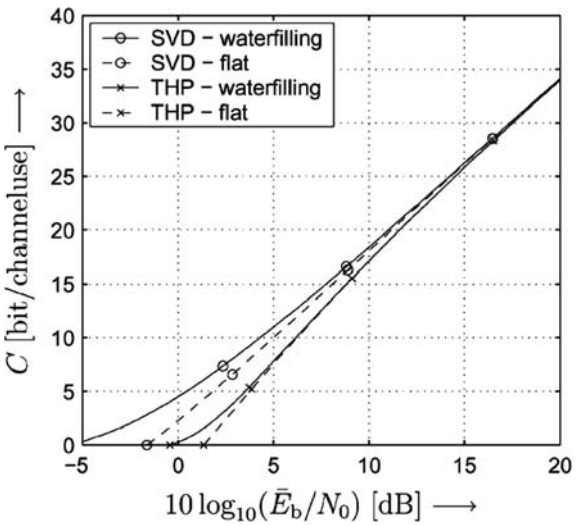

Fig. 4.4. Achievable rates for SVD-based equalization and for MIMO precoding [[152]©IEEE].

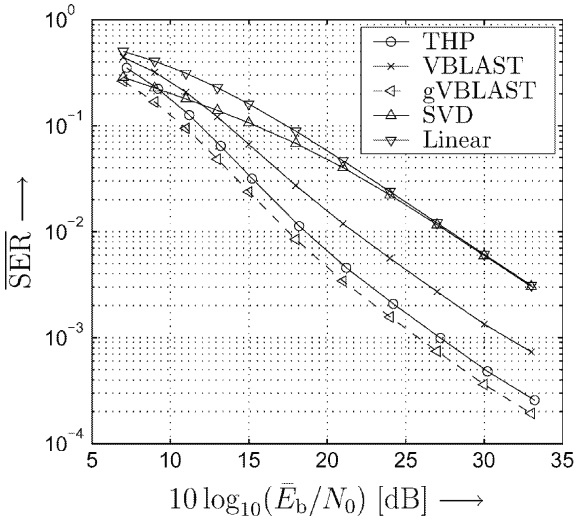

Fig. 4.5. Average symbol error rates for different equalization techniques [[152]©IEEE].

4.3 Joint Design of Linear Precoder and Decoder

A MIMO communication system model with linear precoder and decoder is shown in Fig 4.6. The input bit streams are coded and modulated to and symbol streams are then passed through the linear precoder. The linear precoder is a matrix $\mathbf{F}$ that can add redundancy to the input symbol streams to improve systems performance. The output of the precoder is then sent to the channel through M_t transmit antennas. M_r receive antennas collect the signals at the receiver and pass it to a decoder matrix $\mathbf{G}$ which removes any redundancy that has been introduced by the precoder. For a single carrier system in flat fading channel the system equation is

$$\hat{\mathbf{x}} = \mathbf{GHFx} + \mathbf{Gw}, \tag{4.18}$$

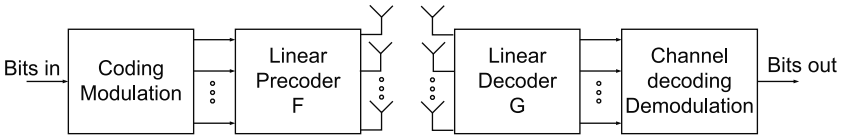

Fig. 4.6. Block diagram of linear precoder/decoder for MIMO channel [[112]©IEEE].

where $\mathbf{x}$ is the $K \times 1$ transmitted vector, $\hat{\mathbf{x}}$ is the $K \times 1$ received vector, F is the $M_t \times K$ precoder matrix, G is the $K \times M_r$ decoder matrix and $\mathbf{H}$ and $\mathbf{w}$ are as defined before. In the following sections, unless otherwise stated, we assume

$$E(\mathbf{x}\mathbf{x}^H) = \mathbf{I}; \quad E(\mathbf{w}\mathbf{w}^H) = \mathbf{I}; \quad E(\mathbf{x}\mathbf{w}^H) = \mathbf{0}. \tag{4.19}$$

We see that the precoder F adds a redundancy of $M_t - K$ across space. For simplicity of the analysis, we assume $K = \text{rank}(\mathbf{H})$.

In section 4.3.1, we show that if the minimization of the any weighted sum of symbol estimation errors of all subchannels is chosen as the desired criterion, the linear precoder and decoder decouples into parallel eigen subchannels. By selecting appropriate error weights, we can maximize the information rate, minimize the sum of error rates. We can also design precoders/decoders for quality-of-service (QoS) based equal error rate (among all subchannels) applications

4.3.1 Generalized Weighted MMSE Design

We want to design $\mathbf{F}$ and $\mathbf{G}$ matrices so as to minimize any weighted combination of symbol estimation errors. Define the $K \times 1$ error vector as

$$\mathbf{e} = \mathbf{x} - \hat{\mathbf{x}} = \mathbf{x} - (\mathbf{GHFx} + \mathbf{Gw}). \tag{4.20}$$

The error covariance matrix or the minimum square error (MSE) matrix is defined as

$$\begin{aligned} \text{MSE} &= E\{\mathbf{e}\mathbf{e}^H\} \\ &= E[(\mathbf{x} - \mathbf{GHFx} - \mathbf{Gw})(\mathbf{x} - \mathbf{GHFx} - \mathbf{Gw})^H] \\ &= (\mathbf{GHF} - \mathbf{I})(\mathbf{GHF} - \mathbf{I})^H + \mathbf{G}\mathbf{R}_{nn}\mathbf{G}^H, \end{aligned} \tag{4.21}$$

where we have used the assumption given in Eq. (4.19).

Considering the $K \times K$ diagonal positive definite weight matrix $\mathbf{W_e}$, the minimization problem can be formulated as

$$\begin{aligned} &\min_{\mathbf{G},\mathbf{F}} E\{\|\mathbf{W_e}^{1/2}\mathbf{e}\|^2\} \\ &\qquad \text{tr}(\mathbf{F}\mathbf{F}^H) \le p_0 \end{aligned} \tag{4.22}$$

where p_0 is the total power available and the expectation E is performed with respect to the distribution of $\mathbf{x}$ and $\mathbf{w}$. Note that

$$\begin{aligned} E\{\|\mathbf{W_e}^{1/2}\mathbf{e}\|^2\} &= E\{\text{tr}(\mathbf{W_e}^{1/2}\mathbf{e}\mathbf{e}^H\mathbf{W_e}^{H1/2})\} \\ &= \text{tr}(\mathbf{W_e}^{1/2}E\{\mathbf{e}\mathbf{e}^H\}\mathbf{W_e}^{H1/2}) \\ &= \text{tr}(\mathbf{W_e}E\{\mathbf{e}\mathbf{e}^H\}), \end{aligned} \tag{4.23}$$

The method of Lagrange duality and the Karush-Kuhn-Tucker (KKT) conditions can be used to solve the optimization problem in (4.22) as follows; We first form the Lagrangian using Eqs. (4.21) and (4.23).

$$L(\mu, \mathbf{G}, \mathbf{F}) = \mathrm{tr}[\mathbf{W_e}(\mathbf{GHF}-\mathbf{I})(\mathbf{GHF}-\mathbf{I})^H + \mathbf{W_e}\mathbf{G}\mathbf{R}_{nn}\mathbf{G}^H] + \mu[\mathrm{tr}(\mathbf{F}\mathbf{F}^H) - p_0] \tag{4.24}$$

It can be shown that $\mathbf{G}$ and $\mathbf{F}$ are optimal if they satisfy the following conditions [112]

$$\bigtriangledown_{\mathbf{G}} L(\mu, \mathbf{G}, \mathbf{F}) = 0, \tag{4.25}$$

$$\bigtriangledown_{\mathbf{F}} L(\mu, \mathbf{G}, \mathbf{F}) = 0, \tag{4.26}$$

$$\mu \geq 0; \quad \mathrm{tr}(\mathbf{F}\mathbf{F}^H) - p_0 \leq 0, \tag{4.27}$$

$$\mu[\mathrm{tr}(\mathbf{F}\mathbf{F}^H) - p_0] = 0. \tag{4.28}$$

Substituting (4.24) in (4.25) and (4.26), we obtain the following formulas for $\mathbf{F}$ and $\mathbf{G}$,

$$\mathbf{HF} = \mathbf{HF}\mathbf{F}^H\mathbf{H}^H\mathbf{G}^H + \mathbf{R}_{nn}\mathbf{G}^H, \tag{4.29}$$

$$\mathbf{W_e}\mathbf{GH} = \mathbf{F}^H\mathbf{H}^H\mathbf{G}^H\mathbf{W_e}\mathbf{GH} + \mu\mathbf{F}^H, \tag{4.30}$$

By solving the above equations the optimum precoder and decoder can be obtained as shown in [112]. Let us define the following eigenvalue decomposition (EVD)

$$\mathbf{H}^H\mathbf{R}_{nn}^H\mathbf{H} = (\mathbf{V} \quad \overline{\mathbf{V}}) \begin{pmatrix} \mathbf{\Lambda} & \mathbf{0} \\ \mathbf{0} & \overline{\mathbf{\Lambda}} \end{pmatrix} (\mathbf{V} \quad \overline{\mathbf{V}})^H \tag{4.31}$$

where $\mathbf{V}$ is an $M_t \times K$ orthogonal matrix whose columns constitutes a basis for the range space of $\mathbf{H}^H\mathbf{R}_{nn}^H\mathbf{H}$. $\overline{\mathbf{V}}$ is a $M_t \times (M_t - K)$ orthogonal matrix forming a basis for the null space of $\mathbf{H}^H\mathbf{R}_{nn}^H\mathbf{H}$. $\mathbf{\Lambda}$ is a diagonal matrix containing the K nonzero eigenvalues $\{\lambda\}_{i=1}^K$ arranged in a decreasing order from the top-left to bottom-right and $\overline{\mathbf{\Lambda}}$ contains the zero eigenvalues. Note that we assume $K = \mathrm{rank}(\mathbf{H}^H\mathbf{R}_{nn}^H\mathbf{H}) = \mathrm{rank}(\mathbf{H})$. Then, the following Theorem presents the optimum $\mathbf{F}$ and $\mathbf{G}$ matrices [112];

Theorem 1: the optimum $\mathbf{F}$ and $\mathbf{G}$ matrices can be found from the following equations

$$\mathbf{F} = \mathbf{V}\mathbf{\Phi_f} \tag{4.32}$$

$$\mathbf{G} = \mathbf{\Phi_g}\mathbf{V}^H\mathbf{H}^H\mathbf{R}_{nn}^{-1} \tag{4.33}$$

where $\mathbf{\Phi_f}$ and $\mathbf{\Phi_g}$ are $K \times K$ diagonal matrices with non-negative elements on the diagonal and are given by

$$\mathbf{\Phi_f} = (\mu^{-1/2}\mathbf{\Lambda}^{-1/2}{\mathbf{W_e}}^{1/2} - \mathbf{\Lambda}^{-1})_+^{1/2} \tag{4.34}$$

$$\mathbf{\Phi_g} = (\mu^{1/2}\mathbf{\Lambda}^{-1/2}{\mathbf{W_e}}^{-1/2} - \mu\mathbf{\Lambda}^{-1}{\mathbf{W_e}}^{-1})_+^{1/2}\mathbf{\Lambda}^{-1/2}. \tag{4.35}$$

where $(.)_+$ means the negative values are replaced with zero.

Proof: The proof can be found in [112].

Let $\mathbf{\Lambda} = \mathrm{diag}([\lambda_1, \lambda_2, ..., \lambda_K])$ and $\mathbf{W_e} = \mathrm{diag}([w_1, w_2, ..., w_K])$. Suppose $k < K$ subchannels are used for transmission. From (4.34) and the power constraint $\mathrm{tr}(\Phi_f^2) = p_0$, we have

$$\mathrm{tr}(\mathbf{\Phi_f}^2) = \mu^{-1/2} \sum_{i=1}^{k} (\lambda_i^{-1/2} w_{ei} 1/2) - \sum_{i=1}^{k} (\lambda_i^{-1}) = p_0 \tag{4.36}$$

Therefore, we can obtain the following expression for μ

$$\mu^{1/2} = \frac{\sum_{i=1}^{k} (\lambda_i^{-1/2} w_{ei}^{1/2})}{p_0 + \sum_{i=1}^{k} (\lambda_i^{-1})} \tag{4.37}$$

Let $\rho_k = \lambda_k w_k$ and let them be ordered in a decreasing manner: $\rho_1 \geq ... \geq \rho_k \geq ... \geq \rho_K$. To compute $\mathbf{\Phi_f} = \mathrm{diag}([\phi_{f,1}, \phi_{f,2}, ..., \phi_{f,K}])$ optimally and ensure that it is positive semi-definite, we can compute μ according to (4.37) for each $k = 1, 2, ...K$ iteratively, starting with $k = K$ and assuming $\mu \leq \rho_k$, so that $\phi_{f,k} \geq 0$,$k = 1, 2...K$.

From Eqs (4.32) and (4.33), we have

$$\mathbf{FHG} = \mathbf{\Phi_g \Lambda \Phi_g} \tag{4.38}$$

In other words, the optimum precoder $\mathbf{F}$ and decoder $\mathbf{G}$ diagonalize channel matrix $\mathbf{H}$ into eigen subchannels (eigenmodes) for any set of error weights. Fig. 4.7 shows the diagonalization of the channel by precoder/decoder.

We can design linear precoder/decoder according to different design criteria, such as maximize information rate, minimize the sum of symbol estimation error and so on by choosing an appropriate error weight matrix $\mathbf{W_e}$. In the following, we explore a variety of these design criteria.

4.3.2 Maximum Information Rate Design

We saw in sections 4.1 that the water-pouring power allocation policy maximized channel capacity of MIMO systems. Rewriting Eq. (4.9) in matrix

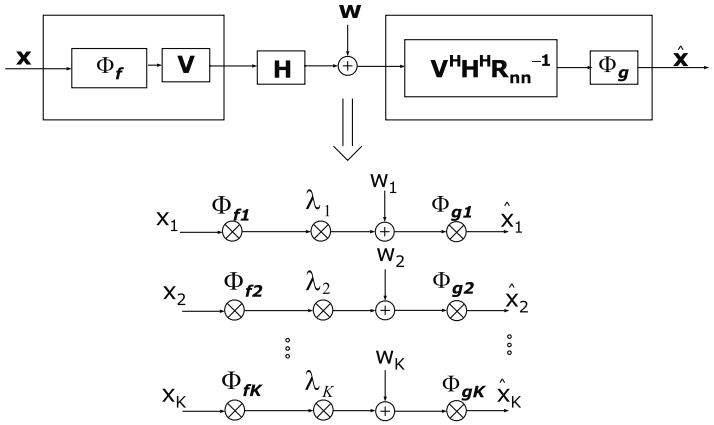

Fig. 4.7. Optimum linear precoder/decoder: decomposition of channels into eigen subchannels [[112]©IEEE].

format and replacing $E\{\|x_i\|^2\}$ with $\text{tr}(\mathbf{F}\mathbf{F}^H) = {\mathbf{\Phi_f}}^2$ we obtain

$$\mathbf{\Phi_f} = (\frac{\mathbf{I}}{\mu^1/2} - \mathbf{\Lambda}^{-1})_+^{1/2} \tag{4.39}$$

The above equation is obtained by choosing $\mathbf{W_e} = \mathbf{\Lambda}$ in Eq. (4.34). It is shown in [111] that the optimum precoder and decoder that maximizes the information rate are given by (4.32) and (4.33) with $\mathbf{\Phi_f}$ obtained from (4.39). In other words, the maximum information rate design is just a special case of generalized weighted MMSE design. Total capacity (information rate) is given by

$$C = \sum_{i=1}^{K} R_i = \sum_{i=1}^{K} \log_2(1 + \phi_{f,i}^2 \lambda_i) \tag{4.40}$$

where R_i is the information rate for the ith subchannel and $\phi_{f,i}$ is the ith element on the diagonal of $\mathbf{\Phi_f}$. Also, Note that since $\mathbf{\Phi_g}$ is not present in the above expression for the maximum information rate, we can select $\mathbf{\Phi_g}$ to be any arbitrary full-rank diagonal matrix.

According to the water-pouring solution, stronger subchannels must be assigned higher rates. The choice of $\mathbf{W_e} = \mathbf{\Lambda}$ tells us that they also need to be heavily weighed. For example, in adaptive modulation systems, more power and higher order modulation are used on subchannels with higher gains to improve the total data rate.

4.3.3 QoS-Based Design

In multimedia applications, different types of information (video, audio, data, *etc.*) with different SNR requirements for successful transmission need to be simultaneously sent on different subchannels. For these quality-of-service (QoS) applications, it is necessary to design our system such that different subchannels have different SNRs. Let us define the SNR matrix as

$$\text{SNR} = (\mathbf{F}^H\mathbf{H}^H\mathbf{G}^H(\mathbf{G}\mathbf{R}_{nn}\mathbf{G}^H)^{-1}\mathbf{G}\mathbf{H}\mathbf{F} \tag{4.41}$$

where we have used the assumption $\mathbf{R}_{xx} = \mathbf{I}$. Using the optimum $\mathbf{F}$ and $\mathbf{G}$ from Eqs. (4.32) and (4.33), SNR is simplified to

$$\text{SNR} = {\mathbf{\Phi_f}}^2\mathbf{\Lambda} = ({\mathbf{W_e}}^{1/2}\mu^{-1/2}\mathbf{\Lambda}^{1/2} - \mathbf{I})_+ = \gamma\mathbf{D} \tag{4.42}$$

where $\mathbf{D} = \text{diag}([d_1, d_2, ..., d_K])$ is a diagonal matrix of relative SNR's across subchannels, with $\sum_{i=1}^{K} d_i = 1$, and $\gamma > 0$ is a scalar. Solving this equation for $\mathbf{W_e}$, we attain

$${\mathbf{W_e}}^{1/2} = (\mathbf{I} + \gamma\mathbf{D})\mathbf{\Lambda}^{-1/2}\mu^{1/2} \tag{4.43}$$

Since μ is a function of $\mathbf{W_e}$ given from (4.37) with $k = K$ as

$$\mu^{1/2} = \frac{\text{Tr}(\mathbf{\Lambda}^{-1/2}{\mathbf{W_e}}^{1/2})}{\text{Tr}(\mathbf{\Lambda}^{-1}) + p_0} \tag{4.44}$$

we can substitute the expression for $\mathbf{W_e}$ from (4.43) into (4.44) to obtain

$$\begin{aligned}\mu^{1/2} &= \frac{\mathrm{Tr}(\mathbf{\Lambda}^{-1/2}(\mathbf{I}+\gamma\mathbf{D})\mathbf{\Lambda}^{-1/2}\mu^{1/2})}{\mathrm{Tr}(\mathbf{\Lambda}^{-1})+p_0} \\ &= \frac{\mu^{1/2}(\mathrm{Tr}(\mathbf{\Lambda}^{-1})+\gamma\mathrm{Tr}(\mathbf{\Lambda}^{-1}\mathbf{D}))}{\mathrm{Tr}(\mathbf{\Lambda}^{-1})+p_0}\end{aligned} \tag{4.45}$$

Therefore, $\gamma = p_0/\mathrm{tr}(\mathbf{\Lambda}^{-1}\mathbf{D})$. Inserting this into (4.43), we obtain

$$\mathbf{W_e}^{1/2} = \mu^{1/2}\left(\frac{p_0}{\mathrm{Tr}(\mathbf{\Lambda}^{-1}\mathbf{D})}\mathbf{D}+\mathbf{I}\right)\mathbf{\Lambda}^{-1/2} \tag{4.46}$$

Substituting (4.46) into (4.34) and (4.35), we obtain the following results for the optimum precoder $\mathbf{F}$ and decoder $\mathbf{G}$ given in (4.32) and (4.33),

$$\mathbf{\Phi_f} = \gamma^{1/2}\mathbf{D}^{1/2}\mathbf{\Lambda}^{-1/2} \tag{4.47}$$

$$\mathbf{\Phi_g} = \gamma^{1/2}\mathbf{D}^{1/2}\mathbf{\Lambda}^{-1/2}(\gamma\mathbf{D}+\mathbf{I})^{-1} \tag{4.48}$$

$$\gamma = \frac{p_0}{\mathrm{tr}(\mathbf{D}\mathbf{\Lambda}^{-1})} \tag{4.49}$$

We can also simplify the expression for $E\{\mathbf{e}\mathbf{e}^H\}$ given in (4.21) using the optimum $\mathbf{F}$ and $\mathbf{G}$ to

$$E\{\mathbf{e}\mathbf{e}^H\} = \mathbf{W_e}^{-1/2}\mathbf{\Lambda}^{-1/2}\mu^{1/2} \tag{4.50}$$

From (4.42) and (4.50), we see

$$\mathrm{SNR} = E\{\mathbf{e}\mathbf{e}^H\}^{-1} - \mathbf{I} \tag{4.51}$$

Hence equal SNR on each subchannels implies equal MSEs regardless of the choice of error-weights.

4.3.4 (Unweighted) MMSE Design

If we let $\mathbf{W_e} = \mathbf{I}$, then the optimal precoder and decoder derived in Eqs. (4.32) and (4.33) will minimize the *sum of symbol estimation errors* across all subchannels and is given by

$$\mathbf{F} = \mathbf{V}\mathbf{\Phi_f} \tag{4.52}$$

$$\mathbf{\Phi_f} = (\mu^{-1/2}\mathbf{\Lambda}^{-1/2} - \mathbf{\Lambda}^{-1})_+^{1/2} \tag{4.53}$$

While, this approach can improve the performance of MIMO systems, it is not guaranteed that the MSEs and SNRs on each subchannels is minimized. Power allocation policy in MMSE design allocates no power to an subchannel if its gain is less than a certain threshold. Among the remaining subchannels, more power is allocated to the weakest subchannels, *i.e.* subchannels with the smallest eigenmodes.

An alternative way of joint MMSE design was illustrated in [117] in which the optimization is done in two steps. First, $\mathrm{tr}(\mathrm{MSE}(\mathbf{F},\mathbf{G}))$ is minimized with respect to $\mathbf{G}$ while $\mathbf{F}$ is fixed. In other words, first, we want to solve

$$\min_{\mathbf{G}} \mathrm{MSE}(\mathbf{F},\mathbf{G}) \tag{4.54}$$

By setting the gradient of $\mathrm{MSE}(\mathbf{F},\mathbf{G}) = E\{\mathbf{e}\mathbf{e}^H\}$ to zero, we write

$$\bigtriangledown_{\mathbf{G}^*} E\{\mathbf{e}\mathbf{e}^H\} = \mathbf{G}\mathbf{H}\mathbf{F}\mathbf{F}^H\mathbf{H}^H - \mathbf{F}^H\mathbf{H}^H + \mathbf{G}\mathbf{R}_{nn} = 0 \tag{4.55}$$

Therefore, the optimum $\mathbf{G}$ is obtained as

$$\mathbf{G}^* = \mathbf{F}^H\mathbf{H}^H(\mathbf{H}\mathbf{F}\mathbf{F}^H\mathbf{H}^H + \mathbf{R}_{nn})^{-1} \tag{4.56}$$

It is shown that the optimum $\mathbf{G}^*$ is the same as the MMSE (Wiener) receiver [64].

Substituting the above expression for $\mathbf{G}^*$ in (4.21), we get

$$\begin{aligned} E\{\mathbf{e}\mathbf{e}^H\} &= (\mathbf{G}^*\mathbf{H}\mathbf{F} - \mathbf{I})(\mathbf{G}^*\mathbf{H}\mathbf{F} - \mathbf{I})^H + \mathbf{G}^*\mathbf{R}_{nn}\mathbf{G}^{*H} \\ &= \mathbf{G}^*(\mathbf{H}\mathbf{F}\mathbf{F}^H\mathbf{H}^H + \mathbf{R}_{nn})\mathbf{G}^{*H} + \mathbf{I} - \mathbf{G}^*\mathbf{H}\mathbf{F} - \mathbf{F}^H\mathbf{H}^H\mathbf{G}^{*H} \\ &= \mathbf{F}^H\mathbf{H}^H((\mathbf{H}\mathbf{F}\mathbf{F}^H\mathbf{H}^H + \mathbf{R}_{nn})^H)^{-1}\mathbf{H}\mathbf{F} + \mathbf{I} - (\mathbf{H}\mathbf{F}\mathbf{F}^H\mathbf{H}^H \\ &\quad + \mathbf{R}_{nn})^{-1}\mathbf{H}\mathbf{F} - ((\mathbf{H}\mathbf{F}\mathbf{F}^H\mathbf{H}^H + \mathbf{R}_{nn})^H)^{-1}\mathbf{H}\mathbf{F} \\ &= \mathbf{I} - (\mathbf{H}\mathbf{F}\mathbf{F}^H\mathbf{H}^H + \mathbf{R}_{nn})^{-1}\mathbf{H}\mathbf{F} \end{aligned} \tag{4.57}$$

Using the matrix inversion lemma

$$(\mathbf{A} + \mathbf{B}\mathbf{C}\mathbf{D})^{-1} = \mathbf{A}^{-1} - \mathbf{A}^{-1}\mathbf{B}(\mathbf{D}\mathbf{A}^{-1}\mathbf{B} + \mathbf{C}^{-1})^{-1}\mathbf{D}\mathbf{A}^{-1}$$

we obtain

$$\mathrm{MSE}(\mathbf{F}) = (\mathbf{I} + \mathbf{F}^H\mathbf{H}^H\mathbf{R}_{nn}^{-1}\mathbf{H}\mathbf{F})^{-1} \tag{4.58}$$

Here $\mathrm{MSE}(\mathbf{F})$ is minimum in the sense that

$$\mathrm{MSE}(\mathbf{F}) = \mathrm{MSE}(\mathbf{F},\mathbf{G}^*) \leq \mathrm{MSE}(\mathbf{F},\mathbf{G}) \tag{4.59}$$

The second step is the more difficult task of minimizing $\mathrm{tr}(\mathrm{MSE}(\mathbf{F}))$ with the power constraint. It is proven in [117] that the optimum result for $\mathbf{F}$ is the same as (4.52) and (4.53). Another method is to minimize the determinant of error covariance matrix (after optimized over $\mathbf{G}$ under power constraint, *i.e.*,

$$\min_{\mathbf{F}} \det(\mathrm{MSE}(\mathbf{F})), \quad \mathrm{tr}(\mathbf{F}\mathbf{F}^H) = p_0 \tag{4.60}$$

As shown in [117], the results are

$$\mathbf{F} = \mathbf{V}\mathbf{\Phi}_{\mathbf{f}} \tag{4.61}$$

$$\mathbf{\Phi}_{\mathbf{f}} = (\eta^{-1/2} - \mathbf{\Lambda}^{-1})_+^{1/2} \tag{4.62}$$

where

$$\eta^{1/2} = \frac{k}{p_0 + \sum_{i=1}^{k}(\lambda_i^{-1})}.$$

4.3.5 Equal Error Design

Some applications require reliable transmission of K symbols using identical modulation and coding scheme and fixed rate. This means that all K subchannels must have equal error rate and hence equal SNRs. The latter requirements can be satisfied simply by choosing $\mathbf{D} = \mathbf{I}$ in Eqs. (4.47)-(4.49) in QoS design to yield

$$\mathbf{\Phi_f} = \gamma^{1/2}\mathbf{\Lambda}^{-1/2} \tag{4.63}$$

$$\mathbf{\Phi_g} = \gamma^{1/2}\mathbf{\Lambda}^{-1/2}(\gamma+1)^{-1} \tag{4.64}$$

$$\gamma = \frac{p_0}{\mathrm{tr}(\mathbf{\Lambda}^{-1})} \tag{4.65}$$

The power allocation policy for equal error design assigns more power to subchannels with less gains while allocates less power to subchannels with stronger eigenmodes so that the subchannel SNRs and MSEs are equal. Furthermore, no subchannels is dropped regardless of its channel realizations. It can be shown that $\mathbf{GHF} = (\gamma)/(\gamma+1)\mathbf{I}$. In other words, the optimum precoder and decoder equal error design transforms the MIMO channel into a scaled identity matrix.

4.3.6 Maximum SNR-Based Design

Sometimes, minimizing the bit error probability is preferred. However, the optimization problem is hard to deal with since they are rarely solvable in closed form. Instead, an indirect way of reducing probability of error is to maximize the minimum distance between hypothesis. Since the minimum eigenvalue $\lambda_{\min}(\mathrm{SNR}(\mathbf{F},\mathbf{G}))$ provides a lower bound for the minimum distance between the hypothesis for the maximum likelihood (ML) detector (provided that the noise is Gaussian and the symbols are $i.i.d$), it was suggested in [117] to use the (4.42) as a sensible measure related to the probability of error. The corresponding optimization formulation is given in the following equations

$$\arg\max_{\mathbf{G},\mathbf{F}} \lambda_{\min}(\mathrm{SNR}(\mathbf{F},\mathbf{G})), \quad \mathrm{tr}(\mathbf{F}\mathbf{F}^H) = p_0 \tag{4.66}$$

and the solutions are given by [117]

$$\mathbf{F} = \mathbf{V}\mathbf{\Phi_f} \tag{4.67}$$

with $\mathbf{\Phi_f}$ is a diagonal $K \times K$ matrix having diagonal entries

$$\Phi_{ii} = \frac{p_0}{\sum_{j=1}^{K} \lambda_{jj}^{-1}} \lambda_{ii}^{-1} \tag{4.68}$$

and

$$\mathbf{G} = \mathbf{\Phi_g}\mathbf{V}^H\mathbf{H}^H\mathbf{R}_{nn}^{-1} \tag{4.69}$$

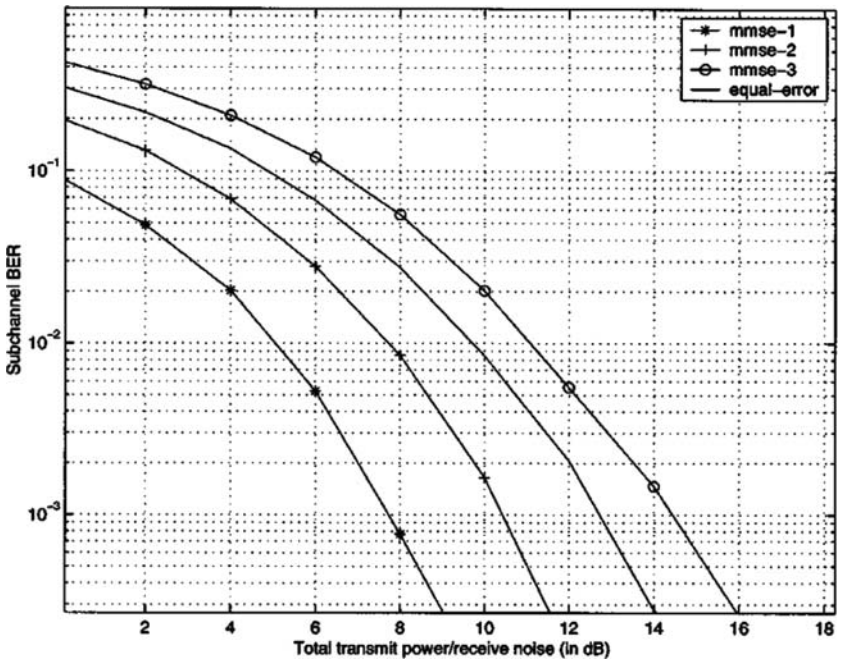

Fig. 4.8. Comparison of equal-error and MMSE design BER performance [[112]©IEEE].

The above solution leads to

$$\text{SNR} = {\mathbf{\Phi_f}}^H \mathbf{\Lambda} \mathbf{\Phi_f} = \frac{p_0}{\sum_{j=1}^{K} \lambda_{jj}^{-1}} \mathbf{I}. \tag{4.70}$$

Fig. 4.8 compares the performance of equal error designs and MMSE design for $M_t = M_r = 4$ spatial multiplexing system. $K = 3$ streams of data are sent over the channel with QAM modulation. As we see from the figure, although equal error and MMSE have the same total average BER performance, the subchannel BER performances for each of the 3 streams are different.

Fig. 4.9 shows the performance of the QoS-based design for a 3×3 MIMO spatial multiplexing system. One audio stream and one video stream are sent into the channel. The optimal precoder and decoder are obtained for each channel realization. The figure shows that video stream are provided with 5-dB higher received SNR.

4.3.7 Unified Framework with Convex Optimization

The joint linear precoder/decoder design is in general a complicated non-convex problem. Optimization can be done with respect to various criteria.

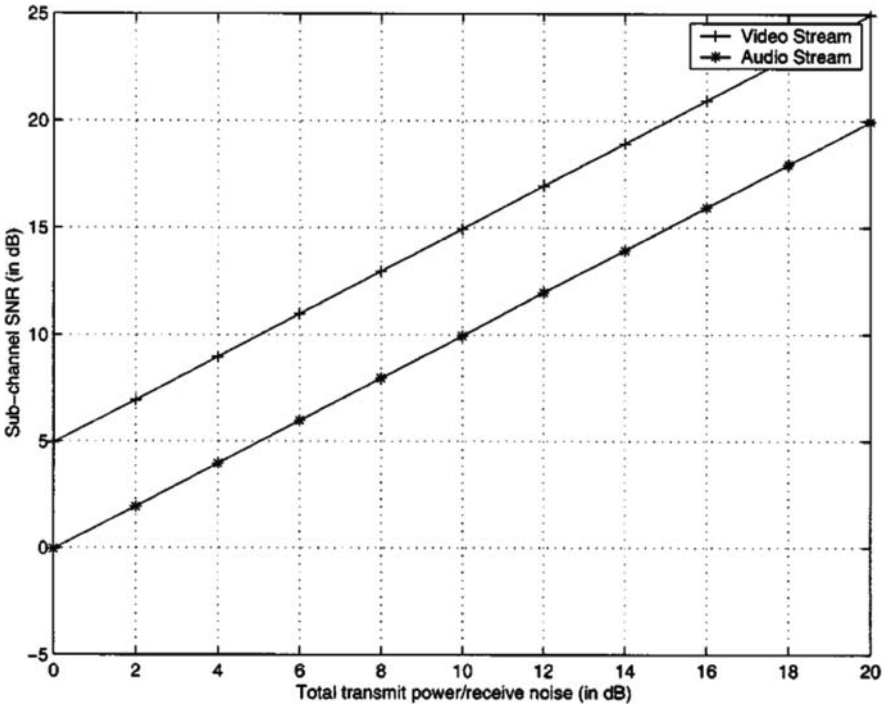

Fig. 4.9. QoS-design SNR performance [[112]©IEEE].

As we saw previously for some specific criteria, the linear precoder/ decoder optimization decouples the MIMO channel into parallel subchannels if the criterion is the minimization of weighted sum of MSEs of all subchannels.

It is of great interest to retain this diagonalized structure for other criteria such as minimization of maximum or average BER. In [99] a unified framework was developed for multicarrier MIMO systems which generalizes the existing result. Instead of dealing with each designing criterion separately, the minimization of some arbitrary objective function of the MSEs of all channel subchannels $f_0(MSE_i)$, were considered, where MSE is the MSE of the ith spatial subchannel, (Objective function of the SNRs and of the BERs are easily incorporated in MSE). The objective function f_0 must be chosen reasonably such that it is increasing in each one one if its arguments while having the rest fixed.

Two families of objective functions are considered here that embodies all the above and other reasonable criteria: Schur-concave and Schur-convex functions that arise in majorization theory.

For any $\mathbf{x} \in \mathcal{R}^n$, let $x_{[1]} \geq ... \geq x_{[n]}$ denote the components of $\mathbf{x}$ in descending order. Also, let $\mathbf{x}, \mathbf{y} \in \mathcal{R}^n$. We say vector $\mathbf{x}$ is majorized by vector $\mathbf{y}$ and represent it by $\mathbf{x} \prec \mathbf{y}$ if

$$\sum_{i=1}^{k} x_{[i]} \leq \sum_{i=1}^{k} y_{[i]}, \quad 1 \leq k \leq n-1$$
$$\sum_{i=1}^{n} x_{[i]} = \sum_{i=1}^{n} y_{[i]} \tag{4.71}$$

Using the above definitions, we can define Schur-concave and Schur-convex functions. A real valued function f defined on a set $\mathcal{A} \subseteq \mathcal{R}^n$ is said to be Schur-convex on $\mathcal{A}$ if

$$\mathbf{x} \prec \mathbf{y} \text{ on } \mathcal{A} \Rightarrow \ f(\mathbf{x}) \leq f(\mathbf{y}), \tag{4.72}$$

Similarly, f is said to be Schur-concave on $\mathcal{A}$ if

$$\mathbf{x} \prec \mathbf{y} \text{ on } \mathcal{A} \Rightarrow \ f(\mathbf{x}) \geq f(\mathbf{y}), \tag{4.73}$$

From the above definitions, we see that, if f is Schur-convex on $\mathcal{A}$, then $-f$ is Schur-concave on $\mathcal{A}$ and vice versa.

Similar to the procedure in subsection 4.3.4, we first derive the optimum decoder $\mathbf{G}^*$ assuming the linear precoder $\mathbf{F}$ is fixed and we obtain Eqs. (4.56) and (4.58). From (4.58), the MSE for the ith diagonal element is given by

$$\text{MSE}_{ii} = \frac{1}{1 + \mathbf{f}_i^H \mathbf{H}^H \mathbf{R}_{nn,i} \mathbf{H} \mathbf{f}_i} \tag{4.74}$$

where $\mathbf{f}_i$ is the ith column of matrix $\mathbf{F}$.

Since many objective functions are expressed as functions of signal to noise and interference ratio (SINR), we shall express MSE as a function of SINR. It is shown in [99] that the ith diagonal element of SINR can be upper bounded by

$$[SINR]_i \leq \mathbf{f}_i^H \mathbf{H}^H \mathbf{R}_{nn,i} \mathbf{H} \mathbf{f}_i \tag{4.75}$$

Therefore, the SINR can be related as a function of MSE as

$$[SINR]_i = \frac{1}{MSE_i} - 1 \tag{4.76}$$

Under the Gaussian noise assumption, the symbol error probability can also be related to SINR as

$$P_e(SINR) = \alpha Q(\sqrt{\beta \ SINR}) \tag{4.77}$$

where α and β are scalars and depends on the modulation scheme. Using the Chernoff upper bound we can approximate the symbol error probability for higher SINR values as

$$P_e \simeq (1/2)\alpha e^{-\frac{\beta}{2} SINR} \tag{4.78}$$

The BER can be approximately obtained from symbol error probability as

$$BER \simeq Pe/\log_2(M) \tag{4.79}$$

where M is the constellation size. Both exact BER function and the Chernoff upper bound are convex decreasing functions of SINR. In addition, for BER less than 2×10^{-2}, both functions are convex increasing functions of the MSE. Therefore, for practical purposes, we can assume the exact BER and the Chernoff upper bound as convex functions of the MSE.

From the above discussion, we conclude that it suffices to focus on objective function of MSEs without loss of generality. The following theorem, presents the optimum linear precoder for any objective function of MSEs.

Theorem 2: Consider the following constraint convex optimization problem

$$\begin{aligned} \min_{\mathbf{F}} \; & f_0(\text{diag}(\text{MSE}(\mathbf{F}))) \\ & \text{tr}(\mathbf{F}\mathbf{F}^H) \leq p_0 \end{aligned} \tag{4.80}$$

where $\text{MSE}(\mathbf{F}) = (\mathbf{I} + \mathbf{F}^H\mathbf{H}^H\mathbf{R}_{nn}^{-1}\mathbf{H}\mathbf{F})^{-1}$. Without loss of generality, it is assumed that the diagonal element of MSE matrix are in decreasing order. $f_0 : \mathcal{R}^K \longrightarrow \mathcal{R}$ is an arbitrary objective increasing function with respect to each variable. Also, we assume $K < v = \text{rank}(\mathbf{H}^H\mathbf{R}_{nn}^H\mathbf{H}) = \text{rank}(\mathbf{H})$.

If f_0 is Schur-concave,

$$\mathbf{F} = \mathbf{V}\mathbf{\Phi}_f \tag{4.81}$$

If f_0 is Schur-convex,

$$\mathbf{F} = \mathbf{V}\mathbf{\Phi}_f\mathbf{U}^H \tag{4.82}$$

where $\mathbf{V}$ is an $M_t \times K$ matrix orthogonal matrix consisting of the eigenvectors corresponding to the K largest eigenvalues $\{\lambda\}_{i=1}^K$ of $\mathbf{H}^H\mathbf{R}_{nn}^H\mathbf{H}$. $\mathbf{\Phi}_f$ is an $v \times v$ diagonal matrix with diagonal elements given by $\{\phi_{f,i}\}^2$, $i = 1, 2, ...v$, and $\mathbf{U}$ is a unitary matrix such that $\text{MSE}(\mathbf{F}) = (\mathbf{I}+\mathbf{F}^H\mathbf{H}^H\mathbf{R}_{nn}^{-1}\mathbf{H}\mathbf{F})^{-1}$ has identical diagonal elements.

Proof: see [99].

For Schur-concave objective functions, both $\mathbf{FHG}$ and $\text{MSE}(\mathbf{F})$ are fully diagonalized. In this case, the corresponding MSEs and SINRs, for $i = 1, 2, ...K$ are given by using (4.76)

$$MSE_i = \frac{1}{1 + \phi_{f,i}^2\lambda_i} \tag{4.83}$$

$$SINR_i = \phi_{f,i}^2\lambda_i \tag{4.84}$$

where λ_i, are the K largest eigenvalues of $\mathbf{H}^H\mathbf{R}_{nn}^H\mathbf{H}$ in increasing order, $\phi_{i,f}^2$ represent the allocated power and w_i is the white noise.

For Schur-convex objective functions, $\mathbf{FHG}$ is diagonalized only up to a specific rotation of data symbols. The MSE matrix is non diagonal with equal diagonal elements and is given by

$$MSE_i = \frac{1}{K}\text{tr}(\text{MSE}(\mathbf{F})) = \frac{1}{K}\left(\sum_{i=1}^{K}\frac{1}{1+\phi_{f,i}^2\lambda_i}\right) \tag{4.85}$$

Similarly, the SINRs are given by using (4.76)

$$SINR_i = \frac{K}{\sum_{i=1}^{K}\frac{1}{1+\phi_{f,i}^2\lambda_i}} - 1 \tag{4.86}$$

We see that in both cases of Schur-concave and Schur-convex objective functions, the original complicated matrix expressions for MSE have been reduced to simple scalar expressions.

Now we can consider different design criteria using the optimum linear decoder derived in (4.56) and the unified framework discussed in Theorem 2. We will show that a great variety of useful objective functions are either Schur-concave or Schur-convex and thus the above Theorem can be applied to simplify the design.

MSE-Based Design

We can select the objective function to be the weighted sum of MSEs as

$$f_0(MSE_i) = \sum_{i=1}^{K} w_{ei} MSE_i, \tag{4.87}$$

or we can choose to minimize the weighted geometric mean of the MSEs by choosing the objective function as

$$f_0(MSE_i) = \prod_{i=1}^{K} (MSE_i)^{w_{ei}} \tag{4.88}$$

It is shown in [99] that both of the above objective functions is minimized when the weights are in increasing order ($w_{ei} \leq w_{i+1}$) and they are then Schur-concave functions. Therefore, by Theorem 2 the diagonal structure is optimal and the MSEs are obtained by (4.83). The resultant convex constraint convex problem for the weighted sum of MSEs is given by

$$\begin{aligned} \min_{\phi_i^2} & \sum_{i=1}^{K} w_{ei}\frac{1}{1+\phi_{f,i}^2\lambda_i} \\ & \sum_{i=1}^{K}\phi_{f,i}^2 \leq p_0 \end{aligned} \tag{4.89}$$

and the solution from the KKT optimality conditions is obtained as

$$\phi_i = (\mu^{-1/2} w_{ei}^{1/2} \lambda_i^{-1/2} - \lambda_i^{-1})_+^{1/2} \tag{4.90}$$

where $\mu^{-1/2}$ is the water-level chosen to satisfy the power constraint with equality. Note that the above convex optimization problem and its solution is nothing but the scaler version of (4.23) and (4.34).

Similarly, we can form the scalar convex optimization expressions for objective function (4.88) with the same power constraint and obtain the solution with KKT optimality condition as

$$\phi_i = (\mu^{-1} w_{ei} - \lambda_i^{-1})_+^{1/2} \tag{4.91}$$

where μ^{-1} is the water-level chosen to satisfy the power constraint with equality. We see that when $w_{ei} = 1$, the (4.91) becomes the classical capacity-achieving water-filling solution.

Another MSE-based criterion is the minimization of the determinant of the MSE matrix. Using the fact that $\mathbf{X} \geq \mathbf{Y} \Rightarrow \det\mathbf{X} \geq \det\mathbf{Y}$ it follows that $\det(\mathrm{MSE}(\mathbf{F}))$ is minimized for the choice of (4.56). Moreover, the determinant of $\mathrm{MSE}(\mathbf{F}) = (\mathbf{I} + \mathbf{F}^H \mathbf{H}^H \mathbf{R}_{nn}^{-1} \mathbf{H}\mathbf{F})^{-1}$ does not change if $\mathbf{F}$ is post-multiplied by a unitary matrix. Therefore, we can always choose an unitary (rotation) matrix such that $\mathrm{MSE}(\mathbf{F})$ is diagonal and then

$$\det(\mathrm{MSE}(\mathbf{F})) = \prod_{i=1}^{K} [\mathrm{MSE}(\mathbf{F})]_{ii} \tag{4.92}$$

Also, since the mutual information is given by

$$\max_{\mathbf{\Sigma_x}} ; I = \log\det(\mathbf{I} + \mathbf{R}_{nn}^{-1} \mathbf{H} \mathbf{\Sigma_x} \mathbf{H}^H) \tag{4.93}$$

where $\mathbf{\Sigma_x} = \mathbf{F}\mathbf{F}^H$. Using the fact that $\det(\mathbf{I}+\mathbf{X}\mathbf{Y}) = \det(\mathbf{I}+\mathbf{Y}\mathbf{X})$, the mutual information can be stated as $I = -\log\det(\mathrm{MSE}(\mathbf{F}))$. Therefore, the maximization of mutual information is equivalent to minimization of $\det(\mathrm{MSE}(\mathbf{F}))$ and by (4.92) is the same as the minimization of the unweighted product of the MSEs. The solution to all these criteria is given the classical capacity-achieving water-filling for the power allocation

$$\phi_i = (\mu^{-1} w_{ei} - \lambda_i^{-1})_+^{1/2} \tag{4.94}$$

Since the average BER performance is dominated by the symbols with the highest MSE, the next reasonable criterion is the minimization of the maximum of the MSEs. In other words, the objective function is

$$f_0(MSE_i) = \max_i \{MSE_i\} \tag{4.95}$$

The above function is Schur-convex [99]. Thus, the MSE of the optimal solution is not diagonal. However, tt is possible to make the diagonal of MSE matrix identical by the optimal rotation matrix. The solution to the resulting scalar convex problem can be written

$$\phi_i = (\overline{\mu}^{1/2} \lambda_i^{-1/2} - \lambda_i^{-1})^+ \tag{4.96}$$

where $\{\overline{\mu}^{1/2}\}$ are multiple water levels chosen to satisfy the optimization constraints.

SNR-Based Criteria

An Objective functions of SINR is related to that of MSE by

$$\tilde{f}_0(\{\text{SINR}_i\}) = f_0(\{\text{MSE}_i\}).$$

One useful such objective function is the weighted geometric mean of the SINRs,

$$\tilde{f}_0(\{\text{SINR}_i\}) = -\prod_{i=1}^{K}(\text{SINR}_i)^{w_{ei}} \tag{4.97}$$

which can be expressed as a function of the MSEs using (4.76)

$$\begin{aligned} f_0(\{\text{MSE}_i\}) &= \tilde{f}_0(\{\text{MSE}_i^{-1} - 1\}) \\ &= -\prod_{i=1}^{K}(\text{MSE}_i^{-1} - 1)^{w_{ei}} \end{aligned} \tag{4.98}$$

$f_0(\{x_i\}) = -\prod_{i=1}^{K}(x_i^{-1} - 1)^{w_{ei}}$ can be shown to be minimized when the weights are in increasing order and is then a Schur-concave function. Thus, the objective function of (4.97) is concave when $MSE_i < 0.5$, a condition easily satisfied. Hence, by Theorem 2, the diagonalized structure is optimal and the SINR is given by (4.84). The solution to the constraint convex optimization problem, is

$$\phi_i = \left(\frac{w_{ei}}{\sum_{i=1}^{K} w_{ei}} p_0\right)^{1/2} \tag{4.99}$$

Note that if $w_{ei} = 1$, the solution is $\phi_i = (p_0/K)^{1/2}$, *i.e.*, uniform power allocation.

There are other SINR-based criteria discussed in [99]. In particular, it is shown that the maximization of $\prod_{i=1}^{K}(1 + SINR_i)$ is equivalent to the minimization of the determinant of MSE and also the maximization of mutual information, both discussed before, with the solution given by capacity-achieving water pouring expression given by (4.94). Also, maximization of the minimum SINR is equivalent to the minimization of maximum MSE treated before.

BER-Based Criterion

The minimization of the maximum of the BERs is equivalent to the maximization of the minimum of the SINRs and to the minimization of the maximum of the MSEs, if all subchannels have the same constellations. Hence their solution is given by (4.96). we only consider the minimization of average BER. Let us first consider the minimization of the arithmetic mean of BERs. The objective function is

$$\tilde{f}_0(\{\mathrm{BER}_i\}) = \sum_{i=1}^{K} \mathrm{BER}_i \tag{4.100}$$

which can be expressed as a function of the MSEs using (4.76), (4.77) and (4.79) as

$$f_0(\{\mathrm{MSE}_i\}) = \sum_{i=1}^{K} \mathrm{BER}(\mathrm{MSE}_i^{-1} - 1) \tag{4.101}$$

The function $f_0(\{x_i\}) = \sum_{i=1}^{K} \mathrm{BER}(x_i^{-1} - 1)$, (assuming $\theta \geq x_i > 0$, for sufficiently small θ such that $\mathrm{BER}(x_i^{-1} - 1) \leq 2 \times 10^{-2}$) is a Schur-convex function [99]. Therefore, by Theorem 2, the optimal solution has a non-diagonal MSE matrix with diagonal elements given by (4.85) which have to be minimized. The scalarized convex optimization problem is given by

$$\begin{aligned} \min_{t_i, \phi_i^2} & \sum_{i=1}^{K} \alpha_i Q\left(\sqrt{\beta_i (t_i^{-1} - 1)}\right) \\ \theta \geq t_i \geq & \frac{1}{K}\left(\sum_{i=1}^{K} \frac{1}{1 + \lambda_i \phi_i^2}\right) \\ & \sum_{i=1}^{K} \phi_i^2 \leq p_0 \end{aligned} \tag{4.102}$$

Unfortunately, this problem does not have a closed form solution and one has to resort to iterative methods such as interior-point methods [99].

4.4 Precoder in MIMO Space-Time Code Systems

Space-time (ST) coding is can effectively exploit the spatial diversity offered by MIMO systems by appropriately mapping data streams across time and space. In this section, we show how precoding can be used in conjunction with space-time codes. First, we consider how to design linear precoder in a channel with fading correlation for a space-time MIMO system. Next, in section 4.4.2, we show how to design linear and unitary precoder in order to maximize diversity and coding gain.

4.4.1 Linear Precoder for Space-Time Coded System with Fading Correlation

So far, we have assumed that the there is no spatial correlation among transmit and receive antennas. In other words, element of the MIMO channel matrix fades independently. However, in many practical downlink scenarios, there may be high correlation between base station (BS) antennas since the BS antennas are typically placed high above the ground and see no local scatterers.

As a results the columns of **H** matrix are correlated. However, the received signal at the mobile is a linear combination of several multipaths reflected from several local scatterers leading to uncorrelated fading across the receive antenna. Hence the rows of **H** are uncorrelated. Studies show that fading correlation reduces MIMO channel capacity and system performance [120]. In this section, we show that a linear precoder that knows only the transmit antenna correlation matrix can be employed to improve the performance.

Suppose in such environment, the MIMO flat fading channel can be written as

$$\mathbf{H} = \mathbf{H_w}\mathbf{R}_a^{1/2} \tag{4.103}$$

where $\mathbf{R}_a^{1/2}$ is the $M_t \times M_t$ transmit antenna correlation matrix and $\mathbf{H_w}$ is an $M_r \times M_t$ *i.i.d* complex matrix.

We will assume a block-fading model wherein $\mathbf{H_w}$ remains constant over the entire periods spanning the space-time codeword and then changes independently over another space-time block.

Fig. 4.10 shows the block diagram of the MIMO system with space-time code and precoder. Let the length of space-time codeword be N time-symbols. At time instant n, the space time encoder takes in a set of input bits and creates a $K \times 1$ output code symbol vector

$$\mathbf{c}(n) = [c_1(n), c_2(n), ..., c_K(n)]^T$$

where $K \leq M_t$. A time sequence of N code symbol vectors $[\mathbf{c}(Nt), \mathbf{c}(Nt - 1), ..., \mathbf{c}(Nt - N + 1)]^T$ form a $K \times N$ space-time codeword,

$$\mathbf{x}(t) = [\mathbf{c}(Nt), \mathbf{c}(Nt - 1), ..., \mathbf{c}(Nt - N + 1)].$$

The $K \times N$ space-time codeword is then processed by the $M_t \times K$ precoder matrix **F** to produce $M_t \times N$ output matrix which is then sent over M_t antennas. Note that the precoder **F** adds redundancy of $M_t - K$ and may provide additional diversity gains. The system equation is given by

$$\mathbf{y} = \mathbf{HFx} + \mathbf{w} \tag{4.104}$$

where $\mathbf{x}$ is the $K \times N$ codeword matrix, $\mathbf{y}$ is $M_r \times N$ received signal matrix and $\mathbf{w}$ is $M_r \times N$ noise matrix. We assume $\mathbf{R_{nn}} = \sigma^2\mathbf{I}$. Substituting (4.103) in (4.104) yields

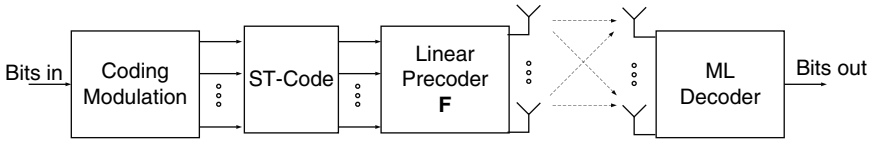

Fig. 4.10. Linear precoder and space-time code in correlated fading channel [[110]©IEEE].

$$\mathbf{y} = \mathbf{H_w}\mathbf{R}_a^{1/2}\mathbf{F}\mathbf{x} + \mathbf{w} \tag{4.105}$$

Let $\mathbf{x}^k(t)$ be the $K \times N$ transmitted space-time codeword at time t. At the receiver, the maximum likelihood (ML) detection is performed. If the ML decoder chooses the nearest distinct $K \times N$ codeword $\mathbf{x}^l(t)$ instead of $\mathbf{x}^k(t)$, the pairwise error matrix can be written as $\mathbf{\Delta x}(k,l,t) = [\mathbf{x}^k(t) - \mathbf{x}^l(t)]$. An upper bound for pairwise error probability (PEP) is given by [128]

$$P(\mathbf{x}^k(t) \rightarrow \mathbf{x}^l(t)) \leq \frac{1}{(\lambda_{gm}\frac{1}{4\sigma^2})^{vM_r}} \tag{4.106}$$

where, v is the rank of matrix $\mathbf{\Delta x}(k,l,t)\mathbf{\Delta x}^H(k,l,t)$ and λ_{gm} stands for the geometric mean of the product of the v nonzero eigenvalues $\{\lambda_i\}_{i=1}^v$ of $\mathbf{\Delta x}(k,l,t)\mathbf{\Delta x}^H(k,l,t)$, *i.e.* $\lambda_{gm} = (\prod_{i=1}^v \lambda_i)^{1/v}$.

The diversity gain is defined as

$$G_d = N_r \left(\min_{\mathbf{x}^k(t),\mathbf{x}^l(t)} \text{rank}(\mathbf{\Delta x}(k,l,t)\mathbf{\Delta x}^H(k,l,t) \right) \tag{4.107}$$

As seen from (4.106), the diversity gain determines the slope of the upper bound for the log-log pairwise error probability-SNR curve. Maximum diversity is obtained if the matrix $\mathbf{\Delta x}(k,l,t)$ is full rank for all distinct $k,l,$.

The coding gain is the minimum of the product of eigenvalues of

$$\mathbf{\Delta x}(k,l,t)\mathbf{\Delta x}^H(k,l,t)$$

among all distinct pairs of $(\mathbf{x}^k(t), \mathbf{x}^l(t))$. In other words, the coding gain can be written as

$$G_c = \min(\prod_{i=1}^{v} \lambda_i)^{1/v} \tag{4.108}$$

For a given diversity gain, the coding gain measures the saving in SNR of the space-time code.

We can design optimal linear precoder given such a known space-time encoder. With the inclusion of the linear precoder $\mathbf{F}$, the effective minimum distance error matrix becomes $\overline{\mathbf{\Delta x}} = \mathbf{F}\mathbf{\Delta x}$. Similar to the proof steps in [128], the PEP can be upper bounded by

$$P(\mathbf{x}^k(t) \rightarrow \mathbf{x}^l(t)) \leq e^{-d^2_{\min}(t)/2} \tag{4.109}$$

where

$$d^2_{min} = (1/\sigma^2)\|\mathbf{H_w}(t)\mathbf{R}_a^{1/2}\overline{\mathbf{\Delta x}}\|_F^2 = \|\mathbf{H_w}(t)\mathbf{R}_a^{1/2}\mathbf{F}\mathbf{\Delta x}\|_F^2 \tag{4.110}$$

where $\|.\|_F$ is the Forbenius norm. Let

$$\mathbf{D} = (1/\sigma^2)\mathbf{R}_a^{1/2}\mathbf{F}\mathbf{\Delta x}\mathbf{\Delta x}^H\mathbf{F}^H\mathbf{R}_a^{H1/2}$$

Define the eigenvalue decomposition (EVD) of $\mathbf{D}$ as $\mathbf{D} = \mathbf{V_d}\mathbf{\Lambda_d}\mathbf{V_d}^H$, where $\mathbf{V_d}$ is an $M_t \times M_t$ orthogonal matrixwhose columns are the eigenvectors of $\mathbf{D}$ matrix and $\mathbf{\Lambda_d}$ is a $M_t \times M_t$ diagonal matrix where its diagonal elements $\{\lambda_{d,i}\}$, $i = 1, 2...M_t$ are eigenvalues of $\mathbf{D}$.

An upper bound on the average PEP can be obtained by taking the expectation of the PEP with respect to $\mathbf{H_w}$. Thus, the average PEP is obtained as

$$\overline{P}(\mathbf{x}^k(t) \to \mathbf{x}^l(t)) \leq \left(\prod_{i=1}^{M_t}(1/(1+\lambda_{d,i}))\right)^{M_r} \tag{4.111}$$

But $\prod_{i=1}^{M_t}(1+\lambda_{d,i}) = \det(\mathbf{I}+\mathbf{D})$, Hence,

$$\overline{P}(\mathbf{x}^k(t) \to \mathbf{x}^l(t)) \leq (\det(\mathbf{I}+\mathbf{D}))^{M_r} = \left(\det(\mathbf{I}+\mathbf{R}_a^{1/2}\mathbf{F}\mathbf{\Delta x}\mathbf{\Delta x}^H\mathbf{F}^H\mathbf{R}_a^{H1/2})\right)^{M_r} \tag{4.112}$$

Now we can find the optimal $\mathbf{F}$ that minimizes the average PEP by solving the following optimization problem

$$\begin{aligned} \max_{\mathbf{F}} \; J &= \det\left(\mathbf{I}+(1/\sigma^2)\mathbf{R}_a^{1/2}\mathbf{F}\mathbf{\Delta x}\mathbf{\Delta x}^H\mathbf{F}^H\mathbf{R}_a^{H1/2}\right) \\ &\text{tr}(\mathbf{F}\mathbf{F}^H) = p_0 \end{aligned} \tag{4.113}$$

where p_0 is the total transmit power across M_t transmit antennas. We initially assume that $\text{rank}(\mathbf{R}_a) = K$ for simplicity. Let us define the EVD for $\mathbf{\Delta x}\mathbf{\Delta x}^H = \mathbf{V_x}\mathbf{\Lambda_x}\mathbf{V_x}^H$, where $\mathbf{V_x}$ is the $K \times K$ orthonormal eigenmatrix and $\mathbf{\Lambda_x}$ is the $K \times K$ diagonal matrix of eigenvalues, $\lambda_{x,i}$, for $i = 1, 2, ...K$. let us also define the singular value decomposition (SVD)

$$\mathbf{R}_a^{1/2} = (\mathbf{U_r} \quad \overline{\mathbf{U_r}}) \begin{pmatrix} \mathbf{\Lambda_r} & \mathbf{0} \\ \mathbf{0} & \overline{\mathbf{\Lambda_r}} \end{pmatrix} (\mathbf{V_r} \quad \overline{\mathbf{V_r}})^H \tag{4.114}$$

where $\mathbf{U_r}$ and $\mathbf{V_r}$ are $M_t \times K$ orthogonal matrix whose columns are basis for the range space of $\mathbf{R}_a^{1/2}$. $\overline{\mathbf{V_r}}$ and $\overline{\mathbf{U_r}}$ are $M_t \times (M_t - K)$ orthogonal matrix which constitutes a basis for the null space of $\mathbf{R}_a^{1/2}$. $\mathbf{\Lambda_r}$ is a diagonal matrix containing the K nonzero eigenvalues $\{\lambda_r\}_{i=1}^K$ arranged in a decreasing order from the top-left to bottom-right and $\overline{\mathbf{\Lambda_r}}$ contains the zero eigenvalues.

It is shown in [110] that the solution to the above optimization problem is given by

$$\begin{aligned} \mathbf{F} &= \mathbf{V_r}\mathbf{\Phi_f}\mathbf{V_x}^H \\ \mathbf{\Phi_f} &= (\gamma\mathbf{I} - \mathbf{\Lambda_r}^{-2}\mathbf{\Lambda_x}^{-1})_+^{1/2} \end{aligned} \tag{4.115}$$

where $\mathbf{\Phi_f}$ is a $K \times K$ matrix. We see that the power allocation on the eigenmodes of $\mathbf{R}_a^{1/2}$ is given by water-pouring policy and depends on the eigenvalues of $\mathbf{\Delta x}\mathbf{\Delta x}^H$ and $\mathbf{R}_a^{1/2}$. Note that when $\text{rank}(\mathbf{R}_a) \neq K$, the precoder

should allocate power on the strongest K eigenvectors of the transmit antenna correlation matrix since otherwise, the cost function is not maximized.

Typically orthogonal space-time codes designed for $i.i.d$ channels have $\mathbf{\Delta x \Delta x}^H = \beta \mathbf{I}$. Thus, $\mathbf{\Lambda_x} = \beta \mathbf{I}$ and $\mathbf{V_x} = \mathbf{I}$, where β is a scalar. In this case, the rotation matrix $\mathbf{V_r}$ ensures that the optimal precoder allocates power only to the eigenmodes of $\mathbf{R}_a$.

Fig. 4.11, [110] shows the advantage of precoding for a rate 3/4 space-time coded system with M_t is 2 and 3 and $M_r = 2$ and $K = 3$. The antenna correlation coefficient $r_{ij}/(\sqrt{r_{ii}r_{jj}}) = 0.7$, where r_{ij} is the ijth element of $\mathbf{R}_a^{1/2}$. For BER of 10^{-2}, the precoding gain is 4.7 dB over an non precoded system.

4.4.2 Linear Constellation Precoding (LCP) for Space-Time Codes

As we discussed before, space-time (ST) coding is a powerful technique that can offer both spatial diversity and coding gain. The most examples of ST codes are ST trellis codes and ST block code with orthogonal design. ST trellis codes enjoy maximum diversity and large coding gains but it is difficult to use them with large constellation size due to their decoding complexity

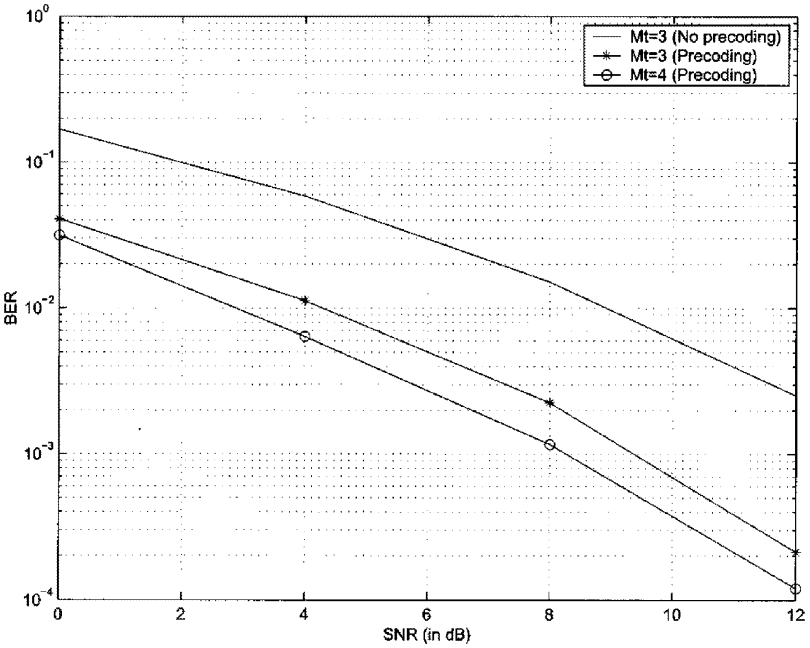

Fig. 4.11. Precoding gain for rate 3/4 space-time code and antenna correlation function 0.7 [[110]©IEEE]

growing exponentially with the transmission rate. Space-time-orthogonal design (ST-OD) codes, on the other hand offer maximum transmit diversity with affordable low-complexity decoders. However, when used with complex constellations and number of transmit antennas M_t greater than two, the transmission rates of ST-OD are reduced.

An alternative transmit diversity scheme that does not sacrifice rates are linear constellation precoding (LCP) as shown in Fig. 4.12. The coded and modulated symbol streams from a normalized constellation $\mathcal{C}$ is first parsed into $M_t \times 1$ signal vectors $\mathbf{x}$ and then is linearly precoded by an $M_t \times M_t$ matrix $\mathbf{F}$. The precoded block is then sent to the space-time code mapper which maps it to an $M_t \times M_t$ code matrix $\mathbf{s}$ that is sent over M_t antennas during M_t time intervals. Specifically, the (i,j)th entry $x_{i,j} = u_{i,j}\mathbf{f}_j^T\mathbf{x}$ is transmitted through the ith antenna at the jth time interval, where $u_{i,j}$ denotes the (i,j)th entry of a unitary matrix $\mathbf{U}$, and vector $\mathbf{f}_j^T$ denotes the jth row of $\mathbf{F}$. Let us define $\mathbf{D_x} = \text{diag}(\mathbf{f}_1^T\mathbf{x}, ..., \mathbf{f}_{M_t}^T\mathbf{x})$, we can then write the $M_t \times M_t$ transmitted ST-LCP code matrix as

$$\mathbf{s} = \mathbf{U}\mathbf{D_x} \tag{4.116}$$

The received symbol at the receive antennas can be expressed as

$$\mathbf{y} = \mathbf{H}\mathbf{s} + \mathbf{w} = \mathbf{H}\mathbf{U}\mathbf{D_x} + \mathbf{w} \tag{4.117}$$

where $\mathbf{y}$ is $M_r \times M_t$ received signal matrix and $\mathbf{w}$ is the $M_r \times M_t$ noise matrix with $[\mathbf{w}]_{i,j}$ is a circularly symmetric complex Gaussian noise. At the receiver end, we will rely on $\mathbf{y}$ to detect $\mathbf{s}$ with maximum likelihood (ML) detection algorithm. We assume that the channel coefficients are only known to the receiver.

The pairwise matrix event $[\mathbf{s}^k - \mathbf{s}^l]$, where $\mathbf{s} = \mathbf{U}\ \text{diag}(\mathbf{f}_1^T\mathbf{x}, ..., \mathbf{f}_{M_t}^T\mathbf{x})$, From (4.106) and using the facts that $\mathbf{U}$ is full rank, and $\mathbf{D_x}$ is diagonal, the diversity gain for the LCP system is given by $M_r|N_{\mathbf{\Delta x}}|$, where $N_{\mathbf{\Delta x}}$ is given by

$$N_{\mathbf{\Delta x}} = \{m : \|\mathbf{f}_m^T(\mathbf{x}^k - \mathbf{x}^l)\|^2 \neq 0\} \tag{4.118}$$

and $|N_{\mathbf{\Delta x}}|$ denotes the cardinality of $N_{\mathbf{\Delta x}}$. Also, the maximum diversity gain $M_t M_r$ is achieved if the following maximum diversity conditions holds true

$$\|\mathbf{f}_m^T(\mathbf{x}^k - \mathbf{x}^l)\| \neq 0 \quad \forall\ m \in [1,\ M_t], \forall\ \mathbf{x}^k, \mathbf{x}^l \in \mathcal{C}^{M_t} \tag{4.119}$$

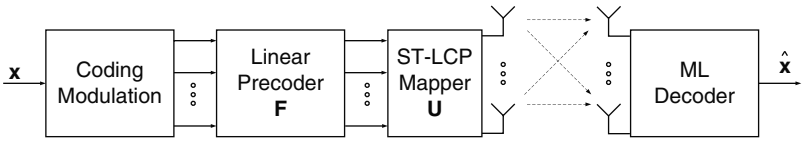

Fig. 4.12. Linear constellation precoder for space-time MIMO system [[154]©IEEE]

Since $\mathbf{f}_m^T(\mathbf{x}^k - \mathbf{x}^l)$ is the mth coordinate of the precoder vector $\mathbf{F}^T(\mathbf{x}^k - \mathbf{x}^l)$, we conclude from the above equation that to achieve maximum diversity, each $M_t \times 1$ output vector $\mathbf{F}^T\mathbf{x}^k$ must be distinct in all its M_t coordinates.

From (4.108) and the fact that $\lambda_m = \|\mathbf{f}_m^T(\mathbf{x}^k - \mathbf{x}^l)\|^2$ for $m = 1, 2, ...M_t$, we can express coding gain for LCP matrix when $G_d = M_t M_r$ as

$$G_c = \min \left(\prod_{i=1}^{M_t} \|\mathbf{f}_m^T(\mathbf{x}^k - \mathbf{x}^l)\| \right)^{2/M_t} \tag{4.120}$$

We will design the linear constellation precoder $\mathbf{F}$ such that it guarantees maximum diversity and high coding gains. We shall not impose any constraint on $\mathbf{F}$ except the following power constraint

$$\mathrm{tr}(\mathbf{F}\mathbf{F}^H) = M_t \tag{4.121}$$

which ensures that total transmit energy over M_t time intervals is $E\{\|\mathbf{F}\mathbf{x}\|^2\} = E\{\|\mathbf{x}\|^2\} = M_t$.

Existence of Diversity-Maximizer Unitary Precoder

Unitary constellation precoding have certain advantage over nonunitary LCPs. A unitary LCP preserves distances among M_t constellation points. On the other hand, a non-unitary LCP, makes some paris of constellation points closer or farther to each other.

Theorem 3: If the constellation size is finite, there always exists at least one unitary $\mathbf{F}$ precoder satisfying (4.119), *i.e.* achieves the maximum diversity gain $M_t M_r$.

Proof: From (4.119), it suffices to show there exists an $M_t \times M_t$ unitary matrix such that each $M_t \times 1$ output vector $\mathbf{F}^T(\mathbf{x}^k - \mathbf{x}^l)$ must be non zero in all its M_t coordinates for all distinct $\mathbf{x}^k$ and $\mathbf{x}^l$. For detailed proof, see [154].

Coding-Gain-Maximizer Unitary Precoder

Now, we look for a unitary $\mathbf{F}$ that maximizes coding gain among diversity-maximizing unitary precoders. The optimum unitary precoder can be found by solving the following optimization problem

$$\begin{aligned} \mathbf{F}_{opt} = \arg\max_{\mathbf{F}} \min_{\mathbf{x}^k \neq \mathbf{x}^l} \prod_{m=1}^{M_t} \|\mathbf{f}_m^T(\mathbf{x}^k - \mathbf{x}^l)\|^{2/M_t} \\ \mathrm{tr}(\mathbf{F}\mathbf{F}^H) = M_t \end{aligned} \tag{4.122}$$

Finding $\mathbf{F}_{opt}$ involves multidimensional nonlinear optimization over M_t^2 complex entries of $\mathbf{F}$. However knowing $\mathbf{F}$ is unitary, we can parameterize it using M_t^2 real entries taking values from finite intervals.

LCP Design Based on Parameterization

Let us consider a real orthogonal precoder with $M_t = 2$,

$$\mathbf{F}_{\Phi} = \begin{bmatrix} \cos\Phi & \sin\Phi \\ -\sin\Phi & \cos\Phi \end{bmatrix} \tag{4.123}$$

where $-\pi/2 \leq \Phi \leq \pi/2$. This precoder rotates every constellation point so that each rotated point is different from other rotated points in both coordinates. Therefore, it is a diversity maximizing precoder.

Another example is a 2×2 complex unitary which can be parameterized as

$$\mathbf{F}_{\Psi,\Phi} = \mathbf{D}\mathbf{U}_{\Psi,\Phi}, \tag{4.124}$$

where

$$\mathbf{U}_{\Psi,\Phi} = \begin{bmatrix} \cos\Psi & e^{-j\Phi}\sin\Psi \\ -e^{j\Phi}\sin\Psi & \cos\Psi \end{bmatrix} \tag{4.125}$$

where $\mathbf{D}$ is a 2×2 diagonal unitary matrix, $-\pi \leq \Psi \leq \pi$, $-\pi/2 \leq \Phi \leq \pi/2$.

Any $M_t \times M_t$ unitary matrix can be written as

$$\mathbf{F} = \mathbf{D} \prod_{1 \leq k \leq M_t - 1,\ k+1 \leq l \leq M_t} \mathbf{G}_{kl(\Psi_{kl},\Phi_{kl})} \tag{4.126}$$

where $\mathbf{D}$ is an $M_t \times M_t$ diagonal unitary matrix, $-\pi \leq \Psi_{kl} \leq \pi$, $-\pi/2 \leq \Phi_{kl} \leq \pi/2$ and $\mathbf{G}_{kl(\Psi_{kl},\Phi_{kl})}$ is a complex *Givens* matrix; *i.e.* an identity matrix $\mathbf{I}_{M_t}$ with the (k,k)th, (l,l)th and (l,k)th entries replaced by $\cos\Psi_{kl}$, $\cos\Psi_{kl}$, $\sin\Psi_{kl}\, e^{-j\Phi_{kl}}$ and $-\sin\Psi_{kl}\, e^{-j\Phi_{kl}}$ respectively.

Since multiplication with a diagonal unitary matrix preserves product distances, $\mathbf{D}$ can be ignored in optimization problem of (4.122). Thus, the number of parameters that need to be optimized is $(M_t(M_t-1))$ which is the parameters of the complex Givens matrix. These $M_t(M_t-1)$ parameters are hard to be computed for large number of M_t or constellation size. Algebraic-based design of LCP can be the solution.

Algebraic Construction of LCP: method 1 (LCP-1)

Let $\mathbb{Z}[j]$ is the ring of Gaussian integers whose elements are in the form of $p + jq$ with $p, q \in \mathbb{Z}$. Let also $\mathbb{Q}(j)$ be the smallest subfield of $\mathbb{C}$ including both $\mathbb{Q}$ and j. Suppose the minimal polynomial over subfield $\mathbb{Q}(j)$ is denoted by $(m_{\alpha,\mathbb{Q}(j)}(x))$. Let $\{\alpha_m\}_{m=1}^{N} T$ are the roots of the minimal polynomial over subfield $\mathbb{Q}(j)$.

Then the the linear constellation precoder can be constructed as follows

$$\mathbf{F} = \frac{1}{\gamma}\begin{bmatrix} 1 & \alpha_1 & \dots & \alpha_1^{M_t-1} \\ 1 & \alpha_2 & \dots & \alpha_2^{M_t-1} \\ \vdots & \vdots & & \vdots \\ 1 & \alpha_{M_t} & \dots & \alpha_{M_t}^{M_t-1} \end{bmatrix} \tag{4.127}$$

From Algebraic theory, it is easy to show [154] that the first row of $\mathbf{F}$ forms a basis for $\mathbb{Q}(j)$, *i.e.*, $\mathbf{f}_1^T(\mathbf{x}^k - \mathbf{x}^l) \in \mathbb{Q}(j)$. It follows that for all $(\mathbf{x}^k - \mathbf{x}^l) \in \mathbb{Z}[j]$, $\mathbf{f}_1^T(\mathbf{x}^k - \mathbf{x}^l)$ is a root of a monic polynomial coefficients with coefficients in $\mathbb{Z}[j]$. Defining $\eta_m(\alpha) = \alpha_m (m \in [1, M_t])$, we have $\eta_m(\mathbf{f}_1^T(\mathbf{x}^k - \mathbf{x}^l)) = \mathbf{f}_1^T(\mathbf{x}^k - \mathbf{x}^l)$. $\prod_{m=1}^{N} T\eta_m(\mathbf{f}_1^T(\mathbf{x}^k - \mathbf{x}^l))$ is actually called a relative norm of $(\mathbf{f}_1^T(\mathbf{x}^k - \mathbf{x}^l))$ which is equivalent to the definition of product distance in (4.120). It can be shown that if $\mathbf{f}_1^T(\mathbf{x}^k - \mathbf{x}^l)$ is in $\mathbb{Q}(j)$ and also a root of a monic polynomial coefficients with coefficients in $\mathbb{Z}[j]$, then its relative norm is $\in \mathbb{Z}[j]$. Therefore, for $\mathbf{x}^k \neq \mathbf{x}^l$, the minimum product distance being nonzero is at least one since it belongs to $\in \mathbb{Z}[j]$.

After taking into account the constant $1/\gamma$ and and the energy normalization, the coding gain is equal to $4d^2/(\gamma^2 E_s)$, where d and E_s depends on constellation.

If constellation belongs to $\mathbb{Z}[j]$ and normalized by $\sqrt{E_s}$, the coding gain is lower bounded as [154]

$$G_c \geq \frac{1}{\gamma^2 E_s} \tag{4.128}$$

Also, for QAM an PAM constellation whose points are normalized by $\sqrt{E_s}$ and has a minimum distance equal to $2d$, the maximum coding gain is lower and upper bounded by

$$(\ln 2)\frac{4d^2}{N_T E_s} \leq G_c^{\max} \leq \frac{4d^2}{N_T E_s} \tag{4.129}$$

Let us define $\mathcal{S} = \{M_t : M_t = \deg(m_{\alpha,\mathbb{Q}(j)}(x)), \alpha = e^{j2\pi/P}, P \in \mathbb{N}\}$. It can be proved that odd integers $M_t > 1$ do not belong to $\mathcal{S}$ while even integers do belong to $\mathcal{S}$. It is shown in [154] that LCP-1 can only achieve the upper bound in (4.129) if in $M_t \in \mathcal{S}$.

Algebraic Construction of LCP: method 2 (LCP-2)

LCP-1 does not guarantee a unitary precoder matrix. As we mentioned before, unitary precoder is often preferred over non unitary ones. A unitary precoder for any value of M_t can be constructed as

$$\mathbf{F} = \mathbf{F}_{M_t}^T \mathrm{diag}(1, \alpha, ..., \alpha^{M_t-1}), \quad \alpha = e^{j2\pi/P} \tag{4.130}$$

where $\mathbf{F}_{M_t}$ is the M_t-point inverse fast Fourier transform (FFT) matrix whose (i,j)th entry is given by $\frac{1}{\sqrt{M_t}} e^{j\frac{2\pi}{M_t}(i-1)(j-1)}$. A lower bound for coding gain of the LCp-2 is given by [154]

$$G_c \geq (\frac{1}{HM_t})^{2(\chi-1)}(\frac{1}{M_t E_s}) \tag{4.131}$$

where $\chi = \sum_{i=1}^{I} D_i/M_t$ and $H = \max_{\mathbf{x}^k,\mathbf{x}^l \in \mathcal{C}} \|\sqrt{E_s}(\mathbf{x}^k - \mathbf{x}^l)\|$. I is the number of distinct minimum polynomial $p_i(x)$ of $\beta_m = \alpha e^{j2\pi(m-1)/M_t}$, $m = 1, ...M_t$, over $\mathbb{Q}(j)$ and D_i is the degree of $p_i(x)$, $i = 1, ...I$ and $D_i \geq M_t$.

To design a LCP with large coding gain, the number of distinct minimal polynomial β_m and their degree must be as small as possible to make χ small [154].

It turns out that the space-time code with unitary constellation precoder can achieve higher average mutual information than orthogonal design space time codes, for $Nt > 2$ and large SNR [154].

the PEP performance of LCP and ST-OD compared via simulation and the results are plotted in Fig. 4.13 and Fig. 4.14. In both figure, $M_t = 3, 4$. For $M_t = 4$, complex precoders $\mathbf{F}$ were constructed according to LCP-1. For $M_t = 3$, the parameterization method were used. Rate 3/4 ST-OD codes were constructed according to [127] and were compared with rate 1 ST-LCP codes. 64 QAM constellation were used for ST-LCP to maintain the same spectral efficiency of 6 bits/s/Hz that ST-OD achieves with 256 QAM constellation. The SNR gain of ST-LCP gain is less than 1 dB in Fig. 4.13, it increases to 3

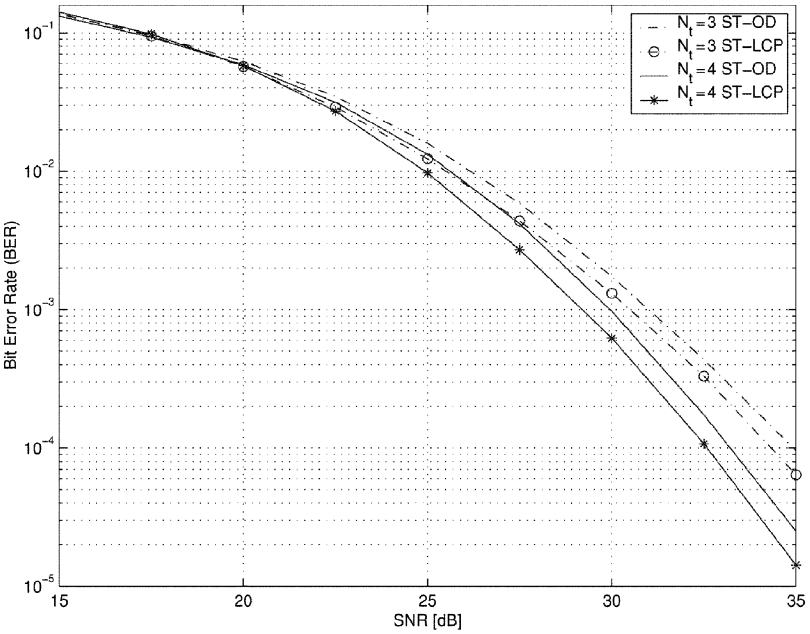

Fig. 4.13. BER performance of ST-OD (256-QAM) versus ST-LCP (64-QAM), with $M_t = 3, 4$, $M_r = 1$ [[154]©IEEE].

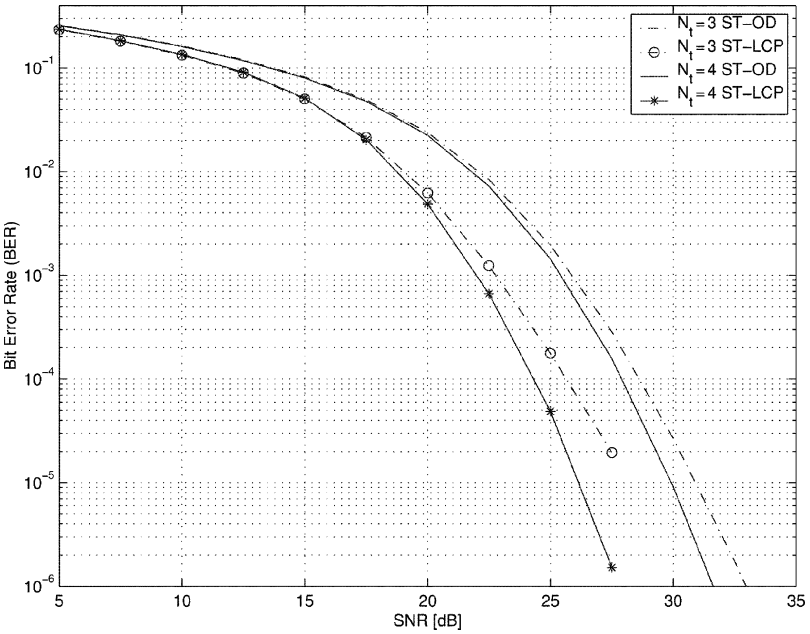

Fig. 4.14. BER performance of ST-OD (256-QAM) versus ST-LCP (64-QAM), with $M_t = 3, 4$, $M_r = 2$ [[154]©IEEE].

dB when $M_r = 2$ in Fig. 4.14. We see that ST-LCP outperforms ST-OD for all cases.

4.5 Precoding Techniques for the Limited Feedback Channel Capacity

The precoding technique in the MIMO channel enables the transmitter to adjust its transmit signal pattern so that the strongest channel mode is exploited to enhance the system performance if the channel state information is known to the transmitter. For time division duplexing (TDD) communication systems, where uplink and downlink channels share the same frequency band at different time, the channel information can be estimated by the transmitter due to channel reciprocity property if the channel state is unchanged. On the contrary, for frequency division duplexing (FDD) systems, where different frequency bands are allocated for the downlink and the uplink channels, the channel response in different frequency is not the same. Hence, a feedback channel is necessary to deliver the estimated channel knowledge at the receiver back to the transmitter.

For a time varying channel, the channel knowledge at the transmitter should be updated every time when the channel changes. The feedback

overhead, which increases linearly as the product of the antenna numbers at both ends and the channel delay spread, could be large. Therefore, the precoder design using full channel information is not practical for the system with limited feedback channel capacity. The precoding scheme, which demands less feedback capacity while enjoying the precoding gain, is more appreciated. Two precoding schemes based on either the channel statistic knowledge [145] or the idea called unitary precoding [80], were recently proposed to save the feedback overhead and will be reviewed next.

4.5.1 Precoding with Channel Statistics Knowledge

Since the real-time channel information is not possible at the transmitter due to either fast channel variation or insufficient feedback capacity, the channel statistic knowledge, namely, channel mean or covariance, which varies less frequently, is more likely to be delivered to the transmitter. The precoder design with either the channel mean or covariance matrix available at the transmitter is recently studied in [91, 145, 59] from the channel capacity point of view. For a specified input covariance matrix, the channel capacity is achieved by the use of vector Gaussian symbols [144]. Therefore, the goal of the precoder design here is to determine the best input covariance matrix that maximizes the mutual information when the channel statistic is known to the transmitter [91, 145, 59]. Some related research results are reviewed next.

The downlink, multiple-input, single-output (MISO) scenario considered in [91, 145] is used as an example to illustrate this design idea[1]. The block diagram of the MISO precoder is given in Fig. 4.15, where M_t transmit antennas are separated far enough at the base station to exploit spatial diversity and a single receive antenna is employed at the mobile unit due to its size and power limitation. Furthermore, we assume only one data link is established at a time and the multiple access can be achieved via either time division

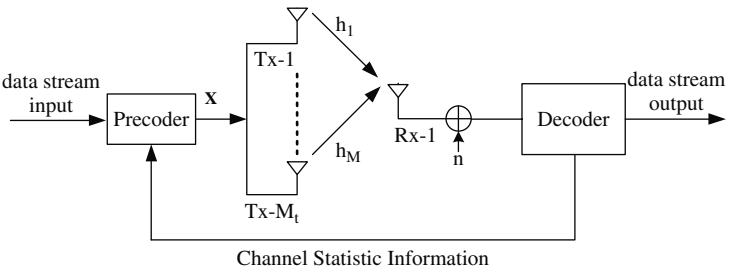

Fig. 4.15. The block diagram of precoder design using channel statistic knowledge [[145]©IEEE].

[1] Based on the similar design concept in [91, 145], Jafar and Goldsmith later extended the precoder design to the MIMO channel in [59].

multiple access (TDMA) or frequency division multiple access (FDMA). Let $\mathbf{x}$ be the $M_t \times 1$ input signal vector at the transmitter. The baseband received signal in the flat fading channel is described as

$$y = \mathbf{x}^{\dagger}\mathbf{h} + n, \tag{4.132}$$

where n is the zero mean circularly complex Gaussian noise sample whose power is equal to σ_n^2 and $\mathbf{h}$ is a $M_t \times 1$ channel vector. Let $\mathbf{h}$ be a circularly symmetric Gaussian random vector as well, whose probability density function (PDF) is completely specified by its mean $\boldsymbol{\nu}$ and variance $\boldsymbol{\Sigma}$ and is denoted as $\mathbf{h} \sim CN(\boldsymbol{\nu}, \boldsymbol{\Sigma})$.

Let $\mathbf{Q}$ be the input covariance matrix of $\mathbf{x}$. Conditioned on the channel realization $\mathbf{h}$, the maximum mutual information is given as

$$\mathcal{I}(\mathbf{x}; y|\mathbf{h}) = \log\left(1 + \frac{\mathbf{h}^{\dagger}\mathbf{Q}\mathbf{h}}{\sigma_{\mathrm{n}}^2}\right). \tag{4.133}$$

The precoder design problem is formulated as

$$\mathbf{Q}^o = \max_{\mathbf{Q}} E_{\mathbf{h}}\{\mathcal{I}(\mathbf{x}; y|\mathbf{h})\} \quad \text{s.t.} \quad E\{\mathbf{x}^{\dagger}\mathbf{x}\} = \mathrm{trace}\{\mathbf{Q}\} = P, \tag{4.134}$$

where the averaged output signal power is limited to P. Let the eigendecomposition of matrix $\mathbf{Q}^o$ be

$$\mathbf{Q}^o = \mathbf{U}_{\mathbf{Q}^{\mathrm{o}}} \boldsymbol{\Lambda}_{\mathbf{Q}^{\mathrm{o}}} \mathbf{U}_{\mathbf{Q}^{\mathrm{o}}}^{\dagger}, \tag{4.135}$$

where

$$\mathbf{U}_{\mathbf{Q}^{\mathrm{o}}} = [\mathbf{u}_{\mathbf{Q}^{\mathrm{o}},1}, \cdots, \mathbf{u}_{\mathbf{Q}^{\mathrm{o}},M_t}], \tag{4.136}$$

$$\boldsymbol{\Lambda}_{\mathbf{Q}^{\mathrm{o}}} = \mathrm{diag}(\lambda_{\mathbf{Q}^{\mathrm{o}},1}, \cdots, \lambda_{\mathbf{Q}^{\mathrm{o}},M_t}), \tag{4.137}$$

and

$$\lambda_{\mathbf{Q}^{\mathrm{o}},1} \geq \lambda_{\mathbf{Q}^{\mathrm{o}},2} \cdots \geq \lambda_{\mathbf{Q}^{\mathrm{o}},M_t}. \tag{4.138}$$

Please note that the ith eigenvector $\mathbf{u}_{\mathbf{Q}^{\mathrm{o}},i}$ specifies the direction of the ith transmit signal while the ith diagonal element $\lambda_{\mathbf{Q}^{\mathrm{o}},i}$ determines the corresponding emitted power along $\mathbf{u}_{\mathbf{Q}^{\mathrm{o}},i}$. Later, we design the optimal input covariance matrix in different scenarios by specifying its eigenvalues and eigenvectors.

Before discussing the precoding algorithm using channel statistic information, let us consider two special cases as follows. First, when the transmitter knows nothing about the channel, the expected value of the mutual information is upper bounded as

$$E_{\mathbf{h}}\{\mathcal{I}(\mathbf{x}; y|\mathbf{h})\} \leq E_{\mathbf{h}}\left\{\log\left(1 + \frac{||\mathbf{h}||^2 P}{M_t \sigma_n^2}\right)\right\}, \tag{4.139}$$

where $||\mathbf{x}||$ is the 2-norm of vector $\mathbf{x}$ [91]. Please note that the above equality holds if and only if

$$\mathbf{Q}^o = \frac{P}{M_t}\mathbf{I}_{M_t}. \tag{4.140}$$

As (4.140) implies, the channel capacity is achieved by transmitting M_t signals in M_t orthogonal directions with equal power, *i.e.,* there is no directional preference for the transmit signal. In the following context, we denotes it as the diversity transmission scheme. Second, when the ideal channel knowledge is available at the transmitter, we can develop the following upper bound as [91]

$$E_{\mathbf{h}}\{\mathcal{I}(\mathbf{x}; y|\mathbf{h})\} \leq E_{\mathbf{h}}\left\{\log\left(1 + \frac{||\mathbf{h}||^2 P}{\sigma_n^2}\right)\right\}, \tag{4.141}$$

where the equality is hold if and only if

$$\mathbf{Q}^o = P\frac{\mathbf{h}\mathbf{h}^\dagger}{||\mathbf{h}||^2}. \tag{4.142}$$

This result implies that when the channel state information is perfectly known at the transmitter, the beamforming scheme, which combines M_t channel gains coherently at the receiver, is able to achieve capacity. As comparing these two capacity achieving schemes, the beamforming scheme not only provides a higher channel capacity but also requires less complexity for symbol decoding than the diversity transmission scheme. However, it demands the instant channel knowledge available at its transmitter. Delivering the real-time channel information from the receiver to the transmitter may not be practical in a time varying channel due to feedback delay. Furthermore, the channel information estimated at the receiver is not perfect as well.

Generally speaking, the solution to the constraint optimization problem in (4.134) for arbitrary $\boldsymbol{\nu}$ and $\boldsymbol{\Sigma}$ is difficult to find. In what follows, we consider the precoder design in (4.134) for two special cases, which depends on the time duration of our interest [145, 59]. First, when the interested time duration is short, the channel information can be somehow track based on the fed back information at the transmitter [145]. The channel knowledge at the transmitter can be modeled as

$$\mathbf{h} \sim \mathcal{CN}(\boldsymbol{\nu}, \sigma_e^2\mathbf{I}), \tag{4.143}$$

which is an non-zero mean circularly complex Gaussian vector. The mean $\boldsymbol{\nu}$ denotes the channel response available while the matrix $\sigma_e^2\mathbf{I}$ denotes the covariance of the estimation error with error power equal to σ_e^2. Here we adopt the same terminology in [145] and name it the channel mean feedback from now on. If the channel mean feedback is possible, the optimal transmission scheme given in [145] is stated in the next Theory 4.4.

Theorem 4: (Visotsky and Madhow [145]) Given the channel mean feedback is feasible, the eigenvectors and the eigenvalues of the optimal input covariance matrix $\mathbf{Q}^o$ satisfy the following conditions:

1. For the eigenvectors of $\mathbf{Q}^o$ we have $\mathbf{u}_{\mathbf{Q}^o,1} = \boldsymbol{\nu}/||\boldsymbol{\nu}||$ and $\mathbf{u}_{\mathbf{Q}^o,2}, \cdots, \mathbf{u}_{\mathbf{Q}^o,M_t}$ form an arbitrary set of orthonormal basis whose span is perpendicular to $\boldsymbol{\nu}$,
2. For the eigenvalues of $\mathbf{Q}^o$ we have $\lambda_{\mathbf{Q}^o,1} = \lambda_o$ and $\lambda_{\mathbf{Q}^o,2} = \lambda_{\mathbf{Q}^o,3} = \cdots = \lambda_{\mathbf{Q}^o,M_t} = (P - \lambda_o)/(M_t - 1)$.

Proof: The proof of the above theorem is omitted here. Interested readers are referred to Sec. III in [145] for the detailed treatment.

When the channel mean feedback is made available, the best transmission scheme, which achieves the highest mutual information, is to transmit the signal along the direction of $\boldsymbol{\nu}$ with power equal to λ_o. Depending on the total available power, if $\lambda_o < P$, we then distribute the residual power equally to other $M_t - 1$ orthogonal directions. This implies that we switch from the beamforming scheme (Rank($\mathbf{Q}^o$)=1) to the diversity transmission (Rank($\mathbf{Q}^o$)=M_t). Although the closed form solutions for the transmit power in different directions, $\lambda_{\mathbf{Q}^o,1}, \cdots, \lambda_{\mathbf{Q}^o,M_t}$, are not given here, they can be computed by some numerical scheme, such as the projected gradient descent algorithm [9] as pointed out in [145].

Another channel model is suitable for the fast time varying channel or a long channel observation period. In this case, the channel mean tracking is not practical and can be treated as zero. It is however that the channel covariance matrix $\boldsymbol{\Sigma}$, which is determined by the relative geometry between the transmitter and the receiver [120], is more stable [145, 59]. As a result, the receiver can gradually passes the channel covariance matrix information to the transmitter and this scheme is denoted as the channel covariance feedback in the sequel. Mathematically, the knowledge of the channel at the transmitter can be modeled as

$$\mathbf{h} \sim \mathcal{CN}(0, \boldsymbol{\Sigma}). \tag{4.144}$$

For the channel covariance feedback, Visotsky and Madhow provides the optimal transmission scheme in [145], which is stated in the following theory.

Theorem 5: (Visotsky and Madhow [145]) For $\mathbf{h} \sim \mathcal{CN}(0, \boldsymbol{\Sigma})$ and channel covariance feedback at the transmitter, the best transmission scheme is to deliver signals along the eigenvector direction of $\boldsymbol{\Sigma}$, *i.e.,*

$$\mathbf{U}_{\mathbf{Q}^o} = \mathbf{U}_{\boldsymbol{\Sigma}}, \tag{4.145}$$

where $\mathbf{U}_{\boldsymbol{\Sigma}}$ denotes all the eigenvectors of matrix $\boldsymbol{\Sigma}$. In order to completely specify the input covariance matrix, the transmitted power corresponding to different direction should be given. Since different direction corresponds to different channel gain, *i.e.,* different eigenvalue of $\boldsymbol{\Sigma}$, the transmit power along various direction can be determined by applying the water filling principle. That is, the better the channel is, the more power we should assign.

Example 1: Channel Mean Feedback

Here we borrow the numerical results from Sec. IV in [145] to illustrate the information rate between different transmission schemes in a system with two

transmit antennas. The channel model we consider is the first order auto-regressive channel model, which is described as

$$\mathbf{h}(t) = a\mathbf{h}(t-1) + \mathbf{w}(t), \tag{4.146}$$

where a is the forgetting factor and $\mathbf{w}(t) \sim \mathcal{CN}(0, \sigma_w^2)$ is an i.i.d. Gaussian vector. Due to the feedback delay d, the channel feedback function is

$$\mathbf{f}(t) = \mathbf{h}(t-d). \tag{4.147}$$

Based on (4.146) and (4.147), the knowledge of the channel at the transmitter can be shown to be

$$\mathbf{h}(t) \sim \mathcal{CN}(\boldsymbol{\nu}, \sigma_n^2\mathbf{I}), \tag{4.148}$$

where $\boldsymbol{\nu} = a^d\mathbf{h}(t-d)$ and $\sigma_n^2 = (\sigma_w^2(1-a^{2d}))/(1-a^2)$. Please note that the value of a^d in (4.148) determines the quality of channel information, namely, the greater a^d is, the better the channel information becomes. Three different transmission schemes are compared, and they are diversity scheme (*i.e.*,$\mathbf{Q} = \frac{P}{M_t}\mathbf{I}_{M_t}$), beamforming scheme (*i.e.*,$\mathbf{Q} = P\frac{\boldsymbol{\nu}\boldsymbol{\nu}^\dagger}{||\boldsymbol{\nu}||^2}$), and the optimal scheme introduced in Theory 1. The result shown in Fig. 4.16 and 4.17 corresponds to the information rate as a function of different schemes with different feedback information quality, namely, $a^d = 0.9$ and 0.3. It is observed from both Fig. 4.16 and 4.17 that when the transmitter has better understanding about the current channel, beamforming achieves the highest information

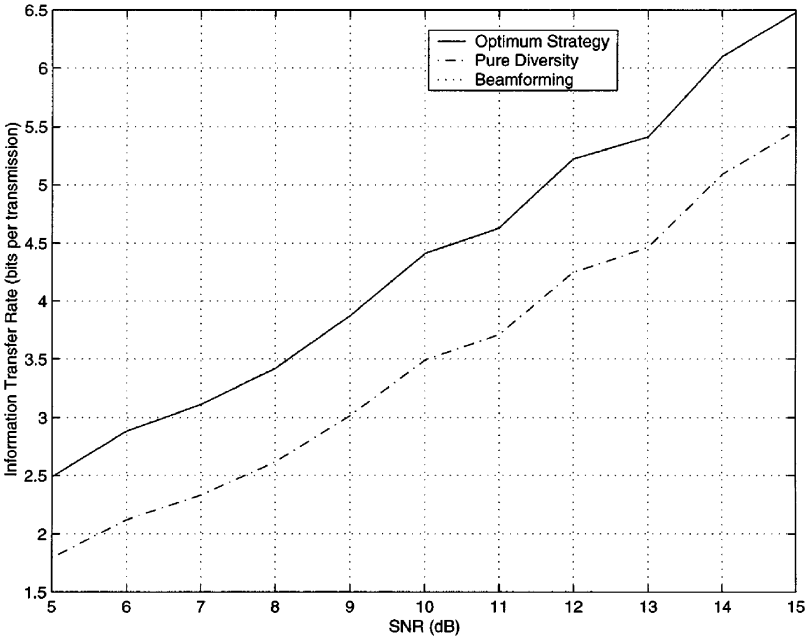

Fig. 4.16. Information rate of different transmission schemes in the channel mean feedback case, $a^d = 0.9$ [[145]©IEEE].

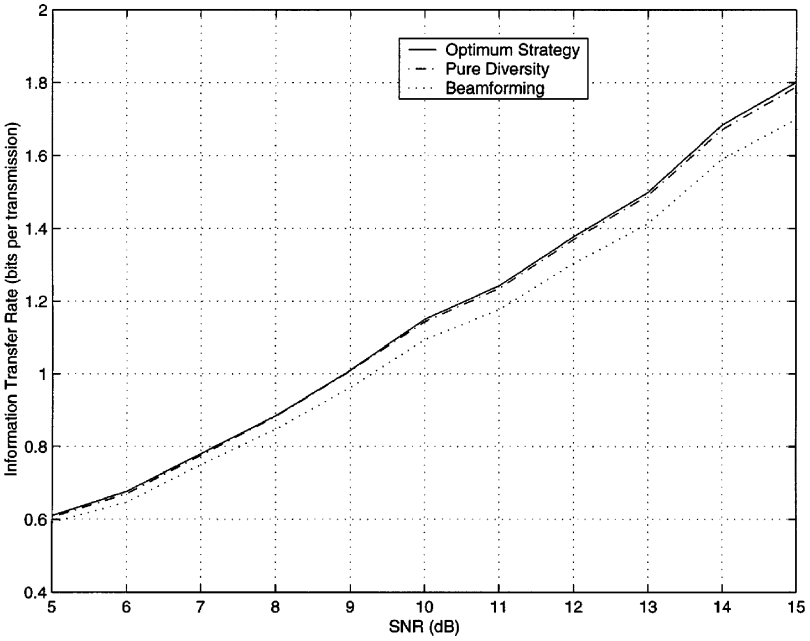

Fig. 4.17. Information rate of different transmission schemes in the channel mean feedback case, $a^d = 0.3$ [[145]©IEEE].

rate while the diversity scheme is 2 dB away from optimal. However, when the channel uncertainty at the precoder increases, the diversity transmission scheme outperforms the beamforming since the direction of beamforming is not very accurate.

Example 2: Channel Covariance Feedback

The numerical result for different transmission schemes based on the channel covariance feedback in [145] is given here. Three transmit antennas are deployed to deliver the information symbols using different transmission method, namely, the diversity scheme (*i.e.,* $\mathbf{Q} = \frac{P}{M_t}\mathbf{I}_{M_t}$), the beamforming scheme, which corresponds to send the information along the direction of the strongest eigenvector direction, and the optimal scheme given in Theory 2. In order to demonstrate how the eigenvalue spread of the channel covariance matrix affects the achieved information rate, we consider two different cases, say, $\sigma_1 = \sigma_2 = \sigma_3$ and $\sigma_1/\sigma_2 = \sigma_1/\sigma_3 = 2$, where σ_i denotes the ith eigenvalue of Σ. The results we have are shown in Fig. 4.18 and 4.19. As Fig. 4.18 and 4.19 suggest, when the eigenvalue of Σ are all equal, diversity scheme is optimal. On the contrary, when the eigenvalue spread of Σ increases, beamforming provides almost the same performance as the optimum scheme.

From the previous Example 1 and 2 we observe that the beamforming scheme is the optimal transmission scheme when either the knowledge of the

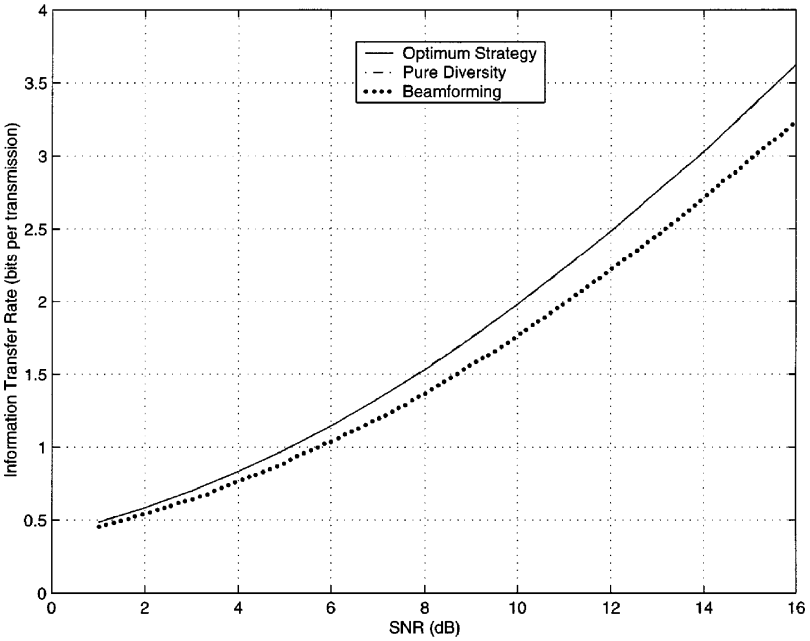

Fig. 4.18. Information rate of different transmission schemes in the channel covariance feedback case, $\sigma_1 = \sigma_2 = \sigma_3$ [[145]©IEEE].

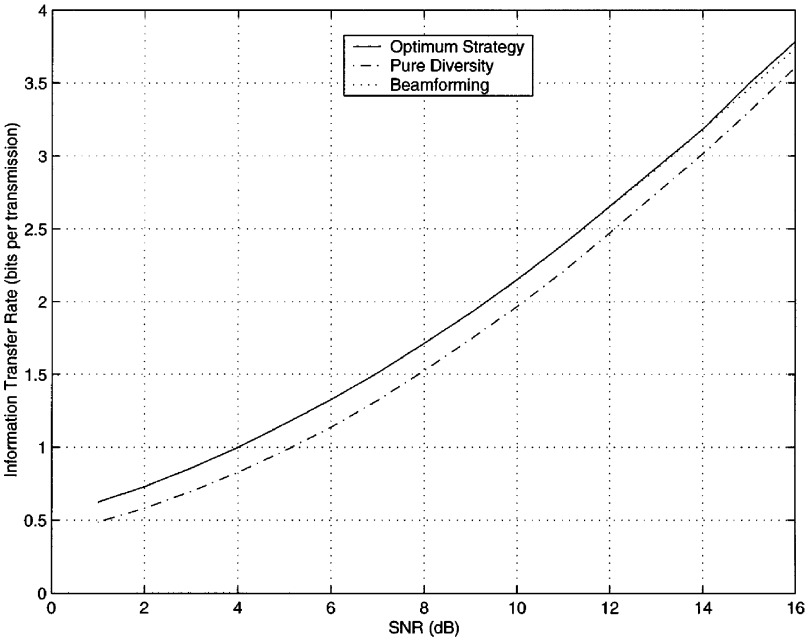

Fig. 4.19. Information rate of different transmission schemes in the channel covariance feedback case, $\sigma_1/\sigma_2 = \sigma_1/\sigma_3 = 2$ [[145]©IEEE].

fed back channel mean improves or the eigenvalue spread of the fed back covariance matrix grows. As we mention earlier, the beamforming scheme, which transmits only one data symbol at a time, requires lower decoding complexity as compared to the diversity transmission scheme, where multiple data symbols should be separated at the receiver. In [145], Visotsky and Madhow demonstrated that beamforming is optimum via simulation only. Later, based on the same concepts of channel mean and covariance feedback, Jafar and Goldsmith generalized the precoder design in [145] to the MIMO channel and provided the necessary and sufficient condition for the optimality of beamforming in [59]. Interested readers are referred to [59] for the detailed treatment of this topic.

4.5.2 Unitary Precoding

The previously introduced precoding scheme is suitable for the fast time varying system. However, when the channel coherent time is long such that the receiver can pass some channel knowledge to the other end of the link, the precoder design with channel statistic only fails to adjust its transmitted signal to the current channel state and its performance degrades as a result. Since the channel knowledge is always quantized before passing to the transmitter, the quantization level poses another design dilemma between precision and feedback overhead. In addition, when the quantized channel information is applied to the precoder design, it is hard to determine the required quantization level for a given system performance spec. Next, we are going to review another precoding scheme, called unitary precoding, which quantizes the precoder rather than the channel information, provides more flexibility than the direct channel quantization scheme in the feedback limit channel.

A set of codebook containing N codewords are first constructed for unitary precoding systems. Since these N codewords, which is independent of the current channel state information, they can be computed off-line and be made available at both ends of the communication link. Based on the estimated channel knowledge, the receiver selects a *proper* code from the codebook based on certain criteria and then sends the corresponding code index to the transmitter for symbol precoding. It is worthwhile to point out that the size of codebook N is limited by the number of bits per feedback, l, *i.e.,*

$$N \leq 2^l. \tag{4.149}$$

Obviously, the feedback quantity l provides an trade-off between the demand feedback capacity and the resulting system performance. There are two questions followed immediately after this unitary precoding scheme: 1), what is the criteria for the codeword selection ? and 2) how to construct a codebook ? Next, we borrow the results for the precoded OSTBC system in [80] to answer these two questions as follows[2].

[2] Even though the unitary precoding idea can be applied to other communication systems, such as the transmit beamforming [79], and the spatial multiplexing

4.5.3 System model and the Optimal Precoder for Unitary Precoded OSTBC Systems

The use of OSTBC is to increase the diversity gain of the MIMO channel such that the probability of channel deep fading is low if channel gains between different paths are independent [3, 127]. However, the full-rate OSTBC only exists for a certain number of transmit antennas [127]. For arbitrary number of transmit antennas, we can apply an additional precoding matrix to achieve the full-rate code while enjoying additional array gain [62, 80].

The block diagram of the precoded OSTBC system is given in Fig. 4.20. Let us consider a $M_r \times M_t$ MIMO system in a block fading channel, where the number of the transmit antennas is less than that of the receive antennas. The channel gain between different transceiver pair is assumed to be an i.i.d., complexity Gaussian random variable whose probability density function (PDF) is $\mathcal{CN}(0,1)$. The M $(M < M_t)$ data symbols are mapped onto M_t transmit antennas via the precoding matrix $\mathbf{P}_i$, which is specified by the receiver according to the current channel realization. As a result, the received signal corresponding to one OSTBC symbol $\mathbf{Y}$ can be formulated as

$$\mathbf{Y} = \sqrt{\frac{\rho}{M}}\mathbf{H}\mathbf{P}_i\mathbf{X} + \mathbf{N}, \tag{4.150}$$

where ρ denotes the signal-to-noise power ratio, $\mathbf{X}$

$$\mathbf{X} = [\mathbf{x}_1, \cdots, \mathbf{x}_T] \tag{4.151}$$

is a $M \times T$ space-time coded symbol matrix whose tth column $\mathbf{x}_t$ specifies the OSTBC encoder output for time t, $\mathbf{N}$ is a $M_r \times T$ noise sample matrix

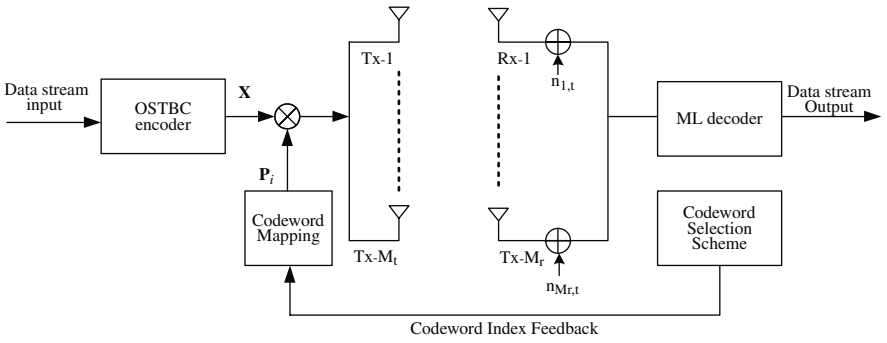

Fig. 4.20. The block diagram of the precoded OSTBC system using unitary precoding.

systems [80], the codeword selection and codebook construction processes are in fact quiet similar with the precoded OSTBC system [80]. Only their design criteria are different.

and its (i,t) element, $n_{i,t}$, which denotes the noise sample at the ith receive antenna at the time instance t, is modeled as an i.i.d. complexity Gaussian random variable, *i.e.,* $n_{i,t} \sim \mathcal{CN}(0,1)$.

If the maximum-likelihood (ML) decoding scheme is used to extract the transmit symbols in $\mathbf{Y}$, the conditional symbol error probability decreases exponentially as the channel Frobenius norm goes up, *i.e.,*

$$\Pr(\text{error}|\mathbf{H}) = \exp\left\{-\gamma||\mathbf{H}\mathbf{P}_i||_F^2\right\}, \tag{4.152}$$

where γ is a constant independent of $\mathbf{H}$ [69]. In order to minimize the symbol error rate (SER), $\mathbf{P}_i$ is selected to maximize the minimum distance between two OSTBC codewords. Mathematically, we can have

$$\begin{aligned}\mathbf{P}_i^* &= \arg \max_{i\in\{1,\cdots,N\}} \left(\min_{l\neq m} ||\mathbf{H}\mathbf{P}_i(\mathbf{X}_l - \mathbf{X}_m)||_F\right) \\ &= \arg \max_{i\in\{1,\cdots,N\}} ||\mathbf{H}\mathbf{P}_i||_F,\end{aligned} \tag{4.153}$$

where the second equality comes from the fact that both $\mathbf{X}_l$ and $\mathbf{X}_m$ are orthogonal. Hence, it is clear to see that the precoder is chosen such that the Frobenius norm of the equivalent channel response is maximized. Next, we are going to introduce the optimal unitary codeword, $\mathbf{P}_{opt}$, if the capacity of the feedback channel is not limited [80]. Please note that even $\mathbf{P}_{opt}$, which demands much more channel capacity for the precoder information feedback, is not practical enough in a feedback limited system, it does provide insight to our codebook design.

Let the singular value decomposition (SVD) of a $m \times n$ $(m > n)$ matrix $\mathbf{A}$ be

$$\mathbf{A} = \mathbf{\Sigma_A}\mathbf{U_A}\mathbf{V_A}^\dagger, \tag{4.154}$$

where $\mathbf{\Sigma_A}$ and $\mathbf{V_A}$ are the unitary matrices of size $m \times m$ and $n \times n$, respectively, and $\mathbf{U_H}$ of size $m \times n$ has m singular values $\lambda_{\mathbf{A},1}, \cdots, \lambda_{\mathbf{A},n}$ on its main diagonal and zeros elsewhere. Please note that n singular values are arranged in a decreasing order, *i.e.,*

$$\lambda_{\mathbf{A},1} \geq \cdots \geq \lambda_{\mathbf{A},n}. \tag{4.155}$$

In addition, the peak power constraint is enforced in the precoder design, *i.e.,*

$$\max_{\mathbf{x}} \frac{||\mathbf{P}\mathbf{x}||}{||\mathbf{x}||} \leq 1, \tag{4.156}$$

where $\mathbf{x} \in \mathbb{C}^{M_t}$. Eq. (4.156) implies that

$$\lambda_{\mathbf{P},1} \leq 1. \tag{4.157}$$

By applying SVD to both $\mathbf{H}$ and $\mathbf{P}$, we can bound $||\mathbf{H}\mathbf{P}||_F$ as [80]

$$\begin{aligned}||\mathbf{HP}||_F &= ||\mathbf{\Sigma_H U_H V_H^\dagger \Sigma_P U_P V_P^\dagger}||_F \\ &= ||\mathbf{U_H V_H^\dagger \Sigma_P U_P}||_F \\ &\leq ||\mathbf{U_H V_H^\dagger \Sigma_P}[\mathbf{I}_M\ \mathbf{0}]^t||_F \\ &\leq \sqrt{\sum_{i=1}^{M} \lambda_{\mathbf{U_H V_H^\dagger \Sigma_P \Sigma_P^\dagger V_H U_H^\dagger}, i}} \\ &= ||\bar{\mathbf{U}}_\mathbf{H}||_F, \end{aligned} \tag{4.158}$$

where $\mathbf{0}$ is the zero matrix of size $M \times M_t$ and $\bar{\mathbf{U}}_\mathbf{H}$ is composed of the first M column vectors in $\mathbf{U_H}$. The property that the Frobenius norm of one matrix is unchanged after being multiplied by an unitary matrix is applied to get the second equation in (4.158) while the first inequality in (4.158) is true by applying the upper bound on M singular values in $\mathbf{P}$. In order to achieve the upper bound in (4.158), $\mathbf{P}_{opt}$ can be designed as

$$\mathbf{P}_{opt} = \bar{\mathbf{V}}_\mathbf{H}. \tag{4.159}$$

The optimal codeword $\mathbf{P}_{opt}$ is composed of M orthonormal basis vectors in $\mathbb{C}^{M_t}$ and is denoted as $\mathbf{P}_{opt} \in \mathcal{U}(M_t, M)$, where $\mathcal{U}(M_t, M)$ denotes all possible M orthonormal basis vectors in $\mathbb{C}^{M_t}$. Please note that $\mathbf{P}_{opt}$ given in (4.159) is not unique since

$$||\mathbf{HP}_{opt}||_F = ||\mathbf{HP}_{opt}\mathbf{U}||_F, \tag{4.160}$$

as long as $\mathbf{U}$ is a $M \times M$ unitary matrix. Given the peak emitted power constraint in (4.156), the optimal precoder emits maximum power in M orthogonal directions. In fact, it is also shown in [80] that for any $\mathbf{P} \in \mathcal{U}(M_t, M)$, allocating unequal power along M precoding vectors cannot maximize the Frobenius norm in $\mathbf{HP}$. When a different constraint, such as the limited total output power, is applied to the precoder design, the optimal procoder adjusts its signal power on different directions based on the corresponding channel gain [117, 112]. However, since the output power for different direction is limited by the linear region of the power amplify at the transmitter, the output power for M different beams is finite. Therefore, the total ouptut power constraint may lead to the output power back-off in this case. Therefore, the discussion of codeword design for the unitary precoding is limited to $\mathcal{U}(M_t, M)$.

Let us consider a special case when each column vector in $\mathbf{P}$ is selected from the columns of $\mathbf{I}_{M_t}$. This corresponds to the antenna subset selection proposed in [46], where the receiver specifies M out of M_t *best* antennas for signal transmission and pass the subset index to the transmitter. Please note that it takes

$$\left\lceil \log_2 \left(\frac{M_t!}{M!(M_t - M)!} \right) \right\rceil \tag{4.161}$$

many bits to specify the antenna subset pattern. Even though both the antenna subset selection and the unitary precoding schemes achieve full diversity

in the MIMO channel [46, 80], the antenna subset selection scheme has less flexibility in design since each element in the precoder is either 1 or 0. Consequently, its performance is worse than that of the unitary precoding as we will show later in the simulation.

4.5.4 Codebook Construction for the Unitary Precoding

Here, we will demonstrate that the codebook construction for the unitary precoding system can be related to the subspace packing problem in the Grassmannian manifold as follows.

Recall that N codewords in the unitary precoding codebook are designed off-line and hence independent of the channel realization and $\mathbf{P}_{opt}$ as well. First, we can modify the codeword selection criteria in (4.153) as

$$\mathbf{P}_i^* = \arg \max_{i\in\{1,\cdots,N\}} ||\mathbf{H}\mathbf{P}_i||_F^2 \tag{4.162}$$

$$= \arg \min_{i\in\{1,\cdots,N\}} \left(||\mathbf{H}\mathbf{P}_{opt}||_F^2 - ||\mathbf{H}\mathbf{P}_i||_F^2\right), \tag{4.163}$$

where

$$\left(||\mathbf{H}\mathbf{P}_{opt}||_F^2 - ||\mathbf{H}\mathbf{P}_i||_F^2\right) \tag{4.164}$$

can be treated as the distortion due to an non-ideal codeword $\mathbf{P}_i$. Love *at al.* in [80] show that for a given channel realization $\mathbf{H}$, the minimum distortion can be bounded from top as

$$\min_{i\in\{1,\cdots,N\}} \left(||\mathbf{H}\mathbf{P}_{opt}||_F^2 - ||\mathbf{H}\mathbf{P}_i||_F^2\right) \le \lambda_{\mathbf{H},1}^2 \min_{i\in\{1,\cdots,N\}} \frac{1}{2}||\bar{\mathbf{V}}_{\mathbf{H}}\bar{\mathbf{V}}_{\mathbf{H}}^\dagger - \mathbf{P}_i\mathbf{P}_i^\dagger||_F^2. \tag{4.165}$$

For a given codebook, its performance can be evaluated via its averaged distortion, *i.e.,*

$$E_{\mathbf{H}}\left\{\min_{i\in\{1,\cdots,N\}} \left(||\mathbf{H}\mathbf{P}_{opt}||_F^2 - ||\mathbf{H}\mathbf{P}_i||_F^2\right)\right\} \tag{4.166}$$

and its upper bound immediately follows as

$$E_{\mathbf{H}}\left\{\min_{i\in\{1,\cdots,N\}} \left(||\mathbf{H}\mathbf{P}_{opt}||_F^2 - ||\mathbf{H}\mathbf{P}_i||_F^2\right)\right\} \le$$

$$E_{\mathbf{H}}\left\{\lambda_{\mathbf{H},1}^2\right\} E_{\mathbf{H}}\left\{\min_{i\in\{1,\cdots,N\}} \frac{1}{2}||\bar{\mathbf{V}}_{\mathbf{H}}\bar{\mathbf{V}}_{\mathbf{H}}^\dagger - \mathbf{P}_i\mathbf{P}_i^\dagger||_F^2\right\}, \tag{4.167}$$

where the distribution of $\lambda_{\mathbf{H},1}^2$ and $\bar{\mathbf{V}}_{\mathbf{H}}$ of $\mathbf{H}$ are independent. By observing (4.167) we learn that the upper bound of the averaged distortion is controlled by both the averaged value of $\lambda_{\mathbf{H},1}^2$ and the distribution of first M vectors in $\mathbf{V}_H$. Since the first term at the right-hand side is independent of the codebook design, we thus construct N unitary codes so that the second term at the right-hand side is minimized. Recall that N codewords are limited to be a

subset of $\mathcal{U}(M_t, M)$ and the column space of codeword $\mathbf{P}_i$, $\mathcal{P}_i$, represents a M-dimensional subspace in $\mathbb{C}^{M_t}$. Let $\mathcal{G}(M_t, M)$ be the Grassmann manifold, which contains all the column space in $\mathcal{U}(M_t, M)$. The vicinity of two column spaces $\mathcal{P}_i$ and $\mathcal{P}_j$ from $\mathbf{P}_i$ and $\mathbf{P}_j$ can be evaluated by their chordal distance, which is defined as

$$d(\mathbf{P}_i, \mathbf{P}_j) = \frac{1}{\sqrt{2}} ||\mathbf{P}_i \mathbf{P}_i^\dagger - \mathbf{P}_j \mathbf{P}_j^\dagger||_F. \tag{4.168}$$

Let d_{min} denote the minimum distance between two different column spaces from two different codewords and $\mathcal{B}_i$ be the union of of all subspaces in $\mathcal{U}(M_t, M)$ whose chordal distance is less than $d_{min}/2$, *i.e.,*

$$\mathcal{B}_i = \left\{ \mathcal{P}_U \in \mathcal{G}(M_t, M) \middle| d(U, \mathcal{P}_i) < \frac{d_{min}}{2} \right\}. \tag{4.169}$$

It can be shown easily that $\mathcal{B}_i$ and $\mathcal{B}_j$ do not overlap if $i \neq j$. These N disjoint open balls cover a subspace of $\mathcal{U}(M_t, M)$, and its *density* is measured by the probability when $\mathbf{F}_{opt}$ lies in one of these balls [80], *i.e.,*

$$Pr\left\{ \mathbf{P}_{opt} \in \bigcup_{i=1}^{N} \mathcal{B}_i \right\}. \tag{4.170}$$

In [7], Barg and Nogin have shown that when M_t is large, the probability function defined above can be approximated by

$$Pr\left\{ \mathbf{P}_{opt} \in \bigcup_{i=1}^{N} \mathcal{B}_i \right\} \approx N \left(\frac{\delta}{2\sqrt{M}} \right)^{2M_t M + o(M_t)}. \tag{4.171}$$

Using (4.168) and (4.171), we can have the following simplification [80]

$$\begin{aligned}
& E_{\mathbf{H}} \left\{ \min_{i \in \{1, \cdots, N\}} \frac{1}{2} ||\bar{\mathbf{V}}_{\mathbf{H}} \bar{\mathbf{V}}_{\mathbf{H}}^\dagger - \mathbf{P}_i \mathbf{P}_i^\dagger||_F^2 \right\} \\
&= E_{\mathbf{H}} \left\{ \min_{i \in \{1, \cdots, N\}} d(\mathbf{P}_{opt}, \mathbf{P}_i)^2 \right\} \\
&\leq Pr\left\{ \mathbf{P}_{opt} \in \bigcup_{i=1}^{N} \mathcal{B}_i \right\} \left(\frac{d_{min}}{2} \right)^2 + \left(1 - Pr\left\{ \mathbf{P}_{opt} \in \bigcup_{i=1}^{N} \mathcal{B}_i \right\} \right) \cdot M \\
&\approx M + N \left(\frac{\delta}{2\sqrt{M}} \right)^{2M_t M + o(M_t)} \left(\frac{1}{4} d_{min}^2 - M \right).
\end{aligned} \tag{4.172}$$

It is shown in [80] that the upper bound developed in (4.172) reduces as d_{min} increases in the general situation. This implies that we should design our codebook so that the minimum chordal distance between two codewords is maximized. As pointed out in [80], the noncoherent space-time modulation

design using Fourier based signal processing scheme in [53] can be applied to find out a good space packing with large minimum distance. Even though this scheme demands high computational complexity for codebook construction, especially when M_t, M_r and M are large, it requires less memory to store all N codewords thanks to its unique code structure. Interested readers are referred to [80] and [53] for more discussion.

Example 3: Unitary precoded OSTBC systems
Here we borrow the simulation result in [80] to compare the performance of different diversity utilization schemes in a MIMO channel. The system parameters are given as: $M_t = 4$, $M_r = 2$, $M = 2$ and the signal constellation is 4-QAM. To illustrate the performance gain due to the increase of codebook size, different feedback quantity, say, 3 and 6-bit, are considered in the unitary precoding. Both codebooks are found by the scheme proposed in [53]. The SER curves corresponding to different systems are plotted as a function of SNR in Fig. 4.21. Both antenna subset selection scheme for 2 transmit antennas [46] and the 2×2 OSTBC without precoding are also plotted for reference purpose in Fig. 4.21. Please note that it takes 3-bit to specify the selected antenna subset. It is observed that the use of precoding not only provides more than 2 dB gain over the OSTBC system without precoding at SER

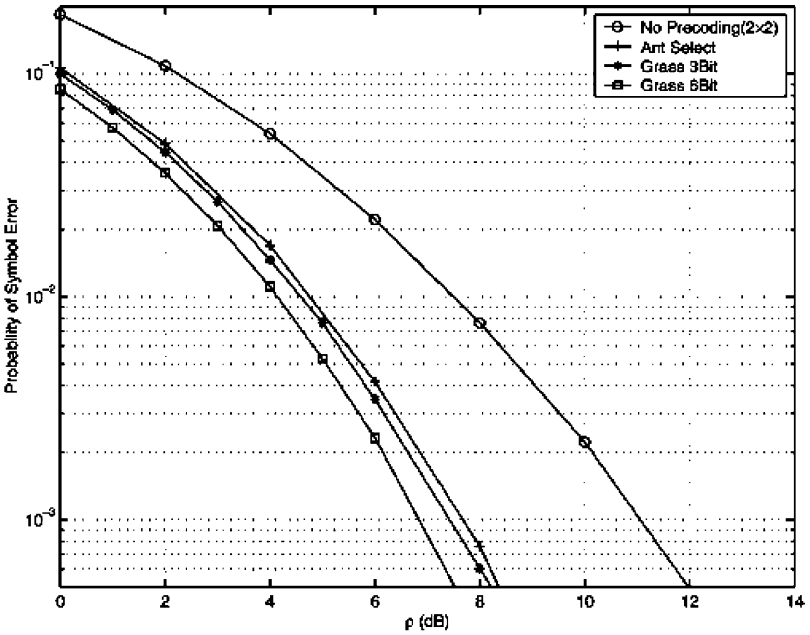

Fig. 4.21. SER for different precoding scheme. $M_t = 4$, $M_r = 2$, $M = 2$ and the signal constellation is 4-QAM [[80]©IEEE].

equal to 10^{-2}, but achieves higher diversity gain as well. In addition, a larger codebook provides a better SER performance at the cost of more feedback overhead. If the feedback channel capacity is limited to be 3-bit, applying the unitary precoding algorithm renders a little extra performance gain over the antenna subset selection.

Part II

Future Communication Systems with Precoding

5

Precoded Multiuser (PMU)-OFDM System

5.1 Introduction

To transmit data simultaneously for multiple users with a shared common channel, the multiuser OFDM technology offers an attractive solution, which is the main focus of this research. Generally speaking, there exist two families of multiuser OFDM systems, i.e., multicarrier code division multiplexing access (MC-CDMA) [1, 48, 49, 67, 155] and orthogonal frequency division multiple access (OFDMA) [57, 66, 114] as detailed below.

When compared with the CDMA technology, MC-CDMA inherits the advantages of multicarrier systems in combating ISI caused by frequency selective fading channels. MC-CDMA systems can be further divided into two types [49]. In the first type, one bit is transmitted per time slot. The transmitted bit is spread into several chips, which are allocated to different subchannels. The number of subchannels equals to the number of chips [155]. This type of MC-CDMA system can exploit the full frequency diversity gain when the maximum ratio combing (MRC) [49, 108] is used in the receiver side. In the second type, several bits are converted from serial-to-parallel and then each bit is spread into several chips. The chips corresponding to the same bit are allocated to the same subchannel [67], which is often called the MC-DS CDMA system. Two more generalized MC-CDMA system was proposed in [1, 48, 49]. In the first scheme [48, 49], each S/P converted bit is spread into several chips and then each subcarrier is modulated with one chip, where the frequency separation corresponding to each bit is maximized to achieve frequency diversity. In the second scheme [1], similarly, each S/P converted bit is spread into several chips. Then, the chips corresponding to the same symbol are modulated in successive subcarriers. Although MC-CDMA systems spread symbols using orthogonal codes to ensure orthogonality, when used in uplink transmission, i.e., from the mobile station (MS) to the base station (BS), orthogonality may be destroyed at the receiver due to frequency selective fading, thus leading to multiaccess interference (MAI). The MAI problem cannot be solved by increasing the transmit power since increasing the transmit power for one user

C.-C.J. Kuo et al., *Precoding Techniques for Digital Communication Systems*,
DOI: 10.1007/978-0-387-71769-2_5,

will also increase the interference for other users. To suppress MAI, sophisticated multiuser detection (MUD) [144] and signal processing techniques have been proposed at the receiver end [30, 49]. Furthermore, due to MAI, the CFO estimation and estimation and compensation are much more complicated in MC-CDMA systems [31, 126].

In contrast, OFDMA is MAI-free when the time and the frequency are well synchronized in the system. It was originally proposed for the cable TV application [114]. Currently, it has been included in the IEEE 802.16a standard for the fixed wireless metropolitan area network (WMAN) [57, 66]. However, similar to conventional OFDM, OFDMA systems are sensitive to frequency asynchronism, i.e., the carrier frequency offset (CFO) problem [87, 101]. The CFO effects result from the oscillator mismatch in the transceiver pair and/or the Doppler effect due to mobile users. Research on accurate CFO estimation and compensation has received a lot of attention in the design of practical OFDM systems [87, 118, 141]. However, different CFOs of multiple users in OFDMA systems make the CFO estimation much more difficult than that of a single user OFDM system. This is because of the fact that, when a user has a CFO, the CFO not only causes the performance degradation of this user (the self-CFO effect) but also results in MAI for others [135, 156]. Then, OFDMA systems are no longer MAI-free in the presence of CFO. The CFO estimation are no longer MAI-free in the presence of CFO. The CFO estimation problem for OFDMA systems has been extensively studied, e.g., [6, 88, 106, 107, 141]. An edge sidelobe suppressor was proposed in [156] to mitigate the CFO effect of an OFDMA system. However, most solutions demand extra complexity at the receiver. The CFO effect is recognized as one of the main technical challenges that limits the mobility of OFDM systems.

Moreover, in the uplink transmission, it is difficult to guarantee that all users' signals are aligned at the receiver and this leads to time asynchronism. Time asynchronism will lead to MAI in OFDMA as well [97]. Although the timing mismatch problem can be handled using a sufficiently long cyclic prefix to cover time offsets, this solution increases redundancy and decreases the actual data rate. Like the frequency offset issue, some research has been conducted using sophisticated signal processing to estimate time and frequency offsets, e.g. [6, 88, 142]. Due to MAI, time offsets cannot be well compensated in the receiver [88]. Offsets have to be estimated by the receiver and sent back to every user via feedback so that each user can compensate the offsets at the transmitter. In the IEEE 802.16 standard, this is done using a feedback mechanism called ranging [57]. Although the time offset problem can be solved using feedback, the solution imposes a higher computational load on the system. In addition, it may not guarantee that all users are perfectly synchronized. If some users fail to synchronize with the base station, MAI will occur and the system performance will degrade.

Furthermore, OFDM-based systems have been designed for applications with little mobility. However, mobile OFDM technology has recently attracted a lot of attention for three reasons. First, it is desirable to provide high qual-

ity broadband services in a mobile environment when we consider the next generation wireless communication system. Second, emerging wireless communication systems are expected to lie in higher spectral bands so that they are more sensitive to the physical movement of users and their surroundings. Third, more subchannels are needed to enhance OFDM bandwidth efficiency, which implies the use of a longer OFDM block. Then, the effective channel variation rate over one OFDM block increases. Rapid variation of the channel over one OFDM symbol destroys the orthogonality among subcarriers, and results in ICI and MAI in multiuser OFDM systems.

Based on the above discussion, a technique that is robust to both time and frequency offsets as well as Doppler effect is desirable. That is, the MAI caused by these effects can be reduced to a negligible amount so that the multiuser system behaves like a "single-user" system. However, little research has been done in the design of a multiuser OFDM system that is inherently robust to these effects. In this chapter, we introduce the PMU-OFDM system which can significantly reduce the MAI due to above factors. As a result, there is no need to use sophisticated signal processing or multiuser detection to overcome the MAI problem. Therefore, an algorithm for single-user OFDM system, which is much simpler than that in multiuser OFDM system, can be used in this novel multiuser OFDM system. PMU-OFDM system reveals that by proper transceiver design with precoding, the MAI issue in multiuser systems can be overcome without increasing receiver complexity.

5.2 System Model and Its Properties

The block diagram of the PMU-OFDM system with T users in uplink direction, i.e., from mobile station (MS) to base station (BS), is shown in Fig. 5.1. Let the input of the ith user ($1 \le i \le T$) be an $N \times 1$ vector $\mathbf{x}_i$, which contains N modulation symbols. The transmitter has 4 stages. At the first stage, each symbol in vector $\mathbf{x}_i$ is repeated M times to form a new vector $\mathbf{y}_i$ of size $NM \times 1$ as

$$y_i[m + kM] = x_i[k], \quad 0 \le k \le N - 1 \text{ and } 0 \le m \le M - 1. \tag{5.1}$$

At the second stage, $\mathbf{y}_i$ is passed through an $NM \times NM$ diagonal matrix $\mathbf{W}_i$ with its diagonal elements drawn from an $M \times M$ unitary matrix $\mathbf{D}$ ($\mathbf{D}^\dagger\mathbf{D} = M\mathbf{I}$). Let the column vectors of $\mathbf{D}$ be $\mathbf{d}_1, \mathbf{d}_2, \cdots, \mathbf{d}_M$. Then, $\mathbf{W}_i$ is obtained by repeating $\mathbf{d}_i$ N times along the diagonal, i.e., $\mathbf{W}_i = \text{diag}\left(\mathbf{d}_i^t\ \mathbf{d}_i^t \ldots \mathbf{d}_i^t\right)$. For instance, let $M = 2$, $N = 4$ and $\mathbf{D}$ be the Hadamard matrix, whose columns form a set of Hadamard-Walsh code. We have

$$\mathbf{W}_1 = \text{diag}(+1\ +1\ +1\ +1\ +1\ +1\ +1\ +1)$$

and

$$\mathbf{W}_2 = \text{diag}(+1\ -1\ +1\ -1\ +1\ -1\ +1\ -1).$$

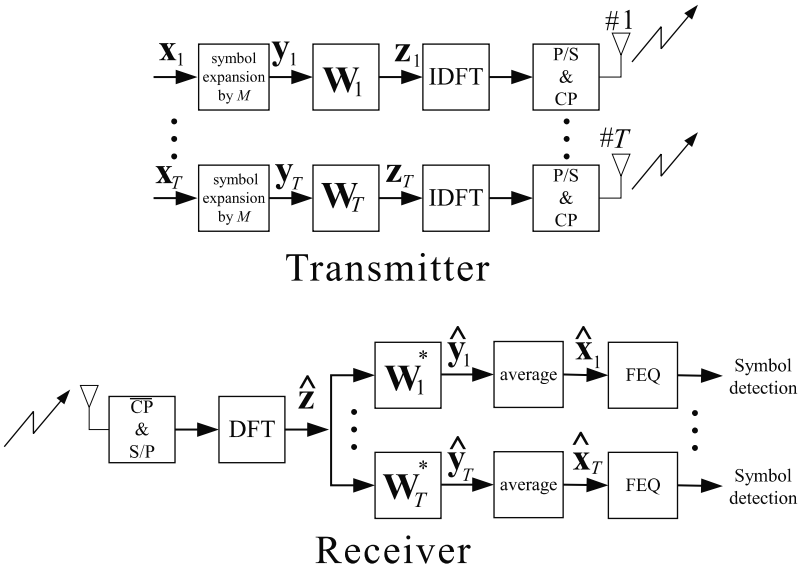

Fig. 5.1. The block diagram of the proposed system [[135] ©IEEE].

Let $w_i[l]$ be the lth diagonal element of $\mathbf{W}_i$, $0 \leq l \leq NM-1$. As $\mathbf{D}^\dagger\mathbf{D} = M\mathbf{I}$, these diagonal elements satisfy the following property:

$$\sum_{m=0}^{M-1} w_i[m+kM]w_j^*[m+kM] = \begin{cases} M, & i=j \\ 0, & i \neq j \end{cases}, \tag{5.2}$$

for all k with $0 \leq k \leq N-1$. After passing through the diagonal matrix, the lth component of the orthogonally coded output vector $\mathbf{z}_i$ is given by

$$z_i[l] = w_i[l]y_i[l], \quad 0 \leq l \leq NM-1. \tag{5.3}$$

At the third stage, each coded vector is passed through the NM-point unitary inverse discrete Fourier transform (IDFT) matrix. Finally, at the fourth stage, each transformed vector is converted from parallel to the serial and the cyclic prefix (CP) of length $\nu = L-1$ is added, where L is the maximum multipath length which includes delay spread.

As for the channel, we assume that the channel has tap delay line with uniform delay, which is commonly used in both wired and wireless communications. PMU-OFDM system is suitable to be used in both wired and wireless environments. For the wired environment, the channel path is the equivalent channel equalized by the time-domain equalizer (TEQ) [27]. Moreover, the crosstalk interference occurs in most wired applications can be regarded as an MAI [28]. For convenience, we will let $h_i(n)$ be the channel path of user i, and $\lambda_i[l]$ be the lth element of NM-point DFT of $h_i(n)$, where $0 \leq l \leq NM-1$, throughout the whole chapter.

At the receiver side, the receiver removes the CP and passes each block of size NM through the unitary discrete Fourier transform (DFT) matrix. For the detection of the symbols transmitted by the ith user, the DFT output vector is multiplied by $\mathbf{W}_i^*$ and then averaged. Let $\hat{\mathbf{y}}_i$ be the output of $\mathbf{W}_i^*$ and $\hat{\mathbf{x}}_i$ be the averaged output. Then, the kth element of $\hat{\mathbf{x}}_i$ is given by

$$\hat{x}_i[k] = \frac{1}{M} \sum_{m=0}^{M-1} \hat{y}_i[m + kM], \quad 0 \le k \le N-1. \tag{5.4}$$

From Fig. 5.1, we can rewrite Eq. (5.4) as

$$\hat{x}_i[k] = \frac{1}{M} \sum_{m=0}^{M-1} \hat{z}[m + kM] w_i^*[m + kM], \quad 0 \le k \le N-1. \tag{5.5}$$

In the final stage, $\hat{\mathbf{x}}_i$ is passed through frequency equalization (FEQ) and ready for detection. The operation of FEQ will be introduced in the following section.

5.2.1 Approximately MAI-Free Property

The PMU-OFDM system has the approximately MAI-free property which is described as follows [135]. According to [10, 27], the lth element of $\hat{\mathbf{z}}$ is given by

$$\hat{z}[l] = \sum_{i=1}^{T} \lambda_i[l] z_i[l] + e[l], \quad 0 \le l \le NM-1. \tag{5.6}$$

From Eqs. (5.3) and (5.6), the lth element of $\hat{\mathbf{y}}_j$ can be expressed as

$$\hat{y}_j[l] = \sum_{i=1}^{T} \lambda_i[l] y_i[l] w_i[l] w_j^*[l] + e[l] w_j^*[l]. \tag{5.7}$$

Let $l = m + kM$. From Eqs. (5.128) and (5.7), the kth element of $\hat{\mathbf{x}}_j$ is given by

$$\begin{aligned}
\hat{x}_j[k] = {} & \frac{1}{M} \sum_{m=0}^{M-1} \lambda_j[m + kM] y_j[m + kM] w_j[m + kM] w_j^*[m + kM] \\
& + \frac{1}{M} \sum_{i=1, i \ne j}^{T} \sum_{m=0}^{M-1} \lambda_i[m + kM] y_i[m + kM] w_i[m + kM] w_j^*[m + kM] \\
& + \frac{1}{M} \sum_{m=0}^{M-1} e[m + kM] w_j^*[m + kM],
\end{aligned} \tag{5.8}$$

where the first term is the desired signal, the second term is the MAI from other users, and the third term is the additive noise. When N is sufficiently

larger than the multipath length L, the coherent bandwidth is large, i.e., correlation between subchannels is large. In this case, the frequency response for adjacent subchannels only varies a little. Therefore, we have the following approximation

$$\lambda_i[m+kM] \approx \widetilde{\lambda}_i[k], \quad 0 \le m \le M-1, \quad 0 \le k \le N-1, \tag{5.9}$$

where $\widetilde{\lambda}_i[k]$ is the kth component of the averaged frequency gain, i.e.,

$$\widetilde{\lambda}_i[k] = \frac{1}{M}\sum_{m=0}^{M-1} \lambda_i[m+kM].$$

Using Eqs. (5.1) and (5.9), we can rewrite Eq. (5.8) as

$$\begin{aligned}
\hat{x}_j[k] &\approx \widetilde{\lambda}_j[k]x_j[k]\frac{1}{M}\sum_{m=0}^{M-1} w_j[m+kM]w_j^*[m+kM] \\
&\quad + \frac{1}{M}\sum_{i=1,i\neq j}^{T} \widetilde{\lambda}_i[k]x_i[k]\sum_{m=0}^{M-1} w_i[m+kM]w_j^*[m+kM] \\
&\quad + \frac{1}{M}\sum_{m=0}^{M-1} e[m+kM]w_j^*[m+kM] \\
&= \widetilde{\lambda}_j[k]x_j[k] + \frac{1}{M}\sum_{m=0}^{M-1} e[m+kM]w_j^*[m+kM].
\end{aligned} \tag{5.10}$$

Observed from Eq. (5.10), the MAI is approximately zero. Hence, if there is no channel noise, we can approximately reconstruct $x_i[k]$ by multiplying $\hat{x}_i[k]$ by $\left(\widetilde{\lambda}_i[k]\right)^{-1}$. Similar to OFDM systems, the one-tap gain multiplication is what usually called frequency equalization (FEQ). Since the proposed system is approximately MAI-free, its capacity increases as transmit power increases in the SNR range that we are interested. This result is very different from that of conventional MC-CDMA systems, in which increasing the transmit power of one user will also increase the MAI for other users.

Although PMU-OFDM uses orthogonal codes to distinguish different users, the approximate zero MAI property makes it significantly different from conventional MC-CDMA systems in many aspects. Instead, it has more similarities to OFDMA as explained below.

1. MAI-free. The PMU-OFDM system can achieve approximately MAI-free when N is much larger than the multipath length L. That is, for a fixed L, as N increases, the system will have less MAI. Hence, by increasing N, PMU-OFDM can accommodate more users with negligible MAI. This MAI-free property is similar to that of the OFDMA system, which is MAI-free when frequency are well synchronized. Moreover, in an OFDMA

system, the block duration is in general much longer than the multipath length. Such systems are usually used in WLAN or WMAN applications [66]. On the other hand, CDMA or MC-CDMA systems are usually used in the cellular phone system, where co-channel interference is the major concern.

2. Detection. Due to MAI, sophisticated multiuser detection (MUD) may be involved in MC-CDMA so that detection of individual symbols is dependent [49]. In the PMU-OFDM and OFDMA system, there is no need of using MUD, and detection of individual symbols is independent.
3. Loading. PMU-OFDM can achieve approximately MAI-free when N is sufficiently large. Hence, by increasing N, the system can be fully loaded with negligible MAI. Also the OFDMA system can be fully loaded with no MAI. In contrast, the number of supportable users in MC-CDMA systems is much less than the spreading factor M due to MAI [1, 48, 49].
4. Frequency equalization. As shown in Fig. 5.1, the PMU-OFDM system performs "frequency equalization" [27] instead of "combining" before symbol detection. This stands in contrast with MC-CDMA systems, where "combining" is usually used before detection [1, 48, 49]. There are several different combining methods such as MRC (maximum ratio combining), EGC (equal gain combining) and ORC (orthogonality restoring combining) in MC-CDMA systems [49]. The combining techniques multiply every spread chip by a weighted gain and then sum up M chips before detection. Hence, there are NM gain multiplications for MC-CDMA systems [1, 48, 49]. On the other hand, form Eq. (5.128), the PMU-OFDM system performs summation before the gain multiplication, i.e., frequency equalization. Thus, it only needs N gain multiplications.
5. Hadamard-Walsh code in the uplink transmission. In the uplink transmission, it is difficult to guarantee that every user transmits his/her signal simultaneously, i.e., there is a time offset between users. This will lead to timing mismatch among users. If the Hadamard-Walsh code is used in the uplink transmission in conventional CDMA systems, a small timing mismatch among users will result in great MAI even if the channel is perfect. Therefore, Hadamard-Walsh code is usually used in downlink transmission but seldom used in the uplink transmission unless the timing mismatch problem can be well resolved by some other mechanism. In conventional CDMA or MC-CDMA systems, quasi-orthogonal codes that have less cross correlation such as the Gold code or the Kasami code are usually used to mitigate the timing mismatch problem. In contrast, since the PMU-OFDM system is robust to timing mismatch [133], we can adopt the low complexity Hadamard-Walsh code in the uplink transmission, i.e., letting $\mathbf{D}$ be the Hadamard matrix.
6. Frequency diversity. Although PMU-OFDM may lose the frequency diversity when compared with MC-CDMA, it can achieve the full loading capacity while maintaining the MAI-free property. The diversity gain of PMU-OFDM is close to that of OFDMA.

5.2.2 Approximately MAI-Free Property: Quantitative Analysis for Hadamard-Walsh Code

It is easy to explain the approximately MAI-free property of the PMU-OFDM system using the approximation in Eq. (5.9). However, it may not be easy to see the relationship between the MAI and N. That is, although we know MAI will decrease as N increases, it does not quantify the rate of MAI decrease. In this section, we show that if all M Hadamard-Walsh codewords are used, the MAI power will decrease at a rate proportional to N^{-2}, i.e., a 6 dB decrease with a doubled N. Moreover, if only $M/2$ symmetric or anti-symmetric codewords of the M Hadamard-Walsh code are used, the MAI power will decrease at a rate proportional to N^{-4}, i.e., a 12 dB decrease as N doubles.

Using the definition of DFT, we can express $\lambda_i[l]$ as

$$\lambda_i[l] = \sum_{n=0}^{L-1} h_i(n) e^{-j\frac{2\pi}{NM}nl}. \tag{5.11}$$

Let $l = m + kM$, $0 \le k \le N-1$ and $0 \le m \le M-1$. Eq. (5.11) can be rewritten as

$$\lambda_i[m+kM] = \sum_{n=0}^{L-1} h_i(n) e^{-j\frac{2\pi}{NM}n(m+kM)}. \tag{5.12}$$

Using the Taylor series representation, i.e.,

$$e^{-j\theta} = 1 - j\theta - \frac{1}{2!}\theta^2 + j\frac{1}{3!}\theta^3 + \frac{1}{4!}\theta^4 - j\frac{1}{5!}\theta^5 - \cdots,$$

we can rewrite Eq. (5.12) as

$$\begin{aligned}\lambda_i[m+kM] = \sum_{n=0}^{L-1} h_i(n) e^{-j\frac{2\pi}{N}kn} \Bigg\{ &\left[1 - \frac{1}{2!}\left(\frac{2\pi}{NM}mn\right)^2 + \cdots\right] \\ &+ j\left[\frac{2\pi}{NM}mn - \frac{1}{3!}\left(\frac{2\pi}{NM}mn\right)^3 + \cdots\right]\Bigg\}. \end{aligned} \tag{5.13}$$

Since the maximum value of n is $L-1$ and the maximum value of m is $M-1$, the maximum value of $2\pi/NMmn$ is less than $2\pi/N(L-1)$. When $N \gg L$, $2\pi/N(L-1)$ is small. In this case, we may use second order approximation of $e^{j2\pi/NMmn}$. That is, we approximate $\lambda_i[m+kM]$ by

$$\lambda_i[m+kM] \approx \sum_{n=0}^{L-1} h_i(n) e^{-j\frac{2\pi}{N}kn} \left\{1 - \frac{1}{2!}\left(\frac{2\pi}{NM}mn\right)^2 + j\left(\frac{2\pi}{NM}mn\right)\right\}. \tag{5.14}$$

The Hadamard-Walsh code is orthogonal and $\sum_{m=0}^{M-1} w_i[m]w_j^*[m] = 0$, for $i \neq j$. Also, from Eqs. (5.8) and (5.14), we have the following approximation

$$MAI_{j\leftarrow i}[k] \approx \frac{1}{M} x_i[k] \sum_{n=0}^{L-1} h_i(n) e^{-j\frac{2\pi}{N}kn} \phi_{i,j}(n), \tag{5.15}$$

where

$$\phi_{i,j}(n) = \sum_{m=0}^{M-1} \left\{ -\frac{1}{2!} \left(\frac{2\pi}{NM} mn \right)^2 + j \left[\frac{2\pi}{NM} mn \right] \right\} w_i[m]w_j^*[m].$$

Now, we would like to evaluate $E\left\{ |MAI_{j\leftarrow i}[k]|^2 \right\}$. Let us assume the transmitted symbol $x_i[k]$ and channel coefficients $h_i(n)$ are uncorrelated. Furthermore, $E\{x_i[k]x_i^*[k']\} = 0$, for $k \neq k'$. Let $\sigma_{x_i}^2 \triangleq E\left\{ |x_i[k]|^2 \right\}$ be the averaged transmitted power. Assume that the channel coefficients have the same averaged power, which is defined as $\sigma_{h_i}^2 = E\left\{ |h_i(n)|^2 \right\}$. It is worth to emphasize that the equal power assumption for channel coefficients will lead to a pessimistic MAI result. In practical situation, channel coefficients usually have exponential decay. As a result, the actual MAI should be much smaller. We will mention later how to extend the result with i.i.d. assumption to practical case. Now let us first introduce several lemmas and proposition to explain the pessimistic result.

Lemma 5.1: When all M Hadamard-Walsh codewords are used, the maximum value of the MAI from user i to user j, $\max_{i,j} E\left\{ |MAI_{j\leftarrow i}[k]|^2 \right\}$, can be approximated by

$$\sigma_{x_i}^2 \sigma_{h_i}^2 \left[\frac{1}{N^2} \frac{\pi^2}{4} \left(1 - \frac{1}{M} \right)^2 \sum_{n=0}^{L-1} n^2 + \frac{1}{N^4} \frac{\pi^4}{4} \left(1 - \frac{1}{M} \right)^2 \sum_{n=0}^{L-1} n^4 \right], \tag{5.16}$$

and the maximum value occurs when $w_i[m]$ and $w_j[m]$ satisfy the following condition

$$w_i[m]w_j[m] = \begin{cases} +1, & 0 \leq m \leq M/2 - 1 \\ -1, & M/2 \leq m \leq M - 1 \end{cases}. \tag{5.17}$$

Proof. From Eq. (5.15), we have

$$\begin{aligned} E\left\{ |MAI_{j\leftarrow i}[k]|^2 \right\} &\approx \frac{1}{M^2} \sigma_{x_i}^2 \sum_{n=0}^{L-1} \sum_{n'=0}^{L-1} E\{h_i(n)h_i^*(n')\} e^{-j\frac{2\pi}{N}k(n-n')} |\phi_{i,j}(n)|^2 \\ &= \frac{1}{M^2} \sigma_{x_i}^2 \sigma_{h_i}^2 \sum_{n=0}^{L-1} |\phi_{i,j}(n)|^2 . \end{aligned} \tag{5.18}$$

From Eq. (5.18), maximizing $E\left\{ |MAI_{j\leftarrow i}[k]|^2 \right\}$ is equivalent to maximizing $|\phi_{i,j}(n)|^2$ for all n. Thus, let us look at the term $|\phi_{i,j}(n)|^2$. From Eq. (5.15), $\phi_{i,j}(n)$ can be rearranged as

$$\phi_{i,j}(n) = \Re\{\phi_{i,j}(n)\} + j\Im\{\phi_{i,j}(n)\}, \tag{5.19}$$

where

$$\Re\{\phi_{i,j}(n)\} = -\frac{1}{2!}\left(\frac{2\pi}{NM}\right)^2 n^2 \sum_{m=0}^{M-1} w_i[m]w_j[m]m^2$$

and

$$\Im\{\phi_{i,j}(n)\} = \frac{2\pi}{NM} n \sum_{m=0}^{M-1} w_i[m]w_j[m]m.$$

Since

$$|\phi_{i,j}(n)|^2 = |\Re\{\phi_{i,j}(n)\}|^2 + |\Im\{\phi_{i,j}(n)\}|^2,$$

maximizing $|\phi_{i,j}(n)|^2$ is equivalent to maximizing both $\left|\sum_{m=0}^{M-1} w_i[m]w_j[m]m\right|$ and $\left|\sum_{m=0}^{M-1} w_i[m]w_j[m]m^2\right|$. According to [65], the product of two arbitrary codewords of M Hadamard-Walsh codes is again a codeword in M codewords, i.e., $w_i[m]w_j[m]$, $0 \le m \le M-1$, is one of the codewords of the M Hadamard-Walsh code. Since m and m^2 are monotonically increasing functions for $m \ge 0$, $\left|\sum_{m=0}^{M-1} w_i[m]w_j[m]m\right|$ and $\left|\sum_{m=0}^{M-1} w_i[m]w_j[m]m^2\right|$ are maximized if the number of successive $+1$s and -1s of $w_i[m]w_j[m]$ are maximized, which occurs when $w_i[m]$ and $w_j[m]$ satisfy the condition in Eq. (5.17). Hence, we have

$$\left|\sum_{m=0}^{M-1} w_i[m]w_j[m]m^2\right| = \sum_{m=0}^{M-1} m^2 - 2\sum_{m=0}^{M/2-1} m^2 = \frac{1}{4}M^3\left(1-\frac{1}{M}\right). \tag{5.20}$$

Similarly, it can be shown that

$$\left|\sum_{m=0}^{M-1} w_i[m]w_j[m]m\right| = \sum_{m=0}^{M-1} m - 2\sum_{m=0}^{M/2-1} m = \frac{1}{4}M^2\left(1-\frac{1}{M}\right). \tag{5.21}$$

Thus, from Eqs. (5.18), (5.19), (5.20) and (5.21), $\max_{i,j} E\left\{|MAI_{j\leftarrow i}[k]|^2\right\}$ can be approximated as that in Eq. (5.16). ■

As given in Eq. (5.16), the maximum value of $E\left\{|MAI_{j\leftarrow i}[k]|^2\right\}$ depends on two terms. One is proportional to N^{-2} and another is proportional to N^{-4}. As N grows, the term proportional to N^{-2} will dominate the performance. Hence, the maximum value of $E\left\{|MAI_{j\leftarrow i}[k]|^2\right\}$ decreases in an order of $O(N^{-2})$. Note that when all M codewords are used, every target user has the dominating MAI term, i.e., the maximum value of $E\left\{|MAI_{j\leftarrow i}[k]|^2\right\}$. For instance, let $M = 16$ and user i uses $\mathbf{w}_1$ and user j uses $\mathbf{w}_9$. Then, $w_i[k]w_j[k]$ satisfies Eq. (5.17) and the dominating MAI occurs. Now, if user i uses $\mathbf{w}_2$ and user j uses $\mathbf{w}_{10}$, again $w_i[k]w_j[k]$ satisfies Eq. (5.17) and the dominating MAI occurs. Consider the overall MAI power for user j, i.e.,

$\sum_{i=1,i\neq j}^{M} E\left\{|MAI_{j\leftarrow i}[k]|^2\right\}$. Since the maximum value of $E\left\{|MAI_{j\leftarrow i}[k]|^2\right\}$ is the dominating MAI of $\sum_{i=1,i\neq j}^{M} E\left\{|MAI_{j\leftarrow i}[k]|^2\right\}$, we may regard the overall MAI power decreases in an order of $O(N^{-2})$. This result explains the approximately MAI-free property of the PMU-OFDM system. That is, when all M codewords are used, the overall MAI power decreases as N increases in an order of $O(N^{-2})$.

According to [50], the set of M Hadamard-Walsh codes can be divided into two groups of $M/2$ codewords. One is the set of symmetric (even) codes satisfying

$$w_i[m] = w_i[M-1-m], \quad 0 \leq m \leq M/2-1. \tag{5.22}$$

The other is the set of anti-symmetric (odd) codes:

$$w_i[m] = -w_i[M-1-m], \quad 0 \leq m \leq M/2-1. \tag{5.23}$$

Now, we consider the use of $M/2$ symmetric or anti-symmetric codewords [135].

Lemma 5.2: Suppose that only $M/2$ symmetric or anti-symmetric codewords of the M Hadamard-Walsh codes are used. The product of any two codewords from the $M/2$ symmetric or anti-symmetric codewords, i.e., $w_i[m]w_j[m]$, is a symmetric codeword in M codewords. Moreover, $w_i[m]$ and $w_j[m]$ satisfy the following property

$$\sum_{m=0}^{M/2-1} w_i[m]w_j[m] = \begin{cases} M/2, & i=j \\ 0, & i\neq j \end{cases}. \tag{5.24}$$

Proof. From Eqs. (5.22) and (5.23), it is obvious that the product of any two codewords from either symmetric or anti-symmetric codes is symmetric. That is, $w_i[m]w_j[m]$ is symmetric and satisfies $w_i[m]w_j[m] = w_i[M-1-m]w_j[M-1-m]$, $0 \leq m \leq M/2-1$. Since the product of any two codewords is again a codeword [65], $w_i[m]w_j[m]$ is a symmetric codeword in M Hadamard-Walsh codes.

Now let us prove Eq. (5.24). The whole summation in Eq. (5.2) can be divided into two terms, i.e.,

$$\sum_{m=0}^{M-1} w_i[m]w_j[m] = \sum_{u=0}^{M/2-1} w_i[u]w_j[u] + \sum_{v=M/2}^{M-1} w_i[v]w_j[v]. \tag{5.25}$$

According to Eq. (5.22) or Eq. (5.23), when only $M/2$ symmetric or anti-symmetric codewords of M Hadamard-Walsh codes are used, the second summation term in Eq. (5.25) is given by

$$\sum_{v=M/2}^{M-1} w_i[v]w_j[v] = \sum_{v=M/2}^{M-1} w_i[M-1-v]w_j[M-1-v]$$
$$= \sum_{v'=M/2-1}^{0} w_i[v']w_j[v']. \tag{5.26}$$

From Eqs. (5.25) and (5.26), we prove the property in Eq. (5.24). ■

Lemma 5.3: Suppose that only $M/2$ symmetric or anti-symmetric codewords of M Hadamard-Walsh codes are used. We have the following property

$$\sum_{m=0}^{M-1} w_i[m]w_j[m]m = 0. \tag{5.27}$$

Proof. $\sum_{m=0}^{M-1} w_i[m]w_j[m]m$ can be divided into two terms as

$$\sum_{m=0}^{M-1} w_i[m]w_j[m]m = \sum_{u=0}^{M/2-1} w_i[u]w_j[u]u + \sum_{v=M/2}^{M-1} w_i[v]w_j[v]v. \tag{5.28}$$

Let $v = M-1-u$ and using either Eq. (5.22) or Eq. (5.23), $\sum_{m=0}^{M-1} w_i[m]$ $w_j[m]m$ can be manipulated as

$$\sum_{m=0}^{M-1} w_i[m]w_j[m]m = \sum_{u=0}^{M/2-1} w_i[u]w_j[u]u$$
$$+ \sum_{u=M/2-1}^{0} w_i[M-1-u]w_j[M-1-u](M-1-u)$$
$$= (M-1)\sum_{u=0}^{M/2-1} w_i[u]w_j[u]$$
$$= 0. \tag{5.29}$$

From Lemma 5.3, the MAI term in Eq. (5.15) becomes

$$MAI_{j\leftarrow i}[k] \approx \frac{1}{M} x_i[k] \sum_{n=0}^{L-1} h_i(n) e^{-j\frac{2\pi}{N}kn} \sum_{m=0}^{M-1} \frac{-1}{2!} \left(\frac{2\pi}{NM} mn\right)^2 w_i[m]w_j[m]. \tag{5.30}$$

Hence, we have the following proposition.

Proposition 5.1: Suppose that only $M/2$ symmetric or anti-symmetric codewords of M Hadamard-Walsh codes are used. The maximum value of $E\left\{|MAI_{j\leftarrow i}[k]|^2\right\}$ can be approximated by

$$\max_{i,j} E\left\{|MAI_{j\leftarrow i}[k]|^2\right\} \approx \sigma_{x_i}^2 \sigma_{h_i}^2 \left[\frac{1}{N^4}\frac{\pi^4}{64}\sum_{n=0}^{L-1} n^4\right], \tag{5.31}$$

which occurs when $w_i[m]$ and $w_j[m]$ satisfy the following condition:

$$w_i[m]w_j[m] = \begin{cases} +1, & 0 \le m \le M/4-1 \text{ or } M/2 \le m \le 3M/4-1 \\ -1, & M/4 \le m \le M/2-1 \text{ or } 3M/4 \le m \le M-1 \end{cases}. \tag{5.32}$$

Proof. According to Eq. (5.30), if the proposed code selection scheme is used, the imaginary part of $\phi_{i,j}(n)$ in Eq. (5.19) disappears. Following the same argument in the proof of Lemma 5.1, we know that maximizing $E\left\{|MAI_{j\leftarrow i}[k]|^2\right\}$ is equivalent to maximizing $\sum_{m=0}^{M-1} w_i[m]w_j[m]m^2$. Hence, the maximum $E\left\{|MAI_{j\leftarrow i}[k]|^2\right\}$ occurs when the number of successive $+1$s or -1s is maximized. Since $w_i[m]w_j[m]$ is one of the symmetric codewords, the last half $M/2$ elements can be obtained from the first $M/2$ elements. Also, from Eq. (5.24), we know that $\sum_{m=0}^{M/2-1} w_i[m]w_j[m] = 0$, for $i \neq j$. Hence, the codeword product $w_i[m]w_j[m]$ will have the largest number of successive $+1$'s or -1's if the condition in Eq. (5.32) is met. Given that the codeword product $w_i[m]w_j[m]$ satisfies Eq. (5.32), we have

$$\left|\sum_{m=0}^{M-1} w_i[m]w_j[m]m^2\right| = \sum_{m=0}^{M-1} m^2 - 2\sum_{m=M/4}^{3M/4-1} m^2 = \frac{1}{16}M^3. \tag{5.33}$$

Based on Eqs. (5.19), (5.30) and (5.33), the maximum value of $E\left\{|MAI_{j\leftarrow i}[k]|^2\right\}$ can be approximated as that in Eq. (5.31). ■

As shown in Eq. (5.31), when only $M/2$ symmetric or anti-symmetric codewords are used, the maximum value of $E\left\{|MAI_{j\leftarrow i}[k]|^2\right\}$ decreases in an order of $O(N^{-4})$. As compared with Eq. (5.16) where the MAI term decreases in an order of $O(N^{-2})$, the use of the code design in Proposition 5.1 enables the system to achieve MAI-free with a much faster rate as N increases. Let us give an example to illustrate this point.

Example 5.1: MAI Decreasing Rate

In this example, we show that the theoretical result derived using the Taylor approximation is close to the simulation result. Moreover, it is demonstrated that the use of only $M/2$ symmetric or anti-symmetric codewords allows the system to be MAI-free at a faster rate. For the theoretical result, Eqs. (5.16) and (5.31) are used to obtain the maximum MAI power for fully- and half-loaded systems, respectively. In the simulation, the Monte Carlo method and the term $MAI_{j\leftarrow i}[k]$ in Eq. (5.8) are used to run more than 2500 different channel realizations. That is, the simulated MAI power is obtained by the following average

$$\frac{1}{N}\sum_{k=0}^{N-1}|MAI_{j\leftarrow i}[k]|^2,$$

for more than 2500 channels. Let $M = 16$ and the modulation is BPSK, i.e., $\sigma_{x_i}^2 = 1$. The multipath length $L = 4$ and the coefficients of the channel are i.i.d. complex Gaussian random variables with an unit variance, i.e., $\sigma_{h_i}^2 = 1$.

Let us consider the maximum MAI power from user i to user j. The maximum MAI occurs if $w_i[m]w_j[m]$ satisfies Eq. (5.17) for the fully-loaded case. If symmetric or anti-symmetric codewords are in use, it occurs when $w_i[m]w_j[m]$ satisfies Eq. (5.32). The maximum MAI power as a function of N for theoretical and simulated results are shown in Fig. 5.2, where the MAI power is obtained for N from 8 to 256 in theory while the simulated MAI power is plotted for $N = 8,\ 16,\ 32,\ 64,\ 128$, and 256. We see from this figure, that theoretical and simulation results are close to each other. This confirms the assumption that the second order Taylor series expansion in Eq. (5.14) is good enough for the MAI analysis in the proposed system. Moreover, we see that the use of symmetric or anti-symmetric codewords enables the system to be MAI-free at a faster rate than a fully-loaded system. This result corroborates our derivation in Lemma 5.1 and Proposition 5.1.

Now, we would like to demonstrate that the maximum MAI power occurs when $w_i[m]$ and $w_j[m]$ satisfies Eq. (5.17) for the fully-loaded case, and satisfies Eq. (5.32) for the use of symmetric or anti-symmetric codewords.

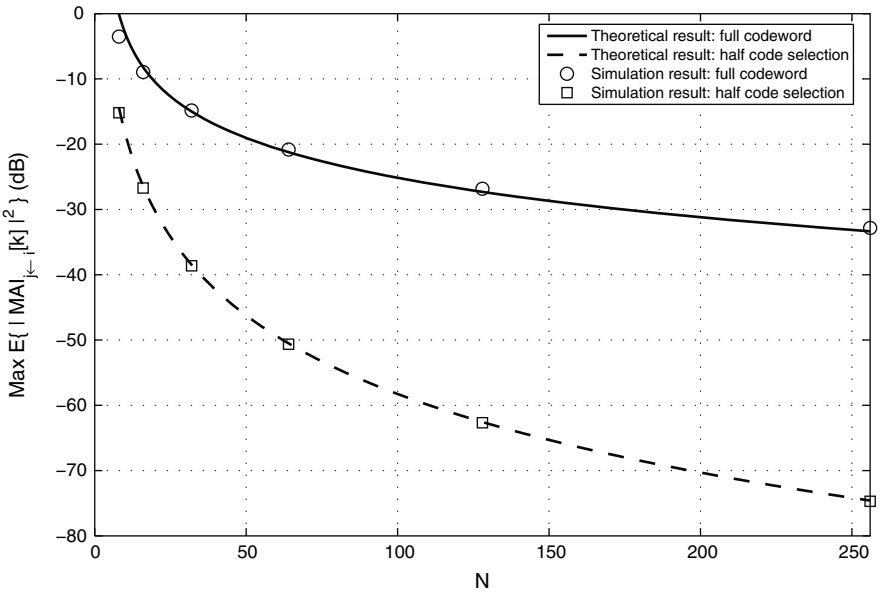

Fig. 5.2. The maximum MAI power as a function of N for theoretical and simulated results with $L = 4$.

For the fully loaded system, there are $M = 16$ possible combinations for $w_i[m]w_j[m]$ and this codeword product is again one of the original codeword. Hence, we will simulate the MAI power for these 16 possible combinations of $w_i[m]w_j[m]$ (in Kronecker ordering [8]) and number them as #1 to #16. Note that since #1 is the all-one code, it denotes the desired signal power instead of MAI. The MAI power for the 16 possible combinations of $w_i[m]w_j[m]$ are shown in Fig. 5.3. Note that since $w_i[m]w_j[m]$ is either symmetric or anti-symmetric, we use squared and circled curves respectively, to identify them. From the figure, we see that the maximum MAI power is the curve with number #9, which is the same curve as the circled points in Fig. 5.2, since the codeword #9 satisfies the condition in Eq. (5.17). This corroborates our derivation.

Consider the use of symmetric or anti-symmetric code. With this code design, the codeword product, $w_i[m]w_j[m]$, is a symmetric codeword according to Lemma 5.2. Hence, the MAI power for $M/2 = 8$ different combinations of $w_i[m]w_j[m]$ can be represented by the 8 squared curves in Eq. (5.3). From the figure, we see that, with the code design, the maximum MAI power is the curve with number #13, which is the same curve as the squared points in Fig. 5.2. Note that codeword #13 satisfies the condition in Eq. (5.32), which corroborates our theoretical derivation.

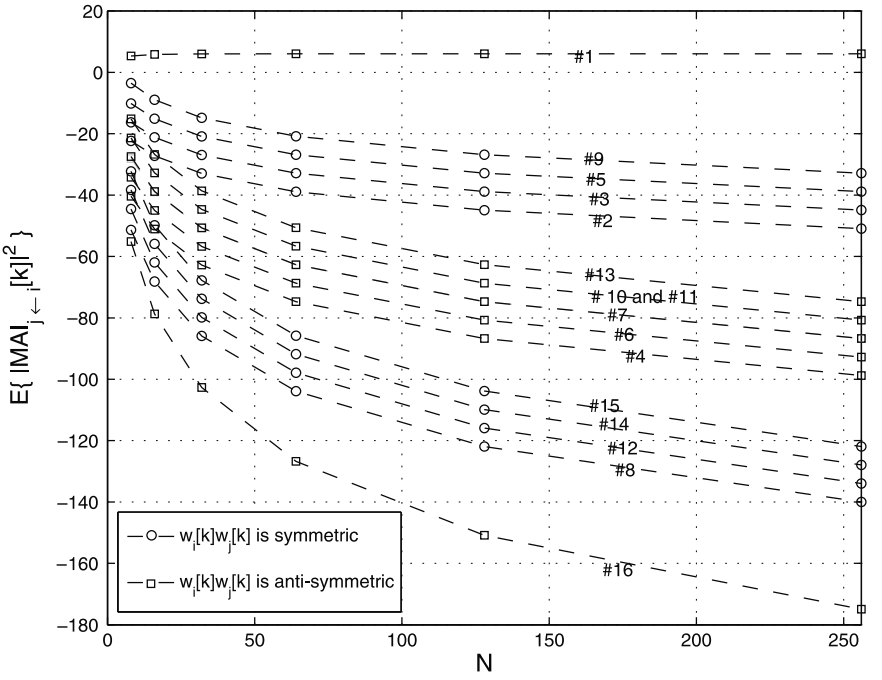

Fig. 5.3. The maximum MAI power as a function of N for symmetric and anti-symmetric $w_i[m]w_j[m]$ with $L = 4$.

Now let us consider a more practical channel model, i.e., channel coefficients do not have the same averaged power. However, it is still reasonable to assume that the channel coefficients are uncorrelated with $E\{h_i(n)h_i^*(n')\} = 0$ for $n \neq n'$. Also, since the channel coefficient power may be different for different taps. Let us assume the averaged channel power of tap n be $\sigma_{h_i}^2(n)$. In this case, Eq. (5.18) should be rewritten as

$$E\left\{|MAI_{j\leftarrow i}[k]|^2\right\} \approx \frac{1}{M^2}\sigma_{x_i}^2 \sum_{n=0}^{L-1} \sigma_{h_i}^2(n)\left|\phi_{i,j}(n)\right|^2. \tag{5.34}$$

Since $\sigma_{h_i}^2(n)$ is a constant for a specific n, using similar derivation from Eqs. (5.18)–(5.33), the maximum value of the MAI from user i to user j, $\max_{i,j} E\left\{|MAI_{j\leftarrow i}[k]|^2\right\}$, in Lemma 5.1 should be rewritten. It can be approximated by

$$\sigma_{x_i}^2\left[\frac{1}{N^2}\frac{\pi^2}{4}\left(1-\frac{1}{M}\right)^2\sum_{n=0}^{L-1}\sigma_{h_i}^2(n)n^2 + \frac{1}{N^4}\frac{\pi^4}{4}\left(1-\frac{1}{M}\right)^2\sum_{n=0}^{L-1}\sigma_{h_i}^2(n)n^4\right]. \tag{5.35}$$

Compared to Lemma 5.1, since $\sigma_{h_i}^2(n)$ usually has exponential decay, the result in Eq. (5.35) leads to a much smaller MAI than that in Eq. (5.16) for fully-loaded PMU-OFDM with Hadamard-Walsh code. Similarly, we should rewrite the maximum value of $E\left\{|MAI_{j\leftarrow i}[k]|^2\right\}$ in Proposition 5.1. It can be approximated by

$$\max_{i,j} E\left\{|MAI_{j\leftarrow i}[k]|^2\right\} \approx \sigma_{x_i}^2\left[\frac{1}{N^4}\frac{\pi^4}{64}\sum_{n=0}^{L-1}\sigma_{h_i}^2(n)n^4\right]. \tag{5.36}$$

Again, the result in Eq. (5.36) leads to a much smaller MAI than that in Eq. (5.30) for half-loaded PMU-OFDM with Hadamard-Walsh code. ■

5.3 PMU-OFDM System in Time Offset Environment

In this section, we will show that the PMU-OFDM system is robust to the time offset if N is sufficiently large. Furthermore, we will derive an expression for the MAI effect due to the time offset in PMU-OFDM. Based on the expression, we show that the MAI effect caused by the time offset can be reduced to a negligible amount so that the multiuser system behaves like a "single-user" system if $M/2$ symmetric or anti-symmetric codewords of the M Hadamard-Walsh codes are used for each user in the prefilering stage of the system.

5.3.1 Time Asynchronism Analysis

In the following analysis, we assume that the CP length is $\nu = L - 1$, where L is the maximum length of the discrete channel considered. In this situation,

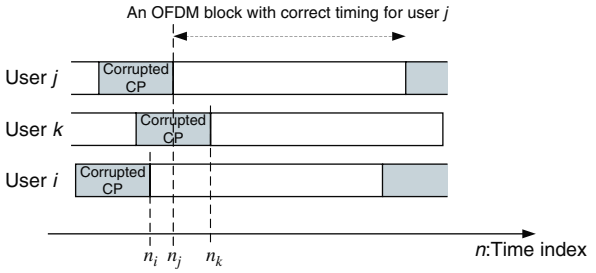

Fig. 5.4. Illustration of the time offset effect.

whenever one user has a non-zero time offset, this user will cause not only symbol distortion to himself/herself, but also MAI to all other users.

Referring to Fig. 5.4, let user j be the target user and thus n_j is the correct block extracting time for user j. Let user i has a time offset of $\tau_i = n_i - n_j$ with respect to the jth user. Then, we say user i is timing advanced if $\tau_i < 0$ and is timing delayed if $\tau_i > 0$. Since the MAI increases as $|\tau_i|$ increases, we will consider the more sever case that $|\tau_i|$ is larger than ν. Later we will show that the derivations also apply to the case $|\tau_i| \leq \nu$. Without loss of generality, suppose the receiver views $\hat{s}(0), \cdots, \hat{s}(M-1)$ as one OFDM block, where $\hat{s}(n)$ is as depicted in Fig. 5.5. For presentational convenience, we will add superscript $(+)$ or $(-)$ to denote, respectively, the data/channel in the previous and next block. For instance, $x_i^{(+)}[k]$ is the kth symbol of $x_i[k]$ in the previous block. Let the ν corrupted CP of the current block be

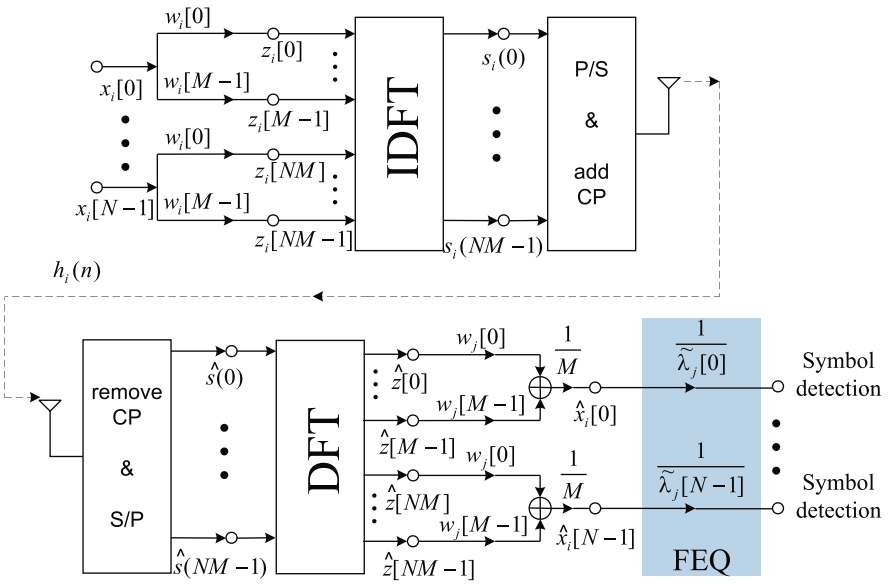

Fig. 5.5. The block diagram of the proposed system.

$[\widetilde{p}_i(0)\cdots\widetilde{p}_i(\nu-1)]$ and the received noise vector be $\hat{\mathbf{e}}$. Referring to Fig. 5.5, the received vector, $\hat{\mathbf{s}} = \sum_{i=1}^{T}\hat{\mathbf{p}}_i + \hat{\mathbf{e}}$. For $\tau_i < 0$, $\hat{\mathbf{p}}_i$ is given by

$$\begin{aligned}&\Big[\, p_i^{(-)}(NM-|\tau_i|+\nu)\cdots p_i^{(-)}(NM-1)\;\Big|\;\widetilde{p}_i(0)\cdots\widetilde{p}_i(\nu-1)\;\Big|\\ &p_i(0)\cdots p_i(NM-1-|\tau_i|)\Big],\end{aligned}\tag{5.37}$$

where

$$\widetilde{p}_i(n)=\sum_{m=0}^{n}h_i(m)s_i((n-m)+NM-\nu)+\sum_{m=n+1}^{\nu}h_i^{(-)}(m)s^{(-)}((n-m)+NM).\tag{5.38}$$

For $\tau_i > 0$, $\hat{\mathbf{p}}_i$ is given by

$$\begin{aligned}&\Big[p_i(\tau_i)\cdots p_i(NM-1)\;\Big|\;\widetilde{p}_i^{(+)}(0)\cdots\;\widetilde{p}_i^{(+)}(\nu-1)\;\Big|\\ &p_i^{(+)}(0)\cdots p_i^{(+)}(\tau_i-\nu-1)\Big],\end{aligned}\tag{5.39}$$

where

$$\widetilde{p}_i^{(+)}(n)=\sum_{m=0}^{n}h_i^{(+)}(m)s_i^{(+)}((n-m)+NM-\nu)+\sum_{m=n+1}^{\nu}h_i(m)s((n-m)+NM).\tag{5.40}$$

After DFT, the mixed signal from all the users are given by

$$\hat{z}[l]=\sum_{i=1}^{T}r_i[l]+e[l],\quad 0\le l\le NM-1,\tag{5.41}$$

where

$$r_i[l]=\frac{1}{\sqrt{NM}}\sum_{n=0}^{NM-1}\hat{s}(n)e^{-j\frac{2\pi}{NM}nl},\tag{5.42}$$

and $e[l]$ is the received noise after DFT. Now consider the symbol detection for the jth user. From Eqs. (5.128) and (5.41), and let $l = v + kM$, where $0 \le v \le M-1$, $0 \le k \le N-1$, the kth element of $\hat{\mathbf{x}}_j$ under time asynchronism is given by

$$\hat{x}_j[k]=\frac{1}{M}\sum_{v=0}^{M-1}r_j[v+kM]w_j^*[v]+\sum_{i=1,i\neq j}^{T}MAI_{j\leftarrow i}[k]+\frac{1}{M}\sum_{v=0}^{M-1}e[v+kM]w_j^*[v],\tag{5.43}$$

where the first term comes from the jth user, and

$$MAI_{j\leftarrow i}[k]=\frac{1}{M}\sum_{v=0}^{M-1}r_i[v+kM]w_j^*[v]$$

is the MAI of user j due to the time asynchronism of user i. Based on Eq. (5.43), once the overall MAI from all the other users is sufficiently smaller than the desired signal, the time offset of user j (sampled as integer) can be easily estimated and then compensated using the algorithms developed for single-user OFDM systems, e.g., [118, 141]. Moreover, as mentioned in the introductory section, there are several additional advantages when MAI is negligible.

Let us proceed to the details of $MAI_{j\leftarrow i}[k]$ and identify the dominating MAI from user i to user j. We consider $\tau_i < 0$. The derivations for $\tau_i > 0$ is similar. For representation purpose, we will use $(n)_{NM}$ to denote n modulo NM. From Eqs. (5.37), (5.42) and (5.43) and let $l = v + kM$, where $0 \le v \le M-1$, $0 \le k \le N-1$, the MAI of user i contributing to user j is given by

$$MAI_{j\leftarrow i}[k] = MAI^{(0)}_{j\leftarrow i}[k] + MAI^{(1)}_{j\leftarrow i}[k] + MAI^{(2)}_{j\leftarrow i}[k], \tag{5.44}$$

where $MAI^{(0)}_{j\leftarrow i}[k]$ is the MAI due to the current block of user i given by

$$\begin{aligned} MAI^{(0)}_{j\leftarrow i}[k] &= \frac{1}{M}\sum_{v=0}^{M-1}\frac{1}{\sqrt{NM}}\sum_{n=|\tau_i|}^{NM-1} p_i(n-|\tau_i|)e^{-j\frac{2\pi}{NM}(k+vM)n} \\ &= MAI^{(00)}_{j\leftarrow i}[k] - MAI^{(01)}_{j\leftarrow i}[k], \end{aligned} \tag{5.45}$$

where $MAI^{(00)}_{j\leftarrow i}[k]$ is given by

$$\frac{1}{M}\sum_{v=0}^{M-1}\frac{1}{\sqrt{NM}}\left[\sum_{n=0}^{NM-1} p_i((n-|\tau_i|)_{NM})e^{-j\frac{2\pi}{NM}(k+vM)n}\right] w_j^*[v],$$

and $MAI^{(01)}_{j\leftarrow i}[k]$ is given by

$$\frac{1}{M}\sum_{v=0}^{M-1}\frac{1}{\sqrt{NM}}\left[\sum_{n=0}^{|\tau_i|-1} p_i\left((n-|\tau_i|)_{NM}\right)e^{-j\frac{2\pi}{NM}(v+kM)n}\right] w_j^*[v].$$

$MAI^{(1)}_{j\leftarrow i}[k]$ is the MAI due to the previous block of the ith user given by

$$\frac{1}{M}\sum_{v=0}^{M-1}\frac{1}{\sqrt{NM}}\left[\sum_{n=0}^{|\tau_i|-\nu-1} p_i^{(-)}(n+NM-|\tau_i|+\nu)e^{-j\frac{2\pi}{NM}(v+kM)n}\right] w_j^*[v], \tag{5.46}$$

and $MAI^{(2)}_{j\leftarrow i}[k]$ is the MAI due to the corrupted CP of user i given by

$$\frac{1}{M}\sum_{v=0}^{M-1}\frac{1}{\sqrt{NM}}\left[\sum_{n=|\tau_i|-\nu}^{|\tau_i|-1} \widetilde{p}_i(n-|\tau_i|+\nu)e^{-j\frac{2\pi}{NM}(v+kM)n}\right] w_j^*[v]. \tag{5.47}$$

Note that when $|\tau_i| < \nu$, $MAI^{(1)}_{j\leftarrow i}[k]$ as given in Eq. (5.46) is zero and $MAI^{(2)}_{j\leftarrow i}[k]$ in Eq. (5.47) will sum up terms only for $n \geq 0$. When the timing mismatch τ_i is significantly smaller than NM, $MAI^{(0)}_{j\leftarrow i}[k]$ is the dominating MAI as compared with $MAI^{(1)}_{j\leftarrow i}[k]$ and $MAI^{(2)}_{j\leftarrow i}[k]$ since the current block contributes $NM - |\tau_i|$ symbols. This number is greater than that from the previous block or the corrupted CP. Moreover, when $|\tau_i| << NM$, $MAI^{(00)}_{j\leftarrow i}[k]$ is much greater than $MAI^{(01)}_{j\leftarrow i}[k]$ since $MAI^{(01)}_{j\leftarrow i}[k]$ is only a small fraction of $MAI^{(00)}_{j\leftarrow i}[k]$ according to Eq. (5.45). Hence, if we can greatly suppress $MAI^{(00)}_{j\leftarrow i}[k]$, the MAI due to time asynchronism can be greatly reduced. The suppression of $MAI^{(00)}_{j\leftarrow i}[k]$ is considered in the next section. Before moving to next section, let us see an example as follows.

Example 5.2: Dominating MAI in Time Offset Environment
Here, we would like to show that $MAI^{(0)}_{j\leftarrow i}[k]$ is the dominating MAI term over $MAI^{(1)}_{j\leftarrow i}[k]$ and $MAI^{(2)}_{j\leftarrow i}[k]$ for both $\tau_i < 0$ and $\tau_i > 0$. The simulation was conducted with the following setting. We consider the performance in the uplink direction, where each user may have a different time offset and channel fading. The channel and the time offset are assumed to be quasi-invariant in the sense that it remains unchanged in one block duration. Simulations are conducted with the following parameter setting throughout this section. $M = 16$ and the BPSK modulation is used. For the PMU-OFDM, the Hadamard-Walsh code is used. For every individual user, the Monte Carlo method is used to run more than 500,000 symbols. We consider the worst time offset situation. That is, except the target user who is assumed to have correct timing, the time offsets of all the other users are randomly assigned to be either $+\tau$ or $-\tau$. All T users are the target user in turn. For instance, as shown in Fig. 5.4, the correct timing for target user j is $n_j = 0$. Other users will have a time offset either $+\tau$ or $-\tau$ with respect to n_j. Moreover, the CP length $\nu = L-1$ is added. In this situation, any non-zero timing mismatch will lead to MAI. We will evaluate the averaged total MAI values of $MAI^{(0)}_{j\leftarrow i}[k]$ and $MAI^{(1)}_{j\leftarrow i}[k]+MAI^{(2)}_{j\leftarrow i}[k]$. The averaged total MAI value of the dominating MAI is obtained via averaging the value,

$$\frac{1}{T}\sum_{j=1}^{T}\frac{1}{N}\sum_{k=0}^{N-1}\left|\sum_{i=1,i\neq j}^{T} MAI^{(0)}_{j\leftarrow i}[k]\right|^2,$$

for more than $500{,}000\,T$ symbols. That is, the total MAI per symbol of the T individual users, for all T users. Similarly, the averaged total MAI value of the non-dominating MAI is obtained via averaging the value,

$$\frac{1}{T}\sum_{j=1}^{T}\frac{1}{N}\sum_{k=0}^{N-1}\left|\sum_{i=1,i\neq j}^{T} MAI^{(1)}_{j\leftarrow i}[k] + MAI^{(2)}_{j\leftarrow i}[k]\right|^2,$$

for more than $500{,}000\,T$ symbols.

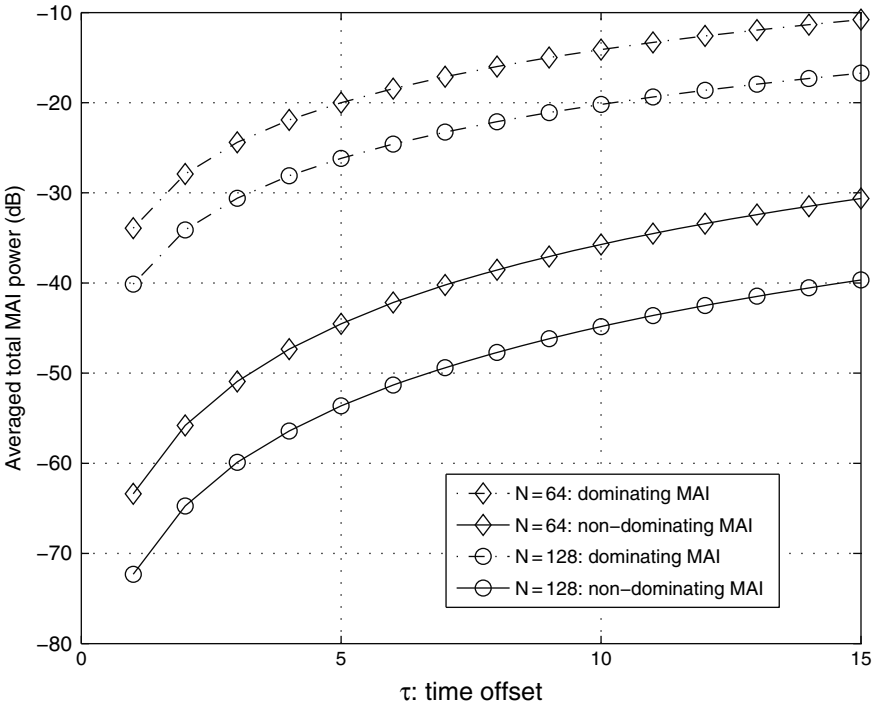

Fig. 5.6. The MAI effect is plotted as a function of the time offset when full M Hadamard-Walsh codewords are used.

Let us consider a flat fading channel whose coefficients are complex Gaussian random variables. Let $T = M = 16$, i.e., the fully-loaded case. The averaged dominating and non-dominating MAI power values are plotted as a function of the time offset for $N = 64$ and 128 in Fig. 5.6. The dominating MAI values are represented by dashed curves. As shown in this figure, the dominating MAI is much greater than the non-dominating MAI by around 20–30 dB for $N = 64$, and by around 22–32 dB for $N = 128$. This result confirms that $MAI^{(0)}_{j\leftarrow i}[k]$ is indeed the dominating MAI over $MAI^{(1)}_{j\leftarrow i}[k]$ and $MAI^{(2)}_{j\leftarrow i}[k]$. Moreover, as N increases from 64 to 128, the dominating MAI decreases by around 6–8 dB, and the non-dominating MAI decreases by around 9–10 dB. This corroborates the theoretical result; namely, both the dominating MAI and the non-dominating MAI decrease as N increases. ■

Asymptotic Behavior with Hadamard-Walsh Code

Now, we will argue that if Hadamard-Walsh code is used, as N increases, all the MAI terms will be approximately zero when N is sufficiently large. That is, even in a time asynchronous environment, the PMU-OFDM can still be approximately MAI-free for a sufficiently large N. Consider $MAI^{(00)}_{j\leftarrow i}[k]$ first. Using the definition of DFT for $p_i(n)$,

$$p_i(n) = \frac{1}{\sqrt{NM}} \sum_{l=0}^{NM-1} z_i[l]\lambda_i[l]e^{j\frac{2\pi}{NM}nl}$$
$$= \frac{1}{\sqrt{NM}} \sum_{f=0}^{N-1} x_i[f]e^{j\frac{2\pi}{N}fn} \sum_{u=0}^{M-1} \lambda_i[u+fM]w_i[u]e^{j\frac{2\pi}{NM}un}, \tag{5.48}$$

and from Eq. (5.45), and the time shift property of DFT [98], we have

$$MAI_{j\leftarrow i}^{(00)}[k] = \frac{1}{M}x_i[k]e^{-j\frac{2\pi}{N}k|\tau_i|} \sum_{v=0}^{M-1} \lambda[v+kM]w_i[v]w_j[v]e^{-j\frac{2\pi}{NM}v|\tau_i|}. \tag{5.49}$$

Using the approximation in Eq. (5.9) and $\tau_i < 0$, we have

$$MAI_{j\leftarrow i}^{(00)}[k] \approx \frac{1}{M}\widetilde{\lambda}_i[k]x_i[k]e^{j\frac{2\pi}{N}k\tau_i} \sum_{v=0}^{M-1} w_i[v]w_j[v]e^{j\frac{2\pi}{NM}v\tau_i}. \tag{5.50}$$

Since the maximum value of v is $M-1$, the term $e^{-j2\pi/NMv|\tau_i|}$ in Eq. (5.50) is approximately 1 if $N \gg |\tau_i|$. This approximation becomes more accurate as N increases. Since the value $\sum_{v=0}^{M-1} w_i[v]w_j[v] = 0$ according to Eq. (5.2), $MAI_{j\leftarrow i}^{(00)}[k] \approx 0$ for sufficiently large N. Now, consider $MAI_{j\leftarrow i}^{(01)}[k]$. From Eq. (5.45), since $p_i\left((n-|\tau_i|)_{NM}\right) = p_i\left(n+NM-|\tau_i|\right)$, for $0 \le n \le |\tau_i|-1$, $MAI_{j\leftarrow i}^{(01)}[k]$ is given by

$$\frac{1}{M}\sum_{v=0}^{M-1} \frac{1}{\sqrt{NM}} \left[\sum_{n=0}^{|\tau_i|-1} p_i\left(n+NM-|\tau_i|\right) e^{-j\frac{2\pi}{NM}(v+kM)n} \right] w_j^*[v]. \tag{5.51}$$

Using Eq. (5.48) and the approximation in Eq. (5.9), we can rewrite Eq. (5.51) as

$$MAI_{j\leftarrow i}^{(01)}[k] \approx \frac{1}{NM^2} \sum_{n=0}^{|\tau_i|-1} \sum_{f=0}^{N-1} x_i[f]\widetilde{\lambda}_i[f]e^{j\frac{2\pi}{N}f(n-|\tau_i|)-kn}\delta_{i,j}^{(01)}(\tau_i), \tag{5.52}$$

where $\delta_{i,j}^{(01)}(\tau_i) = \sum_{u=0,v=0}^{M-1} w_i[u]w_j[v]e^{j\frac{2\pi}{NM}u(n-|\tau_i|)-vn}$. For a fixed n, if N is sufficiently large, $e^{j2\pi/NMu(n-|\tau_i|)-vn}$ is approximately 1 for all possible combination of u and v. For instance, if $n = |\tau_i|-1$, the maximum value of $u(n-|\tau_i|)-vn$ is 0, i.e., when $u=0,\ v=0$, and the minimum value of $u(n-|\tau_i|)-vn$ is $-2(M-1)$, i.e., when $u=v=M-1$. Moreover, for Hadamard-Walsh code is used, $\sum_{u=0,v=0}^{M-1} w_i[u]w_j[v] = \sum_{u=0}^{M-1} w_i[u] \sum_{u=0}^{M-1} w_j[v] = 0$, for $i \neq j$. Hence, $\delta_{i,j}^{(01)}(\tau_i)$ in Eq. (5.52) is approximately zero and thus $MAI_{j\leftarrow i}^{(01)}[k] \approx 0$. Next, consider $MAI_{j\leftarrow i}^{(1)}[k]$. From Eqs. (5.46), (5.48) and the approximation in Eq. (5.9),

$$MAI_{j\leftarrow i}^{(1)}[k] \approx \frac{1}{NM^2} \sum_{n=0}^{|\tau_i|-\nu-1} \sum_{f=0}^{N-1} x_i^{(-)}[f]\widetilde{\lambda}_i^{(-)}[f] e^{j\frac{2\pi}{N}f(n-|\tau_i|+\nu)-kn} \delta_{i,j}^{(1)}(\tau_i), \tag{5.53}$$

where $\delta_{i,j}^{(1)}(\tau_i) = \sum_{u=0,v=0}^{M-1} w_i[u]w_j[v]e^{j\frac{2\pi}{NM}u(n-|\tau_i|+\nu)-vn}$. Using an argument similar to that for $\delta_{i,j}^{(01)}(\tau_i)$, we know that $\delta_{i,j}^{(1)}(\tau_i)$ is also approximately zero for large N. Finally, consider $MAI_{j\leftarrow i}^{(2)}[k]$. From Eqs. (5.38), (5.47) and the fact that $s_i(n)$ is the NM-point IDFT of $z_i[l]$, $MAI_{j\leftarrow i}^{(2)}[k]$ is given by

$$\frac{1}{NM^2} \sum_{n=0}^{\nu-1} \sum_{f=0}^{N-1} \Bigg[x_i[f] \sum_{m=0}^{n} h_i(m) e^{j\frac{2\pi}{N}f(n-m-\nu)-k(n+|\tau_i|-\nu)} \delta_{i,j}^{(20)}(\tau_i) + x_i^{(-)}[f] \sum_{m=n+1}^{\nu} h_i^{(-)}(m) e^{j\frac{2\pi}{N}f(n-m)-k(n+|\tau_i|-\nu)} \delta_{i,j}^{(21)}(\tau_i), \Bigg], \tag{5.54}$$

where $\delta_{i,j}^{(20)}(\tau_i)$ and $\delta_{i,j}^{(21)}(\tau_i)$ are given by

$$\delta_{i,j}^{(20)}(\tau_i) = \sum_{u=0,v=0}^{M-1} w_i[u]w_j[v]e^{j\frac{2\pi}{NM}u(n-m-\nu)-v(n+|\tau_i|-\nu)}$$

and

$$\delta_{i,j}^{(21)}(\tau_i) = \sum_{u=0,v=0}^{M-1} w_i[u]w_j[v]e^{j\frac{2\pi}{NM}u(n-m)-v(n+|\tau_i|-\nu)}.$$

Similarly, $\delta_{i,j}^{(20)}(\tau_i)$ and $\delta_{i,j}^{(21)}(\tau_i)$ are also approximately zero for large N. Thus, for sufficiently large N, PMU-OFDM can still be approximately MAI-free.

5.3.2 Code Design for MAI Mitigation

In the previous section, we have explained that $MAI_{j\leftarrow i}^{(0)}[k]$ is the major MAI. Moreover, $MAI_{j\leftarrow i}^{(0)}[k]$ is divided into $MAI_{j\leftarrow i}^{(00)}[k]$ and $MAI_{j\leftarrow i}^{(01)}[k]$, and the first term is the dominating term. Hence, if we can suppress $MAI_{j\leftarrow i}^{(00)}[k]$, the MAI due to time asynchronism will be reduced greatly. In this section, we will demonstrate a code design which can greatly suppress $MAI_{j\leftarrow i}^{(00)}[k]$. Based on Eq. (5.50), let us define a function $\phi_{i,j}(\tau_i)$ given by

$$\phi_{i,j}(\tau_i) = \sum_{m=0}^{M-1} w_i[m]w_j[m]e^{j\frac{2\pi}{NM}m\tau_i}. \tag{5.55}$$

If the code is properly designed such that $\phi_{i,j}(\tau_i) \approx 0$ for arbitrary combination of i and j, the dominating MAI can be made approximately zero. The following derivation is similar to that in Section 5.2.2 except that now the MAI

is due to time offset. Let us further manipulate $\phi_{i,j}(\tau_i)$ as follows. Express the exponential term in Eq. (5.55) using the Taylor series representation, i.e.,

$$e^{j\frac{2\pi}{NM}m\tau_i} = 1 + j\left(\frac{2\pi}{NM}m\tau_i\right) - \frac{1}{2!}\left(\frac{2\pi}{NM}m\tau_i\right)^2 - j\frac{1}{3!}\left(\frac{2\pi}{NM}m\tau_i\right)^3 + \cdots.$$

Since the maximum value of m is $M-1$, the maximum value of $2\pi/NMm\tau_i < 2\pi\tau_i/N$. When $\tau_i \ll N$, we may use second order approximation of $e^{-j2\pi/NMm\tau_i}$, which leads to

$$\begin{aligned}\phi_{i,j}(\tau_i) &\approx \sum_{m=0}^{M-1} w_i[m]w_j[m]\left[1 - \frac{1}{2!}\left(\frac{2\pi}{NM}m\tau_i\right)^2 + j\frac{2\pi}{NM}m\tau_i\right] \\ &= \sum_{m=0}^{M-1} w_i[m]w_j[m]\left[-\frac{1}{2!}\left(\frac{2\pi}{NM}m\tau_i\right)^2 + j\frac{2\pi}{NM}m\tau_i\right] \\ &\triangleq \widetilde{\phi}_{i,j}(\tau_i), \end{aligned} \tag{5.56}$$

where we have used $\sum_{m=0}^{M-1} w_i[m]w_j^*[m] = 0$, for $i \neq j$. From Eqs. (5.55) and (5.56), we can rewrite Eq. (5.50) as

$$MAI_{j\leftarrow i}^{(00)}[k] \approx \frac{1}{M}\widetilde{\lambda}_i[k]x_i[k]e^{j\frac{2\pi}{N}k\tau_i}\widetilde{\phi}_{i,j}(\tau_i). \tag{5.57}$$

Now, we would like to evaluate $E\left\{\left|MAI_{j\leftarrow i}^{(00)}[k]\right|^2\right\}$, the averaged MAI power from user i to user j. Let us assume the averaged transmitter power are the same for all subchannels and $E\{x_i[k]x_i^*[k']\} = 0$, for $k \neq k'$. Also, assume the averaged channel power are the same for different taps and $E\{h_i[n]h_i^*[n']\} = 0$, for $n \neq n'$. Again, according to the same argument in Section 5.2.2, the equal power assumption of channel coefficients will lead to a pessimistic result. Let $\sigma_{x_i}^2$ be the averaged transmitted power, and $\sigma_{h_i}^2$ be the averaged channel power defined, respectively, by $\sigma_{x_i}^2 = E\left\{|x_i[k]|^2\right\}$ and $\sigma_{h_i}^2 = E\left\{|h_i(n)|^2\right\}$. Then, we have the following lemma.

Lemma 5.4: When all the M Hadamard-Walsh codewords are used, i.e., fully loaded case. The maximum value of the MAI from user i to user j, denoted by $\max_{i,j} E\left\{\left|MAI_{j\leftarrow i}^{(00)}[k]\right|^2\right\}$, can be approximated by

$$\sigma_{x_i}^2\sigma_{h_i}^2\left[\left(\frac{\tau_i}{N}\right)^2\frac{\pi^2}{4}\left(1 - \frac{1}{M}\right)^2 + \left(\frac{\tau_i}{N}\right)^4\frac{\pi^4}{4}\left(1 - \frac{1}{M}\right)^2\right], \tag{5.58}$$

and the maximum value occurs when $w_i[m]$ and $w_j[m]$ satisfy Eq. (5.17).

Proof. From Eq. (5.57) and using that

$$\widetilde{\lambda}_i[k] = \sum_{n=0}^{L-1} h_i(n) e^{-j\frac{2\pi}{N}nk},$$

$E\left\{\left|MAI_{j\leftarrow i}^{(00)}[k]\right|^2\right\}$ can be approximated by

$$\begin{aligned}\frac{1}{M^2}\,\sigma_{x_i}^2 \sum_{n=0}^{L-1}\sum_{n'=0}^{L-1} E\left\{h_i(n)h_i^*(n')\right\} e^{-j\frac{2\pi}{N}k(n-n')}\left|\widetilde{\phi}_{i,j}(\tau_i)\right|^2 \\ = \frac{L}{M^2}\sigma_{x_i}^2\sigma_{h_i}^2\left|\widetilde{\phi}_{i,j}(\tau_i)\right|^2. \end{aligned} \tag{5.59}$$

From Eq. (5.59), maximizing $E\left\{\left|MAI_{j\leftarrow i}^{(00)}[k]\right|^2\right\}$ is equivalent to maximizing $\left|\widetilde{\phi}_{i,j}(\tau_i)\right|^2$. From Eq. (5.56), $\widetilde{\phi}_{i,j}(\tau_i)$ can be rearranged as

$$\widetilde{\phi}_{i,j}(\tau_i) = \Re\left\{\widetilde{\phi}_{i,j}(\tau_i)\right\} + j\Im\left\{\widetilde{\phi}_{i,j}(\tau_i)\right\}, \tag{5.60}$$

where

$$\Re\left\{\widetilde{\phi}_{i,j}(\tau_i)\right\} = -\frac{1}{2!}\left(\frac{2\pi}{NM}\right)^2 \tau_i^2 \sum_{m=0}^{M-1} w_i[m]w_j[m]m^2$$

and

$$\Im\left\{\widetilde{\phi}_{i,j}(\tau_i)\right\} = \left[\frac{2\pi}{NM}\tau_i \sum_{m=0}^{M-1} w_i[m]w_j[m]m\right].$$

Since

$$\left|\widetilde{\phi}_{i,j}(\tau_i)\right|^2 = \left|\Re\left\{\widetilde{\phi}_{i,j}(\tau_i)\right\}\right|^2 + \left|\Im\left\{\widetilde{\phi}_{i,j}(\tau_i)\right\}\right|^2,$$

maximizing $\left|\widetilde{\phi}_{i,j}(\tau_i)\right|^2$ is equivalent to maximizing both $\left|\sum_{m=0}^{M-1} w_i[m]w_j[m]m\right|$ and $\left|\sum_{m=0}^{M-1} w_i[m]w_j[m]m^2\right|$. According to [65], the product of two arbitrary distinct Hadamard-Walsh is a non-all-one Hadamard-Walsh codeword. Note that each of the non-all-one Hadamard-Walsh codeword has equal number of $+1$ and -1. Since m and m^2 are monotonically increasing functions for $m \geq 0$, $\left|\sum_{m=0}^{M-1} w_i[m]w_j[m]m\right|$ and $\left|\sum_{m=0}^{M-1} w_i[m]w_j[m]m^2\right|$ are maximized

if $w_i[m]w_j[m]$ are of the same sign for $0 \leq m \leq M/2-1$. In this case, we have

$$\left|\sum_{m=0}^{M-1} w_i[m]w_j[m]m^2\right| = \sum_{m=M/2}^{M-1} m^2 - \sum_{m=0}^{M/2-1} m^2 = \frac{1}{4}M^3\left(1-\frac{1}{M}\right). \quad (5.61)$$

Similarly, it can be shown

$$\left|\sum_{m=0}^{M-1} w_i[m]w_j[m]m\right| = \sum_{m=M/2}^{M-1} m - \sum_{m=0}^{M/2-1} m = \frac{1}{4}M^2\left(1-\frac{1}{M}\right). \quad (5.62)$$

From Eqs. (5.59), (5.60), (5.61) and (5.62), we proved the approximation in Eq. (5.58). ■

Observed from Eq. (5.58), the maximum value of $E\left\{\left|MAI_{j\leftarrow i}^{(00)}[k]\right|^2\right\}$ depends on two terms. One is proportional to $1/N^2$ and the other is proportional to $1/N^4$. When N grows, the term which is proportional to $1/N^2$ will dominate the performance. Hence, we may regard the maximum value of $E\left\{\left|MAI_{j\leftarrow i}^{(00)}[k]\right|^2\right\}$ decreases at a rate proportional to $1/N^2$. Note that when all the M codewords are used, every target user will unavoidably has interference from a certain user that attains the maximum given in Eq. (5.16). For instance, let $M = 16$ and user i uses $\mathbf{w}_1$ and user j uses $\mathbf{w}_9$. Then, $w_i[k]w_j[k]$ satisfies Eq. (5.17) and the dominating MAI occurs. Now, if user i uses $\mathbf{w}_2$ and user j uses $\mathbf{w}_{10}$, again $w_i[k]w_j[k]$ satisfies Eq. (5.17) and the dominating MAI occurs. Consider the overall MAI power for user j, i.e., $\sum_{i=1,i\neq j}^{M} E\left\{\left|MAI_{j\leftarrow i}^{(00)}[k]\right|^2\right\}$. Since the maximum value of $E\left\{\left|MAI_{j\leftarrow i}^{(00)}[k]\right|^2\right\}$ is the dominating MAI of $\sum_{i=1,i\neq j}^{M} E\left\{\left|MAI_{j\leftarrow i}^{(00)}[k]\right|^2\right\}$, we may regard the overall MAI power decreases in an order of $1/N^2$. Therefore, when all the M codewords are used and N is sufficiently large (for the approximation in Eq. (5.9)), the overall MAI power of the PMU-OFDM due to time asynchronism decreases in an order $1/N^2$. From Eq. (5.16), the term proportional to $1/N^2$ dominates the performance, which is contributed by $\Im\left\{\widetilde{\phi}_{i,j}(\tau_i)\right\}$ in Eq. (5.60). Hence, if we can constrain $\Im\left\{\widetilde{\phi}_{i,j}(\tau_i)\right\} = 0$, the MAI due to time offset can be greatly reduced. This goal can be achieved by properly selecting codewords from the Hadamard-Walsh code.

Now, we consider the use of $M/2$ symmetric or anti-symmetric codewords [135]. From Lemma 5.3, we can rewrite Eq. (5.57) as

$$MAI_{j\leftarrow i}^{(00)}[k] \approx \frac{1}{M}\widetilde{\lambda}_i[k]x_i[k]e^{j\frac{2\pi}{N}k\tau_i}\sum_{m=0}^{M-1}\frac{-1}{2!}\left(\frac{2\pi}{NM}m\tau_i\right)^2 w_i[m]w_j[m]. \quad (5.63)$$

Hence, we have the following proposition.

Proposition 5.2: Suppose that only symmetric (anti-symmetric) Hadamard-Walsh codewords are used, the maximum value of $E\left\{\left|MAI_{j\leftarrow i}^{(00)}[k]\right|^2\right\}$ can be approximated by

$$\max_{i,j} E\left\{\left|MAI_{j\leftarrow i}^{(00)}[k]\right|^2\right\} \approx L\sigma_{x_i}^2\sigma_{h_i}^2\left[\left(\frac{\tau_i}{N}\right)^4\frac{\pi^4}{64}\right], \quad (5.64)$$

and this occurs when $w_i[m]$ and $w_j[m]$ satisfy Eq. (5.32).

Proof. According to Eq. (5.63), if the code selection mentioned in Proposition 5.2 is used, the imaginary part of $\phi_{i,j}(n)$ in Eq. (5.60) disappears. Following the same argument in the proof of Lemma 5.4, we know that $E\left\{\left|MAI_{j\leftarrow i}^{(00)}[k]\right|^2\right\}$ is at its largest when the value $\left|\sum_{m=0}^{M-1} w_i[m]w_j[m]m^2\right|$ is at its largest. According to [135], if only symmetric or anti-symmetric codewords are used, the codeword product $w_i[m]w_j[m]$ is again a symmetric non-all-one Hadamard-Walsh codeword. Hence, the last half $M/2$ elements of $w_i[m]w_j[m]$ can be obtained by its first $M/2$ elements. Therefore, both the first and the last half $M/2$ elements have equal number of $+1$ and -1. Since m^2 are monotonically increasing functions for $m \geq 0$, $\left|\sum_{m=0}^{M/2-1} w_i[m]w_j[m]m^2\right|$ are maximized if $w_i[m]w_j[m]$ are of the same sign for $0 \leq m \leq M/4-1$, and $\left|\sum_{m=M/2}^{M-1} w_i[m]w_j[m]m^2\right|$ are maximized if $w_i[m]w_j[m]$ are of the same sign for $M/2 \leq m \leq 3M/4-1$, which is the condition in Eq. (5.32). Given that the codeword product $w_i[m]w_j[m]$ satisfies Eq. (5.32), we have

$$\sum_{m=0}^{M-1} w_i[m]w_j[m]m^2 = \sum_{m=0}^{M-1} m^2 - 2\sum_{m=M/4}^{3M/4-1} m^2 = \frac{1}{16}M^3. \quad (5.65)$$

From Eqs. (5.60), (5.63) and (5.65), the maximum value of $E\left\{\left|MAI_{j\leftarrow i}^{(00)}[k]\right|^2\right\}$ can be approximated as that in Eq. (5.64). ■

Observing from Eq. (5.64), we see that when symmetric (anti-symmetric) codewords are used, the maximum value of $E\left\{\left|MAI_{j\leftarrow i}^{(00)}[k]\right|^2\right\}$ decreases in an order of $1/N^4$ for sufficiently large N. We can compare this result to fully loaded case, in which MAI power decreases in an order of $1/N^2$. Thus, using

symmetric (anti-symmetric) codewords enable the system to reduce MAI at a much faster rate as N increases in a time asynchronous environment. Although we use the assumption $|\tau_i|/N \ll 1$ in the derivation, simulations demonstrate that the approximation is still accurate for moderate $|\tau_i|/N$.

Example 5.3. In this example, we will show that the second order approximation used in Eq. (5.56) holds for $|\tau_i|/N$ as large as 1/4. Moreover, we demonstrate that using symmetric (anti-symmetric) Hadamard-Walsh codewords enables the system to eliminate MAI due to time asynchronism much faster than the fully-loaded case.

Let us consider the flat fading channel, i.e., $L = 1$. In this case, the approximations in Eqs. (5.9) and (5.50) become equalities. Hence, from Eqs. (5.50) and (5.55), we have

$$E\left\{\left|MAI_{j\leftarrow i}^{(00)}[k]\right|^2\right\} = \frac{1}{M^2}\sigma_{x_i}^2\sigma_{h_i}^2\left|\phi_{i,j}(\tau_i)\right|^2. \tag{5.66}$$

We will compare the approximated maximum interference given in Eqs. (5.16) (fully-loaded) and (5.64) (half-loaded) to the exact quantity given in Eq. (5.66). Let us consider the case that user i has a serious time offset $\tau_i = 16$. Let $M = 16$, $\sigma_{x_i}^2 = 1$ and $\sigma_{h_i}^2 = 1$. Let us consider the maximum MAI power from user i to user j, which occurs when $w_i[m]w_j[m]$ satisfies Eq. (5.17) for the fully-loaded case, and occurs when $w_i[m]w_j[m]$ satisfies Eq. (5.32) when symmetric (anti-symmetric) codewords are used. The maximum MAI power with and without approximation as functions of N for fully- and half-loaded systems are shown in Fig. 5.7. Approximated maximum MAI power is plotted for all integer N from 32 to 256 and exact maximum MAI power is obtained for $N = 32,\ 64,\ 128$, and 256. From the figure, we observe that the approximations are very accurate for both fully- and half-loaded cases when $N \geq 64$. Since $\tau_i = 16$, the approximated results become accurate when the ratio $\tau_i/N \leq 1/4$.

Moreover, we see that symmetric (anti-symmetric) codewords enable the system to reduce MAI at a much faster rate than the fully-loaded system under a time asynchronous environment. We see that in the fully-loaded case, doubling N will decrease MAI power by 6 dB while in half-loaded case, doubling N will decrease MAI power by 12 dB. This result corroborates our derivation in Lemma 5.4 and Proposition 5.2. That is, using symmetric (anti-symmetric) codewords, the maximum MAI power due to time asynchronism decreases at a much faster rate proportional to $1/N^4$ than the fully-loaded system whose rate is proportional to only $1/N^2$.

It is interesting to note that in Eqs. (5.16) and (5.64), the ratio N/τ_i determines the approximated maximum dominating MAI $E\left\{\left|MAI_{j\leftarrow i}^{(00)}[k]\right|^2\right\}$ due to time offset. This result allows us to determine N according to the maximum allowed time offset τ_i. For instance, from Fig. 5.7, we see that in the half-loaded case, $\max_{i,j} E\left\{\left|MAI_{j\leftarrow i}^{(00)}[k]\right|^2\right\}$ is -34 dB for $N = 128$ and

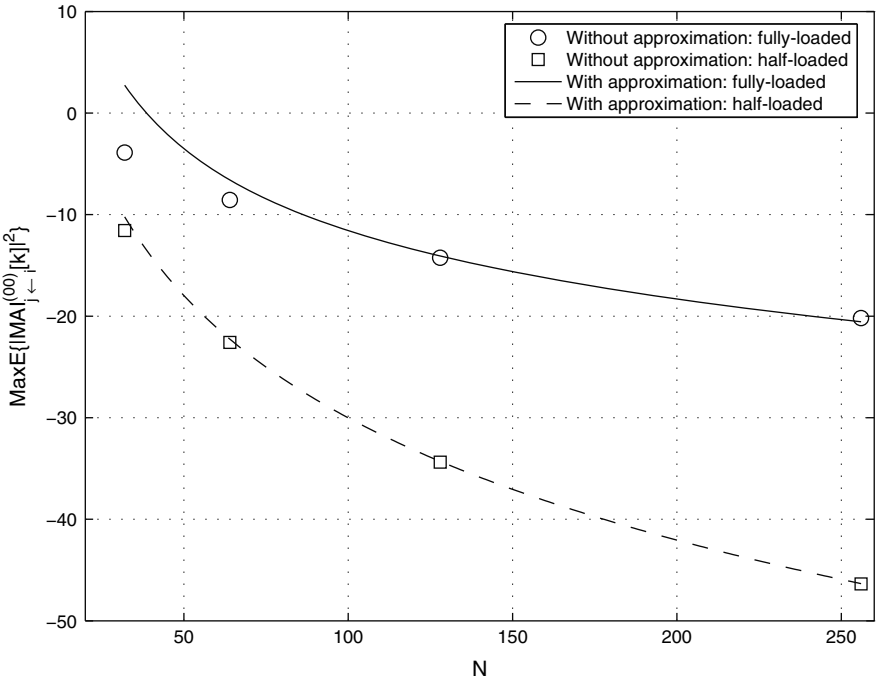

Fig. 5.7. Term $\max_{i,j} E\left\{\left|MAI^{(00)}_{j\leftarrow i}[k]\right|^2\right\}$ with and without approximation as a function of N for fully and half-loaded cases.

$\tau_i = 16$. Now, if the system uses a more strick design parameter for time offset, e.g., τ_i decreases from 16 to 8, to maintain the MAI power to be $-34\,\text{dB}$ in this half-loaded situation, N can be decreased from 128 to 64. Therefore, this result gives us an explicit way to determine N in a time asynchronous environment. ■

Based on Proposition 5.2, it is easy to derive the following corollary.

Corollary 7.1: Suppose that only $M/2$ symmetric or anti-symmetric codewords of M Hadamard-Walsh codes are used, for $i \neq j$, we have the following properties:

$$\sum_{u=0,v=0}^{\frac{M}{2}-1} w_i[u]w_j^*[v] = \sum_{u=\frac{M}{2},v=\frac{M}{2}}^{M-1} w_i[u]w_j^*[v]$$
$$= \sum_{u=0}^{\frac{M}{2}-1}\sum_{v=\frac{M}{2}}^{M-1} w_i[u]w_j^*[v] = \sum_{u=\frac{M}{2}}^{M-1}\sum_{v=0}^{\frac{M}{2}-1} w_i[u]w_j^*[v] = 0. \tag{5.67}$$

The code design procedure as stated in Proposition 5.2 also reduces the three MAI terms, $MAI^{(01)}_{j\leftarrow i}[k]$, $MAI^{(1)}_{j\leftarrow i}[k]$, and $MAI^{(2)}_{j\leftarrow i}[k]$ as well. This can

be explained as follows. Using Eq. (5.67), δ_1, δ_2, δ_3, and δ_4 in Eqs. (5.52), (5.53), and (5.54) can be further reduced since the phase variation in the exponential for all possible u and v becomes one half and the exponential term is closer to 1 as compared with the fully-loaded system. Take δ_1 in Eq. (5.52) as an example, δ_1 can be divided into four terms as

$$\delta_1 = \sum_{u=0,v=0}^{\frac{M}{2}-1} \phi_{i,j}(u,v) + \sum_{u=\frac{M}{2},v=\frac{M}{2}}^{M-1} \phi_{i,j}(u,v) + \sum_{u=0,v=\frac{M}{2}}^{\frac{M}{2}-1,M-1} \phi_{i,j}(u,v) + \sum_{u=\frac{M}{2},v=0}^{M-1,\frac{M}{2}-1} \phi_{i,j}(u,v), \tag{5.68}$$

where $\phi_{i,j}(u,v) = w_i[u]w_j^*[v]e^{j\frac{2\pi}{NM}u(n-|\tau_i|)-vn}$. If symmetric or anti-symmetric Hadamard-Walsh codes are used, the four terms of δ_1 is approximately 0 according to Eq. (5.67). Hence, δ_1 is approximately 0.

However, it is worthwhile to comment that, when compared to the fully load case, the use of the proposed code scheme leads to more accurate approximation and hence smaller δ_1. For example, as mentioned earlier, when $n = |\tau_i| - 1$ in the fully-loaded system, the maximum and minimum values of $u(n-|\tau_i|)-vn$ are 0 and $-2(M-1)$, respectively. Hence, the maximum phase difference is $2\pi/NM2(M-1)$. On the other hand, if the proposed code is used for $n = |\tau_i| - 1$, the maximum and minimum values of $u(n-|\tau_i|)-vn$ are 0 (when $u = v = 0$) and $-(M-1)$ (when $u = v = M/2$), respectively. Thus, the maximum phase difference is $2\pi/NM(M-1)$, which is one half of that of the fully-loaded case. It can be easily verified that the phase differences of the later three terms in Eq. (5.68) are $2\pi/NMM$, $2\pi/NMM$ and $2\pi/NM(M-2)$, respectively. Since the phase differences are near one half of those of the fully loaded system, the use of the proposed code leads to more accurate approximation and smaller δ_1. Please also note that the use of anti-symmetric codewords in a flat channel will result in $MAI_{j\leftarrow i}^{(1)}[k] = MAI_{j\leftarrow i}^{(2)}[k] = 0$ when $\tau_i = -1$, which can be easily verified by Eqs. (5.46) and (5.47). This is also true for $\tau_i = +1$.

The number of users is decreased by one half when only symmetric or anti-symmetric Hadamard-Walsh codewords are used. This price is compensated by several attractive gains. The system can continue to be approximately MAI-free in the presence of time offset. It has been shown that the same code design can greatly mitigate the MAI caused by the frequency offset [135], which is a serious problem that limits the mobility of the OFDMA system [6]. Therefore, the use of symmetric or anti-symmetric Hadamard-Walsh codewords enables the PMU-OFDM to be more robust in both a time and frequency asynchronous environment.

Since the MAI due to time asynchronism becomes negligible, the timing estimation for every individual user becomes much easier, i.e., estimation algorithm used in single-user environment may be applied here without worrying

about the MAI. Moreover, timing misalignment among individual users can be compensated in the receiver end. For instance, the receiver can extract individual users' OFDM block at the corresponding correct timing for detection. Note that even the timing misalignment for all the other users still exist, this misalignment will only cause negligible MAI and will not degrade the system bit error probability performance. Moreover, since the requirement for accurate timing has been greatly relaxed, a much simpler synchronization mechanism can be adopted for the transceiver.

These results stand in contrast to those of the OFDMA system, where minor timing mismatch will cause significant MAI [97]. As mentioned in [142], the timing asynchronism of OFDMA cannot be solved in the receiver end alone and feedback mechanism is demanded. If some users somehow fail to be well-synchronized, great performance degradation occurs and sophisticated multiuser estimation, e.g., [88, 142], is needed to acquire time offset for the users and this will cause extra complexity burden.

Example 5.4: Comparison of MAI Suppression

We will also show that the dominating MAI due to time offset, i.e., $MAI^{(0)}_{j\leftarrow i}[k]$ can be greatly reduced if $M/2$ symmetric or anti-symmetric codewords of the M Hadamard-Walsh codewords are used. Moreover, the experiment results show that the non-domination MAI, $MAI^{(1)}_{j\leftarrow i}[k] + MAI^{(2)}_{j\leftarrow i}[k]$, can also be greatly reduced by using symmetric or anti-symmetric codewords. Let the simulation parameters be the same as that in Example 5.2. First, let $N = 64$. The number of users decreases from $T = M = 16$ to $T = M/2 = 8$, i.e., a half-loaded system. For the comparison purpose, we consider another half-loaded code scheme that uses the first $M/2$ codewords of M Hadamard-Walsh codes to serve as a benchmark. The performance is shown in Fig. 5.8. Note that the dominating MAI using symmetric codewords (dashed-diamond) and the dominating MAI using anti-symmetric codewords (dashed-triangular) are overlapping. Compared with Fig. 5.6 with $N = 64$, the use of symmetric or anti-symmetric codewords can significantly reduce the dominating MAI by a range of 14–37 dB. On the other hand, the use of the first $M/2$ codewords only improves the dominating MAI by around 5–6 dB. We also see that the use of symmetric or anti-symmetric codewords can greatly reduce the non-dominating MAI. The results confirm that both dominating and non-dominating MAIs can be greatly reduced using the proposed code scheme. Note that even if the maximum time offset level is 15 in this example, since $N = 64 > 4 \times 15$, the averaged total MAI can still be suppressed below -25 dB, which is much smaller than the transmit power of 0 dB. This result confirms the claim in Section 5.3.2 that significant MAI suppression can be achieved at a more relaxed value of N.

Figure 5.9 shows the performance for $N = 128$. Comparing it with the result of $N = 128$ in Fig. 5.6, we see that the use of symmetric or anti-symmetric codewords can significantly reduce the dominating MAI by 20–43 dB. The improvement for $N = 128$ is 6 dB better than that for $N = 64$,

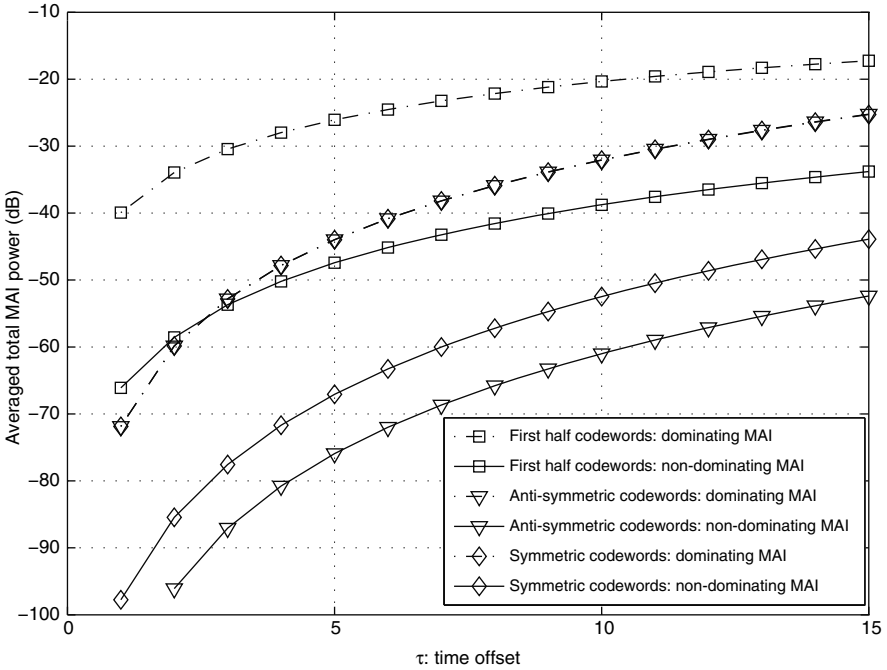

Fig. 5.8. The MAI effect is plotted as a function of the time offset in a half-loaded system for different code schemes with $N = 64$.

where the MAI reduction is 14–37 dB. This can be explained by the fact that, when N increases, the approximation in Eq. (5.56) becomes more accurate. Hence, better MAI suppression can be achieved.

Although the use of anti-symmetric codewords can lead to smaller non-dominating MAI than symmetric codewords, the performance is actually determined by the reduced dominating MAI. Hence, symmetric and anti-symmetric codewords give rise to similar performance. Thus, in the following discussion, we use symmetric codewords only to demonstrate the performance of the proposed code scheme.

From the discussion in Section 5.2.1, we know that the PMU-OFDM system has many characteristics similar to OFDMA. Thus, in the following two examples, we compare the performance of PMU-OFDM and OFDMA under a time asynchronous environment. Let the parameters remain the same as that in Example 5.2. Every user in these two systems transmits N symbols and the size of DFT/IDFT is the same, i.e., NM. Since the two systems transmit N symbols per block and add the CP of the same length ν, their actual data rates are the same. We consider both fully and half-loaded situations. For the fully loaded OFDMA system, each user occupies N subchannels which are maximally separated [114], i.e., user u is assigned subchannels indexed by $(u-1)+kM$, $1 \le u \le M$, and $0 \le k \le N-1$. For the half-loaded

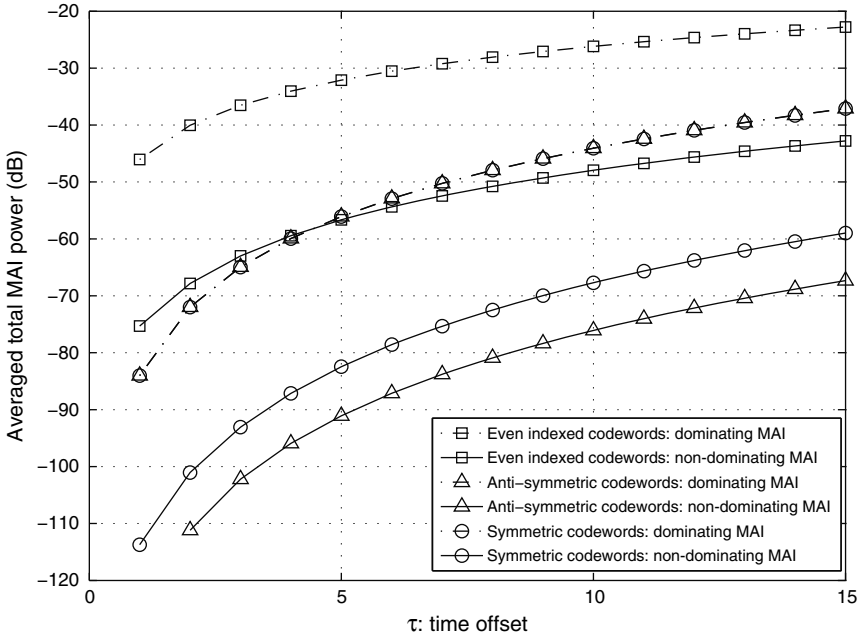

Fig. 5.9. The MAI effect is plotted as a function of the time offset in a half-loaded system for different code schemes with $N = 128$.

OFDMA system, user u is assigned subchannels indexed by $2(u-1)+kM$, with $1 \le u \le M/2$ and $0 \le k \le N-1$. The remaining $NM/2$ subchannels are used as guard bands. ■

Example 5.5: Performance Comparison in a Flat Fading Channel
We first evaluate the MAI power, which is the summation of $MAI_{j\leftarrow i}^{(0)}[k]$, $MAI_{j\leftarrow i}^{(1)}[k]$, and $MAI_{j\leftarrow i}^{(2)}[k]$. As shown in Fig. 5.5, we consider MAI at the detection stage, i.e., after FEQ. The parameters remain the same as that in Example 7.4, i.e., $N = 128$. The averaged MAI after FEQ for PMU-OFDM and OFDMA in fully- (dashed curves) and half-loaded (solid curves) situations are shown in Fig. 5.10. For the fully-loaded situation, PMU-OFDM outperforms OFDMA when the time offset level $\tau \le 5$, but its performance is worse than OFDMA as $\tau > 5$ in a flat channel. For the half-loaded case, we see the use of symmetric codewords can greatly reduce MAI by around 20–43 dB as compared with the fully loaded case. On the other hand, the MAI performance of OFDMA is only slightly improved from the fully loaded system to the half-loaded system. Consequently, PMU-OFDM outperforms OFDMA by around 14–48 dB in the half-loaded situation.

Next, we consider the case where every user, except for the target user, has a time offset of $|\tau_i| = 13$ in the two systems. All T users serve as the target user in turn. We would like to evaluate the bit error probability (BEP)

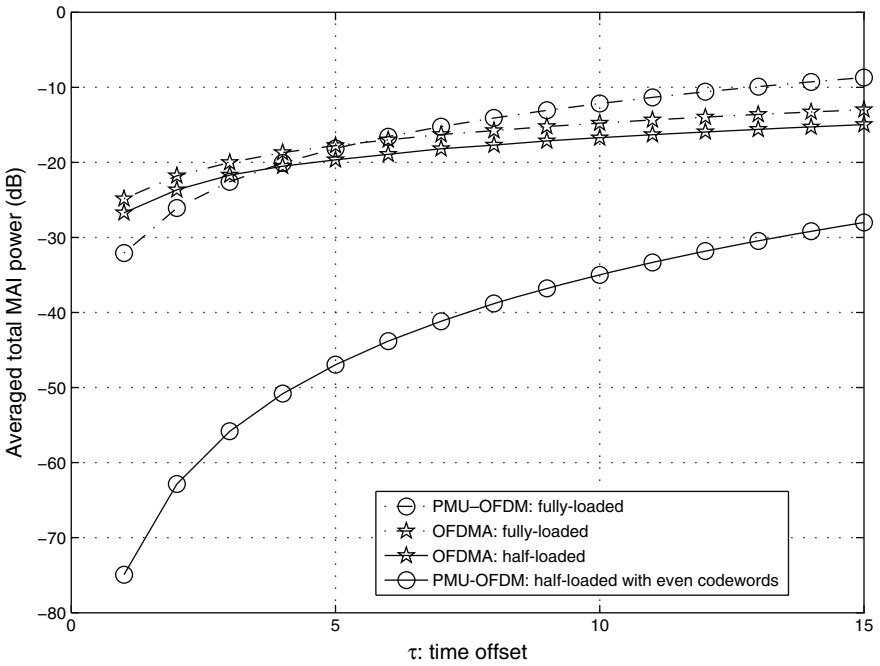

Fig. 5.10. The MAI performance comparison between PMU-OFDM and OFDMA in a flat fading channel.

performance when there is no feedback in Fig. 5.11. For the comparison purpose, we also show the curve of OFDMA without time offset as a benchmark. We see that, in a serious timing mismatch environment such as specified in this example, PMU-OFDM with the proposed code scheme can achieve comparable performance as OFDMA without time offset. However, the performance of OFDMA degrades significantly due to time asynchronism. ■

Example 5.6: Performance Comparison in a Multipath Environment In this example, we examine the time asynchronous effect in a multipath (or frequency-selective) fading channel. The number of multipaths, L, is set to $L = 4$ while the other parameters remain the same as those given in Example 5.5. The channel coefficients are i.i.d. complex Gaussian random variables with an unit variance. The comparison of the MAI power for PMU-OFDM and OFDMA is given in Fig. 5.12. In a fully loaded system, OFDMA has less MAI than PMU-OFDM. However, in a half-loaded system, PMU-OFDM outperforms OFDMA by around 13–25 dB due to the use of the proposed code scheme. The lower MAI value of PMU-OFDM enables the system to estimate time offset more accurately than OFDMA.

Figure 5.13 gives the BEP comparison between the two systems with $|\tau_i| = 13$ in a half-loaded system. We see that PMU-OFDM with the proposed code design does not have a significant performance floor in the presence of

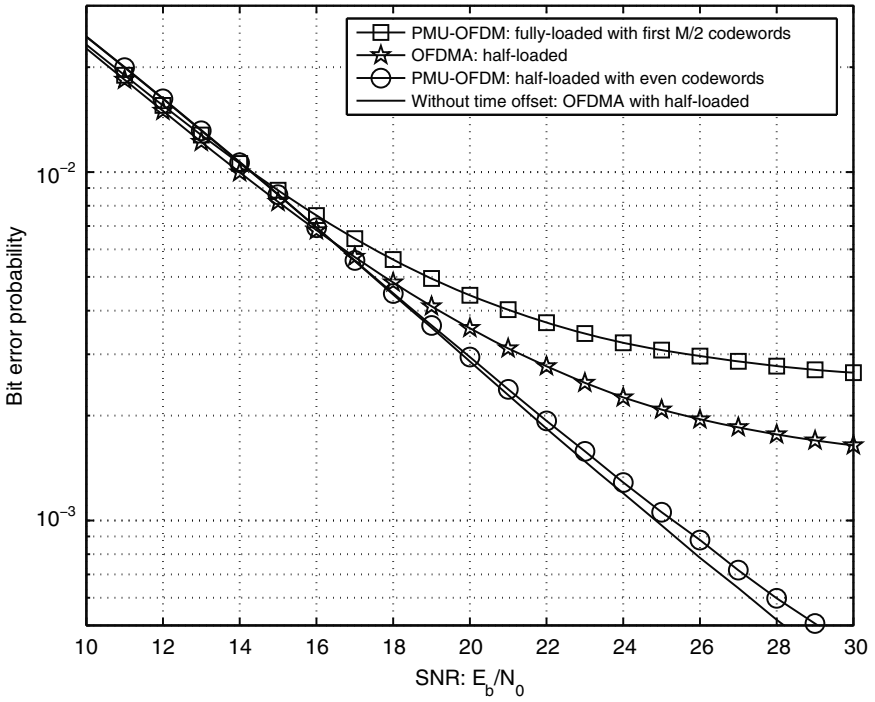

Fig. 5.11. The BEP performance comparison between PMU-OFDM and OFDMA in a flat channel with time offset level $|\tau_j| = 13$.

serious time asynchronous and frequency-selective fading. For comparison, we also plot PMU-OFDM with the first $M/2$ codewords. We see that its performance is close to the half-loaded OFDMA system, which is far worse than the proposed code scheme. This shows that the importance of the proper code design in a time asynchronous environment for the PMU-OFDM system. ■

5.4 PMU-OFDM System in Frequency Offset Environment

In this section, we evaluate the CFO effect of the PMU-OFDM system and derive analytical results for MAI caused by CFO as well as self-CFO impairments. Based on the analytical results, we present a code selection scheme to mitigate MAI by choosing proper orthogonal codes. Again, if we use only the $M/2$ symmetric or the $M/2$ anti-symmetric codewords of the M Hadamard-Walsh codes, MAI can be greatly reduced to a negligible amount. Moreover, based on this code selection, we show that if a proper code priority is used, PMU-OFDM is more robust to CFO. We will explain the code priority concept in this section.

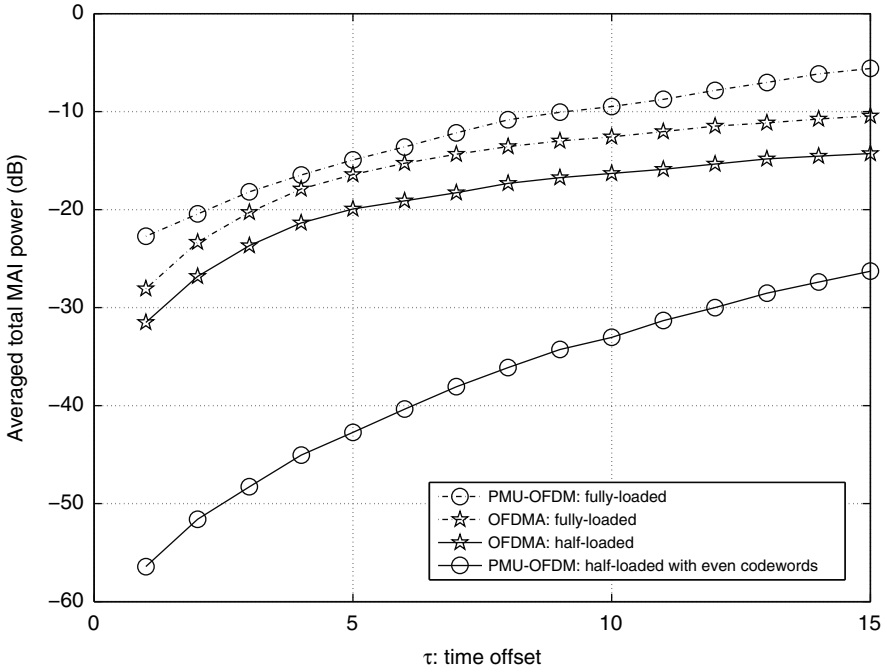

Fig. 5.12. The MAI comparison between PMU-OFDM and OFDMA in a frequency-selective fading channel with $L = 4$.

5.4.1 Analysis of CFO Effects

In the PMU-OFDM system, the overall CFO effect consists of two parts. One is the MAI caused by CFOs of other users. The other is the symbol distortion and the inter carrier interference (ICI) due to the user's own CFO. They will be analyzed separately in this section.

Referring to Fig. 5.1, consider the lth element of the received vector after DFT in a CFO environment, i.e.,

$$\hat{z}[l] = \sum_{i=1}^{T} r_i[l] + e[l], \quad 0 \le l \le NM - 1, \tag{5.69}$$

where $r_i[l]$ is the attenuated symbol of $z_i[l]$. The attenuation is caused by channel fading and the CFO effect. Suppose the ith user has a normalized CFO ϵ_i, which is the actual CFO normalized by $1/NM$ of the overall bandwidth and $-0.5 \le \epsilon_i \le 0.5$, $r_i[l]$ in Eq. (5.69) can be expressed by [87]

$$r_i[l] = r_i^{(0)}[l] + r_i^{(1)}[l], \tag{5.70}$$

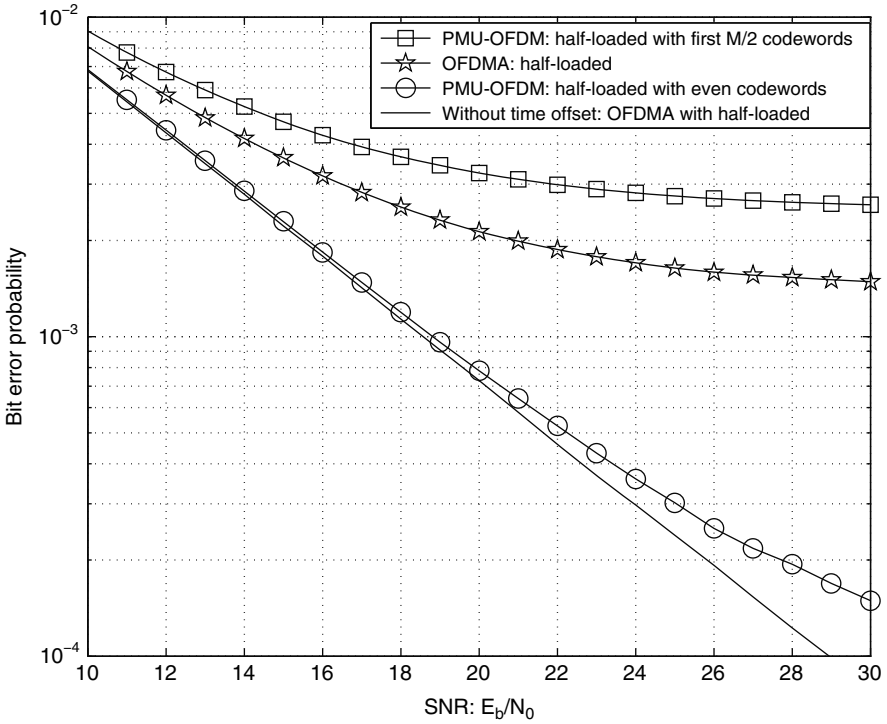

Fig. 5.13. The BEP comparison between PMU-OFDM and OFDMA in a frequency-selective channel with $L = 4$ and time offset level $|\tau_j| = 13$.

where

$$r_i^{(0)}[l] = \alpha_i \lambda_i[l] z_i[l],$$
$$r_i^{(1)}[l] = \beta_i \sum_{m=0, m\neq l}^{NM-1} \lambda_i[m] z_i[m] \frac{e^{-j\pi \frac{m-l}{NM}}}{NM \sin \frac{\pi(m-l+\epsilon_i)}{NM}},$$

α_i and β_i are given by

$$\alpha_i = \frac{\sin \pi\epsilon_i}{NM \sin \frac{\pi\epsilon_i}{NM}} e^{j\pi\epsilon_i \frac{NM-1}{NM}} \text{ and } \beta_i = \sin(\pi\epsilon_i) e^{j\pi\epsilon_i \frac{NM-1}{NM}}. \tag{5.71}$$

$r_i^{(0)}[l]$ is the distorted symbol and $r_i^{(1)}[l]$ is the ICI caused by the CFO. Note that when there is no CFO, $r_i[l]$ equals $\lambda_i[l] z_i[l]$ as defined in Eq. (5.6). From Eqs. (5.128) and (5.69), we see that $\hat{x}_j[k]$ under CFO is given by

$$\hat{x}_j[k] = \underbrace{\frac{1}{M}\sum_{v=0}^{M-1} r_j[v+kM]w_j^*[v+kM]}_{s_j[k]} + \sum_{i=1,i\neq j}^{T} \underbrace{\frac{1}{M}\sum_{v=0}^{M-1} r_i[v+kM]w_j^*[v+kM]}_{MAI_{j\leftarrow i}[k]} + \frac{1}{M}\sum_{v=0}^{M-1} e[v+kM]w_j^*[v+kM], \tag{5.72}$$

where $MAI_{j\leftarrow i}[k]$ is the interference due to user i. In the following, $MAI_{j\leftarrow i}[k]$ and $s_j[k]$ are considered separately.

5.4.2 Analysis of Other User's CFO Effect

Let us consider the MAI of the kth symbol of user j due to user i, i.e., $MAI_{j\leftarrow i}[k]$ in Eq. (5.72). From Eqs. (5.70) and (5.72), we have

$$MAI_{j\leftarrow i}[k] = A_{j\leftarrow i}[k] + B_{j\leftarrow i}[k], \tag{5.73}$$

where

$$A_{j\leftarrow i}[k] = \frac{1}{M}\sum_{v=0}^{M-1} r_i^{(0)}[v+kM]w_j^*[v+kM] \tag{5.74}$$

and

$$B_{j\leftarrow i}[k] = \frac{1}{M}\sum_{v=0}^{M-1} r_i^{(1)}[v+kM]w_j^*[v+kM]. \tag{5.75}$$

Using Eqs. (5.1), (5.3) and the approximation in Eq. (5.9), we have

$$A_{j\leftarrow i}[k] \approx \frac{\alpha_i}{M}\widetilde{\lambda}_i[k]x_i[k]\sum_{v=0}^{M-1} w_i[v+kM]w_j^*[v+kM] = 0. \tag{5.76}$$

Therefore, the interference term $A_{j\leftarrow i}[k]$ is approximately zero. Thus, only the term $B_{j\leftarrow i}[k]$ is of concern. The term $B_{j\leftarrow i}[k]$ can be rearranged as

$$B_{j\leftarrow i}[k] = \frac{\beta_i}{M}\sum_{v=0}^{M-1}\sum_{m=0,m\neq v+kM}^{NM-1} \lambda_i[m]y_i[m]\frac{e^{-j\pi\frac{m-v-kM}{NM}}}{NM\sin\frac{\pi(m-v-kM+\epsilon_i)}{NM}}w_i[m]w_j^*[v]. \tag{5.77}$$

Letting $m = u + fM$, Eq. (5.77) can be manipulated as

$$B_{j\leftarrow i}[k] = \frac{\beta_i}{M} \sum_{v=0}^{M-1} \sum_{f=0}^{N-1} \sum_{u=0, u\neq v+(k-f)M}^{M-1} \lambda_i[u+fM] y_i[u+fM] \cdot \frac{e^{-j\pi \frac{u-v-(k-f)M}{NM}}}{NM \sin \frac{\pi(u-v-(k-f)M+\epsilon_i)}{NM}} w_i[u] w_j^*[v]. \tag{5.78}$$

Using Eq. (5.1) and the approximation in Eq. (5.9), we have

$$B_{j\leftarrow i}[k] \approx \frac{\beta_i}{M} \sum_{f=0}^{N-1} \widetilde{\lambda}_i[f] x_i[f] \sum_{v=0}^{M-1} \sum_{u=0, u\neq v+(k-f)M}^{M-1} \cdot \frac{e^{-j\pi \frac{u-v-(k-f)M}{NM}}}{NM \sin \frac{\pi(u-v-(k-f)M+\epsilon_i)}{NM}} w_i[u] w_j^*[v]. \tag{5.79}$$

Dominating MAI Due to Others' CFOs

We argue that the term of $f = k$ is the dominating MAI in Eq. (5.79) below. Since $u \neq v + (k-f)M$, we have

$$\min_{u,v,k,f} \left| \sin \frac{\pi(u-v+(k-f)M+\epsilon_i)}{NM} \right| = \begin{cases} \sin \frac{\pi(-1+\epsilon_i)}{NM}, & \epsilon_i > 0 \\ \sin \frac{\pi(1+\epsilon_i)}{NM}, & \epsilon_i < 0 \end{cases}.$$

When $f = k$, there are $M-1$ pairs of (u, v) to make the sine function in Eq. (5.79) equal $\sin \pi(1+\epsilon_i)/NM$ and $M-1$ pairs of (u, v) to make the sine function equal $\sin \pi(-1+\epsilon_i)/NM$. On the other hand, when $f = k+1$ or $f = k-1$, both situations have only one pair of (u, v) that makes the sine function equal $\sin \pi(1+\epsilon_i)/NM$ and one pair of (u, v) that makes the sine function equal $\sin \pi(-1+\epsilon_i)/NM$. Hence, the MAI term of $f = k$ contributes the most to Eq. (5.79). If we can find ways to reduce the term of $f = k$, the MAI can be greatly reduced. Intuitively speaking, the MAI in the kth symbol of the target user is most seriously affected by the kth symbols of other users. The farther the distance of other users' symbols from the kth symbol, the less impact they will make. ■

Since the MAI term of $f = k$ in Eq. (5.79) is the dominating MAI, we will rearrange this term to a form that helps us gain insights on how to reduce it. Let us extract the MAI term of $f = k$ in Eq. (5.79) and let it be denoted by $B_{j\leftarrow i}^{(0)}[k]$, we have

$$B_{j\leftarrow i}[k] = B_{j\leftarrow i}^{(0)}[k] + B_{j\leftarrow i}^{(1)}[k], \tag{5.80}$$

where

$$B_{j\leftarrow i}^{(0)}[k] \approx \frac{\beta_i}{M} \widetilde{\lambda}_i[k] x_i[k] \sum_{v=0}^{M-1} \sum_{u=0, u\neq v}^{M-1} \frac{e^{-j\pi \frac{u-v}{NM}}}{NM \sin \frac{\pi(u-v+\epsilon_i)}{NM}} w_i[u] w_j^*[v] \tag{5.81}$$

and

$$B_{j\leftarrow i}^{(1)}[k] = B_{j\leftarrow i}[k] - B_{j\leftarrow i}^{(0)}[k]. \tag{5.82}$$

Referring to Eq. (5.81), let $g(p) = e^{-j\pi\frac{p}{NM}}/NM\sin\frac{\pi(p+\epsilon_i)}{NM}$, $-(M-1) \le p \le M-1$, $p \neq 0$. When N is sufficiently large, the denominator of $g(p)$ is approximately an odd function of p and the numerator is nearly constant for all possible p with $-M+1 \le p \le M-1$, $p \neq 0$. Hence, we can approximate $g(p)$ as an odd function of p, i.e., $g(p) \approx -g(-p)$. Using the equality

$$\begin{aligned}
&\sum_{v=0}^{M-1}\sum_{u=0,u\neq v}^{M-1} g(u-v)w_i[u]w_j^*[v] \\
&= \sum_{p=1}^{M-1}\left\{g(p)\sum_{q=0}^{M-1-p} w_i[p+q]w_j^*[q] + g(-p)\sum_{q=0}^{M-1-p} w_i[q]w_j^*[p+q]\right\},
\end{aligned}$$

and the approximation $g(p) \approx -g(-p)$, we can rewrite Eq. (5.81) as

$$B_{j\leftarrow i}^{(0)}[k] \approx \frac{\beta_i}{M}\widetilde{\lambda}_i[k]x_i[k]\sum_{p=1}^{M-1} g(p)\underbrace{\sum_{q=0}^{M-1-p}\left\{w_i[p+q]w_j^*[q] - w_i[q]w_j^*[p+q]\right\}}_{\mathcal{O}}. \tag{5.83}$$

As given in Eq. (5.83), the quantity $\mathcal{O}$ is determined by the property of orthogonal codewords. If $\mathcal{O} = 0$, the dominating MAI term of $f = k$ in Eq. (5.79) is approximately zero. One way to achieve this is the use of only $M/2$ of the M Hadamard-Walsh codes, which are either symmetric or anti-symmetric.

Proposition 5.3: Suppose only the $M/2$ symmetric or the $M/2$ anti-symmetric codewords of the M Hadamard-Walsh codes are used, $\mathcal{O} = 0$ and thus $B_{j\leftarrow i}^{(0)}[k] \approx 0$.

Proof. When symmetric codewords are used, from Eq. (5.22) and since Hadamard-Walsh code is real, we have

$$\sum_{q=0}^{M-1-p} w_i[p+q]w_j^*[q] = \sum_{q=0}^{M-1-p} w_i[M-1-(p+q)]w_j[M-1-q]. \tag{5.84}$$

Let $q' = M-1-p-q$. We can rewrite Eq. (5.84) as

$$\begin{aligned}
\sum_{q=0}^{M-1-p} w_i[p+q]w_j^*[q] &= \sum_{q'=M-1-p}^{0} w_i[q']w_j[p+q'] \\
&= \sum_{q=0}^{M-1-p} w_i[q]w_j^*[p+q].
\end{aligned} \tag{5.85}$$

Thus, $\mathcal{O}$ in Eq. (5.83) is zero. As for the set of anti-symmetric codewords, from Eq. (5.23), we have the same equality as given in Eq. (5.84) again. This leads

to Eq. (5.85). Therefore, the use of anti-symmetric codewords also results in $\mathcal{O} = 0$. ■

Let us give a simple example for codeword selection. Suppose $M = 8$ and $\mathbf{D}_8$ is an 8×8 Hadamard matrix with column vectors $\mathbf{d}_1, \mathbf{d}_2, \ldots, \mathbf{d}_8$. We can either choose column vectors $\{\mathbf{d}_1, \mathbf{d}_4, \mathbf{d}_6, \mathbf{d}_7\}$, which are symmetric, or column vectors $\{\mathbf{d}_2, \mathbf{d}_3, \mathbf{d}_5, \mathbf{d}_8\}$, which are anti-symmetric, as the four codewords for four users.

If the proposed code selection is used, the dominating MAI $B_{j\leftarrow i}^{(0)}[k]$ can be reduced to a negligible amount. Therefore, the MAI terms of $f \neq k$ in Eq. (5.82) becomes the main MAI impairment. For convenience, with code selection, let us call it residual MAI. Next, we will investigate the residual MAI. From Eqs. (5.79) and (5.81), we have

$$B_{j\leftarrow i}^{(1)}[k] \approx \frac{\beta_i}{M} \sum_{f=0, f\neq k}^{N-1} \widetilde{\lambda}_i[f] x_i[f] \sum_{v=0,u=0}^{M-1} \frac{e^{-j\pi \frac{u-v-(k-f)M}{NM}}}{NM \sin \frac{\pi(u-v-(k-f)M+\epsilon_i)}{NM}} w_i[u] w_j^*[v]. \tag{5.86}$$

Let $l = f - k$. For fixed k, $-k \leq l \leq N-1-k$ and $l \neq 0$, $B_{j\leftarrow i}^{(1)}[k]$ in Eq. (5.86) can be approximated by

$$\frac{\beta_i}{M} \sum_{l=-k, l\neq 0}^{N-1-k} \widetilde{\lambda}_i[k+l] x_i[k+l] \underbrace{\sum_{v=0,u=0}^{M-1} \frac{e^{-j\pi \frac{u-v+lM}{NM}}}{NM \sin \frac{\pi(u-v+lM+\epsilon_i)}{NM}} w_i[u] w_j^*[v]}_{\zeta}. \tag{5.87}$$

Let $f(p,l) = \frac{e^{-j\pi \frac{p}{NM}}}{NM \sin \frac{\pi(p+lM+\epsilon_i)}{NM}}$, we have

$$\begin{aligned} \zeta &= e^{-j\pi \frac{l}{N}} \sum_{v=0}^{M-1} \sum_{u=0}^{M-1} f(u-v,l) w_i[u] w_j^*[v] \\ &= e^{-j\pi \frac{l}{N}} \sum_{p=1}^{M-1} \left[f(p,l) \sum_{q=0}^{M-1-p} w_i[p+q] w_j^*[q] \right. \\ &\quad \left. + f(-p,l) \sum_{q=0}^{M-1-p} w_i[q] w_j^*[p+q] \right]. \end{aligned} \tag{5.88}$$

Using Eqs. (5.85) and (5.88), we can rewrite Eq. (5.87) as

$$\begin{aligned} B_{j\leftarrow i}^{(1)}[k] \approx \frac{\beta_i}{M} &\sum_{l=-k, l\neq 0}^{N-1-k} e^{-j\pi \frac{l}{N}} \widetilde{\lambda}_i[k+l] x_i[k+l] \\ &\cdot \sum_{p=1}^{M-1} [f(p,l) + f(-p,l)] \sum_{q=0}^{M-1-p} w_i[q] w_j^*[p+q]. \end{aligned} \tag{5.89}$$

Assume that $\widetilde{\lambda}_i[k]$ and $x_i[k]$ are uncorrelated for all k, and $x_i[k]$ and $x_i[k']$ are uncorrelated for $k \neq k'$. It can be shown that $E\left\{\left|B^{(1)}_{j\leftarrow i}[k]\right|^2\right\}$ can be approximated by [135]

$$\frac{|\beta_i|^2}{M^2}\sigma^2_{\lambda_i}\sigma^2_{x_i}\sum_{l=1}^{N-1}\left|\sum_{p=1}^{M-1}[f(p,l)+f(-p,l)]\sum_{q=0}^{M-1-p}w_i[q]w_j^*[p+q]\right|^2, \qquad (5.90)$$

where $\sigma^2_{\lambda_i}$ is the averaged channel gain, and $\sigma^2_{x_i}$ is the averaged symbol power of user i defined by

$$\sigma^2_{\lambda_i} = E\left\{\left|\widetilde{\lambda}_i[k]\right|^2\right\} \text{ and } \sigma^2_{x_i} = E\left\{|x_i[k]|^2\right\}, \quad 0 \leq k \leq N-1. \qquad (5.91)$$

Example 5.7: Assume $\sigma^2_{\lambda_i} = \sigma^2_{x_i} = 1$. Let us first consider the CFO case of $\epsilon_i = 0.3$. This CFO level may be regarded as a serious one. Let $M = 16$ and $N = 4$. Figure 5.14 shows the total residual MAI, i.e., $\sum_{i=1,i\neq j}^{T} E\left\{\left|B^{(1)}_{j\leftarrow i}[k]\right|^2\right\}$, as a function of the user index, where the summation term accounts for $T = M/2$ users in this system. As shown in Fig. 5.14, the worst total residual MAI is about -18.5 dB, which is much

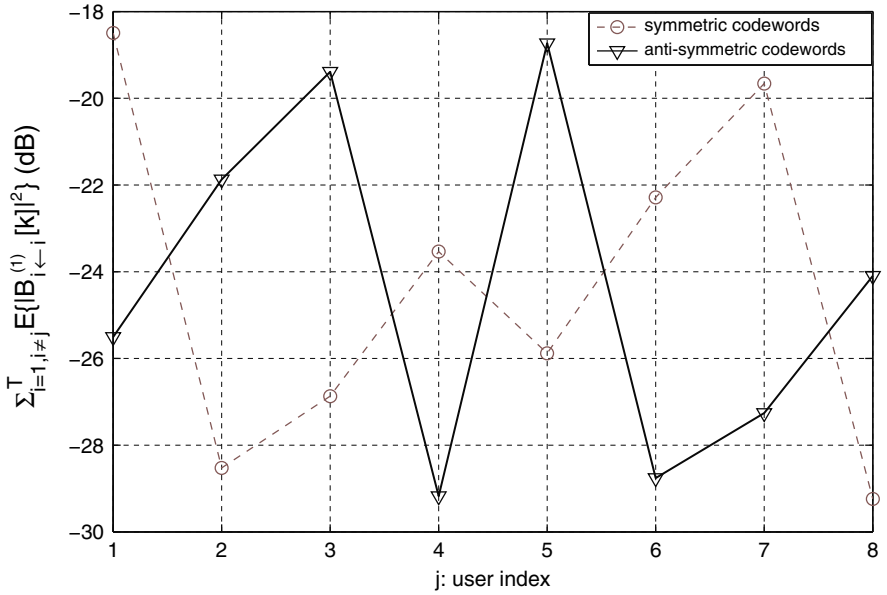

Fig. 5.14. Example 5.7: $\sum_{i=1,i\neq j}^{T} E\left\{\left|B^{(1)}_{j\leftarrow i}[k]\right|^2\right\}$ as a function of user index j with $M = 16$ for symmetric and anti-symmetric codewords [[135] ©IEEE].

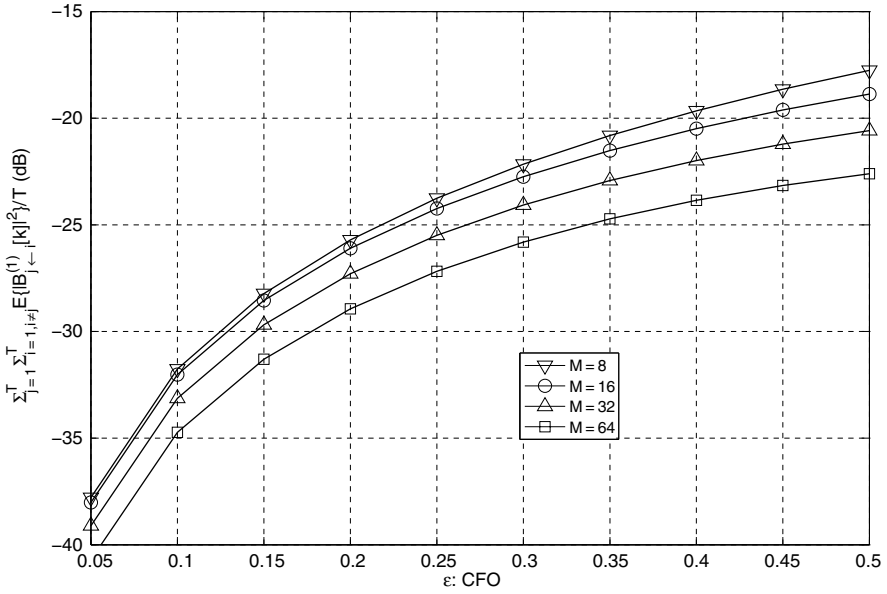

Fig. 5.15. Example 5.7: $\frac{1}{T}\sum_{j=1}^{T}\sum_{i=1,i\neq j}^{T} E\left\{\left|B_{j\leftarrow i}^{(1)}[k]\right|^2\right\}$ as a function of CFO for different M [[135] ©IEEE].

smaller than the transmit power of 0 dB. Since the residual MAI $B_{j\leftarrow i}^{(1)}[k]$ is relatively small, it will make channel estimation and CFO estimation much more accurate. Let us consider the averaged value of total residual MAI for all users, i.e., $\frac{1}{T}\sum_{j=1}^{T}\sum_{i=1,i\neq j}^{T} E\left\{\left|B_{j\leftarrow i}^{(1)}[k]\right|^2\right\}$. Figure 5.15 shows the averaged value of total residual MAI as a function of CFO for different M with symmetric codewords. The performance with anti-symmetric codewords is also similar to this figure. From Fig. 5.15, we see that, as M increases, the averaged total residual MAI decreases. This result means that the increase of M will help reduce $B_{j\leftarrow i}^{(1)}[k]$. Note that since there are $T = M/2$ users in this system, the increase of M will also increase the number of users. It implies that the increase of users can help reduce the residual MAI for a fixed CFO.

Although the codeword selection given in the Proposition 5.3 decreases the number of users from M to $M/2$, it reduces the dominating MAI greatly and the system is approximately MAI-free in the presence of CFOs. Thus, every user only has to tackle his/her own CFO problem without worrying about the CFOs of other users. This is very different from conventional multiaccess OFDM systems, where sophisticated signal processing is used to solve the multiuser CFO problem [6, 31, 88, 142]. ■

Example 5.8: Suppression of Dominating MAI Due to CFO

Here, we would like to show by simulation result that $B_{j\leftarrow i}^{(0)}[k]$ defined in Eq. (5.81) is the dominating MAI term in Eq. (5.79), and it can be greatly reduced using only $M/2$ symmetric or anti-symmetric codewords of the M Hadamard-Walsh codewords.

We consider the performance in the uplink direction so that every user has different CFO and channel fading. We assume the channel and the CFO are quasi-invariant in the sense that it remains unchanged within one block duration. Simulations are conducted with the following parameter setting throughout this section. $M = 16$ and the BPSK modulation is used. The channel coefficients are i.i.d. (independently identically distributed) complex Gaussian random variables with an unit variance. For every individual user, the Monte Carlo method is used to run more than 500,000 symbols. We consider the worst CFO situation. That is, the CFO value of each user is randomly assigned to be either $+\varepsilon$ or $-\varepsilon$.

Let channel be flat and $N = 4$. Then, $A_{j\leftarrow i}[k] = 0$ and $MAI_{j\leftarrow i}[k] = B_{j\leftarrow i}[k]$ according to Eqs. (5.73) and (5.76), where exact equalities are due to flat channel. Using similar notation rule in Eq. (5.80), we define the MAI from the kth symbol of user i to user j as $MAI_{j\leftarrow i}^{(0)}[k]$, and the MAI from all the other symbols of user i as $MAI_{j\leftarrow i}^{(1)}[k]$, i.e., $MAI_{j\leftarrow i}^{(1)}[k] = MAI_{j\leftarrow i}[k] - MAI_{j\leftarrow i}^{(0)}[k]$. Let the number of users, $T = M = 16$, i.e., a fully-loaded system. The total MAI for user j from the kth symbol of all other users, denoted by $\overline{MAI}_j^{(0)}$, is calculated as follows. For the kth symbol of a target user, we accumulate the MAI contributed from the kth symbol of other 15 users. The procedure is repeated and then the MAI power is averaged for k from 0 to $N-1$. That is, $\overline{MAI}_j^{(0)}$ is obtained by averaging the value, $\frac{1}{N}\sum_{k=0}^{N-1}\left|\sum_{i=1,i\neq j}^{T} MAI_{j\leftarrow i}^{(0)}[k]\right|^2$, for more than 500,000 symbols. Similarly, the total MAI from all the other symbols ($f \neq k$) of all the other users, denoted by $\overline{MAI}_j^{(1)}$, is obtained by averaging the value, $\frac{1}{N}\sum_{k=0}^{N-1}\left|\sum_{i=1,i\neq j}^{T} MAI_{j\leftarrow i}^{(1)}[k]\right|^2$, for more than 500,000 symbols.

The total MAI is plotted as a function of the normalized CFO value in Fig. 5.16, where $\overline{MAI}_j^{(0)}$ and $\overline{MAI}_j^{(1)}$ of 16 users are shown by 16 solid and 16 dashed curves, respectively. The solid bold curve in Fig. 5.16, denoted by $\overline{MAI}^{(0)}$, is the averaged value of the 16 solid curves. That is, $\overline{MAI}^{(0)}$ is obtained via $\frac{1}{T}\sum_{j=1}^{T}\overline{MAI}_j^{(0)}$. Similarly, the dashed bold curve, denoted by $\overline{MAI}^{(1)}$, is obtained by averaging the 16 dashed curves. That is, $\overline{MAI}^{(1)}$ is obtained via $\frac{1}{T}\sum_{j=1}^{T}\overline{MAI}_j^{(1)}$. From this figure, we see that $\overline{MAI}^{(0)}$ is around 10–11 dB more than that of $\overline{MAI}^{(1)}$. Hence, for each user, the MAI at the kth symbol is mostly contributed from the kth symbols of other users. Thus, it confirms the derived theoretical result that $B_{j\leftarrow i}^{(0)}[k]$ in Eq. (5.81) is the

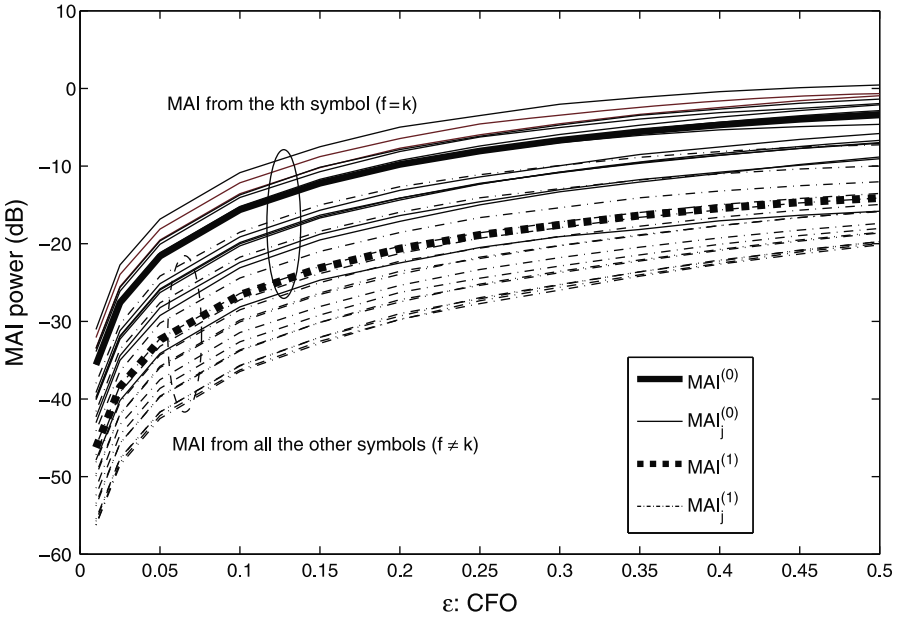

Fig. 5.16. Example 5.8: The MAI effect as a function of the CFO when the full M Hadamard-Walsh codewords are used [[135] ©IEEE].

dominating MAI in Eq. (5.79). In the following, we call $B_{j\leftarrow i}^{(0)}[k]$ "dominating MAI" and $B_{j\leftarrow i}^{(1)}[k]$ "residual MAI" for short.

Next, we demonstrate that the dominating MAI can be greatly reduced using only $M/2$ symmetric codewords of the M Hadamard-Walsh codes. Let the user number decreases from $T = M = 16$ to $T = M/2 = 8$ and only the $M/2 = 8$ symmetric codewords are used. The performance is shown in Fig. 5.17(a). Compared with Fig. 5.16, the residual MAI decreases around 4–5 dB due to the number of users decreasing from 16 to 8. In contrast, the dominating MAI is greatly reduced by 12–47 dB. Note that, the simulation result of the residual MAI is consistent with the theoretical result in Fig. 5.15. Moreover, we see that using symmetric codewords, the dominating MAI is even smaller than that of the residual MAI when the CFO is less than 0.35.

Figure 5.17(b) shows the performance using $M/2$ anti-symmetric codewords. Compared with Fig. 5.17(a), we see that the performance of the set of anti-symmetric codewords is similar to that of the set of symmetric codewords. The result confirms that the dominating MAI can be greatly reduced using the proposed code selection scheme.

5.4.3 Analysis of Self-CFO Effect

In this subsection, we examine the impairment caused by self-CFO. For user j, the self-CFO impairment means the symbol distortion and the interference

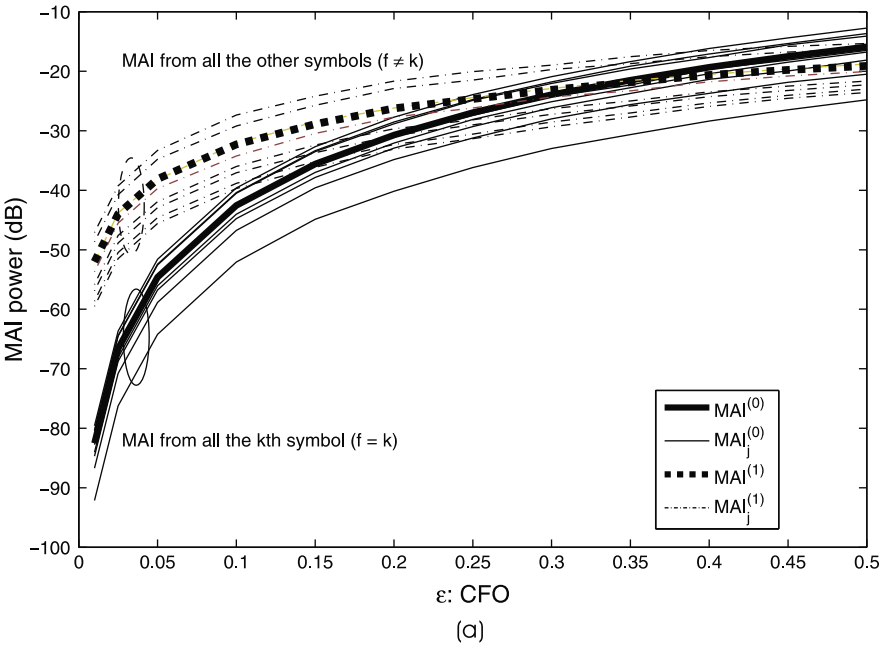

Fig. 5.17. Example 5.8: The MAI effect as a function of the CFO (**a**) when only $M/2$ symmetric Hadamard-Walsh codewords are used and (**b**) when only $M/2$ anti-symmetric Hadamard-Walsh codewords are used [[135] ©IEEE].

caused by his/her own CFO ϵ_j. From Eqs. (5.70) and (5.72), we have

$$s_j[k] = C_j[k] + D_j[k], \tag{5.92}$$

where $C_j[k]$ is the distorted symbol of $x_j[k]$ due to self-CFO given by

$$\begin{aligned} C_j[k] &= \frac{1}{M}\sum_{v=0}^{M-1} r_j^{(0)}[v+kM]w_j^*[v+kM] \\ &= \frac{\alpha_j}{M}\sum_{v=0}^{M-1} \lambda_j[v+kM]y_j[v+kM]w_j[v+kM]w_j^*[v+kM] \\ &\approx \frac{\alpha_j}{M}\widetilde{\lambda}_j[k]x_j[k]\sum_{v=0}^{M-1} w_j[v+kM]w_j^*[v+kM] \\ &= \alpha_j\widetilde{\lambda}_j[k]x_j[k], \end{aligned} \tag{5.93}$$

and $D_j[k]$ is the interference caused by $x_j[f]$, $0 \le f \le N-1$,

$$D_j[k] = \frac{1}{M}\sum_{v=0}^{M-1} r_j^{(1)}[v+kM]w_j^*[v+kM]. \tag{5.94}$$

Using the same procedure of deriving Eqs. (5.75), (5.77), (5.78), and (5.79), we have

$$\begin{aligned} D_j[k] \approx \frac{\beta_j}{M}\sum_{f=0}^{N-1}\widetilde{\lambda}_j[f]x_j[f]\sum_{v=0}^{M-1}\sum_{u=0,u\neq v+(k-f)M}^{M-1} \\ \cdot\frac{e^{-j\pi\frac{u-v-(k-f)M}{NM}}}{NM\sin\frac{\pi(u-v-(k-f)M+\epsilon_j)}{NM}} w_j[u]w_j^*[v]. \end{aligned} \tag{5.95}$$

Using the same procedure of deriving Eqs. (5.81) and (5.83), the term of $f = k$ in Eq. (5.95), which is the interference caused by the kth symbol itself, can be written as

$$\begin{aligned} D_j^{(0)}[k] &\approx \frac{\beta_j}{M}\widetilde{\lambda}_j[k]x_j[k]\sum_{p=1}^{M-1} g(p)\underbrace{\sum_{q=0}^{M-1-p}\left\{w_j[p+q]w_j^*[q] - w_j[q]w_j^*[p+q]\right\}}_{\mathcal{O}'} \\ &= 0, \end{aligned} \tag{5.96}$$

where $\mathcal{O}' = 0$ because $w_j[m] = w_j[m+kM]$, $0 \le m \le M-1$ and $0 \le k \le N-1$. So we have $D_j^{(0)}[k] \approx 0$.

Next, consider the terms of $f \neq k$ in Eq. (5.95), which is the ICI caused by all other symbols except for the kth symbols. Using the same procedure of deriving from Eqs. (5.86), (5.87), (5.88) and (5.89), we have

$$D_j^{(1)}[k] \approx \frac{\beta_j}{M} \sum_{l=0-k, l\neq 0}^{N-1-k} e^{-j\pi\frac{l}{N}} \widetilde{\lambda}_j[k+l] x_j[k+l] \cdot \sum_{p=1}^{M-1} [f(p,l) + f(-p,l)] \sum_{q=0}^{M-1-p} w_j[q] w_j^*[p+q]. \quad (5.97)$$

Eq. (5.97) can be shown to be [136]

$$E\left\{\left|D_j^{(1)}[k]\right|^2\right\} \approx \frac{|\beta_j|^2}{M^2} \sigma_{\lambda_j}^2 \sigma_{x_j}^2 \sum_{l=1}^{N-1} \cdot \left| \sum_{p=1}^{M-1} [f(p,l) + f(-p,l)] \sum_{q=0}^{M-1-p} w_j[q] w_j^*[p+q] \right|^2. \quad (5.98)$$

Example 5.9: The environment setting is the same as that stated in Example 5.7. First, let us consider $E\left\{\left|D_j^{(1)}[k]\right|^2\right\}$ for each individual user, which is plotted as a function of user index in Fig. 5.18. We see that the worst performance is around $-6\,\text{dB}$ for the user with codeword $\mathbf{d}_1$, i.e., the all-one code. Other codewords have performance smaller than $-17\,\text{dB}$. Since the ICI using all other symmetric codewords are below $-27\,\text{dB}$ (except $\mathbf{d}_1$), this result suggests the use of symmetric codewords but excluding the all-one code to have a smaller ICI. According to Eq. (5.93), the distorted symbol due to self-CFO has the mean square expectation value given by $E\left\{|C_j[k]|^2\right\} = -1.3\,\text{dB}$ when $|\epsilon_j| = 0.3$ and $\sigma_{\lambda_i}^2 = \sigma_{x_i}^2 = 1$. Except $\mathbf{d}_1$, the amount $E\left\{\left|D_j^{(1)}[k]\right|^2\right\}$ of other users is much smaller than $-1.3\,\text{dB}$. Moreover, when compared with the residual MAI which is below $-18\,\text{dB}$ in Example 5.7, the $-1.3\,\text{dB}$ of the distorted symbol is still relatively large as compared with the residual MAI. Since the residual MAI and ICI are both smaller than the distorted symbol due to the self-CFO, we can estimate α_j accurately and compensate it in the receiver end without demanding a feedback mechanism. We will discuss this in more detail in the next section. The averaged ICI for all users as a function of CFO for different M, i.e., $\frac{1}{T}\sum_{j=1}^{T} E\left\{\left|D_j^{(1)}[k]\right|^2\right\}$, is shown in Fig. 5.19. Since $\mathbf{d}_1$ is excluded, there are $M/2-1$ users in the system with symmetric codewords. We see that symmetric codewords with $\mathbf{d}_1$ excluded have a smaller averaged ICI than anti-symmetric codewords. From the figure, we see results similar to Fig. 5.15. That is, the increase of M helps reduce ICI for a fixed CFO.

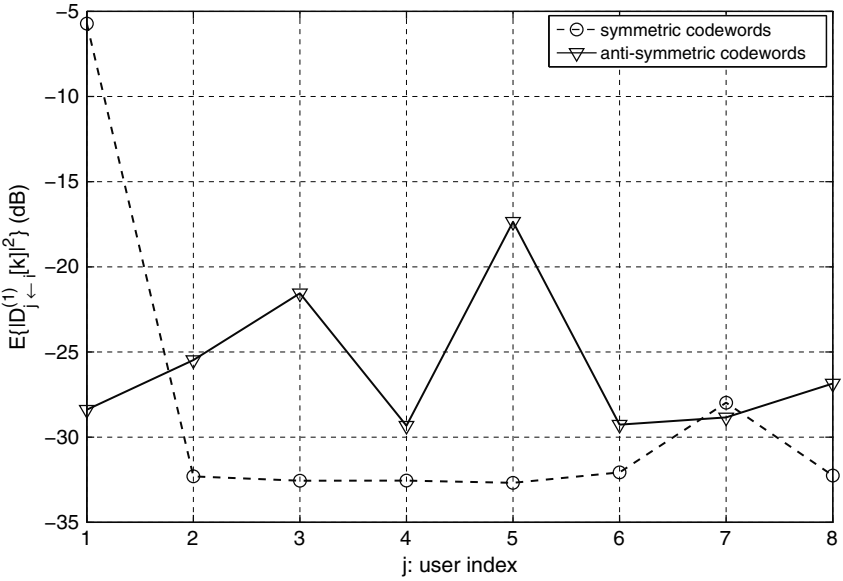

Fig. 5.18. Example 5.9: $E\left\{\left|D_{j\leftarrow i}^{(1)}[k]\right|^2\right\}$ as a function of user index j with $M = 16$ for symmetric and anti-symmetric codewords [[135] ©IEEE].

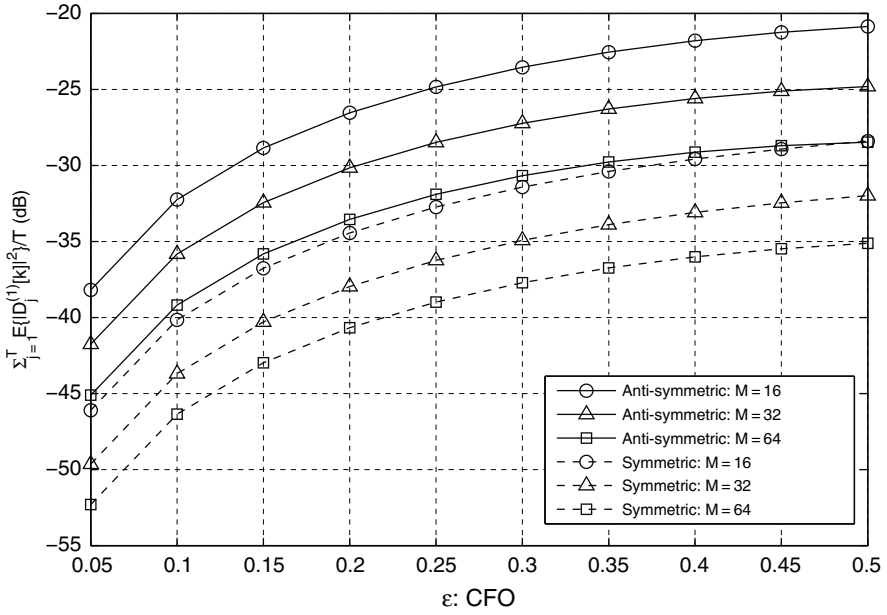

Fig. 5.19. Example 5.9: $\frac{1}{T}\sum_{i=1,i\neq j}^{T} E\left\{\left|D_{j\leftarrow i}^{(1)}[k]\right|^2\right\}$ as a function of CFO for different M, where the all-one code is excluded for the set of symmetric codewords [[135] ©IEEE].

5.4.4 Overall CFO Estimation and Compensation

Here, let us consider the overall CFO effect. For convenience, let us rewrite Eq. (5.72) as

$$\hat{x}_j[k] \approx \alpha_j \widetilde{\lambda}_j[k] x_j[k] + D_j[k] + \sum_{i=1, i\neq j}^{T} MAI_{j\leftarrow i}[k] + \frac{1}{M}\sum_{m=0}^{M-1} e[m+kM] w_j^*[m], \tag{5.99}$$

where the first term is the desired signal, the second term is the self-CFO interference, the third term is the MAI from other users, and the fourth term is the additive noise. Following the discussion in Sections 5.4.2 and 5.4.3, impairments due to MAI and self-CFO interference (second term of Eq. (5.99)) are negligible if only $M/2$ symmetric or anti-symmetric codewords of the M Hadamard-Walsh codes are used. The desired first term of Eq. (5.99) is much larger than all other terms. Thus, we can estimate the self-CFO value ϵ_j of each user accurately with the algorithm for single user OFDM systems developed in [87] and [118, 141]. Once ϵ_j is estimated, we can multiply the lth received symbols of user j by $e^{j2\pi\frac{-l\epsilon_j}{NM}}$ to remove the self-CFO effect, before passing them through the DFT matrix. The penalty is that a separate DFT is needed for each user.

In this case, sophisticated MUD techniques and the feedback mechanism are not needed at the receiver end. On the other hand, if the MAI is not reduced, the CFO estimation for each user could be difficult and MUD techniques are needed, which imposes a heavy computational burden on the receiver. For example, CFOs of other users will cause the MAI to any target user in OFDMA systems and signal processing techniques are often used to estimate the CFO of this target user [6, 88, 142]. Furthermore, since OFDMA does not have a negligible MAI-free property in the CFO environment, the feedback mechanism is demanded after CFO estimation so that every user can compensate his/her own CFO at the transmitter end [142].

In the following two examples, we would like to compare the CFO effect on the proposed system, the OFDMA system, and two MC-CDMA systems over a flat channel. Let the simulation parameters remain the same as that in Example 5.8. Among the two MC-CDMA schemes, one is with subcarriers uniformly allocated (called MC-CDMA/U for short) [48, 49] while the other is with subcarriers successively allocated (called MC-CDMA/S for short) [1]. Every user in these four systems will transmit N symbols and the DFT/IDFT size is the same, i.e., NM. Since all four systems transmit N symbols per block and add the CP of the same length L, their actual data rates are the same. We consider both fully-loaded and half-loaded situations. In a fully-loaded situation, the Hadamard-Walsh code is used in the proposed PMU-OFDM and the two MC-CDMA systems. For OFDMA, two MC-CDMA systems. For OFDMA, each user occupies N subchannels which are maximally separated [114], i.e., user u will be assigned subchannels indexed by $(u-1)+kM$,

$1 \le u \le M$ and $0 \le k \le N-1$. In a half-loaded case, $M/2$ symmetric codewords of the Hadamard-Walsh code (code selection scheme) are used in the proposed system and the two MC-CDMA systems. For OFDMA, the uth user will be assigned subchannels indexed by $2(u-1)+kM$, $1 \le u \le M/2$, and $0 \le k \le N-1$. The remaining $NM/2$ subchannels are used as guard bands.

Example 5.10: Comparison of CFO Effect on the Proposed System, OFDMA and MC-CDMA

Let us first evaluate the MAI in the detection stage, i.e., MAI after frequency equalization. In the absence of MAI and channel noise, the received symbols for detection are still BPSK symbols with either $+1$ or -1. For the proposed system and the OFDMA system, frequency equalization is used. For the two MC-CDMA systems, the orthogonality restoring combing (ORC) scheme is used to achieve equalization [49]. To distinguish from the MAI before equalization, we denote the MAI after equalization by $MAI'_{j\leftarrow i}[k]$. For instance, in the proposed system, $MAI'_{j\leftarrow i}[k] = MAI_{j\leftarrow i}[k]/\widetilde{\lambda}_j[k]$. The averaged total MAI after equalization is obtained via averaging the value, $\frac{1}{T}\sum_{j=1}^{T}\frac{1}{N}\sum_{k=0}^{N-1}\left|\sum_{i=1,i\neq j}^{T} MAI'_{j\leftarrow i}[k]\right|^2$, for $500{,}000\,T$ symbols. Figure 5.20

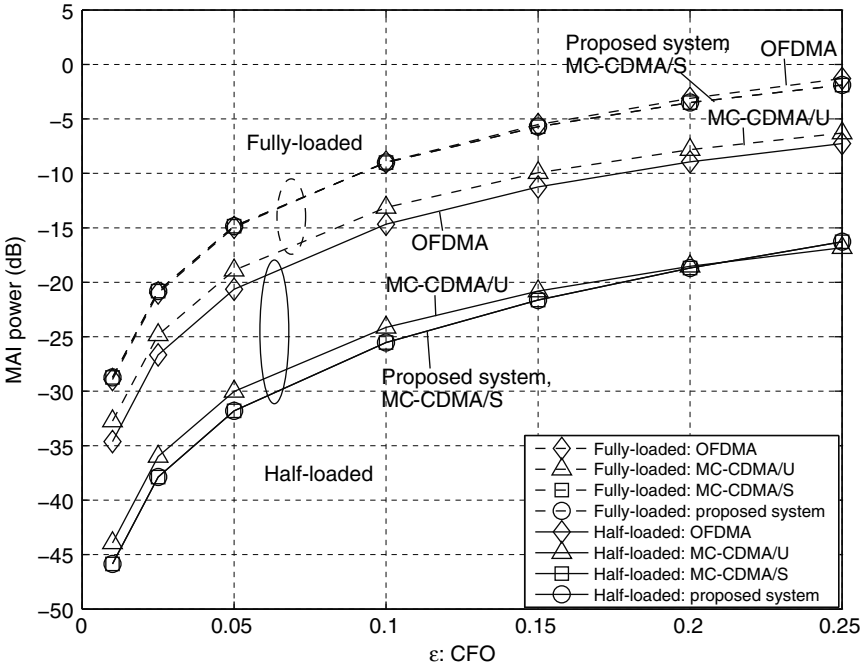

Fig. 5.20. Example 5.10: The MAI comparison among the proposed system, the OFDMA system, and two MC-CDMA systems in a flat fading environment [[135] ©IEEE].

shows the averaged total MAI after equalization as a function of CFO for the four systems in fully-loaded and half-loaded situations. Note that the performance of the proposed system and the MC-CDMA/S are the same for the flat channel so the two curves overlapped. In the fully-loaded case, the MC-CDMA/U outperforms all other three systems. When the number of users decreases from 16 to 8, the MAI of the proposed system is greatly reduced by 15–16 dB and, consequently, the proposed system outperforms OFDMA by 10–11 dB. Recall that in Example 5.8, the dominating MAI of the proposed system is larger than the residual MAI by around 10–11 dB in fully-loaded situation. Using code selection, the dominating MAI is reduced to an amount that is even smaller than the residual MAI. This explain why the proposed system has similar performance with OFDMA in a fully-loaded situation while it outperforms OFDMA by 10–11 dB in a half-loaded situation with code selection.

The self-CFO impairment of the proposed system with symmetric codewords is shown in Fig. 5.21. To compute the self-CFO impairment after frequency equalization, we accumulate the symbol distortion and the interference for the kth symbol of a target user due to his/her own CFO. This procedure is repeated and, then, the impairment power is averaged for k, $0 \leq k \leq N-1$. The self-CFO impairment of the 8 users in the proposed system are indicated by the 8 solid curves in Fig. 5.21. Since the self-CFO impairment of an indi-

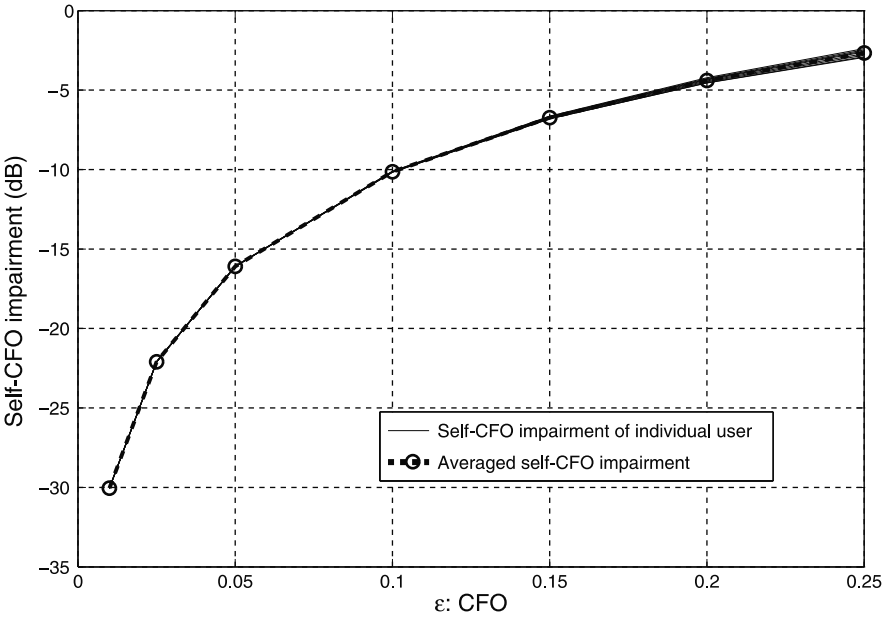

Fig. 5.21. Example 5.10: The self-CFO impairment of the proposed system [[135] ©IEEE].

vidual user is similar, these curves are overlapping. The bold-circled curve in Fig. 5.21 is the averaged value of the 8 solid curves. By comparing this figure with Fig. 5.20, we see that the self-CFO impairment is the main impairment in the proposed system. Since the MAI is relatively small, we can estimate α_j or ϵ_j accurately and then compensate the self-CFO effect as discussed in Section 5.4.4. It is worthwhile to point out that, although not shown here, the self-CFO impairment of OFDMA is very similar to that given in this figure.

Now, assume that each user has a normalized CFO of $|\epsilon_j| = 0.1$ and can accurately estimate the self-CFO in these four systems. We would like to find out the bit error probability when there is no feedback. The BEPs for the four systems are shown in Fig. 5.22. For a fully-loaded situation, the BEP curves of the proposed system and MC-CDMA/S are overlapping. Moreover, for a half-loaded situation, the BEP curves of the proposed system, MC-CDMA/S, and MC-CDMA/U are overlapping. We see that the BEP performance has a similar trend as that of the MAI performance in Fig. 5.20.

Example 5.11: The CFO Effect in a Multipath Environment
In this example, we examine the CFO effect when the channel has the multipath frequency-selective fading. The number of multipath is assumed to be $L = 4$ and N=64 while the other parameters remain the same as

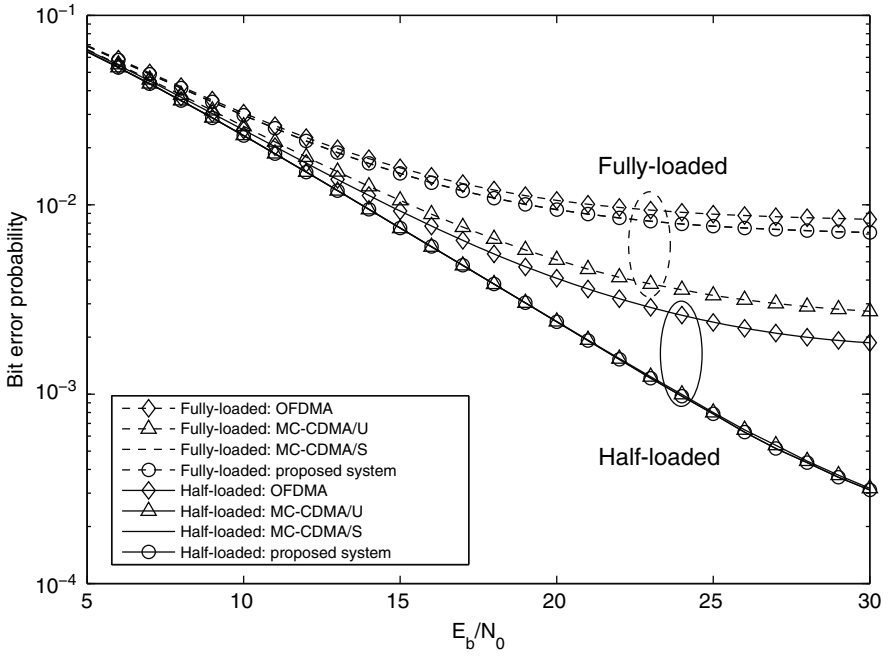

Fig. 5.22. Example 5.10: The BEP comparison among the proposed system, OFDMA and two MC-CDMA systems in a flat channel with a normalized CFO $|\epsilon_j| = 0.1$ [[135] ©IEEE].

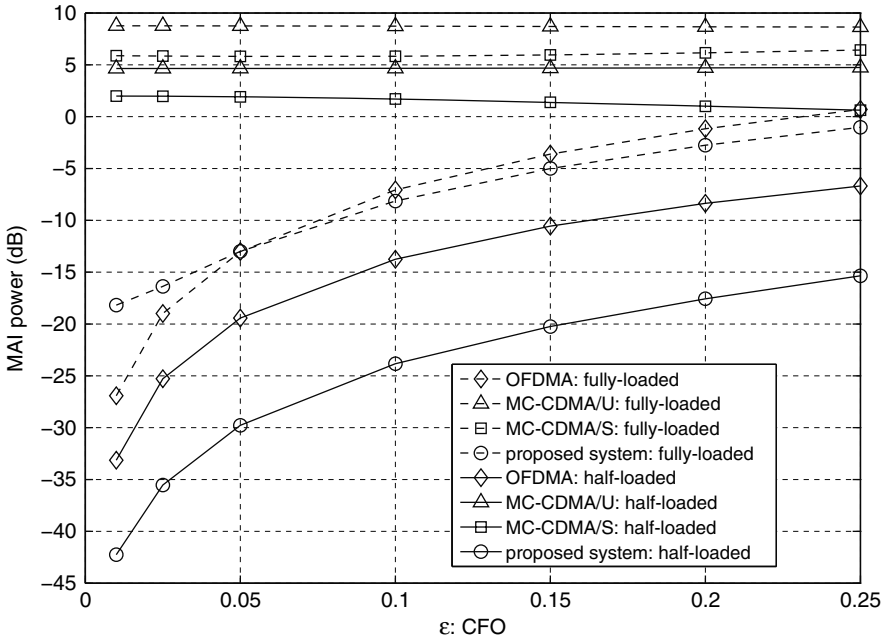

Fig. 5.23. Example 5.11: The MAI comparison among the proposed system, the OFDMA system and two MC-CDMA systems in a multipath fading environment [[135] ©IEEE].

those given in Example 5.10. The MAI performance of the four systems is shown in Fig. 5.23. In a fully-loaded situation with the CFO smaller than 0.05, OFDMA has less MAI than the proposed system because OFDMA is completely MAI-free when frequency and time are well synchronized. However, as CFO grows, the proposed system slightly outperforms OFDMA system. In a half-loaded situation, the proposed system outperforms OFDMA by around 10 dB due to the use of the code selection. The low MAI value of the proposed system with code selection is also beneficial to CFO estimation.

Let us see the comparison with MC-CDMA. The MAI performance curves for the two MC-CDMA systems with ORC are not good, since ORC amplifies the MAI power in the subcarrier with serious fading [49]. In a multipath environment, it is likely that the frequency selective fading contains several zeros to cause huge MAI in the two MC-CDMA systems. However, since a large MAI value may only lead to the error of certain bits, MAI may not be a good performance measure for this case. Instead, the BEP may provide a more valuable measure for fair comparison. As MC-CDMA systems with MRC outperforms those with ORC in a multipath environment, we will use MRC for the two MC-CDMA systems in the MRC for the two MC-CDMA systems in the following discussion.

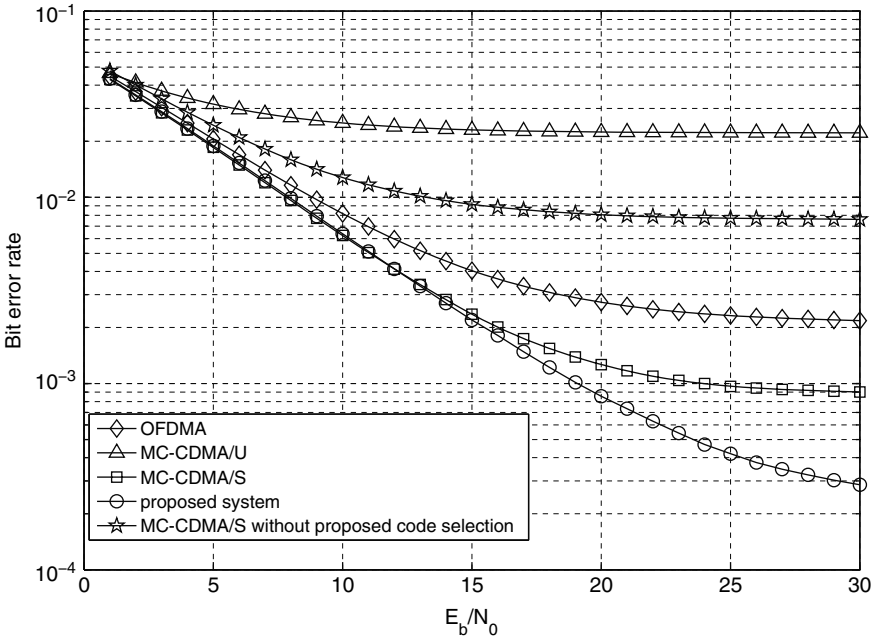

Fig. 5.24. Example 5.11: The BEP comparison among the proposed system, OFDMA and two MC-CDMA systems with $L = 4$ and $|\epsilon_j| = 0.1$ in a half-loaded situation [[135] ©IEEE].

Figure 5.24 shows the BEP comparison among the four systems with $|\epsilon_j| = 0.1$ in a half-loaded situation. We see that MC-CDMA/S with the proposed code selection outperforms OFDMA. Note that if the code selection is not used in MC-CDMA/S, instead, e.g., the first $M/2$ codewords of the M Hadamard-Walsh code are used, the performance as shown in the star curve is much worse than that using code selection. This result shows the advantage of using code selection in certain conventional MC-CDMA system. Furthermore, although the half-loaded MC-CDMA/U has the worst performance in a multipath environment, this scheme can achieve a better frequency diversity order and can perform better when the number of users is small [48]. Finally, we observe that the proposed system with code selection outperforms OFDMA and the two MC-CDMA systems in a half-loaded situation with multipath fading.

5.4.5 Code Priority in CFO Environment

In this section, we show that the performance can be further improved in a CFO environment if a proper code priority is developed based on the proposed code selection scheme [134]. It was demonstrated in the last section that PMU-OFDM is robust to CFO if only $M/2$ symmetric or anti-symmetric codewords

of M Hadamard-Walsh code are used. That is, using this code scheme, the dominating MAI due to CFO can be reduced to a negligible amount. Under this situation, the system performance is determined by residual MAI. Since the use of different Hadamard-Walsh codewords will cause different residual MAI for individual users in a CFO environment. We can further improve the performance using a code priority scheme. In this section, we extend the result in the last section and propose a code priority scheme for PMU-OFDM to improve the system performance in a CFO environment.

Following results in Section 5.4.2, it can be easily shown that

$$E\left\{|A_{j\leftarrow i}[k]|^2\right\} = \frac{|\alpha_i|^2}{M^2}\sigma_{x_i}^2\sigma_{h_i}^2\sum_{n=0}^{L-1}\left|\sum_{v=0}^{M-1} w_i[v]w_j^*[v]e^{-j\frac{2\pi}{NM}vn}\right|^2, \tag{5.100}$$

$$E\left\{\left|B_{j\leftarrow i}^{(0)}[k]\right|^2\right\} = \frac{|\beta_i|^2}{M^2}\sigma_{x_i}^2\sigma_{h_i}^2\sum_{n=0}^{L-1} \cdot\left|\sum_{v=0,u=0,u\neq v}^{M-1}\frac{e^{-j\pi\frac{u-v}{NM}}}{NM\sin\frac{\pi(u-v+\epsilon_i)}{NM}}w_i[v]w_j^*[v]e^{-j\frac{2\pi}{NM}un}\right|^2, \tag{5.101}$$

and

$$E\left\{\left|B_{j\leftarrow i}^{(1)}[k]\right|^2\right\} = \frac{|\beta_i|^2}{M^2}\sigma_{x_i}^2\sigma_{h_i}^2\sum_{f=0,f\neq k}^{N-1}\sum_{n=0}^{L-1} \cdot\left|\sum_{v=0,u=0}^{M-1}\frac{e^{-j\pi\frac{u-v-(k-f)M}{NM}}}{NM\sin\frac{\pi(u-v-(k-f)M+\epsilon_i)}{NM}}w_i[v]w_j^*[v]e^{-j\frac{2\pi}{NM}un}\right|^2. \tag{5.102}$$

It was shown in the last section that, if only $M/2$ symmetric or anti-symmetric codewords are used, $B_{j\leftarrow i}^{(0)}[k]$ can be reduced to be less than $B_{j\leftarrow i}^{(1)}[k]$. In this situation, $B_{j\leftarrow i}^{(1)}[k]$ will determine the system performance. Let us consider an example below.

Example 5.12: MAI Suppression in a CFO Environment

In this example, we evaluate $A_{j\leftarrow i}[k]$, $B_{j\leftarrow i}^{(0)}[k]$, and $B_{j\leftarrow i}^{(1)}[k]$. Let $\sigma_{x_i}^2 = \sigma_{h_i}^2 = 1$, $M = 16$, and $L = 4$. First, let us consider the fully-loaded case. Figure 5.25 shows three MAI terms i.e., $\frac{1}{T}\sum_{j=1}^{T}\sum_{i=1,i\neq j}^{T} E\left\{|A_{j\leftarrow i}[k]|^2\right\}$, $\frac{1}{T}\sum_{j=1}^{T}\sum_{i=1,i\neq j}^{T} E\left\{\left|B_{j\leftarrow i}^{(0)}[k]\right|^2\right\}$, and $\frac{1}{T}\sum_{j=1}^{T}\sum_{i=1,i\neq j}^{T} E\left\{\left|B_{j\leftarrow i}^{(1)}[k]\right|^2\right\}$ as functions of CFO for different N. We see that $\frac{1}{T}\sum_{j=1}^{T}\sum_{i=1,i\neq j}^{T} E\left\{|A_{j\leftarrow i}[k]|^2\right\}$

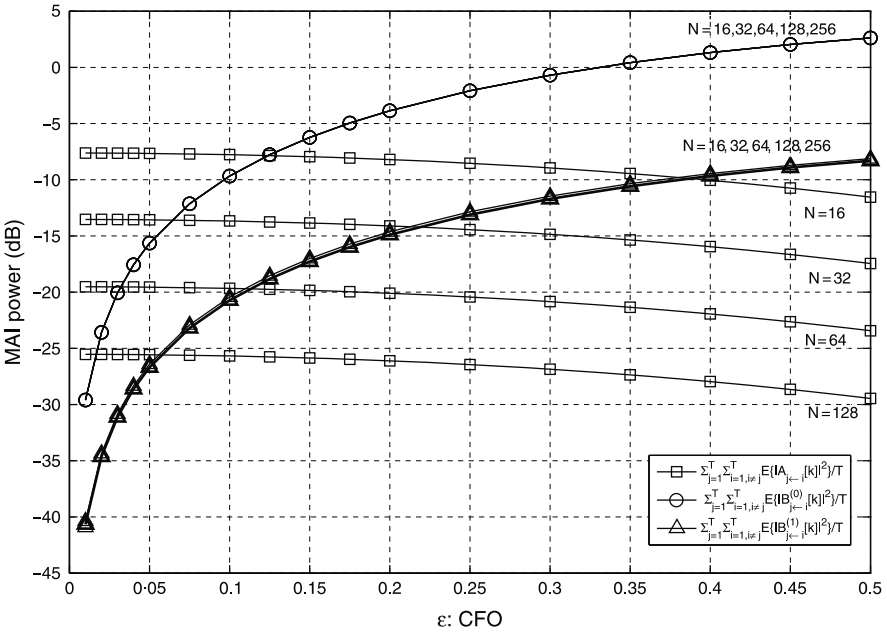

Fig. 5.25. The MAI terms are plotted as functions of CFO for the fully loaded case.

decreases at a rate of $O(N^{-2})$. This is not surprising since $A_{j\leftarrow i}[k] = \alpha_i MAI_{j\leftarrow i}[k]$. When N is sufficiently large, e.g., $N = 64$, $B^{(0)}_{j\leftarrow i}[k]$ is the dominating MAI over $A_{j\leftarrow i}[k]$ and $B^{(1)}_{j\leftarrow i}[k]$ for the CFO range of our interest.

Next, let us consider the use of only $M/2$ symmetric codewords, the performance curves are given in Fig. 5.26. We see $\frac{1}{T}\sum_{j=1}^{T}\sum_{i=1,i\neq j}^{T} E\left\{|A_{j\leftarrow i}[k]|^2\right\}$ decreases at a rate of $O(N^{-4})$. Moreover, the dominating MAI $B^{(0)}_{j\leftarrow i}[k]$ is greatly reduced, which is even less than the residual MAI $B^{(1)}_{j\leftarrow i}[k]$. That is, the system performance is now determined by the residual MAI. From the figure, the residual MAI is not affected by N so that increasing N will no longer improve the performance. ■

According to the discussion in the last section, it is clear that, to further improve the performance, we need to reduce $B^{(1)}_{j\leftarrow i}[k]$. A way to reduce the averaged total residual MAI, $\frac{1}{T}\sum_{j=1}^{T}\sum_{i=1,i\neq j}^{T} E\left\{\left|B^{(1)}_{j\leftarrow i}[k]\right|^2\right\}$, is to increase M. An extra benefit of this method is that it also increases the number of users allowed. Now, we are interested whether there is another way to reduce $B^{(1)}_{j\leftarrow i}[k]$. To answer this question, let us examine $B^{(1)}_{j\leftarrow i}[k]$. For convenience,

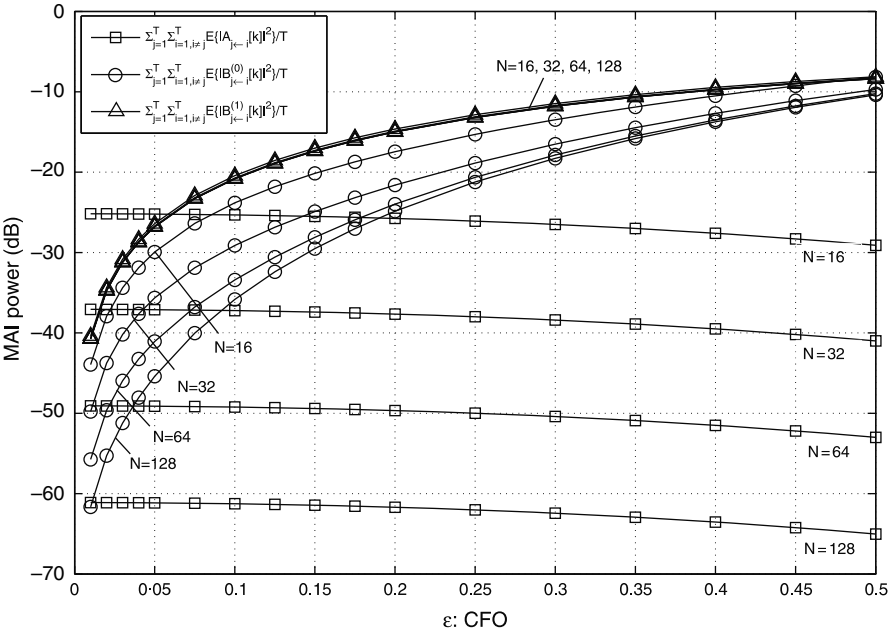

Fig. 5.26. The MAI terms are plotted as functions of CFO for the half-loaded case with $M/2$ symmetric codes.

we repeat the result in the last section here. If the symmetric or anti-symmetric codewords are used, $E\left\{\left|B_{j\leftarrow i}^{(1)}[k]\right|^2\right\}$ can be approximated by

$$\frac{|\beta_i|^2}{M^2}\sigma_{\lambda_i}^2\sigma_{x_i}^2\sum_{l=1}^{N-1}\left|\sum_{p=1}^{M-1}[f(p,l)+f(-p,l)]\sum_{q=0}^{M-1-p}w_i[q]w_j[p+q]\right|^2, \quad (5.103)$$

where $f(p,l)=\frac{e^{-j\pi\frac{p}{NM}}}{NM\sin\frac{\pi(p+lM+\epsilon_i)}{NM}}$. It can be seen from Eq. (5.103) that the residual MAI is determined by the cross-correlation of the assigned Hadamard-Walsh codewords, i.e., $\sum_{q=0}^{M-1-p}w_i[q]w_j^*[p+q]$.

Lemma 5.5: Suppose only $M/2$ symmetric or anti-symmetric codewords of M Hadamard-Walsh codes are used. We have the following property:

$$\sum_{p=1}^{M-1}\sum_{q=0}^{M-1-p}w_i[q]w_j[p+q]=\sum_{p=1}^{M-1}\sum_{q=0}^{M-1-p}w_i[p+q]w_j[q]=0, \quad i\neq j. \quad (5.104)$$

Proof. As shown in [135], if $M/2$ symmetric or anti-symmetric codewords of M Hadamard-Walsh codes are used, we have

$$\sum_{q=0}^{M-1-p} w_i[q]w_j[p+q] = \sum_{q=0}^{M-1-p} w_i[p+q]w_j[q], \quad i \neq j. \tag{5.105}$$

Consider the following equality

$$\sum_{v=0}^{M-1}\sum_{u=0,u\neq v}^{M-1} w_i[u]w_j[v] = \sum_{p=1}^{M-1}\sum_{q=0}^{M-1-p} \{w_i[q]w_j[p+q] + w_i[p+q]w_j[q]\}. \tag{5.106}$$

For $u = v$, since

$$\sum_{v=0}^{M-1} w_i[v]w_j[v] = \sum_{q=0}^{M-1-0} \{w_i[q]w_j[0+q] + w_i[0+q]w_j[q]\} = 0,$$

we have

$$\sum_{v=0}^{M-1}\sum_{u=0}^{M-1} w_i[u]w_j[v] = \sum_{p=1}^{M-1}\sum_{q=0}^{M-1-p} \{w_i[q]w_j[p+q] + w_i[p+q]w_j[q]\}. \tag{5.107}$$

From Eq. (5.107), since $\sum_{v=0}^{M-1}\sum_{u=0}^{M-1} w_i[u]w_j[v] = \sum_{v=0}^{M-1} w_j[v]\sum_{u=0}^{M-1} w_i[u] = 0$, we know that

$$\sum_{p=1}^{M-1}\sum_{q=0}^{M-1-p} \{w_i[q]w_j[p+q] + w_i[p+q]w_j[q]\} = 0. \tag{5.108}$$

From Eqs. (5.105) and (5.108), we can draw a conclusion on Eq. (5.104). ■

From Eq. (5.104), if symmetric or anti-symmetric codewords are used, the value $\sum_{q=0}^{M-1-p} w_i[q]w_j[p+q]$ for two given codewords $w_i[m]$ and $w_j[m]$ must have positive and negative values so that the summation over all p is zero. Since the maximum value of p is $M-1$, if N is sufficiently large, $e^{-j\pi\frac{p}{NM}} \approx 1$. In this case, $f(p,l) + f(-p,l) \approx \frac{1}{NM\sin\frac{\pi(p+lM+\epsilon_i)}{NM}} + \frac{1}{NM\sin\frac{\pi(-p+lM+\epsilon_i)}{NM}}$, which is a monotonically decreasing function of p. Thus, referring to Eq. (5.103), a proper code priority is able to reduce the residual MAI when not all $M/2$ users are active. Intuitively, a "good" code priority here should be able to let $\sum_{q=0}^{M-1-p} w_i[q]w_j[p+q]$ have the most zero values, or the fewest successive positive or negative values so that the absolute-and-squared term in Eq. (5.103) can be efficiently cancelled out after summation for all p. For instance, let $M = 8$ and symmetric codewords are used. Consider the code priority that assigns the first two users the codewords

$$(+1+1+1+1+1+1+1+1) \text{ and } (+1+1-1-1-1-1+1+1).$$

Then, $\sum_{q=0}^{M-1-p} w_i[q]w_j[p+q]$ is $(-1-2-1\ 0+1+2+1)$ for $1 \le p \le M-1$. The alternative code priority is to assign the first two users the codewords

$$(+1-1-1+1+1-1-1+1)\text{and}(+1-1+1-1-1+1-1+1).$$

Then, $\sum_{q=0}^{M-1-p} w_i[q]w_j[p+q]$ is $(-1+2-1\ 0+1-2+1)$ for $1 \le p \le M-1$. Obviously, the latter code priority can more effectively cancel out the residual MAI than the former one.

According to [8], each codeword of the M Hadamard-Walsh codes has an unique zero-crossing number as its identifier. Moreover, symmetric codewords have an even number of zero-crossing while anti-symmetric codewords have an odd number of zero-crossing. From Eqs. (5.103), (5.104) and above discussion, we have the following proposition.

Proposition 5.4: Suppose only $M/2$ symmetric or anti-symmetric codewords of M Hadamard-Walsh codes are used. The maximum value of $E\left\{\left|B_{j\leftarrow i}^{(1)}[k]\right|^2\right\}$ can be approximated by

$$\max_{i,j} E\left\{\left|B_{j\leftarrow i}^{(1)}[k]\right|^2\right\} = \frac{|\beta_i|^2}{M^2}\sigma_{\lambda_i}^2\sigma_{x_i}^2 \sum_{l=1}^{N-1}\left|\sum_{p=1}^{M-1}\left[f(p,l)+f(-p,l)\right]r(p)\right|^2, \tag{5.109}$$

where

$$r(p) = \begin{cases} -p, & 1 \le p \le M/4, \\ p-8, & M/4+1 \le p \le 3M/4, \\ -p+16, & 3M/4+1 \le p \le M-1. \end{cases} \tag{5.110}$$

For symmetric codes, the maximum value occurs when the two codewords, which have zero and two crossings, are used. For anti-symmetric codewords, the maximum value occurs when the two codewords, which have one and three crossings, are used.

Example 5.13: MAI Suppression with Code Priority
Let the parameter setting remains the same as those in Example 5.12 and the normalized CFO level be $\epsilon_j = 0.2$. Let $\phi_{i,j}(T) = \sum_{i=1,i\neq j}^{T} E\left\{\left|B_{j\leftarrow i}^{(1)}[k]\right|^2\right\}$. The relationship between the number of zero-crossings and the codeword indices (in Kronecker ordering [8]) for symmetric codewords and anti-symmetric codewords are manipulated in Table 5.1(a) and (b), respectively. We see that, when M increases from 16 to 32, the performance of codewords with the same crossings does not degrade significantly. The reason is that the newly added codewords have more crossings and tend to cause smaller MAI to other codewords. Take the symmetric code with 10 crossings for instance, this codeword degrades the most, i.e., 2.9 dB. However, since the increase of M will increase the number of codewords with more crossings, which tends to cause much less MAI, the overall performance is actually improved.

Table 5.1. The MAI of assigned codewords indexed by the zero-crossing numbers for (a) $M/2$ symmetric codewords, (b) $M/2$ anti-symmetric codewords, for $M = 16$ (column 3) and $M = 32$ (column 5) [[134] ©IEEE].

No. of zero crossing	Code index ($M = 16$)	$\phi_j(8)$ (dB)	Code index ($M = 32$)	$\phi_j(16)$ (dB)
0	1	–15.6	1	–14.6
2	13	–16.8	25	–15.8
4	7	–21	13	–19.4
6	11	–19.6	21	–18.3
8	4	–26.4	7	–23.8
10	16	–27.3	31	–24.4
12	6	–24.6	11	–22.4
14	10	–23.4	19	–21.5
16			4	–29.3
18			28	–29.6
20			16	–30.2
22			24	–30.1
24			6	–27.5
26			30	–27.9
28			10	–26.3
30			18	–25.7

(a) Symmetric codewords

No. of zero crossing	Code index ($M = 16$)	$\phi_j(8)$ (dB)	Code index ($M = 32$)	$\phi_j(16)$ (dB)
1	9	–15.8	17	–14.9
3	5	–16.5	9	–15.5
5	15	–21.7	29	–19.9
7	3	–19.2	5	–17.9
9	12	–26.7	23	–24.0
11	8	–27.2	15	–24.3
13	14	–25.1	27	–22.7
15	2	–23.0	3	–21.2
17			20	–29.4
19			12	–29.6
21			32	–30.2
23			8	–30.1
25			22	–27.6
27			14	–27.9
29			26	–26.6
31			2	–25.4

(b) Anti-symmetric codewords

Let us see the relationship of $E\left\{\left|B_{j\leftarrow i}^{(1)}[k]\right|^2\right\}$ and the number of crossings. This is shown in Table 5.2. We see that $E\left\{\left|B_{j\leftarrow i}^{(1)}[k]\right|^2\right\}$ is symmetric in the sense that $E\left\{\left|B_{j\leftarrow i}^{(1)}[k]\right|^2\right\} = E\left\{\left|B_{i\leftarrow j}^{(1)}[k]\right|^2\right\}$. Note that if we sum up the whole row or column, we get $\phi_{i,j}(T)$ at the third column in Table 5.1(a). We see from Table 5.2 that, for symmetric codewords, the one with 0 and 2 crossings will lead to the maximum total residual MAI. This result is a direct consequence of Proposition 5.4.

Moreover, we see that different codewords will cause different levels of MAI to other users. Thus, as shown in Table 5.1, different users will receive a different total MAI level. From Table 5.1, we observe that, as M increases, the new codewords, i.e., 8–14 crossings for symmetric codes and 9–15 crossings for anti-symmetric codes, will cause less MAI than the previous codewords, i.e., 0–6 crossings for symmetric codes and 1–7 crossings for anti-symmetric codes. Hence, for a $M/2$-user system with $M \geq 8$, the $M/4$ codewords with more crossings should be assigned to the first $M/4$ active users. The $M/4$ codewords

Table 5.2. $E\left\{|MAI_{j\leftarrow i}[k]|^2\right\}$ (dB) is plotted as a function of codewords in terms of crossing numbers [[134] ©IEEE].

	0 crossing	2 crossings	4 crossings	6 crossings	8 crossings	10 crossings	12 crossings	14 crossings
0 crossing		–18.5	–24.5	–22.4	–31.5	–33.2	–28.9	–27.1
2 crossings	–18.5		–27.3	–26.1	–33.2	–34.0	–31.2	–30.2
4 crossings	–24.5	–27.3		–29.6	–35.2	–35.7	–33.8	–33.2
6 crossings	–22.4	–26.1	–29.6		–34.8	–35.4	–33.2	–32.4
8 crossings	–31.5	–33.2	–35.2	–34.8		–39.2	–38.2	–37.7
10 crossings	–33.2	–34.0	–35.7	–35.4	–39.2		–38.3	–38.1
12 crossings	–28.9	–31.2	–33.8	–33.2	–38.0	–38.3		–36.3
14 crossings	–27.1	–30.2	–33.2	–32.4	–37.7	–38.1	–36.3	

with fewer crossings will be further divided into two sets with $M/8$ codewords, the $M/8$ codewords with more crossings have higher priority to be assigned to users when the number of active users exceeds $M/4$. This procedure will continue until the divided set only has one user.

Take $M = 32$ symmetric code for instance. As shown in Table 5.1, codewords can be divided into the following five sets.

1. The first code set with 0–1 crossing (i.e., 0 for symmetric codes, and 1 for anti-symmetric codes);
2. the second code set with 2–3 crossings;
3. the third code set with 4–7 crossings;
4. the fourth code set with 8–15 crossings; and
5. the fifth code set with 16–31 crossings.

When the index of the code set is higher, the caused MAI is smaller. Thus, we should assign codewords from a higher indexed set to connected users with a higher priority so that the overall performance is better as compared with a random code assignment. Note that the above scheme is only a coarse code priority. That is, in the same code set, codewords with more crossings does not necessarily have a higher priority than codewords with fewer crossings. Take the fifth code set for instance, the codeword with 20 crossings will cause less MAI than the codeword with 30 crossings.

A fine code priority can be obtained off-line using the close form of $E\left\{\left|B^{(1)}_{j\leftarrow i}[k]\right|^2\right\}$ in Eq. (5.102) to construct Tables 5.1 and 5.2. Based on

these two tables, we can easily determine the fine code priority. For instance, when $M = 16$ for symmetric codes, the fine code priority is

$$\text{Fine Code Priority}: \mathbf{w_{16}},\ \mathbf{w_4},\ \mathbf{w_6},\ \mathbf{w_{10}},\ \mathbf{w_7},\ \mathbf{w_{11}},\ \mathbf{w_{13}},\ \mathbf{w_1}. \quad (5.111)$$

Let $M = 16$. Figure 5.27 shows $\sum_{i=1,i\neq j}^{T} E\left\{\left|B_{j\leftarrow i}^{(1)}[k]\right|^2\right\}$, $1 \le j \le 8$, as a function of CFO for symmetric codes. We see from this figure that the performance rank of different codewords is independent of CFO. In other words, a fine code priority is not changed by the CFO value. Hence, we only need to determine the fine code priority once and then it can work for different CFO environment.

Let $M = 16$ and $N = 64$. We consider a quarterly loaded system with symmetric code. That is, only codewords with 14, 12, 10, and 8 crossings are used. Figure 5.28 shows the individual MAI terms as a function of CFO for $N = 64$. Note that the 4 curves $\sum_{i=1,i\neq j}^{T} E\left\{|A_{j\leftarrow i}[k]|^2\right\}$ are overlapping with $\frac{1}{T}\sum_{j=1}^{T}\sum_{i=1,i\neq j}^{T} E\left\{|A_{j\leftarrow i}[k]|^2\right\}$. When comparing the result

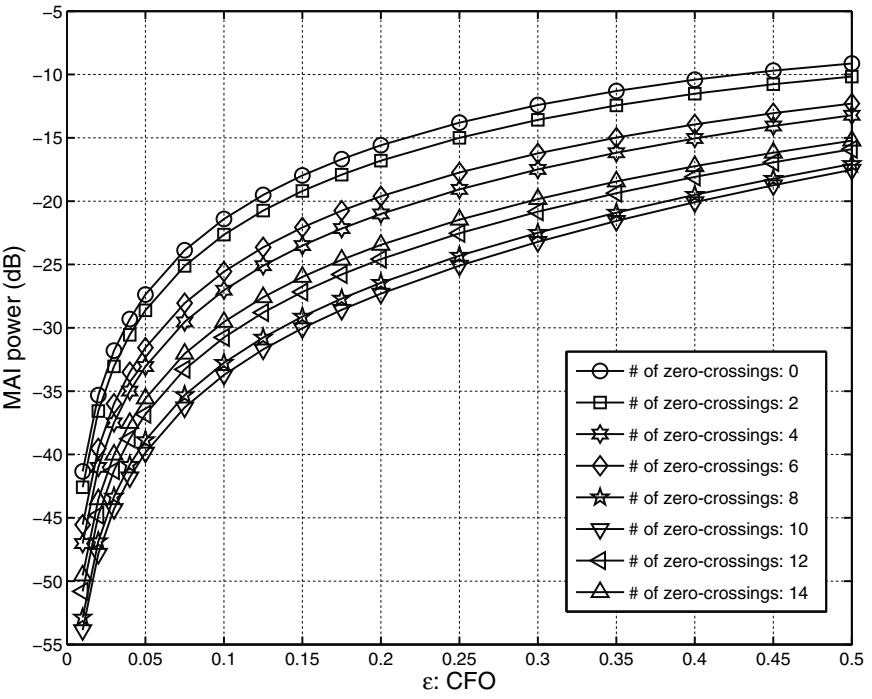

Fig. 5.27. $\frac{1}{T}\sum_{j=1}^{T}\sum_{i=1,i\neq j}^{T} E\left\{\left|B_{j\leftarrow i}^{(1)}[k]\right|^2\right\}$ as a function of CFO for different codewords [[134] ©IEEE].

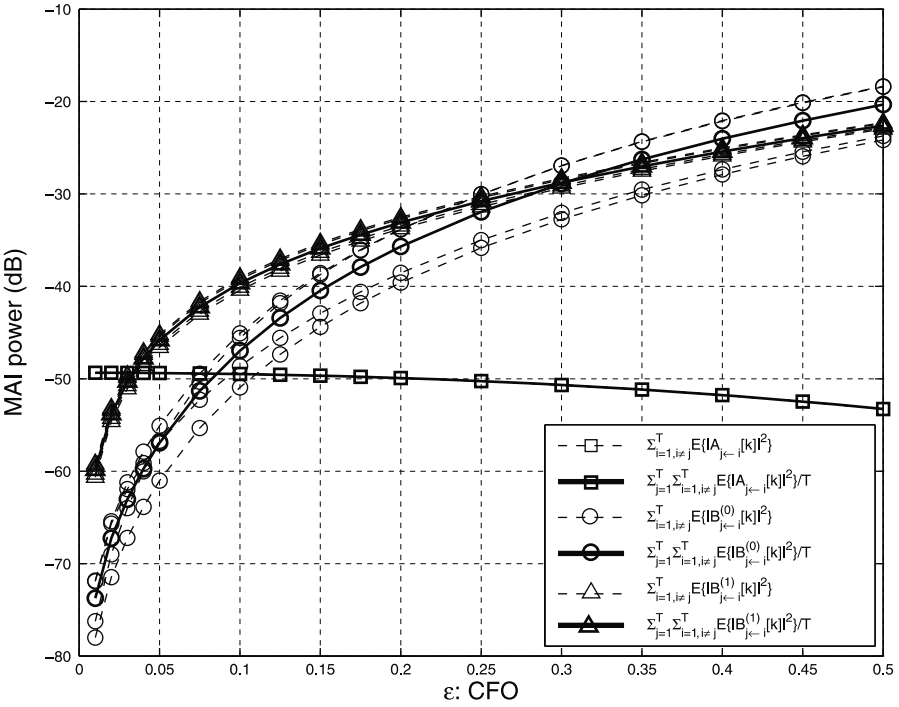

Fig. 5.28. MAI terms are plotted as functions of CFO for the quarterly loaded case with code priority.

with Fig. 5.26, the two MAI terms, $\frac{1}{T}\sum_{j=1}^{T}\sum_{i=1,i\neq j}^{T} E\left\{\left|B_{j\leftarrow i}^{0}[k]\right|^2\right\}$ and $\frac{1}{T}\sum_{j=1}^{T}\sum_{i=1,i\neq j}^{T} E\left\{\left|B_{j\leftarrow i}^{1}[k]\right|^2\right\}$ have been reduced simultaneously so that increasing N from 16 to 64 can further improve the system performance in a CFO environment. This result is different from the half-loaded case in Example 5.12. ■

In an environment with serious CFO mismatch, the system designer may consider this quarterly loaded scheme so that every user is nearly MAI-free in such a bad CFO environment. A scenario is given below. When the user speed is fast to cause a large CFO, it may be impractical to use a feedback mechanism to compensate the CFO in the transmitter side [88, 142]. Hence, it is desirable if we can compensate the CFO effect at the receiver end while the MAI is negligible to lead to significant performance degradation [135]. In this situation, the use of a quarterly loaded PMU-OFDM system is a good trade-off since it enables the system to be more robust to CFO effect.

Example 5.14: MAI Suppression in Quarterly Load Systems

We compare the performance of quarterly loaded PMU-OFDM and quarterly loaded OFDMA systems in this example. Let the parameter setting remains the same as in Example 5.13. In a quarterly loaded case, the four codewords with 14, 12, 10, and 8 crossings are used in the PMU-OFDM system. For OFDMA, the uth user will be assigned subchannels indexed by $4(u-1)+kM$, $1 \le u \le M/4$, and $0 \le k \le N-1$. The remaining $3NM/4$ subchannels are used as guard bands.

We first evaluate the MAI in the detection stage, i.e., MAI after frequency equalization. Figure 5.29 shows the averaged total MAI after equalization as a function of CFO for the two systems in the half- and quarterly loaded situations. We see that the half-loaded PMU-OFDM even outperforms the quarterly loaded OFDMA when CFO is less than 0.375. Consequently, the quarterly loaded PMU-OFDM outperforms quarterly loaded OFDMA around 8–20 dB. We also see that if the code priority scheme is used in the quarterly loaded PMU-OFDM, the system is more robust to the CFO effect. For instance, at CFO=0.15, the quarterly loaded PMU-OFDM with code priority can outperform the half-loaded PMU-OFDM by 14 dB.

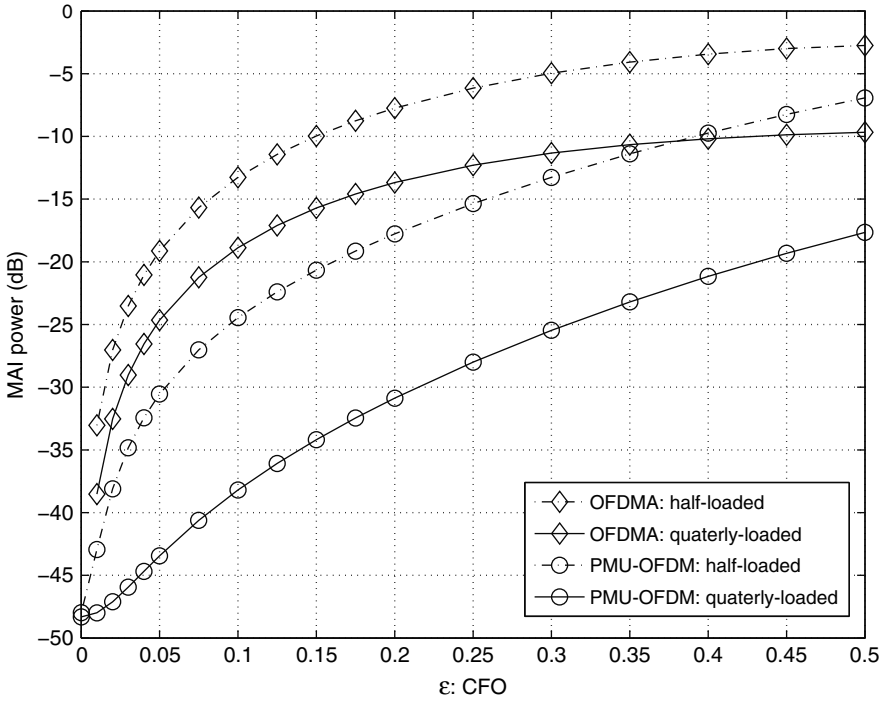

Fig. 5.29. MAI comparison between PMU-OFDM and OFDMA in half- and quarterly-loaded cases [[134] ©IEEE].

Now, consider the bit error probability performance of both systems. Let the CFO value be 0.2, which can be considered to be a serious CFO environment. For instance, in a wireless broadband application [66, 88], let the sampling frequency be 4 MHz and the carrier frequency be 4 GHz. Since there are $NM = 1024$ subchannels, for CFO=0.2, it can be shown that the user speed is around 211 km/h [108]. Note that it has also been verified that the channel coherent time is around 542 μs (see Eq. (5.40.c) in [108]), which is still greater than two times of one OFDM-block duration of 256 μs. Hence, the assumption that the channel is quasi-statistic may still be valid in this situation [108].

Figure 5.30 shows the BEP as a function of signal-to-noise ratio (SNR). Comparing it with Fig. 5.29, we see that the BEP performance in Fig. 5.30 could be roughly evaluated by the MAI curves in Fig. 5.29. Take half-loaded PMU-OFDM for instance, the performance floor occurs when SNR is around 15 dB. This is reasonable since we see from Fig. 5.29 that the MAI power is around -18 dB at CFO=0.2. When SNR=18 dB for BPSK symbols, which have 0 dB power, it means the noise power is around -18 dB. Hence, if we include the MAI of -18 dB. The total power of noise plus interference is

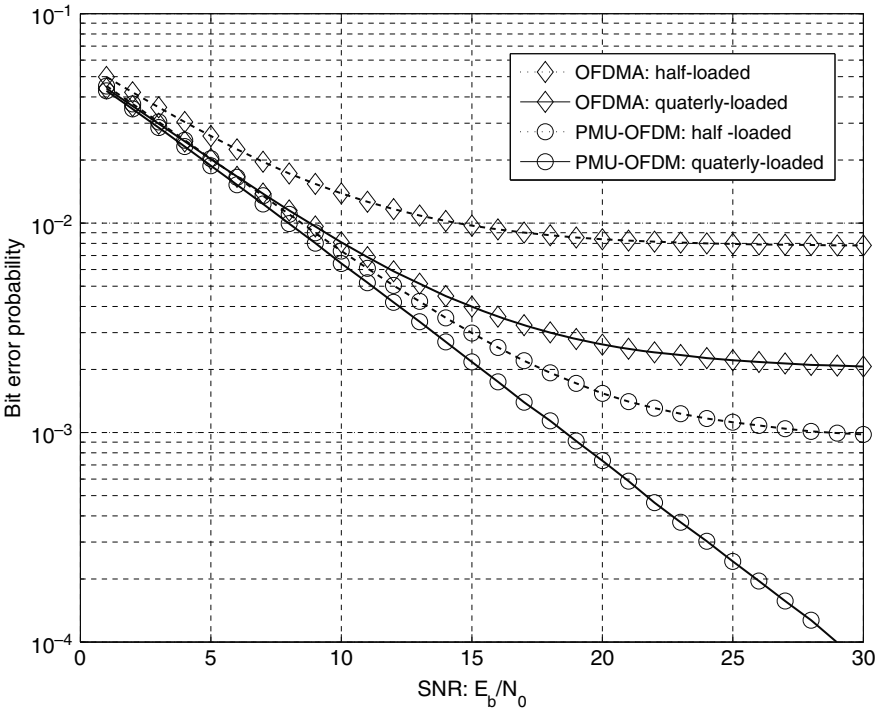

Fig. 5.30. The BEP comparison between PMU-OFDM and OFDMA in half-loaded and quarterly loaded cases ($|\epsilon_j = 0.2|$) [[134] ©IEEE].

-15 dB. Hence, we see from Fig. 5.29 that the BEP of the half-loaded PMU-OFDM at SNR=18 dB performs roughly the same as the quarterly loaded PMU-OFDM at SNR=15 dB, where its MAI power is around -31 dB and is sufficiently smaller than the noise power -15 dB. As SNR increases, the noise will become less than -18 dB. However, the MAI remains -18 dB for half-loaded PMU-OFDM if CFO is fixed at 0.2. In this case, the performance floor will occur at SNR=18 dB. The same evaluation applies to the OFDMA system. Furthermore, we see that quarterly loaded PMU-OFDM with code priority makes the system more robust to this serious CFO environment. In fact, due to the use of symmetric or anti-symmetric codes, half-loaded PMU-OFDM outperforms quarterly loaded OFDMA. ■

Example 5.15: Codeword Assignment with Code Priority
Let the parameter setting remain the same as that in Example 5.14. First, we evaluate the performance of different code priority schemes. The proposed fine code priority is given in Eq. (5.111), which is the code priority that results in the minimum $E\left\{\left|B_{j\leftarrow i}^{(1)}[k]\right|^2\right\}$ according to Tables 5.1 and 5.2. Another code priority used as a benchmark is given by

$$\text{Priority Scheme for Comparision}: \mathbf{w_1},\ \mathbf{w_{13}},\ \mathbf{w_7},\ \mathbf{w_{11}},\ \mathbf{w_4},\ \mathbf{w_{16}},\ \mathbf{w_6},\ \mathbf{w_{10}},$$

which assigns codewords of crossings from the fewest to the most, i.e., from 0 to 14.

Figure 5.31 shows the MAI as a function of the number of active users T for these two schemes. The dashed curves are for CFO=0.05 while the solid curves are for CFO=0.2. We see that the proposed code priority greatly outperforms the benchmark code priority. The benchmark scheme assigns the first two users with the codewords having 0 and 2 crossings, which will cause the most serious MAI in a CFO environment. Hence, we see that, as T increases, the performance of the benchmark priority becomes slightly better. Moreover, we see that the benchmark priority with CFO=0.05 performs even worse than the proposed priority with CFO=0.2 when $T < 5$. These results pronounce the fact that a good code priority design can further enhance the system performance while a bad design may make the performance stay nearly unchanged even if the number of users is decreased to 2. ■

In future communication systems, it is desirable that systems are robust to different CFO levels. For instance, some users are in a fast mobile speed so that they have large CFOs while some users are in a slow speed so that they have small CFOs. In this case, code priority can be used in the following way. That is, we assign codewords of higher priorities to users who have larger CFOs and codewords with lower priorities to users who have smaller CFOs. Since the MAI effect is symmetric in the sense that $E\left\{|MAI_{j\leftarrow i}[k]|^2\right\} = E\left\{|MAI_{i\leftarrow j}[k]|^2\right\}$, if user i has the most serious CFO while it is assigned the highest priority codeword, this codeword is most robust to CFO and it only causes a small MAI to other users.

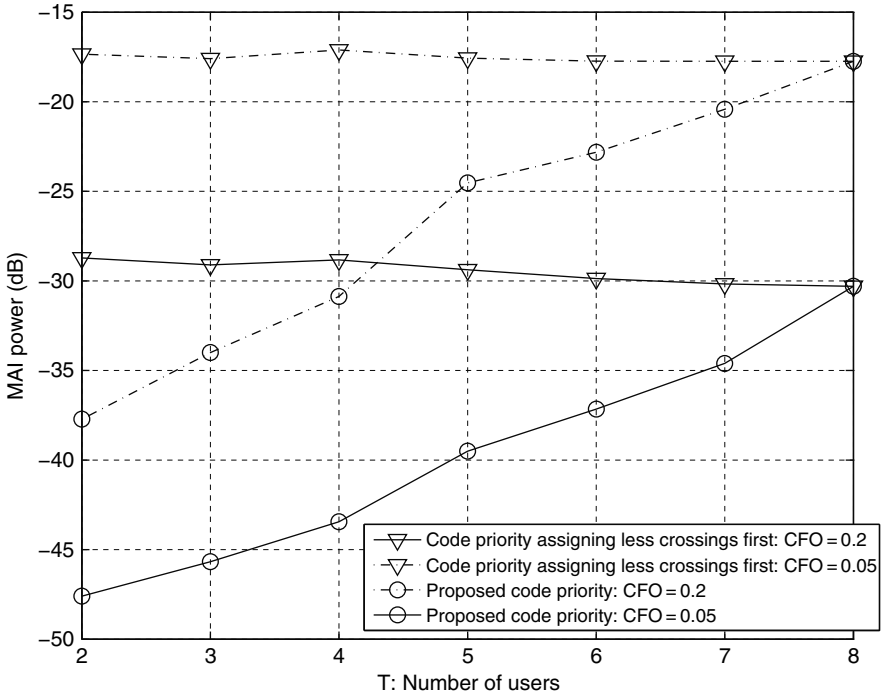

Fig. 5.31. MAI is plotted as a function of the number of active users for different code priority schemes [[134] ©IEEE].

Example 5.16: Codeword Priority for Different CFOs

In this example, we are interested in seeing what happens if we assign higher priority codewords to users who have larger CFOs and the lower priority codewords to users who have lower CFOs in the PMU-OFDM system. This code assignment is intuitive since higher priority codewords are more robust to CFO and they will not cause significant MAI to other users even in a serious CFO environment, e.g., please see Table 5.2. The lower priority codewords tend to cause great MAI to other users. However, if they are assigned to users with lower CFOs, the caused MAI is not as significant due to small CFOs.

Consider a half-loaded system with four different CFO levels, 0.02, 0.03, 0.05, four and 0.1. For PMU-OFDM, $\mathbf{w_1}$ and $\mathbf{w_{13}}$ are with CFO=0.02, $\mathbf{w_{11}}$ and $\mathbf{w_7}$ are with CFO=0.03, $\mathbf{w_{10}}$ and $\mathbf{w_6}$ are with CFO=0.05, and $\mathbf{w_4}$ and $\mathbf{w_{16}}$ are with CFO=0.1. For OFDMA, the first and second users i.e., $u = 1$ and 2 in Example 5.14, are with CFO=0.02, the third and the fourth users are with CFO=0.03, the fifth and the sixth users are with CFO=0.05, and the seventh and the eigth users are with CFO=0.1. Figure 5.32 shows the BEP curves of these two systems. We see that the use of code priority for different CFO levels enables the PMU-OFDM to continue to outperform OFDMA.

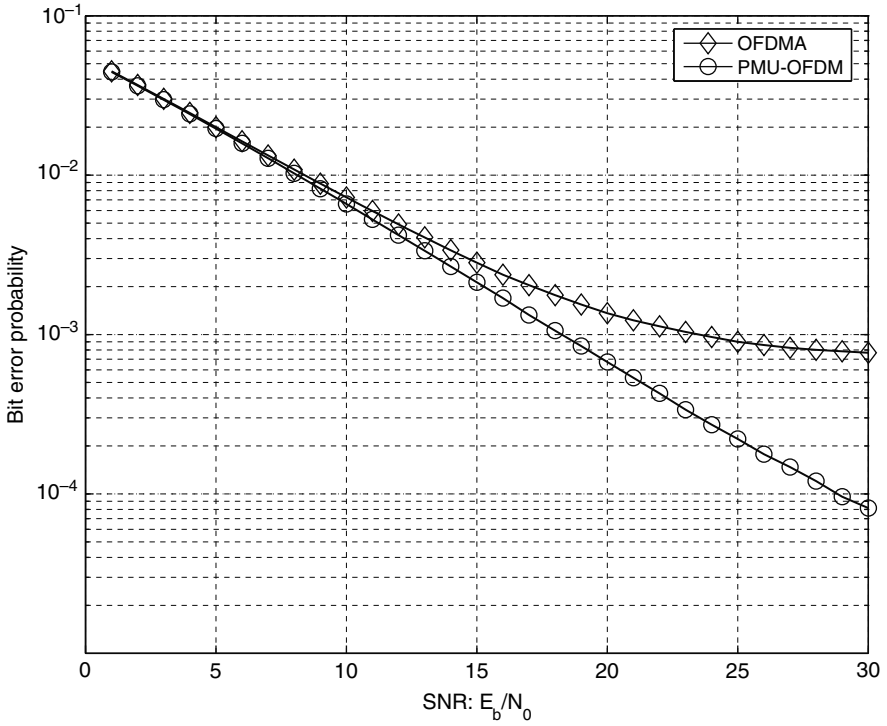

Fig. 5.32. The BEP comparison between PMU-OFDM and OFDMA in an environment with various CFOs [[134] ©IEEE].

This result shows a great advantage of PMU-OFDM with code priority in a practical situation. ■

5.5 PMU-OFDM System in Time-Varying Channel Environment

In this section, we will investigate the performance of PMU-OFDM in the presence of time-varying channels and compare with that of OFDMA system in such an environment.

5.5.1 Time-Varying Rayleigh Fading Channel Model

The discrete-time impulse response of a time-variant channel $h(\tau; n)$ is defined as the response of the channel at time n to an impulse applied at time $n - \tau$. It can be modeled as [60]

$$h(\tau; n) = \sum_{d=0}^{L-1} \beta(d) e^{-j2\pi\phi_d(n)} \delta(\tau - d), \tag{5.112}$$

where $\beta(d)$ is the real envelope of the dth channel gain of the Rayleigh distribution, $\phi_d(n)$ is the phase of the dth multipath component of the uniform distribution. The time-varying nature of the channel can be mathematically modeled by treating $h(\tau; n)$ as a *wide-sense-stationary* (WSS) random process in n with autocorrelation

$$R(\tau_1, \tau_2, \alpha) = E\{h^*(\tau_1, n)h(\tau_2, n + \alpha)\}. \tag{5.113}$$

For most multipath channels, the attenuation and the phase shift associated with different delays are assumed uncorrelated. This uncorrelated scattering (US) leads to the following autocorrelation function [60, 105]

$$R(\tau_1, \tau_2, \alpha) = R(\tau_1, \alpha)\delta(\tau_1 - \tau_2). \tag{5.114}$$

The above equation describes the autocorrelation function for the multipath channel under the wide sense stationary and uncorrelated scattering assumptions. It is often known as the WSSUS model for the multipath fading channel. By applying the Fourier transform to autocorrelation function $R(\tau, \alpha) = E\{h^*(\tau, n)h(\tau, n+\alpha)\}$, we can obtain the *scattering function* of the channel as

$$S(\tau, f) = F\{R(\tau, \alpha)\} = \int_{-\infty}^{\infty} R(\tau, \alpha)e^{-j2\pi f\alpha}d\alpha. \tag{5.115}$$

Based on the above scattering function, we can derive the *multipath intensity profile* (or the power-delay profile), which is defined as

$$p(\tau) = R(\tau, 0) = E\{|h(\tau, n)|^2\}. \tag{5.116}$$

It is the average received power expressed as a function of delay. The two most common power-delay profiles are uniform and exponential. Every multipath component has the same power in the uniform power-delay profile whereas multipath components decay exponentially with delay in the exponential profile.

Another useful function to characterize the time-varying nature of the channel is the *Doppler power spectrum*, which can be derived from the scattering function as

$$S_D(f) = \int_{-\infty}^{\infty} S(\tau, f)d\tau. \tag{5.117}$$

The *Doppler spread*, f_D, provides a measure of spectral broadening caused by the change of the mobile channel over time. It is defined as the range of frequencies over which the received Doppler spectrum is essentially non-zero. When a sinusoidal tone of frequency f_c is transmitted over a time-variant channel, the Doppler spectrum of the received signal will have components in the range from $f_c - f_d$ to $f_c + f_d$, where f_d is called the Doppler shift. It is a function of the relative velocity of the mobile terminal and the angle

θ between the motion direction of the mobile terminal and the direction of arrival of scattered waves. Mathematically, f_d can be written as

$$f_d = f_c \frac{V}{c} \cos\theta, \tag{5.118}$$

where f_c is the carrier frequency, V is the velocity of the mobile terminal, and c is the speed of light.

To model the Doppler phenomenon, it is often assumed that there are many multipath components, each of which has a different delay but the same Doppler spectrum (Fig. 5.33). Each multipath component is actually made up of a large number of simultaneously arriving unresolvable multipath components, having uniformly distributed angles of arrival at the receive antenna. This channel model was suggested by Jakes. The classical *Jakes's Doppler spectrum* has the form [60]

$$S_D(f) = \frac{1}{\sqrt{1-(f/f_D)^2}}, \quad -f_D \le f \le f_D, \tag{5.119}$$

where $f_D = f_c \frac{V}{c}$ is the maximum Doppler shift.

The time-varying channel impulse response of Eq. (5.112) can be written as

$$h(n;\tau) = \sum_{d=0}^{L-1} g(n;d)\delta(\tau - d), \tag{5.120}$$

where $g(n;d) = \beta_d e^{-j2\pi\Phi_d(n)}$ is a complex Gaussian random variable with zero mean and variance σ_d. Then, we have

$$E[g(n;d)g^*(m;d')] = R(d, n-m)\delta(d-d'). \tag{5.121}$$

It turns out that we can factor the autocorrelation function as the product of two one-variable functions of delay and time [105]

$$R(d, n-m) = \phi(n-m)\sigma_d^2$$

where σ_d^2 is the variance of the dth tap and $\phi(n-m)$ is the time-autocorrelation function. The Jakes model for the time-domain time-autocorrelation function [60] can be written as

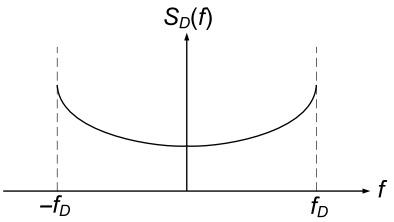

Fig. 5.33. Complex baseband equivalent model of Jakes Doppler spectrum.

$$\phi(n-m) = J_0\left(2\pi f_D T_s(n-m)\right), \tag{5.122}$$

where $J_0(x)$ is the zeroth order Bessel function of the first kind, f_D is the maximum Doppler frequency, and T_s is the sampling rate.

In Eq. (5.112), $\phi_d(n)$ is the Doppler frequency for channel path d. It is the only time-varying parameter in this channel model. The Doppler spread effect is caused by the difference in Doppler frequencies $\phi_d(n)$ for different channel paths. On the other hand, if $\phi_d(n)$ is the same for all channel paths, we have only the Doppler shift effect. Then, the channel impulse response can be written as

$$\begin{aligned} h(\tau; n) &= e^{-j2\pi\phi(n)} \sum_{d=0}^{L-1} \beta_d \delta(\tau - d), \\ &= e^{-j2\pi\phi(n)} h(\tau). \end{aligned} \tag{5.123}$$

In other words, it is equivalent to a time-invariant channel multiplied by a common phase shift component. When there is a carrier frequency offset (CFO) due to the Doppler shift or mismatch between transceiver's oscillators, Eq. (5.112) yet with $\phi(n)$ replaced by the normalized CFO value provides the appropriate channel model.

We will prove that PMU-OFDM is approximately MAI-free in time-varying channel with the use of symmetric or anti-symmetric Hadamard-Walsh codewords as it is in CFO channel. We will also show that the number of sign changes in Hadamard-Walsh codewords has central effect on the value of ICI caused by time-varying channel in PMU-OFDM system.

5.5.2 Analysis of PMU-OFDM Under the Doppler Effect

We can divide the overall Doppler effect in a mobile environment into the Doppler MAI effect and self-Doppler effect. The MAI effect is the interference from symbols of other users while the self-Doppler effect is the interference from neighboring subcarriers (i.e., Doppler ICI) of the same user to also result in symbol distortions.

5.5.3 Doppler MAI

In this section, we analyze the performance of PMU-OFDM and derive its average MAI in Doppler environment. We saw before that in PMU-OFDM, each symbol in the input of user j,($\mathbf{x}_j$) is repeated by M times and after passing through $\mathbf{W}_j$, the resultant $NM \times 1$ vector $\mathbf{z}_j$ can be written as

$$z_j[l] = w_j[l] y_j[l], \quad 0 \le l \le NM - 1, \tag{5.124}$$

where $l = v + kM$ is the frequency index. Next, each coded vector is passed through the NM-point inverse DFT (IDFT) matrix. Then, following the parallel to serial conversion, ν cyclic prefix (CP) are inserted at the beginning of each OFDM symbol. The jth transmitted signal over a block is thus given by

$$s_j(n) = \frac{1}{NM} \sum_{\Omega=0}^{NM-1} w_j[\Omega] y_j[\Omega] e^{j\frac{2\pi}{NM}\Omega n}, \quad -\nu \le n \le NM, \tag{5.125}$$

where $w_j[\Omega]$, $\Omega = 0, 1, \ldots NM-1$ is the jth user's Hadamard-Walsh codewords.

These symbols are fed to the multiple access channel. We consider the uplink scenario where each user experiences a different channel but under the assumption of synchronous communication.

If the cyclic prefix duration is chosen such that $\nu \ge L$, the received signal after removing the cyclic prefix is given by

$$r(n) = \sum_{i=1}^{T} \sum_{d=0}^{L-1} g_i(n;d) s_i(n-d) + e(n), \tag{5.126}$$

where $e(n)$ is the discrete-time additive white Gaussian noise, $g_i(n;d)$ is the channel complex coefficient of user i, and T is the number of multiple access users. The output of DFT can be expressed as

$$r[l] = \sum_{n=0}^{NM-1} r(n) e^{-j\frac{2\pi}{NM}nl}, \quad 0 \le l \le NM-1. \tag{5.127}$$

The detected symbol for user j is then given by

$$\hat{x}_j[k] = \frac{1}{M} \sum_{v=0}^{M-1} w_j[v+kM] \frac{1}{NM} \sum_{i=1}^{T} \sum_{n,\Omega=0}^{NM-1} y_i[\Omega] w_i[\Omega] \sum_{d=0}^{L-1} g_i(n;d) \cdot \left\{ e^{j\frac{2\pi}{NM}\Omega(n-d)} e^{-j\frac{2\pi}{NM}n(v+kM)} \right\} + \hat{e}[k], \tag{5.128}$$

where

$$\hat{e}[k] = \frac{1}{M} \sum_{v=0}^{M-1} e[v+kM] w_j[v+kM], \tag{5.129}$$

and

$$e[v+kM] = \sum_{n=0}^{NM-1} e(n)\, e^{-j\frac{2\pi}{NM}n(v+kM)}. \tag{5.130}$$

By Eq. (5.1), we get

$$y_i[\Omega] = y_i[u+fM] = x_i[f], \tag{5.131}$$

where $\Omega = u + fM$, with $0 \le u \le M-1$ and $0 \le f \le N-1$. Since all symbols of an individual user use the same Hadamard-Walsh code, we have $w_i[u+fM] = w_i[u]$ and $w_j[v+kM] = w_j[v]$. By defining

$$\zeta_{i,j}(n,d) = \frac{1}{M} \sum_{v=0}^{M-1} \sum_{u=0}^{M-1} w_i[u] w_j[v]\, e^{-j\frac{2\pi}{NM}(v-u)n}\, e^{-j\frac{2\pi}{NM}ud}, \tag{5.132}$$

and using Eq. (5.131), we can express Eq. (5.128) in the following form

$$\hat{x}_j[k] = \sum_{i=1}^{T} \sum_{f=0}^{N-1} x_i[f] \frac{1}{NM} \sum_{n=0}^{NM-1} \sum_{d=0}^{L-1} g_i(n;d)\zeta_{i,j}(n,d)\, e^{-j\frac{2\pi}{NM}(fM)d}\, e^{-j\frac{2\pi}{N}(k-f)n} + \hat{e}[k]. \tag{5.133}$$

From the above equation, the MAI to the kth symbol of user j due to user i, denoted by $MAI_{j\leftarrow i}[k]$, is given by

$$MAI_{j\leftarrow i}[k] = \sum_{f=0}^{N-1} x_i[f] \frac{1}{NM} \sum_{n=0}^{NM-1} \sum_{d=0}^{L-1} \cdot \left\{ g_i(n;d)\zeta_{i,j}(n,d) e^{-j\frac{2\pi}{NM}(fM)d} e^{-j\frac{2\pi}{N}(k-f)n} \right\}. \tag{5.134}$$

The averaged $MAI_{j\leftarrow i}[k]$ power is $E\left\{|MAI_{j\leftarrow i}[k]|^2\right\}$. Let

$$\zeta_{i,j}(n,d) = \eta_{i,j}(n) e^{-j\frac{2\pi}{NM}ud},$$

where

$$\eta_{i,j}(n) = \frac{1}{M} \sum_{u,v=0}^{M-1} w_i[u] w_j[v] e^{-j\frac{2\pi}{NM}(v-u)n}. \tag{5.135}$$

We assume that $x_i[f]$ and $g_i(n;d)$ are uncorrelated, and also cross correlation between $x_i[f]$ is zero; i.e., $E\{x_i[f]x_i^*[f']\} = \sigma_{x_i}^2 \delta(f-f')$. Then, by Eqs. (5.121) and (5.122), the averaged power of $MAI_{j\leftarrow i}[k]$ can be found as

$$E\left\{|MAI_{j\leftarrow i}[k]|^2\right\} = L(\frac{\sigma_d \sigma_{x_i}}{NM})^2 \sum_{f=0}^{N-1} \sum_{n,m=0}^{NM-1} J_0\left(2\pi f_D T_s(n-m)\right) \cdot \left\{ \eta_{i,j}(n)\eta_{i,j}^*(m) e^{-j\frac{2\pi}{N}(k-f)(n-m)} \right\}. \tag{5.136}$$

Similar to previous section, we divide the MAI into two terms

$$MAI_{j\leftarrow i}[k] = MAI_{j\leftarrow i}^{(0)}[k] + MAI_{j\leftarrow i}^{(1)}[k]. \tag{5.137}$$

$MAI_{j\leftarrow i}^{(0)}[k]$ is obtained by letting $f = k$ in Eq. (5.134) and is the interference contributed from the kth symbol of user i to the kth symbol of user j. $MAI_{j\leftarrow i}^{(1)}[k]$ is the interference contributed from all the $f \neq k$th symbols of user i to the kth symbol of user j.

From Eq. (5.136), the averaged power of $MAI_{j\leftarrow i}^{(0)}[k]$ is given by

$$E\left\{\left|MAI_{j\leftarrow i}^{(0)}[k]\right|^2\right\} = L\left(\frac{\sigma_d\sigma_{x_i}}{NM}\right)^2 \sum_{n,m=0}^{NM-1} \cdot \left\{J_0\left(2\pi f_D T_s(n-m)\right)\eta_{i,j}(n)\eta_{i,j}^*(m)\right\}. \quad (5.138)$$

Example 5.17: Dominating and Residual MAI in Time-Varying Flat Fading Channel

In this example, we show by simulation that $\overline{MAI}_j^{(0)}$ is indeed the dominating MAI in a Doppler spread environment with flat fading channel. Figure 5.34 shows the simulation results for $MAI_{j\leftarrow i}^{(0)}[k]$ and $MAI_{j\leftarrow i}^{(0)}[k]$ versus normalized Doppler frequency. The simulation parameters are $N = 4$, $M = 16$, $L = 1$, $f_c = 4$ GHz and sampling frequency $F_s = \frac{1}{T_s} = 2$ MHz. The maximum Doppler frequency is related to the mobile speed via $f_D = f_c\frac{V}{c}$, where c is the speed of light and V is the mobile speed. Channel coefficients are allowed

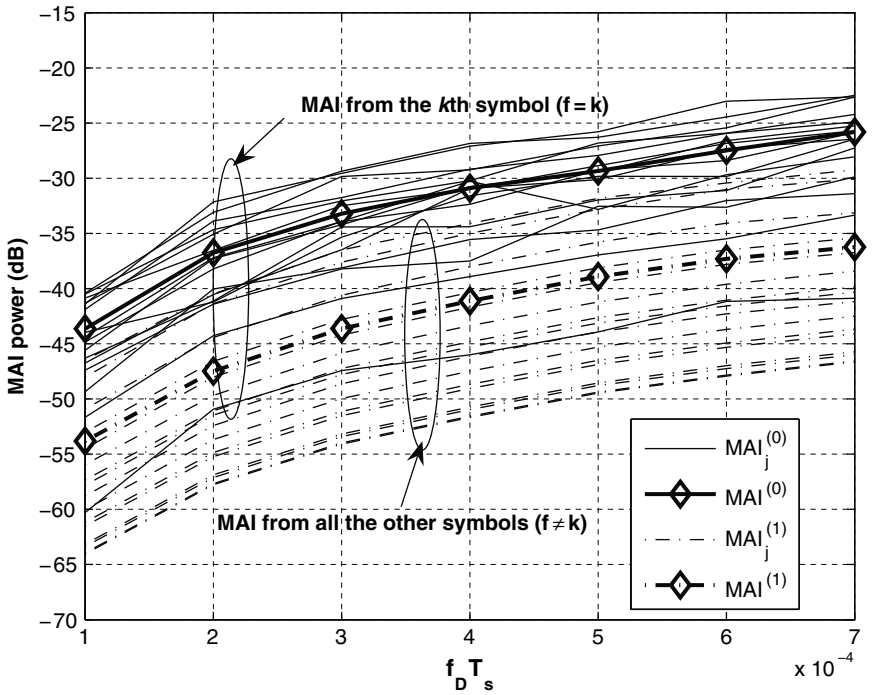

Fig. 5.34. The dominating and the residual MAI curves as a function of the normalized Doppler frequency [[125] ©IEEE].

to change during one OFDM block, and they have the Rayleigh distribution with an unit variance at the same path but different time indices.

The average dominating MAI for user j from all other users, denoted by $\overline{MAI}_j^{(0)}$ and $\overline{MAI}_j^{(1)}$, respectively, are calculated as explained in Example 5.8.

The total MAI is plotted as a function of the maximum normalized Doppler frequency in Fig. 5.34, where $\overline{MAI}_j^{(0)}$ and $\overline{MAI}_j^{(1)}$ of all 16 users are shown by 16 solid curves and 16 dashed curves, respectively. The solid bold curve in Fig. 5.34, denoted by $\overline{MAI}^{(0)}$, is the average value of 16 solid curves and obtained by $\frac{1}{T}\sum_{j=1}^{T}\overline{MAI}_j^{(0)}$. Similarly, the dashed bold curve, denoted by $\overline{MAI}^{(1)}$, is the average value of 16 dashed curves and obtained by $\frac{1}{T}\sum_{j=1}^{T}\overline{MAI}_j^{(0)}$. We see from this figure that the average $\overline{MAI}^{(0)}$ is about 10 dB more than the average $\overline{MAI}^{(1)}$. Thus, we can view $\overline{MAI}^{(0)}$ and $\overline{MAI}^{(1)}$ as the dominating MAI and the residual MAI, respectively, as they are in CFO environment.

Similar to the MAI caused by CFO, the dominating MAI due to the Doppler spread can be reduced to a negligible amount if only $M/2$ symmetric or anti-symmetric codewords of M Hadamard-Walsh codewords are used as the following theorem will demonstrates.

Proposition 5.5: Suppose that only the $M/2$ symmetric or the $M/2$ anti-symmetric codewords of M Hadamard-Walsh codewords are used. Then $MAI_{j\leftarrow i}^{(0)}[k]$ is approximately zero if the normalized Doppler frequency is less than $1/(2\pi NM)$.

Proof. From Lemma 5.5, $\sum_{p=1}^{M-1}\sum_{q=0}^{M-1-p} w_i[p+q]w_j[q] = 0$, $i \neq j$. Then, we can rewrite Eq. (5.138) such that it includes this term. To do so, again we can use the equality

$$\sum_{u=0,u\neq v}^{M-1}\sum_{v=0}^{M-1}\alpha(u-v)w_i[u]w_j[v] = \sum_{p=1}^{M-1}\left\{\alpha(p)\sum_{q=0}^{M-1-p} w_i[p+q]w_j[q] + \alpha(-p)\sum_{q=0}^{M-1-p} w_i[q]w_j[p+q]\right\}, \quad (5.139)$$

where $\alpha(.)$ can be any function. Note that if $i \neq j$ in the above equation, we have

$$\sum_{u=0}^{M-1}\sum_{v=0}^{M-1}\alpha(u-v)w_i[u]w_j[v] = \sum_{u=0,u\neq v}^{M-1}\sum_{v=0}^{M-1}\alpha(u-v)w_i[u]w_j[v]. \quad (5.140)$$

Let $\alpha(u-v) = e^{-j\frac{2\pi}{NM}(v-u)n}$. Using the properties of symmetric and anti-symmetric codewords given in Eqs. (5.85) and by using Eqs. (5.139), (5.140), $\eta_{i,j}(n)$ can be rewritten as

$$\eta_{i,j}(n) = \frac{2}{M} \sum_{p=1}^{M-1} \sum_{q=0}^{M-1-p} w_i[p+q] w_j[q] \cos(\frac{2\pi}{NM} pn), \quad i \neq j. \tag{5.141}$$

By substituting the above equation in Eq. (5.138) and making some rearrangement, we can obtain the averaged power of $MAI_{j\leftarrow i}^{(0)}[k]$ as

$$E\left\{ \left| MAI_{j\leftarrow i}^{(0)}[k] \right|^2 \right\} = L(\frac{2\sigma_d \sigma_{x_i}}{NM^2})^2 \sum_{p=1}^{M-1} \sum_{q=0}^{M-1-p} w_i[p+q] w_j[q] \cdot \left\{ \sum_{r=1}^{M-1} \sum_{s=0}^{M-1-r} w_i[r+s] w_j[s] \rho(p,r) \right\}, \tag{5.142}$$

where

$$\rho(p,r) = \sum_{n,m=0}^{NM-1} J_0\left(2\pi f_D T_s (n-m)\right) \cos(\frac{2\pi}{NM} pn) \cos(\frac{2\pi}{NM} rm). \tag{5.143}$$

Now, we need to show that $\rho(p,r)$ is a constant function so that

$$E\left\{ \left| MAI_{j\leftarrow i}^{(0)}[k] \right|^2 \right\} \simeq 0, \quad \text{for} \quad f_D T_s < \frac{1}{2\pi NM}.$$

The zeroth order Bessel function of the first kind can be expanded by the following power series [2]

$$J_0(z) = 1 - \frac{\frac{1}{4}z^2}{(1!)^2} + \frac{(\frac{1}{4}z^2)^2}{(2!)^2} - \frac{(\frac{1}{4}z^2)^3}{(3!)^2} + \cdots. \tag{5.144}$$

As shown in Fig. 5.35, when $0 < f_D T_s < \frac{1}{2\pi NM}$ (or equivalently $0 < 2\pi f_D T_s (n-m) < 1$), we can approximate $J_0(z)$ for $0 < z < 1$ by $1 - \frac{\frac{1}{4}z^2}{(1!)^2}$. By substituting this approximation for $J_0\left\{2\pi f_D T_s (n-m)\right\}$ with $0 \leq n-m \leq NM$, we obtain

$$J_0\left(2\pi f_D T_s (n-m)\right) \simeq \left(1 - \pi^2 (f_D T_s)^2 (n-m)^2\right), \quad f_D T_s < \frac{1}{2\pi NM}. \tag{5.145}$$

Based on the above approximation, we can express $\rho(p,r)$ in Eq. (5.142) as

$$\begin{aligned} \rho(p,r) \simeq & \sum_{n=0}^{NM-1} \sum_{m=0}^{NM-1} \cos(\frac{2\pi}{NM} pn) \cos(\frac{2\pi}{NM} rm) \\ & - (\pi f_D T_s)^2 \sum_{n=0}^{NM-1} n^2 \cos(\frac{2\pi}{NM} pn) \sum_{m=0}^{NM-1} \cos(\frac{2\pi}{NM} rm) \\ & - (\pi f_D T_s)^2 \sum_{n=0}^{NM-1} \cos(\frac{2\pi}{NM} pn) \sum_{m=0}^{NM-1} m^2 \cos(\frac{2\pi}{NM} rm) \\ & + 2(\pi f_D T_s)^2 \sum_{n=0}^{NM-1} n \cos(\frac{2\pi}{NM} pn) \sum_{m=0}^{NM-1} m \cos(\frac{2\pi}{NM} rm). \end{aligned} \tag{5.146}$$

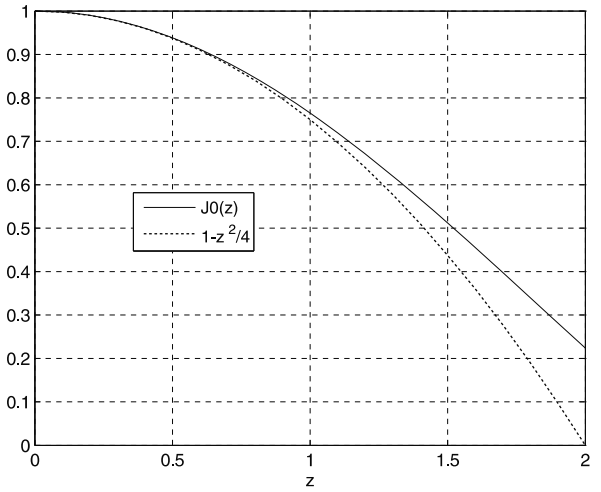

Fig. 5.35. Approximation of $J_0(z)$ by $1 - \frac{\frac{1}{4}z^2}{(1!)^2}$ for $z < 1$ [[125] ©IEEE].

It can easily be shown that $\sum_{n=0}^{NM-1} \cos(\frac{2\pi}{NM}pn) = \sum_{m=0}^{NM-1} \cos(\frac{2\pi}{NM}rm) = 0$. Also, we know from [108] that

$$\sum_{k=0}^{n-1} k\cos(kx) = \frac{n\sin(\frac{2n-1}{2}x)}{2\sin(\frac{x}{2})} - \frac{1-\cos(nx)}{4\sin^2(\frac{x}{2})}, \quad x \neq 0. \tag{5.147}$$

Therefore, for $p = 1, 2, \cdots M-1$, and $r = 1, 2, \cdots, M-1$, we get

$$\begin{aligned}\sum_{m=0}^{NM-1} m\cos(\frac{2\pi}{NM}rm) &= \sum_{n=0}^{NM-1} n\cos(\frac{2\pi}{NM}pn) \\ &= \frac{NM\sin(\frac{2NM-1}{2}\frac{2\pi}{NM}p)}{2\sin(\frac{\pi}{NM}p)} - \frac{1-\cos(2\pi p)}{4\sin^2(\frac{\pi}{NM}p)} \\ &= \frac{NM}{2}\frac{\sin(2\pi p - \frac{p\pi}{NM})}{\sin(\frac{p\pi}{NM})} = -\frac{NM}{2}. \end{aligned} \tag{5.148}$$

By plugging the above expression in Eq. (5.146),

$$\rho(p,r) \simeq 2\pi^2(f_D T_s)^2(\frac{NM}{2})^2,$$

which is independent of p and r. By substituting this approximate value of $\rho(p,r)$ back to Eq. (5.142), we obtain

$$E\left\{\left|MAI_{j\leftarrow i}^{(0)}[k]\right|^2\right\} \simeq 2L(\frac{\pi f_D T_s \sigma_d \sigma_{x_i}}{M})^2 \sum_{p=1}^{M-1}\sum_{q=0}^{M-1-p} w_i[p+q]w_j[q] \cdot \left\{\sum_{r=1}^{M-1}\sum_{s=0}^{M-1-r} w_i[r+s]w_j[s]\right\}. \quad (5.149)$$

It was shown in Lemma 5.5 that $\sum_{p=1}^{M-1}\sum_{q=0}^{M-1-p} w_i[p+q]w_j[q] = 0$, if the symmetric or anti-symmetric Hadamard-Walsh codewords are used. Therefore, the dominating MAI is approximately reduced to

$$E\left\{\left|MAI_{j\leftarrow i}^{(0)}[k]\right|^2\right\} \simeq 0, \quad \text{if } f_D T_s < \frac{1}{2\pi NM}. \quad (5.150)$$

Example 5.18: Suppression of the Dominating MAI in Time-Varying Flat Fading Channel with Code Selection Scheme
We consider the same set of parameters as Example 5.17 and show how employing only $M/2$ symmetric or $M/2$ antisymmetric Hadamard-Walsh codewords can suppress $\overline{MAI}^{(0)}$. Figure 5.36 shows the choosing only $M/2$ symmetric or $M/2$ anti-symmetric Hadamard-Walsh codewords greatly suppresses the dominating MAI. The simulation parameters were the same as those adopted for Fig. 5.34.

By comparing results in this figure and Fig. 5.34, we see that the dominating MAI is reduced by 35–58 dB. In contrast, the residual MAI is only decreased by 5–6 dB due to the decreased user number from 16 to 8. The results confirm that the dominating MAI can be greatly reduced using only $M/2$ symmetric or $M/2$ anti-symmetric codewords so that the total MAI, which is equal to $\overline{MAI}^{(0)} + \overline{MAI}^{(1)}$, is reduced considerably.

In a practical mobile environment, $f_D T_s < \frac{1}{2\pi NM}$ is equivalent to a wide range of normalized Doppler frequency.

Let us consider an example. If $N = 64$ and $M = 16$, PMU-OFDM approximately MAI-free when the normalized maximum frequency is less than 1.5×10^{-4}. For the carrier frequency $f_c = 4$ GHz and the sampling frequency $F_s = \frac{1}{T_s} = 2$ MHz, this maximum Doppler frequency is equivalent to a mobile speed of 81 km/h.

5.5.4 Analysis of Doppler ICI and Symbol Distortion

We studied the interference caused by other users' Doppler effect, namely Doppler MAI in previous section. Here, we investigate the impairment caused by user's self Doppler effect. These effects are symbol distortion and self ICI effect.

If we assume there is no active user except for user j, then by letting $i = j$ in Eq. (5.133), the kth detected symbol of user j is given by

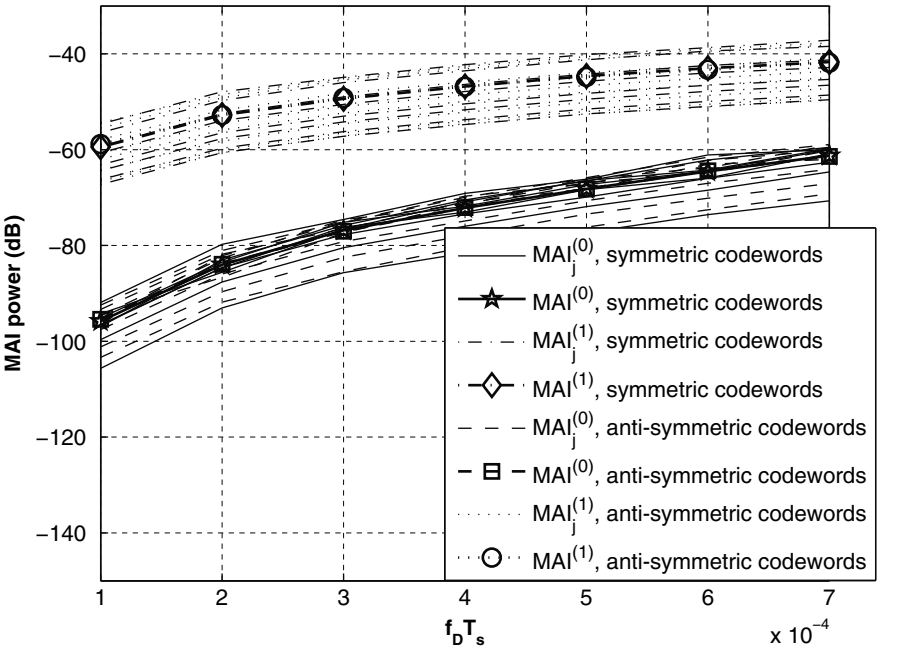

Fig. 5.36. The dominating and residual MAI versus the normalized Doppler frequency when only $M/2$ symmetric or anti-symmetric Hadamard-Walsh codewords are used [[125] ©IEEE].

$$\hat{x}_j[k] = \sum_{f=0}^{N-1} x_j[f] \frac{1}{NM} \sum_{n=0}^{NM-1} \sum_{d=0}^{L-1} g_j(n;d)\zeta_{j,j}(n,d) e^{-j\frac{2\pi}{NM}(fM)d} e^{-j\frac{2\pi}{N}(k-f)n} + \hat{e}[k]. \tag{5.151}$$

We can rewrite Eq. (5.151) as

$$\hat{x}_j[k] = x_j[k]H_j[k] + ICI_j^{(0)}[k] + ICI_j^{(1)}[k] + \hat{e}[k], \tag{5.152}$$

where $H_j[k]$, $ICI_j^{(0)}[k]$, and $ICI_j^{(1)}[k]$ are discussed below. The distortion factor $H_j[k]$, is obtained by putting $f = k$ and $u = v$ in $\zeta_{j,j}(n,d)$ in Eq. (5.151), i.e.,

$$H_j[k] = \frac{1}{NM} \sum_{n=0}^{NM-1} \sum_{d=0}^{L-1} g_j(n;d) \frac{1}{M} \sum_{v=0}^{M-1} e^{-j\frac{2\pi}{NM}(v+kM)d}, \tag{5.153}$$

for $0 \le v \le M-1$ and $0 \le d \le L-1$.

The term $ICI_j^{(0)}[k]$ in Eq. (5.152) is the interference from subcarriers with $f = k$ and $u \ne v$ to the desired subcarrier $f = k$; namely,

$$ICI_j^{(0)}[k] = x_j[k]\frac{1}{NM}\sum_{n=0}^{NM-1}\sum_{d=0}^{L-1} g_j(n;d) \cdot \left\{\{\zeta_{j,j}(n,d)|_{u\neq v}\}e^{-j\frac{2\pi}{NM}(kM)d}\right\}, \tag{5.154}$$

and $ICI_j^{(1)}[k]$ in Eq. (5.152) is the sum of all interferences from subcarriers $f \neq k$, i.e.,

$$ICI_j^{(1)}[k] = \sum_{f=0,f\neq k}^{N-1} x_j[f]\frac{1}{NM}\sum_{n=0}^{NM-1}\sum_{d=0}^{L-1} g_j(n;d) \cdot \left\{\zeta_{j,j}(n,d)e^{-j\frac{2\pi}{NM}(fM)d}e^{-j\frac{2\pi}{N}(k-f)n}\right\}. \tag{5.155}$$

The averaged power of $ICI_j^{(0)}[k]$ can be obtained in a manner similar to that in deriving the MAI averaged power in Eq. (5.136) as

$$E\left\{\left|ICI_j^{(0)}[k]\right|^2\right\} = L(\frac{\sigma_d\sigma_{x_j}}{NM})^2\sum_{n,m=0}^{NM-1} J_0\left(2\pi f_D T_s(n-m)\right) \cdot \left\{\{\eta_{j,j}(n)|_{u\neq v}\}\{\eta_{j,j}^*(m)|_{u\neq v}\}\right\}. \tag{5.156}$$

We can rewrite Eq. (5.139) for $i = j$ as

$$\sum_{u,v=0,u\neq v}^{M-1}\alpha(u-v)w_j[u]w_j[v] = \sum_{p=1}^{M-1}\left\{\{\alpha(p)+\alpha(-p)\}\sum_{q=0}^{M-1-p} w_j[p+q]w_j[q]\right\}.$$

Let $\alpha(u-v) = e^{-j\frac{2\pi}{NM}(v-u)n}$. Then,

$$\eta_{j,j}(n)|_{u\neq v} = \frac{2}{M}\sum_{p=1}^{M-1}\sum_{q=0}^{M-1-p} w_j[p+q]w_j[q]\cos(\frac{2\pi}{NM}pn). \tag{5.157}$$

By substituting the above equation in Eq. (5.156) and using the approximate formula Eq. (5.145) for the Bessel function and Eq. (5.148), we have

$$E\left\{\left|ICI_j^{(0)}[k]\right|^2\right\} \simeq 2L(\frac{\pi f_D T_s\sigma_d\sigma_{x_j}}{M})^2\sum_{p=1}^{M-1}\sum_{q=0}^{M-1-p} w_j[p+q]w_j[q] \cdot \left\{\sum_{r=1}^{M-1}\sum_{s=0}^{M-1-r} w_j[r+s]w_j[s]\right\}. \tag{5.158}$$

To find the double summation term in Eq. (5.158), we note

$$\sum_{p=1}^{M-1}\sum_{q=0}^{M-1-p} w_j[p+q]w_j[q] = \frac{1}{2}\sum_{u,v=0,u\neq v}^{M-1} w_j[u]w_j[v]$$
$$= \frac{1}{2}\sum_{u=0}^{M-1} w_j[u]\sum_{v=0}^{M-1} w_j[v] - \frac{1}{2}\sum_{u=0}^{M-1} w_j^2[u].$$

Since $\sum_{u=0}^{M-1} w_j[u]$ is equal to M for the all-one codeword and is 0 for all other codewords, we have

$$\sum_{p=1}^{M-1}\sum_{q=0}^{M-1-p} w_j[p+q]w_j[q] = \begin{cases} M(M-1)/2, & all-one code, \\ -M/2, & otherwise. \end{cases} \quad (5.159)$$

From Eqs. (5.158) and (5.159),

$$E\left\{\left|ICI_j^{(0)}[k]\right|^2\right\} \simeq \frac{L}{2}(\pi f_D T_s \sigma_d \sigma_{x_j})^2,$$

when the all-one codeword is not used and $f_D T_s < 1/(2\pi NM)$. On the other hand, if the all-one codeword is used, we have

$$E\left\{\left|ICI_j^{(0)}[k]\right|^2\right\} \simeq \frac{L}{2}(\pi f_D T_s \sigma_d \sigma_{x_j}(M-1))^2.$$

Also, if $f_D T_s < 1/(2\pi NM)$, then $E\left\{\left|ICI_j^{(0)}[k]\right|^2\right\} < \frac{L\sigma_d^2\sigma_{x_j}^2}{8N^2}$ for the all-one codeword and $E\left\{\left|ICI_j^{(0)}[k]\right|^2\right\} < \frac{L\sigma_d^2\sigma_{x_j}^2}{8N^2M^2}$ for other codewords.

The averaged power of $ICI_j^{(1)}[k]$ can also be computed as

$$E\left\{\left|ICI_j^{(1)}[k]\right|^2\right\} = L(\frac{\sigma_d\sigma_{x_j}}{NM})^2 \sum_{f=0,f\neq k}^{N-1}\sum_{n,m=0}^{NM-1} J_0\left(2\pi f_D T_s(n-m)\right)$$
$$\cdot \left\{\eta_{j,j}(n)\eta_{j,j}^*(m)e^{-j\frac{2\pi}{N}(k-f)(n-m)}\right\}. \quad (5.160)$$

As compared with the averaged power of $ICI_j^{(1)}[k]$, the averaged power of $ICI_j^{(0)}[k]$ is negligible for all codewords for practical values of N and L. This can be clearly explained by the following example.

Example 5.19: Doppler ICI
Let us consider an example. Let $N = 64$, $L = 4$, $M = 16$. The maximum Doppler frequency was chosen to be 10^{-4}, which corresponds to the user speed of 54 km/h. Also, $\sigma_d^2 = \sigma_{x_j}^2 = 1$. Then, $E\left\{\left|ICI_j^{(0)}[k]\right|^2\right\} \simeq -40.5$ dB for the all-one codeword, and $E\left\{\left|ICI_j^{(0)}[k]\right|^2\right\} \simeq -64$ dB for other codewords.

Using Eq. (5.160) and the same set of parameters, we can compute the value of $E\left\{\left|ICI_j^{(1)}[k]\right|^2\right\}$ to be about $-10\,\text{dB}$ for the user with the all-one codeword dB, and between $-25\,\text{dB}$ and $-50\,\text{dB}$ for all other users. Clearly, $E\left\{\left|ICI_j^{(1)}[k]\right|^2\right\}$ is much larger than the corresponding values of $E\left\{\left|ICI_j^{(0)}[k]\right|^2\right\}$. Since $ICI_j^{(1)}[k]$ is the dominant ICI, we only need to consider this ICI effect and ignore $ICI_j^{(0)}[k]$.

Figure 5.37 shows the average ICI power for each individual Hadamard-Walsh codeword used in PMU-OFDM. For the kth symbol of the target user, we accumulate the ICI from all other symbols $f \neq k$ of the same user. The average ICI power is then averaged for $0 \leq k \leq N-1$; namely, $\overline{ICI}_j^{(1)} = \frac{1}{N}\sum_{k=0}^{N-1}\left|ICI_j^{(1)}[k]\right|^2$.

We see that different users experience a different amount of ICI. Especially, the user that employs the all-one codeword suffers more ICI than all others by 15–40 dB. Intuitively, if a codeword has more sign changes, the main lobes of interfering subcarriers may cancel each other so that the ICI power is

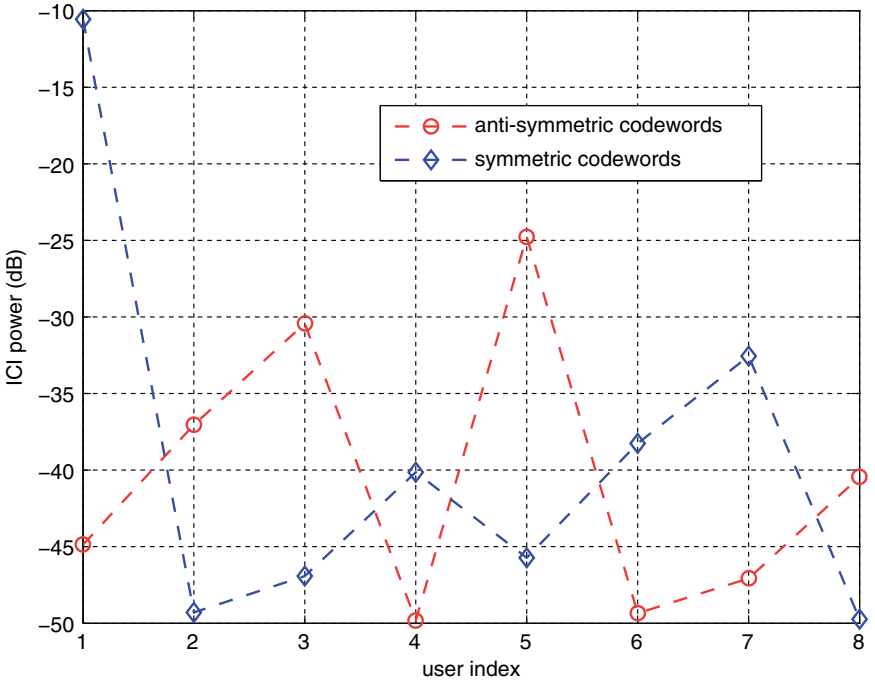

Fig. 5.37. The $ICI^{(1)}$ power as a function of user index for symmetric and anti-symmetric codewords with $f_D T_s = 1 \times 10^{-4}$ [[125] ©IEEE].

decreased. This is similar to the self-ICI cancellation technique used to mitigate ICI in OFDM [157]. Since the all-one codeword belongs to the set of symmetric Hadamard-Walsh codewords, we recommend to choose the set of anti-symmetric Hadamard-Walsh since they have the approximately MAI-free and a lower average ICI power at the same time.

5.5.5 Codeword Priority Schemes for ICI Cancellation

Since $ICI_j^{(1)}[k]$ is the dominant ICI due to the Doppler spread effect, we would like to further investigate this term in this section. It is found that codewords with a higher number of sign changes tend to lead to a smaller ICI value. This can be explained as follows. Based on the combination of u and v values, the expression $\eta_{j,j}(n)\eta_{j,j}^*(m)$ in Eq. (5.160) can be written as the sum of four terms:

$$\begin{aligned}\eta_{j,j}(n)\eta_{j,j}^*(m) = &\{\eta_{j,j}(n)|_{u=v}\}\{\eta_{j,j}^*(m)|_{u=v}\} + \{\eta_{j,j}(n)|_{u=v}\}\{\eta_{j,j}^*(m)|_{u\neq v}\} \\ &+ \{\eta_{j,j}(n)|_{u\neq v}\}\{\eta_{j,j}^*(m)|_{u=v}\} + \{\eta_{j,j}(n)|_{u\neq v}\}\{\eta_{j,j}^*(m)|_{u\neq v}\}.\end{aligned}$$

Let $r_{j,j}[p] = \sum_{q=0}^{M-1-p} w_j[p+q]w_j[q]$, $1 \le p \le M-1$. Since $\{\eta_{j,j}(n)|_{u=v}\} = 1$, and by using Eq. (5.157), $E\left\{\left|ICI_j^{(1)}[k]\right|^2\right\}$ can be written as

$$\begin{aligned}E\left\{\left|ICI_j^{(1)}[k]\right|^2\right\} = L(\frac{\sigma_d\sigma_{x_j}}{NM})^2 \sum_{f=0,f\neq k}^{N-1} \Bigg\{ &\sum_{n,m=0}^{NM-1} J_0\left(2\pi f_D T_s(n-m)\right) e^{-j\frac{2\pi}{N}(k-f)(n-m)} \Bigg[\\ &+ \frac{2}{M}\sum_{p=1}^{M-1} r_{j,j}[p]\cos(\frac{2\pi}{NM}pn) + \frac{2}{M}\sum_{p=1}^{M-1} r_{j,j}[p]\cos(\frac{2\pi}{NM}pm) \\ &+ \frac{4}{M^2}\left|\sum_{p=1}^{M-1} r_{j,j}[p]\right|^2 \cos(\frac{2\pi}{NM}pn)\cos(\frac{2\pi}{NM}pm)\Bigg]\Bigg\}.\end{aligned}$$

Define

$$\beta(p, k-f) = \sum_{n=0}^{NM-1} ne^{-j\frac{2\pi}{N}(k-f)n}\cos(\frac{2\pi}{NM}pn),$$

and

$$\gamma(k-f) = \sum_{n=0}^{NM-1} ne^{-j\frac{2\pi}{N}(k-f)n}.$$

Since

$$\sum_{n=0}^{NM-1} e^{-j\frac{2\pi}{N}(k-f)n} = \sum_{n=0}^{NM-1} e^{-j\frac{2\pi}{N}(k-f)n}\cos(\frac{2\pi}{NM}pn) = 0,$$

for $p = 1, 2, ...M-1$, and $k - f = -2N, ..., -1, 1, ...2N$, and by using the approximate formula Eq. (5.145), we can express the average ICI power for $0 < f_D T_s < \frac{1}{2\pi NM}$ by

$$E\left\{\left|ICI_j^{(1)}[k]\right|^2\right\} \simeq 2L(\frac{\pi(f_D T_s)\sigma_d\sigma_{x_i}}{NM})^2 \sum_{f=0,f\neq k}^{N-1}\left\{|\gamma(k-f)|^2 + \frac{4}{M}\Re\{\gamma^*(k-f)\sum_{p=1}^{M-1} r_{j,j}[p]\beta(p,k-f)\} + \frac{4}{M^2}\left|\sum_{p=1}^{M-1} r_{j,j}[p]\beta(p,k-f)\right|^2\right\}, \quad (5.161)$$

where $\Re\{.\}$ denotes the real part. It was proven in [125] that the real part of $\beta(p, k-f)$ is equal to $-NM/2$. Based on this result, we can rewrite the ICI averaged power as

$$E\left\{\left|ICI_j^{(1)}[k]\right|^2\right\} \simeq 2L(\frac{\pi(f_D T_s)\sigma_d\sigma_{x_i}}{NM})^2 \sum_{f=0,f\neq k}^{N-1}\left\{|\gamma(k-f)|^2 + \frac{4}{M}\Re\left\{\gamma^*(k-f)\left[\text{ø} + \sum_{p=1}^{M-1} r_{j,j}[p]\Im\{\beta(p,k-f)\}\right]\right\} + \frac{4}{M^2}\left|\text{ø} + \sum_{p=1}^{M-1} r_{j,j}[p]\Im\{\beta(p,k-f)\}\right|^2\right\}, \quad (5.162)$$

where $\Im\{.\}$ is the imaginary part and ø can be obtained by Eq. (5.159) as

$$\text{ø} = \begin{cases} \frac{-(M-1)M^2N}{4}, & \text{all-one codeword,} \\ \frac{M^2N}{4}, & \text{otherwise.} \end{cases}$$

The quantity, $r_{j,j}[p]\sum_{q=0}^{M-1-p} w_j[p+q]w_j[q]$, $1 \le p \le M-1$ will appear again. $r_{j,j}[p]$ can be interpreted as the autocorrelation of codeword j. Since $\Im\{\beta(p,k-f)\}$ is a monotonically decreasing or increasing function of p for given $k-f$ as shown in [125], we can characterize the ICI values qualitatively by $r_{j,j}[p]$ based on Eq. (5.162).

If $r_{j,j}[p]$, $1 \le p \le M-1$, has a sufficient number of sign changes, the term $\sum_{p=1}^{M-1} r_{j,j}[p]\Im\{\beta(p,k-f)$ in Eq. (5.162) is likely to be cancelled out after the summation over all p, which leads to a smaller ICI value. Since $r_{j,j}[p] = \sum_{q=0}^{M-1-p} w_j[p+q]w_j[q]$, for $1 \le p \le M-1$, there is a relation between the number of sign changes in the codewords and the number of sign changes in $r[p]$.

Let us consider an example for codewords of size $M = 8$.

- For the all-one codeword: $(1, 1, 1, 1, 1, 1, 1, 1)$, $r_{1,1}[p] = (seven\ 6\ 5\ 4\ 3\ 2\ 1)$ and has no sign change.

- For the second codeword: (1 -1 1 -1 1 -1 1 -1) with seven sign changes, $r_{2,2}[p]$ = (-7 6 -5 4 -3 2 -1) that has six sign changes.

- For the 7th codeword: (1 1 -1 -1 -1 -1 1 1), $r_{7,7}[p]$ = (3 -2 -3 -4 -1 2 1) and they both have two sign changes.

With the above observation, we can adopt the following rule of thumb for codeword selection in a PMU-OFDM system: "To give a higher priority to codewords that have a higher number of sign-changes". This result is similar to PMU-OFDM in the presence of a pure CFO environment [134].

Example 5.19: Code Priority for ICI in Doppler Environment
In this example, we corroborate the code priority analysis given above for ICI power of PMU-OFDM system in Doppler environment via computer simulation.

The ICI power for 16 codewords is shown in Table 5.3, where the corresponding number of sign changes is also provided. System parameters are chosen to be $N = 64$, $M = 16$, and $L = 4$. The maximum normalized Doppler frequency and the SNR value were fixed at 10^{-4} and 30 dB, respectively.

We see that as a general trend, codewords with more sign changes have less ICI. This observation verifies the theoretical result stated above.

Example 5.20: Performance Comparison of PMU-OFDM to OFDMA in Doppler Environment
Here, we compare the performance of the PMU-OFDM and the OFDMA systems via computer simulations. For fair comparison, we keep the size of IDFT/DFT of both systems the same, i.e., NM, and consider both fully loaded and half-loaded situations. To simulate the half-loaded PMU-OFDM system, the set of anti-symmetric (or symmetric) Hadamard-Walsh codewords is used. The subchannel for a fully loaded and half-loaded OFDMA systems, are assigned in the same manner as Examples 5.10 and 5.11 for the half-loaded OFDMA.

Table 5.3. The ICI averaged power in dB for 16 users [[125] ©IEEE].

# sign changes	0	2	4	6	8	10	12	14
ICI of symmetric codewords (dB)	−10.6	−32.5	−40.2	−38.4	−49.4	−49.9	−46.9	−45.8
# sign changes	1	3	5	7	9	11	13	15
ICI of anti-symmetric codewords (dB)	−24.8	−30.5	−40.5	−37.1	−49.6	−49.8	−47.2	−45.0

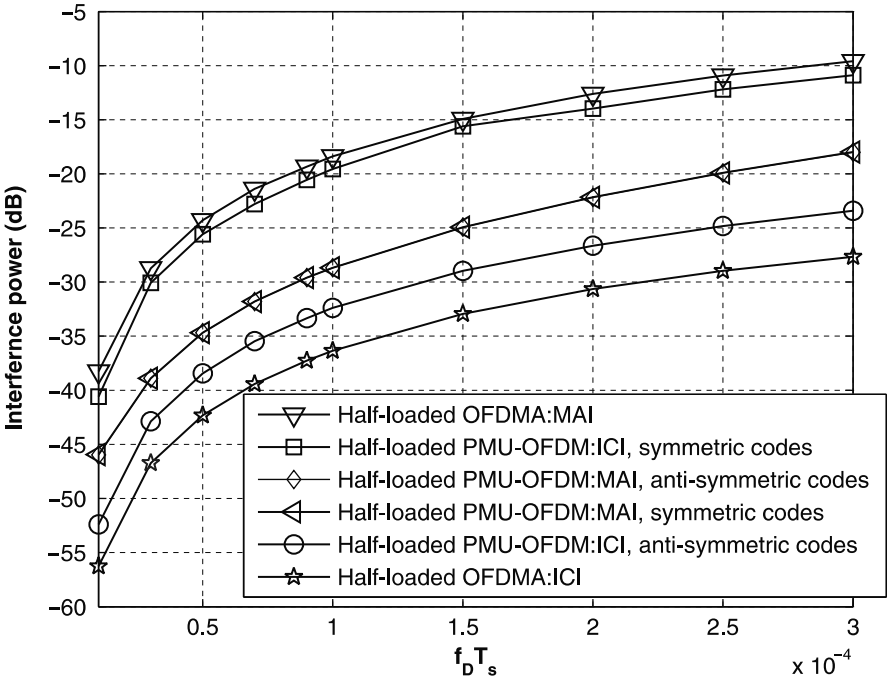

Fig. 5.38. Comparison of the MAI power and the ICI power as a function of the normalized Doppler frequency [[125] ©IEEE].

First, let us see how the MAI and ICI of half-loaded PMU-OFDM compares with that of OFDMA as functions of the normalized Doppler frequency. Let $N = 64$, $M = 16$, and $L = 4$. The ICI power and the MAI power for OFDMA and PMU-OFDM are depicted versus maximum normalized Doppler frequency as in Fig. 5.38. The average ICI power is the averaged value of eight multiple access users (i.e., $T = 8$). The first observation is that the second largest amount of interference is the ICI of PMU-OFDM with only symmetric codewords. The reason should be obvious from our previous discussion in Section 5.5.5. That is, the all-one codeword in the set of symmetric codewords has a high ICI value as compared to the ICI or the MAI of all other users.

On the other hand, the ICI value of PMU-OFDM with the set of anti-symmetric Hadamard-Walsh codewords is about 4 dB more than that of OFDMA. The inferior ICI performance of PMU-OFDM compared to that of OFDMA is explained by noting the subcarriers allocation we adopted for OFDMA. That is, subcarriers allocated to a particular user in OFDMA are spread uniformly across the available bandwidth. Hence, ICI results in less impairment in OFDMA than in a single-user OFDM.

However, for OFDMA, the MAI power is significantly higher than that of PMU-OFDM. As shown in Fig. 5.38, we observe that the MAI value of

PMU-OFDM with either symmetric or anti-symmetric Hadamard-Walsh codewords is about 10 dB less than that of OFDMA. Thus, we expect PMU-OFDM with only anti-symmetric codewords to outperform OFDMA in the bit error probability.

Next, we consider the BEP performance of six systems: fully-loaded PMU-OFDM, fully-loaded OFDMA, half-loaded PMU-OFDM with symmetric codewords, half-loaded PMU-OFDM with anti-symmetric codewords, PMU-OFDM with symmetric codewords, excluding the all-one codeword and half-loaded OFDMA.

Under the setting of $N = 64$, $M = 16$, $L = 4$, and $\frac{E_b}{N_0} = 30\,\text{dB}$, simulation results on the BEP are shown in Fig. 5.39, where the BEP performance is plotted as a function of the Doppler frequency for the above systems.

For this example, we assume that perfect channel knowledge is available at the receiver. A frequency equalizer can be used to compensate the symbol distortion effect, i.e., the detected symbol $\hat{x}_j[k]$ is multiplied by $(H_j[k])^{-1}$. Thus, both systems only suffer from MAI and ICI.

We see that fully-loaded PMU-OFDM and fully-loaded OFDMA have comparable performance for $f_D T_s \geq 10^{-4}$. For $f_D T_s < 10^{-4}$ that corresponds to the mobile speed of 54 km/h with respect to our chosen parameters, OFDMA

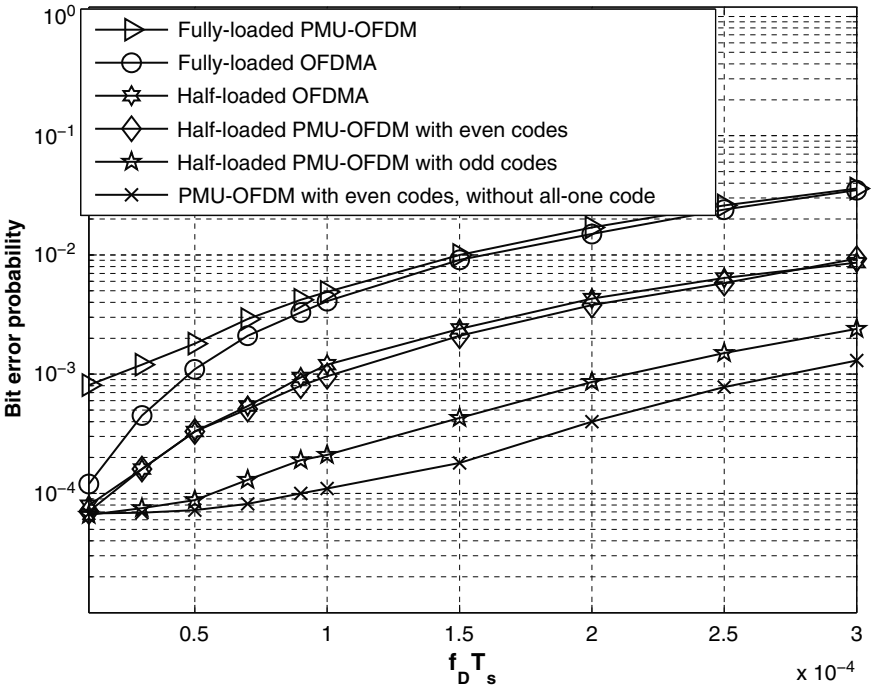

Fig. 5.39. The BEP comparison for PMU-OFDM and OFDMA as a function of the normalized Doppler frequency [[125] ©IEEE].

outperforms PMU-OFDM. This is no surprise since as we saw in previous sections of this chapter, OFDMA is MAI-free if time or frequency asynchronism is negligible.

For half-loaded systems, we see that PMU-OFDM with anti-symmetric codewords results in much better BEP performance than PMU-OFDM with symmetric codewords and OFDMA in the Doppler environment with the maximum normalized Doppler frequency ranging from 1×10^{-5} to 3×10^{-4}. This Doppler frequency range corresponds to a mobile speed between 5.4 km/h and 162 km/h. As explained before, the poorer performance of half-loaded PMU-OFDM with symmetric codewords is due to high ICI of the user with the all-one codeword. Thus, if we exclude the all-one codeword, PMU-OFDM with seven symmetric codewords outperforms all other systems as shown in Fig. 5.39.

Finally, we examine how PMU-OFDM and OFDMA perform when the active number of users varies from 1 to $T = M$. The codeword priority scheme for PMU-OFDM is stated below. When the system load is less than 50%, we use codewords with a higher number of sign changes among the $M/2$ anti-symmetric codewords. When the system load is more than 50%, we choose all $M/2$ anti-symmetric codewords plus an symmetric codeword pre-determined to have a low average ICI value based on the results given in Table 5.3. The procedure is repeated until all 16 codewords are selected. The BEP results are plotted as functions of the user number for PMU-OFDM and OFDMA in Fig. 5.40.

From Fig. 5.40, we see that PMU-OFDMA significantly outperforms OFDMA in a lightly loaded (50% or less) system. When the system reaches its full loading, the BEP performance of PMU-OFDM and OFDMA becomes comparable.

5.5.6 Channel Estimation in Fast Time-Varying Channel

In the previous example, we assumed perfect channel knowledge at the receiver. However, in practice, we have only access to the estimates of channel coefficients.

From Eq. (5.153), if $NM \gg vd$, then $e^{-j\frac{2\pi}{NM}vd} \simeq 1$, $\frac{1}{M}\sum_{v=0}^{M-1} e^{-j\frac{2\pi}{NM}vd} \simeq 1$. Note that since $0 \le v \le M-1$, and $0 \le d \le L-1$, $NM \gg vd$ is equivalent to $N \gg L-1$. Therefore, $H_j[k]$ can be written as

$$H_j[k] \simeq \frac{1}{NM} \sum_{n=0}^{NM-1} \sum_{d=0}^{L-1} g_j(n;d) e^{-j\frac{2\pi}{N}kd}. \tag{5.163}$$

That is, for every time index n and any user j, we take the DFT of channel coefficient $g_j(n;d)$ over path d with frequency index k. The result is then

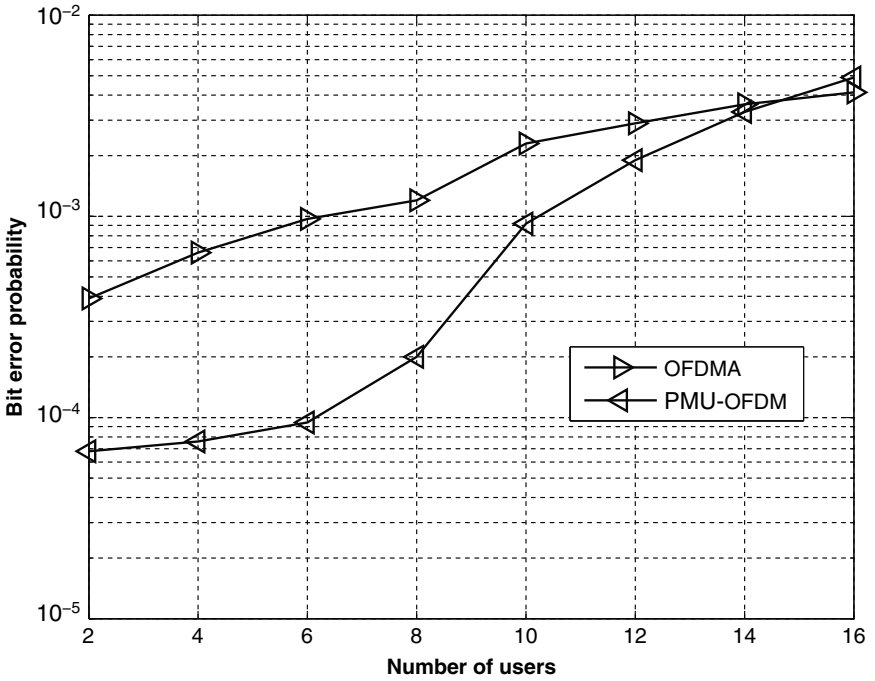

Fig. 5.40. The BEP performance comparison as a function of the user number for PMU-OFDM and OFDMA, where the codeword priority scheme is adopted for PMU-OFDM [[125] ©IEEE].

averaged over one OFDM symbol to yield $H_j[k]$. When $N \gg L-1$, another interpretation of $H_j[k]$ is

$$H_j[k] \simeq \sum_{d=0}^{L-1} g_j^{avg}(d) e^{-j\frac{2\pi}{N}kd}, \tag{5.164}$$

where $g_j^{avg}(d) = \frac{1}{NM}\sum_{n=0}^{NM-1} g_j(n;d)$ is the average of the dth channel tap over one OFDM block. Therefore, $H_j[k]$ represents the DFT of $g_j^{avg}(d)$. Often, subcarriers are much longer than the channel length and $H_j[k]$ can be computed from Eq. (5.153) or (5.153).

In Example 5.19, we ideally mitigated the symbol distortion effect in the receiver using a frequency domain equalizer whose one tap gain for user j is set to $(H_j[k])^{-1}$. In practice, we must obtain and estimate $(H_j[k])^{-1}$.

To this end, channels estimation for time-varying channel must be preformed. When the channel is time-varying within an OFDM block, the preamble-based training method may not work well. Periodic insertion of training symbols during transmission of every block has been suggested for OFDM in time-varying channels. It was shown in [93] that the best set of

frequency domain pilot tones are those which are equally spaced. We adopt this technique to estimate the fast fading channel. Let P be the number of equally spaced pilot tones at subchannels $\Lambda[k] = k \times N/P$, for $0 \leq k \leq P-1$. An estimate of $H_j[k]$ can be obtained at pilot tones via

$$\hat{H}_j[\Lambda[k]] = \frac{\hat{x}_j[\Lambda[k]]}{x_j[\Lambda[k]]} + \frac{(ICI^{(0)}[\Lambda[k]] + ICI^{(1)}[\Lambda[k]] + \hat{e}[\Lambda[k]])}{x_j[\Lambda[k]]}. \tag{5.165}$$

Then, the estimate of $g_j^{avg}(d)$ is obtained through an IDFT of length P as

$$\hat{g}_j^{avg}(d) = \frac{1}{P} \sum_{k=0}^{P-1} \hat{H}_j[\Lambda[k]] e^{\frac{j2\pi dk}{P}}. \tag{5.166}$$

More sophisticated algorithms were suggested to improve the channel estimation performance in a Doppler environment. For example, two ICI mitigation techniques were proposed in [90] to improve the channel estimation performance in the presence of the Doppler effect. Other channel estimation methods for OFDM in time-varying channels were reported in [73] and [71].

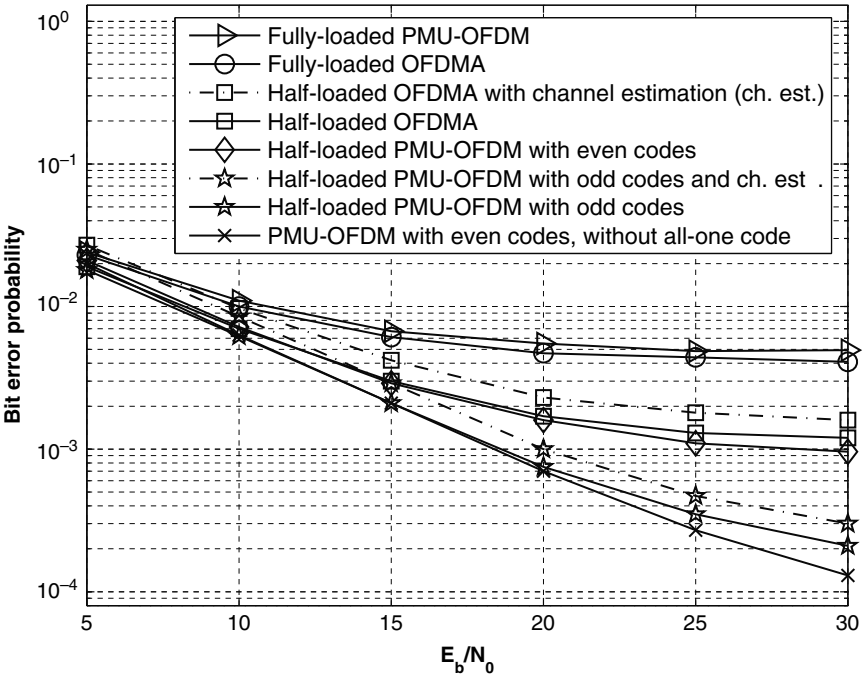

Fig. 5.41. The BEP comparison for PMU-OFDM and OFDMA as a function of the SNR value [[125] ©IEEE].

Example 5.21: Performance Comparison of PMU-OFDM to OFDMA with Non-Perfect Channel Estimation in Doppler Environment

By adopting $N = 64$ and $L = 4$, assume the channel length is much shorter than subcarriers and $H_j[k]$ can be computed from Eq. (5.153) or (5.153).

We consider the same six scenarios given in Fig. 5.39 in Example 5.19. and two more scenarios with channel estimation. The channel estimation was performed using Eqs. (5.165) and (5.166). We used eight pilots in every OFDM block. The BEP results of all eight scenarios are plotted in Fig. 5.41 as a function of the SNR value, $\frac{E_b}{N_0}$, with the maximum normalized Doppler frequency fixed at 10^{-4}.

For fully-loaded cases, the BEP curves of PMU-OFDM and OFDMA are close to each other. For half-loaded cases, the BEP curves of PMU-OFDM with symmetric codewords and OFDMA are also close with each other while PMU-OFDM with anti-symmetric codewords outperforms the above four cases considerably.

Excluding the all-one codeword, PMU-OFDM with seven symmetric codewords perform much better than half-load PMU-OFDM with all eight symmetric codewords due to the high ICI value of the user with all-one codeword. Also, we obseve from Fig. 5.41 that the channel estimation penalty is about 1.5–2.0 dB for $E_b/N_0 \leq 20$ dB. However, the performance gap between half-loaded PMU-OFDM with anti-symmetric codewords and half-loaded OFDMA remains the same with realistic channel estimation.

6

MAI-Free MC-CDMA System

6.1 Introduction

Multicarrier CDMA (MC-CDMA) has been proposed as a promising multiaccess technique. MC-CDMA systems can be divided into two types [49]. For the first type, one symbol is transmitted per time slot. The input symbol is spread into several chips, which are then allocated to different subchannels. The number of subchannels is equal to the number of chips [26, 155]. For the second type, a vector of symbols is formed via the serial-to-parallel conversion, and each symbol is spread into several chips. The chips corresponding to the same symbol are allocated to the same subchannel [67], which is often called MC-DS CDMA. When compared with conventional CDMA systems, MC-CDMA can combat inter-symbol-interference (ISI) more effectively. Moreover, the frequency diversity gain can be fully exploited if the maximum ratio combing (MRC) technique [49, 109] is used at the receiver in MC-CDMA systems. Despite the above advantages, the performance of MC-CDMA systems is still limited by MAI in a multipath environment. Even though MAI can be reduced by MUD [144] and other signal processing [49] techniques, the diversity gain provided by multipath channels could be sacrificed since the received chips are no longer optimally combined under MRC. Furthermore, channel status information is needed for MRC and MUD. In a multiuser environment, multiuser channel estimation is more complicated and its accuracy degrades as the number of users increases, which will in turn degrade the system performance.

In this chapter, we approach the MAI reduction problem for MC-CDMA systems from another angle. That is, we investigate a novel way to select a set of "good" spreading codes so as to completely eliminate the MAI effect while keeping the transceiver structure simple and the computational burden low. Code design based on Hadamard-Walsh code is proposed to achieve the MAI-free property in a synchronous MC-CDMA system [26, 155]. More specifically, let N and L denote, respectively, the spreading factor and the multipath length. The $N = 2^{n_s}$ Hadamard-Walsh codewords are partitioned judiciously into G subsets, where $G = 2^{n_g}$ with $n_s > n_g \geq 1$ and $G \geq L$.

C.-C.J. Kuo et al., *Precoding Techniques for Digital Communication Systems*,
DOI: 10.1007/978-0-387-71769-2_6,

Then we can obtain an MAI-free system and each user can fully exploit the diversity gain provided by the multipath channel using any subset of codewords in frequency-selective channels. The number of supportable MAI-free users in each codeword subset is N/G. We also show a procedure to estimate the channel information for individual users under an MAI-free environment. Moreover, we consider the performance of the proposed Hadamard-Walsh code based scheme in a carrier frequency offset (CFO) environment. It is shown that this code scheme can reduce the CFO-induced MAI effect to a negligible amount under an interested CFO level. Some Hadamard-Walsh codewords can even achieve MAI-free in a CFO environment. Finally, based on the theoretical requirements for MAI-free MC-CDMA, we propose a subset of Hadamard-Walsh codes that are completely MAI-free even in the presence of CFO. We show that, by partitioning those codewords into subsets, codewords in some particular subsets will be MAI-free in a CFO environment and the number of supportable MAI-free users with HW codes is $1 + \log_2(N/G)$.

6.2 System Model and Its Properties

The block diagram of the MC-CDMA system in uplink direction is shown in Fig. 6.1, where the desired signal path demonstrates a signal transmitted by user i and detected in receiver side for user i. On the other hand, we call the signal transmitted by user i and detected for user j as MAI. The system transmits one data symbol in one time slot. Suppose that there are T users. Let the symbol from user i be x_i. In the first stage, x_i is spread by N chips to form an $N \times 1$ vector, denoted by $\mathbf{y}_i$. Let the kth element of $\mathbf{y}_i$ be $y_i[k]$. The relation between $y_i[k]$ and x_i is given by

$$y_i[k] = w_i[k]x_i, \quad 0 \le k \le N-1, \tag{6.1}$$

where $w_i[k]$ is the kth element of the ith orthogonal code. Note that we consider the short code scenario here, where the spreading code for a target user is the same for any time slot. After spreading, $\mathbf{y}_i$ is passed through the $N \times N$ IDFT matrix. Then, the output is parallel-to-serial (P/S) converted and the cyclic prefix (CP) of length $L-1$ is added to combat the inter-symbol-interference (ISI), where L is the considered maximum delay spread.

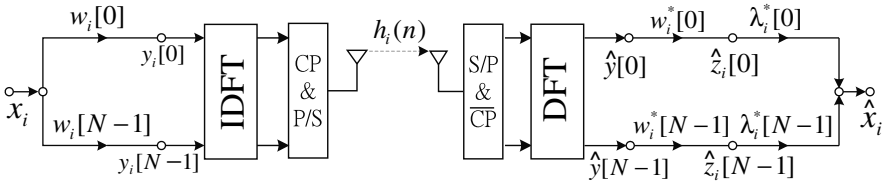

Fig. 6.1. The block diagram of an MC-CDMA system [[136] ©IEEE].

At the receiver side, the receiver removes CP and passes each block of size N through the $N \times N$ DFT matrix. Since there are T users, the kth element of the DFT output $\hat{\mathbf{y}}$ can be written as [10, 27]

$$\hat{y}[k] = \sum_{j=0}^{T-1} \lambda_j[k] y_j[k] + e[k], \tag{6.2}$$

where $\lambda_j[k]$ is the kth component of the N-point DFT of user j's channel impulse response, and $e[k]$ is the received noise after DFT. Based on $\hat{\mathbf{y}}$, we will detect symbols for T users. As shown in Fig. 6.1, to detect symbols transmitted by the ith user, $\hat{\mathbf{y}}$ is multiplied by $w_i^*[k]$ and frequency gain $\lambda_i^*[k]$. The channel information $h_j(n)$ or $\lambda_j[k]$ of every user is assumed to be known to the receiver. The estimation of channel information under an MAI-free environment will be described in Section 6.2.2. After being multiplied with the frequency gains, N chips are summed up to form reconstructed symbol $\hat{x}_i$. Using Eqs. (6.1) and (6.2), $\hat{x}_i$ is given by

$$\hat{x}_i = \underbrace{x_i \sum_{k=0}^{N-1} |\lambda_i[k]|^2}_{\text{multipath effect}} + \underbrace{\sum_{j=0, j\neq i}^{T-1} x_j \sum_{k=0}^{N-1} \lambda_i^*[k] w_i^*[k] \lambda_j[k] w_j[k]}_{MAI_{i\leftarrow j}} + \sum_{k=0}^{N-1} \lambda_i^*[k] w_i^*[k] e[k], \tag{6.3}$$

where $MAI_{i\leftarrow j}$ denotes the MAI from user j to user i. Note that, when the channel noise $e[k]$ is AWGN, the process from $\hat{y}[k]$ to $\hat{x}_i$ is called the maximum ratio combining (MRC) technique [49], which ensures the minimum bit error probability for detected symbols [108], or the maximum achievable diversity gain provided by multipath channels [105].

For any target user i, if $MAI_{i\leftarrow j} = 0$, the reconstructed symbol $\hat{x}_i$ will be affected only by his/her own transmitted symbols x_i and the corresponding channel response $\lambda_i[k]$. Thus, this allows the system to use some simple detection schemes without involving multiuser detection. When the channel has flat fading, $\lambda_i[k]$ and $\lambda_j[k]$ are independent of k and $MAI_{i\leftarrow j} = 0$ if orthogonal codes such as the Hadamard-Walsh codes are used. However, in practical situations, the channel environment is usually frequency-selective and the orthogonality of orthogonal codes will be lost under MRC.

The system model can also be used in downlink transmission, where the signal for every user experiences the same fading. In this situation, MAI-free can be achieved using ORC [49], i.e., the combining gain is $\lambda^{-1}[k]$ instead of $\lambda^*[k]$ in Eq. (6.3) (the subscript disappears since every user experiences the same channel in downlink transmission). However, for subchannels with serious fading, ORC tends to amplify the noise in these subchannels. Thus, the performance will degrade dramatically. That is, the use of ORC may lead to the loss of the diversity gain from multipath channels. In the following sections, we will design $w_i[k]$ such that $MAI_{i\leftarrow j} = 0$ under the multipath

environment. Moreover, the proposed code design allows MRC to be used in both uplink and downlink transmissions. Thus, a full diversity gain from the multipath channel can be achieved.

6.2.1 MAI Analysis over Frequency-Selective Fading

Let $\mathbf{F}$ be the $N \times N$ DFT matrix with the element at the kth row and the nth column given by $[\mathbf{F}]_{k,n} = \frac{1}{\sqrt{N}} e^{-j\frac{2\pi}{N}kn}$ and the maximum length of channel impulse response be L, i.e., $h_i(n) = 0$, for $n > L-1$. The MAI term in Eq. (6.3) can be expressed using matrix representation as

$$MAI_{i \leftarrow j} = x_j \mathbf{h}_i^{\dagger} \underbrace{\mathbf{F}_0^{\dagger} \mathbf{W}_i^{*} \mathbf{W}_j \mathbf{F}_0}_{\mathbf{A}_{i,j}} \mathbf{h}_j, \tag{6.4}$$

where

$$\mathbf{h}_i = (h_i(0)\ h_i(1) \cdots h_i(L-1))^t,$$

$$\mathbf{F}_0 = \mathbf{F} \begin{pmatrix} \mathbf{I}_L \\ \mathbf{0} \end{pmatrix}_{N \times L},$$

and

$$\mathbf{W}_i = \mathrm{diag}(w_i[0] \cdots w_i[N-1]).$$

To have zero MAI for a frequency-selective fading channel, we need to have $MAI_{i \leftarrow j} = 0$ for all nonzero $\mathbf{h}_i$ and $\mathbf{h}_j$. This means that $\mathbf{A}_{i,j}$ in Eq. (6.4) should be the $L \times L$ zero matrix for all $i \neq j$. Define $\mathbf{R}_{i,j} = \mathbf{W}_i^{*} \mathbf{W}_j$, where $\mathbf{R}_{i,j}$ is diagonal, i.e.,

$$\mathbf{R}_{i,j} = \mathrm{diag}\left(r_{i,j}[0] \cdots r_{i,j}[N-1]\right),$$

with

$$r_{i,j}[k] = w_i^{*}[k] w_j[k].$$

We can rewrite $\mathbf{A}_{i,j}$ as

$$\mathbf{A}_{i,j} = \begin{pmatrix} \mathbf{I}_L\ \mathbf{0} \end{pmatrix} \underbrace{\mathbf{F}^{\dagger} \mathbf{R}_{i,j} \mathbf{F}}_{\mathbf{B}_{i,j}} \begin{pmatrix} \mathbf{I}_L \\ \mathbf{0} \end{pmatrix}, \tag{6.5}$$

Since $\mathbf{R}_{i,j}$ is diagonal, it is well known that $\mathbf{B}_{i,j}$ is a circulant matrix [47]. That is, the first column of $\mathbf{B}_{i,j}$, $(b_{i,j}(0) \cdots b_{i,j}(N-1))^t$, is the N-point IDFT of $\mathbf{r}_{i,j}$, where $\mathbf{r}_{i,j} = (r_{i,j}[0] \cdots r_{i,j}[N-1])^t$. Matrix $\mathbf{A}_{i,j}$ is an $L \times L$ upper left submatrix of $\mathbf{B}_{i,j}$, i.e.,

$$\mathbf{A}_{i,j} = \begin{pmatrix} b_{i,j}(0) & b_{i,j}(N-1) & \cdots & b_{i,j}(N-L+1) \\ b_{i,j}(1) & b_{i,j}(0) & & \vdots \\ \vdots & & \ddots & \\ b_{i,j}(L-1) & & \cdots & b_{i,j}(0) \end{pmatrix}. \tag{6.6}$$

To have $\mathbf{A}_{i,j} = \mathbf{0}$ means that $b_{i,j}(0) = \cdots = b_{i,j}(L-1) = 0$ and $b_{i,j}(N-L-1) = \cdots = b_{i,j}(N-1) = 0$. That is, the first L samples and the last $L-1$ samples of the IDFT of $\mathbf{r}_{i,j}$ are zeros. Hence, to achieve MAI-free property for arbitrary channel, the following conditions should be satisfied

$$\begin{cases} b_{i,j}(n) = 0, & 0 \le n \le L-1 \\ b_{i,j}(N-n) = 0, & 1 \le n \le L-1 \end{cases}. \tag{6.7}$$

Lemma 6.1: Suppose the channel length is L and the spreading gain is N. To achieve MAI-free property, N should be greater or equal to $2L$.

Proof: From Eq. (6.7), there should be at least $2L-1$ elements for the codewords. However, if $N = 2L-1$, all elements of the codewords are zeros. Therefore, $N \ge 2L$. ■

Note that Lemma 6.1 holds for both real and complex code design. In what follows, we show how to achieve the MAI-free conditions in Eq. (6.7) using the Hadamard-Walsh codes. Before proceeding, let us recall a well known property of the Hadamard matrix [8] as follows.

An $N \times N$ Hadamard matrix $\mathbf{H}_N$ with $N = 2^p$, $p = 1, 2, \cdots$, can be recursively defined using the Hadamard matrix of order 2, i.e.,

$$\mathbf{H}_N = \mathbf{H}_2 \otimes \mathbf{H}_{N/2} = \begin{pmatrix} \mathbf{H}_{N/2} & \mathbf{H}_{N/2} \\ \mathbf{H}_{N/2} & -\mathbf{H}_{N/2} \end{pmatrix}, \tag{6.8}$$

where $\otimes$ is the Kronecker product [8, 54] and

$$\mathbf{H}_2 = \begin{pmatrix} +1 & +1 \\ +1 & -1 \end{pmatrix}.$$

Our proposed code scheme is stated below. Suppose $N = 2^{n_s}$ and $G = 2^{n_g}$, where both n_s and n_g are integers, and $n_s > n_g \ge 1$. The columns of an $N \times N$ Hadamard matrix $\mathbf{H}_N$ form the N Hadamard-Walsh codes. We divide the N codewords into G subsets. Each subset has N/G codewords. That is, the gth subset, denoted by G_g, has codewords $\left\{\mathbf{w}_{\frac{N}{G}g}, \cdots, \mathbf{w}_{\frac{N}{G}(g+1)-1}\right\}$, where $\mathbf{w}_i$ is the ith column of $\mathbf{H}_N$ and $0 \le g \le G-1$. For instance, let $N = 8$ and $G = 2$. Then, G_0 contains codewords $\{\mathbf{w}_0, \mathbf{w}_1, \mathbf{w}_2, \mathbf{w}_3\}$ and G_1 contains codewords $\{\mathbf{w}_4, \mathbf{w}_5, \mathbf{w}_6, \mathbf{w}_7\}$.

Lemma 6.2: Let $\mathbf{r}_{i,j}$ be an $N \times 1$ vector with the kth element be $r_{i,j}[k] = w_i^*[k]w_j[k]$. For $\mathbf{w}_i$ and $\mathbf{w}_j$ that belong to the same subset, $\mathbf{r}_{i,j}$ is equal to one of the codewords in G_0 excluding codeword $\mathbf{w}_0$.

Proof: Let us first prove that for $\mathbf{w}_i$ and $\mathbf{w}_j \in G_0$, $\mathbf{r}_{i,j}$ is again a codeword within G_0. According to Eq. (6.8), the $N/G \times N/G$ upper left submatrix of $\mathbf{H}_N$ is a $N/G \times N/G$ Hadamard matrix. Thus, the product of any two columns of this submatrix is again a column of this submatrix (see [65]). Since the codewords in subset 0 are the first N/G columns of $\mathbf{H}_N$, which is obtained

by repeating the $N/G \times N/G$ submatrix by G times. Hence, for $\mathbf{w}_i$ and $\mathbf{w}_j$ in subset 0, $\mathbf{r}_{i,j}$ is a codeword in subset 0.

Now, let us consider $\mathbf{r}_{i,j}$ for $\mathbf{w}_i$ and $\mathbf{w}_j$ that are in the same subset other than subset 0. Recall that $w_i[k]$ is the kth element of the ith codeword. It can also be used to denote the kth element of the ith column of $\mathbf{H}_N$. According to Eq. (6.8), for $0 \le i \le N/2-1$, we have the following property

$$\begin{cases} w_i[k] = w_{i+N/2}[k], & 0 \le k \le N/2-1, \\ w_i[k] = -w_{i+N/2}[k], & N/2 \le k \le N-1. \end{cases} \tag{6.9}$$

We see from Eq. (6.9) that the product of any two columns in the last half $N/2$ columns is equal to that of the two corresponding columns in the first half $N/2$ columns, i.e.,

$$w_i[k]w_j[k] = w_{i+N/2}[k]w_{j+N/2}[k], \quad 0 \le i,j \le N/2-1. \tag{6.10}$$

Suppose that we divide the N codewords into two sets, denoted by S_0 and S_1, respectively. The first $N/2$ half codewords form S_0 while the last $N/2$ half codewords form S_1. Hence, as proved in the beginning of the lemma that for $\mathbf{w}_i$ and $\mathbf{w}_j$ in S_0, $\mathbf{r}_{i,j}$ is again a codeword in S_0. For $\mathbf{w}_i$ and $\mathbf{w}_j$ in S_1, $\mathbf{r}_{i,j}$ is equal to a codeword in S_0 based on Eq. (6.10). Using a similar procedure, we can divide S_0 into 2 sets, S_{00} and S_{01}. Thus, for $\mathbf{w}_i$ and $\mathbf{w}_j$ in S_{00}, $\mathbf{r}_{i,j}$ is a codeword in S_{00}. Now, we prove that for $\mathbf{w}_i$ and $\mathbf{w}_j$ in S_{01}, $\mathbf{r}_{i,j}$ is a codeword in S_{00}. From Eq. (6.8), for $0 \le i \le N/4-1$, we have the following property

$$\begin{cases} w_i[k] = w_{i+N/4}[k], & 0 \le k \le N/4-1 \quad \text{or} \quad N/2 \le k \le 3N/4-1, \\ w_i[k] = -w_{i+N/4}[k], & N/4 \le k \le N/2-1 \quad \text{or} \quad 3N/4 \le k \le N-1. \end{cases} \tag{6.11}$$

We see from Eq. (6.11) that the product of any two columns in the second quarter is equal to the product of the two corresponding columns in the first quarter, i.e.,

$$w_i[k]w_j[k] = w_{i+N/4}[k]w_{j+N/4}[k], \quad 0 \le i,j \le N/4-1. \tag{6.12}$$

From Eq. (6.14), for $\mathbf{w}_i$ and $\mathbf{w}_j$ in S_{01}, $\mathbf{r}_{i,j}$ is again a codeword in S_{00}. Similarly, we can divide S_1 into two sets, i.e. S_{10} and S_{11}, and show that for $\mathbf{w}_i$ and $\mathbf{w}_j$ in either S_{10} or S_{11}, $\mathbf{r}_{i,j}$ is again a codeword in S_{00}. Using the same procedure, we can continue to divide the codewords until we have G subsets, and show that for $\mathbf{w}_i$ and $\mathbf{w}_j$ in the same subset, $\mathbf{r}_{i,j}$ is a codeword of subset 0. ■

Lemma 6.3: Let $\tilde{w}_i(n)$, $0 \le n \le N-1$ and $1 \le i \le N/G-1$ be the N-point IDFT of the codewords in G_0 excluding $\mathbf{w}_0$. Then, $\tilde{w}_i(n)$ has the following property:

$$\begin{cases} \tilde{w}_i(n) = 0, & 0 \le n \le G-1, \\ \tilde{w}_i(N-n) = 0, & 1 \le n \le G-1. \end{cases} \tag{6.13}$$

Proof: For $n = 0$, it is easy to see $\tilde{w}_i(0) = \sum_{k=0}^{N-1} w_i[k] = 0$ since there are an equal number of $+1$ and -1 for any codeword except $\mathbf{w}_0$. For $n \neq 0$, since $\tilde{w}_i(n)$ is the IDFT of the codewords in G_0, we have

$$\tilde{w}_i(n) = \frac{1}{N} \sum_{m=0}^{N-1} w_i[k] e^{j\frac{2\pi}{N}mn}. \tag{6.14}$$

Let $m = k + gN/G$, $0 \leq k \leq N/G-1$, $0 \leq g \leq G-1$, we can rewrite Eq. (6.14) as

$$\tilde{w}_i(n) = \frac{1}{N} \sum_{k=0}^{N/G-1} \sum_{g=0}^{G-1} w_i[k + gN/G] e^{j\frac{2\pi}{N}(k+gN/G)n}. \tag{6.15}$$

Since codewords $w_i[k]$ in G_0 are the first N/G columns of $\mathbf{H}_N$, they are formed by repeating the upper left $N/G \times N/G$ submatrix of $\mathbf{H}_N$ by G times. Hence, $w_i[k] = w_i[k + gN/G]$, $0 \leq k \leq N/G - 1$, $0 \leq g \leq G - 1$. We can rewrite Eq. (6.15) as

$$\tilde{w}_i(n) = \frac{1}{N} \sum_{k=0}^{N/G-1} w_i[k] a_n, \tag{6.16}$$

where

$$a_n = \sum_{g=0}^{G-1} e^{j\frac{2\pi}{G}gn} = \begin{cases} G, & n = cG \text{ with } c = 0, \pm 1, \pm 2, \cdots, \\ 0, & \text{otherwise.} \end{cases}$$

Therefore, we obtain

$$\tilde{w}_i(n) = \begin{cases} \frac{G}{N} \sum_{k=0}^{N/G-1} w_i[k], & n = cG \text{ with } c = 0, \pm 1, \pm 2, \cdots, \\ 0, & \text{otherwise.} \end{cases} \tag{6.17}$$

From Eq. (6.17) and $\tilde{w}_i(0) = 0$, we are led to Eq. (6.13). ■

From Eq. (6.13) and Lemma 6.2, we have the following property

$$\begin{cases} b_{i,j}(n) = 0, & 0 \leq n \leq G-1, \\ b_{i,j}(N-n) = 0, & 1 \leq n \leq G-1, \end{cases} \tag{6.18}$$

where $b_{i,j}(n)$ denotes the nth element of the IDFT of $\mathbf{r}_{i,j}$ within the same subset.

Example 6.1: DFT of Hadamard-Walsh Codewords

Let us give an example to illustrate Lemma 6.3. Let $N = 16$, the N-point DFT of the N Hadamard-Walsh codewords are shown in Fig. 6.2. From this figure, we see that, except the all-one codeword, the IDFT of any codeword has zero at $n = 0$. If $G = 8$, we have eight subsets and each subset has two

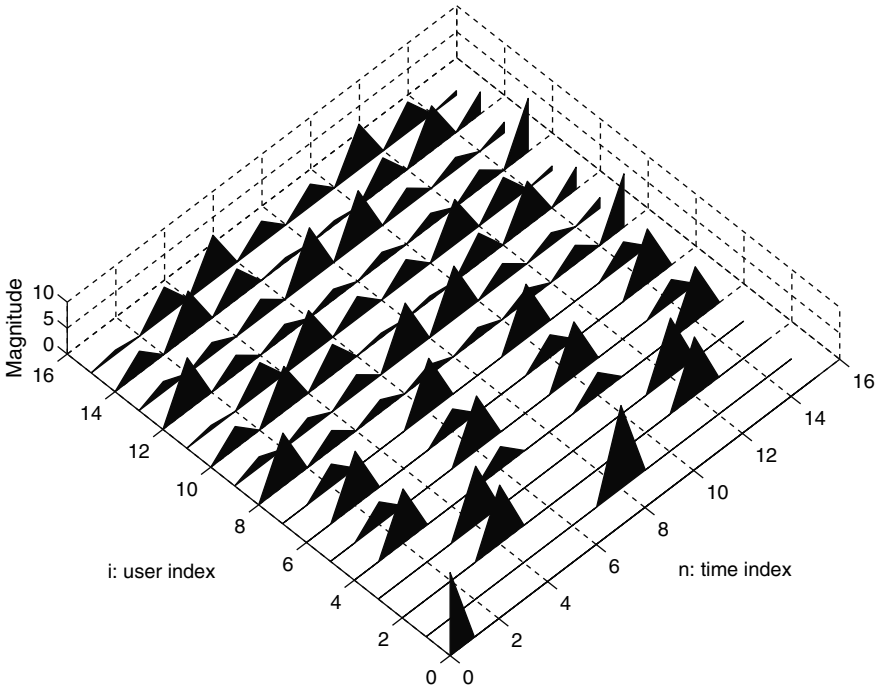

Fig. 6.2. $|\tilde{w}_i(n)|$ as a function of user index i and time index n with $N = 16$ [[136] ©IEEE] [[136] ©IEEE].

codewords. From Lemma 6.3, for $\mathbf{w}_i$ and $\mathbf{w}_j$ in the same subset, $\mathbf{r}_{i,j}$ is equal to $\mathbf{w}_1$. From the figure, the first eight elements of $\tilde{w}_1(n)$ are zeros. If $G = 4$, then we have four subsets and each subset has four codewords. Again from Lemma 6.3, for $\mathbf{w}_i$ and $\mathbf{w}_j$ in the same subset, $\mathbf{r}_{i,j}$ is equal to either $\mathbf{w}_1$, $\mathbf{w}_2$, or $\mathbf{w}_3$. From the figure, the first four elements of $\tilde{w}_1(n)$, $\tilde{w}_2(n)$, and $\tilde{w}_3(n)$ are zeros. ■

Based on the above discussion, we have established one of the main results of this work as stated below.

Theorem 6.1: Let the channel length be L. We divide the N Hadamard-Walsh codewords into G subsets with $G \geq L$, where N and G are power of 2 and each subset consisting of N/G codewords. Then, using any one of the G subsets of codewords, the corresponding MC-CDMA system is completely MAI-free.

Note that Theorem 6.1 holds for arbitrary multipath coefficients. Moreover, the maximum number of MAI-free users, T, in each subset depends on the spreading gain N and multipath length L. Hence, the system can be designed accordingly. Different applications may have different concerns. We describe two application scenarios below.

Application Scenario 1. In cellular systems, frequency reuse for different cells is an important issue since improper frequency reuse will lead to significant co-channel interference [108]. The proposed scheme divides the codewords into several subsets to achieve MAI-free property. It is intuitive to use distinct subsets of codewords in neighboring cells to reduce co-channel interference. Let us give an example to illustrate this point. Let $G = L = 4$. Thus, the orthogonal codes are divided into 4 subsets, i.e., subsets 0, 1, 2 and 3. Figure 6.3 gives an example of frequency planning using the proposed code scheme. For a larger L, G should be increased accordingly to be MAI-free. In this situation, we have more subsets, and the distance among the same subset in reuse can be increased to reduce co-channel interference further.

Application Scenario 2. In wireless local area network (WLAN) applications, the distance among cells is not as close as that in cellular systems. Hence, co-channel interference may not be a major concern. According to Theorem 6.1, the maximum number of users that a cell can support while maintaining the MAI-free property depends on N/G and hence the multipath number L. Thus, a smaller value of L or G enables the system to support more users in one cell. In this situation, N should be much larger than L to support more users. For a fixed sampling frequency, this can be done by increasing the OFDM-block duration. Hence, if the complexity is ignored, N can be as large as possible if the duration of one block does not exceed the channel coherent time. Generally speaking, this concept stands in contrast with that in an MC-CDMA system, where N should be chosen to be close to L so that subchannels have less correlation and a more random signature waveform. However, as stated in Theorem 6.1, when the proposed code design is used, the system is completely MAI-free so that we can choose N that is much larger than L to support more users in WLAN applications.

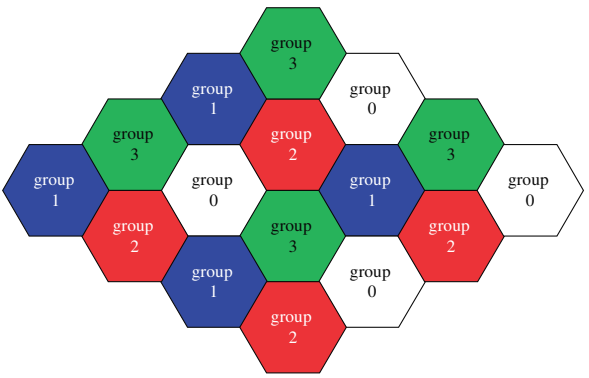

Fig. 6.3. An example of frequency reuse using the proposed code scheme with $G = L = 4$ [[136] ©IEEE].

Example 6.2: Illustration of the MAI-Free Property
In this example, we show that MC-CDMA is MAI-free with the proposed code scheme. We considered the performance in the uplink direction. Also, the Hadamard-Walsh codewords are generated using the Kronecker product in Eq. (6.8) so that the codeword indices are adopted based on this fact. The simulation was conducted under the following setting: $N = 64$, $G = L = 2$ or 4. The transmit power had an unit variance. The taps of the channel were i.i.d. random variables with an unit variance. We evaluate the $MAI_{i \leftarrow j}$ as given in Eq. (6.3). For $L = 2$, one realization of $|MAI_{i \leftarrow j}|$ as a function of user indices i and j is shown in Fig. 6.4(a). As shown in the figure, there are two zones where the MAI is zero; i.e., the zone with codewords from 1 to 32, and the zone with codewords from 33 to 64. The peak values appear along the diagonal since they correspond to the reconstructed desired signal power for each user. Thus, the system is MAI-free if either one of the two subsets of codewords is in use. For $L = 4$, the performance is shown in Fig. 6.4(b). We see four zones where the MAI is equal to zero. Hence, if we use either one of these four subsets, we can achieve an MAI-free system. These results corroborate the claim in Theorem 6.1. ■

Example 6.3: Illustration of the Diversity Gain
In this example, we would like to show that, when the proposed code scheme is used, every user can achieve a low bit error probability to reflect the diversity gain L. The BPSK modulation and Hadamard-Walsh codes of $N = 16$ were adopted. The uplink channel coefficients were i.i.d. complex Gaussian random variables of unit variance. For each individual user, the Monte Carlo method was run for more than 250,000 symbols. The bit error probabilities of two systems were shown in Fig. 6.5. The solid curve is obtained from a system with flat fading, i.e., $L = 1$, with N full codewords used. The dashed curve is resulted from a system of multipath length $L = 2$ and with the proposed $N/2$ Hadamard-Walsh codes G_0. Since there is no MAI, simulation results are consistent with the theoretical results in [3] and [105].

We see that, when L grows from 1 to 2 with the proposed code scheme, the bit error probability improves dramatically due to the increase of the diversity order. Actually, the dashed curve is the same as that for a system with $L = 1$ and two receive antennas with MRC [3]. That is, a diversity order of 2 is achieved via code design in the frequency domain rather than the space domain (see p. 777 in [105]). This example also explains the interplay between the diversity order and the number of users allowed. That is, when L grows, we need to divide N codewords into more subsets to achieve MAI-free. Hence, few users can be supported within each cell. However, these users can enjoy a higher diversity order as L increases.

Note that frequency diversity is inherent in MC-CDMA systems. However, without a proper code design, the system has MAI that will degrade the BEP performance as the number of users increases. Under this situation, MAI will dominate system performance and increasing diversity gain alone may not

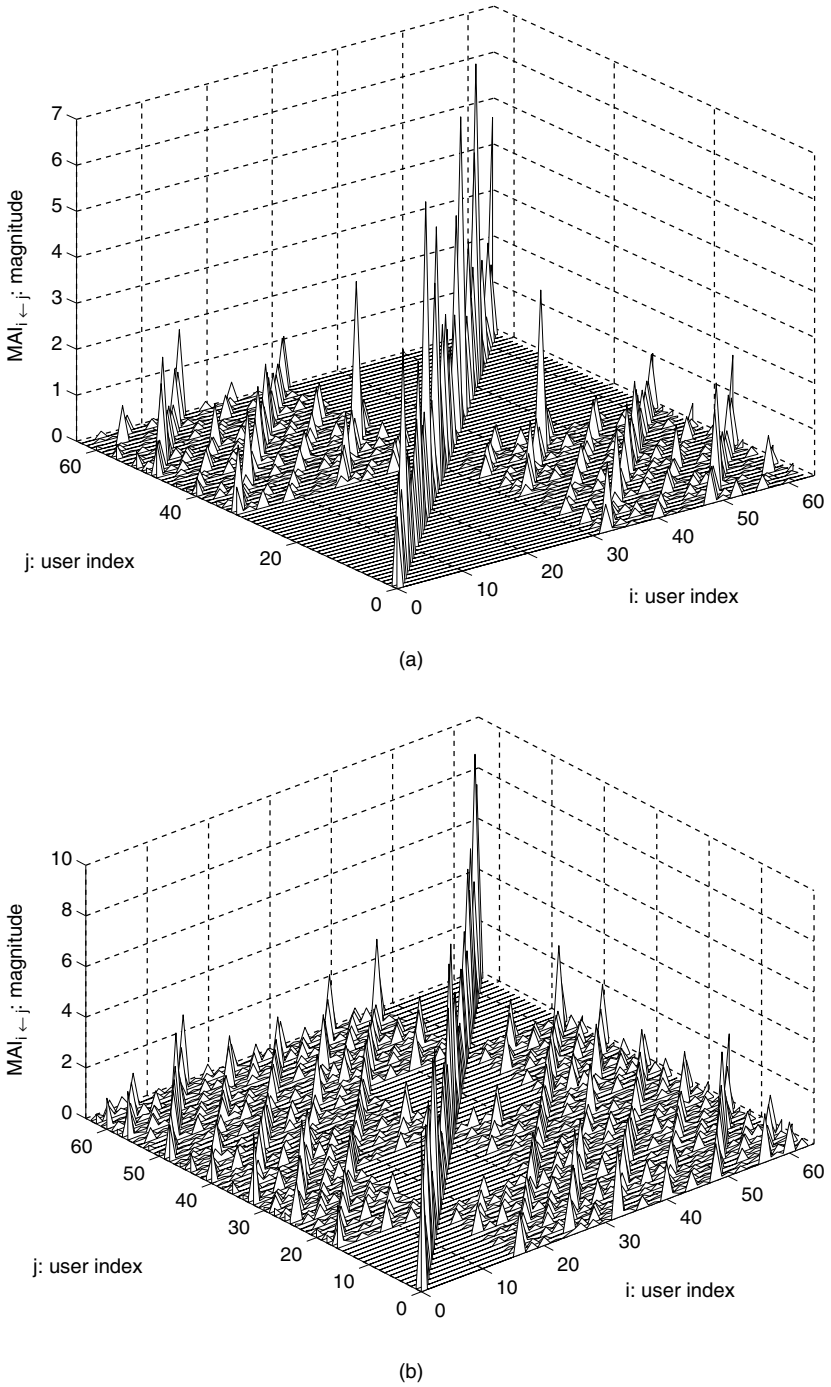

Fig. 6.4. $|MAI_{i\leftarrow j}|$ as a function of user indices i and j with $N = 64$: (**a**) $L = 2$ and (**b**) $L = 4$ [[136] ©IEEE].

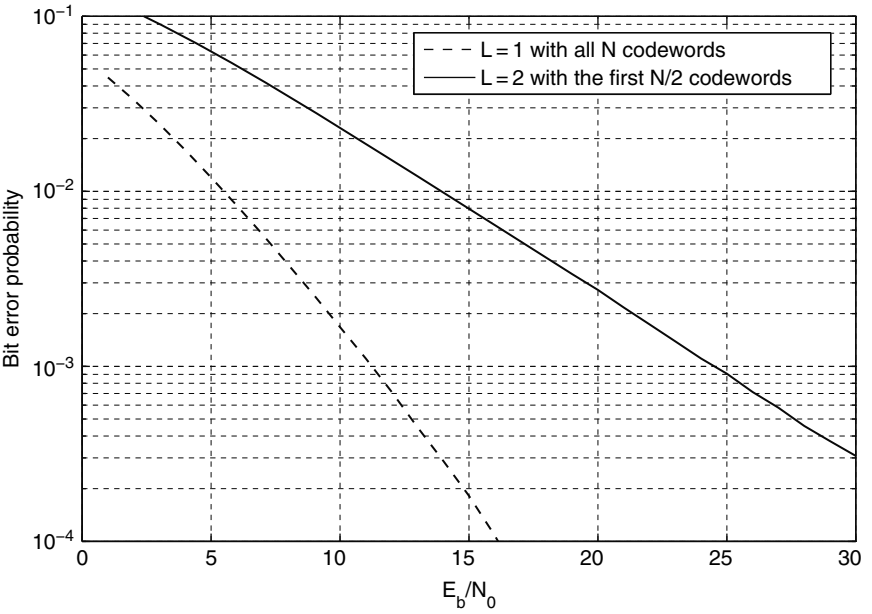

Fig. 6.5. The bit error probability as a function of E_b/N_0 to illustrate the diversity order of the proposed code scheme [[136] ©IEEE].

necessarily improve overall performance [49]. If the proposed code design is used together with M_r receive antennas, a diversity order of LM_r can be achieved for each individual user. ■

6.2.2 Channel Estimation Under MAI-Free Condition

In the last section, we assume that the channel information $\lambda_i[k]$ for every user is known to the receiver. Without accurate channel information, neither ORC nor MRC can be performed at the receiver end. For non-MAI-free schemes, channel information is needed for the MUD-based technique in the receiver. If channel information is not available, it has to be estimated by some techniques [132]. For uplink transmission, every user experiences a different fading. Thus, multiuser channel estimation is required if the system is not MAI-free. For downlink transmission, although the mixed signal of all users from the base station experiences the same channel fading, orthogonality of users' codes may be destroyed as a result of frequency-selective fading. Unless the base station uses the same training sequence x_i and spreading code $w_i[k]$ for every user at the same time slot, it would be difficult for an individual user to acquire his/her own downlink channel information without extra signal processing techniques. However, this reduces the system flexibility since all users have to be coordinated for training with the same signature waveform at the same

time slot. Thus, it is desirable to design a system where channel estimation is conducted under an MAI-free environment. In this section, we will show that the channel information can be obtained in an MAI-free environment if the proposed code scheme is used. Thus, there is no need to do multiuser estimation in the uplink direction and the training procedure is more flexible in the downlink transmission.

To get $\lambda_i[k]$ is equivalent to obtaining its time domain impulse response $h_i(n)$, $0 \le n \le L-1$. We will show how to obtain every user's $h_i(n)$ without worrying about MAI. Again, the result derived here is for the more general uplink case. It can be adapted for the downlink case as well. Referring to Fig. 6.1 and from Eq. (6.2), if the real Hadamard-Walsh code is used, the $N \times 1$ chip vector of user i before gain combining is

$$\hat{\mathbf{z}}_i = x_i \mathbf{F}_0 \mathbf{h}_i + \sum_{j=0, j\neq i}^{T-1} x_j \mathbf{W}_i \mathbf{W}_j \mathbf{F}_0 \mathbf{h}_j + \mathbf{W}_i \mathbf{e}, \tag{6.19}$$

where $\mathbf{e}$ is the noise vector after DFT. Taking the N-point IDFT of $\hat{\mathbf{z}}_i$ in Eq. (6.19), we have

$$\mathbf{F}^\dagger \hat{\mathbf{z}}_i = x_i \begin{pmatrix} \mathbf{I}_L \\ \mathbf{0} \end{pmatrix} \mathbf{h}_i + \sum_{j=0, j\neq i}^{T-1} x_j \underbrace{\mathbf{F}^\dagger \mathbf{W}_i \mathbf{W}_j \mathbf{F}_0 \mathbf{h}_j}_{\mathbf{c}_{i,j}} + \mathbf{F}^\dagger \mathbf{W}_i \mathbf{e}, \tag{6.20}$$

where the second term is the interference term from other users. Since the channel path is of length L, if the first L elements of $\mathbf{c}_{i,j}$ are zeros for all $\mathbf{h}_j$, we can obtain channel $\mathbf{h}_i$ without worrying about the interference from other users.

Theorem 6.2: Suppose that the channel length is equal to L and the code scheme as stated in Theorem 6.1 is used, where $G \ge L$. Then, if we use any one subset of codewords in the MC-CDMA system, the first L elements of $\mathbf{c}_{i,j}$ are zeros. As a result, we can estimate the channel $\mathbf{h}_i$ in a completely MAI-free environment. That is,

$$z_i(n) = x_i h_i(n) + \tilde{e}_i(n), \quad 0 \le n \le L-1, \tag{6.21}$$

where $z_i(n)$ is the nth element of $\mathbf{F}\hat{\mathbf{z}}_i$ and $\tilde{e}_i(n)$ is the nth element of $\mathbf{F}^\dagger \mathbf{W}_i \mathbf{e}$.

Proof: Let us express the DFT matrix $\mathbf{F}$ as $(\ \mathbf{F}_0\ \mathbf{F}_1)$. Then, $\mathbf{c}_{i,j}$ in Eq. (6.20) can be manipulated as

$$\mathbf{c}_{i,j} = \begin{pmatrix} \mathbf{F}_0^\dagger \\ \mathbf{F}_1^\dagger \end{pmatrix} \mathbf{W}_i \mathbf{W}_j \mathbf{F}_0 \mathbf{h}_j = \begin{pmatrix} \mathbf{F}_0^\dagger \mathbf{R}_{i,j} \mathbf{F}_0 \\ \mathbf{F}_1^\dagger \mathbf{R}_{i,j} \mathbf{F}_0 \end{pmatrix} \mathbf{h}_j. \tag{6.22}$$

From the discussion in Section 6.2.1, $\mathbf{F}_0^{\dagger}\mathbf{R}_{i,j}\mathbf{F}_0 = \mathbf{0}$ if any one subset of codewords are used. Hence, the first L elements of $\mathbf{c}_{i,j}$ are zeros, and we get Eq. (6.21). ■

According to Eq. (6.21), if x_i is a known training symbol, we can obtain $h_i(n)$, $0 \leq n \leq L-1$, without worrying about the interference from symbols of other users. That is, channel estimation can be done in a completely MAI-free environment.

Discussion on System Parameters and Performance Tradeoff. From the discussion above, when the number of users increases, we may increase the spreading gain N or decrease the number of partitioned subsets G to accommodate more users. The adjustment of parameters N and G dynamically is an interesting problem, which is under our current investigation. When the system is heavily loaded in the sense that the number of active users is approaching N/L, the proposed code design provides a set of optimal codes for the system in terms of MAI reduction and multipath diversity.

Another tradeoff results from the change of the multipath length L. Under the condition $G = L$, if L becomes larger (or smaller), the number of allowed users decreases (or increases). For a fixed N, since the diversity gain of a user is equal to L, there exists a tradeoff between the number of users and the diversity gain [105].

Finally, it is interesting to examine the case where the number of active users exceeds N/L. Under this scenario, to get an MAI-free system, MUD can be used in the uplink direction while the ORC scheme [49] can be performed in the downlink direction with the penalty that the full diversity gain may be lost. It is worthwhile to emphasize that since Hadamard-Walsh code in nature has group MAI-free property in MC-CDMA system, the complexity for MUD in this case can be greatly reduced.

6.2.3 Proposed Code Design in the Presence of CFO

In this section, we consider the CFO effect and show that it can be handled by the use of the proposed code design. In particular, we show that the MAI due to the CFO effect can be reduced to zero or a negligible amount. Consider the kth chip of the received vector after DFT in a CFO environment, i.e.,

$$\hat{y}[k] = \sum_{j=0}^{T-1} r_j[k] + e[k], \tag{6.23}$$

where $e[k]$ is the received noise after DFT, and $r_j[k]$ is the received signal due to channel fading and the CFO effect. Suppose the jth user has a normalized CFO ϵ_j, which is the actual CFO normalized by $1/N$ of the overall bandwidth and $-0.5 \leq \epsilon_j \leq 0.5$. $r_j[k]$ in Eq. (6.23) can be expressed by [87]:

$$r_j[k] = \frac{1}{\sqrt{N}} \sum_{n=0}^{N-1} \left[\frac{1}{\sqrt{N}} \sum_{m=0}^{N-1} \lambda_j[m] y_j[m] e^{j\frac{2\pi}{N}nm} \right] e^{j\frac{2\pi}{N}n\epsilon_j} e^{-j\frac{2\pi}{N}nk}$$
$$= \underbrace{\alpha_j \lambda_j[k] y_j[k]}_{r_j^{(0)}[k]} + \underbrace{\beta_j \sum_{m=0, m\neq k}^{N-1} \lambda_j[m] y_j[m] \frac{e^{-j\pi\frac{m-k}{N}}}{N \sin\frac{\pi(m-k+\epsilon_j)}{N}}}_{r_j^{(1)}[k]}, \quad (6.24)$$

where α_j and β_j are given by

$$\alpha_j = \frac{\sin \pi\epsilon_j}{N \sin\frac{\pi\epsilon_j}{N}} e^{j\pi\epsilon_j\frac{N-1}{N}} \text{ and } \beta_j = \sin(\pi\epsilon_j) e^{j\pi\epsilon_j\frac{N-1}{N}}. \quad (6.25)$$

The first term of Eq. (6.24) is the distorted chip and the second term is the ICI caused by the CFO. Note that, when there is no CFO, $r_j[k]$ equals $\lambda_j[k]y_j[k]$ as in Eq. (6.2). From Eqs. (6.3) and (6.23), if the real Hadamard-Walsh code is used, we see that $\hat{x}_i[k]$ under CFO is given by

$$\hat{x}_i = \underbrace{\sum_{k=0}^{N-1} r_i[k]\lambda_i^*[k]w_i[k]}_{s_i} + \sum_{j=0, j\neq i}^{T-1} \underbrace{\sum_{k=0}^{N-1} r_j[k]\lambda_i^*[k]w_i[k]}_{\widetilde{MAI}_{i\leftarrow j}} + \sum_{k=0}^{N-1} e[k]\lambda_i^*[k]w_i[k], \quad (6.26)$$

where s_i is the desired signal and $\widetilde{MAI}_{i\leftarrow j}$ is the MAI of user i due to the jth user's CFO. Using Eqs. (6.24) and (6.26), it can be shown that the MAI term is given by

$$\widetilde{MAI}_{i\leftarrow j} = MAI_{i\leftarrow j}^{(0)} + MAI_{i\leftarrow j}^{(1)}, \quad (6.27)$$

where

$$MAI_{i\leftarrow j}^{(0)} = \sum_{k=0}^{N-1} r_j^{(0)}[k]\lambda_i^*[k]w_i[k]$$
$$= \alpha_j x_j \sum_{k=0}^{N-1} \lambda_j[k]w_j[k]\lambda_i^*[k]w_i[k] \quad (6.28)$$

and

$$MAI_{i\leftarrow j}^{(1)} = \sum_{k=0}^{N-1} r_j^{(1)}[k]\lambda_i^*[k]w_i[k]$$
$$= \beta_j x_j \eta_j, \quad (6.29)$$

where

$$\eta_j = \sum_{k=0}^{N-1} \sum_{m=0, m\neq k}^{N-1} \lambda_j[m]w_j[m] \frac{e^{-j\pi\frac{m-k}{N}}}{N \sin\frac{\pi(m-k+\epsilon_j)}{N}} \lambda_i^*[k]w_i[k].$$

Note that if there is no CFO for user j, i.e., $\alpha_j = 1$ and $\beta_j = 0$, $MAI_{i\leftarrow j}^{(1)} = 0$ and $MAI_{i\leftarrow j}^{(0)}$ is equal to the MAI term defined in Eq. (6.3). This gives us an intuition that $MAI_{i\leftarrow j}^{(0)}$ is the dominating MAI term when the CFO is small. Hence, if we can find a way that makes $MAI_{i\leftarrow j}^{(0)} = 0$, the MAI due to the CFO can be reduced to a negligible amount. According to Eqs. (6.3), (6.28) and Theorem 6.1, we have the following Lemma.

Lemma 6.4: Let the channel length be L and the code scheme as stated in Theorem 6.1 is used. Then, if we use any one of the G subsets of codewords for the MC-CDMA system with $G \geq L$, the dominating MAI term $MAI_{i\leftarrow j}^{(0)}$ in Eq. (6.28) is zero.

Now, let us look at another interference term $MAI_{i\leftarrow j}^{(1)}$, which is called the "residual MAI" for convenience. Define $g_j(p) = \frac{e^{-j\pi\frac{p}{N}}}{N\sin\frac{\pi(p+\epsilon_j)}{N}}$. Then, we have the following Lemma.

Lemma 6.5: Let the channel length be L and the code scheme as stated in Theorem 6.1 is used. Then, if we use any one of the G subsets of codewords for the MC-CDMA system with $G \geq L$, the residual MAI term $MAI_{i\leftarrow j}^{(1)}$ in Eq. (6.29) becomes

$$MAI_{i\leftarrow j}^{(1)} = \beta_j x_j \sum_{p=1}^{N-1} g_j(-p) \left\{ \left(\mathbf{h}_i^{(p)}\right)^{\dagger} \underbrace{\mathbf{F}_0^{\dagger}\mathbf{W}_i^{(p)}\mathbf{W}_j\mathbf{F}_0}_{\mathbf{D}_{i,j}^{(p)}} \mathbf{h}_j \right\}, \tag{6.30}$$

where

$$\mathbf{W}_i^{(p)} = \mathrm{diag}\left(w_i[p]\cdots w_i[N-1]\ w_i[0]\cdots w_i[p-1]\right) \tag{6.31}$$

and

$$\mathbf{h}_i^{(p)} = \left(h_i(0)e^{-j\frac{2\pi}{N}0p}\ h_i(1)e^{-j\frac{2\pi}{N}1p}\cdots h_i(L-1)e^{-j\frac{2\pi}{N}(L-1)p}\right). \tag{6.32}$$

Proof: The proof can be found in [136]. ■

Since the MAI due to the CFO is divided into two terms, i.e., the dominating MAI in Eq. (6.28) and the residual MAI in Eq. (6.29), if we can make both terms equal zero, the system can be MAI-free under a CFO environment. From Lemma 6.4, $MAI_{i\leftarrow j}^{(0)} = 0$ with the proposed code. Thus, our goal now is to find a way to make $MAI_{i\leftarrow j}^{(1)} = 0$. Let us further manipulate $\mathbf{D}_{i,j}$ in Eq. (6.30) as

$$\mathbf{D}_{i,j}^{(p)} = \left(\mathbf{I}_L\ \mathbf{0}\right)\mathbf{F}^{\dagger}\mathbf{W}_i^{(p)}\mathbf{W}_j\mathbf{F}\begin{pmatrix}\mathbf{I}_L\\ \mathbf{0}\end{pmatrix}. \tag{6.33}$$

According to Eqs. (6.30) and (6.33), if $\mathbf{D}_{i,j}^{(p)} = 0$ for all $1 \leq p \leq N-1$, we have $MAI_{i\leftarrow j}^{(1)} = 0$.

Theorem 6.3: Suppose the codeword set G_0 is used, the two codewords $\mathbf{w}_0$ and $\mathbf{w}_1$ will have zero $MAI_{i\leftarrow j}^{(1)}$ term. That is, $\sum_{j=0,j\neq 0}^{T-1} MAI_{0\leftarrow j}^{(1)} = 0$ and $\sum_{j=0,j\neq 1}^{T-1} MAI_{1\leftarrow j}^{(1)} = 0$.

Proof. For the all-one code $\mathbf{w}_0$, we have

$$\mathbf{W}_0^{(p)}\mathbf{W}_j = \mathbf{W}_j, \quad 1 \le p \le N-1.$$

Hence, we have $\mathbf{D}_{0,j}^{(p)} = \begin{pmatrix}\mathbf{I}_L & \mathbf{0}\end{pmatrix}\mathbf{F}^{\dagger}\mathbf{W}_j\mathbf{F}\begin{pmatrix}\mathbf{I}_L \\ \mathbf{0}\end{pmatrix}$, for $1 \le p \le N-1$. Since $\mathbf{W}_j$ is a diagonal matrix with diagonal elements drawn from G_0. From the discussion in Section 6.2.1, $\mathbf{D}_{0,j}^{(p)} = 0$ for all p. Hence, $\sum_{j=0,j\neq 0}^{T-1} MAI_{0\leftarrow j}^{(1)} = 0$.

For $\mathbf{w}_1$, which is a codeword with a sign change for every consecutive code symbol, i.e., $\mathbf{w}_1 = (+1\ -1\ +1\ -1\cdots)^t$, its circulant shift is either $\mathbf{w}_1$ or $(-1\ +1\ -1\ +1\cdots)^t = -\mathbf{w}_1$. Hence, we have

$$\mathbf{W}_1^{(p)}\mathbf{W}_j = \begin{cases} \mathbf{W}_1\mathbf{W}_j, & p \text{ even}, \\ -\mathbf{W}_1\mathbf{W}_j, & p \text{ odd}, \end{cases} \quad 1 \le p \le N-1.$$

Since $\mathbf{W}_1\mathbf{W}_j$ is again a codeword in G_0, from the discussion in Section 6.2.1, $\mathbf{D}_{1,j}^{(p)} = 0$ for all p. Hence, $\sum_{j=0,j\neq 0}^{T-1} MAI_{1\leftarrow j}^{(1)} = 0$. ■

Theorem 6.3 suggests to use the 0th codeword set so that there are two codewords to preserve the MAI-free property under the CFO environment. Since codewords $\mathbf{w}_0$ and $\mathbf{w}_1$ are completely MAI-free under the CFO environment when G_0 is used, we can use them as training sequences to estimate the channel and/or CFO for each user. That is, in uplink direction, every user use these two codewords in turn to acquire his/her own channel and/or CFO information. In the downlink direction, one of these two codewords can be reserved as the pilot signal for CFO estimation. In this case, any single-user CFO estimation algorithm (e.g., the one given in [87]) can be applied while sophisticated MUD or signal processing techniques can be avoided. This result stands in contrast with the CFO estimation for GO-MC-CDMA systems [158], where multiuser estimation is demanded to acquire accurate CFO information.

Example 6.4: MAI in the Presence of CFO

In this example, we demonstrate that the dominating MAI due to the CFO effect can be completely eliminated by the use of the proposed code design. The system configuration was the same as that in Example 6.3 with multipath length $L = 2$. Since the simulation was conducted in the uplink direction, every user has his/her own CFO value. Let us consider the worst case, where every user is randomly assigned a CFO either $+\varepsilon$ or $-\varepsilon$. According to Eq. (6.3), when there is no CFO, the desired signal will be scaled by $\sum_{k=0}^{N-1} |\lambda_i[k]|^2$. Thus, we normalize the MAI by $\sum_{k=0}^{N-1} |\lambda_i[k]|^2$ for fair comparison. The dominating total MAI of user i, denoted by $MAI_i^{(0)}$, is obtained

by averaging $\left|\frac{1}{\sum_{k=0}^{N-1}|\lambda_i[k]|^2}\sum_{j=0,j\neq i}^{T-1} MAI_{i\leftarrow j}^{(0)}\right|^2$ for more than 250,000 symbols. Similarly, the residual total MAI, denoted by $MAI_i^{(1)}$, is obtained by averaging $\left|\frac{1}{\sum_{k=0}^{N-1}|\lambda_i[k]|^2}\sum_{j=0,j\neq i}^{T-1} MAI_{i\leftarrow j}^{(1)}\right|^2$ for more than 250,000 symbols. To illustrate the MAI effect clearer, we did not add noise in this example.

First, let us consider the fully-loaded case, i.e., $T = N = 16$. The slim-triangular curves in Fig. 6.6 show the dominating and the residual total MAI of each individual user. The bold-diamond curve, denoted by $MAI^{(0)}$, is the averaged dominating total MAI for the 16 slim-triangular curves of $MAI_i^{(0)}$. Note that the 16 slim-triangular curves of $MAI_i^{(0)}$ are tightly clustered and thus overlap with the bold-diamond curve. Similarly, the bold-square curve, denoted by $MAI^{(1)}$, is the averaged residual total MAI for the 16 slim-circle curves of $MAI_i^{(1)}$. We see that $MAI^{(0)}$ is larger than $MAI^{(1)}$ by 5–32 dB. Hence, it confirms that the dominating MAI term defined in Eq. (6.28) is indeed the key MAI impairment, which is due to CFO.

Now, we consider several half-loaded schemes. First, we examine Shi and Latva-aho's scheme [119] for a half-loaded system, i.e., $\mathbf{w}_0$, $\mathbf{w}_1$, $\mathbf{w}_6$, $\mathbf{w}_7$, $\mathbf{w}_{10}$, $\mathbf{w}_{11}$, $\mathbf{w}_{12}$, and $\mathbf{w}_{13}$. The MAI performance is shown in Fig. 6.7. By comparing

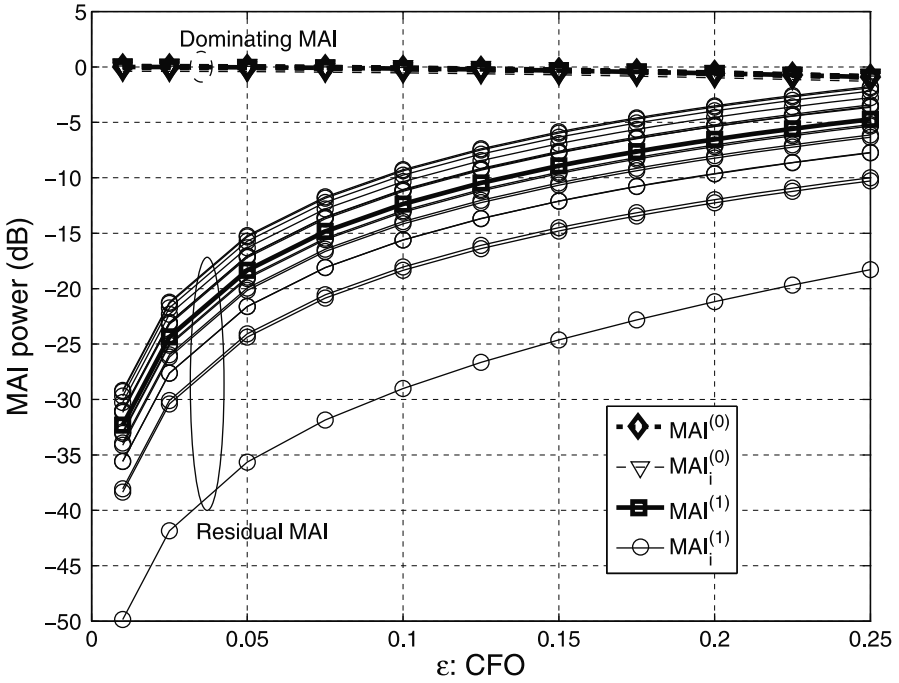

Fig. 6.6. The dominating and the residual MAI as a function of CFO in a fully-loaded situation [[136] ©IEEE].

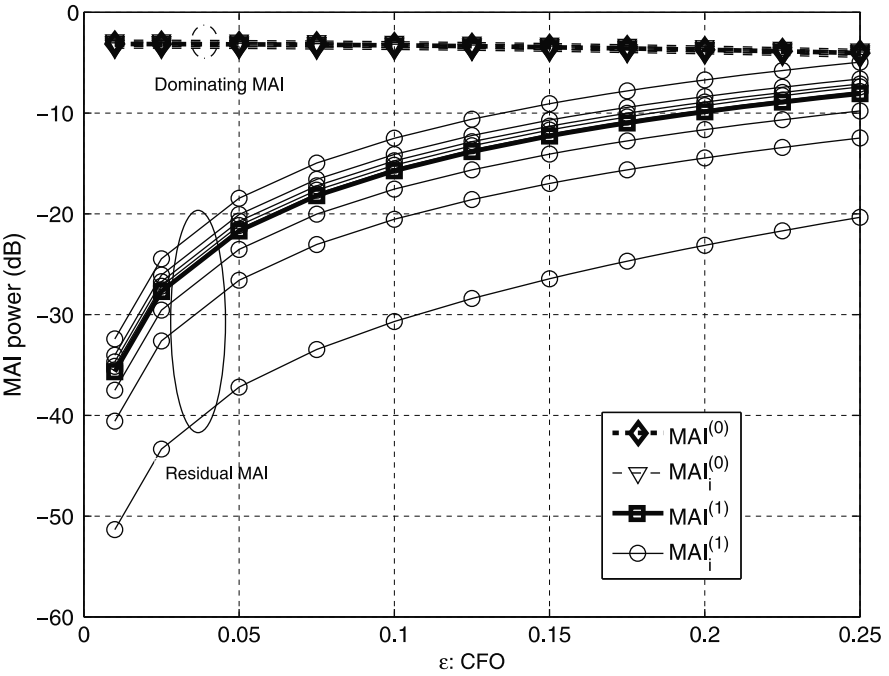

Fig. 6.7. The dominating and the residual MAI as a function of CFO in a half-loaded situation with Shi and Latva-aho's scheme [[136] ©IEEE].

Fig. 6.7 with Fig. 6.6, we see that both the dominating MAI and the residual MAI decrease by only about 3 dB, which shows a reasonable but not satisfactory MAI reduction as the number of users decreases to half in the system.

Next, let us consider the proposed code selection schemes with half-loaded. Since $L = 2$, we divide the codewords into two subsets. G_0 contains the first $N/2$ codewords and G_1 contains the last $N/2$ codewords. The performance is shown in Fig. 6.8(a) and (b), respectively. Note that the dominating MAI term $MAI_i^{(0)}$ is equal to zero so that it is not shown here. Moreover, there are only six curves in Fig. 6.8(a) for $MAI_i^{(1)}$, since the two codewords $\mathbf{w}_0$ and $\mathbf{w}_1$ are completely MAI-free under the CFO environment.

By examining Fig. 6.6 and Fig. 6.8(a) and (b), we see that the dominating MAI can be completely eliminated by the proposed code scheme. In this case, the residual MAI will determine the system performance. Furthermore, the residual MAI decreases around 5 dB. These results show that the MAI due to the CFO effect can be greatly reduced using the proposed code schemes. Moreover, if the codewords of G_0 are used, users of $\mathbf{w}_0$ and $\mathbf{w}_1$ can still have zero MAI under the CFO environment. ■

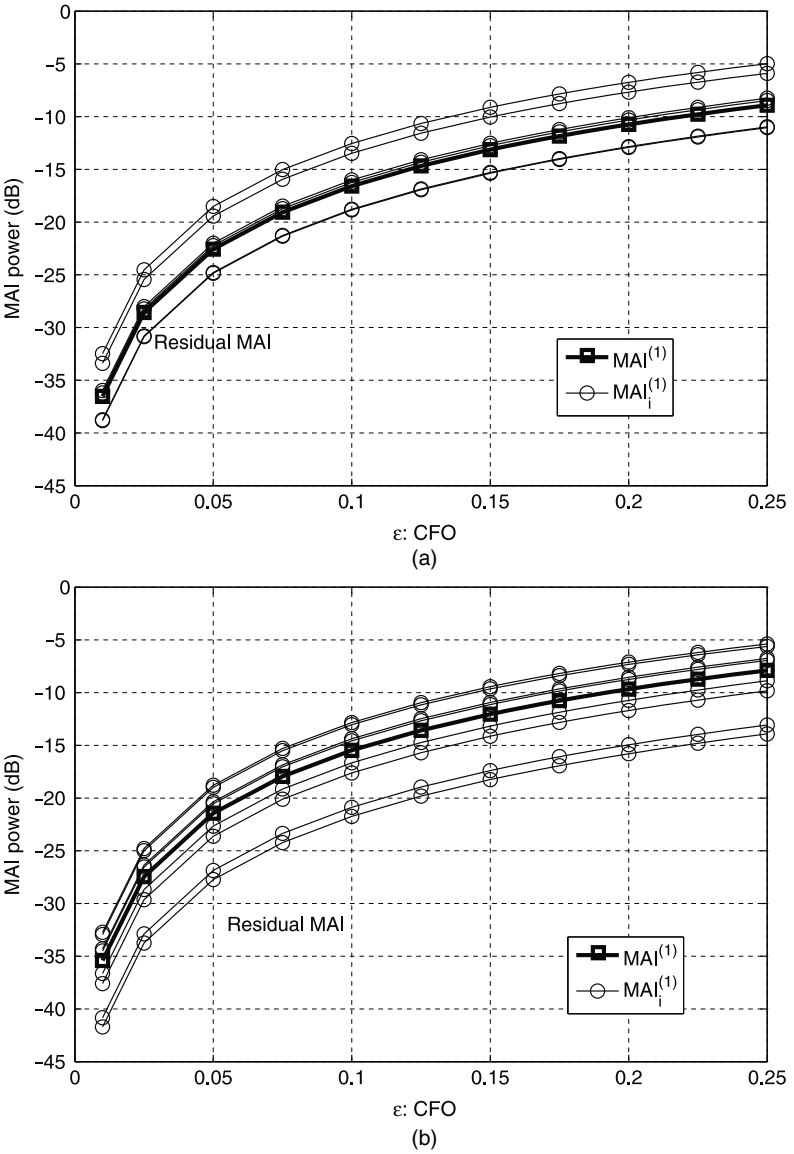

Fig. 6.8. MAI reduction via the proposed code schemes using codewords in (**a**) G_0 and (**b**) G_1 [[136] ©IEEE].

Example 6.5: BEP in the Presence of CFO

In this example, we consider the bit error probability (BEP) performance in the presence of the CFO effect for several code schemes of MC-CDMA and the GO-MC-CDMA scheme [158]. The parameter setting remains the same as

that in Example 6.4. For MC-CDMA, we consider the proposed schemes G_0 and G_1, Shi and Latva-aho's scheme [119], and the even indexed codewords, i.e., $\mathbf{w}_0$, $\mathbf{w}_2$, $\cdots$, $\mathbf{w}_{N-2}$. For GO-MC-CDMA, since $L = 2$, we divide 16 subcarriers into eight groups, where each group can support two users. Since the system is half-loaded, each group has exactly one user so that the system is MAI-free when there is no CFO. We assume that every scheme can accurately estimate individual user's CFO. With G_0, this can be achieved using estimation algorithms for single-user OFDM systems since there are two MAI-free codewords even in a multiuser CFO environment. In contrast, other schemes need to use multiuser CFO estimation. The CFO effect is compensated at the receiver without any feedback. Figure 6.9 shows the BEP as a function of the CFO with SNR ($= E_b/N_0$) fixed at 15 dB for different schemes. It is clear that the proposed code schemes G_0 and G_1 outperform Shi and Latva-aho's scheme and the set of even-indexed codewords significantly. They also outperform GO-MC-CDMA slightly. We see from this figure that codeword set G_0 slightly outperforms codeword set G_1. This is because that $\mathbf{w}_0$ and $\mathbf{w}_1$ are free from MAI in the presence of CFO. ■

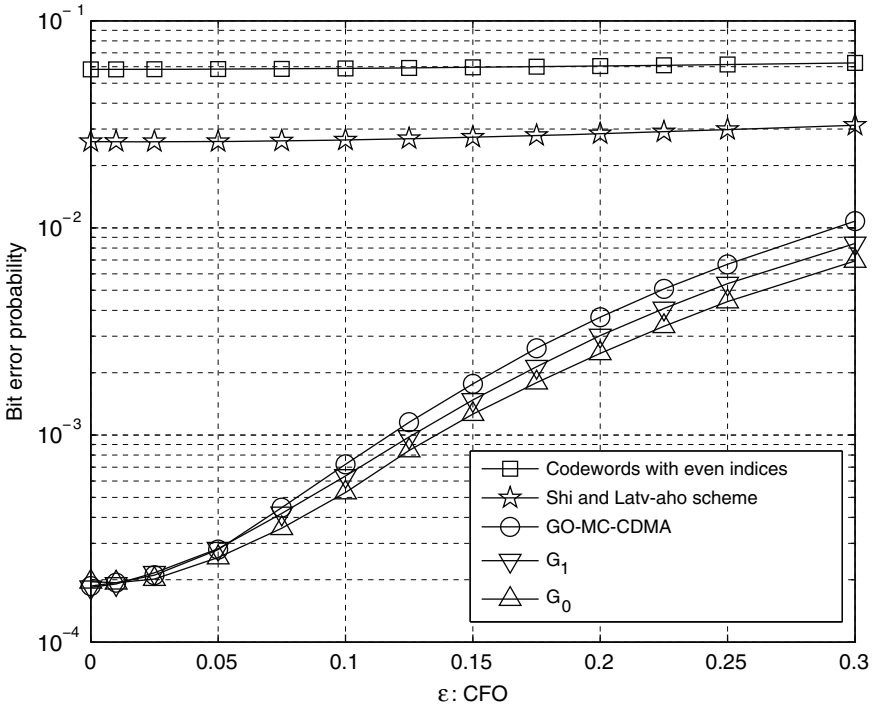

Fig. 6.9. The BEP as a function of CFO (with fixed $E_b/N_0 = 15$ dB) [[136] ©IEEE].

Example 6.6: CFO Estimation with a Single-User Algorithm
It was shown in Example 6.5 that the GO-MC-CDMA system can achieve comparable performance with the proposed code scheme in a CFO environment. However, this result is obtained under the assumption that every user's CFO can be estimated accurately. For the MC-CDMA system with codeword set G_0, users with codewords $\mathbf{w}_0$ and $\mathbf{w}_1$ do not have MAI from others in a CFO environment and, consequently, accurate CFO can be estimated if each user adopts these codewords to estimate his/her own CFO in turn. In this case, estimation algorithms developed for single-user OFDM can be used for the proposed scheme. In contrast, we need more sophisticated estimation algorithms for multiuser OFDM systems for GO-MC-CDMA since none of the users in GO-MC-CDMA is free from MAI in a CFO environment. In this example, we will evaluate the CFO estimation error for the proposed system and the GO-MC-CDMA system when the single-user CFO estimation algorithm given in [87] is used.

The parameter setting remains the same as that in Example 6.5. Since both MC-CDMA and GO-MC-CDMA spread one symbol into several chips, the detection output is actually one symbol. Hence, we only need two symbols for CFO estimation. Referring to Fig. 6.1, we denote the two successive output symbols, i.e., the current and the next ones, by $\hat{x}_i$ and $\hat{x}_i'$. The CFO estimation can be obtained via [87]

$$\hat{\epsilon}_i = \frac{1}{2\pi}\tan^{-1}\left[\Im\left\{\hat{x}_i^*\hat{x}_i'\right\}/\Re\left\{\hat{x}_i^*\hat{x}_i'\right\}\right],$$

where $\Re\{x\}$ and $\Im\{x\}$ are the real and the imaginary parts of x. For the proposed scheme, all eight codewords in G_0 are active. For the GO-MC-CDMA, each user occupies one of the eight groups and there are eight users [158]. Without loss of generality, $\mathbf{w}_0$ is used for CFO estimation in the proposed scheme. For GO-MC-CDMA, the user who occupies the 0th and the 8th subcarriers with the all-one codeword is used for CFO estimation. The Monte Carlo method is used to run for more than 20,000 realizations. The estimation mean square errors, i.e., $E\left\{|\epsilon_i - \hat{\epsilon}_i|^2\right\}$, as a function of CFO for both systems are shown in Fig. 6.10. We see that the estimation error in GO-MC-CDMA increases as the CFO value becomes larger. This is because the CFO-induced MAI increases as the CFO value increases, which deteriorates estimation accuracy. On the other hand, the estimation error in the proposed MC-CDMA system with G_0 remains constant in a multiuser CFO environment. This shows that the use of codeword set G_0 has a better CFO estimation result in a multiuser environment. ■

Example 6.7: Code Priority of MC-CDMA
In this example, we consider a code priority scheme for a fully-loaded MC-CDMA system using the proposed code scheme. The system setting is the same as that in Example 6.5 except that SNR is set to 18 dB while CFO is set to zero. The Monte Carlo method is used with more than 10,000,000 symbols for all users in the simulation.

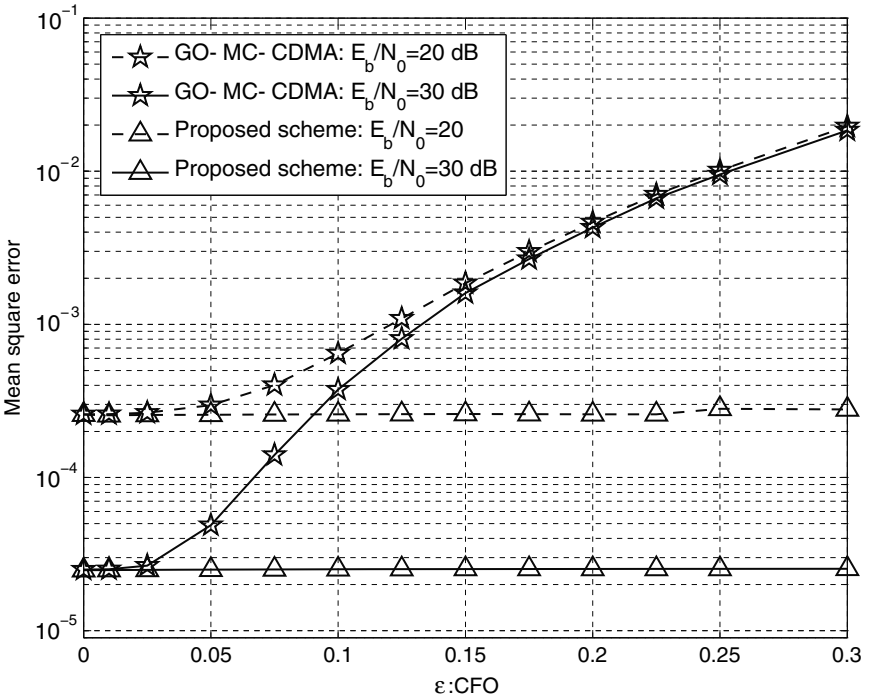

Fig. 6.10. The mean squared error of CFO estimation as a function of CFO for the proposed and the GO-MC-CDMA schemes [[136] ©IEEE].

We first consider two code priority schemes that assign codewords according to the following order:

$$\text{Priority Scheme I: } \mathbf{w_0},\ \mathbf{w_8},\ \mathbf{w_1},\ \mathbf{w_9},\ \mathbf{w_2},\ \mathbf{w_{10}},\ \mathbf{w_3},\ \mathbf{w_{11}},\ \mathbf{w_4},\ \mathbf{w_{12}},\ \mathbf{w_5},\ \mathbf{w_{13}},\ \mathbf{w_6},\ \mathbf{w_{14}},\ \mathbf{w_7},\ \mathbf{w_{15}}. \quad (6.34)$$

$$\text{Priority Scheme II: } \mathbf{w_0},\ \mathbf{w_9},\ \mathbf{w_2},\ \mathbf{w_{11}},\ \mathbf{w_4},\ \mathbf{w_{13}},\ \mathbf{w_6},\ \mathbf{w_{15}},\ \mathbf{w_1},\ \mathbf{w_8},\ \mathbf{w_3},\ \mathbf{w_{10}},\ \mathbf{w_5},\ \mathbf{w_{12}},\ \mathbf{w_7},\ \mathbf{w_{14}}. \quad (6.35)$$

Scheme I assigns the next user an even-indexed (or odd-indexed) codeword in G_1 whenever the current user is assigned an even-indexed (or odd-indexed) codeword in G_0. Since even-indexed (or odd-indexed) codewords in G_1 cause more serious MAI to even-indexed (or odd-index) codewords, the first code priority has poor performance. It is adopted as a performance benchmark. Scheme II assigns even- and odd-indexed codewords from G_0 and G_1 alternatively for the first eight users. It serves as another performance benchmark. Furthermore, we also implement the code priority scheme proposed by Shi and Latva-aho's in [119]. Since this scheme only considers a system up to the half-loaded situation, its performance curve is plotted up to eight users.

Finally, we consider the proposed code priority scheme, where we first assign eight codewords in G_0 to the first eight active users. When the number of active users exceeds eight, we will use codewords in G_1. One such code priority scheme can be written as

$$\text{Proposed Priority Scheme: } \mathbf{w_0},\ \mathbf{w_1},\ \mathbf{w_2},\ \mathbf{w_3},\ \mathbf{w_4},\ \mathbf{w_5},\ \mathbf{w_6},\ \mathbf{w_7},\ \mathbf{w_8},\ \mathbf{w_9},\ \mathbf{w_{10}},\ \mathbf{w_{11}},\ \mathbf{w_{12}},\ \mathbf{w_{13}},\ \mathbf{w_{14}},\ \mathbf{w_{15}}. \tag{6.36}$$

If there is no CFO, the system is MAI-free using only eight codewords in either G_0 or G_1 according to Theorem 6.1. The order of the first eight codewords can be changed arbitrarily. Also, we can assign codewords all from G_1 first and then from G_0.

The bit error probability is plotted as a function of the number of active users for the above four code priority schemes in Fig. 6.11. Scheme I has the worst performance as expected. The performance of the proposed code priority stays the same when the number of active users is smaller than 9 due to the MAI-free property. When T exceeds 8, the performance of the proposed scheme degrades dramatically. However, its performance remains at least as

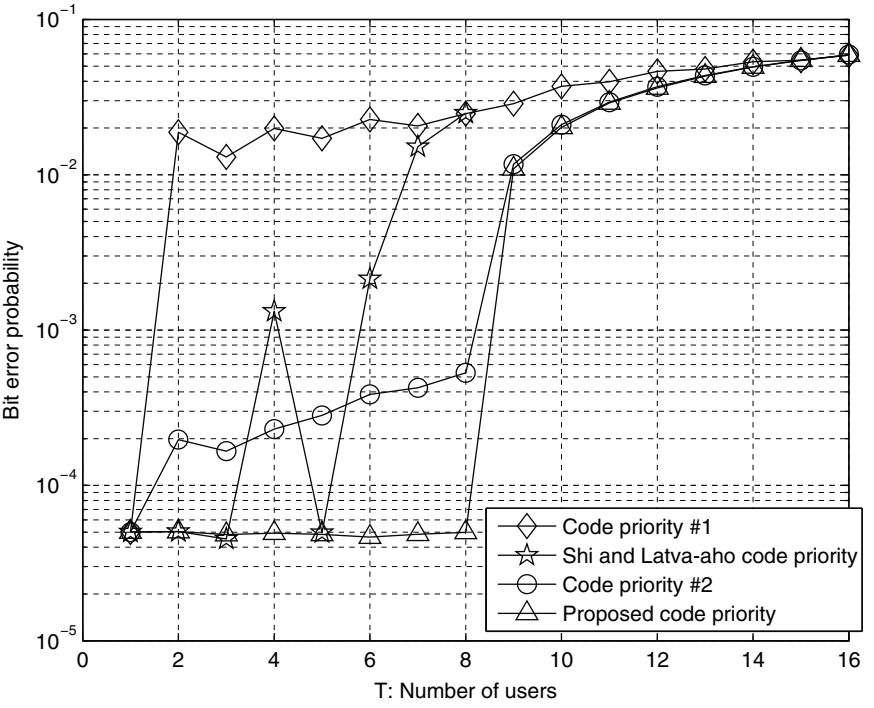

Fig. 6.11. The BEP as a function of the number of users with SNR=18 dB [[136] ©IEEE].

good as Schemes I and II. We also see that for Shi and Latva-aho's scheme, it has the same performance as the proposed code priority when the numbers of users are 1, 2, 3, and 5. This is reasonable since codewords of these user numbers fall in the set of G_0 and, hence, they are free from MAI. However, for other numbers of users, its performance is worse than the proposed code priority scheme. Moreover, in the Shi and Latva-aho's priority, if the number of active users changes, some users will need to change their codewords, which complicates the actual deployment of this scheme. ■

6.2.4 Practical Considerations on Applicability of the Proposed Scheme

The proposed scheme is applicable to both up and down links in a multiuser system. The basic assumption of having a synchronous channel holds in the downlink. As to the uplink, we may consider a quasi-synchronous channel, where the time offset is within one chip. Such a channel holds in the uplink direction for a micro cell, e.g., see pp. 1179–1195 in [121]. In practice, quasi-synchronism can be achieved by the use of the GPS. Therefore, there are several systems or code designs based on this assumption; e.g., group-orthogonal (GO)-MC-CDMA system [158], the LV (Lagrange/Vandermonde) code [116], the code scheme for MC-CDMA in [119], and the LAS (large area synchronized) code in [122]. Even if the system is not perfectly synchronized, time delay can still be included in the channel impulse response. In this case, we may have larger L and, hence, the number of supportable users to meet the MAI-free property decreases.

As presented above, there is a close connection between the multipath length, the spreading gain (i.e., the number of subcarriers) and the number of users that can be supported by the proposed technique. In particular, in order to achieve a zero MAI, the system load has to be significantly reduced for a larger multipath length. This is a potential disadvantage for the proposed scheme. In practice, under a reasonable sampling frequency, the multipath length is in general moderate. For example, in an outdoor environment, the most commonly used multipath duration is around 1–3 μs [108]. For the IS-95 standard, the chip rate is 1.2288 M chips/s in the uplink direction. Hence, the resolvable multipath length is around 1–3 taps. In an indoor environment, the maximum multipath duration for an office building is around 0.27 μs. If we take the sampling frequency of WLAN of 20 MHz as an example, the resolvable multipath length is around 5 taps. However, the indoor multipath duration is in general under 0.1 μs. In this case, the resolvable multipath length is around 2–3 taps. It is worthwhile to point out that under a fixed multipath L and DFT/IDFT size N, the GO-MC-CDMA system [158] without MUD supports exactly the same number of MAI-free users as the proposed system. Although the number of MAI-free users in both systems decreases as channel length L increases, every MAI-free user in these systems can enjoy an increased channel diversity order L.

As commented by Chen in [23] "... all existing CDMA systems fail to offer satisfactory performance and capacity, which is usually far less than half of the processing gain of CDMA systems." Hence, the choice of the spreading code to reduce MAI can be a direction for the design of next-generation CDMA systems. We approach the MAI reduction problem from a similar viewpoint. That is, for fixed channel conditions, we attempt to select a subset of codewords that can lead to an MAI-free system and hence provide a high date rate with simple transceiver design. This design concept stands in contrast with that of conventional CDMA systems. For instance, as the number of users increases in IS-95, the achievable data rate decreases in order to support the fully-loaded user capacity. If a higher data rate is desired in IS-95, we need to use the more sophisticated MUD, which will increase the transceiver burden. However, since the Hadamard-Walsh code in nature has several codeword sets that can achieve MAI-free in MC-CDMA, the complexity for MUD using the Hadamard-Walsh code is much less than that using other code schemes. ■

6.3 MAI-Free MC-CDMA with CFO Using Hadamard-Walsh Codes

In this section, we show how to select a subset of Hadamard-Walsh codes for MC-CDMA to eliminate completely MAI under any CFO level.

Let $w[k]$, $0 \le k \le N-1$, be any codeword of length N and $G < N$ be any integer that divides N. For convenience, we define periodic and antiperiodic codewords below. A codeword is said to be periodic with period N/G if

$$w[((k + gN/G))_N] = w[k], \tag{6.37}$$

where $0 \le k \le N-1$, $0 \le g \le G-1$. A codeword is said to be antiperiodic with antiperiodic N/G if

$$w[((k + N/G))_N] = -w[k]. \tag{6.38}$$

For example, codeword (1 -1 1 -1) is periodic with period $4/2 = 2$ while codeword (1 -1 -1 1) is antiperiodic with antiperiod $4/2 = 2$.

Lemma 6.6: Let $\mathbf{w}_i = (w_i[0], \cdots, w_i[N-1])^t$ be any periodic or antiperiodic codeword with period or antiperiod N/G. Then, $\mathbf{w}_i^{(p)}$ is periodic or antiperiodic if $\mathbf{w}_i$ is periodic or antiperiodic, respectively, with the same period or antiperiod N/G.

Proof: By the definition of $\mathbf{w}_i^{(p)}$, we have

$$w_i^{(p)}[k] = w_i[((N - p + k))_N]. \tag{6.39}$$

If $\mathbf{w}_i$ is periodic with period N/G, we have

$$w_i^{(p)}[((k+gN/G))_N] = w_i[((N-p+k+gN/G))_N]$$
$$= w_i[((N-p+k))_N] = w_i^{(p)}[k].$$

Similarly, if $\mathbf{w}_i$ is antiperiodic with antiperiod N/G, we have

$$w_i^{(p)}[((k+N/G))_N] = w_i[((N-p+k+N/G))_N]$$
$$= -w_i[((N-p+k))_N] = -w_i^{(p)}[k],$$

for $0 \le g \le G-1$ and $0 \le k \le N-1$. ■

Consider the N *times* N Hadamard-Walsh matrix, $\mathbf{H}_N$. As described in Section 6.2.1, we can form the subset $G_0 = \{\mathbf{w}_0, \mathbf{w}_1, \cdots, \mathbf{w}_{\frac{N}{G}-1}\}$ for a channel with maximum length L. We can further divide codewords in G_0 into two disjoint subsets of equal size as

$$G_{00} = \{\mathbf{w}_0, \mathbf{w}_1, \cdots, \mathbf{w}_{\frac{N}{2G}-1}\} \text{ and } G_{01} = \{\mathbf{w}_{\frac{N}{2G}}, \mathbf{w}_{\frac{N}{2G}+1}, \cdots, \mathbf{w}_{\frac{N}{G}-1}\}.$$

Then, we have the following properties.

Lemma 6.7: For any codeword $\mathbf{w}_i$ in G_{01} and any codeword $\mathbf{w}_j$ in G_{00}, we have $\widetilde{MAI}_{i\leftarrow j} = 0$.

Proof: We need to show

$$\widetilde{MAI}_{i\leftarrow j} = MAI_{i\leftarrow j}^{(0)} + MAI_{i\leftarrow j}^{(1)} = 0.$$

Define

$$r_{i,j}^{(p)}[k] = w_i^{(p)}[k] w_j^*[k] \quad k = 0, 1, \cdots, N-1.$$

By Theorem 6.1, if $\mathbf{w}_i$ and $\mathbf{w}_j$ are in two disjoint subsets G_g, $g = 0, 1, ..., G-1$, $MAI_{i\leftarrow j} = 0$ in a frequency selective channel. Since G_{01} and G_{01} are disjoint subsets of G_0, and $MAI_{i\leftarrow j}^{(0)} = \alpha_j MAI_{i\leftarrow j}$ by Eq. (6.28), we conclude $MAI_{i\leftarrow j}^{(0)} = 0$.

To have $MAI_{i\leftarrow j}^{(1)} = 0$, $\mathbf{D}_{i,j}^{(p)}$ must be the $L \times L$ zero matrix for all $i \neq j$ and $p = 0, 1, ..., N-1$. But $\mathbf{D}_{i,j}^{(p)}$ is an $L \times L$ upper left submatrix of matrix $\mathbf{C}_{i,j}^{(p)} = \mathbf{F}^\dagger \mathbf{W}_i^{(p)} \mathbf{W}_j \mathbf{F}$ which is a circulant matrix [47]. That is, the first column of $\mathbf{C}_{i,j}^{(p)}$, $(c_{i,j}(0) \cdots c_{i,j}(N-1))^t$, is the N-point IDFT of $\mathbf{r}_{i,j}^{(p)}$. To have $\mathbf{D}_{i,j}^{(p)} = \mathbf{0}$ the first L samples and the last $L-1$ samples of the IDFT of $\mathbf{r}_{i,j}^{(p)}$ are zeros.

By taking the IDFT of $\mathbf{r}_{i,j}^{(p)}$, we have

$$r_{i,j}^{(p)}(n) = \frac{1}{N} \sum_{m=0}^{N-1} r_{i,j}^{(p)}[m] e^{j\frac{2\pi}{N}mn}. \tag{6.40}$$

Let $m = k + gN/G$, $0 \le k \le N/G - 1$ and $0 \le g \le G-1$. We can rewrite Eq. (6.40) as

$$r_{i,j}^{(p)}(n) = \frac{1}{N} \sum_{k=0}^{N/G-1} \sum_{g=0}^{G-1} r_{i,j}^{(p)}[k + gN/G] e^{j\frac{2\pi}{N}(k+gN/G)n}. \tag{6.41}$$

Since codewords $\mathbf{w}_i$ and $\mathbf{w}_j$ belong to G_0, they are among the first N/G columns of the Hadamard matrix and formed by repeating the upper left $N/G \times N/G$ submatrix of $\mathbf{H}_N$, G times. Hence, they are periodic with period N/G. By Lemma 6.1, $\mathbf{w}_i^{(p)}$ is also periodic with period N/G. Since the product of two periodic functions whose periods are the same is another periodic function with the same period, we have

$$r_{i,j}^{(p)}[k + gN/G] = r_{i,j}^{(p)}[k]. \tag{6.42}$$

Then, we can rewrite Eq. (6.41) as

$$r_{i,j}^{(p)}(n) = \frac{1}{N} \sum_{k=0}^{N/G-1} r_{i,j}^{(p)}[k] e^{j\frac{2\pi}{N}kn} \sum_{g=0}^{G-1} e^{j\frac{2\pi}{G}gn}, \tag{6.43}$$

where $0 \le k \le N/G - 1$ and $0 \le g \le G - 1$. Since

$$\sum_{g=0}^{G-1} e^{j\frac{2\pi}{G}gn} = \begin{cases} G, \, n = 0, \pm G, \cdots \\ 0, \ \text{otherwise}, \end{cases} \tag{6.44}$$

we have

$$r_{i,j}^{(p)}(n) = \begin{cases} \frac{G}{N} \sum_{k=0}^{N/G-1} r_{i,j}^{(p)}[k] e^{j\frac{2\pi}{N}kn}, \, n = 0, \pm G, \cdots \\ 0, \qquad\qquad\qquad\qquad \text{otherwise}. \end{cases} \tag{6.45}$$

To prove $r_{i,j}^{(p)}(0) = 0$, we need to show $\mathbf{r}_{i,j}^{(p)}$ has an equal number of $+1$ and -1. In general, $\mathbf{r}_{i,j}^{(p)}$ does not belong to the Hadamard matrix whose codewords have an equal number of $+1$ and -1. For example, for $N = 8$, $\mathbf{w}_8^{(1)} \cdot \mathbf{w}_7$ has two -1's and six 1's, where $\cdot$ denotes the component-wise vector product. However, if $\mathbf{w}_i \in G_{01}$ and $\mathbf{w}_j \in G_{00}$, $\mathbf{r}_{i,j}^{(p)}$ does have an equal number of $+1$ and -1 as shown below. According to Eq. (6.8), codewords in G_{00} are the first $N/2G$ columns of H_N and obtained by repeating the $N/2G \times N/2G$ submatrix $2G$ times. Hence, any codeword $\mathbf{w}_j \in G_{00}$ is periodic with period $N/2G$. Similarly, we can show that any codeword $\mathbf{w}_i \in G_{01}$ is antiperiodic with antiperiodic $N/2G$. By Lemma 6.1, $\mathbf{w}_i^{(p)}$ is also antiperiodic with the same antiperiod. Therefore, for $0 \le k \le N - 1$, we have

$$\begin{aligned} &w_i^{(p)}[((k + N/2G))_N] w_j[((k + N/2G))_N] = \\ &-w_i[((N - p + k))_N] \, w_j[k] = -w_i^{(p)}[k] w_j[k]. \end{aligned}$$

Hence, $\mathbf{r}_{i,j}^{(p)}$ is antiperiodic with antiperiod $N/2G$. It can be easily shown that any antiperiodic code has an equal number of ± 1. Thus, $r_{i,j}^{(p)}(0) = \frac{1}{N} \sum_{k=0}^{N-1} r_{i,j}^{(p)}[k] = 0$. ■

Let us consider an example for $N = 16$ and $L = 2$. By choosing $G = 2$,

$$G_{00} = \{\mathbf{w}_0, \mathbf{w}_1, \mathbf{w}_2, \mathbf{w}_3\}$$

and

$$G_{01} = \{\mathbf{w}_4, \mathbf{w}_5, \mathbf{w}_6, \mathbf{w}_7\}.$$

By Lemma 6.7, any codeword chosen from G_{01} achieves zero MAI with respect to any codeword from G_{00}. On the other hand, we will not necessarily have an MAI-free system when both codewords are chosen from G_{00} (or both from G_{01}). For instance, $\widetilde{MAI}_{2\leftarrow 3} \neq 0$ or $\widetilde{MAI}_{4\leftarrow 5} \neq 0$ for $N = 16$ and $L = 2$.

Note that Lemma 6.7 does not identify a subset of codewords that can be assigned to all active users while keeping the system MAI-free. This choice will be examined in the following theorem. In particular, we want to determine such an MAI-free set from subsets of G_0 and specify the number of codewords in the resulting MAI-free set.

Theorem 6.4: For a channel of length L and $G = 2^q \geq L$, there are $1 + \log_2(N/G)$ codewords from N HW codes that will lead to an MAI-free MC-CDMA system under any CFO level.

Proof: We form subsets G_0, G_{00}, and G_{01} as described above. To build an MAI-free subset, we must choose only one of the codes from G_{01}. To determine the remaining codes from G_{00}, we divide G_{00} into two subsets G_{000} and G_{001}, each with $N/4G$ codes, by following the same procedure. Then, we can choose one from G_{001}, since it can be proved by arguments similar to that in Lemma 6.2 that any codeword from G_{001} is MAI-free from any codeword in G_{000}. By repeating this procedure, we can obtain an MAI-free set. Since the division of a subset generates one codeword to be included in the MAI-free codeword set in each stage, we have $\log_2(N/G)$ codes in the MAI-free set. Furthermore, each of the two subsets has only one codeword in the last stage, we can add both codewords ($\mathbf{w}_0$ and $\mathbf{w}_1$) to the MAI-free set. Thus, the total number of MAI-free codewords is $1 + \log_2(N/G)$. ■

Consider the previous example, where $N = 16$ and $L = G = 2$. By Lemma 6.2, we can choose one codeword, say $\mathbf{w}_4$, from

$$G_{01} = \{\mathbf{w}_4, \mathbf{w}_5, \mathbf{w}_6, \mathbf{w}_7\}$$

for the MAI-free set. We can divide

$$G_{00} = \{\mathbf{w}_0, \mathbf{w}_1, \mathbf{w}_2, \mathbf{w}_3\}$$

into two subsets, i.e., $G_{000} = \{\mathbf{w}_0, \mathbf{w}_1\}$ and $G_{001} = \{\mathbf{w}_2, \mathbf{w}_3\}$. Then, we include either $\mathbf{w}_2$ or $\mathbf{w}_3$ in G_{001} in the MAI-free set. If we divide G_{000} further into two more subsets, $\{\mathbf{w}_0\}$ and $\{\mathbf{w}_1\}$, we can include both $\mathbf{w}_0$ and $\mathbf{w}_1$ in the MAI-free set by Lemma 6.2. Therefore, there will be $1 + \log_2(16/2) = 4$ MAI-free codewords.

Example 6.8: MAI-Free MC-CDMA with Hadamard-Walsh Codes In this example, we corroborate theoretical results derived in Lemma 6.7 and Theorem 6.4 with computer simulations. Let $N = 16$, $L = 2$ and the CFO value is fixed to be ± 0.1. Every user was randomly assigned by a CFO value of either 0.1 or -0.1. The MAI power was normalized by $\sum_{k=0}^{N-1} |\lambda_i[k]|^2$ since the desired signal was scaled by the same amount.

The values of $MAI_{i \leftarrow j}$ power for all HW codewords in G_0 are tabulated in Table 6.1. When the MAI value is below -290 dB, it is equivalent to zero numerically. We have several interesting observations from Table 6.1. First, users with codewords $\mathbf{w}_0$ and $\mathbf{w}_1$ are mutually MAI-free with other users. This result is not surprising since it was already shown in the proof of Lemma 6.6. Second, there is no MAI among any two users, if one uses a codeword from $G_{01} = \{\mathbf{w}_4, \mathbf{w}_5, \mathbf{w}_6, \mathbf{w}_7\}$ while the other from $G_{00} = \{\mathbf{w}_0, \mathbf{w}_1, \mathbf{w}_2, \mathbf{w}_3\}$. This result validates Lemma 6.7. Third, if users use codewords from G_{01} (or from G_{00}), MAI may not be zero. For example, we see $MAI_{4 \leftarrow 6} = -27.6$ dB and $MAI_{5 \leftarrow 7} = -45.0$ dB. Finally, we observe $\{\mathbf{w}_0, \mathbf{w}_1, \mathbf{w}_2, \mathbf{w}_4\}$ or $\{\mathbf{w}_0, \mathbf{w}_1, \mathbf{w}_3, \mathbf{w}_7\}$ provides two subsets of MAI-free codewords in the presence of CFO. This confirms our claim that there are $1 + \log_2(16/2) = 4$ users that are mutually MAI-free.

Table 6.1. $MAI_{i \leftarrow j}$ power (dB) as a function of Hadamard-Walsh codewords in G_0 [[124] ©IEEE].

	$\mathbf{w}_0$	$\mathbf{w}_1$	$\mathbf{w}_2$	$\mathbf{w}_3$	$\mathbf{w}_4$	$\mathbf{w}_5$	$\mathbf{w}_6$	$\mathbf{w}_7$
$\mathbf{w}_0$	×	−324	−324	−325	−325	−328	−326	−328
$\mathbf{w}_1$	−325	×	−325	−324	−328	−324	−328	−326
$\mathbf{w}_2$	−325	−325	×	−30.1	−326	−328	−324	−327
$\mathbf{w}_3$	−325	−325	−30.1	×	−328	−326	−328	−324
$\mathbf{w}_4$	−324	−329	−326	−328	×	−33.1	−27.6	−53.6
$\mathbf{w}_5$	−328	−324	−328	−326	−33.1	×	−54.25	−45.0
$\mathbf{w}_6$	−326	−329	−324	−328	−27.6	−54.2	×	−33.1
$\mathbf{w}_7$	−328	−326	−328	−323	−53.6	−45.0	−33.1	×

7

Simplified Multiuser Detection for MC-CDMA with Carrier Interferometry Codes with CFO

In previous chapter, we demonstrated that by partitioning Hadamard-Walsh (HW) codewords into subsets, codewords in some particular subsets allow MAI-free communication in a CFO environment. For a system with a spreading gain N and a maximum channel length L, the number of supportable MAI-free users with HW codes is $1 + \log_2(N/G)$, where G is a power of 2 and $L \leq G < N$. However, the number of such MAI-free users are relatively small in most practical multipath channels. Consequently, to have a fully-loaded MC-CDMA, one may resort to multiuser detection techniques.

Multiuser detection (MUD) techniques have been developed to mitigate MAI. The optimum multiuser detection scheme in [144] maximizes the likelihood functions of N users jointly by choosing the bits that minimize the mean square error (MSE) between the estimated received signal and the actual received composite signal. The optimum MUD scheme improves the user capacity gain substantially at the cost of a high computational complexity, which grows exponentially with the number of users.

Suboptimum linear MUD techniques, such as the decorrelating detector and the minimum mean-square error (MMSE) detector, have been designed to lower the complexity of the optimum MUD while keeping the user capacity gain as close to that of the optimum MUD as possible. The decorrelating and MMSE detectors do not require the knowledge of the received amplitudes. One other desirable feature of the decorrelating detector is that it can be decentralized such that every user can be detected independently from other users [144]. For N users, both techniques demand the inversion of an $N \times N$ matrix, which requires $O(N^3)$ computations with Gauss-elimination and $O(N^2)$ computations with fast algorithms.

There is another class of MAI suppression techniques, known as interference cancellation (IC), whose complexity grows linearly with the user number [4]. The IC techniques attempt to remove interference after hard decoding. They can be classified into two types: parallel interference cancellation (PIC) and successive interference cancellation (SIC). The PIC detector was introduced to CDMA systems as a "multistage detector" in [143] and it was shown

C.-C.J. Kuo et al., *Precoding Techniques for Digital Communication Systems*,
DOI: 10.1007/978-0-387-71769-2_7,

to have low complexity and good performance. The PIC receiver [32, 89] processes all N users simultaneously by cancelling their interference after all of them have been decoded independently. The SIC receiver decodes users successively in several stages with interference being cancelled at each stage [89]. The SIC receiver has a lower complexity than the PIC receiver at the cost of higher latency.

A large amount of efforts has been made to reduce the complexity of the multiuser detectors. Cai et al., [158] proposed to assign a set of subcarriers to a group of users while preserving the frequency diversity of MC-CDMA as much as possible. With this design, MAI is only present among users in the same group so that it can be suppressed via simplified MUD techniques. A new ML-MUD scheme called sphere decoding was proposed for MC-CDMA, whose complexity is a polynomial function of the user number [14]. It applies lattice sphere decoding to the received signal that is modeled as multidimensional lattice packing points. However, when the user number is large, the sphere decoding ML algorithm is cumbersome to perform. Moreover, neither of these techniques are shown to be effective in the presence of CFO.

In asynchronous DS-CDMA where the size of cross-correlation matrix is quite large, suboptimal approaches to implement the decorrelating detectors have been proposed which are based on partitioning the long received sequence into blocks of data that have more manageable size [63, 150]. A linear filter implementation for the decorrelating detector was proposed in [82] where the filter coefficients depend on the cross-correlations.

In this chapter, we show how the set of orthogonal carrier interferometry (CI) codewords [92] can increase the number of MAI-free users to N/G, for a multipath channel of length L and spreading gain N, where G is a power of 2 and $L \leq G < N$, and in a CFO environment. It is worthwhile mentioning that two sets of orthogonal CI codewords were introduced in [92] to increase user capacity of MC-CDMA from N to $2N$ with negligible performance degradation in a multipath fading channel. CI codes were also used as training sequences for channel estimation to decouple the inter-antenna interference in a CFO-free MIMO-OFDM system [72].

We also show that the use of CI codes will lead to simplified MAI multiuser detection techniques if employed by a fully-loaded MC-CDMA in a CFO environment. We first use the PIC receiver to suppress MAI and evaluate the performance of PIC in MC-CDMA with CI and HW codes over a multipath Rayleigh fading channel with CFO. Using CI codewords, the complexity for fully-loaded PIC (i.e., N active users) is linearly proportional to the channel length, L, rather than the user number, N. Since N is in general much larger than L, the complexity is substantially reduced. Next, we show that, by exploiting the sparsity of the cross-correlation matrix of MC-CDMA with CI codes, we can lower the complexity of ML detectors so that its complexity grows exponentially with the channel multipath length instead of the number of active users. To be more specific, the complexity of the ML detector for a fully-loaded MC-CDMA system with BPSK signals and spread gain N and

multipath length L in a CFO environment is in the order of $O(2^{2L-1})$ (instead of $O(2^N)$ where N is the number of active users). This results in significant complexity reduction in practical situations. Finally, we show that the cross-correlation matrix for MC-CDMA with $N - L + 1$ users can be transformed to a band matrix so that the complexity of the decorrelating detector is reduced to $O(2(N - L + 1)(L - 1)^2)$. This is far less than the complexity of the decorrelating detector for a general dense matrix of the same dimension.

Although MC-CDMA with CI codes (CI-MC-CDMA) and PIC has been considered before [130], a detailed BEP analysis of PIC in the presence of CFO is not yet available in the literature. Here, we analyze the bit error probability (BEP) of fully-loaded MC-CDMA with a single-stage PIC using CI and HW codes.

Also, we derive an upper bound for the minimum error probability MUD for MC-CDMA in a CFO environment and compare it with simulated BEP results for ML detector. We also develop an iterative channel/CFO estimation scheme with orthogonal MAI-free HW or CI codewords, and adopt it in computer simulation.

In the following, we first study the carrier interferometry codes and its properties for MC-CDMA in the presence of CFO. Then, single stage PIC is described and theoretical BEP for a MC-CDMA with single-stage PIC is analyzed in Section 7.2 along with some examples demonstrating the performance of multiple-stage PIC. We describe the ML detector for MC-CDMA with and without CFO in Section 7.3. The sparsity of the cross correlation matrix of CI codes along with its associated tail biting trellis is studied in this section. Also, an upper bound on the minimum error probability is derived for MC-CDMA in a CFO environment. In Section 7.4, we discuss the reduced complexity decorrelating detector using a proper subset of CI codes that results in a band cross-correlation matrix. Finally, simple channel and CFO estimation techniques are proposed and the performance of PIC with the proposed channel/CFO estimation techniques are discussed in Section 7.5

7.1 Orthogonal Carrier Interferometry Codes for MAI-free MC-CDMA with CFO

In this section, we briefly review the system model of MC-CDMA in a CFO environment that was described in detail in Chapter 6. The kth component of the DFT output, $\hat{\mathbf{y}}$, can be written as

$$\hat{y}[k] = \sum_{j=0}^{T-1} r_j[k] + e[k], \tag{7.1}$$

where $e[k]$ is the DFT of additive noise, and $r_j[k]$ is the received signal contributed from the jth user due to the channel fading and the CFO effects and is given by Eq. (6.24) as

$$r_j[k] = \alpha_j \lambda_j[k] y_j[k] + \beta_j \sum_{m=0, m\neq k}^{N-1} \lambda_j[m] y_j[m] g_j(m-k), \tag{7.2}$$

where $\lambda_j[m]$ is the mth component of the N-point DFT of the channel impulse response of user j. α_j and β_j are given by Eqs. (6.25) in Chapter 6, and $g_j(m-k) = e^{-j\pi m - k/N}/N \sin \pi(m-k+\epsilon_j)/N$ was also defined in Chapter 6.

When there is no CFO (i.e., $\epsilon_j = 0$), $r_j[k] = \lambda_j[k] y_j[k]$. Since $\beta_j g_j(0) = \alpha_j$ and by Eqs. (6.1) and (7.2), we have

$$\hat{\mathbf{y}} = \mathbf{C}\mathbf{x} + \mathbf{e}, \tag{7.3}$$

where the element in the ith row and the jth column is

$$\mathbf{C}(i,j) = \beta_j \sum_{m=0}^{N-1} g_j(m-i) \lambda_j[m] w_j[m], \tag{7.4}$$

and

$$\hat{\mathbf{y}} = (\hat{y}[0], \hat{y}[1], \ldots, \hat{y}[N-1])^T,$$

and

$$\mathbf{e} = (e[0], e[1], \ldots, e[N-1])^T$$

is circularly symmetric complex Gaussian random vector with zero mean and covariance $\sigma^2\mathbf{I}$.

To detect transmitted symbols, one way is to use single user detection techniques such as the maximum ratio combining (MRC). As shown in Chapter 6, the MRC detector detects the ith transmitted symbol as

$$\begin{aligned} \hat{z}_i &= \sum_{k=0}^{N-1} \hat{y}[k] \lambda_i^*[k] w_i^*[k] \\ &= s_i + \sum_{j=0, j\neq i}^{T-1} \widetilde{MAI}_{i\leftarrow j} + \hat{e}_i, \end{aligned} \tag{7.5}$$

where $\hat{e}_i = \sum_{k=0}^{N-1} e[k] \lambda_i^*[k] w_i^*[k]$ and s_i can be written as

$$\begin{aligned} s_i &= \sum_{k=0}^{N-1} r_i[k] \lambda_i^*[k] w_i^*[k] \\ &= \beta_i x_i \sum_{k=0}^{N-1} \sum_{m=0}^{N-1} g_i(m-k) \lambda_i[m] y_i[m] \lambda_i^*[k] w_i^*[k]. \end{aligned} \tag{7.6}$$

We saw in Chapter 6 that the MAI for a MC-CDMA in the presence of CFO is given by

$$\widetilde{MAI}_{i\leftarrow j} = MAI_{i\leftarrow j}^{(0)} + MAI_{i\leftarrow j}^{(1)}, \tag{7.7}$$

where

$$MAI_{i\leftarrow j}^{(0)} = \alpha_j x_j \sum_{k=0}^{N-1} \lambda_j[k] w_j[k] \lambda_i^*[k] w_i^*[k], \tag{7.8}$$

and

$$MAI_{i\leftarrow j}^{(1)} = \beta_j x_j \sum_{m=0, m\neq k}^{N-1} \lambda_j[m] y_j[m] \left\{ \frac{e^{-j\pi\frac{m-k}{N}}}{N \sin\frac{\pi(m-k+\epsilon_j)}{N}} \lambda_i^*[k] w_i^*[k] \right\}. \tag{7.9}$$

In this chapter we will find it more convenient to combine Eqs. (7.8) and (7.9) into

$$\widetilde{MAI}_{i\leftarrow j} = \beta_j x_j \sum_{k=0}^{N-1} \sum_{m=0}^{N-1} g_j(m-k) \lambda_j[m] y_j[m] \lambda_i^*[k] w_i^*[k]. \tag{7.10}$$

Equation (7.8) can be expressed in matrix form as shown in Chapter 6

$$MAI_{i\leftarrow j}^{(0)} = \alpha_j x_j \mathbf{h}_i^\dagger \underbrace{\mathbf{F}_0^\dagger \mathbf{W}_i^\dagger \mathbf{W}_j \mathbf{F}_0}_{\mathbf{A}_{ij}} \mathbf{h}_j, \tag{7.11}$$

where $\mathbf{F}_0 = \mathbf{F} \begin{pmatrix} \mathbf{I}_L \\ \mathbf{0} \end{pmatrix}_{N\times L}$, $\mathbf{h}_i = (h_i(0) \cdots h_i(L-1))^T$, and

$$\mathbf{W}_i = \mathrm{diag}(w_i[0]\, w_i[1] \cdots w_i[N-1]),$$

and where $\mathbf{I}_L$ is an $L \times L$ identity matrix, and $\mathbf{F}$ is the $N \times N$ DFT matrix whose element at the kth row and the nth column is $[\mathbf{F}]_{k,n} = \frac{1}{\sqrt{N}} e^{-j\frac{2\pi}{N}kn}$.

It was also shown in Chapter 6 that $MAI_{i\leftarrow j}^{(1)}$ given by (7.9) can be rewritten as

$$MAI_{i\leftarrow j}^{(1)} = \beta_j x_j \sum_{p=1}^{N-1} g_j(-p) \left\{ (\mathbf{h}_i^{(p)})^\dagger \underbrace{\mathbf{F}_0^\dagger (\mathbf{W}_i^{(p)})^\dagger \mathbf{W}_j \mathbf{F}_0}_{\mathbf{C}_{ij}^{(p)}} \mathbf{h}_j \right\}, \tag{7.12}$$

where

$$g_j(p) = \frac{e^{-j\pi\frac{p}{N}}}{N \sin\frac{\pi(p+\epsilon_j)}{N}}, \tag{7.13}$$

$$\mathbf{W}_i^{(p)} = \mathrm{diag}(w_i[p] \cdots w_i[N-1]\, w_i[0] \cdots w_i[p-1]), \tag{7.14}$$

and

$$\mathbf{h}_i^{(p)} = (h_i(0) e^{-j\frac{2\pi 0 p}{N}} \cdots h_i(L-1) e^{-j\frac{2\pi(L-1)p}{N}})^T. \tag{7.15}$$

We can combine Eqs. (7.11) and (7.12) into one equation as

$$\widetilde{MAI}_{i\leftarrow j} = \beta_j x_j \sum_{p=0}^{N-1} g_j(-p) \left\{ (\mathbf{h}_i^{(p)})^\dagger \underbrace{\mathbf{F}_0^\dagger (\mathbf{W}_i^{(p)})^\dagger \mathbf{W}_j \mathbf{F}_0}_{\mathbf{D}_{ij}^{(p)}} \mathbf{h}_j \right\}, \tag{7.16}$$

where if $p = 0$, $\beta_j g_j(0) = \alpha_j$, $\mathbf{W}_i^{(0)} = \mathbf{W}_i$, and $\mathbf{h}_i^{(0)} = \mathbf{h}_i$.

Since a relatively small number of users can be MAI-free in a channel with CFO using HW codes, we look for other codes to address this issue. In this section, we study the carrier interferometry (CI) codes of size N, which is of the following form

$$w_i[k] = e^{j\frac{2\pi}{N}ki}, \quad k, i = 0, 1, \cdots, N-1. \tag{7.17}$$

Then, the MAI-free property of this code can be stated below.

Theorem 7.1: Let the channel length be L and $G = 2^q \geq L$. There exists N/G carrier interferometry codewords such that the corresponding MC-CDMA is MAI free in a CFO environment.

Proof: Define

$$r_{i,j}^{(p)}[k] = w_i^{(p)}[k] w_j^*[k] \quad k = 0, 1, \cdots, N-1.$$

To have zero MAI in a frequency selective channel with CFO, we demand

$$\widetilde{MAI}_{i\leftarrow j} = 0.$$

As shown in Eq. (7.16), we can define

$$\mathbf{D}_{ij}^{(p)} = (\mathbf{I}_L \ \mathbf{0}) \mathbf{F}^\dagger (\mathbf{W}_i^{(p)})^\dagger \mathbf{W}_j \mathbf{F} \begin{pmatrix} \mathbf{I}_L \\ \mathbf{0} \end{pmatrix}.$$

Thus, $\mathbf{D}_{ij}^{(p)}$ must be a zero matrix of dimension $L \times L$ for all $i \neq j$ to achieve MAI-free in a CFO environment. Similar to the proof of Lemma 6.7 in Chapter 6, we can define matrix $\mathbf{C}_{i,j}^{(p)} = \mathbf{F}^\dagger \mathbf{W}_i^{(p)} \mathbf{W}_j \mathbf{F}$ and note that $\mathbf{D}_{i,j}^{(p)}$ is an $L \times L$ upper left submatrix of matrix $\mathbf{C}_{i,j}^{(p)}$ which is a circulant matrix [47]. Thus, the first column of $\mathbf{C}_{i,j}^{(p)}$, $(c_{i,j}(0) \cdots c_{i,j}(N-1))^T$, is the N-point IDFT of $\mathbf{r}_{i,j}^{(p)}$. To have $\mathbf{D}_{i,j}^{(p)} = \mathbf{0}$, the first L samples and the last $L-1$ samples of the IDFT of $\mathbf{r}_{i,j}^{(p)}$ must be zeros.

Now, consider two codewords with indices i and i'. By taking the IDFT of $\mathbf{r}_{i,j}^{(p)}$, we have

$$r_{i,i'}^{(p)}(n) = \frac{1}{\sqrt{N}} \sum_{m=0}^{N-1} r_{i,i'}^{(p)}[m] e^{j\frac{2\pi}{N}mn}. \tag{7.18}$$

Let $m = k + gN/G$, $0 \le k \le N/G - 1$ and $0 \le g \le G - 1$. We can rewrite Eq. (7.18) as

$$r_{i,i'}^{(p)}(n) = \frac{1}{\sqrt{N}} \sum_{k=0}^{N/G-1} \sum_{g=0}^{G-1} r_{i,i'}^{(p)}[k + gN/G] e^{j\frac{2\pi}{N}(k+gN/G)n}. \tag{7.19}$$

Since $w_i^{(p)}[k] = e^{j2\pi/N(N-p+k)i}$, and

$$r_{i,i'}^{(p)}[k + gN/G] = w_i^{(p)}[((k + gN/G))_N] w_{i'}^{*}[((k + gN/G))_N],$$

we have

$$\begin{aligned} r_{i,i'}^{(p)}[k + gN/G] &= e^{j\frac{2\pi}{N}(N-p+k+gN/G)i} e^{-j\frac{2\pi}{N}(k+gN/G)i'} \\ &= e^{j\frac{2\pi}{N}(N-p+k)i} e^{-j\frac{2\pi}{N}ki'} e^{j\frac{2\pi}{G}g(i-i')}. \end{aligned} \tag{7.20}$$

If $i - i' = mG$, where m can be any nonzero integer, we get $e^{j2\pi/Gg(i-i')} = e^{j2\pi mg} = 1$. Then, we have

$$r_{i,i'}^{(p)}[k + gN/G] = e^{j\frac{2\pi}{N}(N-p+k)i} e^{-j\frac{2\pi}{N}ki'} = r_{i,i'}^{(p)}[k]. \tag{7.21}$$

Then, we can rewrite Eq. (7.19) as

$$r_{i,i'}^{(p)}(n) = \frac{1}{N} \sum_{k=0}^{N/G-1} r_{i,i'}^{(p)}[k] e^{j\frac{2\pi}{N}kn} \sum_{g=0}^{G-1} e^{j\frac{2\pi}{G}gn}, \tag{7.22}$$

where $0 \le k \le N/G - 1$ and $0 \le g \le G - 1$. Since

$$\sum_{g=0}^{G-1} e^{j\frac{2\pi}{G}gn} = \begin{cases} G, \, n = 0, \pm G, \cdots \\ 0, \ \text{otherwise}, \end{cases} \tag{7.23}$$

we have

$$r_{i,i'}^{(p)}(n) = \begin{cases} \frac{G}{\sqrt{N}} \sum_{k=0}^{N/G-1} r_{i,i'}^{(p)}[k] e^{j\frac{2\pi}{N}kn}, \, n = 0, \pm G, \cdots \\ 0, \qquad\qquad\qquad\qquad \text{otherwise.} \end{cases}$$

Furthermore, for $i \neq i'$, we have

$$r_{i,i'}^{(p)}(0) = \frac{1}{\sqrt{N}} \sum_{k=0}^{N-1} r_{i,i'}^{(p)}[k] = \sum_{k=0}^{N-1} e^{j\frac{2\pi(i-i')}{N}(N-p+k)} = 0. \tag{7.24}$$

Thus, $\widetilde{MAI}_{i \leftarrow j} = 0$. Since there are N/G codewords such that $i - i' = mG$, $m = 1, 2, \cdots$, the total number of MAI-free codewords from N exponential codes is N/G. ■

The MAI-free property of CI codes in a CFO environment can be expected since a multiuser system with the CI spreading codes in the frequency domain is equivalent to a TDMA system in the time domain. Besides being codewords in an MC-CDMA system, the CI codes are especially valuable as training sequences in a MIMO-OFDM system. For instance, it was shown in [72] that such codes can decouple inter-antenna interference in a CFO-free channel. Owing to Theorem 7.1, we can use CI codes as training sequences for multiuser MIMO-OFDM systems in a CFO environment to eliminate both inter-antenna interference and MAI.

Theorem 7.2: For two CI codewords with indices i and i', $i, i' = 0, 1, \cdots, N-1$, we have $\widetilde{MAI}_{i \leftarrow i'} = 0$ in a CFO environment if $((|i - i'|))_{N-(L-1)} \geq L$, where L is the channel length.

Proof: For $p = 0, 1, \cdots, N-1$, we have

$$r_{i,i'}^{(p)}(n) = \frac{1}{\sqrt{N}} \sum_{k=0}^{N-1} e^{j\frac{2\pi}{N}(N-p+k)i} e^{-j\frac{2\pi}{N}i'k} e^{j\frac{2\pi}{N}kn}$$
$$= \frac{1}{\sqrt{N}} \sum_{k=0}^{N-1} e^{j\frac{2\pi}{N}(i-i'+n)k} e^{-j\frac{2\pi}{N}pi} = \begin{cases} \sqrt{N} e^{-j\frac{2\pi}{N}pi}, & ((i-i'+n))_N = 0, \\ 0, & \text{otherwise.} \end{cases}$$

To meet condition $((|i - i'|))_{N-(L-1)} \geq L$, $|i - i'|$ should take values from $\{L, L+1, \cdots, N-L\}$. Consider the case $i - i' \geq 0$. Under the conditions that $i - i'$ is equal to a value in this set, $r_{i,i'}^{(p)}(n) \neq 0$, for $n = N-L, N-L-1, \cdots, L$, by the above equation. On the other hand, if $i - i' \leq 0$, then $r_{i,i'}^{(p)}(n) \neq 0$, for $n = N+L, N+L+1, \cdots, 2N-L$. Since

$$r_{i,i'}^{(p)}(n+N) = \frac{1}{\sqrt{N}} \sum_{k=0}^{N-1} e^{j\frac{2\pi}{N}(N-p+k)i} e^{-j\frac{2\pi}{N}i'k} e^{j\frac{2\pi}{N}k(n+N)}$$
$$= \frac{1}{\sqrt{N}} \sum_{k=0}^{N-1} e^{j\frac{2\pi}{N}(N-p+k)i} e^{-j\frac{2\pi}{N}i'k} e^{j\frac{2\pi}{N}k(n)} = r_{i,i'}^{(p)}(n),$$

$r_{i,i'}^{(p)}(n)$ is periodic with period N. We conclude $r_{i,i'}^{(p)}(n) \neq 0$ for $n = L, L+1, \cdots, N-L$, while $r_{i,i'}^{(p)}(0) = r_{i,i'}^{(p)}(1) = \cdots = r_{i,i'}^{(p)}(L-1) = 0$, and $r_{i,i'}^{(p)}(N-L+1) = r_{i,i'}^{(p)}(N-L+2) = \cdots = r_{i,i'}^{(p)}(N-1) = 0$, for $((|i - i'|))_{N-(L-1)} \geq L$. Therefore $\widetilde{MAI}_{i \leftarrow i'} = 0$. ■

Example 7.1: MAI-Free with CI Codewords
Let $N = 16$, $L = 2$ and the CFO value is fixed to be ± 0.1. That is, every user was randomly assigned by a CFO value of either 0.1 or -0.1. The MAI power in the unit of dB between users with different codewords is shown in Table 7.1. The MAI power was normalized by $\sum_{k=0}^{N-1} |\lambda_i[k]|^2$ since the desired signal was scaled by the same amount. According to Theorem 7.1 in Section 7.1,

Table 7.1. $MAI_{i \leftarrow j}$ power (dB) as a function of CI codewords [[124] ©IEEE].

	$\mathbf{w}_0$	$\mathbf{w}_2$	$\mathbf{w}_4$	$\mathbf{w}_6$	$\mathbf{w}_8$	$\mathbf{w}_{10}$	$\mathbf{w}_{12}$	$\mathbf{w}_{14}$
$\mathbf{w}_0$	×	−317	−306	−303	−309	−301	−294	−295
$\mathbf{w}_2$	−317	×	−317	−302	−308	−309	−297	−291
$\mathbf{w}_4$	−306	−317	×	−306	−306	−302	−298	−297
$\mathbf{w}_6$	−303	−302	−306	×	−311	−302	−298	−297
$\mathbf{w}_8$	−310	−308	−305	−311	×	−305	−298	−299
$\mathbf{w}_{10}$	−300	−308	−303	−302	−304	×	−296	−293
$\mathbf{w}_{12}$	−295	−297	−298	−303	−298	−297	×	−302
$\mathbf{w}_{14}$	−296	−291	−297	−301	−299	−293	−302	×
$\mathbf{w}_1$	−18.6	−19.0	−309	−302	−311	−304	−296	−292
$\mathbf{w}_3$	−306	−18.4	−12.9	−306	−306	−301	−300	−293
$\mathbf{w}_5$	−305	−309	−16.2	−19.2	−304	−304	−297	−304
$\mathbf{w}_7$	−309	−299	−301	−19.6	−16.3	−299	−298	−308
$\mathbf{w}_9$	−304	−304	−306	−302	−16.6	−15.3	−296	−292
$\mathbf{w}_{11}$	−293	−304	−304	−297	−302	−18.2	−11.1	−296
$\mathbf{w}_{13}$	−297	−303	−306	−305	−307	−300	−19.9	−19.0
$\mathbf{w}_{15}$	−15.3	−297	−298	−303	−307	−302	−300	−17.6

users with even indexed codewords, i.e., $\{\mathbf{w}_0, \mathbf{w}_2, \mathbf{w}_4, \mathbf{w}_6, \mathbf{w}_8, \mathbf{w}_{10}, \mathbf{w}_{12}, \mathbf{w}_{14}\}$ are mutually MAI-free. This is illustrated in the top half of Table 7.1. We also observe that users whose codewords' indices difference is greater than $L-1$ have zero MAI as proved by Theorem 7.2.

Corollary: For an MC-CDMA system in a CFO environment consisting of N active users with CI codewords. If $L \leq N/2$, each user has $2(L-1)$ interfering users only.

Proof: The condition $L \leq N/2$ guarantees that there are i and i' satisfying $((|i-i'|))_{N-(L-1)} \geq L$. For every codeword with index i, there are $L-1$ codewords such as codeword i' for which $0 < i - i'$ and $((i-i'))_{N-(L-1)} \geq L$ and $L-1$ codewords such as codeword i'' for which $i - i'' < 0$ and $((i''-i))_{N-(L-1)} \geq L$. Therefore, the number of interferers is $2(L-1)$.

The Corollary leads to an important result. In practice, $N >> L$. That is the spreading gain is much greater that the channel length. Thus, a user has to combat much fewer interferers than what it would have to combat if other codes instead of CI codes were used. On the other hand, the user with CI codewords experiences a considerable amount of MAI from nonzero interferers in a fully loaded MC-CDMA system. Fortunately, interference cancellation can be employed to suppress MAI. In the next section.We will consider the parallel interference cancellation (PIC) technique for this purpose and show that its complexity can be reduced by the use of CI codewords since there are only $2(L-1)$ instead of $N-1$ interferers.

7.2 Complexity Reduction in PIC MUD Detection

In this section, we evaluate the performance of a fully-loaded MC-CDMA system with the BPSK modulation and parallel interference cancellation (PIC). It will be shown that the complexity of PIC can be reduced substantially if the CI codewords are used.

The receiver for the ith user in an MC-CDMA system with PIC is depicted in Fig. 7.1. First, initial bit estimates for all users are derived from the single user detection (SUD) receivers, which is basically the same as the one depicted in Fig. 6.1 in Chapter 6. We call this stage as stage 0 of the PIC detector and denote the detected symbols by $\hat{x}_{0i}$, $i = 1, \cdots, N$.

Let $\mathbf{F}_0\mathbf{h}_j = \boldsymbol{\lambda}_j$ and $\mathbf{F}_0\mathbf{h}_i^{(p)} = \boldsymbol{\lambda}_i^{(p)}$. We can express the detected symbol for user i at the 0th stage of PIC as

$$\hat{x}_{0i} = \sum_{k=0}^{N-1} |\lambda_i[k]|^2 x_i + \sum_{j=1, j\neq i}^{T} x_j \gamma_{i,j} + \hat{e}_i[k], \tag{7.25}$$

where

$$\gamma_{i,j} = \beta_j \sum_{p=0}^{N-1} g_j(-p)(\boldsymbol{\lambda}_i^{(p)})^\dagger (\mathbf{W}_i^{(p)})^\dagger \mathbf{W}_j \boldsymbol{\lambda}_j,$$

and $\hat{e}_i[k] = \sum_{k=0}^{N-1} e[k]\lambda_i^*[k]w_i^*[k]$.

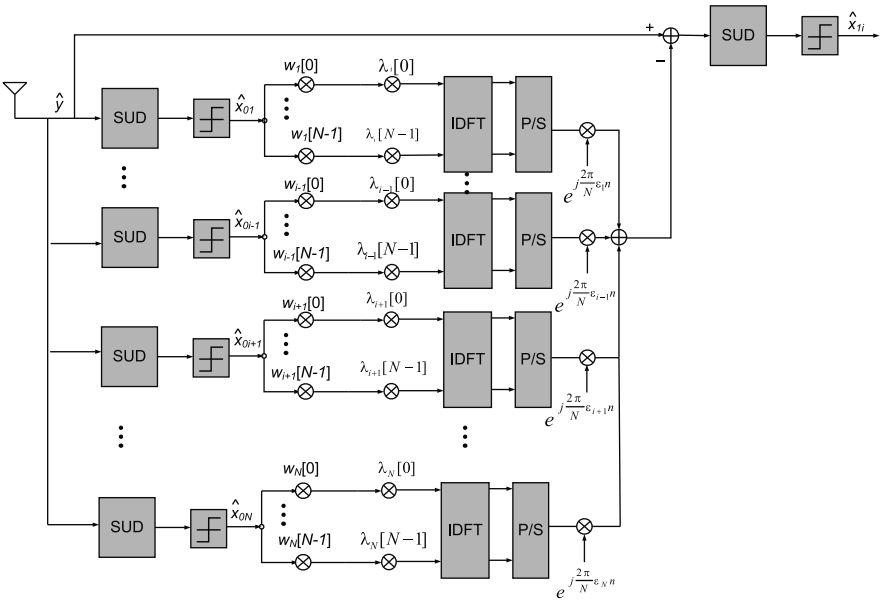

Fig. 7.1. The MC-CDMA receiver with single-stage PIC for the ith user.

Tentative hard decisions are made on $\hat{x}_{0j}, j = 1, 2, \cdots, T, j \neq i$, to produce initial bits estimates; namely,

$$\text{sgn}[\text{Re}\{\hat{x}_{0j}\}].$$

These bits are then spread into multiple chips by their corresponding codewords and scaled by channel gains before passing through the IDFT matrix and the parallel-to-serial converter. To take the CFO effect into account, each signal is multiplied by $e^{j2\pi/Nn\epsilon_j}$, $n = 0, 1, \cdots, N-1$. Here, it is assumed that the exact knowledge of channel gains and CFO values for all users is available in the receiver. Later, simulation results with imperfect channel estimation will also be given. These estimated signals add up to form the MAI estimate for desired user i, which can be subtracted from its received signal $\hat{y}$.

The resultant signal is used by the receiver of user i to produce new detected symbol at stage 1 of the PIC detector denoted by $\hat{x}_{1i}$ as

$$\hat{x}_{1i} = \hat{x}_{0i} - \sum_{j=1, j\neq i}^{T} \frac{1}{N} \sum_{k,k'=0}^{N-1} \text{sgn}[\text{Re}\{\hat{x}_{0j}\}] w_j[k'] \lambda_j[k'] \left\{ \sum_{n=0}^{N-1} e^{j\frac{2\pi}{N}n(k'-k+\epsilon)} w_i^*[k] \lambda_i^*[k] + \hat{e}_i[k] \right\} \tag{7.26}$$

alternatively, $\hat{x}_{1i}$ can be expressed as

$$\hat{x}_{1i} = \hat{x}_{0i} - \sum_{j=1, j\neq i}^{T} \text{sgn}[\text{Re}\{\hat{x}_{0j}\}] \beta_j \sum_{p=0}^{N-1} g_j(-p) (\boldsymbol{\lambda}_i^{(p)})^\dagger (\mathbf{W}_i^{(p)})^\dagger \mathbf{W}_j \boldsymbol{\lambda}_j + \hat{e}_i[k]. \tag{7.27}$$

If a correct decision is made on a particular interfere's bit, the interference from that user to the ith user can be completely cancelled. On the other hand, if an incorrect decision is made, the interference from that user will be enhanced rather than cancelled.

By substituting $\hat{x}_{0i}$ from Eq. (7.25) in Eq. (7.28), we obtain

$$\hat{x}_{1i} = x_i \sum_{k=0}^{N-1} |\lambda_i[k]|^2 + \sum_{j=1, j\neq i}^{T} \gamma_{i,j} (x_j - \text{sgn}[\text{Re}\{\hat{x}_{0j}\}]) + \hat{e}_i[k]. \tag{7.28}$$

Assuming x_j is a BPSK modulated symbol, $(x_j - \text{sgn}[\text{Re}\{\hat{x}_{0j}\}])$ is a three-valued random variable (0,2,−2) whose magnitude represents whether or not a tentative decision is made correctly on the jth user's bit at the previous stage. For higher-order modulation schemes such as M-ary PAM and M-ary PSK, $(x_j - \text{sgn}[\text{Re}\{\hat{x}_{0j}\}])$ can take several values which makes the BEP analysis more difficult.

We know that $\boldsymbol{\lambda}_i$ is a multivariate Gaussian random vector with zero mean and covariance matrix $\mathbf{R}$ whose elements are given by

$$[\mathbf{R}]_{k,k'} = E\{\lambda_i[k]\lambda_i^*[k']\} = \sum_{l=0}^{L-1}\sum_{l'=0}^{L-1} E\{h_i(l)h_i^*(l')\}e^{-j\frac{2\pi}{N}kl}e^{j\frac{2\pi}{N}k'l'}. \quad (7.29)$$

We assume a uniform model for the multipath intensity (power-delay) profile, i.e., the channel coefficients have the same power at each tap. Also, the typical wide-sense stationary uncorrelated scattering (WSSUS) channel model [60] is adopted. Then, we have

$$E\{h_i(l)h_i^*(l')\} = \sigma_{h_i}^2\delta(l-l'),$$

and

$$[\mathbf{R}]_{k,k'} = \sum_{l=0}^{L-1}\sigma_{h_i}^2 e^{-j\frac{2\pi}{N}(k-k')l} = \begin{cases} \sigma_{h_i}^2 L & k = k' \\ \sigma_{h_i}^2\frac{1-e^{-j2\pi(k-k')L/N}}{1-e^{-j2\pi(k-k')/N}} & k \neq k'. \end{cases} \quad (7.30)$$

Since $\gamma_{i,j}$ is a linear transform of $\boldsymbol{\lambda}_j$ given $\boldsymbol{\lambda}_i$, $\gamma_{i,j}|\boldsymbol{\lambda}_i$ is a circularly symmetric complex Gaussian random variable with zero mean and variance

$$\mathrm{var}[\gamma_{i,j}|\boldsymbol{\lambda}_i] = |\beta_j|^2\sum_{p,p'=0}^{N-1}(\mathbf{W}_i^{(p)}\boldsymbol{\lambda}_i^{(p)})^\dagger\mathbf{W}_j\mathbf{R}_j\mathbf{W}_j^\dagger(\mathbf{W}_i^{(p')}\boldsymbol{\lambda}_i^{(p')})g_j(-p)g_j^*(-p'). \quad (7.31)$$

The probability of error for user i at state 0 of the PIC detector using Eq. (7.25), can be written as

$$\begin{aligned} P[\mathrm{sgn}[\mathrm{Re}\{\hat{x}_{0i}\}]) \neq x_i] &= \frac{1}{2}P[\mathrm{Re}\{\hat{x}_{0i}\} < 0|\ x_i = +1] + \frac{1}{2}P[\hat{x}_{0i} > 0|\ x_i = -1] \\ &= P[\mathrm{Re}\{\hat{x}_{0i}\} > 0|\ x_i = -1] \\ &= P\left[\mathrm{Re}\left\{\hat{z}_k + \sum_{j=1,j\neq i}^{T}\gamma_{i,j}x_j\right\} > \sum_{k=0}^{N-1}|\lambda_i[k]|^2\right]. \end{aligned} \quad (7.32)$$

Due to the presence of x_j terms, $\sum_{j=1,j\neq i}^{K} x_j\gamma_{i,j}$ in Eq. (7.25) is not Gaussian for given $\boldsymbol{\lambda}_i$. However, if it is conditioned on all possible x_j, $j \neq i$, we will have a collection of Gaussian random variables that can be approximated by the Gaussian distribution [144]. Hence, we see that $I_{0i} = \mathrm{Re}\left\{\hat{e}[k] + \sum_{j=1,j\neq i}^{K}\gamma_{i,j}x_j\right\} - \sum_{k=0}^{N-1}|\lambda_i[k]|^2$ in the above equation is conditional Gaussian conditioned on $\boldsymbol{\lambda}_i$. By using $\Delta_{x_{0i}}$ to denote $(x_i - \mathrm{sgn}[\mathrm{Re}\{\hat{x}_{0i}\}])$ and noting that $E\left\{\mathrm{Re}^2\{z[k]\}\right\} = \frac{1}{2}\Sigma^2$, the probability of error conditioned on $\boldsymbol{\lambda}_i$ is simply given by

$$P[\Delta_{x_{0i}} \neq 0|\boldsymbol{\lambda}_i] = Q\left(\frac{\sum_{k=0}^{N-1}|\lambda_i[k]|^2}{\sqrt{\sum_{j=1,j\neq i}^{T}\sigma_{\gamma_{i,j}}^2 + \sigma^2/2}}\right), \quad (7.33)$$

where

$$\sigma^2_{\gamma_{i,j}} = E\left\{\mathrm{Re}^2\{\gamma_{i,j}|\boldsymbol{\lambda}_i\}\right\} = \frac{1}{2}\mathrm{var}[\gamma_{i,j}|\boldsymbol{\lambda}_i].$$

Then, the BEP can be obtained by

$$P[\Delta_{x_{0i}} \neq 0] = \int_0^\infty Q\left(\frac{\sum_{k=0}^{N-1}|\lambda_i[k]|^2}{\sqrt{\sum_{j=1,j\neq i}^{T}\sigma^2_{\gamma_{i,j}} + \sigma^2/2}}\right) P[\boldsymbol{\lambda}_i]d_{\boldsymbol{\lambda}_i}. \tag{7.34}$$

This integral can be calculated by the Monte Carlo method [102].

We are ready now to derive the BEP of the detected symbol after stage 1 of PIC. From Eq. (7.28), we have

$$P[\mathrm{Re}\{\hat{x}_{1i}\} > 0|\ x_i = -1] = P\left[\mathrm{Re}\left\{\hat{z}_k + \sum_{j=1,j\neq i}^{T}\gamma_{i,j}\Delta_{x_{0j}}\right\} > \sum_{k=0}^{N-1}|\lambda_i[k]|^2\right]. \tag{7.35}$$

To get the closed form for BEP is difficult since e_{0j}'s are dependent with given $\boldsymbol{\lambda}_i$. Following the arguments in [32] for the BEP derivation of DS-CDMA with PIC, $\Delta_{x_{0j}}$s are actually not strongly dependent. For example, consider $\Delta_{x_{0j}}$ and $\Delta_{x_{0j'}}$. There are only two terms (i.e., $x'_j\gamma_{j,j'}$ in $\Delta_{x_{0j}}$ and $x_j\gamma_{j',j}$ in $\Delta_{x_{0j}}$) that are dependent. Since given $\boldsymbol{\lambda}_i$, $\gamma_{i,j}$, and $\gamma_{i,j'}$ are independent, we can assume with reasonable precision that $\gamma_{i,j}\Delta_{x_{0j}}$, $j = 1, 2, \ldots T$, $j \neq i$ terms are independent. Using the above simplifying assumption, we shall derive two formulas for the BEP based on two probabilistic models for residual interference ($\sum_{j=1,j\neq i}^{T}\gamma_{i,j}\Delta_{x_{0j}}$) in the next two sections.

7.2.1 Derivation of BEP Assuming Gaussian Model for Residual Interference

Using the above simplifying assumptions, we can assume the distribution of the total residual interference (after cancellation) converges to the Gaussian distribution for a sufficiently large number, T, of users. Under this assumption and by noting

$$E\{\Delta^2_{x_{0j}}\mathrm{Re}^2\{\gamma_{i,j}\}|\boldsymbol{\lambda}_i\} = 4P[e_{0j} \neq 0]E\{\mathrm{Re}^2\{\gamma_{i,j}\}|\boldsymbol{\lambda}_i\} \tag{7.36}$$

and

$$E^2\{\Delta_{x_{0j}}\mathrm{Re}\{\gamma_{i,j}\}|\boldsymbol{\lambda}_i\} = E\{\Delta_{x_{0j}}\mathrm{Re}\{\gamma_{i,j}\}\Delta_{x_{0j'}}\mathrm{Re}\{\gamma_{i,j'}\}|\boldsymbol{\lambda}_i\} = 0, \tag{7.37}$$

we can derive the conditional BEP as

$$P[\mathrm{error}|\boldsymbol{\lambda}_i] = Q\left(\frac{\sum_{k=0}^{N-1}|\lambda_i[k]|^2}{\sqrt{\sum_{j=1,j\neq i}^{T}4P[\Delta_{x_{0j}} \neq 0]\sigma^2_{\gamma_{i,j}} + \sigma^2/2}}\right), \tag{7.38}$$

and the BEP is given by

$$P[\text{error}] = \int_0^\infty Q\left(\frac{\sum_{k=0}^{N-1}|\lambda_i[k]|^2}{\sqrt{\sum_{j=1,j\neq i}^{T} 4P[\Delta_{x_{0j}}\neq 0]\sigma^2_{\gamma_{i,j}} + \sigma^2/2}}\right) P[\boldsymbol{\lambda}_i]d_{\boldsymbol{\lambda}_i}. \quad (7.39)$$

7.2.2 Derivation of BEP Using Non-Gaussian Model for Residual Interference

The assumption of Gaussian residual interference is not true when the number of interfering users are not sufficiently large. For example, as proved in the previous section, every user encounters only $2(L-1)$ nonzero interference terms if the CI codewords are used. Thus, for small values of L, the Gaussian assumption for residual interference is not reasonable. The distribution of residual interference must be derived and therefore, a new BEP formula can be obtained.

In the following, we first derive the BEP formula for a system with only 2 interferes. Then, the result is extended to T interferers.

Suppose users i' and i'' are interfering users for user i. The detected received symbol for user i is given by

$$\hat{x}_{1i} = x_i \sum_{k=0}^{N-1}|\lambda_i[k]|^2 + \Delta_{x_{0i'}}\gamma_{i,i'} + \Delta_{x_{0i''}}\gamma_{i,i''} + \hat{e}[k], \quad (7.40)$$

Let $\Delta_{x_{0i'}}\gamma_{i,i'} = U_1$, $\Delta_{x_{0i''}}\gamma_{i,i''} = U_2$, and $\hat{e}[k] = Z$. Then, the probability density function of U_1 conditioned on $\boldsymbol{\lambda}_i$, denoted by $f_{U_1}(u_1|\boldsymbol{\lambda}_i)$, can be obtained by

$$\begin{aligned} f_{U_1}(u_1|\boldsymbol{\lambda}_1) &= f_{U_1}(u_1|\Delta_{x_{0i'}} = 2;\boldsymbol{\lambda}_i)P[\Delta_{x_{0i'}} = 2|\boldsymbol{\lambda}_i] \\ &+ f_{U_1}(u_1|\Delta_{x_{0i'}} = -2;\boldsymbol{\lambda}_i)P[\Delta_{x_{0i'}} = -2|\boldsymbol{\lambda}_i] \\ &+ f_{U_1}(u_1|\Delta_{x_{0i'}} = 0;\boldsymbol{\lambda}_i)P[\Delta_{x_{0i'}} = 0|\boldsymbol{\lambda}_i] \\ &= f_{U_1}(2\gamma_{i,i'}|\boldsymbol{\lambda}_i)P[\Delta_{x_{0i'}} = 2|\boldsymbol{\lambda}_i] + f_{U_1}(-2\gamma_{i,i'}|\boldsymbol{\lambda}_1)P[\Delta_{x_{0i'}} = -2|\boldsymbol{\lambda}_i] \\ &+ \delta(u_1)P[\Delta_{x_{0i'}} = 0|\boldsymbol{\lambda}_i]. \end{aligned} \quad (7.41)$$

We use $\mathcal{N}(a,b)$ to denote the Gaussian distribution, where a and b are the mean and variance, respectively. Since

$$f_{U_1}(2\gamma_{i,i'}|\boldsymbol{\lambda}_i) = f_{U_1}(-2\gamma_{i,i'}|\boldsymbol{\lambda}_i) = N(0, 4\sigma^2_{\gamma_{i,i'}}),$$

we obtain

$$f_{U_1}(u_1|\boldsymbol{\lambda}_i) = P[\Delta_{x_{0i'}}\neq 0|\boldsymbol{\lambda}_i]N(0, 4\sigma^2_{\gamma_{i,i'}}) + (1 - P[\Delta_{x_{0i'}}\neq 0|\boldsymbol{\lambda}_i])\delta(u_1),$$

where

$$P[\Delta_{x_{0i'}}\neq 0|\boldsymbol{\lambda}_i] = Q\left(\frac{\sum_{k=0}^{N-1}|\lambda_{i'}[k]|^2}{\sqrt{\sum_{j=1,j\neq i'}^{T}\sigma^2_{\gamma_{i',j}} + \sigma^2/2}}\right).$$

Similarly,

$$f_{U_2}(u_2|\boldsymbol{\lambda}_i) = P[\Delta_{x_{0i''}} \neq 0|\boldsymbol{\lambda}_i]N(0, 4\sigma^2_{\gamma_{i,i''}}) + (1 - P[\Delta_{x_{0i''}} \neq 0|\boldsymbol{\lambda}_i])\delta(u_2).$$

Again, $\Delta_{x_{0i'}}$ and $\Delta_{x_{0i''}}$ are assumed to be independent. Thus, U_1 and U_2 are independent and given the independence among Z and U_1 and U_2, the pdf of their sum can be obtained by $f_{U_1}(u_1|\boldsymbol{\lambda}_i) * f_{U_2}(u_2|\boldsymbol{\lambda}_i) * f_Z(z|\boldsymbol{\lambda}_i)$, where $*$ denotes the convolution operation. Therefore, we have

$$\begin{aligned} f_V(v|\boldsymbol{\lambda}_i) &= f_{U_1}(u_1|\boldsymbol{\lambda}_i) * f_{U_2}(u_2|\boldsymbol{\lambda}_i) * f_Z(z|\boldsymbol{\lambda}_i) \\ &= P[\Delta_{x_{0i'}} \neq 0|\boldsymbol{\lambda}_i]P[\Delta_{x_{0i''}} \neq 0|\boldsymbol{\lambda}_i]\mathcal{N}(0, 4\sigma^2_{\gamma_{i,i'}} + 4\sigma^2_{\gamma_{i,i''}} + \sigma^2/2) \\ &+ P[\Delta_{x_{0i'}} \neq 0|\boldsymbol{\lambda}_i](1 - P[\Delta_{x_{0i''}} \neq 0|\boldsymbol{\lambda}_i])\mathcal{N}(0, 4\sigma^2_{\gamma_{i,i'}} + \sigma^2/2) \\ &+ P[\Delta_{x_{0i''}} \neq 0|\boldsymbol{\lambda}_i](1 - P[\Delta_{x_{0i'}} \neq 0|\boldsymbol{\lambda}_i])\mathcal{N}(0, 4\sigma^2_{\gamma_{i,i''}} + \sigma^2/2) \\ &+ (1 - P[\Delta_{x_{0i'}} \neq 0|\boldsymbol{\lambda}_i])(1 - P[\Delta_{x_{0i''}} \neq 0|\boldsymbol{\lambda}_i])\mathcal{N}(0, \sigma^2/2). \end{aligned} \quad (7.42)$$

Thus, the conditional BEP after one stage of PIC detector, with CI codewords and $L = 2$ is given by

$$\begin{aligned} P[\text{error}|\boldsymbol{\lambda}_i] &= P[\Delta_{x_{0i'}} \neq 0|\boldsymbol{\lambda}_i]P[\Delta_{x_{0i''}} \neq 0|\boldsymbol{\lambda}_i]Q\left(\frac{\sum_{k=0}^{N-1}|\boldsymbol{\lambda}_i[k]|^2}{\sqrt{4(\sigma^2_{\gamma_{i,i'}} + \sigma^2_{\gamma_{i,i''}}) + \sigma^2/2}}\right) \\ &+ (1 - P[\Delta_{x_{0i'}} \neq 0|\boldsymbol{\lambda}_i])(1 - P[\Delta_{x_{0i''}} \neq 0|\boldsymbol{\lambda}_i])Q\left(\frac{\sum_{k=0}^{N-1}|\lambda_i[k]|^2}{\sqrt{\sigma^2/2}}\right) \\ &+ P[\Delta_{x_{0i'}} \neq 0|\boldsymbol{\lambda}_i](1 - P[\Delta_{x_{0i''}} \neq 0|\boldsymbol{\lambda}_i])Q\left(\frac{\sum_{k=0}^{N-1}|\lambda_i[k]|^2}{\sqrt{4\sigma^2_{\gamma_{i,i'}} + \sigma^2/2}}\right) \\ &+ (1 - P[\Delta_{x_{0i'}} \neq 0|\boldsymbol{\lambda}_i])P[\Delta_{x_{0i''}} \neq 0|\boldsymbol{\lambda}_1]Q\left(\frac{\sum_{k=0}^{N-1}|\lambda_i[k]|^2}{\sqrt{4\sigma^2_{\gamma_{i,i''}} + \sigma^2/2}}\right). \end{aligned} \quad (7.43)$$

Next, we extend the above result to any number, I, of interferers. Let the set of all interfering users' indices for user i be S_i. Then we have

$$\begin{aligned} \hat{x}_{1i} = x_i \sum_{k=0}^{N-1} &|\lambda_i[k]|^2 + \Delta_{x_{0S_i[1]}}\gamma_{i,S_i[1]} + \Delta_{x_{0S_i[2]}}\gamma_{i,S_i[2]} + \ldots + \Delta_{x_{0S_i[I]}}\gamma_{i,S_i[I]} \\ &+ \hat{e}_i[k], \end{aligned} \quad (7.44)$$

and the conditional BEP can be obtained as

$$P[\text{error}|\boldsymbol{\lambda}_i] = \sum_{r_1=0}^{1}\sum_{r_2=0}^{1}\cdots\sum_{r_{S_i[I]=0}}^{1} P[\Delta_{x_{0S_i[1]}} \neq 0|\boldsymbol{\lambda}_i]^{r_1}\cdots$$
$$P[\Delta_{x_{0S_i[I]}} \neq 0|\boldsymbol{\lambda}_i]^{r_{S_i[I]}}\Bigg\{$$
$$(1-P[\Delta_{x_{0S_i[1]}} \neq 0|\boldsymbol{\lambda}_i])^{1-r_1}\cdots(1-P[\Delta_{x_{0S_i[I]}} \neq 0|\boldsymbol{\lambda}_i])^{1-r_{S_i[I]}}$$
$$Q\left(\frac{\sum_{k=0}^{N-1}|\boldsymbol{\lambda}_i[k]|^2}{\sqrt{4(r_1\sigma^2_{\gamma_{i,S_i[1]}}+\ldots+r_{S_i[I]}\sigma^2_{\gamma_{i,S_i[I]}})+\sigma^2/2}},\right)\Bigg\}, \quad (7.45)$$

and

$$P[\text{error}] = \int_0^\infty P[E|\boldsymbol{\lambda}_i]P[\boldsymbol{\lambda}_i]d_{\boldsymbol{\lambda}_i}. \quad (7.46)$$

Example 7.2: Theoretical vs Simulated BEP of Fully-Loaded MC-CDMA with Single Stage PIC

In this example, we conduct the Monte Carlo simulation to evaluate the BEP performance of MC-CDMA with PIC in the presence of CFO and to corroborate theoretical results derived above. We consider both analytical and simulated BEP performance.

In the simulation, channel taps were generated as independently identically distributed (i.i.d.) random variables of unit variance. Every user was randomly assigned by a CFO value of either 0.1 or -0.1. As before, to compute the analytical BEP, the Monte Carlo integration method was used [102]. That is, random variables $\lambda_i[k]$, $k = 0, 1, \cdots, N-1$ are generated by taking the DFT of complex Gaussian distributed channel taps for K times. Then, computer generated samples of $\lambda_i[k]$, $k = 0, 1, \cdots, N-1$ are substituted in the Q function and the sum of trials is divided by K.

Figure 7.2 depicts analytical and simulated BEP results for a fully-loaded MC-CDMA system with CI and HW codewords as a function of the SNR value, E_b/N_0, Under the setting of $N = 16$, $L = 2$, $T = 16$, and $CFO = \pm 0.1$. To shorten simulation time, only the BEP for first users were compared.

Since $L = 2$, we can use Eqs. (7.43) and (7.56) as the analytical BEP expressions of MC-CDMA with CI codewords. For this case, we observe a close agreement between the analytical BEP expression and simulation results. However, if BEP is computed from the approximate expressions (7.39), analytical and simulation results do not have strong agreement, particularly in the high SNR regime as shown in Fig. 7.2 for HW codewords. The disagreement is due to the assumption of an analytical Gaussian model for the total residual user interference in Eq. (7.40) whereas this simplifying assumption is not present in computer simulation.

The analysis of the performance of multiple stage PIC is even more complicated than the performance analysis given in this section. We shall evaluate the performance of multiple stage PIC with both HW and CI codes by computer simulation in next example.

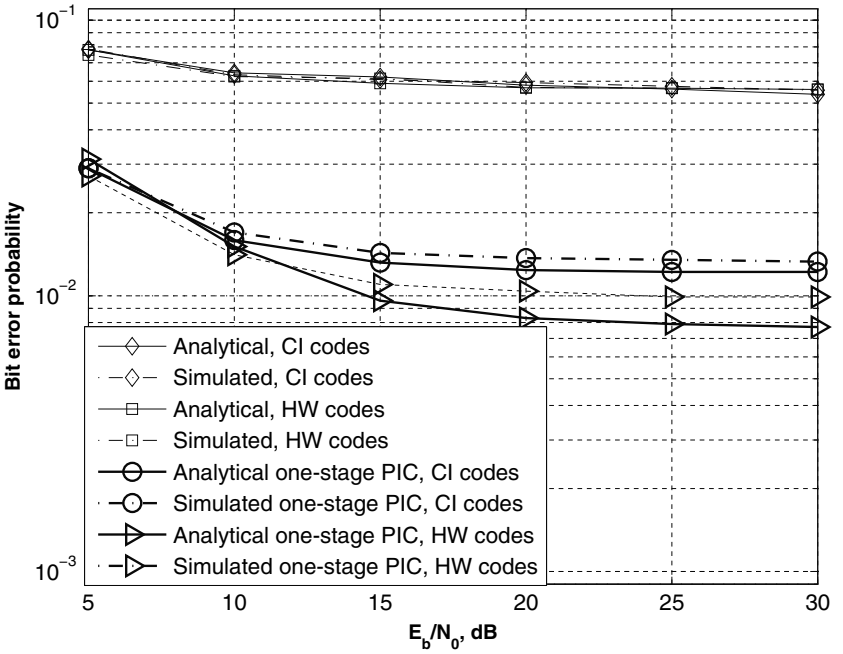

Fig. 7.2. Analytical and simulated BEP versus E_b/N_0 with $N = 16$, $L = 2$ and $CFO = \pm 0.1$.

Example 7.3: Multistage PIC and Effect of Limit Cycle Points
In this example, we use two-stage PIC to illustrate the significant performance improvement of PIC and the effect of convergence to limit cycle points, which is described below. A point at the qth stage of PIC is expressed as $\hat{\boldsymbol{x}}_q = (\hat{x}_{q1}, \hat{x}_{q2}, \cdots, \hat{x}_{qT})$. A limit cycle point is a point that is periodic with a period equal to a certain number of iterations. For example, for a cycle limit point with period 2, we have $\hat{\boldsymbol{x}}_{q+2} = \hat{\boldsymbol{x}}_q$.

The simulation was performed under two sets of parameters: (1) $N = 16$, $L = 2$ and (2) $N = 32$, $L = 4$, respectively. We set $CFO = \pm 0.1$ and the user number $T = 16$. In Figs. 7.3 and 7.4, BEP results are given for both set of parameters. For HW codewords, we see that 2-stage PIC can enhance the BEP performance significantly. However, the performance gain obtained by the second stage of PIC is not significant for CI codewords. We see from Figs. 7.2, 7.3 and 7.4 that the performance of single-stage and two-stage PIC is better with HW codewords.

It is known that the performance of a multistage PIC detector depends on the cross-correlation of codewords [13, 144]. In general, multistage PIC may or may not converge to the optimum (jointly maximum likelihood) solution [144]. It was shown in [13] that, for a CDMA system employing random

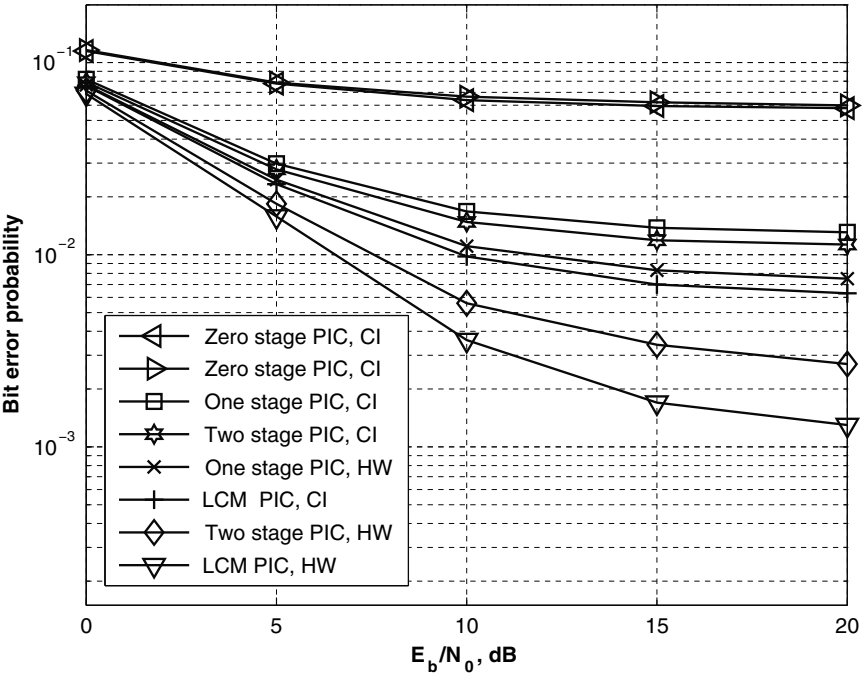

Fig. 7.3. BEP versus the SNR with $N = 16$, $L = 2$, $CFO = \pm 0.1$ dB.

spreading sequences, the poor performance of multistage PIC is mostly due to the existence of limit cycle points with a period of 2. This often happens when the number of users approaches the spread factor. We observed in computer simulation that the large number of limit cycle points account for the worse performance of PIC with CI codewords. For example, for $N = 32$, $L = 4$ and $T = 16$, the ratio of the number of limit cycle points to the total simulated samples is 7/3125 for HW codewords while this ratio becomes 52/3125 for CI codewords.

Due to the periodic nature of limit cycle points, they can be detected easily. On the other hand, if a fixed point is reached, it is difficult to determine wether it is optimal or non-optimal. Three limit cycle mitigation (LCM) techniques were proposed in [13] to improve the poor convergence behavior of PIC. The simplest one among the three was employed in this work. That is, if a limit cycle point is detected, the receiver only attempts to cancel the interference from users whose bit estimates are fixed during multiple PIC iterations and it does not attempt to cancel the interference from those users with toggling bit estimates.

With this technique, the performance of PIC greatly improves for both HW and CI codewords as shown in Figs. 7.3 and 7.4, where the PIC detector with the limit cycle mitigation algorithm (LCM) is called LCM PIC. The BEP

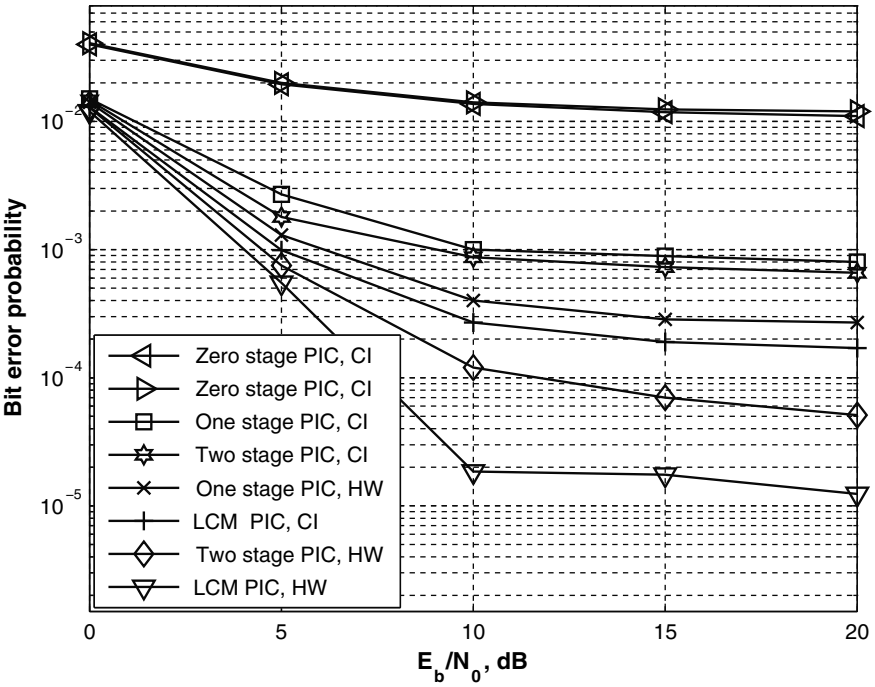

Fig. 7.4. BEP versus the SNR with $N = 32$, $L = 4$, $CFO = \pm 0.1$ dB.

performance of MC-CDMA with HW codewords is still superior to that of CI codewords. However, multistage PIC for MC-CDMA with CI codewords is much less complex than that with HW codewords, since each PIC stage for any user with the CI codeword has to deal with only $2(L-1)$ nonzero interferers as stated in the Corollary of Theorem 7.2 in Section 7.1 while HW codewords must deal with all $N-1$ interferers. We also observe that increasing N from 16 to 32 improves the BEP performance for both codewords. The reason is that the number of mutually zero MAI terms increases as the subcarrier number increases for a fixed number of users.

Example 7.4: The Effect of User Number on the Performance of PIC

Figure 7.5 shows the BEP results versus the user number with $N = 32$, $L = 4$, $CFO = \pm 0.3$ and $E_b/N_0 = 10$ dB. Based on N and L values, there are eight MAI-free users with CI codewords and four MAI-free users with HW codewords. Thus, CI codewords outperforms HW codewords when the number of active users is between 6 and 8 as demonstrated in the Fig. 7.5. However, as the number of users exceeds 8, the performances of both systems become comparable. Figure 7.5. also shows the performance of PIC with the LCM algorithm for both CI and HW codewords. The two systems have comparable performance with PIC for number of users between 6 and 8 but HW

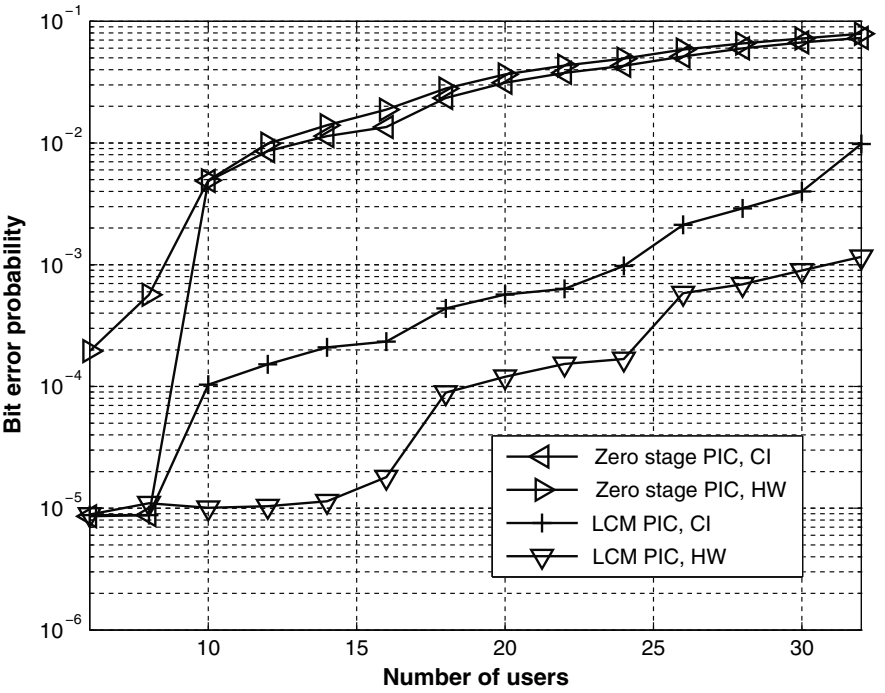

Fig. 7.5. BEP versus the active user number with $N = 32$, $L = 4$, $CFO = \pm 0.3$, and $E_b/N_0 = 10\,\text{dB}$.

outperforms CI as the number of users increases. However, for both codes, the PIC detector greatly improves the performance of light or heavy loaded MC-CDMA.

7.3 Complexity Reduction in ML MUD Detection

We consider the ML detection based on the received signal given in Eq. (7.3) in this section. It is assumed that the receiver has the perfect knowledge of channel coefficients and CFO values. We will examine the multipath and the CFO effects separately. By Theorem 7.2, we know that, for two CI codewords with indices i and i', where $i, i' = 0, 1, \cdots, N-1$, $\widetilde{MAI}_{i \leftarrow i'} = 0$ in a CFO environment if $((|i - i'|))_{N-(L-1)} \geq L$, where $((n))_N$ denotes n modulo N and L is the channel length. We show in this section how the above property of CI codes can reduce the complexity of the ML-MUD receiver significantly.

7.3.1 ML-MUD in Multipath Fading Channel

For given transmitted signal $\mathbf{x}$, we would like to maximize the likelihood of the received signal. From Eq. (7.3) and since noise $\mathbf{n}$ is Gaussian, the ML

estimate can be written as

$$\hat{\mathbf{x}} = \arg\min_{\mathbf{x}} ||\hat{\mathbf{y}} - \mathbf{C}\mathbf{x}||^2. \tag{7.47}$$

By expanding the right hand side of (7.47) and noting that $||\hat{\mathbf{y}}||^2$ is independent of $\mathbf{x}$, we can reformulate the optimization problem as

$$\hat{\mathbf{x}} = \arg\min_{\mathbf{x}} \Omega(\mathbf{x}),$$

where

$$\Omega(\mathbf{x}) = ||\mathbf{C}\mathbf{x}||^2 - 2\Re\{(\mathbf{C}\mathbf{x}, \hat{\mathbf{y}})\},$$

and where $\mathbf{C}$ is defined in Eq. (7.4) in a CFO environment. If there is no CFO, Eq. (7.4) can be written as

$$\mathbf{C}(i,j) = w_j[i]\lambda_j[i].$$

Thus, we have

$$(\mathbf{C}\mathbf{x}, \hat{\mathbf{y}}) = \mathbf{x}^\dagger(\mathbf{C}^\dagger\hat{\mathbf{y}}) = \sum_{j=0}^{T-1} x_j \sum_{k=0}^{N-1} \hat{y}_j[k]w_j^*[k]\lambda_j^*[k].$$

Note that $\sum_{k=0}^{N-1} \hat{y}_j[k]w_j^*[k]\lambda_j^*[k]$ is actually the estimate of the input signal for user j obtained by MRC (i.e., $\hat{z}_j$). On the other hand,

$$||\mathbf{C}\mathbf{x}||^2 = \mathbf{x}^\dagger\mathbf{H}^{(\mathbf{0})}\mathbf{x},$$

where $\mathbf{H}^{(\mathbf{0})} = \mathbf{C}^\dagger\mathbf{C}$. Then, the ML optimization problem is equivalent to minimizing

$$\Omega(\mathbf{x}) = \mathbf{x}^\dagger\widetilde{\mathbf{H}}\mathbf{x} - 2\Re\{(\mathbf{x}^\dagger, \hat{\mathbf{z}})\}$$

with respect to $\mathbf{x}$, where $\hat{\mathbf{z}}$ is the output vector of MRC with its ith element given in (7.5). In the absence of CFO, $\alpha_j = 1$ for any user j and the MAI from user j to desired user i is equal to $MAI_{i\leftarrow j}^{(0)}$. Then, we have from Eq. (7.8) that

$$MAI_{i\leftarrow j}^{(0)} = x_j \sum_{k=0}^{N-1} \lambda_j[k]w_j[k]\lambda_i^*[k]w_i^*[k].$$

It can be easily shown that $\mathbf{H}^{(\mathbf{0})}(i,j) = MAI_{i\leftarrow j}^{(0)}/x_j$. In fact, $\mathbf{H}^{(\mathbf{0})}$ can be viewed as the cross-correlation channel matrix.

7.3.2 ML-MUD in Multipath Fading Channel with CFO

We rewrite Eq. (7.5) in vector format as

$$\hat{\mathbf{z}} = \mathbf{H}\mathbf{x} + \hat{\mathbf{e}}, \tag{7.48}$$

where the i,jth entry of $\mathbf{H}$ is equal to

$$\mathbf{H}(i,j) = \begin{cases} s_i, & i = j, \\ \frac{\widetilde{MAI}_{i \leftarrow j}}{x_j}, & i \neq j. \end{cases}$$

The ML detector has the following form

$$\hat{\mathbf{x}} = \arg\min_{\mathbf{x}} \Omega(\mathbf{x}), \tag{7.49}$$

where

$$\Omega(\mathbf{x}) = ||\hat{\mathbf{z}} - \mathbf{H}\mathbf{x}||^2 = \sum_{i=0}^{T-1} |\hat{z}_i - \mathbf{h}_i \mathbf{x}|^2, \tag{7.50}$$

and where $\mathbf{h}_i$ is the ith row of $\mathbf{H}$.

7.3.3 Viterbi Algorithm for Tail Biting Trellis (TBT)

We know from Theorem 7.2 and its Corollary that for $T = N$ active users with CI codewords and $L \leq N/2$, each user has only $2(L-1)$ (instead of $N-1$) interfering users. Both $\mathbf{H}^{(\mathbf{0})}$ and $\mathbf{H}$ are sparse matrices so that ML-MUD can be performed with a much lower complexity. As shown in Fig. 7.6 for $N = 16$, $T = 16$, and $L = 2$, the nonzero elements (indicated by black squares) of $\mathbf{H}$ (or $\mathbf{H}^{(\mathbf{0})}$ for the case without CFO) are concentrated along the three diagonal lines. Elements in the off-diagonal region with $|i-j| \geq L$ are all equal to zero except for two corners.

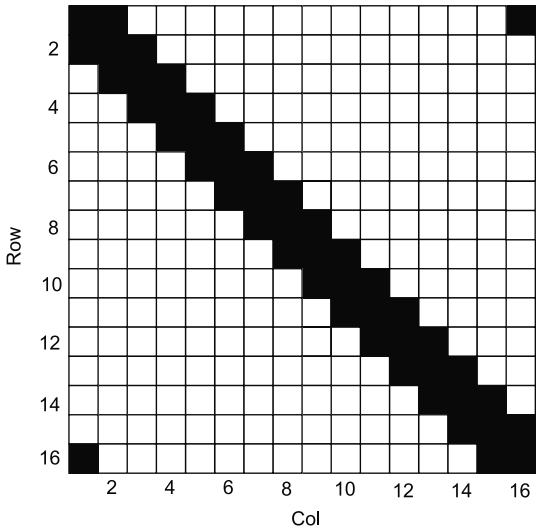

Fig. 7.6. The cross-correlation matrix of CI codewords with $N = T = 16$ and $L = 2$.

The well-known Viterbi algorithm (VA) can be used to solve the ML optimization problem. Generally speaking, its complexity is proportional to the number of states. The number of transition per stage has to be taken into account since the complexity is proportional to this number. The number of state transitions per stage is referred to as the trellis size. It turns out that regardless of how we define the states, the complexity of ML MUD is $O(2^T)$ for a general non-sparse cross-correlation channel matrix and the BPSK modulation. On the other hand, by exploiting the sparsity of $\mathbf{H}$, we can show that the complexity of VA grows exponentially with $2L-1$. For example, for $N=T=16$ and $L=2$ given in Fig. 7.6, Eq. (7.50) can be written as

$$\Omega(\mathbf{x}) = \sum_{i=0}^{N-1} |\hat{z}_i - \mathbf{H}(i,((i-1))_N)x_{((i-1))_N} - \mathbf{H}(i,i)x_i \\ -\mathbf{H}(i,((i+1))_N)x_{((i+1))_N}|^2.$$

Thus, if a proper trellis is defined, the number of states at each stage can be reduced to $2(L-1)=2$ for this example. The trellis construction for the sparse cross-correlation channel matrix of MC-CDMA with CI codewords is explained below.

The structure of $\mathbf{H}$ (or $\mathbf{H}^{(\mathbf{0})}$ for the case without CFO) implies a trellis that is defined on a circulant time axis (or called the *tail biting trellis* (TBT) [16]). TBT was defined and discussed for error correcting codes in [16]. TBT also arises in the context of maximum likelihood (ML) detection in overloaded array processing [52]. A method for trellis construction for a similar matrix structure was proposed in [52] as explained below.

We denote the state of the trellis at stage i and the state space at the ith stage by $s[i]$ and S_i, respectively. We use $U[i]$ to denote the column indices of nonzero elements on the ith row of $\mathbf{H}$. For example, for the example given in Fig. 7.6, we have $U[0]=\{0,1,15\}$ and $U[15]=\{0,14,15\}$. The ith state is defined as [52]

$$s[i] = \{x_u |\ u \in U[((i-1))_N] \cap U[i]\}. \tag{7.51}$$

Using the above definition, we obtain

$$s[i] \cup s[((i+1))_N] = \{U[((i-1))_N] \cap U[i]\} \cup \{U[i] \cap U[((i+1))_N]\} = U[i]. \tag{7.52}$$

In other words, state sequence $\{s[i]\}$ for TBT is defined such that, during the ith stage of the Viterbi algorithm recursion, $U[i]$ corresponds to symbol indices in both $s[i]$ and $s[i+1]$. From the sequence of states defined by Eq. (7.51), we can construct the trellis by listing state values at stage i and connect the valid state transition from stage i to stage $i+1$.

By defining $\mu = 2(L-1)$, we can determine the ith state from Eq. (7.51) by

$$s[i] = (x_{((i-\mu_-))_N}, \cdots, x_i, \cdots, x_{((i+\mu_+))_N}), \tag{7.53}$$

where $\mu_- = \lceil \frac{\mu-1}{2} \rceil$ and $\mu_+ = \lfloor \frac{\mu-1}{2} \rfloor$. Note that μ is the number of interferers for each user in the MC-CDMA system with CI codes and $\mu+1$ is

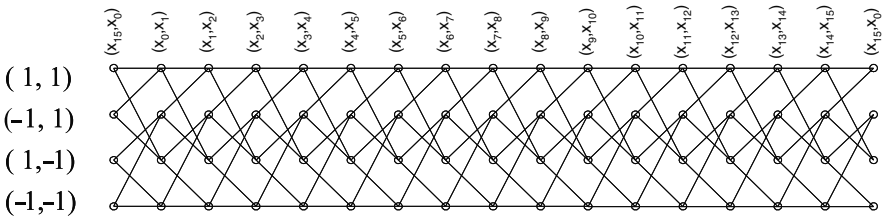

Fig. 7.7. TBT for the case with $N = T = 16$ and $L = 2$.

the bandwidth of the cross-correlation channel matrix. For example, the state definition for the cross-correlation channel matrix given in Fig. 7.6 is

$$s[i] = (x_{((i-1))_N}, x_i), \quad 0 \leq i \leq N-1.$$

With the state sequence for the example in Fig. 7.6, we construct the corresponding trellis in Fig. 7.7, where the value of each state is placed at the top of each stage. Note that the state is tail biting in the sense that it starts and ends with the same state, i.e., (x_{15}, x_0).

Given these state and trellis definitions, we have to solve the ML optimization problem, which is equivalent to finding a closed path with the minimum cost through TBT. A *closed path* around a TBT is a path that starts and ends with the same state. In other words, it is identified by a sequence of state-indices for which $j_s[i] = j_s[i+N]$, $0 \leq i \leq N_{stgs} - N$.

Since the initial state is not actually defined in the TBT, finding the optimum ML solution requires a modified version of the VA that is explained below. That is, the actual ML path for the TBT can be determined in two steps. First, an arbitrary state value is selected as the initial state and the optimum closed path is determined by running the VA. Then, the first step is repeated for every possible value of the initial state. The optimum path is then chosen to be the one with the minimum cost. However, this algorithm has a complexity proportional to $O(2^{2\mu})$ [16]. For example, the TBT depicted in Fig. 7.7 requires 4 calls of the Viterbi Algorithm.

Some approximate ML algorithms with less complexity and satisfactory results for decoding TBT were discussed in [16, 52]. These algorithms initialize all metrics at states in initial stage S_0 to zero, decode with VA starting at S_0 and go around the TBT. Some of these algorithms require that, after each run of VA, the resultant winning path should be checked to see if the starting state is the same as the ending state (i.e., if the winning path is closed) [148]. A less complicated approximate ML algorithm, called the Iterative Tail Biting Viterbi Algorithm (ITB-VA), was proposed in [52] that applies VA iteratively around a TBT multiple times without excluding paths that are not closed. This approach is taken in our work.

We define $N_{stgs} = \lceil N_{round} N \rceil$, where $N_{round} > 1$ is a real number. N_{round} and N_{stgs} are in fact the desired numbers of iterations and stages around the TBT, respectively. We can extend the received symbol sequence $\hat{z}[i]$ (for the

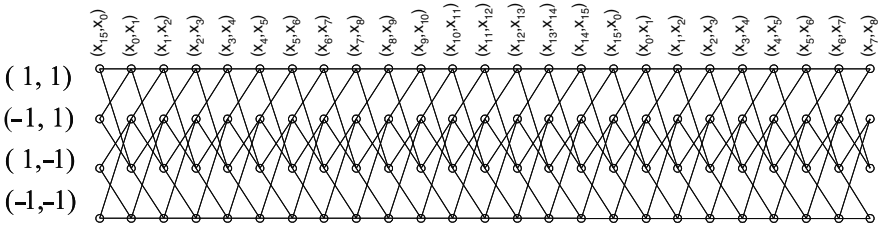

Fig. 7.8. The periodically extended TBT for the case with $N = T = 16$ and $L = 2$ and $N_{round} = 1.5$.

case with CFO) and state sequence $s[i]$ periodically as

$$\hat{z}[i] = \hat{z}[((i))_N], \quad s[i] = s[((i))_N], \quad 0 \le i \le N_{stgs}.$$

Thus, a periodically extended TBT is constructed such that its ith stage is identical to its $((i))_N$ stage for every i. Figure 7.8 shows such an extended TBT for the example given in Fig. 7.6 with $N_{stgs} = 1.5$.

After going around the TBT N_{round} times, the optimum path is chosen and the estimated sequence is translated into a sequence of symbol estimates, $\hat{x}_0, \ldots, \hat{x}_{N-1}$. To do this, we recall that VA has the property that all surviving paths merge after a certain stage δ [74]. Thus, the optimum surviving path at the ith stage is used to estimate the $(i - \delta)$th information bits, where δ is called the *traceback-depth* or the *truncation length* [74]. A more detailed description of the ITB-VA algorithm can be found in [52]. As discussed before, the number of state transitions per stage determines the complexity of VA. By assuming that all components of sparse matrix $\mathbf{H}$ (or $\widetilde{\mathbf{H}}$) can be precomputed and their computational complexity is negligible as compared to the complexity of ITB-VA, the complexity of ITB-VA for MC-CDMA with CI codes and the BPSK modulation is $O(2^{(2L-1)})$ at each stage. Since there are $N_{round}N$ stages, where N_{round} is usually less than 2 [16], the total complexity for all stages is $O((N_{round}N)2^{(2L-1)})$, which is far less than the complexity of a conventional ML MUD (i.e., $O(N2^N)$).

7.3.4 Upper Bound on Minimum Error Probability

It is difficult to obtain a closed-form solution of the minimum error probability for MC-CDMA. However, we can derive its upper bound for BPSK transmitted symbols. We take a similar approach to the procedure for synchronous CDMA in the AWGN channel [144] and fading channel [11] and extend it to synchronous MC-CDMA in a CFO environment.

We define E_i to be the set of error vectors that affect the ith user in form of

$$E_i = \{\boldsymbol{\Delta} \in \{-1, 0, 1\}^T, \Delta_i \neq 0\},$$

where $\Delta_i = x_i - \hat{x}_i$. The set of errors that are compatible with transmitted vector $\mathbf{x} \in \{-1, 1\}^T$ is denoted by

$$\begin{aligned} A(\mathbf{x}) &= \{\boldsymbol{\Delta} \in E, \Delta_i = x_i \text{ or } 0\} \\ &= \{\boldsymbol{\Delta} \in E,\ 2\boldsymbol{\Delta} - \mathbf{x} \in \{-1, 1\}^T\}, \end{aligned}$$

where $E = \cup_{i=1}^{T} E_i$ is the set of nonzero error vectors. The probability of errors for the ith user, denoted by $P_i(e)$, in a fading channel is given by the corresponding bit error probability in the AWGN channel when conditioned on fading coefficients. The minimum error probability in the AWGN channel is given by

$$P\left\{\cup_{\boldsymbol{\Delta}\in E_i}\{\mathbf{x} - 2\boldsymbol{\Delta} = \arg\min_{\mathbf{b}} \Omega(\mathbf{b}), \boldsymbol{\Delta} \in A_i(\mathbf{x})\}\right\}.$$

Applying the union bound over E_i, we have

$$P_i(\text{error}) \le \sum_{\boldsymbol{\Delta}\in E_i} P\{\Omega(\mathbf{x} - 2\boldsymbol{e}) \le \Omega(\mathbf{x}), \boldsymbol{\Delta} \in A_i(\mathbf{x})\}, \tag{7.54}$$

where we have used the fact that, if $\mathbf{x} - 2\boldsymbol{\Delta}$ is the most likely vector, it is more likely than $\mathbf{x}$.

It can be easily shown that, when no CFO is present, we have

$$\begin{aligned} \Omega(\mathbf{x} - 2\boldsymbol{\Delta}) - \Omega(\mathbf{x}) &= 4\Re\{\boldsymbol{\Delta}^T\hat{\mathbf{x}}\} + 4\boldsymbol{\Delta}^T\mathbf{H}^{(\mathbf{0})}\boldsymbol{\Delta} \\ &\quad -2\mathbf{x}^T\mathbf{H}^{(\mathbf{0})}\boldsymbol{\Delta} - 2\boldsymbol{e}^T\mathbf{H}^{(\mathbf{0})}\mathbf{x} \\ &= 4\boldsymbol{\Delta}^T\mathbf{H}^{(\mathbf{0})}\boldsymbol{\Delta} + 4\Re\{\boldsymbol{\Delta}^T\hat{\mathbf{e}}\}, \end{aligned}$$

where the second equality is true since $\hat{\mathbf{z}} = \mathbf{H}^{(\mathbf{0})}\mathbf{x} + \hat{\mathbf{e}}$. We see that this event is dependent on noise $\hat{\mathbf{e}}$ only while $\boldsymbol{\Delta} \in \mathbf{A}(\mathbf{x})$ depends on $\mathbf{x}$ only. Thus, we conclude that these two events are independent.

Extending Eq. (7.54) to the fading channel, we can express the error probability as

$$\begin{aligned} P_i(\text{error}|\mathbf{H}^{(\mathbf{0})}) \le &\sum_{\boldsymbol{\Delta}\in E_i} P\{\Omega(\mathbf{x} - 2\boldsymbol{\Delta}) - \Omega(\mathbf{x}) \le 0|\mathbf{H}^{(\mathbf{0})}\} \\ &\times \left\{P\{\boldsymbol{\Delta} \in \mathbf{A}(\mathbf{x})\}\right\}, \end{aligned} \tag{7.55}$$

which follows from the fact that the admissibility of $\boldsymbol{\epsilon}$ is independent of $\mathbf{H}^{(\mathbf{0})}$. For equally likely transmitted bits, we have

$$P\{\boldsymbol{\Delta} \in \mathbf{A}(\mathbf{x})\} = \prod_{i=0}^{T-1} P\{(x_i - \Delta_i)\Delta_i = 0\} = 2^{-w(\boldsymbol{\Delta})},$$

where $w(\boldsymbol{\Delta}) = \sum_{i=0}^{T-1} |\Delta_i|$. To compute $P\{\Omega(\mathbf{x} - 2\boldsymbol{\Delta}) - \Omega(\mathbf{x}) \le 0|\mathbf{H}^{(\mathbf{0})}\}$, we note that, since $\hat{\mathbf{e}}$ is proper (circularly symmetric) complex Gaussian random vector with zero mean and covariance $\sigma^2\mathbf{H}^{(\mathbf{0})}$,

$$E\{(\Re\{\boldsymbol{\Delta}^T\hat{\mathbf{e}}\})^2\} = \frac{1}{2}E\{\boldsymbol{\Delta}^T\hat{\mathbf{e}}\hat{\mathbf{e}}^\dagger\boldsymbol{\Delta}\} = \frac{1}{2}\sigma^2\boldsymbol{e}^T\mathbf{H}^{(\mathbf{0})}\boldsymbol{\Delta}.$$

Thus, the error probability for user i is bounded by

$$P_i(\text{error}|\mathbf{H}^{(\mathbf{0})}) \leq \sum_{\boldsymbol{\Delta}\in E_i} 2^{-w(\boldsymbol{\Delta})} Q\left(\frac{\sqrt{2\boldsymbol{\Delta}^T\mathbf{H}^{(\mathbf{0})}\boldsymbol{\Delta}}}{\sigma}\right).$$

When CFO is present, we have

$$\Omega(\mathbf{x} - 2\boldsymbol{\Delta}) - \Omega(\mathbf{x}) = 4\boldsymbol{\Delta}^T\mathbf{H}'\boldsymbol{\Delta} + 4\Re\{\boldsymbol{\Delta}^T\mathbf{e}'\},$$

where $\mathbf{H}' = \mathbf{H}^\dagger\mathbf{H}$ and $\mathbf{e}' = \mathbf{H}^\dagger\hat{\mathbf{e}}$. By taking a similar approach, we can show that the upper bound for the error probability is

$$P_i(\text{error}|\mathbf{H}) \leq \sum_{\boldsymbol{\Delta}\in E_i} 2^{-w(\boldsymbol{\Delta})} Q\left(\frac{\sqrt{2}\boldsymbol{\Delta}^T\mathbf{H}'\boldsymbol{\Delta}}{\sigma\sqrt{\boldsymbol{\Delta}^T\mathbf{H}^\dagger\mathbf{H}^{(\mathbf{0})}\mathbf{H}\boldsymbol{\Delta}}}\right).$$

The unconditional BEP for user i can be obtained by

$$P_i(\text{error}) = \int_0^\infty P_i(e|\mathbf{H})P\{\mathbf{H}\}d_{\mathbf{H}}. \tag{7.56}$$

This integral can be calculated using the Monte Carlo method [102].

The upper bound for synchronous DS-CDMA in the AWGN channel was made tighter in [144] by eliminating the so-called *decomposable* error vectors (i.e., $\boldsymbol{\Delta} \in E_i$ that meet certain criteria) from the summation. This result was extended to the fading channel case in [11] by expressing channel matrix $\mathbf{H}$ as $\mathbf{A}^\dagger\mathbf{R}\mathbf{A}$ where $\mathbf{A}$ and $\mathbf{R}$ only contain fading coefficients and cross-correlation coefficients, respectively, and whereby allowing the set of *indecomposable* errors to be independent of fading [11]. However, we are not able to separate fading coefficients and cross-correlation in our system to make the bound tighter.

Example 7.5: ML MUD BEP Versus Minimum Probability of Error

Figure 7.9 shows the upper bound to BEP as a function of the SNR value, E_b/N_0, under the setting of $N = 8$, $L = 2$, $T = 8$ for both zero CFO and CFO= ± 0.3 cases. The upper bound curves in each case are plotted against their corresponding simulated BEP. To obtain simulated BEP, $N_{round} = 1.5$ and $\delta = 3$. To shorten simulation and computation time, only the BEP for the first user was computed. We see that the upper bound is not very tight particularly for the system with CFO. The reason is that the decomposable error sequences could not be identified and discarded in the presence of fading channels, unlike the asynchronous DS-CDMA case in [11]. It is also clear from the figure that ML performs better in the absence of CFO.

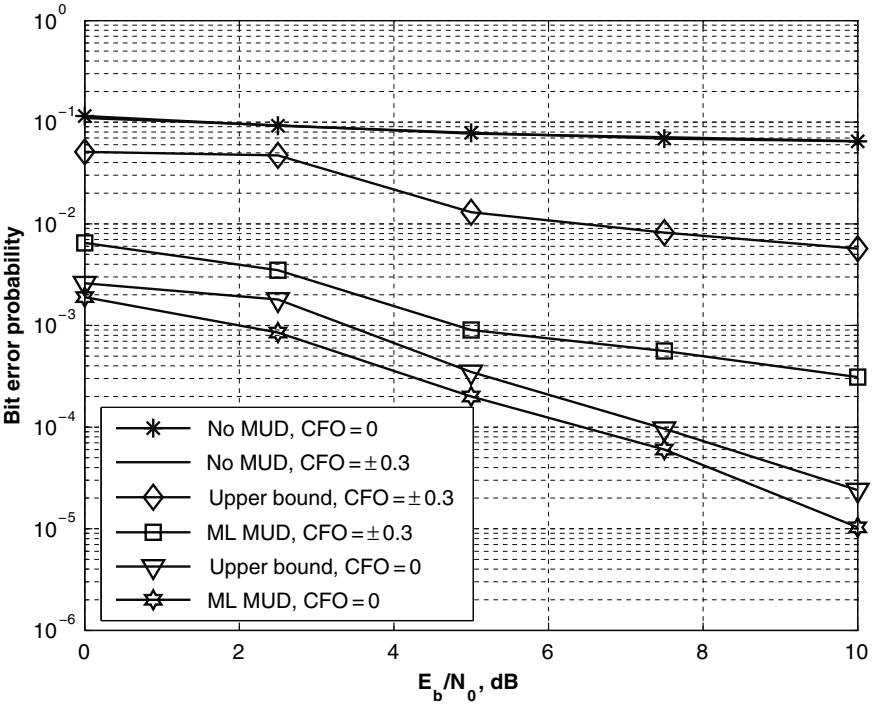

Fig. 7.9. Upperbound and simulation BER $N = 10$, $L = 2$, $CFO = 0, \pm 0.3$.

Example 7.6: ML MUD Performance
Figure 7.10 shows significant performance improvement of the ML detector, where performance of MC-CDMA with ML-MUD is compared to MC-CDMA with the single user MRC detection. The system parameters were $N = 16$, $L = 2$, and $T = 16$. As compared with Fig. 7.9 with $N = 8$, we see that ML performs better since there were more pairwise MAI-free users. Separate simulations were performed to acquire the BEP performance for $CFO = 0$ and $CFO = \pm 0.3$. We see that the BEP achieved by ML for both systems is very low when SNR is close to 10 dB. Again, we see that the ML detector performs better without CFO.

7.4 Complexity Reduction in Decorrelating MUD Detection

A band matrix is a matrix whose nonzero elements are confined to a diagonal band comprising the main diagonal and several sub-diagonals. For band matrix $\mathbf{A}$ with $[\mathbf{A}]_{i,j} = 0$ if $i - j > m_l$ and $j - i > m_u$, integers m_l and m_u are called the lower and upper bandwidths, respectively, and $m = m_l + m_u + 1$ is the total bandwidth.

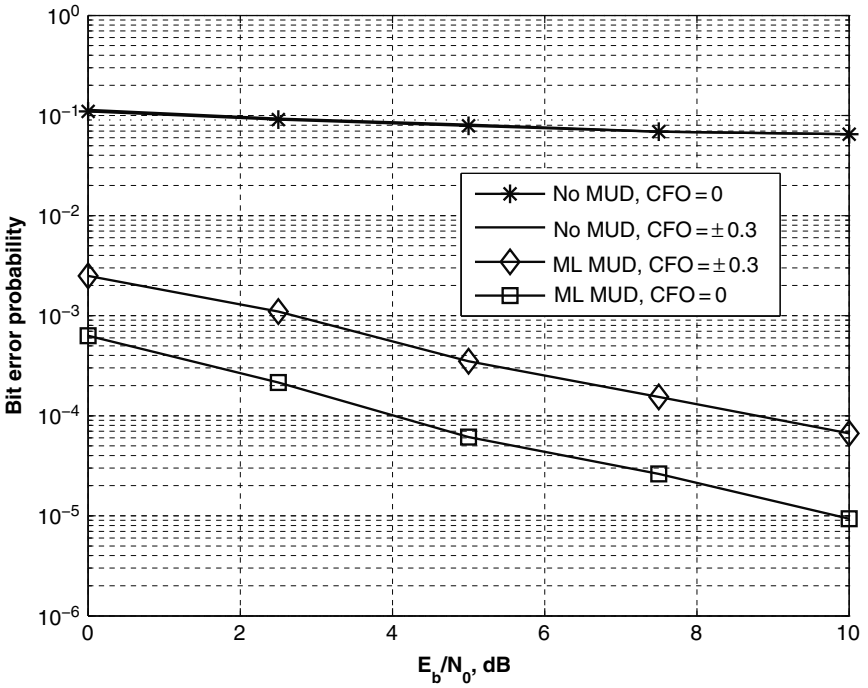

Fig. 7.10. BEP versus SNR $N = 16$, $L = 2$.

Channel matrix $\mathbf{H}$ (or $\widetilde{\mathbf{H}}$ for the case without CFO) can be converted to a band matrix by reducing the number of users to $N - (L-1)$, and employing CI codes $w_i[k] = e^{\frac{j2\pi ki}{N}}$, $k = 0, 1, \ldots N-1$, with the set of indices (i) which is either $\{0, 1, \ldots N-L\}$ or $\{L, L+1, \ldots, N\}$. The bandwidth of the resulting band matrix is $L-1+L-1+1 = 2L-1$. To give an example, for a channel of length $L = 3$, its cross-correlation matrix with $N = 16$ can be transformed into a band matrix of size $N - (L-1) = 14$ and bandwidth $2L-1 = 5$, as shown in Fig. 7.11, by omitting the first two CI codes, $w_0[k] = e^{\frac{j2\pi 0k}{16}}$ and $w_1[k] = e^{\frac{j2\pi 1k}{16}}$, $k = 0, 1, \cdots, 15$.

Band matrices are usually stored by recording diagonals in the band while the rest is simply set to zero. For example, for the following matrix of size 6×6 with $m_l = m_u = 1$:

$$\begin{bmatrix} 11 & 12 & 0 & 0 & 0 & 0 \\ 21 & 22 & 23 & 0 & 0 & 0 \\ 0 & 32 & 33 & 34 & 0 & 0 \\ 0 & 0 & 43 & 44 & 45 & 0 \\ 0 & 0 & 0 & 54 & 55 & 56 \\ 0 & 0 & 0 & 0 & 65 & 66 \end{bmatrix} \tag{7.57}$$

we can store it compactly of the following 6×3 matrix:

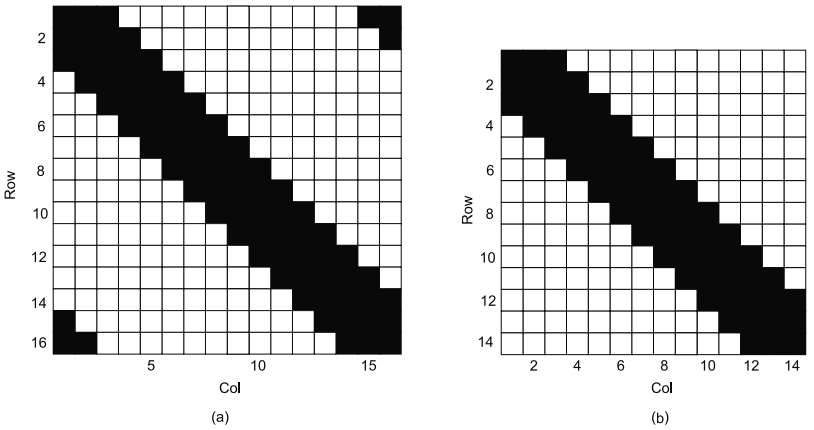

Fig. 7.11. Conversion of a channel matrix into a band matrix with $N = 16$, $L = 3$ by reducing the user number to 14.

$$\begin{bmatrix} 0 & 11 & 12 \\ 21 & 22 & 23 \\ 32 & 33 & 34 \\ 43 & 44 & 45 \\ 54 & 55 & 56 \\ 65 & 66 & 0 \end{bmatrix} \tag{7.58}$$

A banded matrix system can be solved by LU decomposition faster and with less storage space than a general dense matrix of the same dimension.

Consider a MC-CDMA system with a spreading gain of N and $N_b = N - (L-1)$ users employ codewords with indices $i = L, L+1, \ldots, N$ (or $0, 1, \ldots, N-L$) in a CFO environment. By using MRC in the receiver and disregarding the additive noise vector $\hat{\mathbf{n}}$ in Eq. (7.59), the received signal $\hat{\mathbf{z}}$ becomes

$$\hat{\mathbf{z}} = \mathbf{H}_b \mathbf{x}, \tag{7.59}$$

where $\mathbf{H}_b$ is the cross-correlation matrix. The above equation is in fact a linear system equation involving complex band matrix $\mathbf{H}_b$, which can be solved by the Gaussian elimination algorithm with partial pivoting.

The Gaussian elimination algorithm first factors $\mathbf{H}_b$ into the product of an upper triangular matrix $\mathbf{U}$ and a lower triangular matrix $\mathbf{L}$; namely,

$$\mathbf{H}_b = \mathbf{L}\mathbf{U}. \tag{7.60}$$

Next, the solution of the system $\mathbf{H}_b \mathbf{x} = \hat{\mathbf{z}}$ can be rewritten by

$$\mathbf{L}(\mathbf{U}\mathbf{x}) = \hat{\mathbf{z}}, \tag{7.61}$$

which demands forward and backward substitutions. The total number of operations required to solve $\mathbf{H}_b \mathbf{x} = \hat{\mathbf{z}}$ depends upon the number of pivoting

required. Generally speaking, if $N_b \gg m_l + m_u$, the number of operations required by the factorization in Eq. (7.60) is $O(N_b m_l(m_l + m_u))$ while the number of operations required by solving $\mathbf{x}$ in Eq. (7.61) by forward/backward substitutions is about $O(N_b(2m_l + m_u))$ [85].

Note that, for the cross-correlation matrix $\mathbf{H}_b$ of our interest, the lower and the upper bandwidths are both equal to $L-1$. Hence, the complexity of the factorization process and the solution process is equal to $O(2(N-L+1)(L-1)^2)$ and $O(3(N-L+1)(L-1))$, respectively. In contrast, to solve a general linear system of equations with Gaussian elimination with a dense matrix of size $(N-L+1)\times(N-L+1)$, it demands $O((N-L+1)^3/3)$ for the LU factorization and $O((N-L+1)^2)$ for forward and backward substitutions. The complexity of matrix inversion with fast algorithms is $O((N-L+1)^2)$. Thus, the complexity of the decorrelating MUD detection for MC-CDMA has considerably been reduced with CI codes in practical channel scenarios, where $N \gg 2(L-1)^2$.

In the absence of CFO, $\mathbf{H}_b = \mathbf{C}^\dagger\mathbf{C}$, is a Hermitian positive definite banded matrix with $m = m_l = m_u = L-1$, for which there is an even faster Gaussian elimination algorithm for solving the linear system. The total number of operations is approximately equal to $O((N-m)m^2/2 - m^3/3)$ for the LU factorization and $O(2(N-m)m - m^2)$ for the forward and the backward substitutions [85]. In contrast, the complexity of solving a general dense matrix of the same size is $O((N-L+1)^3/6)$ for the LU factorization and $O((N-L+1)^2)$ for the forward and the backward substitutions and the complexity of matrix inversion with fast algorithms is $O((N-L+1)^2)$.

7.4.1 Error Probability for Decorrelating MUD

The detected symbol for the above MUD detection technique is given by

$$\hat{\mathbf{x}} = \mathbf{x} + \mathbf{H}_b^{-1}\hat{\mathbf{e}}, \tag{7.62}$$

where $\hat{\mathbf{e}}$ is an $N-L+1\times 1$ Gaussian random vector with zero mean and covariance $\sigma^2\mathbf{H}^{(\mathbf{0})}$ where $\mathbf{H}^{(\mathbf{0})} = \mathbf{C}^\dagger\mathbf{C}$. Hence, we have

$$\begin{aligned} E\{(\mathbf{H}_b^{-1}\hat{\mathbf{e}})(\mathbf{H}_b^{-1}\hat{\mathbf{e}})^\dagger\} &= E\{\mathbf{H}_b^{-1}\hat{\mathbf{e}}\hat{\mathbf{e}}^\dagger\mathbf{H}_b^{-1\dagger}\} \\ &= \sigma^2\mathbf{H}_b^{-1}\mathbf{H}^{(\mathbf{0})}\mathbf{H}_b^{-1\dagger}. \end{aligned} \tag{7.63}$$

Let $\mathbf{H}_n = \mathbf{H}_b^{-1}\mathbf{H}^{(\mathbf{0})}\mathbf{H}_b^{-1\dagger}$. Since $\hat{\mathbf{e}}$ is a proper complex random vector, we have

$$E\{\Re\{\hat{\mathbf{e}}\hat{\mathbf{e}}^\dagger\}\} = \frac{1}{2}E\{\hat{\mathbf{e}}\hat{\mathbf{e}}^\dagger\} = \frac{1}{2}\sigma^2\mathbf{H}_n.$$

Then, under the BPSK modulation, the conditional bit error probability for the ith user is equal to

$$P_i(\text{error}) = E\left\{Q\left(\sqrt{\frac{2}{\sigma^2\mathbf{H}_n(i,i)}}\right)\right\}.$$

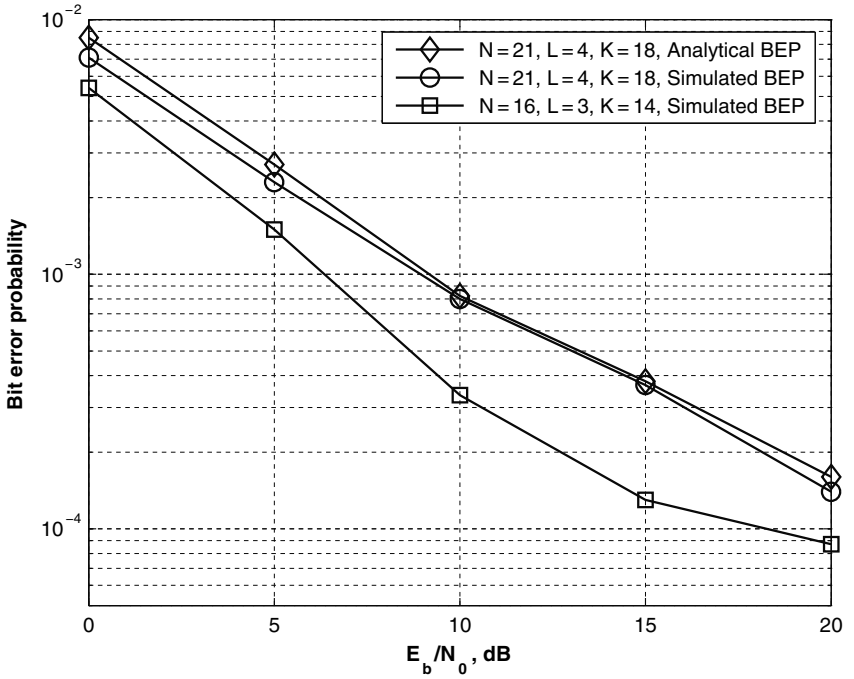

Fig. 7.12. Analytical and simulated BER performance of decorrelating detector with reduced complexity Gaussian elimination algorithm for MC-CDMA with $CFO = \pm 0.3$.

Example 7.7: Decorrelating Detector Performance

Figure 7.12 shows the theoretical and simulated BEP as a function of the SNR value, E_b/N_0, in the presence of CFO, which is uniformly distributed between -0.5 and 0.5, with a decorrelating detector with $N = 21$, $L = 4$, $T = 18$ for MC-CDMA. To shorten the simulation time, only the BEP for the first user was computed. We see that simulated and analytical BEP results are in good agreement. The average BEP performance of a MC-CDMA with $N = 16$, $L = 3$, $T = 14$ is also shown in Fig. 7.12.

Example 7.8: Performance Comparison of PIC, ML, and Decorrelating Detectors

Figure 7.13 compares the BEP performance of PIC, ML, and decorrelating detectors with the MRC detector as the benchmark. As expected, the optimum ML MUD detector greatly outperforms all other detectors. We also observe that the decorrelating detector with $N - L + 1 = 15$ users outperforms the PIC detector when $E_b/N_0 > 15$ dB.

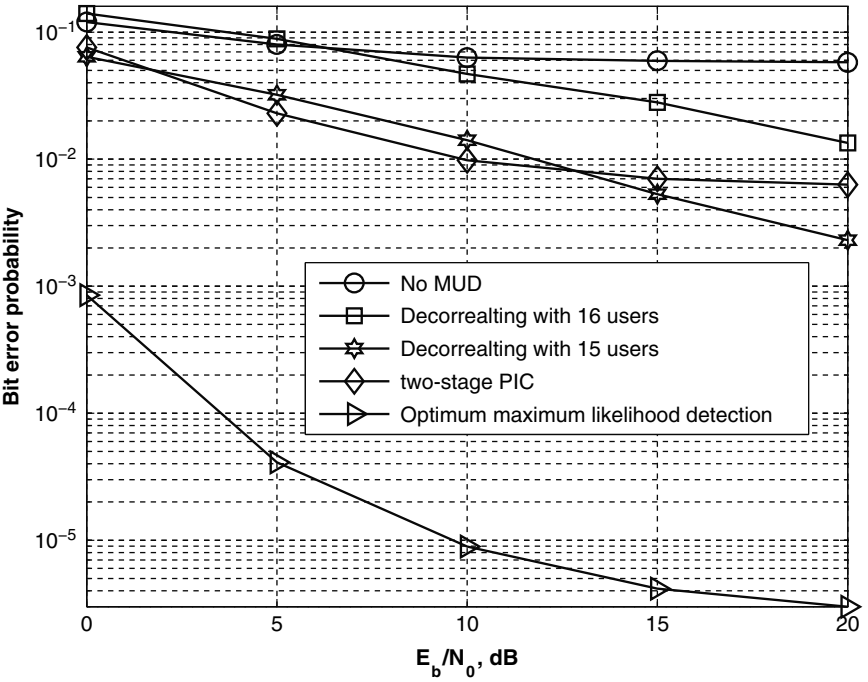

Fig. 7.13. Comparison of MUD techniques for $N = 16$ and $L = 2$ and $CFO = 0$.

7.5 Channel and CFO Estimation

The performance of single-stage PIC was analyzed in Section 7.2 under the assumption that perfect knowledge of channel coefficients and CFO values for each user is available in the receiver. In practice, channel and CFO estimation must be performed using training sequences. Many Channel and CFO estimation algorithms have been proposed for single user OFDM systems with a quasi-static channel. A maximum likelihood CFO estimation algorithm was proposed in [87]. Pilot-based channel estimation techniques for OFDM were discussed in [17, 55, 71]. These CFO/channel estimation algorithms can be extended to multiuser OFDM and MC-CDMA to avoid the use of complex multiuser estimation schemes. However, performance of such CFO or channel estimation techniques can be degraded by MAI.

In this section, we propose simple estimation techniques using the proposed HW codewords in Chapter 6 or CI codewords as introduced in Section 7.1. Since users with these codewords do not have MAI from other users in a CFO environment, more accurate CFO or channel coefficients can be estimated if groups of users employ these codewords in turn. In other words, only $\log_2(N/G) + 1$ users with HW codewords or N/G users with CI codewords can be active simultaneously to send out pilot symbols.

The CFO estimation algorithm for OFDM given in [87] is based on the repetition of data symbol x_i and comparing the phases between successive received symbols. In MC-CDMA, the detection output is actually one symbol rather than an $N \times 1$ OFDM symbol. If we denote two successive output symbols by $\hat{x}_i$ and $\hat{x}'_i$, the CFO can be estimated by [87]

$$\hat{\epsilon}_i = \frac{1}{2\pi} \tan^{-1}[\Im\{\hat{x}_i^* \hat{x}'_i\}/\Re\{\hat{x}_i^* \hat{x}'_i\}]. \tag{7.64}$$

Channel estimation is performed by transmitting pilot symbols. The channel is assumed to be quasi-static. The CFO estimation should be performed before the channel estimation so that each user can compensate for his/her own CFO in the receiver. Thus, the ICI and the self-distortion factors caused by CFO are not present during the pilot transmission. Let a_i denote the pilot symbol for user i, the received signal after going through the DFT and $\mathbf{W_i}$ matrices becomes

$$z[k] = a_i w_i[k] w_i^*[k] \lambda_i[k] + \sum_{j=1, j\neq i}^{T} a_j w_j[k] w_i^*[k] \lambda_j[k] + z[k] w_i^*[k], \tag{7.65}$$

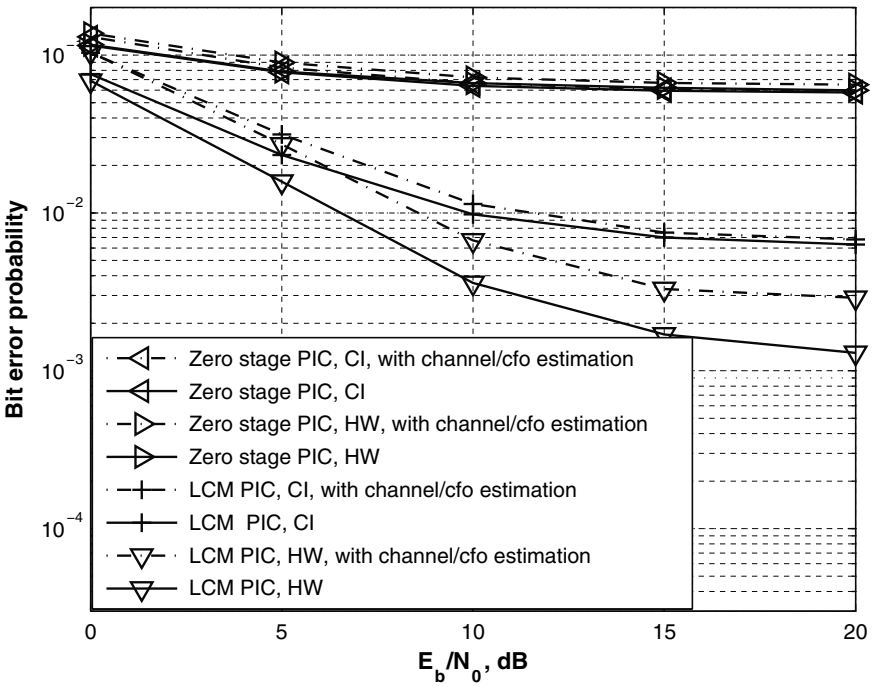

Fig. 7.14. The effect of channel/CFO estimation on the BEP performance, with $N = 16$, $L = 2$, $CFO = \pm 0.1$ dB.

for $k = 0, 1, \cdots, N-1$. To extract $h_i(0), h_i(1), \cdots, h_i(L-1)$ from the above equation, MRC is not useful. Instead, we do the following

$$\hat{h}_i(l) = \frac{1}{\sqrt{N}} \frac{\sum_{k=0}^{N-1} z[k] e^{j\frac{2\pi}{N}kl}}{a_i}, \quad l = 0, 1, \cdots, L-1. \tag{7.66}$$

It is reasonable to perform the above procedure multiple times and then average the estimated channel coefficient so that the variance of the estimator will decrease. Note that the CFO estimation task discussed above requires the knowledge of the channel impulse response, while the channel estimation algorithm needs to know the estimated CFO values to get rid of the ICI and the self-distortion factors caused by CFO.

To address this problem, one possible solution is to perform the CFO estimation and the channel estimation iteratively; namely, first, the CFO values are estimated without the knowledge of the channel impulse response and the estimated CFO values are used to estimate the channel impulse response. In the second iteration, the estimated channel impulse response is employed to estimate the CFO values which in turn are used to update the previous channel estimation results. In the following example, we shall evaluate the performance of the above iterative estimation techniques via simulations.

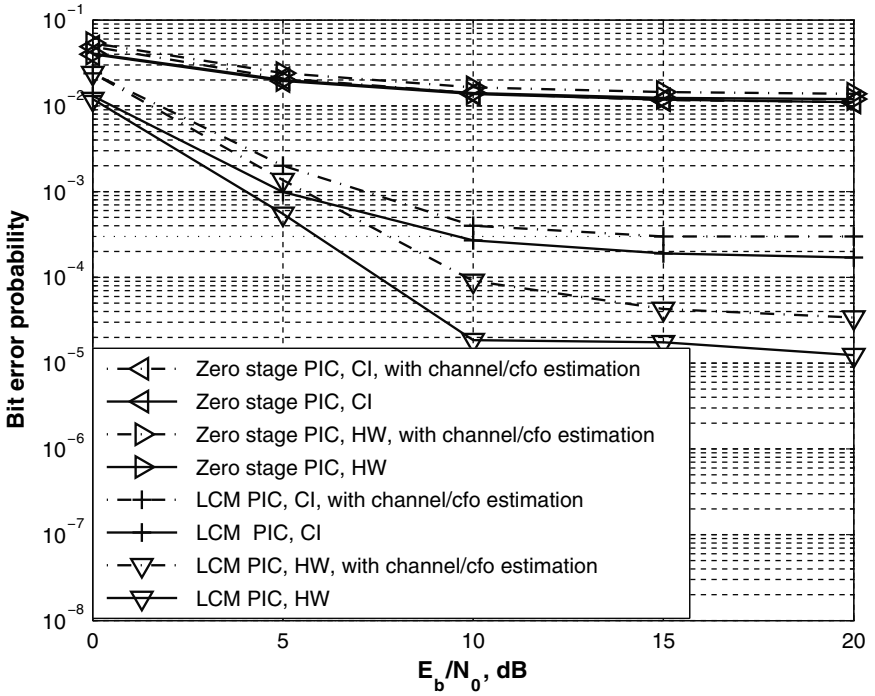

Fig. 7.15. The effect of channel/CFO estimation on the BEP performance, with $N = 32$, $L = 4$, $CFO = \pm 0.1$ dB.

Example 7.9: The Effect of Channel/CFO Estimation on the Performance of PIC

In this example, we investigate the effect of PIC to illustrate the significant performance advantage of PIC. The simulation was performed under two sets of parameters: (1) $N = 16$, $L = 2$ and (2) $N = 32$, $L = 4$, respectively. We set $CFO = \pm 0.1$. Figures 7.14 and 7.15 show the effect of iterative channel and CFO estimations on the BEP performance, where the PIC detector employed the cyclic limit mitigation technique, and the channel and CFO estimation methods were explained in Section 7.5. There are 32 pilot symbols sent for channel estimation and the resultant estimated channel coefficients were averaged to yield the estimate of channel impulse response. We see from these figures that the performance loss of MC-CDMA without PIC due to the channel/CFO estimation is negligible as the performance loss of the PIC detectors is less than 2.5 dB for $E_b/N_0 < 10$ dB.

8

Ultra-Wideband (UWB) Precoding System Design Using Channel Phase

8.1 Introduction

The ultra-wideband (UWB) communication system, which conveys its data symbol by a set of carrier-less pulse waveforms is also known as UWB impulse radio. The narrow pulse, which is of the order of nanoseconds, leads to remarkable multipath resolution at the receiver, i.e., signals coming from different paths can be differentiated easily if their inter-arrival time is greater than one pulse duration. As a result, tens or even hundreds of multipath components are usually found in an indoor environment. Since different path experiences independent channel gain and the probability that all pathes suffer from deep fading simultaneously is low, these many multipath components can be exploited to combat signal deep fading efficiently. However, to acquire sufficient signal power for symbol decoding, one method is to employ a large number of Rake fingers at the receiver [151]. The receiver design of this kind is not only expensive but also consumes a lot of battery power to decode the transmitted symbol. Therefore, it is not favorable for the mobile application, where hardware complexity and power consumption are the major concerns.

The idea called time-reversal prefilter (TRP) or Pre-Rake was recently applied to reduce the UWB receiver complexity in [58, 123, 139] and is described as follows. Given that the channel response is available at the transmitter, the TRP passes the original transmit signal through one prefilter whose impulse response is the same as the order-reversed channel response. Therefore, the equivalent channel response aftering precoding becomes the autocorrelation of the original channel. All the multipath components will be constructively combined after certain delay and it is named as the peak received signal afterward. As a result, the receiver with fewer fingers can enjoy full multipath diversity. The TRP transmitter requires the complete channel response, which is estimated and then passed to the transmitter by the receiver in a frequency division duplex (FDD) system. Owing to a large number of channel taps in the channel, the overhead of the channel information feedback is large and, hence, the TRP scheme is not attractive to the real world implementation.

C.-C.J. Kuo et al., *Precoding Techniques for Digital Communication Systems*,
DOI: 10.1007/978-0-387-71769-2_8,

In this chapter, we introduce a new UWB precoding architecture called channel phase precoded UWB (CPP-UWB) to overcome the drawback of TRP. The CPP transmitter convolutes the transmit signal with the time-reversed phase only, rather than both phase and amplitude information, for symbol precoding. For the carrierless UWB channel response, the phase is equal to either $+1$ or -1, which corresponds to the sign of each tap. As compared to the amplitude information, which is represented by several bits in practice, the phase information is described by one single bit. Therefore, the capacity of the feedback channel is saved. If the feedback phase information is accurate, there will be a strong channel tap in the resultant channel since all the channel taps are coherently combined at the receiver. For those off-peak received signals, their power is much weaker than the peak signal due to arbitrary combining of multpath. By taking advantage of the concentrated signal power, the CPP receiver simply takes one sample at the peak for symbol decision.

Please notice that a similar idea called "delay tuning," which concentrates the received signal power by adjusting the delay and phase of the time-hopped signal properly, was also proposed in [95]. Yet two main differences between the delay tuning and our proposed CPP technique are given as follows. First, the multipath arrival is described as a random variable in [95]. However, the channel model with a fixed inter-arrival time is verified based on the channel sounding experiment in [18]. The random path arrival assumption in [95] requires more complicated schemes for both channel estimation and received signal power focusing. Second, the concentrated signal power at the receiver implies less intersymbol interference (ISI) at the receiver output. Thus, the data rate of CPP-UWB can be improved by reducing the symbol interval without much performance degradation. On the contrary, the delay tuning system, employs a fixed length time-hopping code, does not take advantage of the concentrated signal power to raise its data rate.

The key to the received signal power concentration of CPP systems depends on the accuracy of estimated phase information and a training based phase estimation scheme is used to identify the current phase knowledge. For a given number of training symbols, the lower bound on the output signal-to-noise power ratio (SNR) is derived when the data symbol is encoded by the estimated phase. Please keep in mind that the use of training symbols causes data rate loss and a system designer can minimize the training overhead based on the derived lower bound.

Due to the concentrated signal power at the CPP receiver, the ISI level can be kept tolerable when the symbol interval is less than the channel response length. However, the ISI power gradually dominates the system performance when the data rate increases. Under such circumstance, the CPP system performance can be saved by suppressing the residual ISI at the receiver. Here, one ISI mitigation scheme, say, codeword length optimization (CLO), is developed to suppress interfering signals.

The CLO problem in CPP-UWB systems is motivated by the following observation. Employing a longer codeword, which demands more feedback

channel phase components, may not only improve the concentrated peak power but also amplify the off-peak signal power as well. Consider the case where the symbol interval is less than channel duration, the output signal to interference power ratio (SIR) can be deteriorated consequently. Hence, a longer code may not necessarily enhance the performance than a short one. The design goal of CLO is to maximize the output SIR by adjusting the codeword length. Since the best codeword length is usually less or equal to the original channel response, CLO helps to further reduce the feedback burden. However, it is worthwhile to point out that the closed-form solution to optimal code size is not possible to find since the problem itself is highly nonlinear in nature. Even though we can apply an exhaustive search algorithm to find the best code length, this scheme also requires very high computational power due to a huge number of channel taps in the UWB channel. To save the computational complexity, a fast search algorithm for the optimal code length is also proposed. Even though the fast algorithm maximizes the output SIR, instead of the output signal to interference plus noise power ratio (SINR), the difference between the resulting output SINR and the maximal one is small even when the noise power is strong and it converges to the maximum SINR as noise power goes down.

The organization of this chapter is detailed as follows. The system model of CPP-UWB system is given in Section 8.2 followed by the performance comparison between different precoding systems in Section 8.3. The lower bound on the output SNR when the data symbol is encoded by the estimated channel phase is derived in Section 8.4. Next, the CLO problem is formulated and a fast search algorithm for solving CLO is derived in Section 8.5. Finally, the power spectral mask of the proposed CPP system is derived and the related implement issue is discussed in Section 8.6.

8.2 System Model and Features

8.2.1 System Model

Here we consider a carrierless, pulse-based UWB communication system, where the emitted pulse waveform is carefully designed so that the output power spectral density (PSD) satisfies the US Federal Communications Commission (FCC) requirement in [39]. The tap-delay-line (TDL) channel model from Chao and Scholtz [22] is adopted to simplify our discussion and it is described as

$$h(t) = \sum_{i=0}^{L-1} h_i \delta(t - i\Delta) = \sum_{i=0}^{L-1} p_i \alpha_i \delta(t - i\Delta), \tag{8.1}$$

where $h_i = p_i \alpha_i$ is the channel gain of the ith path and Δ denotes the duration of pulse waveform, which is set as the minimum multipath resolution in time domain. In a baseband channel, the channel gain of the ith signal path h_i is a real number and is composed of two random variables: phase p_i and amplitude

α_i. The phase p_i, which belongs to either $+1$ or -1 with equal probability, depends on the number of reflection during the transmission path. The amplitude signal α_i is modeled as a Rayleigh random variable with probability density function (PDF) as

$$f_{\alpha_i}(x) = \frac{x}{\sigma_i^2} e^{-x^2/2\sigma_i^2}. \tag{8.2}$$

Also, the second moment of α_i, i.e., the power of h_i, decreases as its tap index goes up. Mathematically, we have

$$E\{h_i^2\} = E\{\alpha_i^2\} = 2\sigma_i^2 = \Omega\gamma^i, \tag{8.3}$$

where Ω is the power of the first tap and $\gamma = e^{-\Delta/\Gamma}$ is a positive number less than 1 since Γ that controls the rate of power decay is greater than Δ. The effective channel response length is determined by the value of Γ, i.e., the channel tap, whose power is less than $\Omega\gamma^{L-1}$ is ignored. Four different values of Γ, which are suitable for four different channel modes, namely, channel model 1 to 4 (CM 1–4) in [41], are also specified in [25]. Please note that the inter-arrival time between two consecutive multipath components is fixed in our model. This model is suitable for the environment, where the multipath is dense since multipath components in the same time domain grid can be viewed as an effect channel tap [18, 86].

The block diagram of the CPP-UWB system is shown in Fig. 8.1, where the receiver sends the L-bit estimated channel phase knowledge to the transmitter for symbol precoding. Once the transmitter acquires the fed back phase information, it synthesizes the codeword $\mathbf{c}^{(L)}$ with the reversed phase information as

$$\mathbf{c}^{(L)} = [c_0^{(L)}, \cdots, c_{L-1}^{(L)}]^t = \frac{1}{\sqrt{L}}[\hat{p}_{L-1}, \cdots, \hat{p}_0]^t, \tag{8.4}$$

where $\sqrt{L}$ in the dominator is used to normalize the total transmitted power per symbol. Next, the BPSK symbol, $b(i)$, is modulated onto the codeword $\mathbf{c}^{(L)}$ and the pulse waveform $w_s(t)$. Mathematically, the transmitted signal becomes

$$x_s(t) = \sum_{i=-\infty}^{\infty} b(i) \sum_{j=0}^{L-1} c_j^{(L)} w_s(t - j\Delta - iT), \tag{8.5}$$

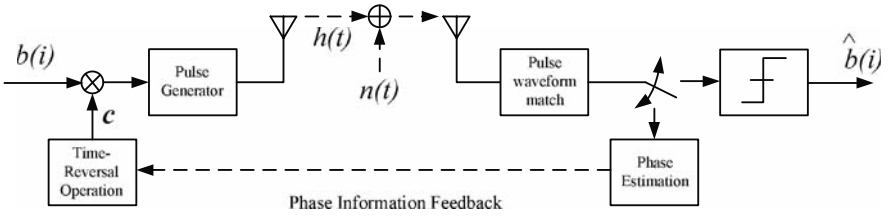

Fig. 8.1. The block diagram of the CPP-UWB system [[20] ©IEEE]

where the symbol interval T is set as an integer multiple of Δ, i.e., $T = M\Delta$, where $M \in \mathbb{N}$.

The signal arrives at the receiver is distorted by the multipath channel and contaminated by the additive white Gaussian noise (AWGN). After received pulse waveform matching and chip sampling, the discrete received signal can be formulated as

$$\mathbf{r}^{(L)}(i) = [r_0^{(L)}(i), \cdots, r_{2L-2}^{(L)}(i)]^t = \mathbf{H}^{(L)}\mathbf{c}^{(L)}b(i) + \boldsymbol{\mathcal{I}}^{(L)}(i) + \mathbf{n}^{(L)}(i), \quad (8.6)$$

where $\mathbf{H}^{(L)}$ is a $(2L-1) \times L$ Toeplitz matrix whose first column contains $\mathbf{h} = [h_0, h_1, \cdots, h_{L-1}]^t$ from the first to the Lth elements and zeros elsewhere, $\boldsymbol{\mathcal{I}}^{(L)}(i) = [\mathcal{I}_0^{(L)}(i), \cdots, \mathcal{I}_{2L-2}^{(L)}(i)]^t$ is the ISI vector, and $\mathbf{n}^{(L)}(i) = [n_0^{(L)}(i), \cdots, n_{2L-2}^{(L)}(i)]^t$ is the AWGN vector whose mean is zero and covariance matrix is $(N_o/2)\mathbf{I}_{2L-1}$. It is worthwhile to comment that the equivalent channel response spans $2L-1$ taps. If the symbol interval is less than L chips, the received signal $\mathbf{r}^{(L)}(i)$ contains ISI since $\boldsymbol{\mathcal{I}}^{(L)}(i)$ is nonzero.

Let $\mathbf{h}^{(L)}$ denote the equivalent channel response after precoding, i.e.,

$$\mathbf{h}^{(L)} = \mathbf{H}^{(L)}\mathbf{c}^{(L)} = [h_0^{(L)}, \cdots, h_{2L-2}^{(L)}]^t, \quad (8.7)$$

where

$$h_i^{(L)} = \begin{cases} \frac{1}{\sqrt{L}} \sum_{j=0}^{i} \hat{p}_{L-1+j-i} p_j \alpha_j, & 0 \le i \le L-1, \\ \frac{1}{\sqrt{L}} \sum_{j=0}^{2L-2-i} p_{i+j-L+1} \hat{p}_j \alpha_{i+j-L+1}, & L \le i \le 2L-2. \end{cases} \quad (8.8)$$

If the fed back phase information is accurate, i.e., $\hat{p}_i = p_i \ \forall i \in \{0, \cdots, L-1\}$, we have

$$h_{L-1}^{(L)}\Big|_{\hat{p}_i = p_i} = \frac{1}{\sqrt{L}} \sum_{j=0}^{L-1} \alpha_j, \quad (8.9)$$

where all the path gains are summed after some delay. As compared to other taps in $\mathbf{h}^{(L)}$, the amplitude of $h_{L-1}^{(L)}$ is much stronger due to the coherent combination of all multipath components. By taking advantage of the concentrated signal power, a single finger rake receiver (i.e., a matched filter (MF)), can be applied to decode the transmit symbol as

$$\hat{b}(i) = \text{sign}\left\{ r_{L-1}^{(L)}(i) \right\}. \quad (8.10)$$

In addition, the focused signal power allows the symbol interval to be reduced to improve the data rate without much ISI penalty.

8.2.2 Features of CPP-UWB System

The CPP-UWB system contains several interesting features, which are detailed next.

Low Cost Receiver Design and Low Bit Rate Feedback Channel Capacity

The TRP transmitter requires full channel information, which includes both phase and amplitude of every channel tap. Usually, a high resolution analogy-to-digital converter (ADC) is necessary at the TRP receiver to resolve each channel gain, for example, a 10-bit ADC is employed at TRP receiver in [56]. The higher resolution ADC also produces more bits for every channel estimation and thus demands more channel capacity for information feedback. On the contrary, the CPP transmitter demands only the knowledge of channel phase, which can be identified by a 1-bit ADC. Therefore, the receiver design employing a lower resolution ADC is cheaper while the required feedback channel capacity is lower.

High Data Transmission Rate

If the phase knowledge at the transmitter is perfect, the phase precoding changes the power profile of the original UWB channel so that a majority of power is focused at one tap while the rest of power is distributed among those off-peak taps. As compared to the system without precoding, the concentrated power profile lessens the ISI effect at the receiver output for a fixed symbol interval. In other words, the reduced off-peak signal power allows a high data rate throughput by shortening the symbol interval for a fixed noise margin.

Secure Data Transmission

The channel measurement result in [103] implies that the spatial correlation between two responses measured by two different receive antennas separated by more than 10 in. does not exceed 0.1. Hence, the channel responses at different locations are almost independent. Since the returned phase information is location dependent, the peak power is achievable only at a specific place while the signal power is spread elsewhere. Thanks to the scattered signal power, it is hard for eavesdroppers to acquire the transmitted data symbol if they are far away from the desired receiver. Even if the phase knowledge is wiretapped by the third party users during the phase information feedback stage, they have to combat a serious ISI during the decoding process. Consequently, CPP technique enhances the transmission security by the nature of its design.

It is worthwhile to mention that the TRP scheme also supports a high rate transmission and a secure communication link. In fact, with more channel knowledge involved in the precoding process, TRP can achieve a higher data rate and more secure communication link than CPP. However, its huge feedback overhead and expensive ADC receiver design impedes its deployment in practice.

8.3 Performance Analysis of CPP-UWB Systems

Since the CPP scheme that utilizes partial channel knowledge in the precoding process, the concentrated signal power may not be as high as TRP. In this section, we will analyze the focused signal power generated by phase codeword and then compare it to other TRP schemes, such as partial Pre-Rake (PPR) [57] in the following analysis. Please note that to simplify our discussion, the fed back phase information is assumed to be perfect.

8.3.1 Channel Power Concentration of Phase Precoding

Given the ideal phase knowledge at the transmitter, from (8.8), the averaged peak power at the receiver can be calculated as

$$\begin{aligned}\bar{P}_{h_{L-1}^{(L)}} &\equiv E\left\{\left(h_{L-1}^{(L)}b(i)\right)^2\right\} = E\left\{\left(\frac{1}{\sqrt{L}}\sum_{j=0}^{L-1}\alpha_j\right)^2\right\} \\ &= \frac{1}{L}E\left\{\sum_{j=0}^{L-1}\alpha_j^2 + \sum_{l,m=0;l\neq m}^{L-1}\alpha_l\alpha_m\right\}. \end{aligned} \tag{8.11}$$

Because the channel gain is assumed to be independent for different path, and the first and the second moments of the Rayleigh random variable α_j equal $\frac{\sqrt{\pi\Omega\gamma^j}}{2}$ and $\Omega\gamma^j$, respectively, the averaged power in (8.11) can be further simplified as

$$\begin{aligned}\bar{P}_{h_{L-1}^{(L)}} &= \frac{\Omega(1-\gamma^L)}{L(1-\gamma)} + \frac{\Omega\pi}{4L}\left(\sum_{l,m=0;l\neq m}^{L-1}\gamma^{(l+m)/2}\right) \\ &= \frac{\Omega(1-\gamma^L)}{L(1-\gamma)} + \frac{\Omega\pi}{4L}\left(\left(\sum_{l=0}^{L-1}\gamma^{l/2}\right)^2 - \sum_{l=0}^{L-1}\gamma^l\right) \\ &= \left(1-\frac{\pi}{4}\right)\frac{\Omega(1-\gamma^L)}{L(1-\gamma)} + \frac{\Omega\pi}{4L}\left(\frac{1-\gamma^{L/2}}{1-\gamma^{1/2}}\right)^2. \end{aligned} \tag{8.12}$$

Let ς denote the ratio between the second and the first terms at the right-hand side of (8.12), i.e.,

$$\varsigma = \frac{\frac{\Omega\pi}{4L}\left(\frac{1-\gamma^{L/2}}{1-\gamma^{1/2}}\right)^2}{\left(1-\frac{\pi}{4}\right)\frac{\Omega(1-\gamma^L)}{L(1-\gamma)}}. \tag{8.13}$$

After some manipulations, it can be shown that ς can be bounded from below as

$$\varsigma \geq \frac{\pi}{4-\pi}\frac{2\Gamma}{\Delta}\left(\frac{1-e^{\eta/2}}{1+e^{\eta/2}}\right), \tag{8.14}$$

where η is defined as

$$\eta = \frac{\Delta L}{\Gamma}.^{1} \tag{8.15}$$

For a typical value of η (e.g., $\eta = 6.146$), we have the following relationship

$$\varsigma \geq 50 \Longleftrightarrow \Gamma/\Delta \geq 6.8. \tag{8.16}$$

Since the pulse duration Δ is usually a smaller number as compared to the decay time constant Γ, the second term at the right-hand side of (8.12) contributes most of the power for $\bar{P}_{h_{L-1}^{(L)}}$. Therefore, $\bar{P}_{h_{L-1}^{(L)}}$ is approximated as

$$\bar{P}_{h_{L-1}^{(L)}} \approx \frac{\Omega\pi}{4L}\left(\frac{1-\gamma^{L/2}}{1-\gamma^{1/2}}\right)^2. \tag{8.17}$$

Please note that the total channel power in the UWB channel is computed as

$$\bar{P}_{chl} = \sum_{j=0}^{L-1} E\left\{h_j^2\right\} = \sum_{j=0}^{L-1} \Omega\gamma^j = \Omega\frac{1-\gamma^L}{1-\gamma}. \tag{8.18}$$

Let χ, which is defined as the ratio between $\bar{P}_{h_{L-1}^{(L)}}$ and $\bar{P}_{chl}$, be the power degradation factor due to incomplete channel information usage in the precoding process. We can have

$$\begin{aligned}\chi = \frac{\bar{P}_{h_{L-1}^{(L)}}}{\bar{P}_{chl}} &\approx \frac{\pi}{4L}\frac{(1+\gamma^{1/2})(1-\gamma^{L/2})}{(1+\gamma^{L/2})(1-\gamma^{1/2})} \\ &= \frac{\pi\Delta}{4\Gamma\eta}\frac{(1-e^{-\eta/2})(1+e^{-\Delta/2\Gamma})}{(1+e^{-\eta/2})(1-e^{-\Delta/2\Gamma})},\end{aligned} \tag{8.19}$$

where L is substituted by $\Gamma\eta/\Delta$ to get the last equation. Recall that since $\Delta/2\Gamma$ is usually a small number, we can obtain the following approximation

$$1 + e^{-\Delta/2\Gamma} \approx 2 \text{ and } 1 - e^{-\Delta/2\Gamma} \approx \Delta/2\Gamma, \tag{8.20}$$

where the higher order terms in the Taylor series expansion of $e^{-\Delta/2\Gamma}$ are ignored. From (8.20) and (8.19), the degradation factor χ in (8.19) can be further simplified as

[1] It is worthwhile to point out that the power of last channel tap $E\{h_{L-1}^2\}$ satisfies the following equation.

$$E\{h_{L-1}^2\} = \Omega\gamma^{L-1} \geq \Omega\gamma^L = \Omega e^{-\eta},$$

where L and γ is replaced by $\Gamma\eta/\Delta$ and $e^{-\Delta/\Gamma}$, respectively, to arrive the last equation. The variable η governs the effective channel length since channel taps whose power is less or equal to $\Omega e^{-\eta}$ are ignored.

$$\chi \approx \frac{\pi(1-e^{-\eta/2})}{\eta(1+e^{-\eta/2})}. \tag{8.21}$$

As (8.21) suggests, the degradation factor χ is also controlled by η. For a larger value of η, i.e., a longer channel duration, the power degradation factor χ could be even lower. This is because the power of each tap shrinks with respective to its tap index and we normalize the phase codeword by $\sqrt{L}$ in its dominator.

8.3.2 Comparison Between TRP and CPP Schemes

The TRP scheme that demands a very high feedback overhead to deliver full channel knowledge back to the transmitter is not practical. Two Pre-Rake schemes, namely, partial Pre-Rake (PPR) and selective Pre-Rake (SPR), are proposed to save the feedback channel capacity of TRP in [58]. It is shown in [21] that given the channel model in Section 8.2, PPR technique concentrates on the highest channel power on the average for a fixed number of feed back channel taps. Since both CPP and PPR transmitters utilize partial channel information, namely the channel phase in CPP and the first several channel taps in PPR, it would be interesting to compare their required feedback quantity when both precoders generates the same amount of peak power at their receivers.

Assume ideal phase information is available at the transmitter. The peak power generated by a l-chip phase codeword is

$$\bar{P}_{h_{l-1}^{(l)}} = \bar{P}_{h_{L-1}^{(L)}}\big|_{L=l}. \tag{8.22}$$

Consider the channel model specified in Section 8.2. The signal power concentrated at the receiver end when only $\bar{L}$ first channel taps are given to the PPR transmitter is shown as [21]

$$\bar{P}_{PPR}(\bar{L}) = \Omega\frac{1-\gamma^{\bar{L}}}{1-\gamma}. \tag{8.23}$$

Therefore, the number of channel taps $\bar{L}$ necessary to produce the same peak power as $\bar{P}_{h_{l-1}^{(l)}}$ can be found by solving the following equation

$$\bar{P}_{PPR}(\bar{L}) = \bar{P}_{h_{l-1}^{(l)}}. \tag{8.24}$$

After some manipulations, we can have

$$\bar{L} = \left\lceil \frac{\Gamma}{\Delta}\ln(1-\rho) \right\rceil, \tag{8.25}$$

where

$$\rho = \frac{1}{l}(1 - \frac{\pi}{4})(1 - \gamma^l) + \frac{\pi}{4l}\left(\frac{1 - \gamma^{l/2}}{1 - \gamma^{1/2}}\right)^2 (1 - \gamma). \tag{8.26}$$

Please note that we adopt the peak power as our criterion to compare the feedback overhead of both PPR and CPP systems in (8.25). Therefore, their BEP performance should be roughly the same when the received signal is ISI-free. However, both system may have different output SINR when the symbol interval M is less than L. The closed-form relationship between $\bar{L}$ and l may not be possible if both systems are evaluated at the same output SINR level. This is because the output SINR is a highly nonlinear function of either $\bar{L}$ and l. In fact, when the ISI power is not large, as shown in Example 8.1, the gap between their BEP curves is small and (8.25) is still valid.

Example 8.1: Comparison Between CPP-UWB and PPR Systems
In this example, we compare the feedback overhead between CPP-UWB and PPR systems when both precoding schemes accumulate the same amount of power at the peak. The system parameters are chosen as $\Delta = 0.7$ ns, $\Gamma = 20.5$ ns (CM3), and $L = 180$. Two different values of symbol intervals, say, $M = 30$ and 60, which correspond to data rate equal to 47.6 and 23.8 Mbps, respectively, are considered. Furthermore, the result shown here is the average of 1000 channel realizations. Let the corresponding feedback number of channel phase l be the same as the symbol interval in chip. The amount of

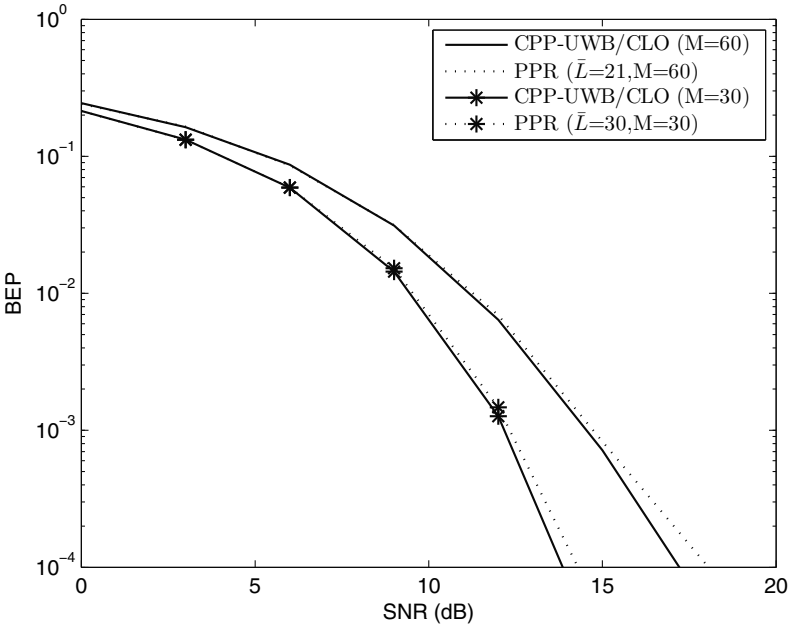

Fig. 8.2. BEP performance between CPP-UWB and PPR at different noise power [[80] ©IEEE].

feedback channel taps for PPR $\bar{L}$ computed by (8.25) are $\bar{L} = 30$ and 21 for M=60 and 30, respectively. If a 10-bit ADC is utilized at the PPR receiver [56], this equals to $300(30*10)$ and $210(21*10)$ bits per channel feedback. On the other hand, CPP-UWB requires only 60 and 30 bits per feedback, which is much smaller than that of PPR.

Next, let us consider their decoding performance. The corresponding BEP performance at different input SNR are plotted in Fig. 8.2. It is observed from Fig. 8.2 that the BEP gap between two systems is small for two different data rates considered in this example. Therefore, the feedback overhead comparison based on the concentrated signal power is valid even when ISI occurs.

8.4 Phase Estimation and Performance Analysis with Estimated Phase Information

The decoding performance of CPP systems relies on the correctness of the returned phase information. In this section, a training based phase estimation scheme, which is simple yet practical, is applied to identify the current phase knowledge. When the CPP transmitter utilizes the phase estimate acquired by N training symbols, the corresponding SNR lower bound is derived to evaluate its system performance.

8.4.1 Channel Phase Estimation Algorithm

The phase estimation scheme using training symbols is described as the following steps.

1. After channel synchronization is achieved, N channel sounding pulses $b_t(i)$ $\forall i = 0, \cdots, N-1$, whose pattern are also known at the receiver, are emitted by the transmitter. The interval between two consecutive pulses are long enough so that the response of different pulse is separated.
2. The receiver performs the pulse waveform match and samples the received signal for every Δ second to digitalize N channel responses. In order to minimize the noise distortion, all received signals are first demodulated and then averaged before phase estimation. Mathematically, the averaged response becomes

$$\hat{\mathbf{r}}_t = \frac{1}{N}\sum_{l=0}^{N-1} b_t(l)\mathbf{r}_t(l) = \frac{1}{N}\sum_{l=0}^{N-1} b_t(l)\left(\mathbf{h} + \mathbf{n}_t(l)\right) = \mathbf{h} + \hat{\mathbf{n}}_t, \quad (8.27)$$

where

$$\hat{\mathbf{n}}_t = [\hat{n}_{t,0}, \cdots, \hat{n}_{t,L-1}]^t = \frac{1}{N}\sum_{l=0}^{N-1} b_t(l)\mathbf{n}_t(l) \quad (8.28)$$

and $\mathbf{n}_t(l) \sim \mathcal{N}(0, N_0/2\mathbf{I}_L)$ is the AWGN noise vector corresponding to the lth training symbol. Also, it can be shown easily that $\hat{n}_t \sim \mathcal{N}(0, N_0/2N\mathbf{I}_L)$.

3. The channel phase is thus measured by the sign of every tap in the averaged response $\hat{\mathbf{r}}_t$. Thus, the channel phase estimate is given as

$$\hat{\mathbf{P}} = \text{sign}\{\hat{\mathbf{r}}_t\}. \tag{8.29}$$

8.4.2 Performance Analysis with Estimated Phase

When the data symbol is precoded with the phase estimate $\hat{\mathbf{p}}$, the output SNR of CPP-UWB can be bounded from below as stated in the following proposition.

Proposition 8.1. Let N be the number of training symbols used in the CPP-UWB system. The output SNR $\bar{\nu}^{(L)}$ satisfies

$$\begin{aligned}\bar{\nu}^{(L)} &= \frac{E\left\{\left(h_{L-1}^{(L)}b(i)\right)^2\right\}}{E\left\{\left(n_{L-1}^{(L)}(i)\right)^2\right\}} = \frac{2E\left\{\left(h_{L-1}^{(L)}\right)^2\right\}}{N_0} \\ &\geq \frac{2}{LN_0}\left\{\Omega\frac{1-\gamma^L}{1-\gamma} + \sum_{i,j=0;i\neq j}^{L-1} \left[\frac{\sqrt{\pi\Omega}}{2}\gamma^{i/2} - \frac{\sqrt{2\pi}}{\Omega\gamma^i}\left(\frac{\Omega N_0\gamma^i}{2N_0+2N\Omega\gamma^i}\right)^{3/2}\right]\right. \\ &\qquad \left. \cdot \left[\frac{\sqrt{\pi\Omega}}{2}\gamma^{j/2} - \frac{\sqrt{2\pi}}{\Omega\gamma^j}\left(\frac{\Omega N_0\gamma^j}{2N_0+2N\Omega\gamma^j}\right)^{3/2}\right]\right\}.\end{aligned} \tag{8.30}$$

Proof: By (8.8), the averaged peak power can be simplified as

$$\begin{aligned}E\left\{\left(h_{L-1}^{(L)}b(i)\right)^2\right\} &= E\left\{\left(\frac{1}{\sqrt{L}}\sum_{j=0}^{L-1}\hat{p}_j p_j \alpha_j b(i)\right)^2\right\} \\ &= \frac{1}{L}\sum_{j=0}^{L-1}\Omega\gamma^j + \frac{1}{L}\sum_{j,m=0;j\neq m}^{L-1} E\left\{p_j\hat{p}_j\alpha_j\right\}E\left\{p_m\hat{p}_m\alpha_m\right\}.\end{aligned} \tag{8.31}$$

Please note that whether the ith phase estimate is correct depends on the magnitude of α_i and the noise power of the ith element of $\hat{\mathbf{n}}_t$. Conditioned on one channel realization, the probability of correct phase estimate is

$$\begin{aligned}Pr\left\{\hat{p}_i = p_i\middle|\alpha_i\right\} &= Pr\{\hat{p}_i = 1\big|\alpha_i, p_i = 1\}Pr\{p_i = 1\} \\ &\quad + Pr\{\hat{p}_i = -1\big|\alpha_i, p_i = -1\}Pr\{p_i = -1\} \\ &= Pr\left\{p_i\alpha_i + \hat{n}_{t,i} > 0\middle|\alpha_i, p_i = 1\right\}Pr\{p_i = 1\} \\ &\quad + Pr\left\{p_i\alpha_i + \hat{n}_{t,i} < 0\middle|\alpha_i, p_i = -1\right\}Pr\{p_i = -1\} \\ &= 1 - Q\left(\sqrt{2N\alpha_i^2/N_0}\right).\end{aligned} \tag{8.32}$$

Similarly, we can have

$$Pr\left\{\hat{p}_i \neq p_i | \alpha_i\right\} = Q\left(\sqrt{2N\alpha_i^2/N_0}\right). \tag{8.33}$$

From (8.32) and (8.33), the expected value of $\hat{p}_i p_i \alpha_i$ conditioned on the channel gain α_i is computed as

$$\begin{aligned} E\left\{\hat{p}_i p_i \alpha_i | \alpha_i\right\} &= \alpha_i Pr\{\hat{p}_i = p_i\} - \alpha_i Pr\{\hat{p}_i \neq p_i\} \\ &= \alpha_i - 2\alpha_i Q\left(\sqrt{2N\alpha_i^2/N_0}\right). \end{aligned} \tag{8.34}$$

By averaging over the probability of α_i, we have the uncoditional expected value as

$$\begin{aligned} E\left\{\hat{p}_i p_i \alpha_i\right\} &= E_{\alpha_i}\left\{E\left\{\hat{p}_i p_i \alpha_i | \alpha_i\right\}\right\} \\ &= E_{\alpha_i}\left\{\alpha_i\right\} - 2E_{\alpha_i}\left\{\alpha_i Q\left(\sqrt{2N\alpha_i^2/N_0}\right)\right\} \\ &\geq \frac{\sqrt{\pi\Omega}}{2}\gamma^{i/2} - \int_0^\infty e^{-Nx^2/N_0} x f_{\alpha_i}(x) dx \\ &= \frac{\sqrt{\pi\Omega}}{2}\gamma^{i/2} - \frac{\sqrt{2\pi}}{\Omega\gamma^i}\left(\frac{\Omega N_0 \gamma^i}{2N_0 + 2N\Omega\gamma^i}\right)^{3/2}, \end{aligned} \tag{8.35}$$

where the inequality is obtained by substituting the Q function with its upper bound in [146], i.e.,

$$Q(x) \leq \frac{1}{2}e^{-x^2/2}, \tag{8.36}$$

and several mathematical manipulations are applied to the right-hand side of the inequality to get the final result. By replacing $E\left\{\hat{p}_i p_i \alpha_i\right\}$ in (8.31) with its lower bound derived in (8.35) and dividing (8.31) by $N_0/2$, we have completed the proof of Proposition 8.1.

An example for the proposed phase estimation scheme is shown next.

Example 8.2: Effect of Proposed Phase Estimation Algorithm
In this example, we demonstrate the impact of training overhead on the performance of the phase estimation algorithm. The system parameters are remained the same as those in the previous example, except we let the symbol interval be greater than L so that ISI is absent. Three input SNR values (10, 15, and 20 dB) are considered and the corresponding output SNR for different number of training symbols N is shown in Fig. 8.3. The output SNR curves, which correspond to the idea phase and the derived lower bound, respectively, are also plotted for referencing purposes. As Fig. 8.3 suggests, when the input SNR is fixed, the use of more training symbols improves the output SNR at the cost of higher overhead and degraded data rate. The derived lower bound that suggests the worse case output SNR for a given number of training symbols. Therefore, we can vary the number of training symbols to save the data

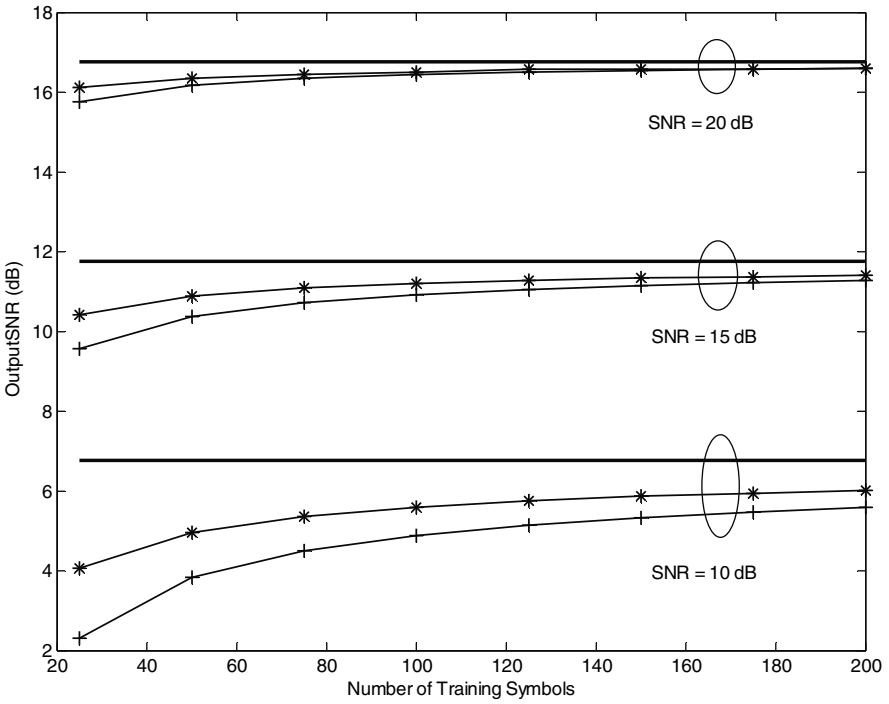

Fig. 8.3. The output SNR vs the number of training symbols [[80] ©IEEE].

rate. In addition, the bound becomes tie as either N or input SNR increases since the gap between $Q(x)$ and its upper bound becomes small as x goes up.

Furthermore, the degradation between input SNR and ideal output SNR is around 3.3 dB. With (8.15), the value of η in this example is computed as

$$\eta = \frac{180 * 0.7}{20.5} \approx 6.146. \tag{8.37}$$

By substituting (8.37) into (8.21), we have the peak power degradation as

$$\chi \approx \left.\frac{\pi(1 - e^{-\eta/2})}{\eta(1 + e^{-\eta/2})}\right|_{\eta=6.146} = 0.4659 = -3.3 \text{ dB}, \tag{8.38}$$

which corroborates the observation we have in Fig. 8.3.

The derived lower bound provides a means to predict the system performance for a fixed number of training symbol. Therefore, the system designer can properly adjust the amount of training symbols based on the specified performance requirement to avoid excess training overhead. By observing (8.32), we learn that the probability of correct phase estimation approaches asymptotically to 1 as N increases. This implies that not only the proposed phase estimation scheme is unbiased, but also the corresponding mean-square-error

(MSE) of the phase estimate is zero as long as the number of training symbol is large enough.

8.5 Codeword Length Optimization (CLO) in an ISI Channel

8.5.1 Problem Statement

Before we discuss the codeword length optimization (CLO) problem, let us fist consider the output signal-to-interference power ratio (CIR) of different phase code sizes as in the following example.

Example 8.3: Output Signal-to-Interference Power Ratio (SIR) vs Different Codeword Size
Here we compare the output signal power and SIR of CPP systems with different codeword length in this example. The system variables are chosen as: $L = 180$, $M = 30$, $\Delta = 0.7$ ns, and $\Gamma = 20.5$ ns (CM3). Two different sizes of phase code, namely, $l = 180$ and $l = 30$, are considered and their resultant channel responses are drawn in Fig. 8.4. The solid stars and circles in the figure denote the corresponding desired signals and interference,

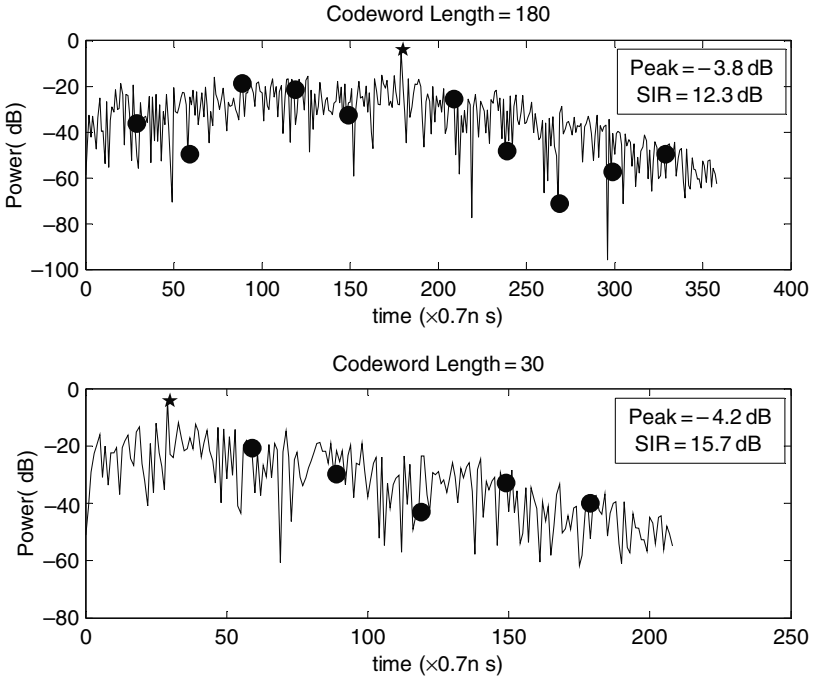

Fig. 8.4. The received signal power for different codeword lengths [[80] ©IEEE].

respectively. It is observed from Fig. 8.4 that the use of more phase information that combines more channel taps at the receiver output could produce more peak signal power as well as more interference from the neighboring symbols. Therefore, the SIR generated by a longer phase code is actually worse.

Although the focused signal power allows us to shrink the symbol interval to rise the data transmission rate without much ISI, the more phase knowledge at the transmitter may not reduce the symbol error rate at the receiver as Example 8.3 suggests. Consider a fixed symbol interval, an optimal codeword length, which renders the highest output SIR at the CPP receiver output, exists. Furthermore, since the optimal codeword length is usually less than L, knowing the best codeword size reduces the feedback burden, too.

Our CLO problem is based on the following assumption that the channel duration L is assumed to be an integer dividable by the symbol interval M, i.e., $L = KM$, where K is a positive integer. The assumption here is not as restrict as it first appears since we can always truncate or zero-pads the original channel response to satisfy this requirement when the amplitude of the last channel tap becomes very small. We will show later that the system bit-error-probability (BEP) of this altered channel is almost indistinguishable from that of the original channel using one example later in this section.

When a data symbol is encoded by a l-chip long codeword $\mathbf{c}^{(l)}$, i.e.,

$$\mathbf{c}^{(l)} = [c_0^{(l)}, \cdots, c_{l-1}^{(l)}]^t = \frac{1}{\sqrt{l}}[p_{l-1}, \cdots, p_0]^t, \tag{8.39}$$

the corresponding received signal is written as

$$\begin{aligned}\mathbf{r}^{(l)}(i) &= [r_0^{(l)}(i), \cdots, r_{L+l-2}^{(l)}(i)]^t \\ &= \mathbf{H}^{(l)}\mathbf{c}^{(l)}b(i) + \boldsymbol{\mathcal{I}}^{(l)}(i) + \mathbf{n}^{(l)}(i) \\ &= \mathbf{h}^{(l)}b(i) + \boldsymbol{\mathcal{I}}^{(l)}(i) + \mathbf{n}^{(l)}(i),\end{aligned}$$

where $\mathbf{H}^{(l)}$ is the $(L+l-1)\times l$ Toeplitz matrix, $\boldsymbol{\mathcal{I}}^{(l)}(i)$ and $\mathbf{n}^{(l)}(i)$ are the interference and AWGN vectors, respectively, $\mathbf{h}^{(l)} = \mathbf{H}^{(l)}\mathbf{c}^{(l)} = [h_0^{(l)}, \cdots, h_{L+l-1}^{(l)}]^t$, and

$$h_i^{(l)} = \begin{cases} \frac{1}{\sqrt{l}}\sum_{j=0}^{i} p_{l-1+j-i}p_j\alpha_j, & 0 \le i \le l-1, \\ \frac{1}{\sqrt{l}}\sum_{j=0}^{l-1} p_j p_{j+i-l+1}\alpha_{j+i-l+1}, & l \le i \le L-1, \\ \frac{1}{\sqrt{l}}\sum_{j=0}^{l-i+L-2} p_j p_{l-1+j}\alpha_{l-1+j}, & L \le i \le L+l-2. \end{cases} \tag{8.40}$$

The codeword $\mathbf{c}^{(l)}$ leads to the coherent combination of the first l channel taps and the peak signal power occurs at $h_{l-1}^{(l)}(i)$. The average output SIR at $r_{l-1}^{(l)}$ is equal to

$$\bar{\nu}^{(l)} = E\left\{\left(h_{l-1}^{(l)} b(i)\right)^2\right\} \times \left\{\sum_{j=1}^{\lfloor (L-1)/M \rfloor} E\left\{\left(h_{l+jM-1}^{(l)} b(i-j)\right)^2\right\} + \sum_{j=1}^{\lfloor (l-1)/M \rfloor} E\left\{\left(h_{l-jM-1}^{(l)} b(i+j)\right)^2\right\}\right\}^{-1}. \tag{8.41}$$

The problem of codeword length optimization is then formulated as

$$L_{opt} = \arg \max_{0<l\leq L} \bar{\nu}^{(l)}, \tag{8.42}$$

where a closed-form solution to L_{opt} is difficult owing to the nonlinear nature of the problem. Even though we can apply an exhaustive search algorithm that tests all the possible value of l and pick up the one with highest output SIR, this algorithm is computationally very intensive and is not favorable. Next, a fast search algorithm is presented to find the solution for the above optimization problem with less computational complexity.

Please note that our discussion of the optimized codeword length is primarily limited to the high data rate scenario, i.e., $T \leq L\Delta$. Since the transmit power per symbol in CPP systems is always normalized to one and the power of each tap decreases exponentially with respect to its tap index, a longer code may not guarantee a higher peak power. Hence, the optimal codeword length that generates the highest output SNR can be found in the ISI-free case, too. The CLO problem for the low data rate case is however not as interesting as that for the high data rate case.

8.5.2 Fast Search Algorithm for Optimal Code Length

Let us first rewrite the output SIR by substituting (8.40) into (8.41) and performing some manipulations as

$$\bar{\nu}^{(l)} = \frac{E\left\{\left(\sum_{j=0}^{l-1} \alpha_j\right)^2\right\}}{\sum_{j=0}^{l-1} I^{(j)}},$$

where

$$\begin{aligned} I^{(j)} &\equiv \sum_{m=1}^{\lfloor j/M \rfloor} E\left\{(\alpha_{j-mM} p_j p_{j-mM} b(i+m))^2\right\} + \sum_{n=1}^{\lfloor (L-j)/M \rfloor} E\left\{(\alpha_{j+nM} p_j p_{j+nM} b(i-n))^2\right\} \\ &= \sum_{m=1}^{\lfloor j/M \rfloor} E\left\{\alpha_{j-mM}^2\right\} + \sum_{n=1}^{\lfloor (L-j)/M \rfloor} E\left\{\alpha_{j+nM}^2\right\} \\ &= \sum_{m=1}^{\lfloor j/M \rfloor} \Omega\gamma^{j-mM} + \sum_{n=1}^{\lfloor (L-j)/M \rfloor} \Omega\gamma^{j+nM} \end{aligned}$$

is the normalized interference power generated by adding the jth channel tap at the peak, and $\sum_{n=1}^{\lfloor (L-j)/M \rfloor} \Omega\gamma^{j+nM}$ and $\sum_{m=1}^{\lfloor j/M \rfloor} \Omega\gamma^{j-mM}$ are the ISI power caused by the previous and following data symbols with respect to $b(i)$, respectively.

The variable β_j that measures the ratio between the average power of the jth path and $I^{(j)}$ is defined as

$$\begin{aligned}\beta_j &\equiv \frac{E\left\{\alpha_j^2\right\}}{I^{(j)}} = \frac{\Omega\gamma^j}{I^{(j)}} = \frac{\Omega\gamma^j}{\sum_{m=1}^{\lfloor j/M \rfloor} \Omega\gamma^{j-mM} + \sum_{n=1}^{\lfloor (L-j)/M \rfloor} \Omega\gamma^{j+nM}} \\ &= \frac{1}{\sum_{m=1}^{\lfloor j/M \rfloor} \gamma^{-mM} + \sum_{n=1}^{\lfloor (L-j)/M \rfloor} \gamma^{nM}}. \end{aligned} \tag{8.43}$$

We get from (8.43) that

$$\beta_0 = \cdots = \beta_{M-1} > \beta_M = \cdots = \beta_{2M-1} > \cdots > \beta_{(K-1)M} = \cdots = \beta_{KM-1}, \tag{8.44}$$

which renders a way to separate all L tap components into K disjoint groups so that elements in the same group have the same β value. For example, group 1 has the 0th to the $(M-1)$th elements, group 2 has the Mth to the $(2M-1)$th elements, and so on.

The following lemma will be needed in deriving the fast search algorithm.

Lemma 8.1. *If* S_1, S_2, I_1 *and* I_2 *are all positive numbers, then*

$$\frac{S_2}{I_2} < \frac{S_1}{I_1} \Longleftrightarrow \frac{S_2}{I_2} < \frac{S_1+S_2}{I_1+I_2} < \frac{S_1}{I_1}.$$

The proof of the above Lemma is straightforward and thus omitted here. When the codeword length is not greater than M, we can determine the best code length based on the following Proposition.

Proposition 8.2. When $0 < l \le M$, $M = \arg\max_{0<l\le M} \bar{\nu}^{(l)}$.

Proof: Let k denote the length of codeword less or equal to M. The output SIR of codeword $\mathbf{c}^{(l)}$, $\bar{\nu}^{(k)}$, is first simplified as

$$\begin{aligned}\bar{\nu}^{(k)} &= \frac{E\left\{\left(\sum_{j=0}^{k-1} \alpha_j\right)^2\right\}}{\sum_{j=0}^{k-1} I^{(j)}} = \frac{E\left\{\sum_{j=0}^{k-1} \alpha_j^2 + \sum_{i,j=0;i\neq j}^{k-1} \alpha_i\alpha_j\right\}}{I^{(0)} \sum_{j=0}^{k-1} d^{2j}} \\ &= \frac{\Omega\left(\sum_{j=0}^{k-1} d^{2j} + \frac{\pi}{2}\sum_{i=1}^{k-1}\sum_{j=1}^{i} d^{i+j-1}\right)}{I^{(0)} \sum_{j=0}^{k-1} d^{2j}} \\ &= \beta_0 + \beta_0 \frac{\pi}{2} \frac{\sum_{i=1}^{k-1}\sum_{j=1}^{i} d^{i+j-1}}{\sum_{j=0}^{k-1} d^{2j}} = \beta_0 + \beta_0 \frac{\pi}{2} g(k), \end{aligned} \tag{8.45}$$

where $d = \gamma^{1/2} < 1$ and $g(k) = (\sum_{i=1}^{k-1} \sum_{j=1}^{i} d^{i+j-1})/(\sum_{j=0}^{k-1} d^{2j}) > 0 \ \forall k$. It is shown in the part A of the Appendix in [20] that $g(k)$ is a monotonically increasing function of k for $1 \leq k \leq M$. Therefore, we can conclude that the maximum SIR must occur at $k = M$. $\square$

Next, consider the case when the code length l exceeds M and it is decomposed as

$$l = kM + \bar{l}, \tag{8.46}$$

where $k \equiv \lceil \frac{l-M}{M} \rceil$ and $\bar{l} \equiv l - kM$, respectively. Then, the output SIR can be reformulated as

$$\bar{\nu}^{(l)} = \frac{S(l)}{I(l)} = \frac{S(kM) + \Delta S(\bar{l})}{I(kM) + \Delta I(\bar{l})}, \tag{8.47}$$

where $S(kM) \equiv E\left\{\left(\sum_{j=0}^{kM-1} \alpha_j\right)^2\right\}$ and $I(kM) \equiv \sum_{j=0}^{kM-1} I^{(j)}$ are the signal power and interference power obtained by combining the first kM channel taps, $\Delta S(\bar{l}) \equiv S(kM+\bar{l}) - S(kM) = E\left\{\sum_{j=kM}^{l-1} \alpha_j^2 + 2\sum_{i=0}^{kM-1} \sum_{j=kM}^{l-1} \alpha_i \alpha_j\right\}$ and $\Delta I(\bar{l}) \equiv \sum_{j=kM}^{l-1} I^{(j)}$ are the amounts of increased signal and noise power due to the extension of code length from kM to $kM+\bar{l}$, respectively. The next proposition provides the upper bound for the output SIR when l is greater than M.

Proposition 8.3. Let the codeword length l be given by (8.46). The output SIR, $\bar{\nu}^{(l)}$, is upper bounded by either $\bar{\nu}^{(kM)}$ or $\bar{\nu}^{((k+1)M)}$.

Proof: We try to establish this Proposition by showing that either one of the following statements is true.

1. If $\bar{\nu}^{((k+1)M)} \geq \bar{\nu}^{(kM)}$, $\max_{kM \leq l \leq (k+1)M} \bar{\nu}^{(l)} = \bar{\nu}^{((k+1)M)}$.
2. If $\bar{\nu}^{(kM)} \geq \bar{\nu}^{((k+1)M)}$, $\max_{kM \leq l \leq (k+1)M} \bar{\nu}^{(l)} = \bar{\nu}^{(kM)}$.

The proof of the first statement under the assumption $\bar{\nu}^{((k+1)M)} \geq \bar{\nu}^{(kM)}$ is given next. If $\frac{\Delta S(\bar{l})}{\Delta I(\bar{l})} \leq \frac{S(kM)}{I(kM)}$, we recall the fact that

$$\bar{\nu}^{(l)} = \frac{S(kM) + \Delta S(\bar{l})}{I(kM) + \Delta I(\bar{l})} \leq \frac{S(kM)}{I(kM)} = \bar{\nu}^{(kM)} \leq \bar{\nu}^{((k+1)M)} \tag{8.48}$$

from Lemma 8.1. Otherwise, consider the case where $\frac{\Delta S(\bar{l})}{\Delta I(\bar{l})} \geq \frac{S(kM)}{I(kM)}$. It is shown in Lemma 2 of [20] that $\frac{\Delta S(\bar{l})}{\Delta I(\bar{l})}$ is an increasing function with respective to $\bar{l}$. Therefore, we have $\frac{\Delta S(\bar{l})}{\Delta I(\bar{l})} \leq \frac{\Delta S(M)}{\Delta I(M)}$, and then use Lemma 8.5.2 to get

$$\bar{\nu}^{(l)} = \frac{S(kM) + \Delta S(\bar{l})}{I(kM) + \Delta I(\bar{l})} \leq \frac{S(kM) + \Delta S(M)}{I(kM) + \Delta I(M)} = \bar{\nu}^{(k+1)M}. \tag{8.49}$$

The first statement is then approved based on (8.48) and (8.49). The second statement that can be proved similarly is omitted here. □

From Proposition 8.3, the maximum output SIR must be bounded by $\bar{\nu}^{(k\cdot M)}$, $k = 1, \cdots, K$, i.e.,

$$\max_{0<l\leq L} \bar{\nu}^{(l)} \leq \max_{0<k\leq K} \bar{\nu}^{(k\cdot M)}. \tag{8.50}$$

Thus, we obtain the fast search algorithm that is given in the following proposition.

Proposition 8.4. A fast search algorithm that identify the optimal code length L_{opt} can be written as

$$L_{opt} = \arg \max_{0<l\leq L} \bar{\nu}^{(l)} = M \cdot \arg \max_{0<k\leq K} \bar{\nu}^{(kM)}, \tag{8.51}$$

and the corresponding maximum output SIR is

$$\bar{\nu}^{(L_{opt})} = \frac{E\left\{\left(\sum_{j=0}^{L_{opt}-1} \alpha_j\right)^2\right\}}{\sum_{j=0}^{L_{opt}-1} I^{(j)}}. \tag{8.52}$$

As compared with the exhaustive search algorithm in (8.42), the fast algorithm reduces the search number by a factor of M.

Another possible criterion for CLO is to consider both AWGN and ISI jointly. That is, we can maximize the output SINR, i.e.,

$$\hat{L}_{opt} = \arg \max_{0<l\leq L} \left(\frac{E\left\{(\sum_{j=0}^{l-1} \alpha_j)^2\right\}}{l \cdot (N_0/2) + \sum_{j=0}^{l-1} I^{(j)}} \right). \tag{8.53}$$

The fast search algorithm in Proposition 8.4 may not give the maximum output SINR, especially in the low SNR environment. In fact, as suggested in the following example, the performance gap between these two criteria as specified in (8.51) and (8.53) is small even in the presence of high noise power.

Example 8.4: Residual ISI Suppression of CPP-UWB Systems
In this example, we show that the performance of CPP-UWB systems can be improved by adjusting its codeword length according to the proposed fast search algorithm in Section 8.5. The system parameters are remained the same as those in the Example 8.1. To simplify our discussion, the feedback phase information is assumed to be perfect. The BEP curves of CPP-UWB system with and without CLO are drawn in Fig. 8.5. In addition, the performance curves of CPP-UWB system with different codeword length optimization criteria given in (8.53) is presented for the performance benchmark. According

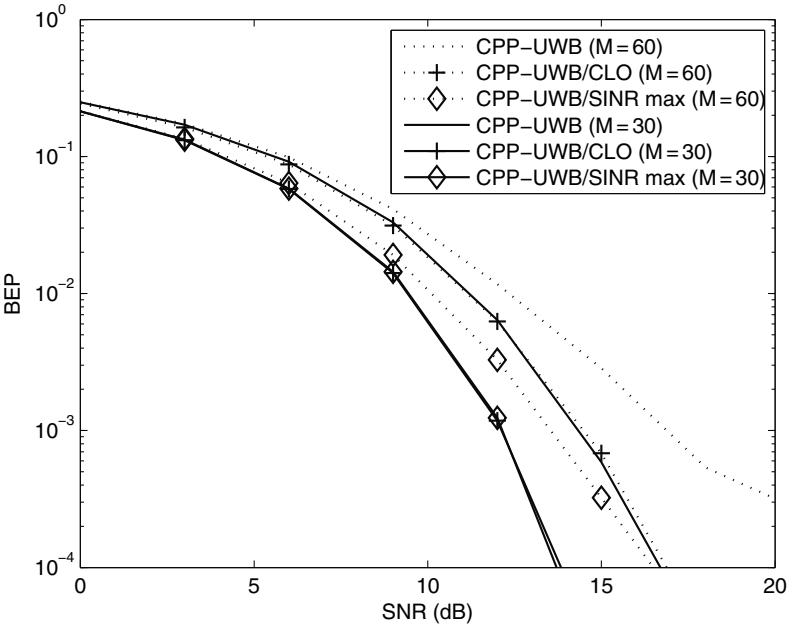

Fig. 8.5. The BEP performance improvement with different ISI suppression schemes at different data rates [[80] ©IEEE].

to our simulation result, the optimal codeword size found by the proposed fast searching algorithm for $M = 30$ and 60 are l=30 and 60, respectively. It is observed from Fig. 8.5 that the fast algorithm provides additional 2 dB gain at BEP equal to 10^{-3} as compared with the conventional CPP-UWB system using full phase knowledge. For a low data rate case, the decoding performance between two different codeword length choosing criteria is very small. On the contrary, for a high data rate case, the performance gap between two phase code designs reduces as signal power increases.

To better illustrate this idea, let us consider the output SINR of CPP-UWB systems at different codeword length. Here we fix the symbol interval at $M = 30$ and the corresponding output SINR is plotted as a function of different code length under different input SNR in Fig. 8.6. The lower six curves represents the cases that the input SNR is equal to 0–25 dB with a step size of 5 dB while the top one denotes the case when the noise power is very weak, i.e., the output SIR. The circle and triangle marks in each curve denotes the maximum output SIR and SINR, respectively. From Fig. 8.6, the codeword length determined by different criteria converges when the input SNR is greater or equal to 20 dB. Even though different design criteria requires different amount of phase information when the SNR is less than 20 dB, the output SINR gap between two different size of phase codes is indeed small.

In the next example, we will validate the previous claim about the channel length duration for the development of our fast search algorithm.

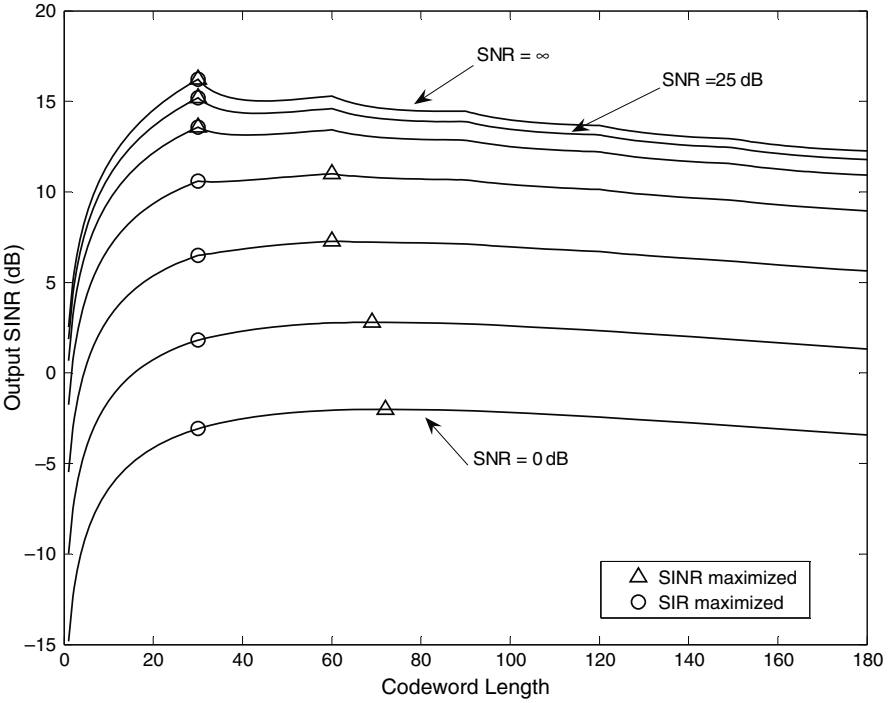

Fig. 8.6. Output SINR with different codeword lengths at different input SNR values [[80] ©IEEE].

Example 8.5: Effect of Channel Length Approximation and Comparison of Fast and Exhaustive Search for CLO

In the previous example, we assume the channel response length L is equal to 180 chips. However, in the real situation, the channel response may not be an integer multiple of the symbol interval. As we claim earlier, we can always pad zeros or truncate the channel tail to meet this channel response length requirement in Section 8.5. In this example, we would like to validate this claim by comparing the CPP-UWB systems under different channel length assumption here. Let us consider a real channel case, whose duration varies between 170 and 190 chips. Under this circumstance, the optimal codeword size that provides the maximum output SIR can be found by an exhaustive search algorithm. The corresponding BEP curve is plotted in Fig. 8.7, where the ideal channel length is also shown for comparison. As Fig. 8.7 suggests, the performance curves between these two channel models are almost indistinguishable. This result implies that modifying the length of UWB channel when the power of taps at the channel tail is small enough will not alter the system performance much. Furthermore, the computational complexity for CLO can be saved by applying the fast search algorithm.

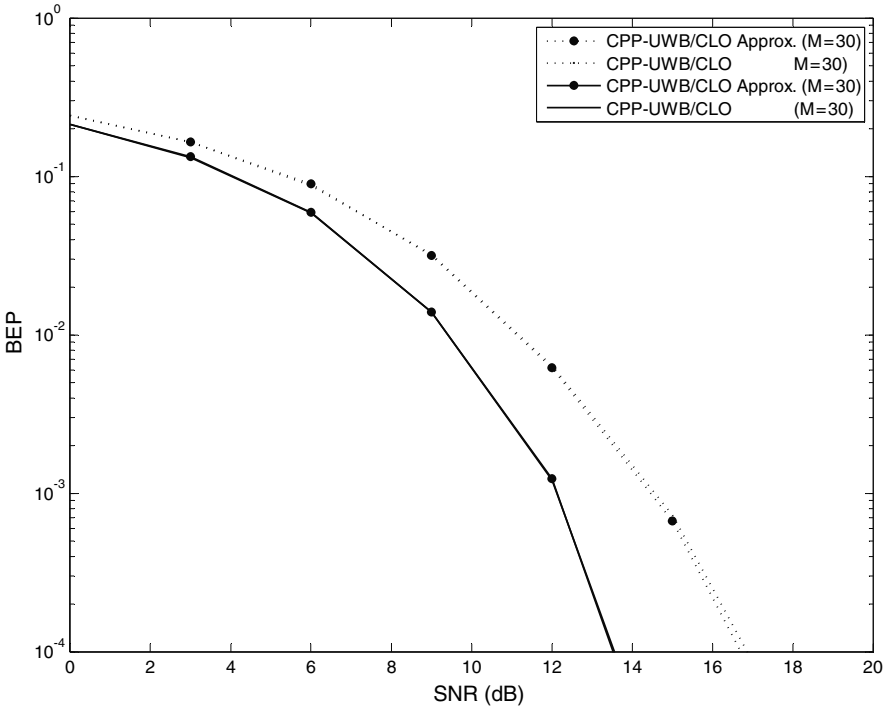

Fig. 8.7. The BEP performance comparison between two systems using the approximated and the real channels, where $\Delta = 0.7\,\text{ns}$, $\Gamma = 20.5\,\text{ns}$ (CM3) [[80] ©IEEE].

8.6 Consideration of FCC Power Spectral Mask

The US Federal Communications Commission (FCC) assigns a huge frequency band that overlaps with those used in the existing narrow-band radio services to the UWB signal. In order to avoid excess in-band interference from UWB transmitters, FCC also enforces a mask on the output power spectrum that limits the maximum possible power of UWB radio at different frequency band as shown in Fig. 8.8. Since precoding changes the power spectral density (PSD) of the transmitted signal, we derive the PSD of the CPP signal and address the related implementation issue when the power mask is applied as follows.

To simplify our discussion, we assume that the symbol interval is shorter than the channel response and the channel length is an integer multiple of the symbol interval, i.e., $L = KM$ with K being a positive integer. If the energy per pulse is equal to E_s, the transmitted signal is depicted as

$$\begin{aligned} x_s(t) &= \sqrt{\frac{E_s}{L}} \sum_{l=-\infty}^{\infty} \sum_{k=0}^{K-1} \sum_{j=0}^{M-1} b(l-k) p_{L-1-kM-j} w_s(t - lM\Delta - j\Delta) \\ &= w_s(t) \otimes x_1(t), \end{aligned} \tag{8.54}$$

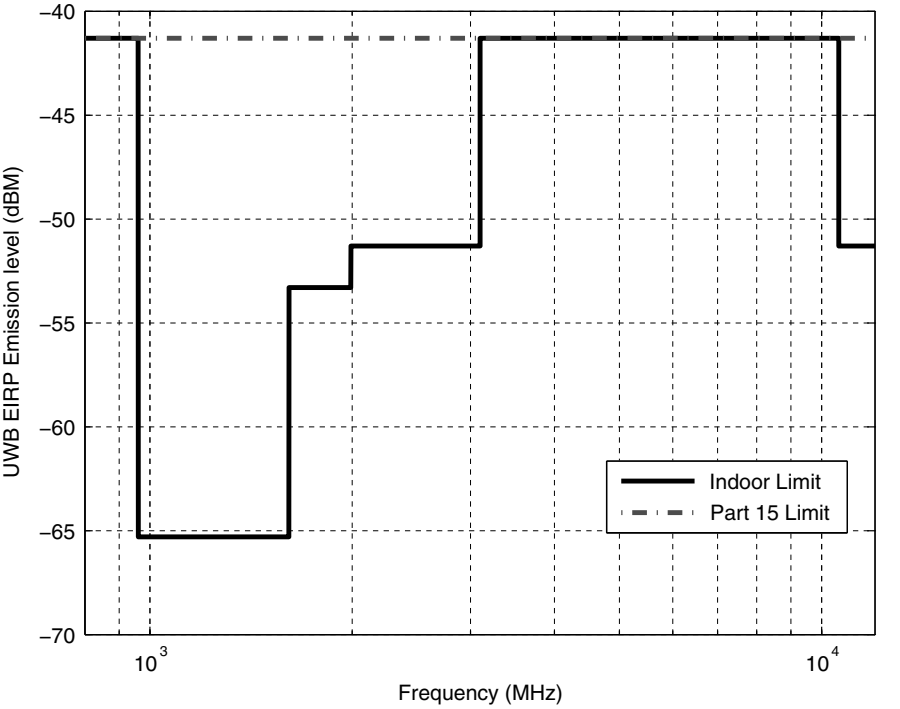

Fig. 8.8. The power spectral mask of FCC for UWB transmitters in [39].

where

$$x_1(t) = \sqrt{\frac{E_s}{L}} \sum_{l=-\infty}^{\infty} \sum_{k=0}^{K-1} \sum_{j=0}^{M-1} b(l-k) p_{L-1-kM-j} \delta(t - lM\Delta - j\Delta). \quad (8.55)$$

Let T_f be an integer multiple of the symbol interval, i.e., $T_f = T\alpha$ where α is a positive integer, the truncated $x_1(t)$ signal is defined as

$$x_1^{(T_f)}(t) = \begin{cases} x_1(t), & -T_f - \epsilon \le t \le T_f - \epsilon \\ 0, & \text{elsewhere} \end{cases}, \quad (8.56)$$

where $0 < \epsilon \ll 1$. Then, $x_1^{(T_f)}(t)$ can be explicitly expressed as

$$x_1^{(T_f)}(t) = \sqrt{\frac{E_s}{L}} \sum_{l=-\alpha}^{\alpha-1} \sum_{k=0}^{K-1} \sum_{j=0}^{M-1} b(l-k) p_{L-1-kM-j} \delta(t - lM\Delta - j\Delta). \quad (8.57)$$

The time-averaged autocorrelation function of $x_1^{(T_f)}(t)$ is equal to

$$\frac{1}{2T_f} E\left\{x_1^{(T_f)}(t_1) x_1^{(T_f)}(t_2)\right\} = \frac{E_s}{2TL\alpha} 2\alpha MK\delta(t_1 - t_2) = \frac{E_s}{T}\delta(\tau), \quad (8.58)$$

where $\tau = t_1 - t_2$. Consequently, the PSD of $x_1(t)$ is computed as

$$\begin{aligned} S_{x_1}(f) &= \lim_{T_f \to \infty} \mathbb{F}\left\{ \frac{1}{2T_f} E\left\{ x_1^{(T_f)}(t_1) x_1^{(T_f)}(t_2) \right\} \right\} \\ &= \lim_{\alpha \to \infty} \mathbb{F}\left\{ \frac{E_s}{T} \delta(\tau) \right\} = \frac{E_s}{T}. \end{aligned} \tag{8.59}$$

Let the Fourier transform of $w_s(t)$ be $W_s(f)$, the PSD of $x_s(t)$ is computed as

$$S_{x_s}(f) = S_{x_1}(f)|W_s(f)|^2 = \frac{E_s}{T}|W_s(f)|^2, \tag{8.60}$$

which is proportional to either $|W_s(f)|^2$ or the inverse of T, i.e., the data rate. Furthermore, the same conclusion in (8.60) can be drawn when the data symbol is encoded by the code found by the fast search algorithm in Section 8.5.

For a fixed data rate system, we learn from (8.60) that the maximum power per data symbol in CPP-UWB is bound by enforcing the FCC mask. A better system performance can be achieved by properly design the pulse waveform $w_s(t)$ so that as much power as possible can be pumped into the wireless channel without violating the power spectral mask constraint. The pulse waveform design problem is interesting; however, it will not be covered in this book since it is out of the current scope of this chapter. Interested readers are referred to [70] and references therein for detailed treatment on this topic. On the contrary, for a fixed pulse waveform, the output power of CPP transmitters should be lowered when the symbol interval is shortened. Consequently, the received signal power decreases as well. To keep the same SNR level as the low data rate system, more attention should be focused on the noise figure reduction at the receiver in its hardware implementation.

9

Conclusion and Future Trend

9.1 Conclusion

9.1.1 Chapter 2

In Chapter 2, we reviewed the principle of Precoding for ISI channels. First, Tomlinson–Hiroshima (TH) precoding was explained in detail. It was shown that in high SNR, TH precoding can approach the capacity of any bandwidth limited Gaussian channel as closely as the capacity of an ideal Gaussian channel. Moreover, we also reviewed trellis shaping and trellis precoding and showed that with trellis precoding, the SNR gap of about 9 dB (at $P_r(E) \simeq 10^{-6}$) between capacity and uncoded modulation can be reduced by approximately 7 dB over any strictly bandlimited high SNR Gaussian channel. We also reviewed the basic of multirate signal processing and represented OFDM systems using matrix forms, which can also be regarded as transceiver with precoding and postcoding. As a result, CP and ZP inserted OFDM systems can be easily represented and different receivers, e.g., ZF and MMSE can be designed accordingly. We also introduced the SC-CP system which can be regarded as an OFDM system with channel independent precoding.

9.1.2 Chapter 3

In Chapter 3, several precoding techniques, namely Tx-MF, Tx-ZF, and Tx-Wiener, are introduced to improve the performance of downlink DS-CDMA systems while keeping the receiver design simple. The Tx-MF precoding automatically combines all the multipath gains of the desired user's channel after some delay and, thus, a simple MF receiver is sufficient to acquire full multipath diversity. Since Tx-MF fails to suppress interference efficiently, its performance degrades as the number of users increases. By exploiting the knowledge of transmit signals from all the other users at the base station, Tx-ZF that eradicates all the interference at the desired receiver output can be applied. However, Tx-ZF cancels MAI at the cost of reducing its available

C.-C.J. Kuo et al., *Precoding Techniques for Digital Communication Systems*,
DOI: 10.1007/978-0-387-71769-2_9,

signal dimension. As a result, the overall signal power at the receiver output is reduced. Finally, the Tx-Wiener precoding is also proposed to strike a balance between signal power gain and interference suppression.

9.1.3 Chapter 4

In Chapter 4, precoding for MIMO channels were discussed. We demonstrated that TH precoding can easily be applied to a BLAST MIMO system. For high SNR, the capacity achieved by TH precoding approaches to capacity of MIMO channel.

Linear precoder can also be designed jointly with a linear decoder to minimize a desired criterion. In particular, if the criterion is to minimize the weighted sum of symbol estimation errors for all subchannels, the linear precoder and decoder decouples MIMO channel into parallel eigen subchannels. By selecting appropriate error weights, we can maximize the information rate and minimize the sum of error rates. The joint linear precoder/decoder design is in general a complicated non-convex problem. Optimization can be done with respect to various criteria. By adopting a unified framework, the linear precoder and decoder can still diagonalize channel if other criteria such as minimization of maximum or average BER are chosen. Hence, the optimization problems are simplified greatly.

Furthermore, precoding was used in conjunction with space-time codes. It was shown that it is possible to design linear precoder in a channel with fading correlation for a space-time MIMO system or to design linear and unitary precoder in order to maximize diversity and coding gain.

Finally, since the complete channel information may not be always available at the MIMO transmitter due to channel variation, two MIMO precoder designs using incomplete channel information, i.e., channel statistics precoding and unitary precoding, are also provided. It is found that when either channel mean or channel covariance matrix is known to the transmitter, either transmit beamforming or spatial multiplexing achieves the highest information rate depending on the quality of the returned information. The unitary precoding is deployed over the precoded OSTBC system, where the codeword is selected to minimize the symbol error rate. The discrete codeword design can be related to a subspace packing problem in the Grassmannian manifold, where the minimum chordal distance between any two codewords is maximized. When being compared to the 2×2 OSTBC systems, the unitary precoding with 3 feedback bits in the 4×2 MIMO system provides more than 3 dB gain at the BER equal to 10^{-3} as simulation results suggest.

9.1.4 Chapter 5

In Chapter 5, we proposed an approximately MAI-free multiaccess OFDM system, called the PMU-OFDM system. In the PMU-OFDM system, every

user receives negligible MAI and behaves as in a "single-user" OFDM system. Like the OFDM system, each individual user in PMU-OFDM transmits N parallel symbols. When N is sufficiently large, PMU-OFDM has the approximate MAI-free property. Moreover, we proposed a code selection scheme using Hadamard-Walsh codes to relax the requirement on the large value of N while the system can still achieve the approximate MAI-free property. More specifically, in a fully-load situation, i.e. without code selection, the MAI power decreases at a speed of $O(N^{-2})$ while the MAI power decreases at a speed of $O(N^{-4})$ in a half-loaded situation with code selection. Furthermore, PMU-OFDM with code selection was proved to operate robustly in time, frequency asynchronous as well rapid time-variant environments. Based on the code selection scheme, we showed that a proper code priority can further enhance the performance of PMU-OFDM in a frequency asynchronous and rapid time-variant environment. Since PMU-OFDM can solve the MAI and asynchronism issues using a simple code selection scheme, it does not demand sophisticated multiuser detection or signal processing techniques, which are commonly adopted in multiuser OFDM systems. When a fully-loaded user capacity is required and hence MUD is required, the use of code selection in PMU-OFDM can reduce the complexity for MUD since each user only needs to deal with the interference from half of the users.

9.1.5 Chapter 6

In Chapter 6, we proposed a code selection scheme, which is based on the Hadamard-Walsh code, to achieve a completely MAI-free as well as full diversity gain in an MC-CDMA system with multipath effect. Based on this code selection, we can estimate the channel information under an MAI-free environment conveniently. We also showed that MC-CDMA systems can be more robust to the CFO effect using the proposed code selection scheme. More specifically, by properly partitioning the codewords, the users in a specific codeword set can achieve MAI-free even in CFO environments.

9.1.6 Chapter 7

In Chapter 7, we show how different precoding scheme, i.e. CI code, can increase the number of MAI-free users in MC-CDMA system with CFO. Moreover, thanks to the MAI-free property of the proposed code selection schemes, if the system is to be operated in a fully-loaded situation, we can greatly simply the computational complexity for MAI suppression since each user does not need to deal with the interference from all other users.

9.1.7 Chapter 8

In Chapter 8, a channel phase precoding technique is proposed to simplify the receiver design while saving the feedback information quantity in TRP. The

CPP scheme is not only simpler in design but also computationally more efficient than the TRP-based system. A performance lower bound on the output SNR is derived to evaluate the system performance when the transmit symbol is encoded by the estimated phase information acquired by a set of training symbols. The concentrated signal power at the CPP receiver is exploited to enhance the data transfer rate by reducing the symbol interval without much ISI degradation. In the high date transmission case, a better system performance can be achieved by optimizing the codeword length so that its output SIR is maximized. The closed form solution is not possible since the optimization problem is a highly nonlinear. Instead of resorting to an exhaustive search scheme, a fast search algorithm is derived to find out the optimal codeword length with low computational burden.

9.2 Future Research Trend

9.2.1 Precoding with Partial Channel Information

In Chapters 4 and 8, we introduce precoding techniques with partial channel information for MIMO and UWB systems, respectively. Partial channel information feedback is in general more feasible in wireless or mobile environments, especially when the numbers of transmit and receive antennas are large. For instance, in current IEEE 802.16e-2005 standard, the subcarriers can be up to 2048. If MIMO precoding with full channel information is performed, we need to compute the precoding solution for all subcharriers and feedback them to transmit side. In this case, the computational complexity and the amount of feedback are huge and may not be feasible. This result also limits the standard not to offer more antenna numbers to achieve higher data throughput, because the computational complexity and feedback amount both increase exponential with the number of transmit and receive antennas. To solve this problem, precoding with partial channel information may offer a good solution.

9.2.2 Combined Precoding and MUD for Multiuser Communications

In Chapters 5–6, we showed that by proper transceiver and code design, some subsets of users in the multiuser systems can achieve an MAI-free or nearly MAI-free property without any channel information in the transmit side, where the MAI arises from various sources such as multipath effect, time and frequency offsets, and Doppler effect. Such precoding schemes can be combined with MUD to achieve a good leverage for the computational complexity between transmitter and receiver. Without proper precoding scheme, MUD will lead to large complexity burden in the receiver side. The scenario is that, by using precoding in the multiuser systems, some subsets of users can be

MAI-free. In this case, the interferers for each target user become fewer. Since the complexity of MUD directly related to the number of interferers, reducing number of interferers can reduce the complexity for MUD. In addition, since the active users may not always be fully-loaded, once the active user number is below the supportable MAI-free user number, there is no need to perform MUD while those active users can still enjoy an MAI-free transmission.

9.2.3 Other Code Scheme to Achieve More MAI-Free User Number

To achieve MAI-free property, the proposed code selection scheme reduces the number of users from M to $M/2$ in the PMU-OFDM system. Also, in MC-CDMA system, the number of MAI-free users is also limited by the multi-path length. The proposed code selection schemes in these two systems are however only examples. It is possible that there exist some other better code schemes that may allow more number of users to achieve MAI-free property. It is an interesting topic to explore such better code schemes.

References

[1] S. Abeta, H. Atarashi, and M. Sawahashi. Forward link capacity of coherent DS-CDMA and MC-CDMA broadband packet wireless access in a multi-cell environments. *IEEE VTC Fall*, 5:2213–2218, Sep. 2000.

[2] M. Abramowitz and I. A. Stegun. *Handbook of Mathematical Functions With Formulas, Graphs, and Mathematical Tables*. United States Department of Commerce, 1972 edition.

[3] S. M. Alamouti. A simple transmit diversity technique for wireless communications. *IEEE J. Select. Areas Commun.*, 16:1451–1458, Oct. 1998.

[4] J. G. Andrews. Interference cancellation for cellular systems: a contemporary overview. *IEEE Commun. Mag.*, 12:19–29, 2005.

[5] J. T. Aslanis S. Kasturia, and J. M. Cioffi. Vector coding for partial response channels. *IEEE T. Inform. Theory*, 36:741–762, 1990.

[6] S. Barbarossa, M. Pompili, and G. B. Giannakis. Channel-independent synchronization of orthogonal frequency division multiple access systems. *IEEE J. Select. Areas Commun.*, 20:474–486, Feb. 2002.

[7] A. Barg and D. Y. Nogin. Bounds on packings of spheres in the Grassmann manifold. *IEEE J. Select. Areas Commun.*, 48:2450–2454, September 2002.

[8] K. G. Beauchamp. *Walsh Functions and Their Applications*. Academic Press, 1975.

[9] D. Bertsekas. *Nonlinear Programming*. Athena Scientific, 1995.

[10] J. A. C. Bingham. Multicarrier modulation for data transmission: an idea whose time has come. *IEEE Commun. Mag.*, 28:5–14, May 1990.

[11] D. Brady, Z. Zvonar. Multiuser detection in single-path fading channels. *IEEE T. Commun.*, 42:1729–1739, 1994.

[12] M. Brandt-Pearce and A. Dharap. Transmitter-based multiuser interference rejection for the down-link of a wireless CDMA system in a multipath environment. *IEEE J. Select. Areas Commun.*, 18(3): 407–417, 2000.

[13] D. R. Brown. Multistage parallel interference cancellation: convergence behaviour and improved performance through limit cycle mitigation. *IEEE T. Signal Proc.*, 53:283–294, Jan. 2005.

[14] L. Brunel. Multiuse detection techniques using maximum likelihood sphere decoding in multicarrier CDMA systems. 3:949–957, May 2004.

[15] A. R. Calderbank and J. E. Mazo. Baseband line codes via spectral factorization. *IEEE J. Select. Areas Commun.*, SAC-7:914–928, 1989.

[16] A. R. Calderbank and A. V. Giannakis. Minimal tail-biting trellises: the golay code and more. *IEEE T. Inform. Theory*, 45:1435–1455, 1999.

[17] S. Caoleri, M. Ergen, and A. Bahai. Channel estimation techniques based on pilot arragnements in OFDM systems. 48:223–229, Sep. 2002.

[18] D. Cassioli, M. Z. Win, and A. F. Molisch. The ultra-wide bandwidth indoor channel: from statistical model to simulations. *IEEE J. Select. Areas Commun.*, 20(6):1247–1257, Aug. 2002.

[19] R. W. Chang. Synthesis of band-limited orthogonal signals for multichannel data transmission. *Bell Syst. Tech. J.*

[20] Y.-H. Chang, S.-H. Tsai, X. Yu, and C.-C. J. Kuo. Ultra-wideband (UWB) transceiver design using channel phase precoding (CPP). *IEEE T. Signal Proc.*, 55(7):3807–3822, 2007.

[21] Y.-H. Chang, X. Yu, and C.-C. J. Kuo. Techniques for received signal focusing in DSUWB systems. *Proc. IEEE VTC'04 Fall*, 3:1777–1781, Sep. 2005.

[22] Y.-L. Chao and R. A. Scholtz. Weighted correlation receivers for ultra-wideband transmitted reference systems. *Proc. IEEE Globecom'04*, 1: 66–70, Nov. 2004.

[23] H. H. Chen and M. Guizani. Guest editorial: multiple access technologies for B3G wireless communications. *IEEE Commun. Mag.*, 9:65–67, Feb. 2005.

[24] R. L.-U Choi, K. B. Letaief, and R. D. Murch. MISO CDMA transmission with simplified receiver for wireless communication handsets. *IEEE T. Commun.*, 49(5):888–898, May 2001.

[25] L.-U. Choi and R. D. Murch. Transmit-preprocessing techniques with simplified receivers for the downlink of MISO TDD-CDMA systems. *IEEE T. Veh. Technol.*, 53(2):285–295, 2004.

[26] A. Chouly, A. Brajal, and S. Jourdan. Orthogonal multicarrier techniques applied to direct sequence spread spectrum CDMA systems. *IEEE Globlecom*, 3:1723–1728, Dec. 1993.

[27] J. S. Chow, J. C. Tu, and J. M. Cioffi. A discrete multitone transceiver system for HDSL applications. *IEEE J. Select. Areas Commun.*, 9: 895–908, Aug. 1991.

[28] J. M. Cioffi. Dynamic spectrum management. http://www.stanford.edu/group/coffi/dsm/tut/chap11.doc.

[29] R. de Buda. Some optimal codes have structure. *IEEE J. Select. Areas Commun.*, 7:893–899, 1989.

[30] A. Dekorsy, V. Kühn, and K.-D. Kammeyer. Exploiting time and frequency diversity by iterative decoding in OFDM-CDMA systems. In *IEEE Globlecom*, 5:2576–2580, Dec. 1999.

[31] J. H. Deng and T. S. Lee. An iterative maximum SINR receiver for multicarrier CDMA systems over a multipath fading channel with frequency offset. *IEEE T. Wirel. Commun.*, 2:560–569, May 2003.

[32] D. Divsalar and M. K. Simon. CDMA with interference cancellation for multiprobe missions. *JPL TDA Progress Report*, 42-120:40–53, Feb. 1995.

[33] G. F. Edelmann, T. Akal, W. S. Hodgkiss, S. Kim, W. A. Kuperman, and H. C. Song. An initial demonstration of underwater acoustic communication using time reversal. *IEEE J. Oceanic Eng.*, 27:602–609, 2002.

[34] R. Esmailzadeh, E. Sourous, and M. Nakagawa. Prerake diversity combining in time-division duplex CDMA mobile communications. *IEEE T. Veh. Technol.*, 48(3):795–801, May 1999.

[35] M. V. Eyuboglu and Jr. G. D. Forney. Combined coding and equalization using trellis precoding. In *Proc. of CSI Workshop on Advanced Communications Technologies,* Ruidoso, NM, May 1989.

[36] M. V. Eyuboglu and Jr. G. D. Forney. Trellis precoding: combined coding, precoding and shaping for intersymbol interference channels. *IEEE T. Inform. Theory*, 38(2):301–314, 1992.

[37] M. V. Eyuboglu and S. U. H. Qureshi. Reduced-state sequence estimation with set partitioning and decision feedback. *IEEE T. Commun.*, 36:13–20, 1988.

[38] M. V. Eyuboglu and S. U. H. Qureshi. Reduced-state sequence estimation for coded modulation on intersymbol interference channels. *IEEE J. Select. Areas Commun.*, 7(6):989–995, 1989.

[39] Federal Communications Commission (FCC). *Revision of Part 15 of the Commission's Rules Regarding Ultra-Wideband Transmission Systems, First Report and Order, ET Decoet 98-153, FCC 02-48.* adopted/released Feb. 14/Apr. 22, 2002.

[40] M. Fink. Time reversal of ultrasonic fields-part I: basic principles. *IEEE T. Ultrason. Ferroelectr. Freq. Control*, 39(5):555–566, Sep. 1992.

[41] J. R. Foerster. Channel modeling sub-committe report final. *IEEE P802.15 WPAN P802.15-02/490r1-SG3a*, Feb. 2003.

[42] G. D. Forney. Trellis shaping. *IEEE T. Inform. Theory*, 38:281–300, 1992.

[43] Jr. G. D. Forney and A. R. Calderbank. Coset codes for partial response channels; or, coset codes with spectral nulls. *IEEE T. Inform. Theory*, 35:925–943, 1989.

[44] G. D. Forney and M. V. Eyuboglu. Combined equalization and coding using precoding. *IEEE Commun. Mag.*, 29:25–34, 1991.

[45] Jr. G. D. Forney and L.-F. Wei. Multidimensional constellation-Part 1: Introduction, figures of merit, and generalized cross constellation. *IEEE J. Select. Areas Commun.*, 7:877–892, 1989.

[46] D. A. Gore and A. J. Paulraj. MIMO antenna subset selection with space-time coding. *IEEE Trans. on Signal Processing*, 50:2580–2588, October 2002.

[47] R. M. Gray. On the asymptotic eigenvalue distribution of Toeplitz matrices. *IEEE T. Inform. Theory*, 18:725–730, Nov. 1972.

[48] X. Gui and T. S. Ng. Performance of asynchronous orthogonal multicarrier CDMA system in frequency selective fading channel. *IEEE T. Commun.*, 47:1084–1091, Jul. 1999.

[49] S. Hara and R. Prasad. Overview of multicarrier CDMA. *IEEE Commun. Mag.*, 35:126–133, Dec. 1997.

[50] H. F. Harmuth. Applications of Walsh function in communications. *IEEE Spectrum*, Nov. 1969.

[51] M. G. Heinemann, A. Larazza, and K. B. Smith. Acoustic communications in an enclosure using single-channel time-reversal acoustics. *Appl. Phys. Lett.*, 80:694–696, 2002.

[52] J. Hicks, R. J. Boyle, S. Bayram, and W. H. Tranter. Overloaded array processing with spatially reduced search joint detection. *IEEE J. Select. Areas Commun.*, 19:1584–1593, 2001.

[53] B. M. Hochwald, T. L. Marzetta, T. J. Richardson, W. Sweldens, and R. Urbanke. Systematic design of unitary space-time constellations. *IEEE Trans. Inform. Theory*, 46:1962–1973, September 2000.

[54] R. A. Horn and C. R. Johnson. *Matrix Analysis*. Cambridge University Press, 1985.

[55] M. H. Hsieh and C. H. Wei. Channel estimation for OFDM systems based on comb-type pilot arrangement in frequency selective fading channels. *IEEE T. Consum. Electr.*, 44:217–225, 1998.

[56] J. Ibrahim, R. Menon, and R. M. Buehrer. UWB signal detection based on sequence optimization for dense multipath channels. 10(4):228–230, 2006.

[57] IEEE standard for local and metropolitan area networks. *IEEE 802.16a Standard*, Apr. 2003.

[58] S. Imada and T. Ohtsuki. Pre-RAKE diversity combining for UWB systems in IEEE 802.15 UWB multipath channel. *Proc. Joint UWBST & IWUWBS'04*, 2:236–240, May 2004.

[59] S. A. Jafar and A. Goldsmith. Transmit optimization and optimality of beamforming for multiple antenna systems. 3(4):1165–1175, 2004.

[60] W. C. Jakes. *Microwave Mobile Communications*. Wiley, NY, 1974 edition.

[61] M. Joham, W. Utschick, and J. A. Nossek. Linear transmit processing in MIMO communications systems. *IEEE T. Signal Processing*, 53(8): 2700–2712, Aug. 2005.

[62] G Jöngren, M. Skoglund, and B. Ottersten. Combining beamforming and orthogonal space-time block coding. *IEEE Trans. Inform. Theory*, 48:611–626, March 2002.

[63] A. Kajiwara and M. Nakagawa. Microcellular CDMA system with a linear multi-user interference canceller. *IEEE J. Select. Areas Commun.*, 12(4):605–611, May 1994.

[64] S. M. Kay. *Fundamentals of Statistical Signal Processing, Estimateion/Detection Theory.* Prentice-Hall, Englewood Cliffs, NJ, 1993.

[65] B. L. N. Kennett. A note on the finite Walsh Transform. *IEEE T. Inform. Theory*, 16:489–491, Jul. 1970.

[66] I. Koffman and V. Roman. Broadband wireless access solutions based on OFDM access in IEEE 802.16. *IEEE Commun. Mag.*, 40:96–103, Apr. 2002.

[67] S. Kondo and L. B. Milstein. Performance of multicarrier DS CDMA systems. *IEEE T. Commun.*, 44:238–246, Feb. 1996.

[68] P. Kyritsi, G. Papanicolaou, P. Eggers, and A. Opera. MISO time reversal and delay-spread compression for FWA channels at 5 GHz. *IEEE Antenn. Wirel. Propag. Lett.*, 3:96–99, 2004.

[69] E. G. Larsson and P. Stoica. *Space-time block coding for wireless communications.* Cambridge University Press, 2003.

[70] T. P. Lewis and R. A. Scholtz. An ultrawideband signal design with power spectral density constraints. *Proc. 38th Asilomar Conf.*, 2: 1521–1525, Nov. 2005.

[71] Y. Li. Pilot-symbol-aided channel estimation for OFDM in wireless systems. *IEEE T. Veh. Technol.*, 49:1207–1215, 2000.

[72] Y. (G.) Li. Simplified channel estimation for OFDM with multiple transmit antennas. 1:67–75, 2002.

[73] Y. Li, L. G. Cimini, and N. R. Sollenberger. Robust channel estimation for OFDM systems with rapid dispersive fading channels. *IEEE T. Commun.*, 46:902–915, 1998.

[74] L. Lin and D. Costello. *Error Control Coding.* Prentice HAll PTP, 2003 edition.

[75] Y.-P. Lin. *Multirate Systems.* Course materials at National Chiao Tung University Taiwan, 2007.

[76] Y.-P. Lin and S.-M Phoong. Perfect discrete multitone modulation with optimal transceivers. *IEEE T. Signal Processing*, 48:1702–1711, Jun. 2000.

[77] Y.-P. Lin and S.-M Phoong. ISI Free FIR Filterbank Transceivers for Frequency Selective Channels. *IEEE T. Signal Processing*, 49: 2648–2658, Nov. 2001.

[78] Y.-P. Lin and S.-M Phoong. BRE minimized OFDM systems with channel independent precoders. *IEEE T. Signal Processing*, 51:2369–2380, Sep. 2003.

[79] D. J. Love and R. W. Heath. Grassmannian beamforming for multiple-input multiple-output wireless systems. *IEEE Trans. Inform. Theory*, 49(10):2735–2747, October 2003.

[80] D. J. Love and R. W. Heath. Limited feedback unitary precoding for orthogonal space-time block codes. *IEEE Trans. on Signal Processing*, 53(1):64–73, January 2005.

[81] R. Lupas and S. Verdú. Linear multiuser detectors for synchronous code-division multiple access channels. *IEEE T. Inform. Theory*, 34: 123–136, Jan. 1989.

[82] R. Lupas and S. Verdu. Near-far resistance of multi-user detectors in asychronous channels. *IEEE T. Commun.*, 38(4):496–508, 1990.

[83] U. Madhow and M. L. Honig. On the average near-far resistance for MMSE detection of direct sequence CDMA signals with random spreading. *IEEE T. Inform. Theory*, 45(6):2039–2045, Sep. 1999.

[84] H. Miyakawa and H. Harashima. Matched-transmission technique for channels with intersymbol interference. *IEEE T. Commun.*, 20(4): 774–780, 1972.

[85] C. B. Moler, J. J. Dongarra, J. R. Bunch, and G. W. Stewart. *LINPACK Users' Guide*. Society for industrial and applied mathematics, 1980 edition.

[86] A. F. Molisch. Ultrawideband propagation channels-theory, measurement, and modeling. *IEEE T. Veh. Technol.*, 54(5):1528–1545, Sep. 2005.

[87] P. H. Moose. A technique for orthogonal frequency division multiplexing frequency offset correction. *IEEE T. Commun.*, 42:2908–2914, Oct. 1994.

[88] M. Morelli. Timing and frequency sunchronization for the uplink of an OFDMA system. *IEEE T. Commun.*, 52:296–306, Feb. 2004.

[89] S. Moshavi. Multi-user detection for DS-CDMA communications. *IEEE Commun. Mag.*, 49:124–136, Oct. 1996.

[90] Y. Mostofi and D. C. Cox. ICI mitigation for pilot-aided OFDM mobile systems. *IEEE T. Wireless. Commun.*, 4:765–774, 2005.

[91] A. Narula, M. J. Lopez, M. D. Trott, and G. W. Wornell. Efficient use of side information in multiple-antenna data transmission over fading channels. *IEEE J. Select. Areas Commun.*, 16(8):1423–1436, October 1998.

[92] B. Natarajan, Z. Wu, C. R. Nassar, and S. Shattil. Large set of CI spreading codes for high-capacity MC-CDMA. *IEEE T. Commun.*, 52: 1862–1866, Nov. 2004.

[93] R. Negi and J. Cioffi. Pilot tone selection for channel estimation in a mobile OFDM system. *IEEE T. Consumer Electronics*, 44:1122–1128, 1998.

[94] H. T. Nguyen, J. B. Andersen, and G. F. Pedersen. The potential use of time reversal techniques in multiple element antenna systems. 9(1): 40–42, Jan. 2005.

[95] S. Niranjayan, A. Nallanathan, and B. Kannan. Delay tuning based transmit diversity scheme for TH-PPM UWB: performance with RAKE reception and comparison with multi RX schemes. *Proc. Joint UWBST & IWUWBS'04*, 341–345, May 2004.

[96] K. Nishimori, K. Cho, Y. Takatori, and T. Hori. Automatic calibration method using transmitting signals of an adaptive array for TDD systems. *IEEE T. Veh. Technol.*, 50(6):1636–1640, Nov. 2001.

[97] R. Nogueroles, M. Bossert, A. Donder, and V. Zyablov. Improved performance of a random OFDMA mobile communication system. *IEEE VTC*, 3:2502–2506, May 1998.

[98] A. V. Oppenheim and R. W. Schafer. *Discrete-Time Signal Processing.* Prentice Hall, 1989.

[99] P. Palomar, J M. Cioffi, and M. A. Lagunas. Joint Tx-Rx beamforming design for multicarrier MIMO channels: a unified framework for convex optimization. *IEEE Trans. on Signal Processing*, 51(9):2381–2401, 2003.

[100] S.-M. Phoong. *Multirate Systems.* Course materials at National Taiwan University Taiwan, 2007.

[101] T. Pollet, M. V. Bladel, and M. Moeneclaey. BER sensitivity of OFDM systems to carrier frequency offset and Wiener phase noise. *IEEE Trans. Commun.*, 43:191–193, Feb./Mar./Apr. 1995.

[102] W. H. Press, B. P. Flannery, S. A. Teukolsky, and W. T. vetterling. *Numerical Recipes, the Art of Scientific Computing.* Cambridge University Press, NY, 1986 edition.

[103] C. Prettie, D. Cheung, L. Rusch, and M. Ho. Spatial correlation of UWB signals in a home environment. *Proc. UWBST'02*, 65–69, May 2002.

[104] R. Price. Non linearly feedback equalized PAM versus capacity for noisy filtered channels. *Proc. ICC'72*, 1972.

[105] J. G. Proakis. *Digital Communications.* McGraw-Hill, 4th edition, 2000.

[106] M. O. Pun, S.-H. Tsai, and C.-C. Jay Kuo. An EM-based maximum likelihood joint carrier frequency offset and channel estimation for uplink of OFDMA systems. In *IEEE VTC Fall*, Sep. 2004.

[107] M. O. Pun, S.-H. Tsai, and C.-C. Jay Kuo. Joint maximum likelihood estimation of carrier frequency offset and channel in uplink OFDMA systems. *IEEE Globecom*, 6:3748–3752, Dec. 2004.

[108] T. S. Rappaport. *Wireless Communications.* Prentice Hall PTR, 2002.

[109] I. M. Ryzhik, I. S. Gradshteyn, and A. Jeffrey. *Tables of Integrals, Series, and Products.* Academic Press, Inc., 1994 edition.

[110] H. Sampath and A. Paulraj. Linear precoding for space-time coded systems with known fading correlation. *IEEE Trans. Commun.*, 6(6): 502–513, 2002.

[111] H. Sampath, P. Stoica, and A. paulraj. A generalized space-time linear precoder and decoder design using the weighted MMSE criterion. In *Proc. of 39th Asilomar Conf. on Signals, Systems and Computers.*, pages 753–758, 2000.

[112] H. Sampath, P. Stoica, and A. Paulraj. Generalized linear precoder and decoder design for MIMO channels using the weighted MMSE criterion. *IEEE Trans. Commun.*, 49(12):2198–2206, December 2001.

[113] H. Sari, G. Karam, and I. Jeanclaude. Transmission techniques for digital terrestrial TV broadcasting. *IEEE Commun. Mag.*, 100–109, Feb. 1995.

[114] H. Sari, Y. Levy, and G. Karam. An analysis of orthogonal frequency-division multiple access. *IEEE Globecom*, 3:1635–1639, Nov. 1997.

[115] A. Scaglione, G. B. Giannakis, and S. Barbarossa. Redundant filterbank precoders and equalizers part I: unification and optimal designs. *IEEE T. Signal Process.*, 47:1988–2006, Jul. 1999.

[116] A. Scaglione, G. B. Giannakis, and S. Barbarossa. Lagrange/ Vandermonde MUI eliminating user codes for quasi-synchronous CDMA in unknown multipath. *IEEE T. Signal Process.*, 48:2057–2073, Jul. 2000.

[117] A. Scaglione, P. Stoica, S. Barbarossa, G. B. Giannakis, and H. Sampath. Optimal design for space-time linear precoders and decoders. *IEEE Trans. on Signal Processing*, 50(5):1051–1064, May 2002.

[118] T. M. Schmidl and D. C. Cox. Robust frequency and timing synchronization for OFDM. *IEEE T. Commun.*, 45:1613–1621, Dec. 1997.

[119] Q. Shi and M. Latva-aho. Simple spreading code allocation scheme for downlink MC-CDMA. *Electronics Letters.*, 38:807–809, Jul. 2002.

[120] D. Shiu, J. G. Foschini, M. Gans, and J. M. Kahn. Fading correaltion and its effect on the capacity of multi-element antenna systems. *IEEE Trans. Commun.*, 48(3):502–513, 2000.

[121] M. K. Simon, J. K. Omura, R. A. Scholtz, and B. K. Levitt. *Spread Spectrum Communications Handbook, Electronic Edition.* McGraw-Hill, electronic edition, 2002.

[122] S. Stanczak, H. Boche, and M. Haardt. Are LAS-codes a miracle? *IEEE Globecom*, 3:589–593, Nov. 2001.

[123] T. Strohmer, M. Emami, J. Hansen, G. Papanicolaous, and A. J. Paulraj. Application of time-reversal with MMSE equalization to UWB communications. *Proc. IEEE Globecom'04*, 5:3123–3127, Nov. 2004.

[124] L. Tadjpour, S.-H. Tsai, and C.-C. J. Kuo. Orthogonal codes for MAI-free MC-CDMA with carrier frequency offsets (CFO). *IEEE Globecom*, 06, Nov. 2006.

[125] L. Tadjpour, S.-H. Tsai, and C.-C. Jay Kuo. An approximately MAI-free multiaccess OFDM system in fast time-varying channels. *IEEE T. Signal Process.*, 55(7):3787–3799, 2007.

[126] O. Takyu, T. Ohtsuki, and M. Nakagawa. Frequency offset compensation with MMSE-MUD for multi-carrier CDMA in quasi-synchronous uplink. *IEEE ICC*, 4:2485–2489, May 2003.

[127] V. Tarokh, H. Jafakhani, and A. R. Calderbank. Space-time block codes from orthogonal design. *IEEE Trans. Inform. Theory*, 45:1456–1467, 1999.

[128] V. Tarokh, N. Sheshadri, and A. R. Calderbank. Space-time codes for high data rate wireless communication: performance criterion and code construction. *IEEE Trans. Inform. Theory*, 44:744–765, Mar. 1998.

[129] E. Telatar. Capacity of multi-antenna Gaussian channels. *European Transactions on telecommunications*, 10(6):585–595, Nov/Dec, 1999.

[130] V. Thippavajjula and B. Natarajan. Parallel interference cancellation techniques for synchronous carrier interferometry/MC-CDMA uplink. In *Proc. of 60th IEEE Vehicular Technolgy Conference*. San Fransisco, CA, Sep. 2004.

[131] M. Tomlinson. New automic equalizer employing modulo arithmetic. *Electronics Letters*. 7:138–39, 1971.

[132] M. Torlak, G. Xu, and H. Liu. An improved signature waveform approach exploiting pulse shaping information in synchronous CDMA systems. *IEEE ICC*, 2:22–27, Jun. 1996.

[133] S.-H. Tsai, Y.-P. Lin, and C.-C. J. Kuo. A repetitively coded multicarrier CDMA (RCMC-CDMA) transceiver for multiuser communications. *IEEE WCNC*, 2:959–964, Mar. 2004.

[134] S.-H. Tsai, Y.-P. Lin, and C.-C. J. Kuo. Code priority of Multiuser OFDM systems in frequency asynchronous environment. In *Proc. of IEEE 62nd Semiannual VTC Fall*, pages 710–713. Dallas, Texas, Sep. 25–28, 2005.

[135] S.-H. Tsai, Y.-P. Lin, and C.-C. J. Kuo. An approximately MAI-free multiaccess OFDM system in carrier frequency offset environment. *IEEE T. Signal Proces.*, 53(11):4339–4353, 2005.

[136] S.-H. Tsai, Y.-P. Lin, and C.-C. J. Kuo. MAI-free MC-CDMA systems based on Hadamard Walsh codes. *IEEE T. Signal Proces.*, 54: 3166–3179, Aug. 2006.

[137] G. V. Tsoulos and M. A. Beach. Calibration and linearity issues for an adaptive antenna system. In *Proc. IEEE VTC'97*, 1597–1600, May 1997.

[138] G. Ungerboeck. Channel coding with multilevel/phase signals. *IEEE T. Inform. Theory*, IT-28:55–67, 1982.

[139] K. Usuda, H. Zhang, and M. Nakagawa. Pre-RAKE performance for pulse based UWB system in a standardized UWB short-range channel. *Proc. IEEE WCNC'04*, 2:920–925, 2004.

[140] P. P. Vaidyanathan. *Multirate Systems and Filter Banks*. Englewood Cliffs, Prentice-Hall, NJ, 1993.

[141] J.-J. van de Beek, M. Sandell, and P. O. Börjesson. ML estimation of time and frequency offset in OFDM systems. *IEEE T. Signal Proces.*, 45:1800–1805, Jul. 1997.

[142] J. J. van de Beek, P. O. Börjesson, M. L. Boucheret, D. Landström, J. M. Arenas, P. Ödling, C. Östberg, M. Wahlqvist, and S. K. Wilson. A time

and frequency synchronization scheme for multiuser OFDM. *IEEE J. Select. Areas Commun.*, 17:1900–1914, Nov. 1999.

[143] M. Varanasi and B. Aazhang. Multistage detection in asynchronous code-division multiple-access communications. *IEEE Trans. Commun.*, 38:509–519, Apr. 1990.

[144] S. Verdu. *Multiuser Detection.* Cambridge University Press, 1998.

[145] E. Visotsky and U. Madhow. Space-time transmit precoding with imperfect feedback. *IEEE Trans. Inform. Theory*, 47(6):2632–2639, September 2001.

[146] A. J. Viterbi. *CDMA: Principles of Spread Spectrum Communication.* Addison-Wesley, Reading, MA, 1995.

[147] B. R. Vojcic and W. M. Jang. Transmitter precoding in synchronous multiuser communications. *IEEE Trans. Commun.*, 46(10):1346–1355, Oct. 1998.

[148] Q. Wang and V. K. Bhargava. An efficient maximum lielihood decoding algorithm for generalized tail biting convolutional codes including quasicyclic codes. *IEEE Trans. Commun.*, 37:875–879, 1989.

[149] Z. Wang and G. B. Giannakis. Linearly precoded or coded OFDM against wireless channel fades. In *Third IEEE Signal Processing Workshop on Signal Processing Advances in Wireless Communications.*, page 267.

[150] S. S. H. Wijayasuriya, G. H. Norton, and J. P. McGeehan. A near-far resistant sliding window decorrelating algorithm for multi-user detectors in DS-CDMA systems. In *Proc. IEEE Globecom Conference*, pages 1331–1338. San Fransisco, CA, Dec. 1992.

[151] M. Z. Win and R. A. Scholtz. On the energy capture of ultrawide bandwidth signals in dense multipath environments. 2(9):245–247, Sep. 1998.

[152] C. Windpassinger, R. F. H. Fischer, T. Vencel, and J. B. Huber. Precoding in multiantenna and multiuser communications. 3(4):1305–1316, 2004.

[153] X. Xia. Precoded and vector OFDM robust to channel spectral nulls and with reduced cyclic prefix length. *IEEE T. Commun.*, 49: 1363–1374, 2001.

[154] Y. Xin, Z. Wang, and G. Giannakis. Space-time diversity systems based on linear constellationprecoding. *IEEE T. Wireless Commun.*, 2(2):502–513, 2003.

[155] N. Yee, J. P. Linnartz, and G. Fettweis. Multi-carrier CDMA in indoor wireless radio networks. *IEICE T. Commun.*, E77-B:900–904, Jul. 1994.

[156] H. Yoo and D. Hong. Edge sidelobe supressor scheme for OFDMA uplink systems. *IEEE Commun. Lett.*, 7:534–536, Nov. 2003.

[157] Y. Zhao and S. G. Haggman. Intercarrier interference self-cancellation scheme for OFDM mobile communication systems. *IEEE T. Commun.*, 49:1185–1191, 2001.

[158] S. Zhou, X. Cai, and G. B. Giannakis. Group-orthogonal multicarrier CDMA. *IEEE T. Commun.*, 52:90–99, Jan. 2004.

Index